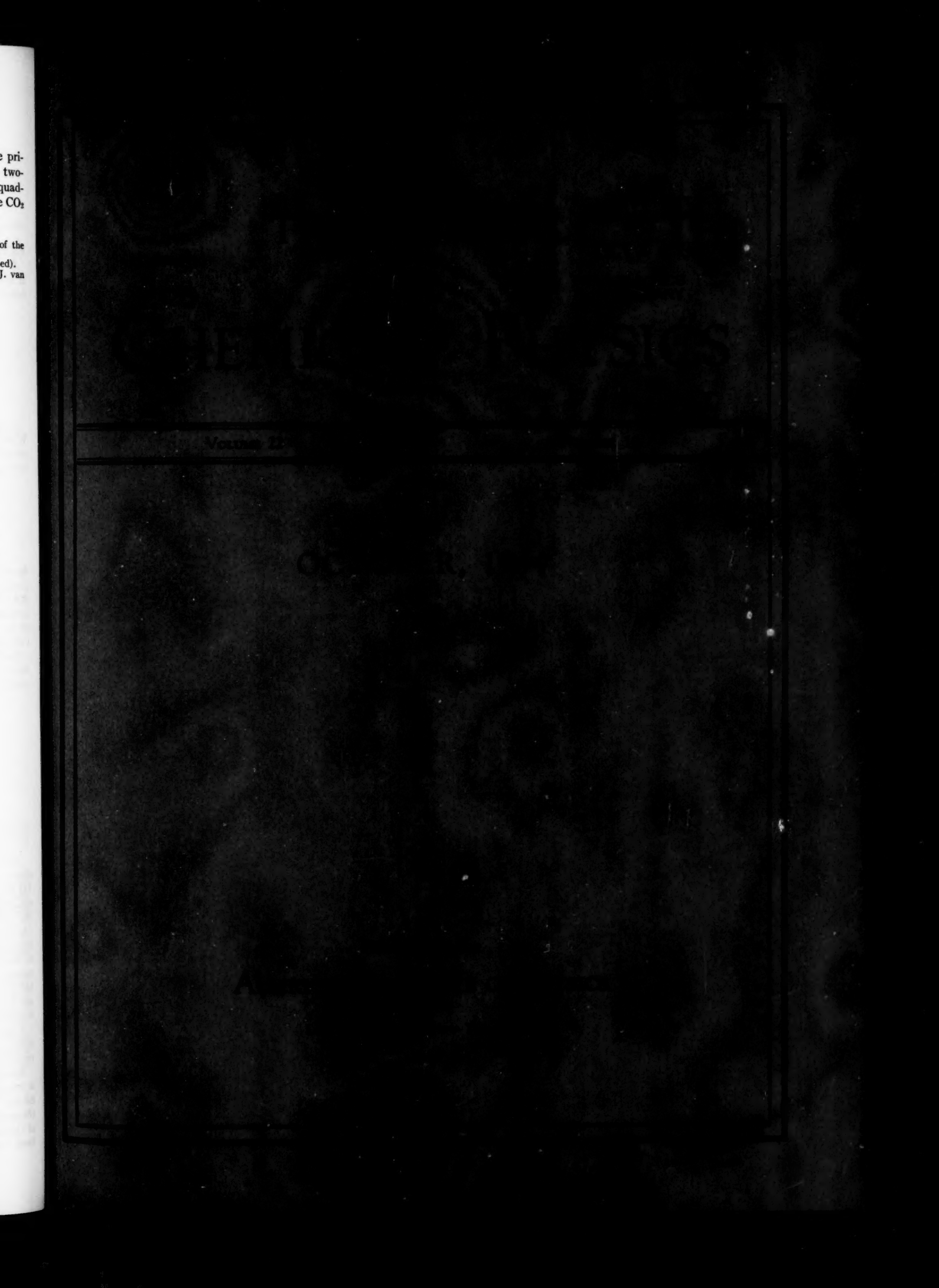

Editor

Associate Editors

Reviews of Modern Physics

Reviews of Modern Physics

Publication Committee

Chairman

Members

Reviews of Modern Physics

Reviews of Modern Physics

Reviews of Modern Physics

THE JOURNAL
OF
CHEMICAL PHYSICS

VOLUME 22, NUMBER 10 OCTOBER, 1954

A Proposal for Fundamental Equations of Dynamics of Gases under High Stress (A Proposal for Statistical Mechanical Treatment of Systems Not in Thermal Equilibrium Associated with Transport Phenomena)

TOYOKI KOGA
Faculty of Engineering, Nagoya University, Nagoya, Japan
(Received September 30, 1952)

In order to derive the fundamental equations of gas dynamics which are valid for the flow at high shearing stress and low gas pressure, an attempt was made to eliminate the assumption that the state concerned departs only slightly from thermal equilibrium, as we frequently find phenomena which cannot be treated under this assumption.

First, the state of gas in an intermediate volume element was microscopically represented in terms of the quantities of transport. Considering their averages over an intermediate time interval, an attempt was made to find the statistical character of the system. In other words, under the assumption that the macroscopic observation is possible or that the macroscopic law can be established, it was shown that the Boltzmann-Planck method in a new sense is applicable to the present systems. The new distribution function thus derived, $f=\exp(\alpha+\Sigma\beta_\xi c_\xi+\Sigma\Sigma\gamma_{\xi\eta}c_\xi c_\eta+\cdots)$ (where $\mathbf{c}$ denotes the velocity of a particle), should satisfy the Boltzmann-Maxwell equation. This can be shown by means of Kirkwood's verification accepted in some extended meaning.

In solving the B-M equation (hereafter, the B-M equation is the abbreviation of the Boltzmann-Maxwell equation) from this new standpoint, the stress components were taken together with mass density and velocity of mass motion as the independent variables in the zeroth approximation, although usually temperature is taken in place of stress. This method of treatment is analogous to that of Enskog and Chapman, although some important modifications are found in the latter half of the treatment. The fundamental equations of gas dynamics have been derived. Instead of viscosity and thermal conductivity, a new conception arises in the equations. That conception is conductivity of stress.

INTRODUCTION

As is well known, the current fundamental equations of gas dynamics consist of the equation of continuity (mass conservation), Navier-Stokes' equation (momentum conservation), the equation of energy (energy conservation), and a few equations of state (Boyle-Charles' law, the relations between viscosity and temperature, and between thermal conductivity and temperature).

The process of deriving the equations is not perfectly clear from the point of view of continuous medium,[1] but it has been examined closely by means of the molecular theory of gases. The first postulation set here is that the transport phenomena observed macroscopically do not represent gross deviations from thermal equilibrium. For instance, we assume that there are the following relations between the components of stress, i.e., momentum of transport:

$$T_{xx}\doteqdot T_{yy}\doteqdot T_{zz}\gg|T_{\xi\eta}|\ (\xi\neq\eta),\qquad \left.\begin{matrix}\xi\\ \eta\end{matrix}\right\}=x,y,z. \tag{1}$$

That is to say, the deviation from thermal equilibrium is not large. As will be shown later, the object of the present article is to eliminate, to some extent, this limitation of the theory.

(1) On the assumption of slight deviation from thermal equilibrium, we have the excellent study of Kirkwood.[2] In his study, the important points are as follows:

(a) Changes in state of gases measured are the secular changes concerning time. There are microscopic fluctuations with time, and the state observed is the average over an interval of moderate scale. Let τ denote

[1] Wien-Harms, *Handbuch der Experimentalphysik* (Akademische Verlagsgesellschaft M. B. H., Leipzig, 1931), Bd. 4, 1 Teil, SS. 350–359.

[2] John G. Kirkwood, J. Chem. Phys. **14**, 180 (1946); **15**, 72 (1947).

the interval of time, which is small macroscopically but large microscopically.

$$\frac{1}{\tau}\int_0^\tau \rho(\mathbf{p},\mathbf{q},t+s)ds=\bar{\rho}=f(\mathbf{p},\mathbf{q},t). \tag{2}$$

Here, ρ is the fine-grained density of a particle and f the coarse-grained.

(b) In the microscopic sense, the density ρ_i of a molecule i is expressed as follows:

$$\rho_i=f_i^{(0)}+\varphi_i, \tag{3}$$

where $f^{(0)}$ is the most probable distribution function of the thermal equilibrium state from which the state concerned departs only slightly, and φ is the fluctuation and the deviation caused by the nonuniformity. Under this assumption,

$$f_i^{(0)}\gg|\varphi_i|. \tag{4}$$

And as for the average over τ, there is a relation

$$\langle\rho_i\rho_l\rangle_{Av}=\bar{\rho}_i\bar{\rho}_l+0(\langle\varphi_i\varphi_l\rangle_{Av})\doteqdot f_if_l. \tag{5}$$

(c) Liouville's equation has to be accepted in the microscopic sense. The B-M equation, prescribing the variation of f, is the result of Liouville's equation averaged over the time interval τ, and is accepted in the macroscopic sense.

(2) The consequences of Kirkwood's study described above have been developed by Enskog and Chapman and other investigators.[3] By their method the fundamental equations of gas dynamics are derived reasonably from the B-M equation. The distribution function f is developed in a series in the following way:

$$\left.\begin{aligned} &f=f^{(0)}+f^{(1)}+f^{(2)}+\cdots,\\ &f^{(0)}\gg|f^{(1)}+f^{(2)}+\cdots|. \end{aligned}\right\} \tag{6}$$

Here, T, the usual notation of temperature, in $f^{(0)}$ does not have the same physical meaning as that in thermal equilibrium. Strictly speaking, this is a parameter concerning energy.[4] Taking n as the density of number of the molecules, there are the relations[5]

$$\left.\begin{aligned} &f^{(k)}\sim n^{(1-k)},\\ &k=1,2,3,\cdots. \end{aligned}\right\} \tag{7}$$

When n is of moderate scale and the macroscopic changes of the state are also moderate, a good approximation is obtained in terms of $f^{(0)}+f^{(1)}$.

As described previously, the studies on the transport phenomena of gases seem to have been completed. Nevertheless there arises some doubt of the validity of assumption (4) in future gas dynamics. We see an example in the following:

The viscosity coefficient of air μ is about 2×10^{-4} in cgs units, and in the present example μ is taken as nearly constant over a vast range of temperature. Assuming that the consideration of usual gas dynamics is adequate for use in the boundary layer flow near a rigid body flying up in the air, we can infer that the stress approaches

$$T_{xz}=5\times10^4 \text{ dyne/cm}^2,$$
$$T_{xy}=2\times10^3 \text{ dyne/cm}^2,$$

at the altitude of 2×10^4 m at the speed of 10^3 m/sec. The higher altitude and speed become, the nearer T_{xz} and T_{yy} approach each other. This contradicts the assumption (1). Further, when considering the circumstances (7), it is surmised that the convergence of the right-hand side of (6) is not sufficiently good under the condition that n is comparatively small.

Next, let us consider the energy of transport. Taking 5×10^{-5} cal cm^{-1} sec^{-1} c^{0-1} for the coefficient of thermal conductivity of air, the heat conducted in the above described case is surmised to be 2×10^7 in cgs units. Equating this value to (density of air)$\times$(velocity)^3, we find 2×10^{13} (cm/sec)^3 for (velocity)^3. We can expect the mean speed of random motion of 10^5 cm/sec, considering the high temperature in the boundary layer. On the other hand, 2×10^{13} (cm/sec)^3 divided by $(10^5)^2$ (cm/sec)^2 gives 10^3 cm/sec. Consequently, from the viewpoint of energy of transport, the deviation from thermal equilibrium does not seem large.

Difficulties of a similar kind are found in shock front.[6]

Prigogine[7] showed precisely that there is a limit to the domain of the current theory. Although a few authors[8] have tried to overcome the difficulties, the results have not yet been proved entirely successful.

The present study is intended to eliminate the assumption that the state under consideration departs only slightly from thermal equilibrium. The problem is reconsidered on the basis of statistical mechanics. Molecules are assumed to be perfectly elastic spheres (in the sense of classical dynamics) which collide only binarily with each other. Consequently the result is applicable only to gases of sufficiently low density. We do not pay attention to the effects of intermolecular potentials on which, for example, Born and Green[9] focused their attentions in their theory of liquids.

In the first part of this article we obtain a function from the statistical point of view as an approximate expression for the most probable distribution of the

[3] S. Chapman and T. G. Cowling, *The Mathematical Theory of Non-Uniform Gases* (Cambridge University Press, London, 1936).

[4] T. Koga and N. Taketa, J. Phys. Soc. (Japan) **4**, 34 (1949); **7**, 143 (1952). And also see Subsection 3 of the Appendix.

[5] See reference 3, p. 116.

[6] L. H. Thomas, J. Chem. Phys. **12**, 449 (1944).

[7] S. R. De Groot, *Thermodynamics of Irreversible Process* (North-Holland Publishing Company, Amsterdam, 1951), Chaps. 3 and 81.

[8] H. M. Mott-Smith, Phys. Rev. **82**, 885 (1951); K. Zolles, Z. Physik **130**, 1 (1951); H. Grad, Communs. Pure Appl. Math. **2**, 331 (1949).

[9] M. Born and H. S. Green, Proc. Roy. Soc. (London) **A188**, 10 (1946).

system concerned. This function is different from that of Maxwell. Our systems cannot be approximately expressed in terms of Maxwell's function. In spite of this, we can prove that Kirkwood's verification of the B-M equation is also valid as to these systems.

In the subsequent part, the B-M equation is solved in consequence of the results explained in the first sections. The treatment is similar to that of Enskog and Chapman[3] so far as the general form of hydrodynamical equations is concerned. Our method deviates from that of Enskog and Chapman as explained in Sections 7 and 8 where we treat in detail the terms contained in the equations.

I. VALIDITY OF THE BOLTZMANN-MAXWELL EQUATION

In verification of the validity of the B-M equation, Kirkwood assumed that the state concerned deviates only slightly from thermal equilibrium. In other words, the coarse-grained distribution function f was assumed to depart only slightly from Maxwell's function. This assumption, no other point in his arguments being changed, is extensible or replaceable by the assumption that the most probable distribution corresponding to the macroscopic condition in question exists and predominates markedly over the other possible distributions under the same condition.

In Kirkwood's original presentation,

fine-grained probability density of a particle = coarse-grained probability density in thermal equilibrium + (small deviation + fluctuation). (1.1)

In the extended meaning we assume that

fine-grained probability density of a particle = approximate coarse-grained probability density in the state concerned (non-thermal-equilibrium) + (small deviation + fluctuation), (1.2)

where the first term in the right-hand side, for which Maxwell's function is not substitutive, must be sufficiently large compared with the terms in parentheses. In Kirkwood's treatment, one can substitute the relation (1.2) for the relation (1.1) without disturbing all the other arguments.

We expect that we can find such an approximate coarse-grained probability function from a statistical viewpoint, postponing, for the present, the treatment of the B-M equation.

II. EXPRESSION OF A SYSTEM OF MOLECULES IN TERMS OF QUANTITIES OF TRANSPORT

For the sake of simplicity we restrict our attention to a gas consisting of the single component, monatomic molecule. The mass of each molecule is m. It is assumed that there are Ωn molecules in a cell of intermediate volume Ω, which is small in a macroscopic sense but large compared with microscopic dimensions. (Let Ω denote the volume of a cell and also the cell itself.) At an instant of time in the microscopic sense, the state of the system of Ωn molecules in the cell is specified by the velocities of the molecules $c_{\nu x}$, $c_{\nu y}$, and $c_{\nu z}$. Here, $\nu=1, 2$, and $3, \cdots, \Omega n$. The spatial distribution of the molecules in Ω will not be discussed here, as no external force and no influence of intermolecular potential are assumed to be present.

In terms of these velocity components, we construct the following quantities which are independent of each other:

$$\left.\begin{aligned} m\sum_{\nu=1}^{\Omega n} c_{\nu\xi} &= \Omega t_\xi, \\ m\sum c_{\nu\xi}c_{\nu\eta} &= \Omega t_{\xi\eta}, \\ m\sum c_{\nu\xi}c_{\nu\eta}c_{\nu\zeta} &= \Omega t_{\xi\eta\zeta}, \\ \left.\begin{matrix}\xi\\ \eta\\ \zeta\\ \cdot\\ \cdot\\ \cdot\end{matrix}\right\} &= x, y, z, \end{aligned}\right\} \tag{2.1}$$

where $3\Omega n$ of the t's are independent of one another from the viewpoint of microscopic dynamics. Their physical meanings are obvious: t_ξ is the momentum in unit volume, $t_{\xi\eta}$ the flux of momentum through unit area per unit time, etc. When the values of all these quantities are given, the state of the system is microscopically determined, although the spatial distribution of molecules is not determined in Ω.

In this case, the density of energy is $(t_{xx}+t_{yy}+t_{zz})/2$, and the flux of energy is $(t_{xx\xi}+t_{yy\xi}+t_{zz\xi})/2$, where $\xi=x, y, z$.

III. MACROSCOPICALLY OBSERVABLE STATE (OR STATE UNDER MACROSCOPIC LAW) AND THE REPRESENTATIVE ENSEMBLE OF SYSTEMS IN Ω AND τ

From the viewpoint of classical dynamics, if we could measure with sufficient accuracy the positions and momenta of all the particles of gas at an instant of time, we should be able to predict, at least in principle, all the future behaviors of the system. There are two reasons why this attempt seems to be hopeless. First, we cannot carry out an accurate observation of each individual particle. Secondly, we cannot solve the equations of motion in such a complicated system.

We may assume as follows: As to our system, there is a certain sufficiently accurate law between cause and effect which can be formulated in terms of a very small number of macroscopic variables compared with the degrees of microscopic freedom. Here those variables appear as continuous functions of time and space in the

macroscopic sense, and the law takes the form of hydrodynamics. Each macroscopic instant of time has some length τ in the microscopic sense, and each macroscopic point of space has some volume Ω in the microscopic sense. The variables under consideration at a macroscopic point of time and space are the results of averaging some microscopic quantities over the intermediate duration and volume. The t's given in (2.1) and n are the averages over volume in this sense. The macroscopic variables in terms of which the macroscopic law is formulated are surmised to be obtained as the results of averaging n, t_ξ, $t_{\xi\eta}$, $\cdots$, etc., over τ. Let $\bar{n}$, $\bar{t}_\xi$, $\bar{t}_{\xi\eta}$, $\cdots$, etc., denote the averages.

As to an isolated system in thermal equilibrium, the essential quantities are the mass density mn, momentum density t_ξ, and energy density $(t_{xx}+t_{yy}+t_{zz})/2$, which are conserved in an isolated system and are equal, respectively, to $m\bar{n}$, $\bar{t}_\xi$, and $(\bar{t}_{xx}+\bar{t}_{yy}+\bar{t}_{zz})/2$.* The macroscopic law of the system can be completed in terms of these macroscopic variables.

In the case of systems not in thermal equilibrium where interactions take place between cells, some other variables must be considered in addition. In Enskog and Chapman's approximation, momentum of transport $\bar{t}_{\xi\eta}$ and energy of transport $(\bar{t}_{xx\xi}+\bar{t}_{yy\xi}+\bar{t}_{zz\xi})/2$ are taken anew into the macroscopic law in addition to the macroscopic variables mentioned above in thermal equilibrium, although the new variables are supplementary and are expressed in terms of derivatives of the main variables, i.e., mass, momentum, and energy. The added quantities are not conserved in an isolated system.

On the other hand, as was shown in the introductory section, we find some cases where not only mass, momentum, and energy but also some other variables should be taken into account as the main or essential variables, with their derivatives as the supplementary terms necessary to complete the macroscopic law.

Only after repeated trials, we can select out of the t's (2.1) *the variables which are essential or main to complete the macroscopic law.*

For example, let

$$\bar{n},\ \bar{t}_\xi,\ \bar{t}_{\xi\eta} \tag{3.1}$$

be known as or assumed to be the most essential or the most important of the independent variables. In other words, among the averages of the t's (2.1) over τ, some are functions of $\bar{n}$, $\bar{t}_\xi$, and $\bar{t}_{\xi\eta}$ and the remainders are supplementary and presented in terms of derivatives of $\bar{n}$, $\bar{t}_\xi$, and $\bar{t}_{\xi\eta}$.

Let us assume, in the zeroth approximation, that the macroscopic condition in Ω and τ is perfectly expressed by the values of the variables (3.1), and that the fluctuations of the values of n, t_ξ, and $t_{\xi\eta}$ are negligibly small.† This means that

$$n=\bar{n},\quad t_\xi=\bar{t}_\xi,\quad t_{\xi\eta}=\bar{t}_{\xi\eta}$$

throughout the interval τ. Then we can represent the microscopic conditions in Ω and τ, excluding the microscopic locations of molecules in the configuration space, by means of positions in the region D of a momentum space of $3n\Omega$ dimensions enclosed by the multidimensional surfaces which are represented by the equations

$$t_\xi=a_\xi,\qquad t_\xi=a_\xi+\delta a_\xi,$$

$$t_{\xi\eta}=a_{\xi\eta},\quad t_{\xi\eta}=a_{\xi\eta}+\delta a_{\xi\eta},$$

where a_ξ and $a_{\xi\eta}$ are given, and δa_ξ and $\delta a_{\xi\eta}$ are sufficiently small and definite. A point in D, each situation of which represents the momenta of the molecules in Ω at each microscopic instant, moves inside D of the momentum space as time goes on.

Consequently we must consider the fluctuations of the quantities (other than n, t_ξ, and $t_{\xi\eta}$) given in (2.1); they have their own fluctuating values as the point moves inside D. According to the assumption given at the beginning, their averages over τ, however, are known to be functions of n, t_ξ, and $t_{\xi\eta}$ only, or to be small and neglected in the zeroth approximation.

If the point did stay in a particular part of D much longer‡ than in the other part, some of the quantities (2.1) which are different from n, t_ξ, and $t_{\xi\eta}$ should have their own average values independent of $\bar{n}$, $\bar{t}_\xi$, and $\bar{t}_{\xi\eta}$ proper to the particular part. In other words, n, t_ξ, and $t_{\xi\eta}$ can specify D only; some other quantities specify the particular part in D. Consequently we should refer to the new variables in formulating the macroscopic law. This contradicts the assumption given at the beginning that only $\bar{n}$, $\bar{t}_\xi$, and $\bar{t}_{\xi\eta}$ are the essential and independent variables necessary for describing the macroscopic law. Therefore, the uniformity of the probability density of the points in D representing the microscopic state in Ω and τ may be taken as sufficient requirement. In other words, the probability density in D is a function of n, t_ξ, and $t_{\xi\eta}$ only.

From the viewpoint of necessary condition, the points in D microscopically representing the momenta of the systems in Ω and τ should not crowd together, at least not predominately at a few special parts of D making conspicuous colonies. Thus the grains of unevenness of density should be sufficiently fine and in sufficiently diffused distribution, if they do exist. Although this does not yet mean "ergodic distribution" in a mathematically strict sense, we surmise that the probability density in D is uniform to such a degree that the coarse-grained probability density of a particle in Ω and τ ob-

* Here it is not necessary to give any upper limits to Ω and τ, and sometimes angular momentum is considered in addition. With the exception of these, which are mutually independent, some of the averages of the t's over τ are dependent upon $\bar{n}$, $\bar{t}_\xi$, and $\bar{t}_{\xi\eta}$, and the other averages disappear.

† Here we have to set the lower limit to Ω to keep the fluctuations small. The circumstances are assumed to be analogous to the cases of grand canonical ensemble in thermal equilibrium.

‡ This consideration is given in a statistical sense.

tained under the condition of perfectly uniform density in D (a region of momentum space) is substitutive, at least, for the first term in the right-hand side of Eq. (1.2).

Here we add that we have not yet discussed the spatial situations of molecules in Ω and τ, as no external force and no influence of intermolecular potential are assumed to be present. (On the effects of intermolecular potentials Born and Green focused their attentions in their theory of liquids.[9])

IV. THE MOST PROBABLE DISTRIBUTION

In accordance with our conclusion in the last section, we are trying to find the most probable distribution function of molecules in Ω and τ under the condition that, for instance, $\bar{n}$, $\bar{t}_\xi$, and $\bar{t}_{\xi\eta}$ are the independent macroscopic variables: First, we divide the region D into parts in such a way that the states of the systems represented by the positions in each individual part are, in the statistical sense, indistinguishable one from the other. Next, we identify the largest of the parts. The most probable distribution is assumed to be the molecular distribution proper to the largest part. The treatment is similar to that of Boltzmann-Planck by means of Lagrange's method of indeterminate multipliers.[10] Under the condition that

$$\left.\begin{array}{l} n \text{ remains constant, } t_\xi \text{ remains within an infinitesimal range, } t_{\xi\eta} \text{ remains within an infinitesimal range (consequently } t_{xx}+t_{yy} \\ +t_{zz} \text{ also remains within an infinitesimal range),} \end{array}\right\} \tag{4.1}$$

we find for the most probable distribution function

$$f^{(0)}=\exp(\alpha+\sum\beta_\xi c_\xi+\sum\sum\gamma_{\xi\eta}c_\xi c_\eta). \tag{4.2}$$

The parameters α, β, and γ are functions of time and position in configuration space, and by means of them $f^{(0)}$ varies with time and space in the macroscopic sense.

Recalling Kirkwood's investigation or the investigation given in Section 1 of this article, we see that $f^{(0)}$ is subject to the B-M equation in the following way,

$$\left.\begin{array}{l} \dfrac{\partial f}{\partial t}+c_x\dfrac{\partial f}{\partial x}+c_y\dfrac{\partial f}{\partial y}+c_z\dfrac{\partial f}{\partial z}=-J, \\ f=f^{(0)}+\varphi, \quad f^{(0)}\gg|\varphi|. \end{array}\right\} \tag{4.3}$$

Here, J denotes the decrease of f by means of collisions in unit time interval and in unit volume.

V. THE ZEROTH APPROXIMATION TO HYDRODYNAMICAL EQUATIONS

In the preceding section, $\bar{n}$, $\bar{t}_\xi$, and $\bar{t}_{\xi\eta}$ were provisionally given as the most essential independent macroscopic variables. In general, our final decision as to what are the essential variables is made only after repeated trials. The choice of the essential variables changes according to the phenomena to which the theory is applied.

As a specific example we give below the derivation of the fundamental equations of dynamics of gases in the case where $\bar{n}$, $\bar{t}_\xi$, and $\bar{t}_{\xi\eta}$ are the essential and independent variables, and consequently the zeroth approximation to the distribution function is given by

$$f^{(0)}=\exp(\alpha+\sum\beta_\xi c_\xi+\sum\sum\gamma_{\xi\eta}c_\xi c_\eta) \tag{5.1}$$

as set forth in Section 4.

As will be shown in this section and the following, so far as determination of the general form for hydrodynamical equations of gases is concerned, our treatment is similar to that of Enskog, Chapman, and Cowling. Our method differs in actual calculation of the function $f^{(1)}$ which is the first supplementary term of the series

$$f=f^{(0)}+f^{(1)}+f^{(2)}+\cdots. \tag{5.2}$$

The function $f^{(0)}$ in our theory is complicated when compared with Maxwell's. It is difficult to find $f^{(1)}$ explicitly by solving the integral equation as derived according to the method of Enskog and Chapman. We can determine $f^{(1)}$ by means of another method, a method originated by Meyer and recently developed by the author and his co-worker, as mentioned in the appendix hereto.

We use the following notations:

ρ, the density of gas,
$\mathbf{v}=(v_x\ v_y\ v_z)$, the velocity of mass motion,
$\mathbf{T}=\begin{bmatrix} T_{xx} & T_{xy} & T_{xz} \\ T_{xy} & T_{yy} & T_{yz} \\ T_{xz} & T_{yz} & T_{zz} \end{bmatrix}$, the stress.

According to the following definitions,

$$\left.\begin{array}{l} \displaystyle\int\int\int_{-\infty}^{+\infty} mf^{(0)}d\mathbf{c}=\rho, \\ \displaystyle\int\int\int mc_\xi f^{(0)}d\mathbf{c}=\rho v_\xi, \\ \displaystyle\int\int\int m(c_\xi-v_\xi)(c_\eta-v_\eta)f^{(0)}d\mathbf{c}=T_{\xi\eta}, \\ d\mathbf{c}=dc_x dc_y dc_z, \end{array}\right\} \tag{5.3}$$

the parameters α, β, and γ, included in the function $f^{(0)}$ (5.1) are expressed[11] in terms of ρ, v_ξ, and $T_{\xi\eta}$,

[10] R. C. Tolman, *The Principles of Statistical Mechanics* (Oxford University Press, London, 1938), p. 79.

[11] S. S. Wilks, *Mathematical Statistics* (Princeton University Press, Princeton, New Jersey, 1950), Sec. 3.23. The present author independently obtained the same result.

with the result

$$f^{(0)}=\frac{\rho^{5/2}}{m(8\pi^3|\mathbf{T}|)^{\frac{1}{2}}}\exp\left\{\frac{-\rho(|T_{xx}|C_x^2+|T_{yy}|C_y^2+|T_{zz}|C_z^2+2|T_{xy}|C_xC_y+2|T_{xz}|C_xC_z+2|T_{yz}|C_yC_z)}{2|\mathbf{T}|}\right\}. \quad (5.4)$$

Here,

$$\left.\begin{aligned} &C_\xi=c_\xi-v_\xi,\\ &|\mathbf{T}|=\begin{vmatrix}T_{xx}&T_{xy}&T_{xz}\\T_{xy}&T_{yy}&T_{yz}\\T_{xz}&T_{yz}&T_{zz}\end{vmatrix},\quad |T_{xx}|=\begin{vmatrix}T_{yy}&T_{yz}\\T_{yz}&T_{zz}\end{vmatrix},\quad |T_{xy}|=-\begin{vmatrix}T_{xy}&T_{yz}\\T_{xz}&T_{zz}\end{vmatrix},\ \cdots,\ \text{etc.}\\ &\mathbf{S}=\frac{1}{|\mathbf{T}|}\begin{Vmatrix}|T_{xx}|&|T_{xy}|&|T_{xz}|\\|T_{xy}|&|T_{yy}|&|T_{yz}|\\|T_{xz}|&|T_{yz}|&|T_{zz}|\end{Vmatrix},\\ &\mathbf{S}:\mathbf{T}=3\quad\left(\sum_\xi\sum_\eta S_{\xi\eta}T_{\eta\xi}=3\right),\\ &\mathbf{S}\cdot\mathbf{T}=\mathbf{U}\quad\left(\sum_\eta S_{\xi\eta}T_{\eta\xi}=\delta_{\xi\zeta}\right).\end{aligned}\right\} \quad (5.4')$$

and consequently

Hereafter we sometimes use such symbols of summation as appear in (5.4′).

The equation, to which the variables ρ, v_ξ, and $T_{\xi\eta}$ included in $f^{(0)}$ are subject in the zeroth approximation, is given as follows according to relations (4.3) and the assumption that $f^{(0)}$ is the zeroth approximation to the distribution function

$$\frac{\partial f^{(0)}}{\partial t}+c_x\frac{\partial f^{(0)}}{\partial x}+c_y\frac{\partial f^{(0)}}{\partial y}+c_z\frac{\partial f^{(0)}}{\partial z}=-J^{(0)}: \quad (5.5)$$

$$\left.\begin{aligned} &J^{(0)}=\int\int(f^{(0)}f_1^{(0)}-f^{(0)\prime}f_1^{(0)\prime})kd\mathbf{k}d\mathbf{c}_1,\\ &f_1^{(0)}=f^{(0)}(\mathbf{c}_1),\quad f^{(0)\prime}=f^{(0)}(\mathbf{c}'),\quad f_1^{(0)\prime}=f^{(0)}(\mathbf{c}_1'),\end{aligned}\right\} \quad (5.5')$$

where $\mathbf{c}'$ is the velocity of the particle which has the velocity $\mathbf{c}$ after collision, and $\mathbf{c}_1'$ is the velocity of another particle having the velocity $\mathbf{c}_1$ after the same collision.§

Multiplying Eq. (5.5) by $md\mathbf{c}$ and integrating throughout the velocity-space, we obtain for the equation of continuity[12]

$$\left.\begin{aligned} &\frac{D_0\rho}{Dt}\left(=\frac{D\rho}{Dt}\right)=-\rho\left(\frac{\partial v_x}{\partial x}+\frac{\partial v_y}{\partial y}+\frac{\partial v_z}{\partial z}\right),\\ &\frac{D}{Dt}\equiv\frac{\partial}{\partial t}+v_x\frac{\partial}{\partial x}+v_y\frac{\partial}{\partial y}+v_z\frac{\partial}{\partial z}.\end{aligned}\right\} \quad (5.6)$$

In this equation $D_0\rho/Dt$ means the zeroth approximation to $D\rho/Dt$. But this is a special case where $D_0\rho/Dt$ coincides with $D\rho/Dt$ according to the condition (5.3) and the law of mass conservation at collision. Next let us multiply Eq. (5.5) by $mc_\xi d\mathbf{c}$ and integrate the result. Then we obtain for the equation of momentum

$$\frac{D_0v_\xi}{Dt}\left(=\frac{Dv_\xi}{Dt}\right)=-\frac{1}{\rho}\left(\frac{\partial T_{\xi x}}{\partial x}+\frac{\partial T_{\xi y}}{\partial y}+\frac{\partial T_{\xi z}}{\partial z}\right). \quad (5.7)$$

Here also D_0v_ξ/Dt coincides with Dv_ξ/Dt according to the condition (5.3) and the law of momentum conservation. Further, multiplying Eq. (5.5) by $mc_\xi c_\eta d\mathbf{c}$, we find for the equation of stress

$$\begin{aligned}\frac{D_0T_{\xi\eta}}{Dt}=&-T_{\xi\eta}\left(\frac{\partial v_x}{\partial x}+\frac{\partial v_y}{\partial y}+\frac{\partial v_z}{\partial z}\right)\\&-\left(T_{\xi x}\frac{\partial v_\eta}{\partial x}+T_{\xi y}\frac{\partial v_\eta}{\partial y}+T_{\xi z}\frac{\partial v_\eta}{\partial z}\right)\\&-\left(T_{\eta x}\frac{\partial v_\xi}{\partial x}+T_{\eta y}\frac{\partial v_\xi}{\partial y}+T_{\eta z}\frac{\partial v_\xi}{\partial z}\right)-I_{\xi\eta}^{(0)},\end{aligned} \quad (5.8)$$

where

$$I_{\xi\eta}^{(0)}=\int mc_\xi c_\eta J^{(0)}d\mathbf{c} \quad (5.9)$$

and

$$\frac{D_0T_{\xi\eta}}{Dt}\neq\frac{DT_{\xi\eta}}{Dt}. \quad (5.10)$$

On account of the relation (5.10), Eq. (5.8) is valid only to the zeroth degree of approximation, although Eqs. (5.6) and (5.7) are not modified for the next approximation.

VI. THE FIRST APPROXIMATION TO HYDRODYNAMICAL EQUATIONS

To complete the hydrodynamical equations to the next degree of approximation, we must take the first

§ The details of illustration will be given in Section 8. The molecules are assumed to be of spherical form and perfectly elastic.

[12] See reference 3, pp. 47–50.

supplementary term $f^{(1)}$ of the series (5.2) into consideration. For the present, and referring to the relations (5.3), we assume that $f^{(1)}$ is subject to the following conditions:

$$\left.\begin{aligned} &\int mf^{(1)}d\mathbf{c}=0, \quad \int mC_\xi f^{(1)}d\mathbf{C}=0, \\ &\int mC_\xi C_\eta f^{(1)}d\mathbf{C}=0. \end{aligned}\right\} \tag{6.1}$$

As Enskog and Chapman assumed, we also take for granted (for the present) that $f^{(1)}$ is obtained by solving the following integral equation

$$\left.\begin{aligned} &\mathfrak{D}^{(0)}+J^{(0)}=-J^{(1)}, \\ &J^{(1)}=\int\int (f^{(0)}f_1^{(1)}-f^{(0)\prime}f_1^{(1)\prime}+f^{(1)}f_1^{(0)} \\ &\qquad -f^{(1)\prime}f_1^{(0)\prime})kd\mathbf{k}d\mathbf{c}_1, \end{aligned}\right\} \tag{6.2}$$

where $\mathfrak{D}^{(0)}$, being the zeroth approximation to

$$\left(\frac{\partial}{\partial t}+c_x\frac{\partial}{\partial x}+c_y\frac{\partial}{\partial y}+c_z\frac{\partial}{\partial z}\right)f^{(0)},$$

is defined by

$$\mathfrak{D}^{(0)}=f^{(0)}\left\{\frac{D_0\log f^{(0)}}{Dt}+\sum C_\xi\frac{\partial\log f^{(0)}}{\partial\xi}\right. \\ \left.-\sum\frac{D_0v_\xi}{Dt}\frac{\partial\log f^{(0)}}{\partial C_\xi}-\sum\sum\frac{\partial\log f^{(0)}}{\partial C_\xi}C_\eta\frac{\partial}{\partial_\eta}v_\xi\right\}. \tag{6.3}$$

Here, $f^{(0)}$ is specified as a function not of $\mathbf{c}$, x, y, z, t but of $\mathbf{C}$, x, y, z, t, and $D_0f^{(0)}/Dt$, the zeroth approximation to $Df^{(0)}/Dt$, is defined by[13]

$$\frac{D_0f^{(0)}}{Dt}=\frac{D_0\rho}{Dt}\frac{\partial f^{(0)}}{\partial\rho}+\sum\sum\frac{D_0T_{\xi\eta}}{Dt}\frac{\partial f^{(0)}}{\partial T_{\xi\eta}}.$$

According to the expression of $f^{(0)}$ (5.4) and Eqs. (5.6), (5.7), and (5.8), after long calculation, we get

$$\mathfrak{D}^{(0)}=f^{(0)}\left[\left(\frac{5}{2}\frac{1}{\rho}-\tfrac{1}{2}\mathbf{S}:\mathbf{CC}\right)\left(\frac{\partial\rho}{\partial\mathbf{r}}\cdot\mathbf{C}\right)\right. \\ +\{-\tfrac{1}{2}\mathbf{SC}+\tfrac{1}{2}\rho(\mathbf{S}\cdot\mathbf{S})\cdot\mathbf{CCC}-(\mathbf{S}\cdot\mathbf{C})\mathbf{U}\}:\frac{\partial\mathbf{T}}{\partial\mathbf{r}} \\ \left.+\tfrac{1}{2}\{\mathbf{S}-\rho(\mathbf{S}\cdot\mathbf{CC})\cdot\mathbf{S}\}:\mathbf{I}^{(0)}\right], \tag{6.4}$$

where $\mathbf{r}$ denotes the vector $(x\ y\ z)$. For the sake of further references, intermediate results of the calculation are given as follows:

$$\left.\begin{aligned} &\frac{D_0\log f^{(0)}}{Dt}=-\rho\left\{\frac{\partial\mathbf{v}}{\partial\mathbf{r}}:(\mathbf{S}\cdot\mathbf{CC})\right\} \\ &\qquad +\tfrac{1}{2}\mathbf{I}^{(0)}:\{\mathbf{S}-\rho(\mathbf{S}\cdot\mathbf{CC})\cdot\mathbf{S}\}, \\ &-\frac{\partial\log f^{(0)}}{\partial\mathbf{C}}\mathbf{C}:\frac{\partial\mathbf{v}}{\partial\mathbf{r}}=\rho(\mathbf{S}\cdot\mathbf{CC}):\frac{\partial\mathbf{v}}{\partial\mathbf{r}}, \\ &-\frac{D_0\mathbf{v}}{Dt}\cdot\frac{\partial\log f^{(0)}}{\partial\mathbf{C}}=-(\mathbf{S}\cdot\mathbf{C})\mathbf{U}:\frac{\partial\mathbf{T}}{\partial\mathbf{r}}, \\ &\mathbf{C}\cdot\frac{\partial\log f^{(0)}}{\partial\mathbf{r}}=\left(\frac{5}{2}\frac{1}{\rho}-\tfrac{1}{2}\mathbf{S}:\mathbf{CC}\right)\left(\frac{\partial\rho}{\partial\mathbf{r}}\cdot\mathbf{C}\right) \\ &\qquad +\{-\tfrac{1}{2}\mathbf{SC}+\tfrac{1}{2}\rho(\mathbf{S}\cdot\mathbf{S})\cdot\mathbf{CCC}\}:\frac{\partial\mathbf{T}}{\partial\mathbf{r}}. \end{aligned}\right\} \tag{6.5}$$

After short calculation, we have from (6.4)

$$\mathfrak{D}^{(0)}=f^{(0)}\left[\{-\tfrac{1}{2}\mathbf{SC}+\tfrac{1}{2}\rho(\mathbf{S}\cdot\mathbf{S})\cdot\mathbf{CCC}\right. \\ -(\mathbf{S}\cdot\mathbf{C})\mathbf{U}\}:\rho\frac{\partial}{\partial\mathbf{r}}\left(\frac{\mathbf{T}}{\rho}\right) \\ \left.+\tfrac{1}{2}\{\mathbf{S}-\rho(\mathbf{S}\cdot\mathbf{CC})\cdot\mathbf{S}\}:\mathbf{I}^{(0)}\right]. \tag{6.4'}$$

Now, assuming that $f^{(1)}$ has already been solved from Eq. (6.2), we write, for the first approximation to the B-M equation,

$$\left(\frac{\partial}{\partial t}+c_x\frac{\partial}{\partial x}+c_y\frac{\partial}{\partial y}+c_z\frac{\partial}{\partial z}\right)(f^{(0)}+f^{(1)})=-J^{(0)}-J^{(1)}, \tag{6.6}$$

where $-J^{(0)}$ is the right-hand side of (6.2). From this equation we can derive the stress equation in the first approximation, the zeroth approximation to which is Eq. (5.8). The derivation is carried out as follows: According to (6.3), Eq. (6.2) becomes

$$-J^{(0)}-J^{(1)}=\frac{D_0f^{(0)}}{Dt}+\sum C_\xi\frac{\partial f^{(0)}}{\partial\xi} \\ -\sum\frac{D_0v_\xi}{Dt}\frac{\partial f^{(0)}}{\partial C_\xi}-\sum\sum\frac{\partial f^{(0)}}{\partial C_\xi}C_\eta\frac{\partial v_\xi}{\partial\eta}. \tag{6.2'}$$

On the other hand, specifying $f^{(0)}+f^{(1)}$ in Eq. (6.6) as a function not of $\mathbf{c}$ but of $\mathbf{C}$, we find

$$-J^{(0)}-J^{(1)}=\frac{Df^{(0)}}{Dt}+\sum C_\xi\frac{\partial f^{(0)}}{\partial\xi}-\sum\frac{Dv_\xi}{Dt}\frac{\partial f^{(0)}}{\partial C_\xi} \\ -\sum\sum\frac{\partial f^{(0)}}{\partial C_\xi}C_\eta\frac{\partial v_\xi}{\partial\eta}+\frac{Df^{(1)}}{Dt}+\sum C_\xi\frac{\partial f^{(1)}}{\partial\xi} \\ -\sum\frac{Dv_\xi}{Dt}\frac{\partial f^{(1)}}{\partial C_\xi}-\sum\sum C_\eta\frac{\partial v_\xi}{\partial\eta}\frac{\partial f^{(1)}}{\partial C_\xi}.$$

[13] See reference 3, p. 49.

Comparing this with (6.2′), we get

$$\frac{Df^{(0)}}{Dt}-\sum\frac{Dv_\xi}{Dt}\frac{\partial f^{(0)}}{\partial C_\xi}+\frac{Df^{(1)}}{Dt}+\sum C_\xi\frac{\partial f^{(1)}}{\partial\xi}$$
$$-\sum\frac{Dv_\xi}{Dt}\frac{\partial f^{(1)}}{\partial C_\xi}-\sum\sum\frac{\partial f^{(1)}}{\partial C_\xi}C_\eta\frac{\partial v_\xi}{\partial\eta}=\frac{D_0f^{(0)}}{Dt}-\sum\frac{Dv_\xi}{Dt}\frac{\partial f^{(0)}}{\partial C_\xi}.$$

Replacing $\mathbf{C}$ by $\mathbf{c}-\mathbf{v}$ again in the left-hand side of this equation and rewriting the right-hand side by means of (6.5), we obtain

$$\frac{Df^{(0)}}{Dt}+\frac{\partial f^{(1)}}{\partial t}+\sum C_\xi\frac{\partial f^{(1)}}{\partial\xi}=f^{(0)}\left[-\rho\left\{\frac{\partial\mathbf{v}}{\partial\mathbf{r}}:(\mathbf{S}\cdot\mathbf{CC})\right\}\right.$$
$$\left.+\tfrac{1}{2}\mathbf{I}^{(0)}:\{\mathbf{S}-\rho(\mathbf{S}\cdot\mathbf{CC})\cdot\mathbf{S}\}-(\mathbf{S}\cdot\mathbf{C})\mathbf{U}:\frac{\partial\mathbf{T}}{\partial\mathbf{r}}\right]. \quad (6.7)$$

By multiplying the left-hand side of Eq. (6.7) by $mc_\xi c_\eta$ and the right-hand side by $m(C_\xi+v_\xi)(C_\eta+v_\eta)$, and integrating|| all the terms throughout the velocity-space, one obtains an equation for the first approximation to the equation of stress, the zeroth approximation to which is Eq. (5.8). The result is

$$\frac{D(T_{\xi\eta}+\rho v_\xi v_\eta)}{Dt}+\frac{\partial W_{\xi\eta x}}{\partial x}+\frac{\partial W_{\xi\eta y}}{\partial y}+\frac{\partial W_{\xi\eta z}}{\partial z}$$
$$=-\left[\mathbf{T}\cdot\frac{\partial\mathbf{v}}{\partial\mathbf{r}}\right]_{\xi\eta}-\left[\mathbf{T}\cdot\frac{\partial\mathbf{v}}{\partial\mathbf{r}}\right]_{\eta\xi}-[\mathbf{T}\cdot\mathbf{U}]_{\xi\eta}\,\mathrm{div}\mathbf{v}$$
$$-\rho v_\xi v_\eta\,\mathrm{div}\mathbf{v}-v_\xi\left[\frac{\partial}{\partial\mathbf{r}}\cdot\mathbf{T}\right]_\eta-v_\eta\left[\frac{\partial}{\partial\mathbf{r}}\cdot\mathbf{T}\right]_\xi-I_{\xi\eta}{}^{(0)},$$

or, being rearranged according to Eqs. (5.6) and (5.7), becomes

$$\frac{DT_{\xi\eta}}{Dt}+\left[\frac{\partial}{\partial\mathbf{r}}\cdot\mathbf{W}\right]_{\xi\eta}=-T_{\xi\eta}\,\mathrm{div}\mathbf{v}-\left[\mathbf{T}\cdot\frac{\partial\mathbf{v}}{\partial\mathbf{r}}\right]_{\xi\eta}$$
$$-\left[\mathbf{T}\cdot\frac{\partial\mathbf{v}}{\partial\mathbf{r}}\right]_{\eta\xi}-I_{\xi\eta}{}^{(0)}, \quad (6.8)$$

where

$$\mathbf{W}_{\xi\eta\zeta}=\int mC_\xi C_\eta C_\zeta f^{(1)}d\mathbf{C}. \quad (6.9)$$

$\mathbf{W}$ is a tensor of order 3 and will be treated concretely in the next section.

For the fundamental equations of gas dynamics we have obtained Eqs. (5.6), (5.7), and (6.8).

|| The following results of integrations are used:

$$\int mC_x{}^4f^{(0)}d\mathbf{C}=3T_{xx}{}^2/\rho,\quad \int mC_x{}^3C_yf^{(0)}d\mathbf{C}=3T_{xx}T_{xy}/\rho,$$
$$\int mC_x{}^2C_y{}^2f^{(0)}d\mathbf{C}=(T_{xx}T_{yy}+2T_{xy}{}^2)/\rho,$$
$$\int mC_xC_yC_z{}^2f^{(0)}d\mathbf{C}=(T_{xy}T_{zz}+2T_{xz}T_{yz})/\rho.$$

VII. DETAILED TREATMENT OF W

We have to calculate $f^{(1)}$ explicitly in order to express $\mathbf{W}$ in terms of derivatives of the main variables ρ, $\mathbf{v}$, and $\mathbf{T}$. By "Meyer's theory,"[14] we know that

$$\left.\begin{aligned}&f^{(1)}=-(\mathfrak{D}^{(0)}+J^{(0)})/\Theta,\\&\Theta=\pi\sigma^2\int f_1{}^{(0)}Vd\mathbf{C}_1\quad\text{(probability of collision)},\\&f_1{}^{(0)}\equiv f^{(0)}(\mathbf{C}_1),\\&V=\{(C_x-C_{1x})^2+(C_y-C_{1y})^2+(C_z-C_{1z})^2\}^{\frac{1}{2}},\\&\qquad\sigma:\text{the diameter of a molecule.}\end{aligned}\right\} \quad (7.1)$$

$\mathbf{W}$ is a tensor of order 3, whereas $\rho\partial(\mathbf{T}/\rho)/\partial\mathbf{r}$ is the only term of order of odd number included in $\mathfrak{D}^{(0)}$ (6.4′) and $J^{(0)}$. According to (7.1) and (6.9), we see that the only term which contributes to $\mathbf{W}$ is $\rho\partial(\mathbf{T}/\rho)/\partial\mathbf{r}$ among the terms of $\mathfrak{D}^{(0)}+J^{(0)}$. In general $f^{(0)}$ in Meyer's theory is slightly different from $f^{(0)}$ in Enskog-Chapman's treatment.[15] That is to say, the conditions (6.1) are not necessarily satisfied in Meyer's treatment. In Meyer's treatment, the parameters ρ, $\mathbf{v}$, and $\mathbf{T}$ are, respectively, the zeroth approximations to the density, mass velocity, and stress. Consequently, the first approximations to the density, mass velocity, and stress are, respectively, $\rho+\Delta\rho$, $\mathbf{v}+\Delta\mathbf{v}$, and $\mathbf{T}+\Delta\mathbf{T}$. Here $\Delta\rho$, $\Delta\mathbf{v}$, and $\Delta\mathbf{T}$ are the supplementary quantities composed of terms of derivatives of ρ, $\mathbf{v}$, and $\mathbf{T}$. Now $\mathbf{W}$ does not appear in the zeroth approximation. $\mathbf{W}$ appears first in the first approximation in terms of derivatives of $\mathbf{T}$. Consequently $\mathbf{W}$, to the first degree of approximation, is not influenced by the slight modifications of ρ, $\mathbf{v}$, and $\mathbf{T}$, although the influences should not be neglected in the next approximations.

According to the foregoing consideration, we select from $\mathfrak{D}^{(0)}$ (6.4′) the following,

$$\mathfrak{D}_W{}^{(0)}\equiv f^{(0)}\{-\tfrac{1}{2}\mathbf{SC}+\tfrac{1}{2}\rho(\mathbf{S}\cdot\mathbf{S})\cdot\mathbf{CCC}$$
$$-(\mathbf{S}\cdot\mathbf{C})\mathbf{U}\}:\frac{\partial(\mathbf{T}/\rho)}{\partial\mathbf{r}}\rho, \quad (7.2)$$

for the terms which contribute to $\mathbf{W}$. Consequently, according to (7.1),

$$W_{\xi\eta\zeta}=-\int mC_\xi C_\eta C_\zeta\mathfrak{D}_W{}^{(0)}\frac{1}{\Theta}d\mathbf{C} \quad (7.3)$$
$$=\sum_\lambda\sum_\mu\sum_\nu\alpha_{\xi\eta\zeta\lambda\mu\nu}\frac{\partial}{\partial r_\nu}(T_{\mu\lambda}/\rho).\quad \left.\begin{matrix}\lambda\\\mu\\\nu\end{matrix}\right\}=x,y,z. \quad (7.4)$$

Here $\boldsymbol{\alpha}$ may be called the coefficient of conduction of stress, because it corresponds to the coefficients of viscosity and of thermal conduction in current gas

[14] See the appendix, Eq. (n).
[15] See subsection 3 of the appendix.

dynamics. α is a tensor of order 6 and appears to be complicated. However, there is no need for pessimism because it is complicated in appearance only. The way of simplification is as follows: First, $\mathbf{T}$ is a symmetric tensor. Next, the usual problems with which we deal (the boundary layer flow and shock front) are either one- or two-dimensional in the approximate treatment. In this way α is simplified sufficiently in practical problems.

VIII. DETAILED TREATMENT OF $I^{(0)}$

The quantity $\mathbf{I}^{(0)}$ in Eq. (6.8) is defined by

$$I_{\xi\eta}^{(0)}=\int\int\int mc_\xi c_\eta(f^{(0)}f_1^{(0)}-f^{(0)\prime}f_1^{(0)\prime})kd\mathbf{k}d\mathbf{c}_1d\mathbf{c}, \quad (8.1)$$

where $f^{(0)}f_1^{(0)}$ is concerned with the decrease of the molecules of the velocity $\mathbf{c}$, and $f^{(0)\prime}f_1^{(0)\prime}$ is concerned with the increase.

We reduce $\mathbf{I}^{(0)}$ to a more convenient form for use. In Fig. 1, λ, μ, and ν are the direction cosines of the velocity of the molecule 1 as related to molecule 0. Also l, m, and n are the direction cosines of the line connecting the centers of the two molecules, 0 and 1, which are just in contact with each other coming into collision. The velocity of the molecule 0 is denoted by $\mathbf{c}$ and that of the molecule 1 is denoted by $\mathbf{c}_1$. The relations among these variables are as follows:

$$\left.\begin{aligned}&\cos\theta=-\lambda l-\mu m-\nu n,\\&\lambda=(c_{1x}-c_x)/V,\\&\mu=(c_{1y}-c_y)/V,\\&\nu=(c_{1z}-c_z)/V,\\&V=\{(c_{1x}-c_x)^2+(c_{1y}-c_y)^2+(c_{1z}-c_z)^2\}^{\frac{1}{2}}.\end{aligned}\right\} \quad (8.2)$$

k and $d\mathbf{k}$ in the right-hand side of (8.1) are explicitly expressed in the following forms:[16]

$$\left.\begin{aligned}&k=V\cos\theta=l(c_{1x}-c_x)+m(c_{1y}-c_y)+n(c_{1z}-c_z),\\&d\mathbf{k}=\sigma^2\sin\theta d\theta d\epsilon.\end{aligned}\right\} \quad (8.3)$$

Here, the range of θ extends from 0 to $\pi/2$, and that of ϵ from 0 to 2π. In general the following relation is known:[17]

$$\begin{aligned}I_{\xi\eta}^{(0)}&=\int\int\int mc_\xi c_\eta(f^{(0)}f_1^{(0)}-f^{(0)\prime}f_1^{(0)\prime})kd\mathbf{k}d\mathbf{c}d\mathbf{c}_1\\&=\int\int\int m(c_\xi c_\eta-c_\xi'c_\eta')f^{(0)}f_1^{(0)}kd\mathbf{k}d\mathbf{c}d\mathbf{c}_1. \quad (8.4)\end{aligned}$$

Assuming that molecules are of the form of spheres and perfectly elastic (in the classical dynamical sense), we find

$$\left.\begin{aligned}&c_x'=c_x-Vl\cos\theta,\\&c_y'=c_y-Vm\cos\theta,\\&c_z'=c_z-Vn\cos\theta.\end{aligned}\right\} \quad (8.5)$$

[16] See reference 3, p. 61.
[17] See reference 3, p. 66.

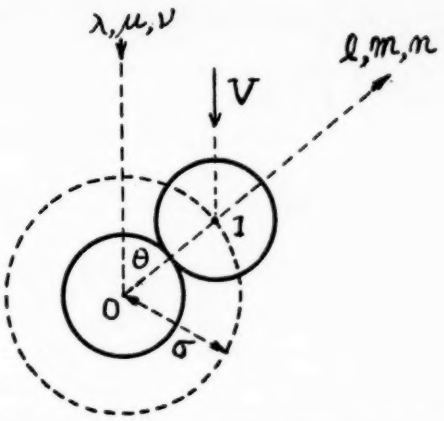

FIG. 1. The molecule 1 comes into contact with the molecule 0 at the relative velocity V. The range of θ: $0\sim\pi/2$. As θ is fixed, the line (l,m,n) forms a circular cone around the line (λ,μ,ν) as ϵ changes from 0 to 2π.

Consequently $m(c_\xi c_\eta-c_\xi'c_\eta')$ is given in terms of θ, ϵ, $\mathbf{c}$, and $\mathbf{c}_1$, and $\mathbf{I}^{(0)}$ is ready to be calculated. After long calculation with the help of theorems of spherical trigonometry, we obtain for $I_{xy}^{(0)}$

$$\begin{aligned}I_{xy}^{(0)}=\sigma^2m\pi\int\int f^{(0)}f_1^{(0)}\{&-\tfrac{1}{2}(C_{1x}-C_x)C_y\\&-\tfrac{1}{2}(C_{1y}-C_y)C_x-\tfrac{1}{4}(C_{1x}-C_x)(C_{1y}-C_y)\}\\&\times Vd\mathbf{C}_1d\mathbf{C}, \quad (8.6)\end{aligned}$$

where $C_\xi=c_\xi-v_\xi$. As $\mathbf{C}$ and $\mathbf{C}_1$ are symmetrically situated in $f^{(0)}f_1^{(0)}$ and V, $I_{xy}^{(0)}$ (8.6) becomes

$$\begin{aligned}I_{xy}^{(0)}=\sigma^2m\pi\int\int f^{(0)}f_1^{(0)}V\{&\tfrac{1}{2}(C_xC_y-C_{1x}C_y)\}\\&\times d\mathbf{C}_1d\mathbf{C}. \quad (8.6')\end{aligned}$$

In the same way, we get for $I_{xx}^{(0)}$

$$\begin{aligned}I_{xx}^{(0)}=\sigma^2m\pi\int\int f^{(0)}f_1^{(0)}V&\\\times\{\tfrac{1}{4}(C_x-C_{1x})^2-\tfrac{1}{12}V^2\}d\mathbf{C}d\mathbf{C}_1.& \quad (8.7)\end{aligned}$$

The other components of $\mathbf{I}^{(0)}$ are given in similar forms.

Further¶ we can conveniently express $\mathbf{C}$ and $\mathbf{C}_1$ in terms of the new variables, $\mathbf{a}$ and $\mathbf{b}$, by

$$C_\xi=a_\xi-b_\xi/2, \quad C_{1\xi}=a_\xi+b_\xi/2.$$

In consequence of the expression, we have

$$V=(b_x^2+b_y^2+b_z^2)^{\frac{1}{2}},$$
$$d\mathbf{C}d\mathbf{C}_1=d\mathbf{a}d\mathbf{b},$$

¶ Credit is given to K. Takao.

and $I_{xy}^{(0)}$ (8.6) is given in the form

$$I_{xy}^{(0)}=\sigma^2 m\pi\int\int f^{(0)}f_1^{(0)} \times(-\tfrac{1}{2}a_y b_x-\tfrac{1}{2}a_x b_y+\tfrac{1}{4}b_x b_y)V d\mathbf{a}d\mathbf{b},$$

$$f^{(0)}f_1^{(0)}=\frac{\rho^5}{8\pi^3|T|m^2}\exp(-\rho\sum\sum S_{\xi\eta}a_\eta a_\xi-\tfrac{1}{4}\rho\sum\sum S_{\xi\eta}b_\eta b_\xi).$$

The integration over all the range of $\mathbf{a}$, from $-\infty$ to $+\infty$, is easily worked out and we get

$$I_{xy}^{(0)}=\frac{\sigma^2\rho^{7/2}}{32\pi^{\frac{1}{2}}|\mathbf{T}||\mathbf{S}|^{\frac{1}{2}}m}\int_{-\infty}^{+\infty} \times\{\exp(-\tfrac{1}{4}\rho\sum\sum S_{\xi\eta}b_\eta b_\xi)\}b_x b_y V d\mathbf{b}.$$

Further, we introduce a set of new variables, ψ and φ, defined by

$$b_x=V\sin\psi\sin\varphi,$$
$$b_y=V\sin\psi\cos\varphi,$$
$$b_z=V\cos\psi.$$

Here we plainly see

$$d\mathbf{b}=V^2\sin\psi d\psi d\varphi dV,$$
$$b_x b_y=V^2\sin\psi\sin\varphi\cos\varphi.$$

Consequently, we obtain for $I_{xy}^{(0)}$

$$\left.\begin{aligned} I_{xy}^{(0)}&=\frac{2\sigma^2\rho^{\frac{1}{2}}}{\pi^{\frac{1}{2}}|\mathbf{T}||\mathbf{S}|^{\frac{1}{2}}m} \times\int_{\psi=0}^{\pi}\int_{\varphi=0}^{2\pi}\frac{\sin^3\psi\sin\varphi\cos\varphi d\psi d\varphi}{A^3},\\ A&=S_{xx}\sin^2\varphi\sin^2\psi+S_{yy}\cos^2\varphi\sin^2\psi\\ &\quad+S_{zz}\cos^2\psi+2(S_{xy}\sin\varphi\cos\varphi\sin^2\psi\\ &\quad+S_{yz}\cos\varphi\sin\psi\cos\psi+S_{zx}\sin\varphi\sin\psi\cos\psi). \end{aligned}\right\} \quad (8.8)$$

Similarly $I_{xx}^{(0)}$ (8.7) is given in the form

$$I_{xx}^{(0)}=\frac{2\sigma^2\rho^{\frac{1}{2}}}{3\pi^{\frac{1}{2}}|\mathbf{T}||\mathbf{S}|^{\frac{1}{2}}} \times\int\int\frac{(3\sin^2\varphi\sin^2\psi-1)\sin\psi d\psi d\varphi}{A^3}. \quad (8.9)$$

IX. SUMMARY AND CONCLUSION

1. The validity of current hydrodynamical equations of gases rests upon the assumption that the states concerned depart only slightly from thermal equilibrium. There are many phenomena where the states depart too far from thermal equilibrium for current theories to be applied.

2. The author proposes a distribution function, relating to the tensors formed from the velocity components of the molecules in a small volume element, according to his own principle for the distribution of the molecules. The tensor of order zero means the mass density, order one is the momentum of mass motion and order two is the flux of momentum (stress), etc.

3. For the fundamental equations applicable to a new domain of gas dynamics, we have derived a new set of equations (5.6), (5.7), and (6.8) by means of our new distribution function where mass density, velocity of mass motion, and stress are the essential variables. So far as the general form for the fundamental equations of gas dynamics is concerned, the method of treatment is similar to that of Enskog and Chapman's. The terms $\mathbf{W}$ and $\mathbf{I}$ contained in Eq. (6.8) are somewhat complicated and are discussed in detail in Sections 7 and 8, wherein is introduced a new method originated by Meyer and developed by the author and his co-worker.

4. In solving the resultant equations under given boundary conditions, the work may be laborious, suitable, perhaps, for a modern calculating machine. Nevertheless, one need not become excessively pessimistic because some method of simplification and approximation will reasonably be found corresponding to given conditions.

5. Our result is applicable only to rarefied gases. The present interest is not focused on the effect of intermolecular potentials to which, for instance, Born and Green paid attention in their theory of liquids.

APPENDIX

Generalization of "Meyer's Theory"[18]

1. The theory based upon Meyer's intuition has several inconsistencies. It is a primitive method of calculating the thermal conductivity of gases.

By means of Meyer's theory as developed further by us, we can deal with the transport phenomena of gases and the result is equivalent to what is obtained by solving the B-M equation as shown in final subsection 4. Compared with Enskog-Chapman's method[3] of solving the B-M equation we have a strong point in that the approximate result is obtained by means of the integration of known function instead of solving integral equations.

It is assumed that a gas exists throughout all space and time. Space and time are divided into small cells (of 4 dimensions) of mosaic form. These cells are small macroscopically but large microscopically. In each cell the zeroth approximation to the distribution function of molecules is assumed to be known. For instance, there are cases where Maxwell's function is given for the zeroth approximation. In general, other functions are given instead of Maxwell's.

We assume that there is no field of external force.

[18] J. H. Jeans, *The Dynamical Theory of Gases* (Cambridge University Press, London, 1925), fourth edition, pp. 291–300.

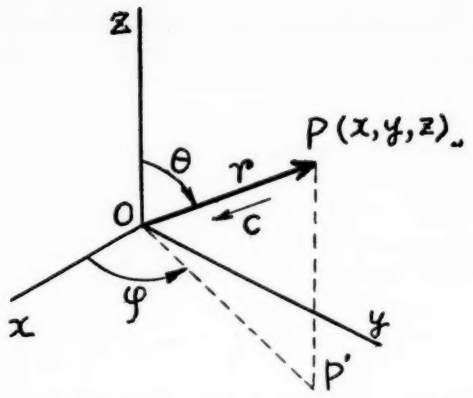

FIG. 2. At the origin 0 we observe molecules of the velocity **c** traveling from P. The polar coordinates of P are r, θ, φ.

2. In Fig. 2, the origin 0 is the point where the molecules coming from the surrounding space are observed at the time 0, and $P(x,y,z,l)$ is a point in the field other than 0.

We assume that a molecule which finished the last collision at P, encountering no other collision on the way, just arrives at 0 at the time 0. As the velocity **c** is assumed to be constant between P and 0 (no external force is assumed to be present), we see that

$$\left.\begin{aligned} &\frac{1}{l}=\frac{c_x}{x}=\frac{c_y}{y}=\frac{c_z}{z}=\frac{c}{r}, \\ &c=(c_x^2+c_y^2+c_z^2)^{\frac{1}{2}}, \\ &r=(x^2+y^2+z^2)^{\frac{1}{2}}. \end{aligned}\right\} \tag{a}$$

Here **c** is the sum of the velocity of random motion and that of mass motion. We now let $[f\Theta]'$ denote the number of molecules which receive the velocity **c** anew by collisions in unit volume and unit time at P, losing their original velocities

$$[f\Theta]'=\int\int f'f_1'k d\mathbf{k}d\mathbf{c}_1, \tag{b}$$

$$f'\equiv f(\mathbf{c}'), \quad f_1'\equiv f(\mathbf{c}_1'), \tag{c}$$

where $\mathbf{c}'$ and $\mathbf{c}_1'$ denote the velocities which are assigned to a pair of colliding molecules just before the collision, **c** and $\mathbf{c}_1$ being their velocities just after the collision.**

In practical calculations we substitute an approximate function $f^{(0)}$ for f. In a special case where $f^{(0)}$ is Maxwell's function, we see that

$$f^{(0)}f_1^{(0)}=f^{(0)\prime}f_1^{(0)\prime}, \quad [f^{(0)}\Theta]'=\int\int f^{(0)}f_1^{(0)}kd\mathbf{k}d\mathbf{c}_1. \tag{d}$$

In general, the condition (d) is not satisfied.

Now let us take a small domain or cell dV_P and a time interval dt at P. The molecules receiving the velocities between **c** and $\mathbf{c}+d\mathbf{c}$ by collisions in $dV_P\times dt$ are assumed to arrive at the point 0 at the time 0. Here those which have encountered other molecules on the way should be omitted from our observation. Let Φ be the probability of a molecule describing the free path l from P to 0 without collision. As is shown in Jeans' textbook,[19]

$$\begin{aligned} \Phi&=\exp\left(-\frac{1}{c}\int_0^l \Theta dl\right) \qquad (l=PO) \\ &=\exp\left[-\frac{1}{c}\int_r^0 \Theta(-dr)\right] \quad (r=OP) \\ &=\exp\left(-\frac{1}{c}\int_0^r \Theta dr\right), \end{aligned} \tag{e}$$

where Θ is the probable number of collisions of one molecule of velocity **c** per unit time and per unit volume.

Referring to (b) and (e), the number of molecules which arrive at 0 traveling from P without any collision enroute are

$$[f^{(0)}\Theta]'\times dV_P\times dt\times\Phi\times d\mathbf{c}. \tag{f}$$

Referring to Fig. 2, it is convenient to give $d\mathbf{c}$ in the form:

$$d\mathbf{c}=c^2\sin(\pi-\theta)dcd(\pi-\theta)d(\pi+\varphi). \tag{g}$$

The molecules are dispersed in the solid angle $\sin(\pi-\theta)\times d(\pi-\theta)d(\pi+\varphi)$. The number dN of the molecules passing the plane set perpendicularly to PO at 0 through unit area in unit time is given by

$$dN=\frac{[f^{(0)}\Theta]'\times dV_P\times dt\times\Phi\times c^2\sin(\pi-\theta)\times dcd(\pi-\theta)d(\pi+\varphi)}{r^2\sin(\pi-\theta)d(\pi-\theta)d(\pi+\varphi)}=\frac{[f^{(0)}\Theta]'\times dV_P\times dt\times\Phi\times c^2dc}{r^2}. \tag{h}$$

Their transit through the plane at 0 lasts during dt and the velocity is **c**. Consequently dN divided by $c\times dt$ gives the density

$$[f^{(0)}\Theta]'\times dV_P\times dc\times\Phi\times c/r^2. \tag{i}$$

We take for dV_P

$$dV_P=r^2\sin\theta dr d'\theta d'\varphi, \tag{j}$$

where $d'\theta$ and $d'\varphi$ must be distinguished from $d\theta$ and $d\varphi$ in (g). Here it may be desirable to note the following: All the molecules starting simultaneously from dV_P for 0 arrive at the plane at 0 not exactly at an instant of time, as there arise some dispersions in the following way; first, they disperse in the range of $r\times dc/c$ in the direction of PO, because the magni-

** For other notations in (b), see Section 8 of the text.

[19] See reference 18, p. 293.

tudes of their velocities are dispersed between c and $c+dc$. This dispersion, however, is cancelled when we assume that each individual molecule starts from P with the delay of $t\times\delta c/c$ corresponding to its velocity $c+\delta c$.†† Next, the breadth dr of dV_P is a cause of the dispersions. A dispersion of this kind vanishes through the delay of starting time $\delta r/c$ corresponding to δr. Further corresponding to $d'\theta$ and $d'\varphi$, the directions of their velocities at 0 disperse between

$$\pi-\theta \quad \text{and} \quad \pi-\theta-d'\theta,$$

and between

$$\pi+\varphi \quad \text{and} \quad \pi+\varphi+d'\varphi.$$

After considering these points, we insert dV_P (j) into (i) and integrate the result throughout the range of r, from 0 to ∞, under the condition (a). Thus we get for the first approximation to the distribution function $f^{(0)}+f^{(1)}$ at 0

$$(f^{(0)}+f^{(1)})_0 c^2 \sin(\pi-\theta)dxd'(\pi-\theta)d'(\pi-\varphi)$$

$$=\int_{r=0}^{r=\infty}\frac{[f^{(0)}\Theta]'\Phi r^2\sin\theta dr d'\theta d'\varphi c^2 dc}{cr^2}, \quad \text{(k)}$$

or

$$(f^{(0)}+f^{(1)})_0=\int_0^\infty\frac{[f^{(0)}\Theta]'\times\Phi}{c}dr. \quad \text{(l)}$$

As an example, we will take Maxwell's function for the zeroth approximation. Then, according to the relation (d), we have:

$$f^{(0)}\Theta=[f^{(0)}\Theta]'$$

and consequently we see that

$$(f^{(0)}+f^{(1)})_0=\int_0^\infty\frac{f^{(0)}\Theta\exp\left(-\int_0^r\Theta dr/c\right)}{c}dr. \quad \text{(l')}$$

Considering that $\exp(-\int_0^r\Theta dr/c)$ rapidly approaches zero as r increases, we expand the functions contained in the integrand of (l') as power series in r/c:

$$\left.\begin{aligned}
f^{(0)}&=f_0^{(0)}+\left(\frac{df^{(0)}}{dt}\right)_0\left(-\frac{r}{c}\right)+\cdots,\\
\Theta&=\Theta_0+\left(\frac{d\Theta}{dt}\right)_0\left(-\frac{r}{c}\right)+\cdots,\\
\Phi&=\exp\left(-\int_0^r\Theta dr/c\right)\\
&=[\exp(-\Theta_0 r/c)]\times\left[1+\frac{1}{2}\frac{r^2}{c^2}\left(\frac{d\Theta}{dt}\right)_0+\cdots\right],\\
\frac{d}{dt}&=\frac{\partial}{\partial t}+c_x\frac{\partial}{\partial x}+c_y\frac{\partial}{\partial y}+c_z\frac{\partial}{\partial z},
\end{aligned}\right\} \quad \text{(m)}$$

†† Our argument is correct, so far as the change of the state during $t\times\delta c/c$ at P is sufficiently small.

where the variables associated with the suffix o denote the values at 0. Inserting these into (l') and neglecting the small terms of higher order, we get

$$(f^{(0)}+f^{(1)})_0=\int_0^\infty f_0^{(0)}\Theta_0\exp(-\Theta_0 r/c)$$

$$\times\left[1+\frac{1}{f_0^{(0)}}\left(\frac{df^{(0)}}{dt}\right)_0\left(-\frac{r}{c}\right)+\frac{1}{\Theta_0}\left(\frac{d\Theta}{dt}\right)_0\left(-\frac{r}{c}\right)+\frac{1}{2}\frac{r^2}{c^2}\left(\frac{d\Theta}{dt}\right)_0\right]dr.$$

Taking into account the definite integrals

$$\int_0^\infty\frac{1}{2}\frac{\Theta_0 r^2}{c^2}\exp\left(-\frac{\Theta_0 r}{c}\right)dr=\int_0^\infty\frac{r}{c}\exp\left(-\frac{\Theta_0 r}{c}\right)dr=\frac{c}{\Theta_0^2},$$

$$\int_0^\infty\Theta_0\exp\left(-\frac{\Theta_0 r}{c}\right)dr=c,$$

we get for the result

$$(f^{(0)}+f^{(1)})_0=f_0^{(0)}\left[1-\frac{1}{\Theta_0}\left(\frac{d\log f^{(0)}}{dt}\right)_0\right].$$

When the origin 0 is displaced from its original position to any other point in the space, the result remains unchanged. Therefore we omit the suffix o and the result is valid at every point in the space. The final result is

$$f^{(0)}+f^{(1)}=f^{(0)}\left[1-\frac{1}{\Theta}\frac{d\log f^{(0)}}{dt}\right]. \quad \text{(n')}$$

In general cases where $f^{(0)}$ is a function different from Maxwell's, $-J^{(0)}(=[f^{(0)}\Theta]'-f^{(0)}\Theta)$ does not vanish and must be taken into consideration. Considering that $J^{(0)}$ is of the same order as that of $df^{(0)}/dt$ and the term $(dJ^{(0)}/dt)(-r/c)$ is negligible, we get instead of (n')

$$f^{0)}+f^{(1)}=f^{(0)}\left[1-\frac{1}{\Theta}\frac{d\log f^{0)}}{dt}-\frac{1}{f^{(0)}\Theta}J^{(0)}\right] \quad \text{(n)}$$

for $f^{(0)}+f^{(1)}$.

3. For example, we calculate explicitly the quantities of transport in cases where Maxwell's function is given for the zeroth approximation to the distribution function as follows:

$$\left.\begin{aligned}
f^{(0)}&=n_0\left(\frac{2kT_0 m}{\pi}\right)^{\frac{3}{2}}\exp\left[-\frac{m}{2kT_0}(C_x^2+C_y^2+C_z^2)\right],\\
c_\xi&=C_\xi+v_\xi,
\end{aligned}\right\} \quad \text{(o)}$$

where n_0, $3kT_0/2$, and v_0 represent, respectively, (i) *the zeroth approximation* to molecular density, (ii) *the zeroth approximation* to the mean value of energy of

one molecule including no contribution from energy of mass motion, and (iii) *the zeroth approximation* to the velocity of mass motion. In Enskog and Chapman's theory n, $3kT/2$ and $\mathbf{v}$ in $f^{(0)}$ are the *exact* values. It should be emphasized that $f^{(0)}$ in the present theory is to be distinguished from the zeroth approximation to distribution function in Enskog and Chapman's theory.‡‡ Consequently $f^{(1)}$ in the present theory does not necessarily satisfy the conditions§§ [see Eq. (5.3)],

$$\int m f^{(1)} d\mathbf{c} = 0, \quad \int m C_\xi f^{(1)} d\mathbf{C} = 0,$$

$$\int m(C_x^2 + C_y^2 + C_z^2) f^{(1)} d\mathbf{C} = 0.$$

From Eqs. (n′) and (o) we get[3]

$$\left.\begin{aligned} f^{(0)} \frac{d \log f^{(0)}}{dt} &= f^{(0)}\left[\left(\frac{m}{2kT_0}C^2 - \frac{5}{2}\right)\mathbf{C}\cdot\frac{\partial \log T_0}{\partial \mathbf{r}} + \frac{m}{kT_0}\mathbf{C}\cdot\mathbf{C}:\frac{\partial \mathbf{v}_0}{\partial \mathbf{r}}\right], \\ f^{(0)} + f^{(1)} &= f^{(0)} - \frac{f^{(0)}}{\Theta}\left[\left(\frac{m}{2kT_0}C^2 - \frac{5}{2}\right)\mathbf{C}\cdot\frac{\partial \log T_0}{\partial \mathbf{r}} + \frac{m}{kT_0}\mathbf{C}\cdot\mathbf{C}:\frac{\partial \mathbf{v}_0}{\partial \mathbf{r}}\right], \\ \mathbf{C}\cdot\mathbf{C} &= \mathbf{CC} - \tfrac{1}{3}\mathbf{U}C^2. \end{aligned}\right\} \quad \text{(p)}$$

According to (p), after short calculation, we get for the first approximation to density

$$\rho = \int m(f^{(0)} + f^{(1)}) d\mathbf{C} = m n_0 = \rho_0. \qquad \text{(q)}$$

The first approximation to momentum (of mass motion) is given as follows:

$$\rho v_\xi = \int m(C_\xi + v_{0\xi})(f^{(0)} + f^{(1)}) d\mathbf{C} = \rho_0\left(v_{0\xi} - \frac{1}{3}\frac{A'}{\rho_0}\frac{\partial \log T_0}{\partial \xi}\right), \qquad \text{(r)}$$

where

$$A' = \frac{m}{2kT_0}\int \frac{f^{(0)}}{\Theta} C^2 C^2 d\mathbf{C} - \frac{5}{2} m \int \frac{f^{(0)}}{\Theta} C^2 d\mathbf{C}. \qquad \text{(s)}$$

The first approximation to flux of momentum (containing stress) is given as follows:

$$\left.\begin{aligned} t_{\xi\xi} &= \int m(C_\xi + v_{0\xi})^2 (f^{(0)} + f^{(1)}) d\mathbf{C} \\ &= p_0 + \rho_0 v_{0\xi}^2 - 2\mu\left(\frac{\partial v_{0\xi}}{\partial \xi} - \tfrac{1}{3}\operatorname{div}\mathbf{v}_0\right) - \tfrac{2}{3}\rho_0 v_{0\xi} A' \frac{\partial \log T_0}{\partial \xi}, \\ t_{\xi\eta} &= \rho_0 v_{0\xi} v_{0\eta} - \tfrac{1}{3}A'\left(v_{0\xi}\frac{\partial \log T_0}{\partial \eta} + v_{0\eta}\frac{\partial \log T_0}{\partial \xi}\right) \\ &\qquad (\xi \neq \eta) \\ &\qquad - \mu\left(\frac{\partial v_{0\xi}}{\partial \eta} + \frac{\partial v_{0\eta}}{\partial \xi}\right), \end{aligned}\right\} \quad \text{(t)}$$

where

$$\left.\begin{aligned} p_0 &= \int \frac{m}{3} C^2 f^{(0)} d\mathbf{C} = n_0 k T_0, \\ \mu &= \int \frac{m^2}{kT_0} C_\xi^2 C_\eta^2 \frac{f^{(0)}}{\Theta} d\mathbf{C} \\ &= \tfrac{1}{2}\int \frac{m^2}{kT_0}\left(\frac{C^2 C^2}{3} - 3C_\xi^2 C_\eta^2\right)\frac{f^{(0)}}{\Theta} d\mathbf{C}, \\ &\qquad (\xi \neq \eta) \end{aligned}\right\} \quad \text{(u)}$$

as $f^{(0)}/\Theta$ is symmetrical with respect to C_x, C_y, and C_z. The first approximation to density of energy (containing energy of mass motion) is

$$E = \tfrac{1}{2}(t_{xx} + t_{yy} + t_{zz}) = \tfrac{3}{2}p_0 + \tfrac{1}{2}\rho_0 v_0^2 - \tfrac{2}{3}\rho_0 A'\left(v_{0x}\frac{\partial \log T_0}{\partial y} + v_{0y}\frac{\partial \log T_0}{\partial y} + v_{0z}\frac{\partial \log T_0}{\partial z}\right). \qquad \text{(v)}$$

Further, the energy of transport in the first approximation is obtained as follows:

$$\begin{aligned} E_x &= \int \tfrac{1}{2} m(c_x^2 + c_y^2 + c_z^2) c_x (f^{(0)} + f^{(1)}) d\mathbf{c} \\ &= \tfrac{3}{2}p_0 v_{0x} + \tfrac{1}{2}\rho_0 v_0^2 v_{0x} + v_{0x}\left\{p_0 - 2\mu\left(\frac{\partial v_{0x}}{\partial x} - \tfrac{1}{3}\operatorname{div}\mathbf{v}_0\right)\right\} \\ &\quad + v_{0y}\left\{-\mu\left(\frac{\partial v_{0y}}{\partial x} + \frac{\partial v_{0x}}{\partial y}\right)\right\} + v_{0z}\left\{-\mu\left(\frac{\partial v_{0z}}{\partial z} + \frac{\partial v_{0z}}{\partial x}\right)\right\} \\ &\quad - \frac{A'}{3}v_{0x}\left(v_{0x}\frac{\partial}{\partial x} + v_{0y}\frac{\partial}{\partial y} + v_{0z}\frac{\partial}{\partial z}\right)\log T_0 \\ &\quad + (-\tfrac{1}{6}A - \tfrac{1}{6}A' v_0^2)\frac{\partial \log T_0}{\partial x}, \end{aligned} \qquad \text{(w)}$$

‡‡ See Section 6 of the text.

§§ As to this point, Meyer was confused. See reference 18, pp. 295–296.

where

$$A=\int mC^2C^2\left(\frac{m}{2kT_0}C^2-\frac{5}{2}\right)\frac{f^{(0)}}{\Theta}d\mathbf{C}. \qquad (x)$$

Now referring to (r), we see that

$$v_\xi=v_{0\xi}-\frac{1}{3}\frac{A'}{\rho_0}\frac{\partial \log T_0}{\partial \xi}, \qquad (y)$$

or the term containing A' being of small magnitude of higher order,

$$v_{0\xi}=v_\xi+\frac{1}{3}\frac{A'}{\rho_0}\frac{\partial \log T_0}{\partial \xi}. \qquad (y')$$

We take $\mathbf{v}$ for the first approximation to mass velocity, whereas $\mathbf{v}_0$ is the zeroth approximation. According to (y) and (y'), $t_{\xi\eta}(t)$, $E(v)$, and $E_\xi(w)$ are given as follows:

$$\left.\begin{aligned}
&t_{xx}=p_0+\rho v_x^2-2\mu\left(\frac{\partial v_x}{\partial x}-\tfrac{1}{3}\operatorname{div}\mathbf{v}\right),\\
&t_{xy}=\rho v_x v_y-\mu\left(\frac{\partial v_x}{\partial y}+\frac{\partial v_y}{\partial x}\right),\quad E=\tfrac{1}{2}(3p_0+\rho v^2),\\
&E_x=v_x(t_{xx}-\rho v_x^2)+v_y(t_{xy}-\rho v_x v_y)\\
&\qquad +v_z(t_{xz}-\rho v_x v_z)+Ev_x+\lambda\frac{\partial \log T_0}{\partial x},\\
&p_0\rho^{-1}=\frac{k}{m}T_0,\quad \lambda=\frac{1}{6}\left(5A'\frac{p_0}{\rho}-A\right).
\end{aligned}\right\} \qquad (z)$$

These results agree with those of Enskog, Chapman, and Cowling. It is emphasized that p_0 and T_0 have already lost the experimental meanings of pressure and temperature of thermal equilibrium.[20]

4. According to the foregoing, Taketa[21] presumed that the exact distribution function f would satisfy the following integral equation [see Eq. (l)],

$$f(\mathbf{c},\mathbf{r},t)=\int_0^\infty [f_\tau\Theta_\tau]'\exp\left(-\int_0^\tau \Theta_s ds\right)d\tau,$$

where

$$f_\tau=f(\mathbf{c}_\tau,\mathbf{r}_\tau,t-\tau),$$

$$f_\tau'=f(\mathbf{c}_\tau',\mathbf{r}_\tau,t-\tau)$$

and

$$\frac{d\mathbf{r}_\tau}{dt}=-\frac{d\mathbf{r}_\tau}{d\tau}=\mathbf{c}_\tau,\quad \frac{d\mathbf{c}_\tau}{dt}=-\frac{d\mathbf{c}_\tau}{d\tau}=\mathbf{F}\ \text{(external force)},$$

$$\left.\begin{aligned}\mathbf{c}_\tau&=\mathbf{c},\\ \mathbf{r}_\tau&=\mathbf{r}\end{aligned}\right\}\quad \text{when}\quad \tau=0.$$

The meaning of $[f\Theta]'$ has been given in (b). He verified that f defined above satisfies the B-M Eq. exactly. Thus the reasonableness of the present method originated in Meyer's intuition has been proved.

By this method, it is not necessary to solve integral equations, although we integrate some known functions. Our method has this merit.

[20] See reference 4. A few mistakes of calculation are found in the article referred to. Those mistakes are corrected in the present calculation.

[21] N. Taketa, J. Phys. Soc. (Japan) 4, 357 (1949).

Thermodynamics of Adsorption

RALPH J. TYKODI
250 Ridge Avenue, State College, Pennsylvania
(Received November 4, 1953)

The thermodynamics of the adsorption of gases on solids is developed in terms of a two-component system. It is shown that all solids swell during the adsorption process, and that spontaneous first-order phase changes in the adsorbed layer are unlikely. The ideal process: i(gas)→i(adsorbed)—constant environment—is introduced and discussed; thermodynamic functions appropriate to the process are defined. Two types of heat capacity of the adsorbed layer are defined and discussed. The chemical potential of a solid is treated at some length.

1. INTRODUCTION

IN recent years the thermodynamics of the adsorption of gases on solids has been treated rather extensively; for a good summary of the results of such treatments see the review article by Hill.[1] In spite of all the work that has been done in this field it is worth going over the thermodynamics of the situation just once more in order to (1) demonstrate a set of thermodynamic relations closely tied to normal experimental procedure and (2) to give new physical meaning to some of the old functional forms.

The following is taken as a primitive postulate: P1. A thermodynamic system (macro or micro) is defined in terms of its composition and surroundings.

Thermodynamic processes, then, consist of energetic[2] interchanges between system and surroundings, the interchanges being calculated from observed changes in the surroundings.

Adsorption systems have been described thermodynamically in the following ways: 1. Adsorbed phase plus gas phase; 2. Swelled phase (adsorbent plus adsorbed molecules) plus gas phase; 3. Total system, gas plus solid, as a two-component system. These descriptions have the following properties.

(1) Here it is assumed that the composition and surroundings of both the gas and adsorbed phases are well defined. The surroundings of the gas phase are specified by the temperature T and the pressure P; while those of the adsorbed phase are specified by T, P, and one other variable relating to the contribution of the solid to the surroundings of the adsorbed phase. The third variable, however, is not independent; it is usually evaluated from more fundamental properties of the total system.

The chief problems of this description refer to the composition of (exact number of moles in) the adsorbed phase and the *a priori* characterization of its surroundings. Hill[3] has examined this system rather completely and has discussed many of its inherent difficulties. A few additional remarks about (1) are made in Sec. 11 of this paper.

(2) In this system the surroundings of the swelled phase and the gas phase are specified by T and P. The remaining problem of the description relates to the composition of the swelled phase. Hill[4] has used (2) as the basis of his adsorption thermodynamics; in addition to the assumptions of (2) he has assumed that the thermodynamic properties of the pure adsorbent in vacuo are well defined.

(3) The total system is well defined thermodynamically. Its surroundings are completely specified by T and P, and its composition as a two-component system is known. Thus (3) leads to the rigorous description of a system whose thermodynamic properties can be exactly determined. Partial molal quantities relative to the two components can be rigorously defined and discussed. The adsorption problem via (3) has been discussed by Guggenheim.[5]

For a more extensive discussion of the merits of various thermodynamic descriptions see reference 1.

In the following section yet another thermodynamic description is developed. It is based upon the two-component treatment (3) but assumes in addition that molar properties of the pure components are well-defined functions of T and P. For a finely divided solid it would seem that the pressure dependence of a molar property cannot be rigorously (operationally) defined, since no truly inert pressure-carrying medium exists. To the extent that the pressure dependence is uncertain, the present treatment, like (1) and (2), is an approximate one.

2. THE THERMODYNAMIC SYSTEM

Consider a well-defined volume containing n_s moles of adsorbent. Introduce a nonadsorbable, pressure-carrying medium (perfect gas). Subject the volume to temperature T and pressure P by means of heat bath, piston, and varying mass of pressure-carrying medium. Calibrate the gas and adsorbent volumes for the temperature and pressure range over which the adsorption process is to be studied. (In calling the volume well defined what is intended is simply that the total volume of the system is to be considered known at all times.)

[1] T. L. Hill, *Advances in Catalysis* (Academic Press, Inc., New York, 1952), Vol. IV.
[2] J. N. Brønsted, Phil. Mag. **29**, 449 (1940).
[3] T. L. Hill, J. Chem. Phys. **17**, 520 (1949).
[4] T. L. Hill, J. Chem. Phys. **18**, 246 (1950).
[5] See reference 1, pp. 253–254.

Now, consider the well-defined volume full of n_s moles of adsorbent and n_g moles of adsorbable gas at temperature T and pressure P. Introduce the notation Z_s, Z_g, Z_s^0 for a property of the solid, of the gas, and of the solid under calibration conditions, respectively. For the total system, gas plus adsorbent, the following relations hold:

$$E=TS-PV+n_g\mu_g+n_s\mu_s, \tag{2.1.1}$$

$$\delta E=T\delta S-P\delta V+\mu_g\delta n_g+\mu_s\delta n_s, \tag{2.1.2}$$

$$G=H-TS=n_g\mu_g+n_s\mu_s, \tag{2.1.3}$$

$$\delta G=-S\delta T+V\delta P+\mu_g\delta n_g+\mu_s\delta n_s, \tag{2.1.4}$$

$$S\delta T-V\delta P+n_g\delta\mu_g+n_s\delta\mu_s=0. \tag{2.1.5}$$

Extensive variables refer to the entire system. It is assumed that the chemical potentials μ_g and μ_s can be properly defined so as to be homogeneous throughout their respective media. In the case of a finely divided solid, Eqs. (2.1.2) and (2.1.4) refer to the introduction of δn_s moles of solid in the same state of subdivision. If the chemical potential of the solid depends on the size of the particles, then the μ_s appearing in Eqs. (2.1) is to be taken as the mean value of the chemical potential associated with each particle, distributed over a representative molar assembly of the particles, i.e., an assembly of particles such that the weight of the assembly is the same as the molecular weight of the solid and the particle size distribution is that prevailing throughout the entire solid. The physical interpretation of the chemical potential of the solid will be discussed later.

If n_g^0 moles of gas would fill the calibrated gas space, $V-V_s^0$, at temperature T and pressure P then the adsorption excess Γ is defined by $\Gamma\equiv n_g-n_g^0$; so $n_g^0=n_g-\Gamma$. The composite system can be partitioned in the following way: gas phase, solid phase, and excess. An extensive property Z of the total system can be written as

$$Z\equiv\{n_g^0\bar{Z}_g+n_s\bar{Z}_s^0+Z_f\} \tag{2.2.1}$$

or, equivalently, as

$$Z=\{(n_g-\Gamma)\bar{Z}_g+n_s\bar{Z}_s^0+Z_f\}, \tag{2.2.2}$$

where the bars refer to molar properties, and Z_f is the necessary correction term or excess due to the adsorption process. Since the excess is calculated on the basis of the calibration condition, $V_f\equiv 0$, i.e., $n_g^0\equiv(V-V_s^0)/\bar{V}_g$.

Applying the above partition to Eqs. (2.1) and using standard forms for properties of the pure gas and solid components, there follows:

$$E_f=TS_f+\Gamma\mu_g+n_s\mu_f, \tag{2.3.1}$$

$$\delta E_f=T\delta S_f+\mu_g\delta\Gamma+\mu_f\delta n_s, \tag{2.3.2}$$

$$G_f=H_f-TS_f=\Gamma\mu_g+n_s\mu_f, \tag{2.3.3}$$

$$\delta G_f=-S_f\delta T+\mu_g\delta\Gamma+\mu_f\delta n_s, \tag{2.3.4}$$

$$S_f\delta T+\Gamma\delta\mu_g+n_s\delta\mu_f=0, \tag{2.3.5}$$

where

$$H_f\equiv E_f+PV_f=E_f,$$

and

$$\mu_f\equiv\mu_s-\mu_s^0.$$

Introducing the following definitions,

$$\bar{Z}_f\equiv Z_f/\Gamma, \tag{2.4.1}$$

$$X\equiv\Gamma/n_s, \tag{2.4.2}$$

$$\mathfrak{C}_f\equiv\bar{E}_f-(\mu_f/X), \tag{2.4.3}$$

$$\mathfrak{G}_f\equiv\mathfrak{C}_f-T\bar{S}_f, \tag{2.4.4}$$

there is obtained from (2.3) and (2.4) a set of basic relations:

$$\bar{E}_f=T\bar{S}_f+\mu_g+(\mu_f/X), \tag{2.5.1}$$

$$\delta\bar{E}_f=T\delta\bar{S}_f-(\mu_f\delta X/X^2), \tag{2.5.2}$$

$$\mathfrak{C}_f=\bar{E}_f-(\mu_f/X), \tag{2.5.3}$$

$$\delta\mathfrak{C}_f=T\delta\bar{S}_f-(\delta\mu_f/X), \tag{2.5.4}$$

$$\bar{G}_f=\bar{E}_f-T\bar{S}_f=\mu_g+(\mu_f/X), \tag{2.5.5}$$

$$\delta\bar{G}_f=-\bar{S}_f\delta T-(\mu_f\delta X/X^2), \tag{2.5.6}$$

$$\mathfrak{G}_f=\mathfrak{C}_f-T\bar{S}_f, \tag{2.5.7}$$

$$\delta\mathfrak{G}_f=-\bar{S}_f\delta T-(\delta\mu_f/X), \tag{2.5.8}$$

$$\delta\mu_f=-X\bar{S}_f\delta T-X\delta\mu_g=-X(\bar{S}_f-\bar{S}_g)\delta T-X\bar{V}_g\delta P. \tag{2.5.9}$$

Equations (2.5) yield the following sets of relations among the differential coefficients:

$$\text{a.}\quad\left(\frac{\partial\bar{E}_f}{\partial\bar{S}_f}\right)_X=T, \qquad \text{b.}\quad\left(\frac{\partial\bar{E}_f}{\partial X}\right)_{\bar{S}_f}=-\mu_f/X^2, \tag{2.6.1}$$

$$\text{a.}\quad\left(\frac{\partial\mathfrak{C}_f}{\partial\bar{S}_f}\right)_{\mu_f}=T, \qquad \text{b.}\quad\left(\frac{\partial\mathfrak{C}_f}{\partial\mu_f}\right)_{\bar{S}_f}=-1/X, \tag{2.6.2}$$

$$\text{a.}\quad\left(\frac{\partial\bar{G}_f}{\partial T}\right)_X=-\bar{S}_f, \qquad \text{b.}\quad\left(\frac{\partial\bar{G}_f}{\partial X}\right)_T=-\mu_f/X^2, \tag{2.6.3}$$

$$\text{a.}\quad\left(\frac{\partial\mathfrak{G}_f}{\partial T}\right)_{\mu_f}=-\bar{S}_f, \qquad \text{b.}\quad\left(\frac{\partial\mathfrak{G}_f}{\partial\mu_f}\right)_T=-1/X, \tag{2.6.4}$$

$$\text{a.}\quad \left(\frac{\partial \mu_f}{\partial T}\right)_P = -X(\bar{S}_f - \bar{S}_g), \tag{2.6.5}$$

$$\text{b.}\quad \left(\frac{\partial \mu_f}{\partial P}\right)_T = -X\bar{V}_g \cong -XRT/P,$$

and

$$\left(\frac{\partial \mu_f}{\partial \bar{S}_f}\right)_X = -X^2\left(\frac{\partial T}{\partial X}\right)_{\bar{S}_f}, \tag{2.7.1}$$

$$\left(\frac{\partial \mu_f}{\partial T}\right)_{\bar{S}_f} = X^2\left(\frac{\partial \bar{S}_f}{\partial X}\right)_{\mu_f}, \tag{2.7.2}$$

$$\left(\frac{\partial \mu_f}{\partial T}\right)_X = X^2\left(\frac{\partial \bar{S}_f}{\partial X}\right)_T, \tag{2.7.3}$$

$$\left(\frac{\partial \mu_f}{\partial \bar{S}_f}\right)_T = -X^2\left(\frac{\partial T}{\partial X}\right)_{\mu_f}, \tag{2.7.4}$$

$$(\bar{S}_f - \bar{S}_g)\left(\frac{\partial X}{\partial P}\right)_T + X\left(\frac{\partial \bar{S}_f}{\partial P}\right)_T = \bar{V}_g\left(\frac{\partial X}{\partial T}\right)_P, \tag{2.7.5}$$

where the approximate equality $\cong$ is used to indicate an application of the perfect gas law.

The basic Eqs. (2.5) yield a set of thermodynamic relations based upon the variables T, P, X, and μ_f, only two of which are independent. This system of equations is closely analogous to that derivable by standard Gibbsian method. By means of the calibration condition explicit use of a dividing surface has been avoided; the end result, however, is much the same. The extension of the system of thermodynamic relations to mixtures of gases and to adsorption systems in external electric or magnetic fields should be straightforward.

Finally, it should be noted that the molar excess functions $\bar{Z}_f$ are in the nature of integral or mean molar quantities. In the present system differential or partial molar quantities are indicated by a superscript partial differential operator, i.e.,

$$Z_f{}^{\partial} \equiv \frac{\partial Z_f}{\partial \Gamma} = \bar{Z}_f + X\left(\frac{\partial \bar{Z}_f}{\partial X}\right). \tag{2.8}$$

3. THE MEASURES OF ADSORPTION

In addition to the adsorption excess Γ, other measures of adsorption are in common use. By weighing the solid during the adsorption process the weight excess of adsorption W_f can be determined. In place of excesses the amount adsorbed Γ' or the weight adsorbed W_a can be dealt with directly. The measures of adsorption are related to one another in the following way:

If, under calibration conditions T, P, nonadsorbable gas of molecular weight M_0, the apparent weight of the solid is W_0, and, under calibration conditions T, P, adsorbate of molecular weight M_g, the apparent weight is W, then the weight excess of adsorption is defined by:

$$W_f \equiv W - W_0 + \frac{V_s{}^0(M_g - M_0)}{\bar{V}_g} \cong \Delta W + \frac{PV_s{}^0\Delta M}{RT}. \tag{3.1}$$

Then,

$$W_f = \Gamma M_g, \tag{3.2}$$

or

$$\Gamma \cong \frac{\Delta W}{M_g} + \frac{PV_s{}^0\Delta M}{M_g RT}. \tag{3.3}$$

Also, if the swelling of the solid is negligible, and the adsorbed phase has a well-defined volume V_a then the amount adsorbed Γ' is related to the adsorption excess Γ as follows:

$$\Gamma' = \Gamma + (V_a/\bar{V}_g), \tag{3.4}$$

or, in terms of the gas phase density ρ_g and the mean adsorbed phase density ρ_a,

$$\Gamma' = \Gamma/1 - (\rho_g/\rho_a). \tag{3.5}$$

Then the weight adsorbed W_a will be

$$W_a = \Gamma' M_g = W_f/1 - (\rho_g/\rho_a). \tag{3.6}$$

Finally, extensive quantity per mole adsorbed will be related to extensive quantity per molar excess as follows:

$$\bar{Z}_a = \bar{Z}_f - (\rho_g/\rho_a)(\bar{Z}_f - \bar{Z}_g), \tag{3.7}$$

and

$$\bar{Z}_a - \bar{Z}_g = [1 - (\rho_g/\rho_a)](\bar{Z}_f - \bar{Z}_g). \tag{3.8}$$

4. THE PROBLEM OF THE CHEMICAL POTENTIAL

Under equilibrium conditions a gas molecule anywhere in the available adsorption space has the same value for its chemical potential; thus the chemical potential of the gas μ_g is just the usual bulk expression. The case of the solid, however, is somewhat more difficult. Equation (2.1.2) or (2.1.4) would perhaps serve to formally define μ_s; however, in order to give μ_s further significance, the following set of postulates will be introduced:

P2. The chemical potential of a system (macro or micro) is a function of its surroundings.

P3. The chemical potential of a solid can be expressed in terms of the chemical potentials of the lattice elements of the solid.

P4. The chemical potential of each species of lattice element can be defined so as to be homogeneous throughout the solid.

From the postulates (P) it follows that all solids swell during the adsorption process; because of adsorption, the environment, and thus the chemical potential of surface lattice elements, changes; i order to maintain homogeneity in the chemical potential the surroundings of an internal lattice element must change also. Therefore, the solid swells.

For ordinary solids the increase in volume due to swelling will be small; therefore, the chemical potential of the solid can be expanded about the calibration

value in terms of the volume, keeping first-order terms only:

$$\mu_s=\mu_s^0+\left(\frac{\partial\mu_s^0}{\partial\bar{V}_s^0}\right)_T(\bar{V}_s-\bar{V}_s^0)+\cdots(\text{constant } T) \quad (4.1)$$

$$=\mu_s^0+\bar{V}_s^0\left(\frac{\partial P}{\partial\bar{V}_s^0}\right)_T\Delta\bar{V}_s$$

$$=\mu_s^0-(\Delta\bar{V}_s/\beta),$$

where $\beta=-(\partial\bar{V}_s^0/\partial P)_T/\bar{V}_s^0$ is the isothermal compressibility of the solid. Then,

$$\mu_f=\mu_s-\mu_s^0=-\Delta\bar{V}_s/\beta \quad (\text{constant } T) \quad (4.2)$$

and, in general,

$$\mu_f(T,X)=-\Delta\bar{V}_s(T,X)/\beta(T,P). \quad (4.3)$$

Thus μ_f and its differential coefficients can be expressed in terms of the compressibility β and the degree of swelling $\Delta\bar{V}_s$. For most substances the isothermal compressibility is independent of the pressure over a large range of pressures; therefore, β can be determined on any size sample of the solid. The degree of swelling can conceivably be measured directly—the linear expansion of a solid rod upon adsorption, the change in tension of a stretched fiber upon adsorption, etc. For some early work on the swelling of charcoal, see Bangham *et al.*[6,7]

An idea as to the order of magnitude of the swelling effect can be obtained from the data of Jura and Harkins[8] pertaining to the saturation adsorption of water at 25°C on an anatase sample of area 13.8 square meters per gram. Taking β for anatase as roughly 1×10^{-6} atmos^{-1}, the degree of swelling at saturation is $\Delta\bar{V}_s\approx1\times10^{-3}$ cc.

In this case, the value of $\Delta\bar{V}_s$ is fairly small; however, for an understanding of the adsorption process, the degree of swelling is quite important. The case is analogous to the change in activity of the solvent in the theory of the dilute solution. Hill[3,4] has emphasized the correspondence between functional forms involving the chemical potential of the solid and the normal relations between component activities in solution theory.

Hill[4] has also discussed the osmotic pressure analogy in describing the properties of the solid. The osmotic pressure is just the pressure necessary to keep the solid from swelling during the adsorption process. In order to keep the properties of the adsorbed phase the same and yet prevent the solid from swelling it is necessary to constrain the solid from within by means of Hill's internal, semipermeable piston, or some such hypothetical device. Such a treatment of osmotic pressure relative to adsorption is purely a formal one and has little physical significance.

Another analogy that suggests itself is the comparison of the swelling caused by adsorption to that caused by *electrostriction*. In the case of *electrostriction*, a solid in an external electric field responds to changes in the field (environment) by changes in volume. An attempt might be made to correlate the swelling of the solid with an hypothetical electric field in the adsorbed phase of such a nature as to cause equivalent swelling. Under such a program the adsorption properties of an adsorbate would be correlated with its electrical properties (polarizability, multipole moments, etc.) and statistical models capable of supplying the required fields would be sought. It is an open question as to whether such an approach would contribute anything physically to the understanding of the adsorption process; the analogy will not be pursued further.

The remarks about solids in this section are meant to apply to a homogeneous section of an isotropic solid. In the case of a powder, the device of the representative molar assembly (Sec. 2) is to be invoked. If the chemical nature of the solid is very complex or uncertain, the chemical potential per gram of solid can be introduced and the development carried through accordingly.

5. THE CONSTANT μ_f PROCESS

The importance of the constant μ_f process is evident from the defining equation

$$\mu_s\equiv\mu_s^0+\mu_f. \quad (5.1)$$

For a process at constant μ_f the differential coefficients of the solid are the same under adsorption conditions as under calibration conditions; in particular the entropy and heat capacity of the solid maintain their calibration condition values. A consequence of the foregoing is that under constant μ_f conditions entropy and heat capacity excesses are purely properties of the adsorbed molecules. As an example the heat capacity excess function which can be meaningfully correlated with the bulk heat capacity of an adsorbate is $\bar{C}_{\mu f}$ and not $\bar{C}_X$, for $\bar{C}_X$ contains not only the contribution of the adsorbed molecules but also a contribution due to swelling of the solid. In the case of transitions in the adsorbed layer, a plot of $\bar{C}_X$ *vs* T will probably exhibit a diffuse maximum due to swelling of the solid contemporaneously with the transition; whereas a plot of $\bar{C}_{\mu f}$ *vs* T should show a more nearly first-order (or bulk-order) type of transition. Heat capacity excesses will be more fully discussed in a later section.

The foregoing considerations lead to the definition of the ideal adsorption process:

$$i(\text{gas})\rightarrow i(\text{adsorbed}) \quad (\text{constant environment}). \quad (5.2)$$

This ideal process, carried out under constant environmental conditions, is just the constant μ_f process. The change in extensive quantity $\Delta\bar{Z}$ for the process is best expressed in terms of the script excess functions of

[6] D. H. Bangham *et al.*, Proc. Roy. Soc. (London) **130A**, 81 (1930).
[7] D. H. Bangham *et al.*, Proc. Roy. Soc. (London) **138A**, 162 (1932).
[8] G. Jura and W. Harkins, J. Am. Chem. Soc. **66**, 1356 (1944).

Eqs. (2.5), i.e., $\Delta\bar{Z}=\bar{z}_f-\bar{Z}_g$. It is thus possible by simple calculation to use the data from the spontaneous adsorption process to describe the ideal adsorption process (5.2).

6. THE GIBBS EQUATION

From Eq. (2.5.9),

$$\delta\mu_f=-X(\bar{S}_f-\bar{S}_g)\delta T-X\bar{V}_g\delta P, \qquad (2.5.9)$$

there follows:

$$\left(\frac{\partial\mu_f}{\partial X}\right)_T=-X\bar{V}_g\left(\frac{\partial P}{\partial X}\right)_T\cong-XRT\left(\frac{\partial \ln P}{\partial X}\right)_T \qquad (6.1)$$

and, at constant T,

$$\begin{aligned}\mu_f&\cong-RT\int_0^X X\left(\frac{\partial \ln P}{\partial X}\right)_T\delta X\\&\cong-RT\int_0^P X\delta \ln P.\end{aligned} \qquad (6.2)$$

Equation (6.2) is the usual integral form of the Gibbs equation. It is obvious that if analytic expressions are available for $\mu_f=\mu_f(T,X)$, Eq. (6.2) can be used to generate a family of isotherm equations, $P=P(T,X)$.

As a particularly simple example assume that for very small amounts adsorbed

$$\mu_s=\mu_s^0+RT\ln\frac{n_s}{n_s+\Gamma}=\mu_s^0-RT\ln(1+X). \qquad (6.3.1)$$

Then

$$\mu_f=\mu_s-\mu_s^0=-RT\ln(1+X), \qquad (6.3.2)$$

and by (6.2) and (6.3.2)

$$\delta\ln P=\delta X/X(1+X), \qquad (6.3.3)$$

$$\ln P=\ln\frac{X}{1+X}+\text{const}, \qquad (6.3.4)$$

$$P=\frac{kX}{1+X}\cong kX \quad (X\ll 1), \qquad (6.3.5)$$

thus arriving at the usual Henry's law expression.

For multilayer adsorption the following limiting conditions hold:

$$\lim_{X\to 0}\mu_f=0, \qquad (6.4.1)$$

$$\lim_{X\to\infty}\mu_f=\mu^*\ \text{(finite)}. \qquad (6.4.2)$$

Close to saturation it might be expected that

$$\mu_f=\mu^*-RT\ln\frac{\Gamma}{\Gamma+n_s}=\mu^*-RT\ln\frac{X}{1+X}. \qquad (6.5.1)$$

Such an expression leads to the isotherm equation:

$$\ln P/P_0=-\frac{1}{X}+\ln\frac{1+X}{X}, \qquad (6.5.2)$$

$$P/P_0\cong 1-X^{-2} \quad (X\gg 1), \qquad (6.5.3)$$

$$X\cong(1-P/P_0)^{-\frac{1}{2}} \quad (P/P_0 \text{ close to } 1), \qquad (6.5.4)$$

where P_0 is the vapor pressure of the bulk liquid at the isotherm temperature.

Hill,[9] by a free-volume argument, has derived an equation similar to (6.5.2). He finds, however, that according to his treatment the amount adsorbed close to saturation should be proportional to $(1-P/P_0)^{-\frac{1}{2}}$. For an experimental investigation of the limiting law close to saturation see the work of Bowers.[10]

In the region intermediate between small and large amounts adsorbed isotherm equations similar to those of Jura and Harkins[11] can be readily obtained, e.g., the assumption

$$\mu_f=\mu^*X/(X+\alpha) \qquad (6.6.1)$$

leads to

$$RT\ln P/P_0=\mu^*\left\{\frac{1}{\alpha}-\ln\frac{X+\alpha}{X}-\frac{1}{X+\alpha}\right\}, \qquad (6.6.2)$$

which has as limiting forms for $X\ll\alpha$ and $X\gg\alpha$ Freundlich-type and Harkins-Jura-type isotherms, respectively, α being just an arbitrary constant. Thus any analytic expression $\mu_f=\mu_f(T,X)$ satisfying the boundary conditions (6.4) will yield a multilayer isotherm. The number of such expressions is legion, and in the absence of *a priori* reasons for favoring one or several above the others, the mechanical production of isotherm equations seems somewhat pointless.

7. DELTA PROCESSES

Using the notation $\bar{Z}_f-\bar{Z}_g=\Delta\bar{Z}$, there follows from (2.5)

$$\Delta\bar{S}=-\bar{V}_g\left(\frac{\partial P}{\partial T}\right)_{\mu_f}\cong-RT\left(\frac{\partial \ln P}{\partial T}\right)_{\mu_f}, \qquad (7.1.1)$$

$$\Delta\bar{H}=\bar{E}_f-\bar{H}_g=T\Delta\bar{S}+(\mu_f/X)$$

$$\cong-RT^2\left(\frac{\partial \ln P}{\partial T}\right)_{\mu_f}+\frac{\mu_f}{X}, \qquad (7.1.2)$$

$$\Delta\mathfrak{C}=\Delta\bar{H}-\frac{\mu_f}{X}\cong-RT^2\left(\frac{\partial \ln P}{\partial T}\right)_{\mu_f}, \qquad (7.1.3)$$

$$\Delta\bar{G}=\mu_f/X, \qquad (7.1.4)$$

$$\Delta\mathcal{G}=\Delta\bar{G}-(\mu_f/X)=0. \qquad (7.1.5)$$

[9] T. L. Hill, J. Chem. Phys. **17**, 590 (1949).
[10] R. Bowers, Phil. Mag. **44**, 467 (1953).
[11] G. Jura and W. Harkins, J. Am. Chem. Soc. **68**, 1941 (1946).

It will be demonstrated that the ordinary calorimetrically determined integral heat of adsorption Q is given by $\Delta\bar{H}$ and not by $\Delta\mathfrak{IC}$, as might be supposed; the perfect gas assumption will be used throughout the demonstration:

$$\left(\frac{\partial \ln P}{\partial T}\right)_{\mu_f} = -\left(\frac{\partial \mu_f}{\partial T}\right)_P \Big/ \left(\frac{\partial \mu_f}{\partial \ln P}\right)_T, \quad (7.2.1)$$

and by (2.5.9),

$$\left(\frac{\partial \ln P}{\partial T}\right)_{\mu_f} \cong \left(\frac{\partial \mu_f}{\partial T}\right)_P \Big/ RTX, \quad (7.2.2)$$

$$\Delta\bar{H} \cong -RT^2\left(\frac{\partial \ln P}{\partial T}\right)_{\mu_f} + \frac{\mu_f}{X}$$

$$\cong \frac{\mu_f}{X} - \frac{T}{X}\left(\frac{\partial \mu_f}{\partial T}\right)_P. \quad (7.2.3)$$

Now from (6.2),

$$\mu_f \cong -RT\int_0^P X\delta \ln P, \quad (6.2)$$

follows

$$\left(\frac{\partial \mu_f}{\partial T}\right)_P \cong \frac{\mu_f}{T} - RT\frac{\partial}{\partial T}\int_0^P X\delta \ln P, \quad (7.2.4)$$

$$\left(\frac{\partial \mu_f}{\partial T}\right)_P \cong \frac{\mu_f}{T} + RT\int_0^P \left(\frac{\partial X}{\partial P}\right)_T \left(\frac{\partial \ln P}{\partial T}\right)_X \delta P, \quad (7.2.5)$$

$$\mu_f - T\left(\frac{\partial \mu_f}{\partial T}\right)_P \cong -RT^2\int^X \left(\frac{\partial \ln P}{\partial T}\right)_X \delta X$$

$$\cong \int_0^X q_{st}\delta X = XQ, \quad (7.2.6)$$

$$Q = \frac{\mu_f}{X} - \frac{T}{X}\left(\frac{\partial \mu_f}{\partial T}\right)_P = \Delta\bar{H}; \quad (7.2.7)$$

q_{st} is the isosteric heat of adsorption, i.e.,

$$q_{st} \equiv \left\{\frac{\partial(\Gamma Q)}{\partial \Gamma}\right\}_T = \left\{\frac{\partial(XQ)}{\partial X}\right\}_T \cong -RT^2\left(\frac{\partial \ln P}{\partial T}\right)_X. \quad (7.2.8)$$

The quantity (XQ) is the integral heat of adsorption per mole of adsorbent; Q is the integral heat of adsorption per molar excess (per mole adsorbed).

Now by (7.1.3), $\Delta\mathfrak{IC} = \Delta\bar{H} - (\mu_f/X) = Q - (\mu_f/X)$. From the discussion in Sec. 4 it is evident that μ_f/X represents the work of swelling of the solid. Thus, $\Delta\mathfrak{IC}$ represents the total heat content change minus the work of swelling—in other words, $\Delta\mathfrak{IC}$ refers to the ideal adsorption process (5.2).

Finally, by (2.7.3), (2.7.5), (7.1.1), and (7.1.3)

$$\Delta\mathfrak{IC} = q_{st} - \frac{T}{X}\left(\frac{\partial \mu_f}{\partial T}\right)_X. \quad (7.2.9)$$

The heat quantities, isosteric and integral, defined in this paper are true heats of *adsorption* in the thermodynamic sense and thus are of opposite sign to the quantities usually called heats of adsorption (true heats of *desorption*). Reasonable attention to the defining equations will make the sign convention of the present paper clear.

8. HEAT CAPACITIES

The two types of heat capacity excesses are defined as follows:

$$\bar{C}_X \equiv \left(\frac{\partial \bar{E}_f}{\partial T}\right)_X = T\left(\frac{\partial \bar{S}_f}{\partial T}\right)_X, \quad (8.1)$$

$$\bar{C}_{\mu_f} \equiv \left(\frac{\partial \mathfrak{IC}_f}{\partial T}\right)_{\mu_f} = T\left(\frac{\partial \bar{S}_f}{\partial T}\right)_{\mu_f}. \quad (8.2)$$

Then, if $\bar{S}_f = \bar{S}_f(T,X)$,

$$\bar{C}_{\mu_f} - \bar{C}_X = T\left(\frac{\partial \bar{S}_f}{\partial X}\right)_T \left(\frac{\partial X}{\partial T}\right)_{\mu_f}. \quad (8.3)$$

Also, if $\mu_f = \mu_f(T,X)$ and by (2.7.3) and (6.1),

$$\bar{C}_{\mu_f} - \bar{C}_X \cong \frac{X}{R}\left(\frac{\partial \bar{S}_f}{\partial X}\right)_T^2 \left(\frac{\partial X}{\partial \ln P}\right)_T, \quad (8.4)$$

and

$$\bar{C}_{\mu_f} - \bar{C}_X \cong \frac{1}{RX^3}\left(\frac{\partial \mu_f}{\partial T}\right)_X^2 \left(\frac{\partial X}{\partial \ln P}\right)_T, \quad (8.5)$$

or by (7.2.9)

$$\bar{C}_{\mu_f} - \bar{C}_X \cong \frac{1}{RT^2}\left(\frac{\partial \ln X}{\partial \ln P}\right)_T (\Delta\mathfrak{IC} - q_{st})^2$$

$$= \frac{1}{R}\left(\frac{\partial \ln X}{\partial \ln P}\right)_T (\bar{S}_f - S_f{}^{\partial})^2. \quad (8.6)$$

From the limiting laws for small and large amounts adsorbed, (6.3.2) and (6.5.1), and (8.5) there follows:

$$\lim_{X\to 0} \bar{C}_{\mu_f} - \bar{C}_X = R, \quad (8.7)$$

$$\lim_{X\to\infty} \bar{C}_{\mu_f} - \bar{C}_X = \frac{1}{R}\left(\frac{d\mu^*}{dT}\right)^2. \quad (8.8)$$

Finally, by Eqs. (2.7)

$$\bar{C}_{\mu_f}/\bar{C}_X = \left(\frac{\partial \mu_f}{\partial X}\right)_{\bar{S}_f} \Big/ \left(\frac{\partial \mu_f}{\partial X}\right)_T, \quad (8.9)$$

and

$$\bar{C}_{\mu_f}/\bar{C}_X=1-\left(\frac{\partial X}{\partial T}\right)_{\mu_f}\left(\frac{\partial X}{\partial T}\right)^{-1}_{\bar{S}_f}. \tag{8.10}$$

Either heat capacity excess can be used to obtain zero-point entropy excesses, e.g.,

$$\bar{S}_f(X)=\bar{S}_f^0(X)+\int_0^T \bar{C}_X d\ln T, \tag{8.11}$$

and by (7.1.2), (7.2.7), and (8.11)

$$\bar{S}_f^0(X)=\bar{S}_g+\frac{Q}{T}-\frac{\mu_f}{TX}-\int_0^T \bar{C}_X d\ln T. \tag{8.12}$$

9. FIRST-ORDER PHASE CHANGES

It is usual to consider a step discontinuity in an adsorption isotherm (i.e., a point other than P_0 at which $(\partial X/\partial P)_T\to\infty$) as evidence for a phase transition in the adsorbed layer. Such a transition would occur at constant T and P and thus at constant μ_f. Under these conditions plots such as μ_f *vs* P at constant T will have a corner point at the pressure in question; therefore, it may be necessary in discussing differential coefficients to distinguish derivatives on the right from those on the left.

Let the subscripts 1 and 2 refer to the system at the beginning of the transition and at the end of the transition, respectively. Also let $\Delta\bar{Z}_i\equiv\bar{Z}_{f(i)}-\bar{Z}_g$ and $\Delta\bar{Z}_f\equiv\bar{Z}_{f(2)}-\bar{Z}_{f(1)}$. Then

$$\Delta\bar{Z}_f=\Delta\bar{Z}_2-\Delta\bar{Z}_1 \tag{9.1}$$

and, by (7.1),

$$\Delta\bar{S}_f\cong-RT\left\{\frac{\partial\ln P_{(2)}}{\partial T}-\frac{\partial\ln P_{(1)}}{\partial T}\right\}_{\mu_f}$$

$$=-RT\Delta\left(\frac{\partial\ln P}{\partial T}\right)_{\mu_f}, \tag{9.2}$$

and so on.

Of more interest, however, are the relations concerning the transition pressure and μ_f, and the way these change with temperature. Let the values of the variables at the transition point simply be μ_f and P. Then

$$\mu_f=\mu_{f(1)}=\mu_{f(2)}, \tag{9.3}$$

and

$$d\mu_f=d\mu_{f(1)}=d\mu_{f(2)}. \tag{9.4}$$

From Eqs. (2.4), (2.5), and (9.4) there follows

$$-\bar{V}_g\frac{dP}{dT}=\frac{X_1}{\Delta X}\Delta\bar{S}_f+\Delta\bar{S}_2\cong-RT\frac{d\ln P}{dT}, \tag{9.5}$$

$$-RT^2\frac{d\ln P}{dT}\cong\frac{X_1}{\Delta X}\Delta\mathfrak{C}_f+\Delta\mathfrak{C}_2=\frac{X_1}{\Delta X}\Delta\bar{H}_f+\Delta\bar{H}_2. \tag{9.6}$$

Also

$$\frac{d\mu_f}{dT}=-X_1\Delta\bar{S}_1-X_1\bar{V}_g\frac{dP}{dT}, \tag{9.7}$$

and by (9.5)

$$\frac{d\mu_f}{dT}=\frac{X_1X_2}{\Delta X}\Delta\bar{S}_f. \tag{9.8}$$

Equations (9) are formally equivalent to those of Hill[3] and Meyer and Long.[12]

Since μ_f is a measure of the response of the solid (swelling) to changes in its environment, the first-order phase change restriction—occurs at constant μ_f—appears to be prohibitive. It is required that during the phase change $(\partial\mu_f/\partial X)_T=0$; by postulate (P2) this requires that the population of the adsorbed phase change without any concomitant change in the thermodynamic environment of the solid. Such a process appears unlikely.

If the solid continues to swell with increasing population of the adsorbed phase, then by (4.2)

$$\left(\frac{\partial\mu_f}{\partial X}\right)_T=-\frac{1}{\beta}\left(\frac{\partial\Delta\bar{V}_s}{\partial X}\right)_T\neq0 \tag{9.9}$$

and, by (6.1)

$$\left(\frac{\partial P}{\partial X}\right)_T=-\frac{1}{X\bar{V}_g}\left(\frac{\partial\mu_f}{\partial X}\right)_T\neq0, \quad \text{for} \quad P\neq P_0. \tag{9.10}$$

Thus it seems unlikely that step-discontinuous isotherms—with the discontinuity attributable to a first-order phase change—can be observed experimentally. In this regard see the recent work of Young and coworkers[13,14] pertaining to the adsorption of argon and *n*-heptane on graphite.

While processes at constant μ_f are not apt to happen spontaneously, it is possible to reduce any case in point to the ideal adsorption process (5.2) by the use of script excess functions.

10. THE CLASSICAL THEORY OF SOLIDS

The postulates (P) and the conclusion that all solids swell upon adsorption have some consequences for the classical theory of solids. A natural extension of the present treatment is to introduce, as a standard state for a crystalline solid, a solid of infinite dimensions; i.e., each lattice element of a given species has the same surroundings anywhere in the solid. The introduction of bounding surfaces (finite sample) requires a response on the part of the solid in order to establish homogeneity in the chemical potential per lattice element; i.e., the solid contracts. The extent of contraction depends on

[12] L. Meyer and E. Long, Phys. Rev. **85**, 1035 (1952).
[13] A. Cromwell and D. Young, Trans. Faraday Soc. **49**, 1080 (1953).
[14] Young, Beebe, and Bienes, Trans. Faraday Soc. **49**, 1086 (1953).

the ratio of lattice elements with incomplete nearest-neighbor shells (surface elements) to those with complete nearest-neighbor shells (bulk elements). Such behavior is analogous to the surface tension of a liquid; however, for a solid the curvature of the bounding surface has little to do, directly, with the extent of contraction; the pertinent variable is simply the previously mentioned ratio.

Thus, as is well known, the thermodynamic properties of a finely divided solid will differ from those of a sample effectively approaching the infinite solid, i.e., having a large bulk to surface ratio. Furthermore, the homogeneity of the chemical potential per lattice element requires that each lattice element of a given species contribute equally to the heat capacity and entropy of the solid, regardless of position; this is contrary to the usual statistical mechanical partition into bulk properties and surface properties.

Since the solid contracts upon the introduction of bounding surfaces, the (nearly) infinite solid can be put into the same state by placing it under pressure:

$$\mu_B(T,P)=\mu_I(T,P)+\int_P^{P'} \bar{V}_I dP \quad P'>P, \quad (10.1)$$

where the subscript notation is fairly obvious.

Thus division of a solid (increasing the surface to bulk ratio) and adsorption are inverse processes: in one, the solid contracts (relative to the standard state); while in the other, it swells (relative to the calibration condition). Some correlation might be expected between the two processes; e.g., an adequate theory of the swelling power of an adsorbate would be expected to furnish a relationship between μ^* and $\mu_B-\mu_I$.

11. THE CONCEPTS OF SPREADING PRESSURE AND AREA

It has been the custom[3,11,15] in treating the adsorption of gases on solids to follow the analogy to insoluble films on a liquid subphase. In the case of a liquid subphase, the area A and the two-dimensional spreading pressure φ (negative of the force per unit length exerted on the film by the movable barrier) of the film are well-defined properties of the surroundings; therefore, by postulate (P1) they are suitable or natural thermodynamic parameters. In particular the spreading pressure is capable of direct measurement.

For the adsorption of gases on solids the analogs of the area and spreading pressure are no longer well-defined properties of the surroundings. The area of a finely divided solid is difficult to determine unambiguously; while the analog of the spreading pressure is merely a formal quantity, i.e., it is not something measured directly; it is always a calculated quantity.

However, if the compressibility of the solid is such that its properties in vacuo temperature T are approximately equal to its properties under calibration conditions temperature T and pressure P, then there is a formal correspondence between the present development and the development in terms of spreading pressure and area:

$$\mu_f \cong -\bar{A}\varphi, \quad (11.1)$$

where $\bar{A}$ is the area per mole of solid. If the area remains constant

$$\delta\mu_f \cong -\bar{A}\delta\varphi, \quad (11.2)$$

and

$$\Gamma''=\Gamma'/A, \quad (11.3)$$

where Γ''-moles adsorbed per unit area—is the adsorption measure commonly used in the spreading pressure system.

Finally, functional forms involving φ in the spreading pressure system are taken as applying to the behavior of the adsorbed molecules—two-dimensional equations of state, etc.; whereas, in the present system, the corresponding forms in μ_f are taken as referring to the response of the solid to changes in its environment.

12. CONCLUSION

An adsorption system has been described in which both components have been put on a more or less equal footing: under the influence of the solid, gas molecules become adsorbed; under the influence of the adsorbed molecules, the solid swells. Both processes are viewed as the response of system to environment.

[15] D. H. Everett, Trans. Faraday Soc. **46**, 453 (1950).

THE JOURNAL OF CHEMICAL PHYSICS VOLUME 22, NUMBER 10 OCTOBER, 1954

Electronic Structure of Disordered One-Dimensional Chains

ROLF LANDAUER AND JOSEPH C. HELLAND*
Research Department, International Business Machines Corporation, Poughkeepsie, New York
(Received March 31, 1954)

The positions of the electronic levels in a variety of finite one-dimensional models of disordered alloys and of liquids have been evaluated numerically over a wide range of energies. The disordered alloys consist of two types of potential wells thrown together in a random sequence, but in equal proportions. In the disordered case the tightly bound states give rise to narrow bands in which the distribution of states cannot be described by a smooth function. The distribution of states can be interpreted in terms of an approximation in which each electron is confined to its own group of adjacent identical atoms. At high energy levels the disordered alloys obey perturbation theory, at least in a qualitative fashion, and the ordered alloy differs from the disordered one because of the effect of Bragg reflections from the superlattice. At high energies the distribution of states can be described by a reasonably smooth density function. Between the high energy range and the tightly bound levels, in some of the cases a transition region occurs, in which the levels are distributed irregularly, but without well-defined gaps and without being susceptible to the simple explanation of localized states. The total number of states (not counting the two spin possibilities as separate states) up to a well-pronounced energy gap is always an integral multiple of one-half the total number of atoms in the chain.

The liquids consist of a series of identical wells separated by a variable well-to-well space. In a liquid the forbidden energy ranges are either smaller than in the strictly periodic crystal, or else nonexistent. The extent to which an energy gap in the strictly periodic crystal will be affected by the introduction of dispersion in the spacing depends on the original gap width as well as on the sensitivity of the gap position, in the strictly periodic case, to uniform dilations. In both the liquid cases and the disordered alloy models a distinction must be made between energy ranges in which the density of states is very low and ranges in which it is strictly zero.

I. INTRODUCTION

THE distribution of electronic energy levels in a perfectly periodic crystal has received a great deal of attention. The effect of isolated defects, or else of periodically repeated defects, has also been frequently examined. The effect of a complete departure from periodicity, such as occurs in disordered alloys and also in liquids, has not received much attention. This is the case discussed in this paper. A variety of one-dimensional models of liquids and disordered alloys have been investigated numerically. In each case, a finite chain of atoms was selected and all the levels within a wide energy range were located.

Since we have used one-dimensional models, none of our results are intended to apply to particular alloys or liquids. Instead, it is hoped that a numerical calculation of the type presented here can indicate some of the ways in which disordered alloys and liquids can deviate from the well-understood band structure.

II. DISORDERED ALLOYS

This part of the investigation is concerned with the grouping of electronic energy levels in a disordered alloy. We have in mind alloys such as CuZn and FeAl in which two types of atoms can occur in either an ordered or a disordered arrangement. The perfectly ordered alloy results in a periodic crystal structure in which the energy levels come grouped in well-defined energy bands. The case of the disordered alloy has been considered by Saxon and Hutner,[1] as well as Luttinger,[2] who have treated the case of a disordered one-dimensional series of δ function potential wells. Allen and Shockley[3] have pointed out that the δ function well has peculiar properties which make it unsuitable for band structure investigations. More recently, James and Ginzbarg[4] have considered the problem of impurity bands in a semiconductor, where the two types of atoms are present in very unequal proportions.

In a disordered potential, the energy levels can be spaced very irregularly. While we are not necessarily interested in the very exact location of each level, we would like to know exactly how many energy levels there are in each of a set of reasonably small energy intervals. A method for performing this counting of energy levels, suitable for numerical calculation, was devised for this purpose. The method is essentially that of "node counting" which has since been described by James and Ginzbarg.[4] James and Ginzbarg assumed infinite potential walls at the end of their lattice. This leads to the requirement that the wave function vanish at the two ends of the chain. One does not expect the particular boundary conditions to be very important if the chain is long enough. It seems reasonable, however, that surface effects will be less likely with periodic boundary conditions, and we have therefore used the latter in our investigation. This requires some additional, but fairly straightforward, elaboration on the node counting process as described by James and Ginzbarg.

In this computation we have considered a variety of shapes and arrangements for our wells. Our notation is explained in Fig. 1, which shows the typical unit that

* Present address: North American Aviation, Inc., Los Angeles International Airport, Los Angeles, California.

[1] D. S. Saxon and R. A. Hutner, Philips Research Repts. **4**, 81 (1949).

[2] J. M. Luttinger, Philips Research Repts. **6**, 303 (1951).

[3] G. Allen, Phys. Rev. **91**, 531 (1953); W. Shockley, *Holes and Electrons in Semiconductors* (D. Van Nostrand Company, Inc., New York, 1950), p. 407, Problem 5.

[4] H. M. James and A. S. Ginzbarg, J. Phys. Chem. **57**, 840 (1953). References to the earlier literature are given here.

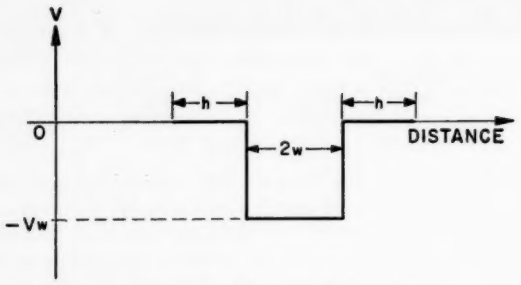

FIG. 1. Typical well used in sequences representing disordered alloys. All wells are symmetrical and have a region of negative potential surrounded by regions of zero potential.

is used in building the chain. The two types of wells which are thrown together to form a chain will be called A and B. All the parameters necessary for the calculations are then specified if we are given a particular sequence of A's and B's and the values of the dimensions h_A, w_A, h_B, w_B, and of the well depths V_A and V_B. Note that in the "hills" separating adjacent wells we always have $V=0$. The bottom of the well is always at a level below this, as indicated in Fig. 1 by its location at $V=-V_w$, where V_w is positive. All of our disordered sequences consist of an equal number of A and B atoms. The potential wells used in the computation are tabulated in Table I, and the atomic sequences in Table II. In all cases, the energy range extends from $-V_A$ or $-V_B$, whichever is less, up to the value listed in Table I under "Maximum energy."

A few of our computations were done with a chain of 40 atoms. All others were done with 150 atoms. The wave equation was taken as

$$d^2\psi/dx^2+[E-V(x)]\psi=0. \quad (1)$$

Node counts were performed at intervals of 0.01 on the energy scale, in all regions where particular detail was desired. Otherwise, a node count was performed at intervals of 0.02 or at intervals of 0.10. Whenever a node count is performed, we then know the total number of energy levels up to the energy at which the count is made. The computation was performed on the IBM 701 Electronic Data Processing Machine. Approximately 7.5 seconds were required for the computation and printing of results relevant to one node count, for a sequence of 150 symmetrical potential wells.

Table I shows a number of potentials, some of which differ only in the total number of wells, or in the particular sequence of wells. These variations were introduced to show the extent to which our results depend on the choice of a particular sequence. A similar variation in the particular arrangement was also used in the "liquid model." A given sequence of atoms can be rearranged in two different ways. One kind of rearrangement leaves adjacent identical atoms together and only shuffles such groups of adjacent atoms around without breaking them up, and without forming larger groups of adjacent identical atoms. A second kind of rearrangement permits a departure from this and changes, for example, the number of times three B atoms are found next to each other. All the rearrangements tried by us were such as to leave a reasonably typical looking random sequence, with no obvious anomalous features. Our results were almost completely insensitive to rearrangements of the first kind, but moderately sensitive to rearrangements of the second kind. By "completely insensitive," we mean that the shape of the $N(E)$ curve, which plots the total number of levels up to the energy E, against E, is left unchanged. Naturally, our results for finite chains of 40, or 150 wells do not give a continuous function $N(E)$, since N must increase by at least an integer, if it increases at all, in a given energy interval. There are, therefore, slight departures from a smooth curve, and the exact nature of those departures is sensitive even to a rearrangement of the first kind. Even these departures, from a smooth curve, are changed primarily in their exact place of occurrence with respect to energy (or, roughly speaking, their "phasing") rather than in their frequency and magnitude.

III. EXPECTED NATURE OF RESULTS

There are two limiting cases in which the general nature of the results can be anticipated. One is the case of very tightly bound electrons, the other is the case of almost free electrons. In discussing these results we shall have a chain of $2N$ atoms in mind, N atoms of type A, and N atoms of type B. If this were an ordered chain, it would have N unit cells in the chain, and therefore N electronic levels per band (in this as well as all succeeding statements, we shall be concerned only with the number of different spatial wave functions, and shall disregard the fact that there are two spin possibilities for each spatial wave function). We shall assume that the sites of the center of the A atoms are given by a_1, $a_2 \cdots a_N$. The center of the B atoms are at b_1, b_2, $\cdots b_N$. The potential can then be written as a sum of nonoverlapping atomic potentials

$$V=\sum_1^N V_A(x-a_i)+\sum_1^N V_B(x-b_i). \quad (2)$$

TABLE I. Disordered potentials used in numerical computation.

Run	V_A	w_A	h_A	V_B	w_B	h_B	Order of atoms[a]	Total No. of wells	Maximum energy
1α	$2\frac{1}{2}$	$\pi/2$	$\pi/2$	4	$\pi/2$	$\pi/2$	α	150	8.0
1β	$2\frac{1}{2}$	$\pi/2$	$\pi/2$	4	$\pi/2$	$\pi/2$	β	40	7.7
1γ	$2\frac{1}{2}$	$\pi/2$	$\pi/2$	4	$\pi/2$	$\pi/2$	γ	40	12.0
1δ	$2\frac{1}{2}$	$\pi/2$	$\pi/2$	4	$\pi/2$	$\pi/2$	δ	40	10.9
2α	1	$\pi/2$	$\pi/2$	6	$\pi/2$	$\pi/2$	α	150	15.0
3α	4	$\pi/2$	$\pi/2$	6	$\pi/2$	$\pi/2$	α	150	8.0
4α	$2\frac{1}{2}$	$\pi/2$	$\pi/2$	$2\frac{3}{4}$	$\pi/2$	$\pi/2$	α	150	12.0
4β	$2\frac{1}{2}$	$\pi/2$	$\pi/2$	$2\frac{3}{4}$	$\pi/2$	$\pi/2$	β	40	11.2
5β	$2\frac{1}{2}$	$\pi/2$	$\pi/2$	3	$\pi/2$	$\pi/2$	β	40	11.5
6α	$2\frac{1}{2}$	$\pi/2$	$1.05\pi/2$	$2\frac{1}{2}$	$\pi/2$	$0.95\pi/2$	α	150	13.4
7α	$2\frac{1}{2}$	$\pi/2$	$1.2\pi/2$	$2\frac{1}{2}$	$\pi/2$	$0.8\pi/2$	α	150	12.0
8α	1	$\pi/8$	$\frac{7}{8}\pi$	1	$\frac{3}{8}\pi$	$\frac{5}{8}\pi$	α	150	14.4

[a] These sequences are given in Table II.

This lack of overlap implies that the potential near each atomic site depends only on the type of atom at that site. The electronic screening present in a good conductor will prevent the potential of one atom from reaching very far beyond its lattice site; it will, however, reach at least into neighboring cells, and we are neglecting this. The exact nature of the screening will depend not only on the atom being screened, but also on the kind of screening that the neighboring atoms can provide.[5]

Let us consider the range of energies in which both A and B atoms have tightly bound electrons. At an energy at which the A atoms have a bound level, the B atoms will in general not have one. Near such an energy there will then be N states, whose wave functions are appreciable only near the A sites.

The case of almost free electrons is readily analyzed by perturbation theory if the A and B atoms have the same length, i.e., $2w_A+2h_A=2w_B+2h_B$. In this perturbation treatment we shall consider a chain containing N of the A atoms and N of the B atoms. We shall take the total length of the chain to be $2Na$. Free electron states with wave functions

$$=(2Na)^{-\frac{1}{2}}e^{\pm ikx} \tag{3}$$

are taken as the unperturbed states. For periodic boundary conditions the values of k are restricted to $k=\pi m/Na$, where m can be zero or a positive integer. With the exception of the state $k=0$, the unperturbed states are doubly degenerate and hence the correct linear combination of the degenerate wave functions must first be found. This is entirely analogous to the usual Brillouin treatment of the strictly periodic case.[6] The two correct linear combinations are separated in energy by a first-order term which is twice the magnitude of the matrix element

$$\int \frac{[\exp(-ikx)]^*}{(2Na)^{\frac{1}{2}}} V \frac{\exp(ikx)}{(2Na)^{\frac{1}{2}}} dx, \tag{4}$$

the integral being taken over the length of the chain. Let the left end cell of the chain be between $x=0$ and $x=a$. The potential in this cell according to Eq. (2) can then be either $V_A[x-(a/2)]$ or $V_B[x-(a/2)]$. Then if we let

$$A_k=\int_0^a V_A\left(x-\frac{a}{2}\right)e^{2ikx}dx,$$

$$B_k=\int_0^a V_B\left(x-\frac{a}{2}\right)e^{2ikx}dx,$$

[5] J. Friedel, Phil. Mag. 43, 153 (1952), points out that screening can occur by bound electrons as well as by electrons free to move through the conduction band.

[6] F. Seitz, *The Modern Theory of Solids* (McGraw-Hill Book Company, Inc., New York, 1950), Sec. 61.

TABLE II. Atomic arrangements used in computation.

Disordered alloys

α Sequence: *ABABAABABBBAABAAABBAABBABBAAB AABABBABABAAABBABBABBBAAABABBBBBAABAAB ABABABBABBABAABBBABBABBAABAABBABBBAAAA ABAABBABBBBABBAABAAAABBABBAABAABAABAAA BABABAB*

β Sequence: *ABABAAABABABBABBAABAABBABAAAB BBABBBAABBA*

γ Sequence: *BABABBBABABAABAABBABBAABABBBA AABAAABBAAB*

δ Sequence: *ABABAAAAABABAABBBABABBBAAABAA BAABBABBBBB*

Liquid models

L' Sequence: *WSSWSSSWSWSSSWSWSSWSSSWWSSWSS WSWSSSWSSSWSSSSWSSWSSWSWSSWWSSSWSSWSSW SSSWSSWSWSWSSSSWSSWSSWSWSSWWSWSSSWSSWSSW SSWSSWSSWSWSWSWSSSWSSSWSSWSSWSSWSSWSSSS WSSSWS*

L'' Sequence: *WSSWSWWSWSSWSSWSSWSWSSWSSSWS SWSSSSWSSWSSWSSWSSSSWSWSSSWSSSSWSSWSWSSS WSWSSWSWWSSWSSSWSSSWSSSSWSSWSSWSSSWSSS WSSWSSWSSWSWSSSWSWSWSWSSWSSSWSSSWWSSSW SSWSWSS*

W = Well. S = Spacer section.

the matrix element (4) becomes

$$\frac{1}{2Na}\sum_{n=1}^{2N} e^{2ik(n-1)a}[f_A(n)A_k+f_B(n)B_k]. \tag{4a}$$

The function $f_A(n)$ is unity if the nth cell is occupied by an A atom, and zero otherwise. $f_B(n)$ similarly indicates the presence of B atoms. Whenever m is an integral multiple of N, so that the unperturbed wavelength fits an integral number of times into the length $2a$, then (4a) reduces to

$$(A_k+B_k)/2a. \tag{4b}$$

(4b) applies to the values of k at which a perfectly periodic crystal with a unit cell of length a has its energy gaps. The energy gap that results is $|A_k+B_k|/a$. A pure A crystal would have a gap $2|A_k|/a$, while a pure B crystal would have a gap $2|B_k|/a$. Hence, V_D, the gap width in the disordered alloy, is related to the gap widths V_A and V_B of the pure crystals in the fashion

$$V_D^2=\tfrac{1}{4}(V_A^2+V_B^2+2V_AV_B\cos\theta). \tag{5}$$

Here θ is the angle which gives the phase difference between A_k and B_k. For all of our potentials, except 6α, 7α, and 8α, the two wells have the same length and the same position within the cell, and differ only in well depth. In this case $\cos\theta=1$. Between the gaps given by Eq. (5) there will be $2N$ states (i.e., different spatial wave functions). Note that according to Eq. (5) the disordered gap can at most be equal to the root-mean-

square value of the corresponding pure crystal gaps. If, however, $\cos\theta$ does not equal unity, then the disordered gap will be smaller.

We have derived Eq. (5) for values of m which are integral multiples of N. When m has any other value the contributions to the matrix element from the various atoms of a given species will not be in phase anymore. In this case the rms value of (4a), for large N, varies as $N^{-\frac{1}{2}}$. In computing this rms value the averaging is carried out over the ensemble of all possible arrangements of N atoms of type A and N atoms of type B. The energy gap in this case is then an effect due the finite size of the lattice and has no significance in the infinite lattice. The correct linear combinations of the two degenerate wave functions, $e^{\pm ikx}$, are, however, standing waves with zero current, for all values of N.

In the limit of almost free electrons we can therefore expect energy bands which contain $2N$ states each. This is in contrast to the ordered AB alloy which has N states per band, and therefore twice as many energy gaps as the disordered alloy. The gaps, however, which are common to both the ordered and disordered alloy are the same width in both, according to first-order perturbation theory. This width is the one given by Eq. (5).

It should be noted that the perturbation theory will be valid only for the higher-energy states and can tell us nothing about the total number of states below a certain energy. The perturbation theory result that there must be $2N$ levels per band does not imply that the total number of levels in the lower lying bands is also a multiple of $2N$. In fact, we have seen that the tightly bound electrons come in bands of N states, and it is easily possible to have an odd number of tightly bound bands. We learn nothing from perturbation theory about the number of states in the transition region between the tightly bound and the almost free electrons. It is not even clear that this number must be a multiple of N.

The results of first-order perturbation theory that we have quoted must not be taken too literally. Perturbation theory is, strictly speaking, only valid when the splitting of degenerate energy levels is small compared to the spacing of the unperturbed levels. If N is large enough so that in the range V_d given by Eq. (5) there are several unperturbed levels, then perturbation theory is not necessarily correct. But N must be this large in order to give V_d the significance of a forbidden energy range; for much smaller N, V_d represents only a minor splitting in a particular energy level. Furthermore, in the other case that was discussed, where m is not an integral multiple of N, the splitting decreases as $N^{-\frac{1}{2}}$, but the density of states is proportional to N, so that here again our conclusions are not really applicable to very long chains. Attempts to go beyond a first-order treatment are difficult because none of the relevant matrix elements is zero.

IV. RELATION TO THREE-DIMENSIONAL CASE

There are a number of apparent ways in which a three-dimensional disordered lattice will differ from our model. First of all, there is the well-known fact (for the strictly periodic case) that in three dimensions bands can overlap, while they cannot do so in one dimension. There are, however, other distinctions which are peculiar to the disordered case.

The one-dimensional chain consists of alternate groups of A and B atoms. In a disordered three-dimensional lattice each atom has many nearest neighbors and in all but a small fraction of cases, an atom will have nearest neighbors of both types (assuming A and B present in equal proportions). There will then be few completely isolated groups of like atoms in the three-dimensional case. Instead, there will be long chains with many arms.

There is one particular sequence of atoms, α in Table II, which was used in most of our computations. This sequence was selected with a slight prejudice. It has slightly fewer large clusters of identical adjacent atoms than most random sequences of 150 atoms. This prejudice in the selection was exercised to obtain a slightly closer resemblance to the three-dimensional case, in which an A atom is very rarely immersed in an environment of pure A over several interatomic distances.

In a real alloy with a relatively small percentage of B, the average distance between nearest B neighbors is inversely proportional to the cube root of their concentration. In the one-dimensional model this distance is inversely proportional to the concentration. Since it is both the distance between nearest B neighbors (e.g., when considering the extent to which tightly bound B-type wave functions overlap) as well as the concentration of B atoms (as for example when considering B-type contributions to perturbation theory matrix elements) that matter, it is difficult to get a realistic one-dimensional model for the case in which there are relatively few B atoms. These difficulties are minimized in the alloy AB which we have investigated.

V. ALMOST FORBIDDEN REGIONS

In the strictly periodic case one has only two types of energy ranges: allowed and forbidden. In the disordered case it will be necessary to distinguish between three types: allowed, strictly forbidden, and almost forbidden. The almost forbidden range is one in which the density of levels is very low, but not quite zero.

The energy gaps between tightly bound states are examples of strictly forbidden ranges. No atomic rearrangement can broaden the very narrow bands beyond a certain extent, leaving large forbidden ranges in between.

Some typical energy gaps at higher energies are shown in Figs. 2–4. Note that the points on the graphs do not represent the energies at which energy levels are located. A point simply serves to indicate the number of

levels that occur below an arbitrarily selected value of energy. Consider now in detail the gap shown for the case 2α, in Fig. 2. Between 5.825 and 6.045 no energy levels occur. This, however, is only a result of the limited size of our chain. This range is not a "strictly forbidden" range, but only an "almost forbidden" range. To see this we must take into account that the forbidden range for a pure A crystal (as shown by the shaded vertical columns drawn with 2α in Fig. 2) does not overlap the forbidden range for the pure B crystal. This is in contrast to the situation shown for 4α in the right-hand part of Fig. 2, where the forbidden A and B ranges do overlap. In a long chain of disordered AB there will be occasional large clusters of pure A and other large clusters of pure B. These large clusters will contribute energy levels very similar to those of pure crystals.[7] Therefore, the large cluster will provide

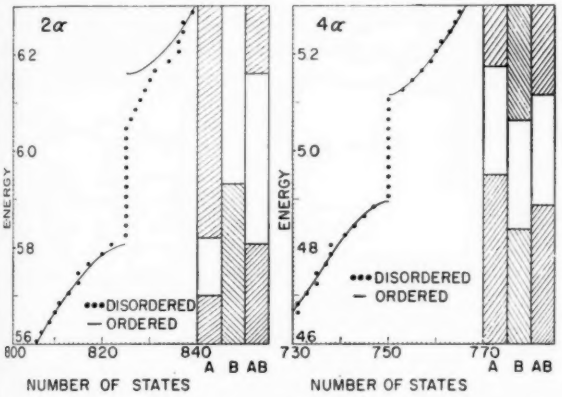

FIG. 2. At left is a part of the results for the disordered potential 2α, showing a range with no energy levels. The allowed ranges for the A crystal, the B crystal, and the ordered AB alloy are indicated by the shaded vertical regions. Note that the dots are not the locations of energy levels, but only serve to indicate the number of levels up to the energy concerned. The solid curve gives the level distribution for an infinite ordered AB chain, normalized to 75 states per band (in contrast to the slightly more irregular results obtained from a finite chain of 150 atoms). At right are similar results for a part of 4α, a potential consisting of very similar A and B atoms.

energy levels in any energy range in which either the pure A or the pure B band has allowed levels. The effect of nonoverlapping forbidden ranges is shown more clearly in Fig. 3 where there is an obvious range of a lower density of states, but no clearly defined forbidden range. It is interesting to note that in the shorter chains 1β and 1γ, whose largest clusters contain only three identical adjacent atoms, there is a well-defined energy range, without any levels, between the energies 0.34 and 0.44. (1β and 1γ are built up out of the same A and B wells as 1α.)

More generally, any ordered alloy composed of A and

[7] In one dimension the effect of changing boundary conditions is to displace levels by magnitudes comparable to their spacing, so that a large cluster of identical atoms contributes the same density of levels to a crystal, regardless of the environment in which it is placed. (This is a somewhat oversimplified version of a statement which can be proven by the use of oscillation theorems.)

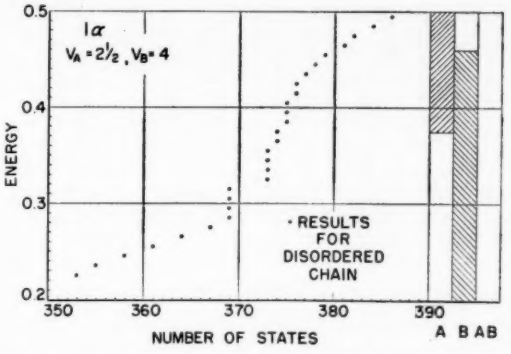

FIG. 3. A part of the results for 1α showing a range of reduced density of levels, but not a strictly forbidden range, in the disordered alloy. The allowed ranges for the A crystal, the B crystal, and the ordered AB alloy are indicated by the shaded regions at the right. The whole range shown is part of an energy gap in the ordered crystal.

B atoms in any proportion must be represented by several clusters in a sufficiently long chain of disordered AB. Any energy range which is an allowed range in such an alloy cannot, therefore, be a strictly forbidden range in disordered AB. The theorem suggested by Saxon and Hutner[1] and proven by Luttinger[2] states that if the A and B wells are δ functions, then any range forbidden to both the pure A and B lattices is also forbidden in any alloy of A and B, regardless of the sequence or proportion of A and B atoms. From our discussion we know that an allowed range of either pure A or pure B cannot be a strictly forbidden range of the disordered alloy. Hence the energy ranges specified by Saxon, Hutner, and Luttinger are the only strictly forbidden ranges in the δ function model.

An ordered alloy or periodic structure is a conductor if and only if the Fermi level occurs in an allowed range. In a disordered alloy what can be expected if the Fermi

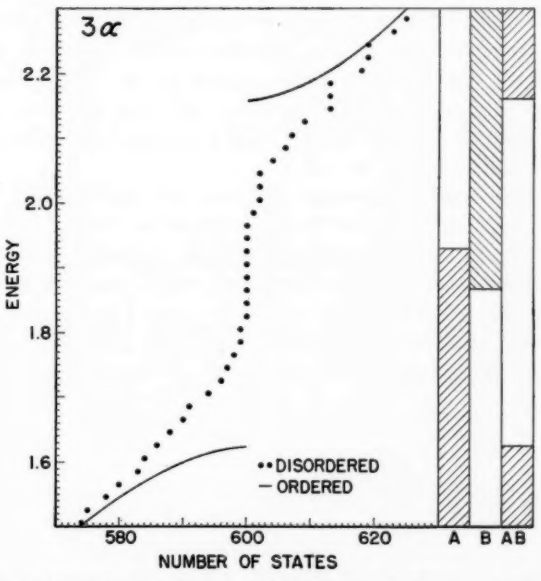

FIG. 4. Results for 3α. The forbidden A and B ranges do not overlap.

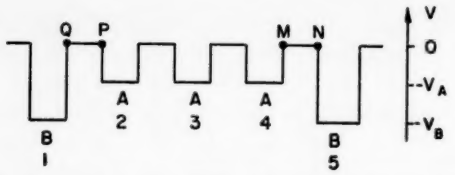

FIG. 5. Three adjacent A wells are surrounded by B wells. This group of A atoms will contribute a set of three levels to a narrow A band.

level occurs in an almost forbidden range? In this case the wave functions at the Fermi level are localized to the large ordered inclusions, and therefore cannot carry a current.

In three dimensions, inclusions of pure A or pure B would be much less likely than in one dimension. Large inclusions of ordered AB, however, will be a serious possibility, since actual alloys always have some local order left above the transition temperature.

VI. NARROW BANDS

We shall here consider the electronic energy levels for the case where there are tightly bound electrons for the A atoms, and no levels for the B atoms, at nearby energies. In our chain of $2N$ wells, there will then be N states in such a narrow band, one for each A atom. Whenever we have a group of adjacent A atoms, the electron has a small chance of passing from one atom in this group to another. Presumably its probability of passing completely out of its original A group, through one or more B atoms, into another A group, is much smaller. Each group of adjacent A atoms is then an almost isolated unit, and contributes its own set of energy levels.

Consider the group of three A atoms shown in Fig. 5. The wave functions for this group will be appreciable in wells 2, 3, 4, but must be small in wells 1 and 5. In each A well the wave functions must be very similar to the wave function of the isolated A atom. Between the A wells the wave function varies in an exponential fashion. The wave function drops off sharply as we go into the hill from a well, reaching a minimum somewhere near the center of the hill.

In the regions marked PQ and MN the minima, if they exist at all, must be much closer to Q and N than to M and P. Consider for the moment a similar problem, illustrated in Fig. 6, involving only A wells. The solutions in an infinite A lattice look like the usual atomic wave functions in each well, but are modulated by an amplitude which varies as cos kx in going from

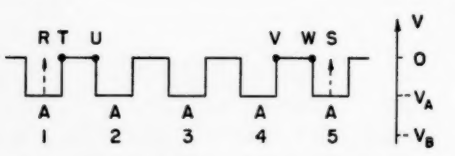

FIG. 6. A group of five adjacent A wells. The wave function which is particularly small in wells 1 and 5 is a good approximation to a solution for the situation shown in Fig. 5.

cell to cell. The wave functions in wells 2 and 4 will have a large amplitude compared to the wave functions in wells 1 and 5, if cos kx has a zero at R and S. (R and S are the midpoints of wells.) At the energies corresponding to these particular values of k the wave functions in TU and VW will be similar to the desired wave functions in PQ and MN in Fig. 5. To find the energies at which cos kx can be zero at both R and S we use the fact that

$$e^{ika}=\tfrac{1}{2}(T_A\pm(T_A{}^2-4)^{\frac{1}{2}}), \tag{6}$$

where T_A is the trace of the matrix which relates $(\psi, d\psi/dx)$ at the right-hand end of an A cell to $(\psi, d\psi/dx)$ at the left-hand edge of the cell. a is the cell length. T_A is a quantity which varies approximately linearly with energy in the vicinity of a narrow band. A pure A crystal will have an allowed band in the narrow range in which $|e^{ika}|=1$, which corresponds to the range in which T_A is between -2 and $+2$. Figure 7 illustrates what happens near a narrow band as T_A varies through the range from -2 to $+2$. Every possible

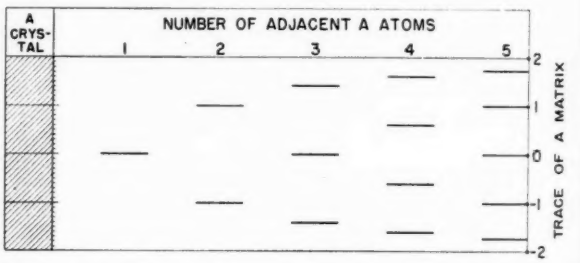

FIG. 7. Distribution of energy levels for groups of 1, 2, 3, 4, and 5 adjacent A atoms. The approximation which replaces Fig. 5 by Fig. 6 and then requires $\psi(R)=\psi(S)=0$ has been used. As the number of adjacent atoms is increased, the distribution approaches that of the infinite crystal, in which the allowed band covers the whole range between $T_A=-2$ and $T_A=+2$.

size of group contributes its own characteristic set of levels. In a chain, such as α in Table II, each of these A groups occurs a certain number of times. Therefore, the level structure for a narrow A band in sequence 1α can be expected to be a superposition of the patterns shown in Fig. 7. A set of actual results are compared to this anticipation in Fig. 8.

As shown in this case, as well as in all similar narrow bands which we have investigated in disordered alloys, the computational results do not fit on a smooth $N(E)$ curve. The states cover almost the same energy range as in a pure A crystal. In contrast, an ordered AB alloy has much narrower tightly bound bands, since in it identical wells never have a chance to be adjacent.

In a three-dimensional structure isolated A groups are far less likely and therefore the exact structure of narrow bands will not be as outlined above. It is, however, likely that even in the three-dimensional case the fine structure of narrow bands is determined by the number of times each type of local arrangement occurs.

VII. GENERAL RESULTS

Typical results over a wide energy range are shown in Fig. 9. The forbidden regions shown for the disordered case are not necessarily strictly forbidden regions, but are regions in which there are no levels for our chain of 150 atoms. In fact, there are no strictly forbidden regions in the positive energy range, since the forbidden A and B ranges do not overlap.

In the negative energy region the behavior has already been described. The $N(E)$ curves there are far from smooth, but do permit a simple interpretation. In the positive energy region above 2.8 the results for the disordered chain are in accordance with the perturbation theory prediction of 150 states per band. In this region the $N(E)$ curves are quite smooth. The transition region is the region between 0.02 and 2.52. In this region, particularly in its lower part, the $N(E)$ curve has many irregularities. The most prominent one is shown in Fig. 3. There are, however, no clearly defined gaps in this transition region. Such transition regions occur in all of our cases where the pure A crystals and the pure B crystals have striking differences in band structure, in the positive energy range. In the other cases where the two pure crystals have allowed bands (in the range $E>0$) which are displaced from each other by an amount which is small compared to the band width, there is no transition region.

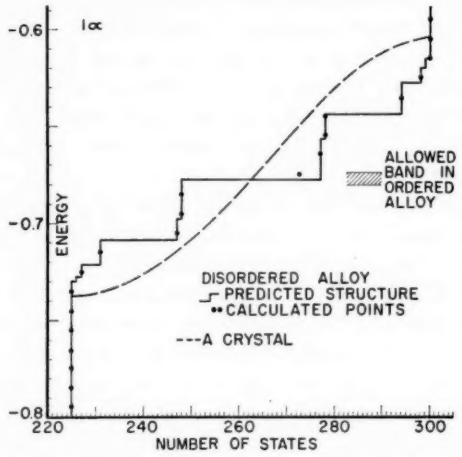

FIG. 8. The distribution of energy levels in the disordered alloy near an energy at which the isolated A atom has a tightly bound level. The staircase line is the prediction based on Fig. 7. The points are the actual computational results. The dashed curve gives the distribution of levels for a pure chain of A atoms. According to the theory used in Fig. 7, the ordered AB band should have zero width. The finite width shown in the shaded region is an indication of the extent to which A wells interact, when separated by B wells, and is a measure of the error we can expect in the theory based on Fig. 7.

Above the transition region (or throughout the positive energy range, when there is no transition region) the band structure follows perturbation theory reasonably well in all cases, as far as the existence and location of forbidden bands go, but does not at all obey perturbation theory as far as the width of forbidden regions goes. In this high-energy region there is an obvious one-to-one correspondence between the forbidden ranges for the pure A crystal and the forbidden ranges for the pure B crystal. The disordered AB crystal

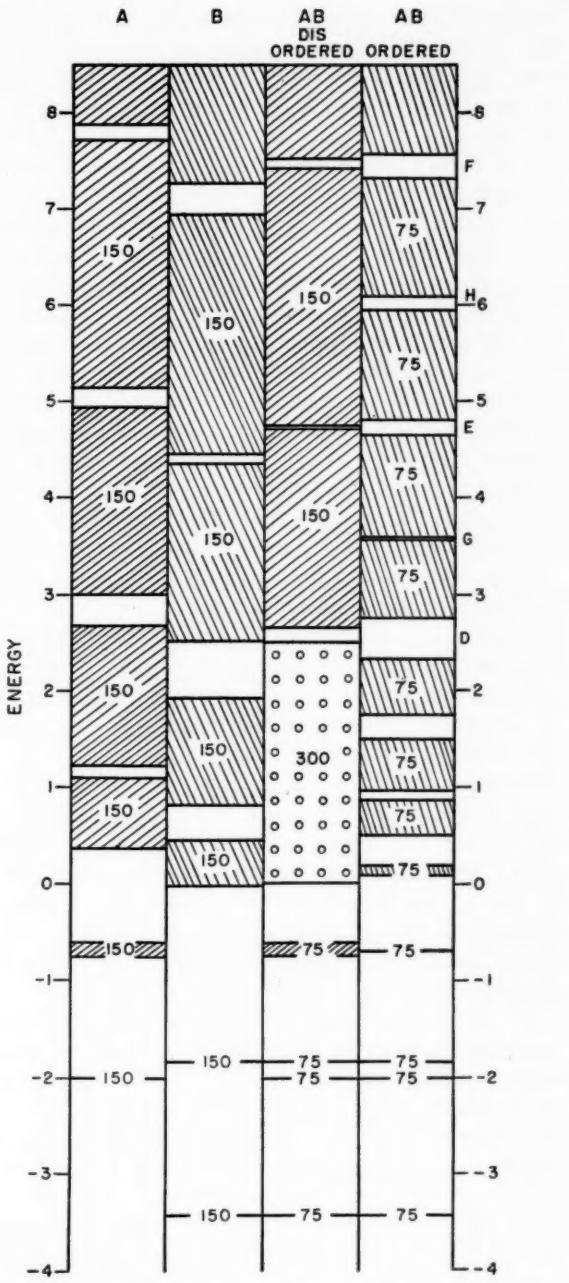

FIG. 9. The complete results from 1α. The shaded regions represent energy ranges in which levels occur. The number of levels in each energy range is also specified. For the case of a pure A crystal, a chain of 150 atoms gives 150 levels in each band, and similarly for B. For the case of an ordered AB chain of 150 atoms there are 75 levels per band. The disordered AB chain of 150 atoms does not have a fixed number of levels per band. The energy range between 0.02 and 2.52 contains 300 levels in the disordered case. These 300 levels are distributed in an irregular fashion, but without any well-defined gaps. The smallest energy gaps in this diagram are not to scale.

has its forbidden ranges centered about halfway between the centers of the pure A gaps and the corresponding pure B gaps. (According to first-order perturbation theory, the position of the center of a forbidden gap depends only on the average lattice potential.) Perturbation theory relates the width of the forbidden range, in the disordered alloy, to the widths of the gaps in the pure crystal by Eq. (5). In all cases the forbidden range in the disordered chain is actually smaller than this, and in a number of cases a predicted forbidden range is entirely absent. If the corresponding gaps of the pure crystals are close together, then the gap in the disordered case is at least comparable to the prediction of Eq. (5). If the two are far apart, compared to their widths, then Eq. (5) gives a much larger value than is actually observed for the disordered alloy. In fact, it has already been pointed out that the forbidden gaps in the disordered alloy cannot be "strictly forbidden" unless the pure A gap and the pure B gap overlap.

The ordered AB alloy has more than twice as many forbidden bands above the transition region as the disordered alloy. (The words "more than" would not have to be used, if all the disordered gaps predicted by perturbation theory really appeared.) Half of the gaps in the ordered case are of the type illustrated by D, E, and F in Fig. 9 and occur close to gaps of A, B, and disordered AB. The ordered gaps that are close to pure A and pure B gaps are in better agreement with Eq. (5) and are wider than the corresponding disordered gaps. The other half of the ordered gaps, illustrated by G and H, correspond to the "superlattice" x-ray reflections. In all our results, the ranges in which energy levels occur in the disordered alloy *always* include *all* the allowed ranges of the ordered alloy.

In all cases where a transition region was found it contained a number of states which was an integral multiple of one-half the total number of wells. Therefore in *all* disordered cases the total number of states up to any energy gap is a multiple of one-half the total number of wells. (This fact does not seem to be an obvious consequence of fundamental principles.) A transition region with 51 states, for example, in a chain with 150 wells, which would favor incompletely filled bands, and therefore conductivity, seems ruled out.

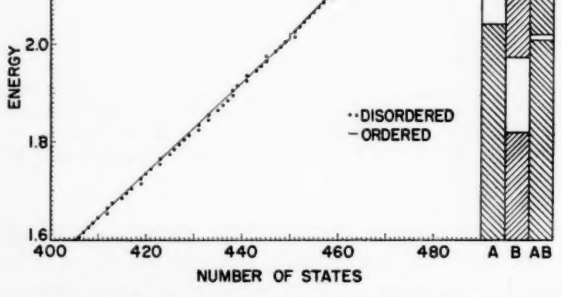

FIG. 10. Distribution of states in the neighborhood of A and B gaps. Perturbation theory leads us to expect that $\cos\theta$ in Eq. (5) is negative for the gaps in this figure.

As the energy increases, the splitting of the two degenerate unperturbed wave functions $e^{\pm ikx}$ becomes smaller, while the average spacing between energy levels become larger. Therefore, levels tend to come in pairs, at sufficiently high energies. This tendency is apparent in all our results, becoming more pronounced as the energy goes up. For example, in 1α it sets in at an energy of about 3.0. The tendency toward simple pairing is disrupted near almost forbidden ranges.

On the basis of perturbation theory one has in addition to the unperturbed degenerate wave functions $e^{\pm ikx}$, a lowest unperturbed wave function, which is a constant and is not degenerate. Therefore, one expects that if one selects an energy at random, at high energies, that there would probably be an integral number of paired levels below it, in addition to the unpaired one, leaving an odd numbered total. This is verified by our results. As we go up in energy, odd numbered totals become more and more prevalent—even though perturbation theory results apply only to the higher-energy states and cannot be expected to give any information about the total number of states up to a certain energy.

Case 8α was analyzed since it contains gaps for which $\cos\theta$ in Eq. (5) has the value -1. Figure 10 shows such a gap near 2.0. Despite the closeness of the pure A gap to the pure B gap, the gap in the ordered alloy is very small, and the gap in the disordered case, if present at all, is too small to be shown reliably within the resolution of a calculation based on 150 atoms.

This kind of destructive interference between A and B wells probably prevents the Saxon, Hutner,[1] and Luttinger[2] theorem from being true for arbitrary well shapes.

VIII. ATOMS OF DIFFERENT SIZES

Runs No. 6α and 7α represent an alloy in which the two types of atoms have different radii.[8] In order to examine the effect of this difference, the well shapes are taken the same for both A and B atoms, and only the hill lengths differ ($w_A=w_B$, $h_A\neq h_B$). This model, just like the liquid model described in Part IX, is one in which the well-to-well spacing is the only thing that is varied. In the present case, however, only three different well-to-well spacings are possible, corresponding to possibilities of $A-A$ bonds, $B-B$ bonds, and $A-B$ bonds. In our liquid model five different well-to-well spacings will be possible. Of the two cases considered at present 6α is closer to the periodic case; 7α has the greater variation in hill size.

The present case of two atomic sizes is similar to the liquid model in still another important aspect. In all

[8] This part of the investigation was suggested by George Vineyard.

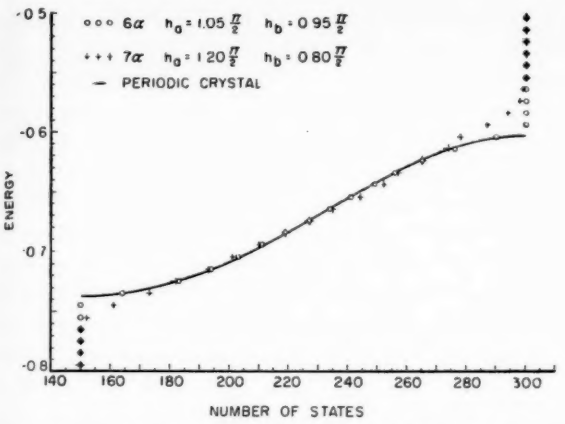

FIG. 11. Distribution of states in the neighborhood of a narrow band. The strictly periodic case is compared to two cases in which there is a difference in the hill lengths of A and B atoms, but no difference in the well shapes. The hill length averaged over all atoms in the chain is the same for all three cases shown.

the cases treated up to now, the Fourier representation of the potential for an infinite chain consisted of a continuous part (Fourier integral) in addition to a series of discrete terms (Fourier series). The discrete terms gave rise to the energy gaps in the perturbation treatment. The potential in the present case, as well as in the liquid case, has no discrete terms; hence, according to perturbation theory, there are no gaps. There are, however, maxima in the Fourier spectrum of the potential, and if the difference between h_A and h_B is small, these are sharp maxima.

There is no question, of course, that there actually strictly forbidden energy gaps, at least in the energy range of tight binding. Results for a narrow band are shown in Fig. 11. Note that the smaller the value of h_B, the wider the band is. This results from the fact that the smaller values of h_B permit occasional adjacent wells to interact more strongly than they do in the strictly periodic case.

Figure 12 illustrates what happens at higher energies. As the difference between h_A and h_B is increased, the forbidden ranges become smaller and finally disappear entirely. In fact, for 7α (the case with the greater dispersion in well-to-well distance) there are no forbidden ranges at all above 0.3, leaving only the forbidden ranges surrounding the tightly bound bands.

To summarize the results for 6α and 7α it will be necessary first to consider the bands for the pure A and pure B crystal. The pure A crystal is then a periodic crystal whose well-to-well spacing is equal to the maximum found in our disordered case. The pure B crystal has a well-to-well spacing equal to the minimum found in our disordered case. Energy gaps which are sufficiently sensitive to this well-to-well spacing, so that in going from the A crystal to the B crystal they are displaced by amounts large compared to the size of the energy gap concerned, do not appear at all in the disordered case. Energy gaps which are displaced by amounts comparable to their width (including at least one case in which the displacement is large enough so that the corresponding A and B gaps do not overlap) are reduced in width, but still exist, in the disordered alloy. (We are not distinguishing here between strictly forbidden and almost forbidden gaps.)

Cases related to 6α and 7α but of a slightly different nature have also been examined, but will not be presented in detail. In these cases we deal with a chain of 150 identical wells in which only two different well-to-well distances can occur, and do appear with equal frequency. The results for these cases are very similar to those described for 6α and 7α, except for one interesting feature. Consider the displacement in the energy gaps caused by varying the dimensions continuously from those of the A (expanded) crystal to those of the B (compressed) crystal. In one case which we examined [$V=2.5$, $w=\pi/2$, max well-to-well distance$=1.2\pi$, min well-to-well distance$=0.8\pi$] one of the B gaps is raised so much that it almost comes into coincidence with the next higher A gap. In the corresponding disordered case we do find that there is a pronounced energy gap in the neighborhood of this "accidental" coincidence. There are 675 states in the disordered crystal below this gap (for a chain of 150 wells).

IX. LIQUID CASE

Our model of a liquid consists of a series of identical potential wells whose separation varies as we go along the chain. The variation in spacing is accomplished as shown in Fig. 13 by taking a chain of identical "atoms" of the type shown in Fig. 1 and inserting a variable number of short spacer sections[9] in which $V=0$. Specifically, a chain of 50 atoms and 100 spacer sections

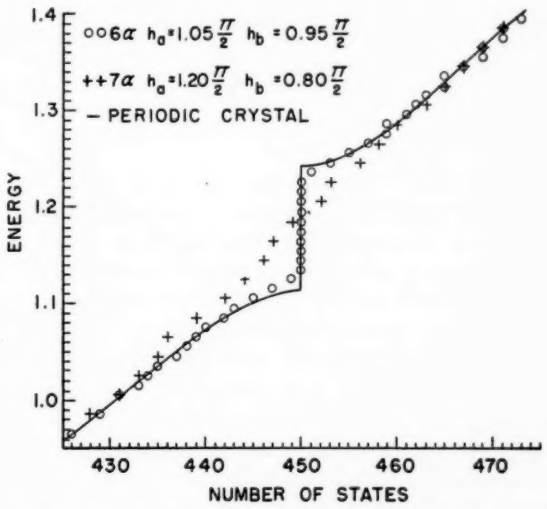

FIG. 12. Distribution of states in the neighborhood of an energy gap. The strictly periodic case is compared to cases in which there is a difference in the hill lengths of the two types of atoms, but not in their well shapes. The hill length averaged over all atoms in the chain is the same for all cases shown.

[9] We are indebted to L. P. Hunter for suggesting the use of spacers.

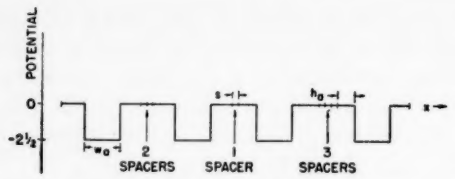

FIG. 13. Part of liquid chain, showing identical atomic wells, with a variable number of "spacers" inserted in between.

was used. The 50 potential wells were each taken to be 2.5 deep and π long. Two different choices were made for the remaining dimensions. In run $9L'$, h_a (one-half the minimum well-to-well distance which can occur in the chain) was taken to be $0.95\pi/2$ and s was taken to be $0.05\pi/2$. In run No. $10L'$, h_a was taken to be $0.7\pi/2$ and s was taken to be $0.3\pi/2$. The succession of atoms and spacer sections was taken to be the same for $9L'$ and $10L'$, namely, the sequence listed as L' in Table II. An additional computation, $10L''$, was performed, based on the same parameters as $10L'$ but using sequence L'' instead, to check the sensitivity of the results to the particular sequence of spacers. L'' is a rearrangement of L' which does not require any group of adjacent spacers to be broken up, nor does it require the bringing together of previously separated spacers. In agreement with the discussion of Sec. II, this rearrangement leaves the $N(E)$ plot unaffected.

In all liquid runs the average well-to-well distance is π. The rms deviation from this is very close to the length of one spacer section, or $0.05\pi/2$ for $9L'$ and $0.3\pi/2$ in $10L'$ and $10L''$.

In the range of tightly bound energy levels, the results are illustrated by Fig. 14. The $N(E)$ curve for a periodic crystal with the same well shape and the same mean spacing as in the liquid models is contrasted with the results of $9L'$ and $10L'$. The curves for the liquids are more irregular and cover a wider range. The widening of the energy range can be expected, since it is the interaction of adjacent wells that determines this broadening, and in the liquid there are some wells closer to each other than they are in the solid.

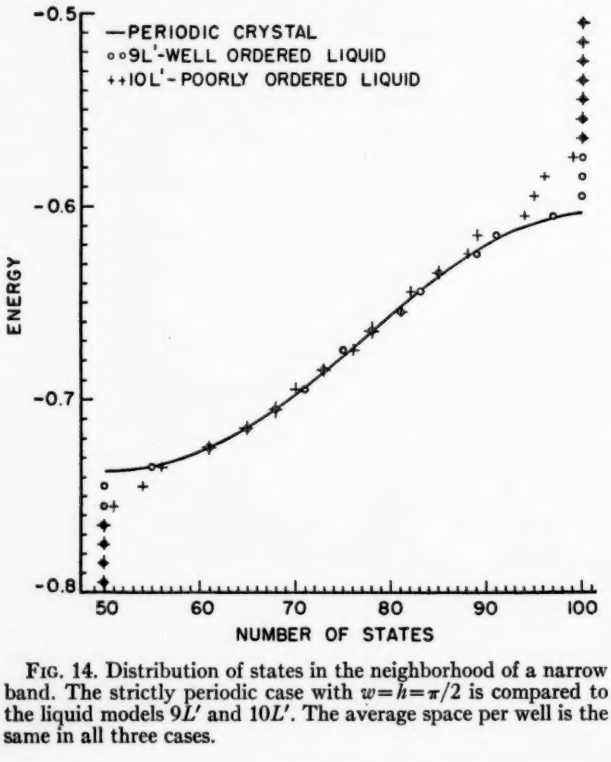

FIG. 14. Distribution of states in the neighborhood of a narrow band. The strictly periodic case with $w=h=\pi/2$ is compared to the liquid models $9L'$ and $10L'$. The average space per well is the same in all three cases.

In the range of relatively free electrons the results are illustrated by Fig. 15. The results for both $9L'$ and

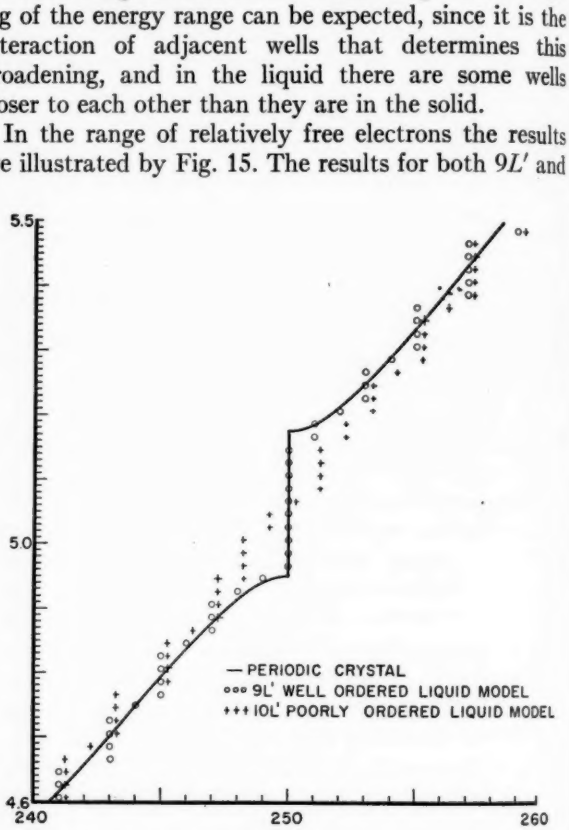

FIG. 15. Distribution of states in the neighborhood of a narrow energy gap. The strictly periodic case with $w=h=\pi/2$ is compared to the liquid models $9L'$ and $10L'$. The average space per well is the same in all three cases. The results for the poorly ordered liquid have been shifted to the right by $\frac{1}{4}$ state to give a clearer graphical representation.

$10L'$ in the positive energy range can be summarized by saying that the extent to which forbidden gaps are affected depends on:

(1) The width of the gap in the periodic case.
(2) The extent to which the gap moves as the lattice is uniformly expanded or compressed.

If the displacement of the gap, under a strain corresponding to the typical deviation in spacing found in the liquid, is large compared to the gap, then the gap disappears in the liquid. If the displacement is small compared to the gap, the gap is relatively unaffected. If the displacement and the gap width are comparable, then border line cases occur which show up as irregularities in the $N(E)$ curve. In the case of $9L'$, the well-ordered liquid, this means that in the range covered (up to 8.6) all except one gap still appear in the liquid, and even the remaining gap appears as a gap of questionable

definiteness (or what might perhaps be better called a region of pronounced irregularity in the spacing of energy levels). In the case of $10L'$, the poorly ordered liquid, this means that the only well-defined gaps are the ones that separate tightly bound levels.

The criteria we have mentioned for determining the sensitivity of a gap to the lattice distortions present in the liquid cannot be the complete story. It is apparent from the usual Bragg reflection argument, or from the author's method of distributed reflections,[10] that energy gaps in periodic crystals at high energies are due to the piling up of reflections from successive cells. Now the width of the forbidden region is a measure of the strength of the reflections, but does not tell us anything about the phase of the reflected wave with respect to the phase of the incident wave. This phase can, however, be important for the case of a liquid. It is possible that the average spacing in the liquid is such that the periodic crystal with this average spacing will have an energy gap of zero or very small width because of proximity to one of the double points discussed by Allen.[3] (These are equivalent to the band crossings discussed by Shockley.[11]) Now, if we vary the spacing away from this value, as happens in the liquid, and do this by a sufficient amount to go beyond the value of spacing corresponding to the double point, then the phase of the reflections from adjacent cells will sometimes be such that they interfere destructively rather than constructively. This destructive interference will provide for a more rapid disappearance of the energy gap than would be expected purely on the basis of a shift of the center of the gap.

The same distinction between strictly forbidden and almost forbidden gaps that exists for the chemically disordered case also exists for the liquid. A very long liquid chain will contain some clusters of atoms which will form an almost periodic inclusion.

ACKNOWLEDGMENTS

The authors are indebted to L. P. Hunter, G. Vineyard, and G. Kuczynski for discussions, to D. A. Quarles for a part of the program, and to N. Rochester and various members of his group for assistance both in programing and in the use of the IBM 701 Electronic Data Processing Machine.

[10] R. Landauer, Phys. Rev. **82**, 80 (1951).

[11] W. Shockley, Phys. Rev. **56**, 317 (1939).

THE JOURNAL OF CHEMICAL PHYSICS VOLUME 22, NUMBER 10 OCTOBER, 1954

Neutron Diffraction Study of Liquid Mercury*

GEORGE H. VINEYARD
Department of Physics, University of Missouri, Columbia, Missouri
(Received April 21, 1954)

The neutron diffraction pattern of liquid mercury at 23°C has been measured. The pattern has general resemblance to the x-ray patterns obtained by Debye and Menke and by Jennings, although the angular resolution is not quite as good. The inner peak which has been reported by several investigators is not seen. The radial density function has been calculated from the data.

INTRODUCTION

ALTHOUGH mercury was one of the first liquids to be studied by x-ray diffraction,[1] the published studies show a notable lack of accord. In their classical study Debye and Menke[2] found the most regular and sharply peaked scattering pattern which has yet been reported. Boyd and Wakeham,[3] sometime later, found remarkably different x-ray patterns characterized by a strong inner peak at roughly half the angle of the main peak. All of the investigators up to this time had used filtered radiation, and it was pointed out by Gregg and Gingrich[4] that this technique may have introduced a spurious inner peak because of contamination of the characteristic radiation by a shorter-wavelength component from the continuum. Gammertsfelder and Gingrich[5] made measurements with crystal monochromatized radiation and found only a small inner peak. However, Campbell and Hildebrand[6] re-investigated liquid mercury with crystal monochromatized MoKα radiation and found again a strong inner peak, although their patterns were appreciably different from those of Boyd and Wakeham. Recently a pattern obtained by Jennings has been reported in a paper by Oster and Riley.[7] Little information on the experimen-

* The experimental part of this work was carried out under the auspices of the U. S. Atomic Energy Commission, while the author was on leave of absence at the Brookhaven National Laboratory.

[1] For references see N. S. Gingrich, Revs. Modern Phys. **15**, 90 (1943).

[2] P. Debye and H. Menke, Physik, Z. **31**, 797 (1930); H. Menke, Physik. Z. **33**, 593 (1933).

[3] R. N. Boyd and H. R. R. Wakeham, J. Chem. Phys. **7**, 958 (1939).

[4] R. Q. Gregg and N. S. Gingrich, Rev. Sci. Instr. **11**, 305 (1940).

[5] Private communication.

[6] J. A. Campbell and J. H. Hildebrand, J. Chem. Phys. **11**, 330 (1943).

[7] G. Oster and D. P. Riley, Acta Cryst. **5**, 1 (1952), (Fig. 3).

tal conditions is given, but the curve completely lacks the inner peak and is rather like the Debye and Menke result, although the peaks are not so high.

Because of the very high absorption coefficient which mercury presents to x-rays, it has not been an ideal substance to study. Nearly all investigators have used the method of reflecting the x-ray beam off of a mercury surface, which introduces some difficulties of alignment and collimation. In this respect neutrons offer an advantage, even though the neutron absorption cross section is also relatively high (220 barns at 1-A wavelength). With neutrons the transmission arrangement can easily be employed, and sample thicknesses are such that questions of surface layer contamination do not enter. The present investigation was made to provide an independent check on the discordant x-ray data.

EXPERIMENTAL

The mercury sample was in the form of a nearly plane slab, being confined between two windows of 0.001-in. vanadium foil clamped to a steel frame. A very moderate bulging of the windows under the hydrostatic pressure of the mercury occurred, and the mean sample thickness in the region penetrated by the beam was 0.052 in. The mercury was triple distilled laboratory grade and was at room temperature, 23 ± 1°C throughout the runs. Thermal neutrons from the Brookhaven reactor were collimated in a graphite channel and monochromatized by reflection from the 200 planes of a lead crystal. The wavelength used was 1.07 A. The pile spectrum was such that the intensity of the second-order component could not exceed about 5 percent of the first-order intensity.

The scattered beam was detected by a counter rotating about a vertical axis through the specimen. The specimen table was geared to rotate at half the angular rate of the counter, so that the plane of the specimen slab always bisected the angle formed by the incident and scattered beams, the specimen being in the transmission position. In order to have adequate intensity it was necessary to open the counter slits to an over-all range in scattering angle of about ±2°.

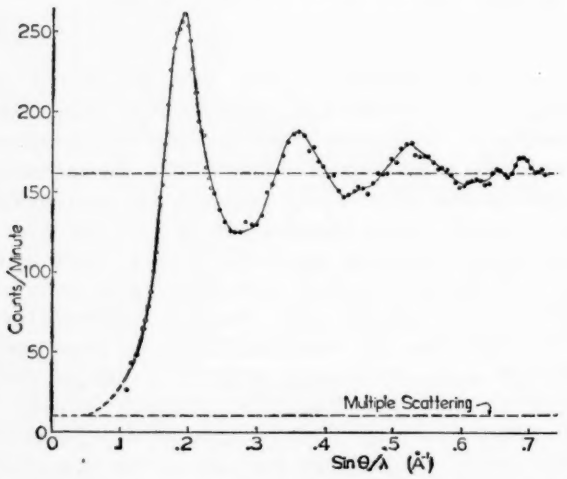

FIG. 1. Neutron scattering pattern from liquid mercury. Solid circles represent 20-minute counting periods, open circles, 10-minute periods. Computed correction for multiple scattering shown. Upper dotted line shows estimated value of scattering at very large $\sin\theta/\lambda$.

RESULTS

Figure 1 shows the resulting scattering pattern for the best of four runs, counting rate being plotted against $\sin\theta/\lambda$, where θ is half the scattering angle and λ is the wavelength. The observations shown have been corrected for background, sample holder scattering, absorption, and variation with angle of the amount of scattering material in the beam. The background and sample holder correction was made by subtracting the results of a blank run with the empty sample holder in place. Over most of the range this correction lay between 30 and 40 counts per minute. For the absorption and geometric correction these results are multiplied by $\cos\theta\exp(\tau\sec\theta-\tau)$, where $\exp(-\tau)$ is the attenuation of the beam in traversing the sample at normal incidence. In the present case τ was measured to be 1.40.

A further correction for multiple scattering is needed. This component may be estimated by a straightforward calculation[8] and turns out to be very nearly isotropic in the experimental range. The calculated multiple scattering is also shown in Fig. 1; this is to be subtracted as a final correction. The assumption is also made that the incoherent cross section of mercury is much smaller than the coherent.

The peaks in the curve of Fig. 1 occur at $\sin\theta/\lambda$ equal to 0.194, 0.361, 0.523, and 0.685. The three peaks of Jennings' data (similarly plotted) are at $\sin\theta/\lambda$ equal to 0.185, 0.365, and 0.53. Campbell and Hildebrand[9] list the peak positions found in the other principal investigations, although they apparently do not distinguish between plots of scattered intensity and scattered intensity divided by atomic structure factor squared.

A Fourier inversion, after the usual method of Zernike and Prins,[1] has been carried out on this data. The level of scattering in the limit of large angles is assumed to be as indicated in Fig. 1. A check on this assumption comes from the value taken by the radial density function at zero radius. A suitable choice of large-angle scattering will bring this to zero. In the present case the assumed value proved to be within one percent of one which would meet this criterion, and a repetition of the inversion with a corrected fitting was not considered necessary. The integrations were extended to $\sin\theta/\lambda=0.723$. The resulting radial density function $\rho(r)$ (mean density of atoms at distance r from any one atom) is shown in Fig. 2. Figure 3 gives

[8] G. H. Vineyard, Phys. Rev. **91**, 239 (1953). A more extensive account of these calculations will be published.

$4\pi r^2\rho(r)$ and $4\pi r^2\rho_0$, where ρ_0 is the mean atomic density of liquid mercury. The area under the first peak in Fig. 3, when this is bounded in the manner shown by the dotted lines, is 8.3 atoms. The succeeding peaks in this plot are not sharp enough to warrant being assigned coordination numbers. The vertical lines at the bottom of the graph show the coordination shells of crystalline mercury in its accepted rhombohedral structure.[9]

The data in Fig. 1 show no evidence of an inner peak and extend into $\sin\theta/\lambda=0.104$. Data from other runs, made with finer angular resolution extended into $\sin\theta/\lambda=0.065$, within which range they approached zero steadily and gave no evidence of an inner peak. The inner peak of Campbell and Hildebrand came at $\sin\theta/\lambda\cong 0.11$ (at temperatures of 0° and 50°C) and so should have been seen if present.

DISCUSSION

The diffraction pattern found here resembles those of Debye and Menke and Jennings, although the first two peaks are lower and less sharp in the present work.

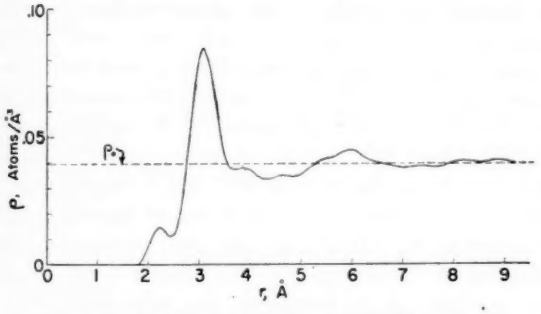

FIG. 2. Radial density function for liquid mercury.

Our rather poor angular resolution can account for this difference. The coordination number for the first peak in Debye and Menke's work is about 10 (it is impossible to take an accurate value from their published curves), to be compared with the present value of 8.3. This difference does not seem to be outside the assignable errors. The very small peaks on either side of the first main peak in $\rho(r)$ are probably spurious and are very likely due to the diffraction error introduced by the limited range of $\sin\theta/\lambda$ over which the data extends.[10] The same reservations apply to other minor fluctuations in the $\rho(r)$ curve.

[9] P. P. Ewald and C. Hermann, *Strukturbericht* 1913–28 (Akademische Verlagsgesellschaft M. B. H., Leipzig, 1931), p. 737.

[10] An analysis of this effect is given by T. Sugawara [Science Repts. Research Inst. Tôhoku Univ. **A3**, 39 (1951)]. Sugawara's treatment here predicts satellite peaks at 2.26 A and 3.94 A, in close agreement with the positions of two small peaks in Fig. 2.

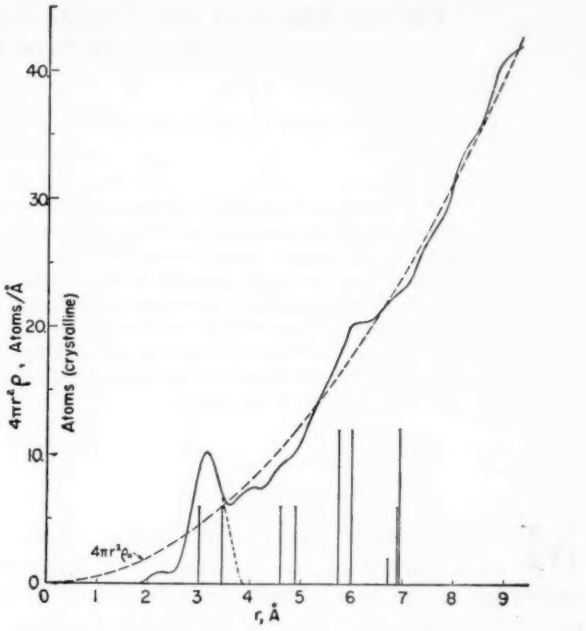

FIG. 3. $4\pi r^2\rho(r)$ (solid line) and $4\pi r^2\rho_0$ (dotted line) *vs* radius Vertica lines at bottom give coordination shells of crystalline. mercury.

As is frequently the case,[1] there is only very imperfect correlation between the coordination shells in the solid and liquid phases.

The finding of an inner peak in the diffraction pattern[3,6] is definitely not supported.

In the foregoing structure analysis it has been assumed that the process of neutron diffraction in liquid mercury mainly occurs without energy interchanges which are appreciable compared to the incident energy.[11] The validity of this assumption can be confirmed by certain rough calculations, although a complete justification would be highly desirable.

This experiment could profitably be repeated using one of the isotopes of mercury which has low neutron absorption. A very decided improvement of accuracy should then be realized.

ACKNOWLEDGMENT

The author is indebted to the Brookhaven National Laboratory for its hospitality and to the members of the Solid State Group there for assistance; to N. S. Gingrich for information and suggestions; and to R. D. Levee who kindly arranged for the machine calculation of the Fourier transforms.

[11] G. Placzek, Phys. Rev. **86**, 377 (1952).

Excited States of the Naphthalene Molecule. I. Symmetry Properties of the First Two Excited Singlet States*

DONALD S. MCCLURE
Department of Chemistry and Chemical Engineering, University of California, Berkeley, California
(Received May 14, 1954)

The detailed polarization properties of the bands in absorption and fluorescence spectra of the naphthalene molecule have been determined by a method which makes use of a substitutional solid solution of naphthalene in durene. A single crystal of about 0.1 percent naphthalene in durene was cut so that the short axes of the naphthalenes lie strictly parallel to the surface and in one direction. The spectra were then determined in polarized light at 20°K under moderately high dispersion. The results clearly indicate that the first state is $^1B_{3u}$ (the transition from the ground state is long-axis polarized) and the second $^1B_{2u}$. Vibrational-electronic interaction involving b_{1g} vibrations apparently couples the first state with the second, and this results in a large short-axis polarized transition moment. This fact has been at the root of most of the previous difficulties with analysis of the spectra.

I. INTRODUCTION

MANY experimental and theoretical attempts have been made to determine the symmetry properties of the lowest excited singlet states of the naphthalene molecule.[1] Most of the pertinent references are to be found in two earlier papers,[2,3] and will not be repeated here. Since late 1952, several other publications on this subject have appeared: Craig and Lyons[4] worked with pure naphthalene crystal, and concluded that the first excited state is $^1A_{1g}$ and the second $^1B_{2u}$: McConnell and McClure[5] presented evidence to show that the first transition must be $g \rightarrow u$. This was based on the intensity behavior of the 0−0 band on substitution. Schnepp and McClure[6] used the latter information along with their interpretation of their work on the low temperature spectra of the pure crystal, and concluded that the first state was $^1B_{2u}$, the second $^1B_{3u}$.

Meanwhile, Pariser had applied the new method of Pariser and Parr[7] to calculate the energies and symmetry properties of the lowest excited states of naphthalene.[8] Moffitt has also carried out some theoretical calculations using a π-electron perimeter model, similar to Platt's,[9] but considerably refined, and apparently capable of accurate predictions.[10] The theoretical workers mentioned agreed with Platt's results based on semiempirical correlation of aromatic molecule spectra. These results are that the lowest excited singlet state is $^1B_{3u}$, and the second is $^1B_{2u}$.

Pariser's work represents the π-electron approximation carried out nearly to its ultimate accuracy. If a disagreement exists between this work and the experimental facts, it would seem futile to look for further theoretical progress from the π-electron approximation either for the case of naphthalene or for other aromatic molecules. For this reason, it seemed of the utmost importance to devise experiments which would give the desired information in the most unambiguous fashion. The method of mixed crystals was used, and when coupled with the vapor phase absorption and fluorescence spectra of naphthalene, the new results show clearly that the theoretical predictions are correct. The results also point out the source of the difficulties which led previous attempts at a symmetry determination astray.

II. THE EXPERIMENTAL METHOD

The method involves the use of a crystalline solid solution, in this case of naphthalene in durene. Durene does not begin to absorb appreciably until well beyond the beginning of the second absorption system of naphthalene. The durene would not be expected to affect the naphthalene spectrum any more than, say, the fluid solvent xylene. The object of using a crystalline solid solution is, of course, to clamp the naphthalenes in definite orientations in the crystal lattice. Then if a single crystal of the solution is cut in a certain way, one can determine the absorption spectrum in polarized light along the projections of the principal molecular axes permitted by the crystal structure and the cut of the crystal. This procedure, when carried out for a very dilute solution, should approximate the "oriented gas" as closely as it can be achieved in practice. We should also have eliminated the difficulties encountered in using the pure crystal. These arise from band formation and the attendant complications of exciton-phonon

* This work was partially supported by the U. S. Office of Naval Research under contract N6 ori-211—T.O. III.

[1] The group theory notation used in this paper will be that of Herzberg, *Infra-Red and Raman Spectra of Polyatomic Molecules* (D. Van Nostrand Company, Inc., 1945). The long molecular axis is designated the x axis and the short axis is the y axis. The z axis is perpendicular to the molecular plane.

[2] H. Sponer and G. Nordheim, Discussions Faraday Soc. **9**, 19 (1950).

[3] O. Schnepp and D. S. McClure, J. Chem. Phys. **20**, 1375 (1952).

[4] D. P. Craig and L. E. Lyons, J. Chem. Phys. **20**, 1499 (1952).

[5] H. McConnell and D. S. McClure, J. Chem. Phys. **21**, 1296 (1953).

[6] O. Schnepp and D. S. McClure, J. Chem. Phys. **21**, 959 (1953).

[7] R. Pariser and R. Parr, J. Chem. Phys. **21**, 466, 767 (1953).

[8] R. Pariser, Talk at the Ohio State Symposium on Molecular Structure and Spectra, June, 1954.

[9] J. R. Platt, J. Chem. Phys. **17**, 484 (1949).

[10] William Moffitt, J. Chem. Phys. **22**, 320 (1954).

interaction and of "factor group" splitting, or Davydov splitting.[11]

The solid solution range of naphthalene in durene was found, by means of cooling curves, to be limited to about two mole percent naphthalene. Some solid solution formation was expected from the similarity of the unit cell dimensions of the two substances, and from the fact that the molecular weights and melting points are nearly identical (see Table I.)

The durene crystal structure[12] is illustrated in Fig. 1. It was hoped, of course, that the naphthalene molecules would take up one of the two possible positions in the unit cell (with identical environments), to form a truly substitutional solid solution. That this is actually the case is proven by the absorption spectra, which are extremely sharp and almost entirely different in polarized light along the *b* and *c'* directions. Both the *ab* and the *bc'* planes were used, but as is evident from the figures, the *bc'* plane is the more useful one. Naphthalenes in substitutional positions are held with the short in-plane axis almost exactly parallel to *c'* (*c'* is perpendicular to the *a* and *b* axes), and the projection of the long axis is almost exactly parallel to the *b* axis. Furthermore, the *b* axis is a principal dielectric axis fixed by the symmetry of the crystal, and there is no chance that dispersion of the optic axes will interfere with the polarized absorption measurements when using the *bc'* plane at normal incidence.

TABLE I. Physical data on naphthalene and durene. Both crystals monoclinic, C_{2h}^5.

	Naphthalene, $C_{10}H_8$	Durene, $C_6H_2(CH_3)_4$
Molecular weight	128.16	134.21
M.P. °C	80.2	79.3
unit cell data		
a A	8.29	11.57
b	5.95	5.77
c	8.68	7.03
β	122.1°	113.3°
z	2	2
Volume per molecule, A³	181.5	215

For a perfectly oriented naphthalene molecule in the durene lattice, the ratio of short molecular axis to long axis absorption in the *b* direction is 0.00045. The ratio of long axis absorption to short axis absorption in the *c'* direction of the crystal is 0.0002. These figures represent the amount of "contamination" of one spectrum by the other and it is seen to be negligible, provided the crystal is perfectly cut and polished. Traces of the oppositely polarized spectra do appear, and this could be caused either by the inaccuracies in the crystal cutting, or by departures of the naphthalenes from perfect substitutional orientation. Electronic effects of the environment may also contribute to this.

[11] H. Winston, J. Chem. Phys. **19**, 156 (1951).
[12] J. M. Robertson, Proc. Roy. Soc. (London) **A141**, 594 (1933); **A142**, 659 (1933).

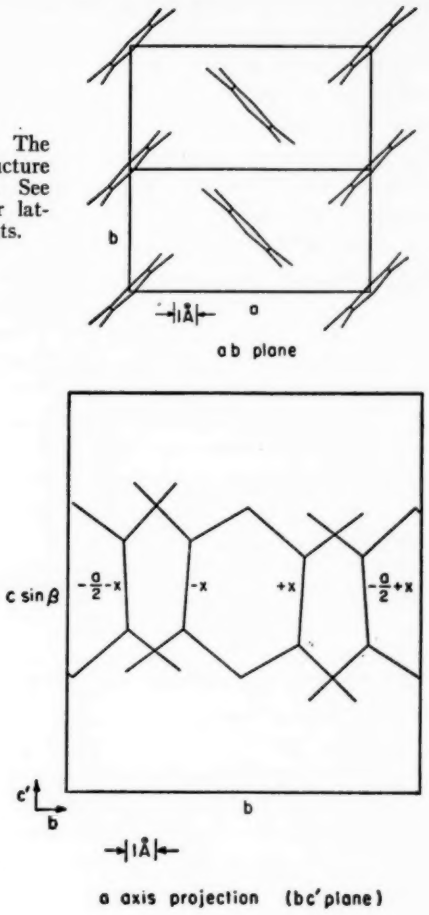

FIG. 1. The crystal structure of durene. See Table I for lattice constants.

The mixed crystals were grown by slowly lowering the melt out of a furnace heated to 150°C. A nearly perfect 5-cm crystal could be grown in a period of 36 hours. Naphthalene concentrations from about 0.01 to 0.5 mole percent were used. No attempt was made to determine the actual concentrations in the crystal samples used. Because of segregation of the naphthalene during crystal growth, the actual concentration will differ from the nominal concentration in the starting mixture. The cleavage plane of a large crystal is easily found, and is known to be the *ab* plane. A slab of crystal bounded by the *ab* faces was examined under the polarizing microscope to determine the position of the *b* axis, and was then cut perpendicular to the *ab* face, parallel to the *b* axis. This yielded the *bc'* face. A slab of crystal from one to four mm thick was polished on these faces and mounted on a quartz disk. This in turn was inserted into a rotating stage which could be mounted inside a quartz Dewar. The final orientation of the crystal was made just before an exposure by rotating the stage to an extinction position between crossed polaroids.

The spectra obtained were moderately sharp at 77°K. Most of the bands were no more than 20 cm^{-1} wide. In order to obtain the best vibrational analysis however, liquid hydrogen was used as the refrigerant.

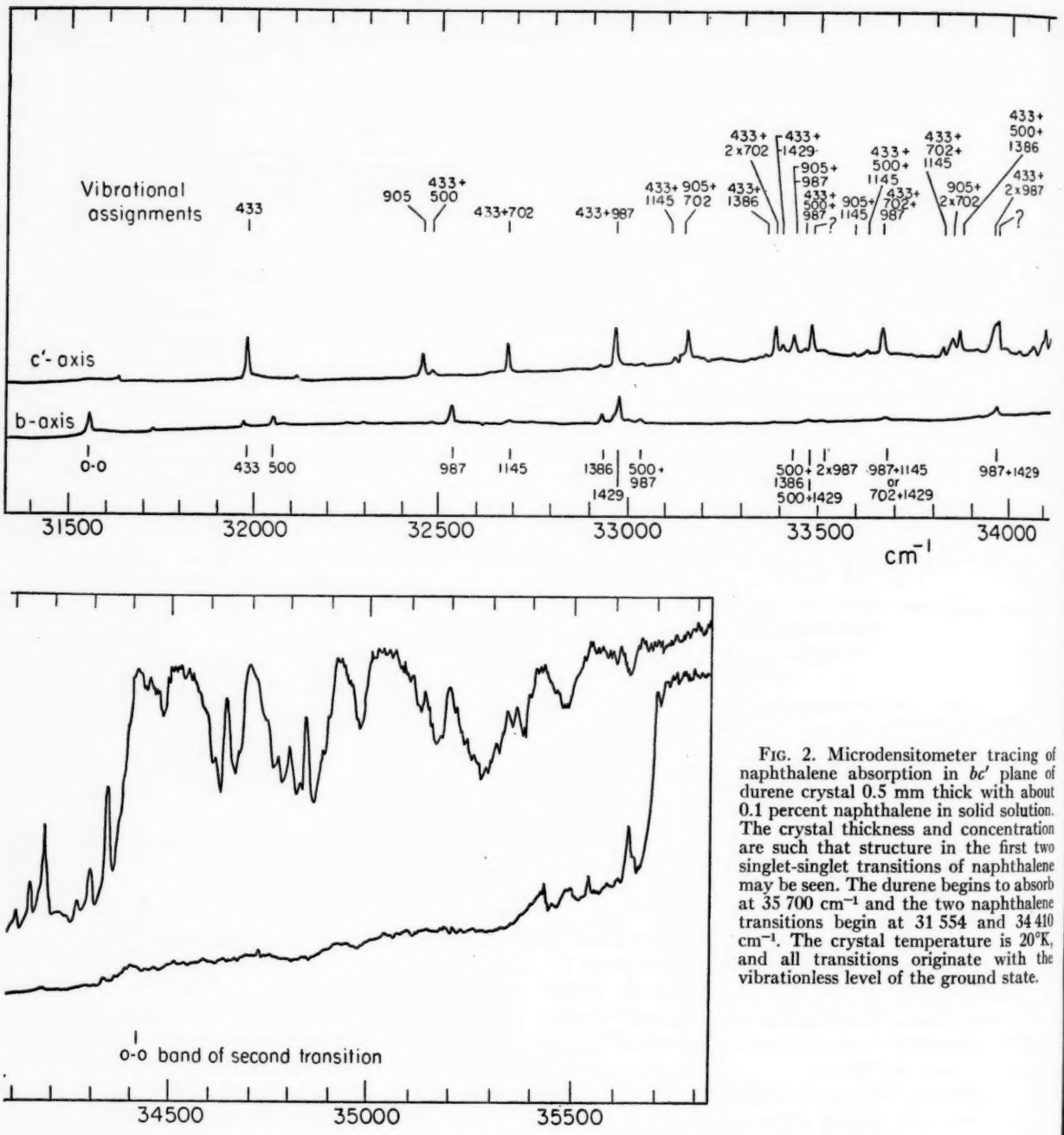

FIG. 2. Microdensitometer tracing of naphthalene absorption in *bc'* plane of durene crystal 0.5 mm thick with about 0.1 percent naphthalene in solid solution. The crystal thickness and concentration are such that structure in the first two singlet-singlet transitions of naphthalene may be seen. The durene begins to absorb at 35 700 cm^{-1} and the two naphthalene transitions begin at 31 554 and 34 410 cm^{-1}. The crystal temperature is 20°K, and all transitions originate with the vibrationless level of the ground state.

At 20°K the bands were from 3 to 8 cm^{-1} wide at half-maximum intensity, and the vibrational analysis was usually accurate to two cm^{-1}.

The spectrograph used had a quartz prism in a 3-meter Littrow mount. The actual resolving power attained was 30 000. A 150-watt Hanovia high-pressure xenon arc or a low-voltage hydrogen arc was used as the source for the absorption spectra and light from a General Electric AH-6 high-pressure mercury arc after being passed through the proper filters was used to excite fluorescence. A pair of quartz lenses formed the image of the crystal on the spectrograph slit. A Wollaston prism was mounted inside the spectrograph about 12 in. behind the slit. The light from the doubly refracting crystal was analyzed by this prism and there resulted two oppositely polarized spectra adjoining each other on the photographic plate. The spectrograph-optical system combination showed a very slight preference for one direction of polarization over the other, but this was too small to require a correction in these experiments.

The lines on the plates were measured to 0.003 mm with a comparator, and the iron lines were fitted to a three-constant Hartmann dispersion formula which was then used to convert distances on the plate to wavelengths. Wavelengths were converted to wave numbers

by using Kaiser's *Tabelle der Schwingungzahlen*. Microdensitometer tracings of some of the plates were made, and the measurements of very weak lines were taken from these.† The absolute accuracy of the position of the bands in the spectra was about 4 cm^{-1}, but relative positions of strong bands were reproducible to one or two cm^{-1}.

The use of mixed crystal systems for investigations of electronic spectra of molecules is evidently a powerful tool in the cases where it can be applied. Solid solutions among organic compounds are relatively rare, however, and when the requirement that the host crystal be transparent in the spectral range of interest is added, the possibilities are even more limited. Two other examples have been studied in this laboratory; azulene in naphthalene, where two azulene transitions can be observed, and anthracene in phenanthrene where only a part of the first anthracene transition is observed. In the first of these examples, the spectral features were sharp and had the polarizations calculated assuming that the azulenes fit into the naphthalene structure in the same way naphthalene molecules do. The second pair did not give sharp spectra even at 20°K. This probably indicates that the anthracene molecules may assume a variety of positions in the phenanthrene lattice.

III. ANALYSIS OF THE SPECTRA

Since the concentration of naphthalene molecules in the crystal is usually no more than 0.001 mole fraction, each naphthalene molecule is surrounded only by durenes out to next nearest neighbors at least 95 times out of 100. The sharpness of the spectra shows that energy transfer between naphthalenes is much less rapid than in the pure crystal, but there is still a possibility of many transfers during the lifetime of the excited state. If the undetectably small broadening of 1 cm^{-1} were due to energy transfers, it would correspond to 3×10^{10} transfers per second, or about 1000 during the lifetime of the excited state. There may be fewer than this and as far as can be seen, there are no spectral effects ascribable to energy transfers.

The sharpness of the bands is evidence that the internal motions of the naphthalene molecules are not coupled strongly to the lattice. The average thermal energy per degree of vibrational freedom at 20°K is 14 cm^{-1}, and since the bands are narrower than this, the vibrational state of the lattice cannot often change during a transition.

In addition to energy transfer and mechanical coupling to the lattice, there are the possible electronic effects of the surrounding molecules to be considered. The site symmetry of a naphthalene molecule in a substitutional position in the lattice is C_i. Thus all selection rules except the parity rule are at least formally broken down. The degree to which this breakdown has occurred in the crystal must be very small for the experimental method to be of value. The absorption spectrum demonstrates that the selection rules for the free molecule hold to a surprising degree. A comparison with the vapor absorption spectrum to be made later is a most convincing demonstration of this. This comparison

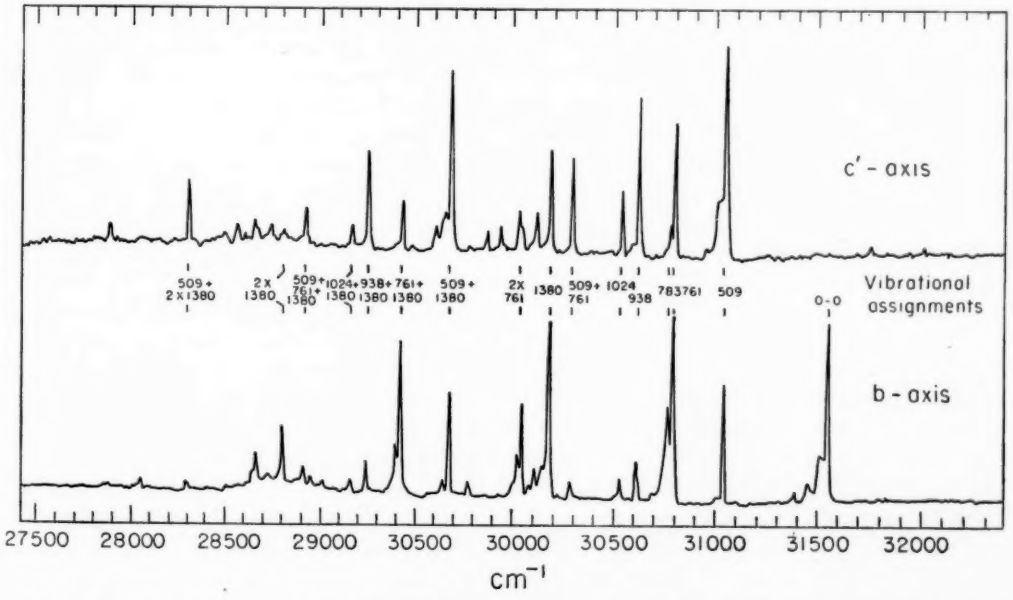

FIG. 3. Microdensitometer tracing of naphthalene fluorescence from bc' plane of durene crystal with about 0.1 percent naphthalene in solid solution. The crystal temperature was 20°K, and since thermal equilibrium is established before emission, all transitions start from the vibrationless upper state. The short molecular axis practically coincides with the c' direction and thus the upper strip is essentially short axis fluorescence. The lower strip is long axis fluorescence.

† The author wishes to thank Professor John Phillipps and the Department of Astronomy for the use of the microdensitometer.

also shows that the molecular vibration frequencies in the embedded molecules are within a few wave numbers of the values determined from the vapor absorption. On the other hand, there are certain features, principally in the fluorescence spectrum, which may be caused by the polarizable environment.

Another electronic effect of the environment, rather unimportant in connection with this study, is the displacement of the 0—0 band. This is 468 cm^{-1} to the red of the vapor and 15 cm^{-1} to the violet of the computed position for the pure crystal.[6]

The absorption and fluorescence spectra observed are shown in Figs. 2 and 3. Partial vibrational analyses are given in both figures. The b and c' absorption spectra are entirely different in appearance. The first transition region shows significant absorption in both b and c' components, while the second region from 34 400 cm^{-1} to the durene cutoff at 35 700 cm^{-1} shows absorption only along c'. The decision as to the direction of the electric moment with respect to molecular axes in the first region has to await fuller analysis, but the second transition is unambiguously determined by these simple observations to lie along the short axis of the molecule. This makes it practically certain to be a $^1A_{1g} \rightarrow {}^1B_{2u}$ transition, as it appears to be electronically allowed. This conclusion is in agreement with that of Craig and Lyons[4] and with Pariser's predictions by the complete molecular orbital method.[8] A fuller study of the second transition will be presented in a later paper.

The lowest frequency absorption band and the highest frequency fluorescence band in the b-polarized spectrum coincide to better than 2 cm^{-1}. The value of this frequency is 31 554 cm^{-1} as determined from the absorption plates. This, of course, is the 0—0 band.

The vibrational analysis of the b-polarized absorption that is observed in fairly dilute crystals is given in Table II. Exactly the same spectrum is observed along the a axis of the crystal. The analysis appears to be the only reasonable one for the prominent vibrations because of the good agreement between the calculated and observed frequencies of the combinations. The most prominent frequencies, namely 502, 987, 1145, 1386, and 1429 cm^{-1} are five of the nine totally symmetric motions which an undistorted, or symmetrically distorted molecule in the upper state would have. The two hydrogen-stretching modes would appear in a region where absorption to the B_{2u} state might interfere, and we can leave them out of consideration. This leaves two moderately low a_g frequencies to be found. The 702 frequency appears alone and in combinations with greater intensity than the other possibilities, and in addition was found strongly in the c' component, so it was chosen as one of the frequencies sought. Two bands, 747 and 794 cm^{-1} from the 0—0 band are almost as strong as 702 in the b spectrum, and it is possible that one of them is the missing frequency. As a result of a detailed study, 794 was chosen (see part II). Out of a total of 41 bands observed, all of the bands with moderate intensity or greater are explained by this analysis. There are 16 bands in the weak or very weak category which are not accounted for as combinations of a_g modes.

Analysis of the c' absorption is also shown in Table II. This was carried out using the seven frequencies obtained from the b absorption and with 31 987 (0–433) and 32 459 (0–905) as origins. The first origin is about twice as strong as the second. Both appear very weakly in the b component. One rather strong band is not accounted for in the analysis. The only bands listed in Table II for the c' absorption are those appearing in a very dilute crystal. Many more were found in thicker or more concentrated crystals, but it does not seem necessary to list them. The bands listed for the b spectrum were those found in a somewhat thicker crystal than for the c' spectrum. The c' spectrum appears definitely more intense than the b spectrum when both are measured in the same crystal. This can be verified by reference to Fig. 2.

Details of the vibrational analysis will be taken up in a later paper (part II), where it is also planned to give the analysis of the fluorescence spectrum. For the purposes of this paper, which are to establish the symmetry properties of the upper state and the transition mechanism, the fluorescence spectrum is only needed to establish the 0—0 band.

IV. INTERPRETATION OF THE SPECTRA

The vibrational analysis of the absorption strongly suggests that the b spectrum is electronically allowed. The clear appearance of the 0—0 band in both absorption and fluorescence and the addition of vibrational intervals in one and two quanta and in combinations to the 0—0 frequency, are practically incontrovertible evidence for this conclusion. The c' absorption spectrum has the appearance of a forbidden transition with two nontotally symmetric modes of vibration causing violation of the electronic selection rule. Furthermore, the 0—0 band does not appear in the c' fluorescence or absorption (except with long exposures, or thick crystals). The b and c' spectra are part of the same electronic transition since they have the same set of totally symmetric frequencies and the fluorescence data shows them to have the same vibrationless upper state. We therefore have an example here of an electronically allowed transition which nevertheless has vibrationally induced components of greater intensity than, and opposite polarization from, the pure electronic component.

We cannot eliminate by these data the possibility that the transition is polarized perpendicular to the ring, but if this were the case, the upper state could not be a π-electron state, so we will neglect this possibility in further discussion. It is possible that other crystalline solid solutions could be found which would differentiate perpendicular transitions from others, but in the durene solution, both the long axis and the per-

TABLE II. This table gives the observed lines in both b and c' absorption spectra of naphthalene in durene. The next column in the part of the table referring to each spectrum gives

TABLE II. This table gives the observed lines in both *b* and *c'* absorption spectra of naphthalene in durene. The next column in the part of the table referring to each spectrum gives the intensity of the line as estimated from microphotometer tracings. Next the vibrational analysis of the spectrum is given, followed by the deviation of the calculated frequency from the measured one. The next four columns enable a comparison with the vapor data to be made. The data are those of de Laszlo, Z. physik Chem. **118**, 369 (1925), Table V. His table V gives the reciprocal of the wavelength rather than the wave number corrected to vacuum. Therefore, we have given the wavelength of the line he has reported, the intensity given by him and the corresponding wave number, corrected to vacuum. The final column gives the wave number expected from the crystal spectrum. This is calculated by adding 468 cm^{-1} to the frequencies determined from the crystal. To allow for errors in measurement, a band in the vapor as much as 3 cm^{-1} away from the position calculated from the *b* crystal spectrum was considered to correspond to the line in the crystal. In the *c'* spectrum there are many perturbations which displace the positions of combination lines from the calculated ones by up to 8 cm^{-1}. To allow for the possibility that these perturbations may be different in crystal and vapor, a deviation of up to 5 cm^{-1} from the calculated position was permitted. In every case where no band in de Laszlo's list was within the stated distance from the calculated position, the distance to the nearest band in A is given. The vapor intensity values do not seem to agree very well with our expectations based on the crystal intensities, but in a few cases, marked by X, a band within the tolerances given appeared much too strong to correspond to the crystal line. Also, in several cases de Laszlo did not report the intensity of an observed band; this is indicated in the table by a dash in the intensity column. In several cases we have indicated two bands in the vapor spectrum which could correspond to one line of the crystal spectrum.

Band, cm^{-1}	*b*—Polarized absorption Intensity	Assignment	Error calculated-measured	Vapor, observed λ,*A*	Intensity	cm^{-1}	Vapor calculated cm^{-1}
31 554	VS	$0-0$ $\quad {}^1A_{1g}-{}^1B_{3g}$	···	3122.07	16	32 021	(32 022)
31 989	VW	$0-433$ $\quad b_{1g}$	−2	3080.34	55	32 455	32 457
32 057	S	$0-502$ $\quad a_g$	−1	3073.79	10	32 523	32 525
32 254[a]	VW	$0-702$ $\quad a_g$	+2	3055.16	15	32 722	32 722
32 301[a]	VW	$0-747$ $\quad ?$	···	not present	0.7A		32 769
32 348[a]	VW	$0-794$ $\quad a_g$	···	3046.46	30	32 816	32 816
32 368[a]	VVW	$0-924$ $\quad ?$	···	not present	0.6A		32 836
32 458[a]	VVW	$0-905$ $\quad b_{1g}$	+1	3036.24	52	32 926	32 926
32 541	VS	$0-987$ $\quad a_g$	0	3028.66	52	33 008	33 009
32 558	M	$0-2\times502$	0	not present	1.3A		33 026
32 576[a]	W (Br.)	$0-1022$ $\quad ?$		X			33 044
32 699	M	$0-1145$ $\quad a_g$	0	not present	1A		33 167
32 755[a]	W	$0-702+502$	3	not present	1A		33 223
32 850[a]	VW	$0-794+502$	0	3000.53	44	33 318	33 318
32 914[a]	VW	$0-1360$ $\quad ?$		X			33 382
32 940	M	$0-1386$ $\quad a_g$	0	2992.22 (62)	70 (70)	33 411 (06)	33 408
32 967[a]	W	$0-1413$ $\quad ?$		2989.94	70	33 435	33 435
32 983	S	$0-1429$ $\quad a_g$	0	2988.51	···	33 452	33 451
33 042	M	$0-987+502$	1	2983.17	70	33 511	33 510
33 126[a]	VW	$0-1572$ $\quad ?$		not present	1.4A		33 594
33 243	VW	$0-987+702$	0	not present	1A		33 711
33 289[a]	VVW	$0-987+747$	−1	not present	0.3A		33 757
33 337[a]	VVW	$0-987+794$	−2	not present	4A		33 805
33 400[a]	VW	$0-1145+702$	1	not present	1A		33 868
33 440	W	$0-1386+502$	2	not present	0.4A		33 908
33 469[a]	W	$0-1915$ $\quad ?$		2945.70	50	33 938	33 937
33 485	M	$0-1429+502$	−1	2944.62	65	33 950	33 953
33 528	M	$0-2\times987$	0	not present	0.7A		33 996
33 583[a]	VVW	$0-2029$ $\quad ?$					
33 596[a]	VVW	$0-2042$ $\quad ?$					
33 630[a]	VVW	$0-2076$ $\quad ?$					
33 686	S	$0-1145+987$ or $1429+702$	0 or −1	not present	2A		34 154
33 730[a]	VW	$0+1429+747$ $\quad ?$	0	not present	6A		34 198
33 743[a]	VW	$0-2189$ $\quad ?$					
33 781[a]	VVW	$0-1429+794$	−4				
33 925	W	$0-1386+987$	2	not present	1A		34 393
33 934	W	$0-2400$ $\quad ?$					
33 970	S	$0-1429+987$	0	not present	0.7A		34 438
34 113	VW	$0-2559$ $\quad ?$					
34 130	VW	$0-1429+1145$	−2				34 698
34 190	W	$0-1145+987+502$	−2				34 658

Band, cm^{-1}	*c'*—Polarized absorption Intensity	Assignment	Error calculated-measured	Vapor, observed λ,*A*	Intensity	cm^{-1}	Vapor calculated cm^{-1}
31 554	VVW	$0-0$					···
31 987	VS	$0-433$ $\quad b_{1g}$		3080.34	55	32 455	32 455
32 459	S	$0-905$ $\quad b_{1g}$		3036.24	52	32 926	32 927
32 486	VW	$0-433+500$	1	not present	1A		32 954
32 689	S	$0-433+702$	0	3015.25	27	33 155	33 157
32 935	VVW	$0-1381$ $\quad ?$		2992.90	45	33 403	33 403
32 972	VS	$0-433+987$	+2	2989.13 (8.94)	75 (70)	33 445 (36)	33 440
33 131	VVW	$0-433+1145$	1	not present	1A		33 599
33 166	S	$0-905+702$	−5	2972.49	60	33 632	33 634
33 374	VVW	$0-433+1386$	−1	2954.27	50	33 839	33 842
33 397	S	$0-433+2\times702$	−6	2952.40	60	33 861	33 865
33 416	W	$0-433+1429$	0	not present	1.1A		33 884
33 446	M	$0-905+987$	0	not present	0.8A		33 914
33 473	W	$0-433+502+987$	3	2945.20	55	33 944	33 941
33 492	M	$0-1938$ (1505 + 433?)		2943.62	75	33 962	33 960
33 603	VW	$0-905+1145$	0	not present	1.2A		34 071
33 636	W	$0-433+502+1145$	−2	not present	1A		34 114
33 675	M	$0-433+702+987$	1	not present	1.4A		34 143
33 831	W	$0-433+702+1145$	3	not present	1.2A		34 299
33 855	M–W	$0-905+2\times702$	8	2912.55	···	34 324	34 323
33 873	M	$0-433+502+1386$	2	2910.71	···	34 346	34 341
33 962	M	$0-433+2\times987$	−1	2903.64	···	34 429	34 430
33 970	M	(0 − 1505 + 905?)		not present	0.7A		34 438
34 115	W	$0-433+702+1429$ or $0-433+987+1145$	3 4	not present	5A		34 583
34 152	M	$0-905+702+987$	−4	not present	6A		34 620
34 188	S	$0-1938+702$	+6	not present	4A		34 656
34 272	W	$0-433+2\times1145$	5	not present	5A		34 740
34 304	M	$0-905+702+1145$	2	not present	5A		34 772
34 345	S	$0-905+502+1386$	2	not present	5A		34 813

[a] Measured from microdensitometer tracing.

pendicular direction are projected in equivalent directions.

If effects of the lattice can be definitely ruled out, the only possible assignment for the upper electronic state is $^1B_{3u}$. It will be seen from the following discussion that it is most unlikely that the surroundings of the naphthalene molecule have anything important to do with the appearance of the spectrum, and in particular with the existence of the 0—0 band.

Since in the durene naphthalene solution the surroundings of a naphthalene molecule present only inversion symmetry, the 0—0 band, if induced by the surroundings, would be expected to be unpolarized. In dilute crystals with up to about 75 percent absorption in the 0—0 band, there is no trace of absorption along the c' axis. In thicker crystals, however, diffuse c' absorption in the 0—0 region does appear. This is clearly an effect of the surroundings, because lattice vibrational intervals of 15, 27, and 62 cm^{-1} can at the same time be distinguished in both polarizations to the violet of the 0—0 frequency. The c' polarized part is not only more diffuse than the b, but in it the second number of the lattice vibrational series, 0—15, is more intense than 0—0. What is probably happening here is that the 0—0 band appears because of unsymmetrical perturbations from the surrounding durenes, and the 0–15 band represents a lattice mode which strongly increases the dissymmetry of the surroundings. The diffuseness is probably caused by the addition of lattice frequencies of the acoustic branch. Lattice modes of any type appear in the spectrum because the local field at the naphthalene molecule depends upon the positions of the durenes, and because the equilibrium position of the naphthalene molecule is different in the two electronic states. In studying the structure in the region of c' (0—0), we have discovered some of the characteristics of a lattice-induced electronic transition. These features are for the most part absent in b (0—0), so that only a small part of its intensity could be lattice-induced.

A second point to notice is that the absorption in the region of the second transition is almost entirely c' polarized, and therefore that the local surroundings do not cause even the feeble appearance of the b (0—0) band in this case. This is not conclusive, however, as it is known that "solvent effects" are different in different electronic states of the same molecule.

A third point to be remembered is that the first transition was shown to be $g \rightarrow u$,[5] and thus the free molecule spectrum will have a 0—0 band of finite intensity. The b (0—0) band observed must therefore be the true 0—0 band.

The final evidence comes from a comparison of the mixed crystal spectrum with the vapor spectrum. While a detailed analysis of the vapor absorption spectrum has not been made, measurements of some of the bands show that a detailed analysis could probably be carried out as suggested by the mixed crystal experiments. The data used is that of de Laszlo. The comparison is shown in Table II. If the band at 32 020 cm^{-1} is taken as the 0—0 band, part of the weak series analogous to the b-polarized absorption can be identified. In particular, the bands 0–502, 0–702, and 0–987 are found within a few wave numbers of the position expected from the mixed crystal spectrum. The two strong bands 0–433 and 0–905 are present.

The comparison of the vapor spectrum with the crystal spectrum carried out in Table II is not entirely satisfactory because of the many bands which should, according to the crystal data, have appeared in the vapor spectrum and do not appear in de Laszlo's table. The intensity values do not agree very well in a number of cases, but as these are very qualitative, this disagreement cannot be considered serious. It can only be said that a thorough-going comparison of the crystal and vapor spectrum should be made on the basis of newer and more complete data on the vapor spectrum using the present data for the crystal spectrum.

One of the possible interpretations of the first absorption region, the possibility that it represents two electronic transitions,[13] can be eliminated at this point. The interval 433 cm^{-1} between the 0—0 band in the b-polarized spectrum and the first strong band of the c'-polarized spectrum is found unaltered in the vapor. If this were the difference between two electronic intervals, it would change in some way in going from vapor to solution. Also, as we have already noted, the vibrational intervals in the two polarizations are the same. This can only be the case when the electronic states are the same.

Thus it appears that the only interpretation consistent with all of the facts presented is that the first excited electronic singlet state of naphthalene is $^1B_{3u}$.

Previous attempts to fix the symmetry class of the first singlet were based on two incorrect assumptions. It had long been assumed that the prominent interval 32 455–31 513 cm^{-1}, measured in the vapor, represented the 0–1 to 1–0 interval of the same vibrational mode.[2,3] The band in the vapor at 32 455 corresponds to the vibration 433 cm^{-1} of the upper state, and this vibration is clearly nontotally symmetric since it appears in only one quantum and acts as the origin for most of the short axis spectrum. On the other hand, 31 513 represents a transition from the vibrationless upper state to 512 cm^{-1} in the lower state, and 512 is positively identified in the Raman spectrum as totally symmetric. The behavior of this mode in the b-polarized fluorescence supports this assignment (see Fig. 3). It is surprising, however, that the analog of 433 does not appear in the c'-polarized fluorescence, whereas 512 appears in its stead. This will be discussed in Part II. The analog of 512 in the upper state is 500 cm^{-1}, but as it is weak compared to 433, the 0–1, 1–0 interval of this vibration is not prominent. The second incorrect assumption was

[13] Knipe, Sponer, and Cooper, J. Chem. Phys. **21**, 376 (1953).

that the molecules in the naphthalene crystal can be considered nearly independent of each other.[4,6] But the nearby B_{2u} state is strongly mixed by intermolecular resonance with the B_{3u} state, with the result that even the 0−0 band in the b direction of the naphthalene crystal (mostly short axis absorption) is stronger than the 0−0 band in the a direction (mostly long axis absorption). This led to the B_{2u} assignment for the first singlet. Both difficulties arose because of the proximity of the first two singlets, which in the first case were mixed strongly by vibrational-electronic interaction and in the second case by the crystal field. The extreme weakness of the purely electronic portion of the transition to the first state makes these perturbations able to determine most of the spectral features.

We can be quite certain that the 433 and 905 cm^{-1} vibrations appearing in the c' spectrum of the mixed crystal are b_{1g} fundamentals of the B_{3u} state. Only vibrations of this symmetry can change the polarization of the $A_g \rightarrow B_{3u}$ transition to the short axis. They are also of the right symmetry to mix the B_{3u} state with the nearby B_{2u} state, and the proximity of the latter partly accounts for the fact that the vibrational electronic interaction is fairly strong. The 433 vibrational mode is not far in frequency from the e_{2g} vibration of benzene which causes the main part of the absorption in the 2600 A region. This frequency has the values 606 and 521 in the lower and upper states of benzene, respectively. The e_{2g} class goes into the classes a_g and b_{1g} in the group D_{2h}. It seems plausible that the 502 and 433 represent an a_g and a b_{1g} mode of the upper state of naphthalene, related to each other and to the e_{2g} of benzene. The type of motion in the benzene e_{2g} vibration is chiefly C−C−C in-plane bending. Since both of these low frequency modes of naphthalene appear strongly in the spectrum, it suggests that the bending motion is important for the same reason as in benzene, and that the excited electronic states of the two molecules are in some way similar. This can be added to Platt's arguments for a similarity between these states of benzene and naphthalene.[9] In this case, there are five nodes cutting the molecular long axis. This partially accounts for the low value of the transition moment.

Further properties of both excited states can be deduced from the fluorescence and absorption data of the normal and deuterated molecules. These will be discussed in a later article.

The two symmetry assignments presented in this paper are in agreement with the detailed calculations of Dr. Rudolf Pariser.[8] Dr. Pariser has kindly permitted me to quote his results in advance of his own publication. The lowest excited singlet is a $^1B_{3u}$ state calculated at 4.018 ev, compared to the experimental 3.969 ev. The calculated f number is about zero. Experimentally the solution spectrum gives about 0.002, but the purely electronic part of the transition corresponds to much less than this; approximately $f=0.0005$. The environment probably affects the intensity of the pure electronic part relative to the vibration-induced part, so that reliable measurements could only be obtained for the vapor. The next higher singlet according to the calculations lies at 4.493 ev and is a $^1B_{2u}$ state. This agrees with our identification of the symmetry and with Sponer's value for the 0−0 band of the transition to this state, 4.452 ev.[2] The calculated f number is 0.2, in agreement with values obtained from solution measurements.

The agreement between theory and experiment is so good that two corrections on the experimental data must be considered. It has been shown[14] that in benzene, the zero point energy of the ground state is 21 535 cm^{-1}, and of the $^1B_{2u}$ state, 20 050 cm^{-1}. The difference, 1485 cm^{-1} or 0.184 ev must be added to the observed transition energy to obtain a purely electronic energy comparable to the calculated electronic energy. This correction for naphthalene is not known, but must be in the neighborhood of 0.2 ev.

The second correction is necessary because the calculated transition energies are for a vertical transition while the 0−0 band is a nonvertical transition. From the structure of the b-polarized spectrum of the first transition, it can be seen that this correction must be in the neighborhood of 0.1–0.2 ev, while for the second transition it is somewhat larger, about 0.2–0.3 ev. Thus a total of perhaps 0.3 ev must be added to the 0−0 energy of the first transition and 0.4 ev to the second in order to obtain a figure comparable to the calculated results.

The writer wishes to thank Dr. Otto Schnepp for his assistance in the early stages of this investigation, and Dr. H. Sponer for her valuable criticism of the manuscript.

---

[14] Garforth, Ingold, and Poole, J. Chem. Soc. **1948**, 510.

Lattice Dynamics of Body-Centered and Face-Centered Cubic Metallic Elements. II

JULES DE LAUNAY
United States Naval Research Laboratory, Washington 25, D. C.
(Received May 6, 1954)

A numerical table is presented which permits the easy calculation of the Debye characteristic temperature of any cubic metallic element at 0°K. The use of the table presupposes a knowledge of the elastic constants, atomic volume, and density of the element at 0°K. The characteristic temperature can be evaluated for either of the theoretical cases described in an earlier paper by the author.

INTRODUCTION

IN an earlier paper[1] which we shall refer to as "Part I," we represented the body-centered and face-centered cubic monatomic metals by a model consisting of an ion point lattice imbedded in an electron gas. We assumed that the electron gas participated in the acoustical wave motion of the ions. This led to a determination of the Hooke's constants α and γ in terms of the acoustically measured elastic constants c_{11}, c_{12}, and c_{44}. On studying the contribution of the conduction electrons to the *thermal* motion of the lattice, we treated two extreme cases: 1. The electron gas does not partake of the thermal motion appreciably; 2. the electron gas follows the ion motion almost exactly. The Debye characteristic temperature at 0°K, Θ_0, was then computed for the two cases, under the additional condition that the isotropy condition be approximately fulfilled [Part I, Eqs. (58) and (59)]. Unfortunately, only aluminum and tungsten seem to come within the range of these formulas. Therefore, we are presenting in this paper a numerical table which will permit the easy calculation of Θ_0 for any cubic metallic element at both theoretical extremes.

THE COMPUTATION OF Θ_0

The value of Θ_0 for both types of cubic lattice and for both theoretical extremes is given by

$$\Theta_0^3=\frac{9N}{4\pi V}\left(\frac{h}{k}\right)^3\left(\frac{c_{44}}{\rho}\right)^{\frac{3}{2}}\cdot\frac{9}{18+\sqrt{3}}\cdot f(s,t). \qquad (1)$$

The ratio of Planck's constant to Boltzmann's constant is h/k. N is Avogadro's number. The atomic volume and density are V and ρ, respectively. When the x-ray value of the edge length a of the fundamental cube of an element is known, it should be used in computing V and ρ. In terms of a, the atomic volume per atom, V/N, is $a^3/2$ and $a^3/4$ for the b.c.c. and f.c.c. lattices, respectively. The corresponding densities are $2m/a^3$ and $4m/a^3$, where m is the mass of an atom. The quantities V, ρ, and c_{44} must be evaluated at 0°K.

The factor f is a function of the anisotropy of the crystal and has the value unity when the elastic constants satisfy the isotropy condition $c_{11}-c_{12}=2c_{44}$ and the electron gas is not participating in the thermal motion. We shall call f the anisotropy factor. The anisotropy factor is a function of two independent variables, s and t. These quantities are defined in terms of the elastic constants as follows:

1. Without electron gas participation in the thermal motion

$$s=\frac{c_{11}-c_{12}}{2c_{44}},\quad t=0. \qquad (2)$$

2. With electron gas participation in the thermal motion

$$s=\frac{c_{11}-c_{44}}{c_{12}+c_{44}},\quad t=\frac{c_{12}-c_{44}}{c_{44}},\quad t_m=\frac{2s}{1-s}. \qquad (3)$$

The symbol t_m represents the maximum value which t can possess. For values of t greater than t_m, f becomes a complex number.

Table I presents the anisotropic factor as a function of s and t/t_m. The following procedure is suggested for

TABLE I. The anisotropy factor f.

s \ t/t_m	0	0.1	0.2	0.3	0.4	0.5	0.6	0.7	0.8	0.9
0.9	0.9382	0.9225	0.8738	0.8117	0.7413	0.6637	0.5785	0.4841	0.3775	0.2499
0.8	0.8724	0.8413	0.7955	0.7399	0.6767	0.6064	0.5288	0.4428	0.3453	0.2288
0.7	0.8019	0.7654	0.7207	0.6692	0.6116	0.5479	0.4778	0.4000	0.3122	0.2071
0.6	0.7260	0.6883	0.6455	0.5978	0.5455	0.4882	0.4254	0.3561	0.2781	0.1849
0.5	0.6437	0.6072	0.5674	0.5241	0.4772	0.4265	0.3714	0.3110	0.2431	0.1621
0.4	0.5536	0.5202	0.4846	0.4465	0.4058	0.3623	0.3154	0.2642	0.2070	0.1386
0.3	0.4542	0.4256	0.3955	0.3637	0.3303	0.2947	0.2567	0.2154	0.1693	0.1141
0.2	0.3429	0.3208	0.2979	0.2739	0.2488	0.2224	0.1942	0.1636	0.1293	0.0881
0.1	0.2147	0.2012	0.1873	0.1727	0.1575	0.1415	0.1243	0.1056	0.0844	0.0589

[1] J. de Launay, J. Chem. Phys. **21**, 1975 (1953).

interpolation. Ten curves of f *versus* s are plotted on large graph paper, one curve for each value of t/t_m of the table. For the first theoretical case, s is computed by means of Eqs. (2) and f read off the curve for which $t/t_m=0$. For the second theoretical case, s is computed by means of Eqs. (3) and ten values of f are obtained from the graphs, one value from each constant t/t_m curve. Then these values of f are plotted against t/t_m and the final value of f read off this curve using the value of t/t_m obtained from Eqs. (3).

For the special value $s=1$, we have the exact expression

$$f(1,t)=\frac{18+\sqrt{3}}{9}\cdot\frac{1}{2+(3+t)^{-\frac{1}{2}}}. \tag{4}$$

The row for $s=1$ is absent from Table I, because for $t/t_m=0.1,\cdots,0.9$ we always have $t=\infty$. According to Eq. (4), this would give $f=1+(\sqrt{3}/18)=1.0962$ as the entry at the head of each column, except for the column headed $t/t_m=0$, where then the entry would be $f=1$.

The low temperature elastic constants are known for Al and Cu.[2,3] The data for these elements are given in Table II together with the Debye characteristic temperatures calculated with the help of Table I.

Table I can also be used to check two earlier computations of f. First, Part I contains formulas for the computation of Θ_0 when $|(c_{11}-c_{12}-2c_{44})/c_{44}|$, < about $\frac{1}{2}$ [Part I, Eqs. (58) and (59)]. This limiting condition was a guess at one percent error in $\Theta_0{}^3$ due to the neglect of an unknown remainder. Comparison of the numerical values obtained from these approximate formulas with those obtained by the more exact table show that the guess was correct. The second check is that of some numerical values worked out by Leighton.[4] It was pointed out to the author by Overton that the first row of Table VI of Leighton's paper is equivalent to the entries in the first column of our Table I for $s=0.5$ and 0.3. Leighton's numbers, when converted to f, yield 0.6373 and 0.4773, respectively. Leighton's quantity θ/β, which is proportional to $f^{\frac{1}{2}}$, is therefore accurate to about one percent.

MANNER OF PREPARATION OF TABLE I

The plan employed for the numerical calculation of the anisotropy factor followed the analytic treatment of Part I, Section VI, in which $\Theta_0{}^3$ was calculated. The goal of the numerical work was the determination of the volume in $\mathbf{k}$ space ($\mathbf{k}$ is the propagation vector) contained within a constant-frequency surface. This amounts to the evaluation of the integral $\int k^3 d\omega$ at constant frequency, where $d\omega$ is the element of solid angle. The work was considerably simplified by the high degree of symmetry of the surface. The whole constant-frequency surface can be generated from that portion contained in the trihedral angle with edges along the (001), (011), and (111), directions, using the symmetry rotations of the cube. This solid angle is 1/48 of the total solid angle 4π. In making the calculations, we subdivided this solid angle of magnitude $\pi/12$ into about 70 elements of roughly equal magnitudes. The coefficients of the cubic equation (Part I, Eq. (45)) were evaluated at the centroids of these elementary solid angles and then the roots obtained for the values of s equal to 0.1, 0.2, $\cdots$, 0.9. These roots are linearly related to ν^2, and it is in the transformation to ν^2 that the parameter t arises. (The parameter t is the ratio of the electron gas bulk modulus to the constant c_{44}). Now k is proportional to ν, the proportionality constant being a number depending on the spherical coordinates θ and ϕ and the parameters s and t. Thus, k^3 was expressed in terms of ν^3 at each centroid and then the sum $\Sigma k^3\Delta\omega$ was computed. After proper normalization, the reciprocal of this sum becomes f.

Much of the calculations for $t=0$ were carried out with a desk calculator by J. Harrison Hancock of this Laboratory. The remainder of the table, for $t>0$, was computed on the Naval Research Laboratory electronic digital computer, the NAREC. The numerical work was carried to six significant figures. Thus the residual error could be entirely ascribed to the coarseness of the size of the elementary angles $\Delta\omega$. In a few of the most highly anisotropic surfaces (e.g., $s=0.1$, $t/t_m=0.9$), the anisotropy is so great that as much as a third of the sum $\Sigma k^3\Delta\omega$ is contained in a single element. This element, which is the one with the direction (011) as one edge, and some of its immediate neighbors were subdivided into 9 elements each and their contributions to the sum recalculated. In this manner it was established that the error in the figures of Table I probably never exceeds two units in the last digit shown.

We have used a direct method of calculating the anisotropy factor. But there are also graphical methods of making these calculations such as the method proposed by Quimby and Sutton.[5]

TABLE II. Tabulation of the data of Al and Cu (cgs units), and the resulting characteristic temperatures.

Quantity	Al	Cu
c_{11}	12.26×10^{11}	17.62×10^{11}
c_{12}	7.085×10^{11}	12.48×10^{11}
c_{44}	3.065×10^{11}	8.17×10^{11}
V	9.863	7.049
ρ	2.734	9.018
Θ_0, case 1	421.0°K	340.8°K
Θ_0, case 2	426.6°K	345.3°K

[2] P. M. Sutton, Phys. Rev. **91**, 816 (1953). Al. The values presented in Table II differ slightly from those of Sutton because of the different manner of extrapolation to 0°K.
[3] W. C. Overton, Jr., Phys. Rev. (to be published). Cu.
[4] R. B. Leighton, Revs. Modern Phys. **20**, 165 (1948).
[5] S. L. Quimby and Paul M. Sutton, Phys. Rev. **91**, 1122 (1953).

Microwave Spectrum and Properties of Vinylene Carbonate*

GEO. R. SLAYTON, J. W. SIMMONS, AND J. H. GOLDSTEIN
Emory University, Emory University, Georgia

(Received April 8, 1954)

The microwave spectrum of vinylene carbonate has been investigated in the region from 19 000 to 32 000 Mc/sec. Eight *R*-branch transitions have been identified and fitted with the following spectroscopic parameters: $a=9346.79$ Mc/sec, $b=4188.46$ Mc/sec, $c=2891.54$ Mc/sec, all ± 0.10 Mc/sec; $\kappa=-0.59818$. The dipole moment of the vapor, as determined from Stark effect studies, is $4.51\pm0.05D$ and lies in the *a*-axis. The molecule has been shown to be planar. The significance of these results is discussed.

INTRODUCTION

VINYLENE carbonate (I) is the cyclic carbonate ester of the hypothetical parent enediol (II).

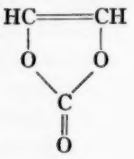

(I)

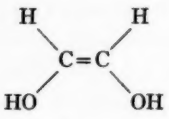

(II)

The synthesis of this unusual compound was first reported in 1953, by Newman and Addor,[1] who prepared it by the dehydrohalogenation of chloroethylene carbonate, and investigated its chemical and physical properties. The desirability of a microwave spectroscopic study of this molecule was pointed out by Mr. K. C. Brannock and Mr. Arthur Neal, of this laboratory, who also synthesized it following the published procedure.

Vinylene carbonate was expected to have a sizable dipole moment, and its vapor pressure was sufficient for microwave study. Nothing was known of its structure, but it was tentatively assumed to be planar. Our initial model of the molecule was based on the following parameters: $r_{C=O}=1.25$A°, $r_{C-O}=1.42$A°, $r_{C=C}=1.38$A°, $r_{C-H}=1.08$A°, OCO angle 120°, and the other ring angles adjusted to fit these values. The calculated values of the rotational constants were: $a=7996.2$ Mc/sec, $b=4263.4$ Mc/sec, $c=2780.7$ Mc/sec, $\kappa=-0.43$, with the dipole moment in the a axis.

TABLE I. Rotational spectrum of vinylene carbonate.

	Transition	Observed frequency Mc/sec	Calculated[a] frequency Mc/sec
1.	$2_{12}\rightarrow3_{13}$	19 169.62	19 169.62
2.	$2_{11}\rightarrow3_{12}$	23 037.67	23 037.68
3.	$3_{13}\rightarrow4_{14}$	25 355.29	25 355.31
4.	$3_{03}\rightarrow4_{04}$	26 450.13	26 450.00
5.	$3_{22}\rightarrow4_{23}$	28 151.36	28 151.41
6.	$3_{21}\rightarrow4_{22}$	30 019.22	30 019.45
7.	$3_{12}\rightarrow4_{13}$	30 409.18	30 409.30
8.	$4_{14}\rightarrow5_{15}$	31 420.68	31 420.27

[a] Calculated using the constants listed in Table II.

* This work was sponsored by the Office of Ordnance Research, U. S. Army.

[1] Melvin S. Newman and Roger W. Addor, J. Am. Chem. Soc. **75**,1263 (1953).

The predicted spectrum included a number of transitions arising from levels of low J-values in the 19 000–32 000 Mc/sec region. Because of their low intensity, the Q-branch lines of this group were excluded from consideration. After a cursory examination of the spectrum revealed a number of lines with resolvable Stark patterns, further studies emphasized the search for the expected group of low-J R-branch transitions.

These studies were performed with a spectrograph modulated by a 100 kc/sec square-wave source. Other pertinent experimental details are given below.

OBSERVED SPECTRUM AND ANALYSIS

The 19 000–32 000 Mc/sec region was scanned repeatedly until all expected transitions arising from levels of low J-value were located. Intensive study of the Stark patterns made this identification possible, and also permitted a tentative classification according to values of J. Attempts to fit these lines to the predicted spectrum were unsuccessful, however, and further study of the spectrum indicated that an appreciable change in κ would be required. By means of a graphical analysis it was determined that the only acceptable assignment required a value of about -0.6 for κ.

With this value of κ, and appropriate new assignments, a quantitative fitting of the entire spectrum was easily obtained. The observed spectrum and final assignments are given in Table I.

The frequency standard used for these measurements was monitored against signals from Station WWV. Each frequency value represents the mean of a number of readings taken over a period of several days. The final frequencies are estimated to be known to within about 0.10 Mc/sec. The rotational constants were calculated from lines 3, 4, and 5 of Table I without assuming planarity. As a check, the value of κ was also calculated from line 2, belonging to a different value of J, without appreciable change from the previous results. The final values are given in Table II.

The uncertainty in these constants is estimated to be within 0.10 Mc/sec. The corresponding values of the principal moments of inertia are, in gm-cm$^2\times10^{-40}$: $I_a=89.754$, $I_b=200.291$, and $I_c=290.126$. The defect, $I_c-I_a-I_b$, is 0.081×10^{-40} gm-cm^2, which is so small that a planar structure is indicated.

As a further test of planarity, approximate measurements of relative intensities were carried out. In the planar model, which belongs to point group C_{2v}, rotation about the a axis exchanges two hydrogen atoms. This necessitates the inclusion of spin factors in calculating relative intensities.[2] The weights are three and one, respectively, for rotational states which are odd and even with respect to this rotation. The experimental relative intensities showed that these factors were required, in agreement with the planar model.

The last column of Table I gives the frequencies calculated with our final values of rotational parameters. The agreement is quite satisfactory, the mean deviation for all lines being only a little larger than the estimated uncertainty in the frequencies. Centrifugal distortion effects are apparently quite small for the lines studied, and have not been considered in the analysis.

STARK EFFECT AND DIPOLE MOMENT

For the quantitative Stark effect studies, the applied square wave voltages were measured by balancing against an accurately measured external supply, and the wave guide was calibrated by means of measurements taken on OCS.[3] The field strengths used are estimated to be accurate within one percent.

Measurements were made on the $M=1$ component of the $2_{11}\rightarrow 3_{12}$ line, and the $M=2$ component of the $3_{13}\rightarrow 4_{14}$ line. The values of $\Delta\nu/E^2$ found for these two components are 2.60824 and 1.75408, respectively. Both figures represent the average of many measurements, with average deviations of about one-half and one percent, respectively. The effect was found to be quadratic, as was to be expected from the absence of degeneracies affecting the levels involved in the transitions studied.

The dipole moment was calculated by the method of Golden and Wilson.[4] The values obtained are $4.50D$ and $4.52D$, respectively, for the two lines studied, with an estimated uncertainty of $\pm 0.05D$.

As a further check on the results, rough measurements were made on the $M=1$ component of the $3_{12}\rightarrow 4_{13}$ line, and the $M=3$ component of the $3_{13}\rightarrow 4_{14}$ line. The average dipole moment calculated from these displacements was $4.5D$. Finally, the entire Stark pattern of the $3_{13}\rightarrow 4_{14}$ line was compared with the behavior predicted from the calculated values of $(A+BM^2)E^2$ and the theoretical intensities. These observations agreed with the predicted behavior in every respect.

DISCUSSION

With the exception of the brief survey of properties by Newman and Addor, there have been no other reported investigations of the physical and structural characteristics of vinylene carbonate. The present microwave study of this molecule has provided accurate values of its moments of inertia, proof of its planar structure, and the value of its dipole moment as determined in the vapor phase.

TABLE II. Rotational constants of vinylene carbonate.

a	9346.79 Mc/sec
b	4188.46 Mc/sec
c	2891.54 Mc/sec
κ	−0.59818

The two independent principal moments do not allow a complete structural calculation. Nevertheless, the definite establishment of planarity is of interest. The possibility of writing resonating structures of the form (III):

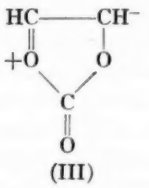

(III)

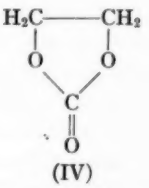

(IV)

led us to assume a planar structure initially. Independent proof of planarity means, at least, that such structures are not inconsistent with the geometry of the molecule.

The value of $4.51D$ obtained for the dipole moment of vinylene carbonate seems at first sight strikingly large. That this result is reasonable is indicated by the fact that for the related saturated ester, ethylene carbonate (IV), an even greater value, $4.80D$, has been reported by Arbuzov and Shavsha.[5] The unsaturated compound is expected to possess a somewhat smaller dipole moment if the two postulated resonating forms, (III) and its image, contribute appreciably to the overall structure. Analogous structures are commonly accepted as occurring in simpler heterocyclic compounds, such as furan. The results of our investigation are consistent with the idea that reasonating double-bonded structures involving participation of the non-bonded oxygen electrons occur also in unsaturated cyclic esters such as vinylene carbonate.

ACKNOWLEDGMENT

The authors wish to record their gratitude to Mr. K. C. Brannock and Mr. Arthur Neal, for preparing the sample of vinylene carbonate, and for numerous enlightening discussions; to Mr. Joseph Fine and Professor R. H. Rohrer for valuable assistance during the course of this investigation; and to the Jefferson Chemical Company for supplying the ethylene carbonate used in the synthesis.

[2] G. Herzberg, *Infrared and Raman Spectra* (D. Van Nostrand Company, Inc., New York, 1945), p. 53.
[3] R. G. Shulman and C. H. Townes, Phys. Rev. **77**, 500 (1950).
[4] S. Golden and E. B. Wilson, Jr., J. Chem. Phys. **16**, 669 (1948).
[5] B. A. Arbuzov and T. G. Shavsha, Chem. Abstracts, **44**, 886^g (1950).

Vacuum Ultraviolet Photochemistry, Part I. Nitrous Oxide at 1470 A

MURRAY ZELIKOFF AND LEONARD M. ASCHENBRAND
Geophysics Research Directorate, Air Force Cambridge Research Center, Air Research and Development Command, Cambridge, Massachusetts

(Received March 2, 1954)

The photolysis of nitrous oxide at 1470 A has been studied and the quantum yields measured for N_2O disappearance and NO, O_2, and N_2 appearance. The average of 38 measurements gives $\phi N_2O = 1.7_0$, $\phi O_2 = 0.5_0$, and $\phi N_2 = 1.4_4$ with ϕNO being pressure dependent. The data obtained here can be explained by a mechanism involving initial dissociation of nitrous oxide into nitrogen molecules and oxygen atoms. The source of NO can be in the reaction $O + N_2O \rightarrow 2NO$. These results are discussed in the light of previous work.

I. INTRODUCTION

THE photolysis of nitrous oxide was first studied in some detail by MacDonald[1] [using Al spark lines (1850–1950 A)] who reported the quantum yield of N_2O disappearance to be four. To explain this value, an energy chain mechanism was postulated using initial production of excited molecules. This interpretation was questioned by Noyes[2] since the absorption of N_2O in the photolytic wavelength region is by a continuum, and therefore, the initial absorption of light should lead to dissociation rather than to excitation. Dark reactions subsequent to the initial step should lead to a maximum value of two for the quantum yield of N_2O disappearance. The most thorough and exhaustive work on N_2O photolysis is that of Noyes[3–5] and his collaborators who reached the following conclusions: 1. The products of the reaction are nitrogen, nitric oxide and oxygen. 2. The initial act of absorption leads to two different dissociative processes; one into N_2 molecules plus O atoms and the other into NO molecules and N atoms. 3. The origin of NO must be the latter process, since formation of NO by reaction of O atoms with N_2O requires an energy of activation of at least 14 kcals.[3] Moreover, addition of hydrogen to N_2O undergoing photolysis leads to formation of small amounts of ammonia.[4] This apparently requires nitrogen atoms. However, in conflict with this conclusion is the catalytic effect of added oxygen on Hg-sensitized N_2O decomposition.[5] This catalytic effect was confirmed in this work. 4. Formation of O atoms must occur to some extent, since it represents the only source of oxygen atoms large enough to account for the observed oxygen produced by atomic recombination.

Farkas, Haber, and Harteck[6] found that N_2O photosensitizes the hydrogen-oxygen reaction in the far ultraviolet and ascribed this effect to the production of O atoms from N_2O. Wulf and Melvin[7] found that absorption of 2300 A radiation by N_2O leads to the appearance of the γ bands of NO in absorption. They ascribed this observation to the initial production of NO. It must be observed that neither of these observations is in any way conclusive regarding a choice of one mode of dissociation in preference to the other. The experiments of Farkas *et al.* constitute good evidence in favor of O atom production, but it does not exclude initial formation of NO. The detection of NO in absorption does not necessarily indicate its formation in the initial step.

The basic question to be answered is: does NO form in the initial step or is it produced by the action of oxygen atoms on nitrous oxide? The work of Musgrave and Hinshelwood[8] and that of Friedman and Bigeleisen[9] indicates that in the thermal decomposition of N_2O the source of NO is not the initial step. Nevertheless, at elevated temperatures, reaction of $O + N_2O$ could proceed with a measurable rate, while it might not proceed to any extent as a dark reaction at ordinary temperatures following initial light absorption.

The present work is a study of the mechanism of N_2O photolysis at 1470 A and an attempt to deduce from it information regarding the effect of longer wavelengths.

II. EXPERIMENTAL

The apparatus used was built around a xenon resonance lamp similar to that used by Dacey and Hodgins[10] and Wijnen and Taylor.[11] Briefly, the reaction vessel was a cylindrical Pyrex tube about 30 cm long and about 7 cm in diameter, containing an annular tube of quartz joined to it by graded seals. The quartz tube was about 20 cm long, 1 cm in diameter, and had a wall thickness <0.1 mm. The electrodes were contained in Pyrex cylinders (2.5 cm in diameter and 10 cm long) which were sealed to the ends of the quartz tube through graded seals. Instead of using cold electrodes and high

[1] J. Y. MacDonald, J. Chem. Soc. (London) **Part 1**, 1 (1928).
[2] W. A. Noyes, Jr., J. Chem. Phys. **5**, 807 (1937).
[3] Henriques, Duncan, and Noyes, J. Chem. Phys. **6**, 518 (1938).
[4] J. W. Zabor and W. A. Noyes, Jr., J. Am. Chem. Soc. **62**, 1957 (1940).
[5] W. M. Manning and W. A. Noyes, Jr., J. Am. Chem. Soc. **54**, 3907 (1932).
[6] Farkas, Haber, and Harteck, Z. Elektrochem. **36**, 711 (1930).
[7] O. R. Wulf and E. H. Melvin, Phys. Rev. **39**, 180 (1932).
[8] F. F. Musgrave and C. N. Hinshelwood, Proc. Roy. Soc. (London) **A135**, 23 (1932).
[9] L. Friedman and J. Bigeleisen, J. Am. Chem. Soc. **75**, 2215 (1953).
[10] J. R. Dacey and J. W. Hodgins, Can. J. Research **B28**, 90 (1950).
[11] M. H. Wijnen and H. A. Taylor, J. Chem. Phys. **21**, 233 (1953).

voltage to maintain the discharge, heated filaments of thoriated tungsten were used which permitted stable operating conditions at 40 volts and 120–130 milliamperes dc. These heated filaments generally lasted several hundred hours and greatly reduced the outgassing time. The principal difficulty encountered in operating the lamp was the removal of carbon monoxide which, when present, carried the discharge current itself and prevented the production of the xenon resonance lines. The presence of CO in the lamp could be detected with a small hand spectroscope since characteristic CO bands appeared in the visible. Also, the voltage across the electrodes always rose considerably when CO was present. Removal of this troublesome impurity was effected by filling the lamp with xenon, running the discharge until the voltage increased above 50 volts, evacuating, refilling, etc., until the discharge voltage remained low and no CO bands appeared. During all the runs, the condition of the discharge was always monitored both electrically and spectroscopically. However, even though the purity of the discharge could be maintained, the intensity of the 1470A line was found to vary somewhat with xenon pressure. To neutralize the errors which might have been produced by this variation the same xenon pressure ($\sim$1 mm) in the lamp was used for all measurements, and calibration runs were made very frequently; at least one Xe-sensitized CO_2 calibration being made for each two nitrous oxide runs. Since the intensity of the lamp was quite low (total flux 5×10^{14} quanta/sec) at least two hours were required to produce enough decomposition to permit reliable analysis. To compensate for light intensity changes during a run, calibrations were made with CO_2 samples being taken at the same time as for N_2O runs (see below). Since in this work N_2O both Xe photosensitized and nonphotosensitized showed the same results, the bulk of the experiments were carried out in the absence of xenon.

Samples from the reaction vessel were taken periodically and analyzed on a Consolidated Engineering Corporation Analytical Mass Spectrometer. The zero time sample was always a good test of the purity of the irradiated gas, since impurities present to the extent of 0.05 percent could be easily detected. The N_2O and CO_2 used were purified from commercial materials by fractional distillation at liquid nitrogen temperatures until mass spectrometric analysis showed total impurity less than 0.05 percent. Even with only 5–10 percent decomposition, analyses could be made accurate to ±5 percent for the less abundant constituents and to within ±2 percent for the nitrous oxide or carbon dioxide. The sample size was kept to less than one percent of the total reaction mixture. The temperature of the reaction vessel during lamp operation was probably not much above 50°C since pressure measurements on the gas contained in it both during and after a run indicated only a slight change. Cooling air from electric air blowers helped to maintain this temperature. The lamp intensity was too low to produce much percentage decomposition in a reasonable time if N_2O or CO_2 pressures exceeded 5 or 6 mm.

Calibration of the Lamp

The actinometer used was carbon dioxide photolysis. It has been shown by Groth[12] that the quantum yield (ϕ) of CO_2 decomposition is 0.98 for 1470 A light, and Dacey and Hodgins[10] have shown that this value is the same for the xenon photosensitized decomposition. The validity of the 0.98 value has recently been questioned by Wijnen and Taylor,[11] and Noyes,[13] and the importance of this value is sufficiently great to warrant discussion here.

Groth based his measurement on a comparison of the quantum yields of NH_3 photolysis, ozone formation, and CO_2 decomposition. His light source produced both xenon resonance lines at 1295 A and 1470 A with 1470 A about ten times as strong as 1295 A.

The criticism of Wijnen and Taylor is based on their measurements at 1470 A of the quantum yields of CO_2 and NH_3 photolysis. They find that ϕNH_3 varies from 2 to 11 depending on the pressure of ammonia, the higher value being obtained at higher pressures. These values are based on the assumption that ϕCO_2 is one. Groth found $\phi NH_3=0.17$ using $\phi CO_2=1$. Wijnen and Taylor point out that their experiments were probably run at a higher temperature than those of Groth and that this may have produced a higher ϕNH_3. Since Ogg, Leighton, and Bergstrom[14] have shown that at 1200-mm NH_3 pressure, $\phi NH_3=0.14$ at 20°C and $\phi NH_3=0.54$ at 400°C, and since Wijnen and Taylor worked at temperatures of about 50°C–200°C, it does not seem that temperature alone could produce this discrepancy with the results of Groth. The implication is that since $\phi NH_3=2$ to 11 for $\phi CO_2=1$, ϕCO_2 should be about 0.1 to reconcile the different values of ϕNH_3. Further doubt of the validity of Groth's value for ϕCO_2 is pointed out by Wijnen and Taylor in that "Groth did not then accept a decompostion of the carbon monoxide molecule which he later proves to take place at 1295 A," although it does not happen at 1470 A. This criticism lacks value in that recent measurements[15] have shown that at 1295 A, which falls between the 9th and 10th members of the IV positive CO bands, CO_2 absorbs about 10 times as strongly as CO; moreover, 1470 A was about 10 times as strong as 1295 A. The question of the accumulation of reaction products cannot be considered since Groth[16] used a flow method in his experiments. It is admittedly difficult to explain the ammonia dis-

[12] W. Groth, Z. physik. Chem. **B37**, 307 (1937).
[13] W. A. Noyes, Jr., and P. A. Leighton, *The Photochemistry of Gases* (Reinhold Publishing Corporation, Inc., New York, 1941), pp. 83, 248.
[14] Ogg, Leighton, and Bergstrom, J. Am. Chem. Soc. **56**, 318 (1934).
[15] Watanabe, Zelikoff, and Inn, Geophysical Research Paper No. 21 of A.F.C.R.C. (1953).
[16] Private communication.

TABLE I. Quantum yields in nitrous oxide photolysis.

Run No.	mm N_2O pressure	Time in min	Experimental ϕN_2O	ϕNO	ϕO_2	ϕN_2	Calculated ϕN_2O $2(\phi N_2-\phi O_2)$	$\frac{1}{2}(\phi NO+2\phi N_2)$	$\phi NO+2\phi O_2$
1	1.72	120	1.6_6	0.44	0.56	1.6_4	2.1_6	1.8_6	1.5_6
		195	1.5_7	0.37	0.44	1.3_9	1.9_0	1.5_8	1.2_5
		300	1.5_1	0.46	0.53	1.3_7	1.6_8	1.6_0	1.5_2
2	1.75	165	1.7_7	0.54	0.61	1.7_2	2.2_2	1.9_9	1.7_6
		210	1.7_8	0.47	0.57	1.5_6	1.9_8	1.8_0	1.6_1
		270	1.7_5	0.42	0.62	1.5_3	1.8_2	1.7_4	1.6_8
3	1.85	120	1.8_7	0.43	0.68	1.3_5	1.3_4	1.5_7	1.7_9
		180	1.6_5	0.34	0.66	1.4_1	1.5_0	1.5_8	1.6_8
		240	1.7_5	0.42	0.62	1.3_5	1.4_6	1.5_6	1.6_6
		300	1.7_6	0.40	0.61	1.3_8	1.5_4	1.5_8	1.6_2
4	1.87	120	1.5_4	0.45	0.50	1.3_7	1.7_4	1.6_0	1.4_5
		180	1.5_4	0.37	0.52	1.2_5	1.4_6	1.4_4	1.4_1
		240	1.4_5	0.41	0.52	1.2_7	1.5_0	1.4_8	1.4_5
		300	1.6_4	0.39	0.55	1.3_3	1.5_6	1.5_3	1.4_9
5	2.02	120	1.7_2	0.50	0.63	1.6_7	2.0_8	1.9_2	1.7_6
		300	1.6_1	0.59	0.65	1.5_2	1.7_4	1.8_2	1.8_9
6	2.15	120	1.7_5	0.34	0.36	1.3_4	1.9_6	1.5_1	0.9_6
		180	1.6_7	0.46	0.43	1.6_1	2.3_6	1.8_4	1.3_2
		300	1.7_1	0.50	0.46	1.3_7	1.8_2	1.6_2	1.4_2
7	2.20	285	1.6_1	0.32	0.30	1.5_0	2.4_0	1.6_6	0.9_2
		360	1.8_0	0.54	0.46	1.4_6	2.0_0	1.7_3	1.4_6
8	2.20	405	1.6_5	0.39	0.25	1.3_7	2.2_4	1.5_7	0.8_9
9	2.22	270	1.7_4	0.56	0.51	1.3_8	1.7_4	1.6_6	1.5_8
		375	1.8_0	0.48	0.44	1.2_8	1.6_8	1.5_2	1.3_6
10	2.40	285	1.6_6	0.40	0.28	1.5_3	2.5_0	1.7_3	0.9_6
		420	1.7_6	0.44	0.35	1.5_4	2.3_8	1.7_5	1.1_4
11	2.70	300	1.6_0	0.46	0.33	1.1_5	1.6_4	1.3_8	1.1_2
12	2.74	450	1.7_2	0.43	0.55	1.4_7	1.8_4	1.6_9	1.5_3
13	2.75	300	1.8_3	0.67	0.45	1.3_7	1.8_4	1.7_1	1.5_7
14	3.40	120	1.7_1	0.61	0.40	1.7_7	2.7_4	2.0_3	1.4_1
		300	1.6_9	0.60	0.48	1.4_6	1.9_6	1.7_6	1.5_6
15	4.43	120	1.6_9	0.68	0.41	1.5_3	2.2_4	1.8_7	1.5_0
		300	1.8_5	0.55	0.43	1.2_8	1.7_0	1.5_6	1.4_1
16	4.60	300	1.7_3	0.70	0.53	1.3_4	1.6_2	1.6_9	1.7_6
17	5.20	225	1.7_2	0.67	0.46	1.3_4	1.7_6	1.6_8	1.5_9
18	5.62	120	1.7_4	0.68	0.56	1.5_2	1.9_2	1.8_6	1.8_0
		180	1.7_1	0.82	0.58	1.6_5	2.1_4	2.0_6	1.9_8
		300	1.7_4	0.79	0.55	1.4_1	1.7_2	1.8_1	1.8_9
Averages:			$1.7_0\pm0.07$	0.50 ± 0.09		$1.4_4\pm0.11$	$1.8_9\pm0.31$	$1.6_9\pm0.13$	$1.4_9\pm0.20$

crepancy, but it must be noted that using $\phi CO_2=1$, Groth found ϕO_3 (formation) $=1.90\pm0.05$ in agreement with the value of Vaughan and Noyes.[17] It may be mentioned that in all experiments a small oxygen impurity would make results uncertain since at 1470 A oxygen absorbs about ten times as strongly as NH_3 and 20 times as strongly as CO_2.[15]

Noyes bases his criticism of Groth's value for ϕCO_2 on work of Verhoek[18] who reports a stationary state in CO_2 photolysis at which the ratio $CO/CO_2=0.02$. Verhoek also reports that ϕCO_2 approaches unity only in a flowing system. It must be noted here that a flowing system is precisely what Groth[16] used. Concerning stationary states, the present work made use of a static system with CO_2 pressures from 2–5 mm. No evidence of a photostationary state was found at least up to 10 percent CO_2 decomposition at which point CO/CO_2

[17] W. E. Vaughan and W. A. Noyes, Jr., J. Am. Chem. Soc. **52**, 559 (1930).

[18] See reference 13, p. 397.

$=0.1$. Presumably a photostationary state would be produced by the accumulation of oxygen in a static system and subsequent regeneration of CO_2 through reaction of CO with oxygen atoms. This regeneration would be assisted by the strong absorption of oxygen. This is not serious in the present measurements since xenon photosensitization was used, and Wijnen and Taylor have shown that even 3 microns of xenon absorb practically all the 1470 A light in their reaction cell which had a light path of about 5 cm. Thus, xenon probably absorbs its resonance line at least 10 times as strongly as does oxygen. Since in this work Xe photosensitization was used in all calibrations, the only point that need be considered, therefore, is the frequency of collision of Xe* atoms with CO_2, CO, and O_2. Clearly, at the early stages of the reaction, Xe* collisions with CO_2 are predominant.

Finally, it may be mentioned that in this work some early experiments on *nonphotosensitized* CO_2 photolysis also showed no stationary state up to about 10 percent decomposition. In one experiment, the reaction was practically stopped by leakage into the reaction vessel of a few percent of oxygen. We suggest this as a possible explanation of results which imply ϕCO_2 to be much less than unity.

III. DATA AND DISCUSSION

We shall discuss here two alternative mechanisms for N_2O photolysis. The results of Noyes and those to be presented here, as well as the continuous absorption of N_2O make the energy-chain mechanism of MacDonald seem unlikely. We shall, therefore, consider only

(1) $N_2O \rightarrow N_2+O$

(2) $O+N_2O \rightarrow 2NO$

(3) $O+N_2O \rightarrow N_2+O_2$

(4) $O+O+M \rightarrow O_2+M$

(5) $N_2O \rightarrow NO+N$

(6) $N+N_2O \rightarrow N_2+NO$

(7) $N+N+M \rightarrow N_2+M$.

Mechanism I involves (1), (2), (3) and (4) only, and mechanism II (favored by Noyes) involves (1), (4), (5), (6), and (7).

Using Eqs. (1) to (4), the quantum yield of disappearance of N_2O may be related to the quantum yields of appearance of products. Thus we may write

$$\phi N_2O=\phi N_2(1)+1/2\phi NO+\phi N_2(3), \quad (a)$$

or

$$\phi N_2O=\phi N_2+1/2\phi NO, \quad (b)$$

where $\phi N_2(1)$ and $\phi N_2(3)$ are the contributions of steps (1) and (3) to the quantum yield of N_2. Quantum yields having no subscript numbers represent total values. Using similar notation, it can be shown that

$$\phi O_2(4)=\phi O_2-(\phi N_2-\phi), \quad (c)$$

where ϕ is the primary quantum yield. Also

$$\phi O_2(3)=\phi O_2-1/2\phi O(4) \quad (d)$$

and

$$\phi O(4)=2\phi-1/2\phi NO-\phi N_2. \quad (e)$$

Combining (c), (d), and (e) we obtain

$$\phi O_2=\phi O_2(3)+\phi O_2(4)=1/2\phi N_2-1/4\phi NO. \quad (f)$$

Substituting for ϕNO in (b) gives

$$\phi N_2O=2\phi N_2-2\phi O_2. \quad (g)$$

Equations (b) and (g) can be combined to give

$$\phi N_2O=\phi NO+2\phi O_2. \quad (h)$$

Table I presents quantum yields obtained in this work. The columns headed ϕN_2O, ϕNO, ϕO_2, and ϕN_2 represent experimental values. The last three columns represent three alternative expressions for ϕN_2O derived *assuming mechanism I*. At the end of the table are listed average values for all columns except ϕNO since the latter is clearly pressure dependent. The data, in general, are for initial rates since extensive decomposition would lead to accumulation of products which can absorb the 1470 A light. In no case was NO_2 found among the products. It should be noted in this connection that the mass spectrometric analysis used in this work is easily capable of detecting NO_2 when present to the extent of one part in 2000. Several features of Table I should be noted particularly as evidence in favor of mechanism I.

(1) The good agreement between calculated and observed values of ϕN_2O. (2) The value of $\phi N_2=1.4_4$ which exceeds unity by considerably more than the experimental error. $\phi N_2>1$ cannot be a consequence of mechanism II, but it can and should be a consequence of mechanism I. (3) The pressure dependence of ϕNO seems to favor mechanism I. Step (5) cannot account for this dependence since the disappearance of N_2O was observed in this work as zero order depending only on light intensity. Since there is no reason to believe that (7) cannot proceed as quickly as (4), the use of (6) to explain the NO-pressure dependence is questionable, its contribution probably being relatively small. Moreover, Willey and Rideal[19] have shown that N_2O does not affect the glow of active nitrogen. Analysis of their products showed no N_2O decomposition by active nitrogen.

In the work of Noyes, it is experimentally shown that $\phi N_2+\phi NO=1.9$ and ϕNO is taken as 0.9 assuming $\phi N_2=1$ *without direct experimental measurement*. Even the value of unity for ϕN_2 leads to some complications if mechanism II is assumed. If steps (1), (6), and (7) only can lead to N_2, the occurrence of (7) must be slight since it would lead to $\phi N_2<1$. Since there is no a priori reason for believing (7) to be slow, it can be

[19] E. J. B. Willey and E. K. Rideal, J. Chem. Soc. (London) **130**, 669 (1927).

seen that a mechanism involving (5), (6), and (7) only would lead to $\phi N_2 < 1$. Therefore, if ϕN_2 is to equal unity, one must assume that the initial absorption of light leads principally to dissociation by (1) and to a lesser extent to dissociation by (5). In this connection, however, it can be pointed out that if NO can be formed only by (5) and (6), and since ϕNO must equal 0.9, at least 45 percent of the initial absorption must lead to (5) assuming (7) does not take place at all. Thus, mechanism II requires that oxygen be formed by (4) but that nitrogen be formed by (6) rather than by (7). This suggestion is not supported by the work of Willey and Rideal[19] as noted above. It should be pointed out that if the initial absorption leads to N as well as O atoms, the process $O+N+M \rightarrow NO+M$ may not be negligible.

Evidence in favor of step (5) is cited by Noyes[4] in that NH_3 is formed when H_2 is added to N_2O undergoing photolysis. Added NO prevents the formation of NH_3. This seems to indicate that the nitrogen atoms apparently needed for the formation of NH_3 do not originate from photolysis of NO, but rather that NO is an effective third body for N atom recombination. Here one may ask why NO should be more effective than N_2O. Moreover, as pointed out by Noyes, NO may play still another role, i.e., (8) $NH_2+NO \rightarrow N_2+H_2O$.

Regarding the role of NO, it must be noted that while added NO inhibits NH_3 formation, very small amounts of NO cannot do this, since some NO is always formed in N_2O photolysis. The very small amount of NH_3 formation observed seems to argue against (5) as the origin of N atoms and in favor of dissociation of NO. It should be noted that NO does dissociate in this spectral region (1850–1950 A).

Up to this point we have not discussed the difference in wavelength between our work at 1470 A and that of Noyes in the 1850–1950 A region. Recent work[20] on the absorption coefficients of N_2O in the vacuum ultraviolet has shown that 1470 A falls in a continuous absorption region which has a long wavelength limit at about 1555 A corresponding to ~8 ev. Thermochemical data[21] and Sponer and Bonner[22] have shown that the transition from the ground state to a state described by

$$N_2O(^3\pi \text{ or } ^3\Sigma) \rightarrow N_2(^1\Sigma)+O(^3P),$$

requires 1.71 ev. Thus, adding 6.2 ev for the excitation energy of $N_2(^3\Sigma^+)$, the long wave limit of the continuum above should be about 8 ev in good agreement with observation. Thus, the absorption of 1470 A should produce an excited molecule which dissociates into $N_2(^3\Sigma^+)$ and $O(^3P)$. There are no excited levels of NO or N which would give such an energetically consistent picture. The 1850–1950 A region is contained in another N_2O absorption continuum which has a long wavelength limit at 2100 A or 5.9 ev. Since this absorption is continuous, it probably involves a transition to a repulsive upper state

$$N_2O(^1\Sigma) \rightarrow N_2(^1\Sigma)+O(^1S).$$

The excitation energy of $O(^1S)$ is 4.2 ev which added to 1.71 ev gives excellent agreement with the observed value 5.9 ev. Thus, it seems likely that the oxygen atoms produced by Noyes in his experiments at 1850–1950 A were ^1S atoms rather than atoms in the lower excited (^1D) or ground state (^3P). Noyes' measurement of the activation energy of reaction (2) employed ^1D and ^3P oxygen atoms.

IV. CONCLUSIONS

The results of the present work can be explained on the basis of mechanism I. Spectroscopic data suggest that N_2O absorption at 1470 A and between 1850–1950 A leads to dissociation into nitrogen molecules and oxygen atoms. Mechanism II cannot explain the present observations, and the use of mechanism II encounters difficulties in explaining past work.

[20] Zelikoff, Watanabe, and Inn, J. Chem. Phys. **21**, 1643 (1953).

[21] F. R. Bichowsky and F. D. Rossini, *Thermochemistry of Chemical Substances* (Reinhold Publishing Corporation, Inc., New York, 1936).

[22] H. Sponer and L. G. Bonner, J. Chem. Phys. **8**, 33 (1940).

Vacuum Ultraviolet Photochemistry, Part II. Nitrous Oxide at 1849 A

MURRAY ZELIKOFF AND LEONARD M. ASCHENBRAND
Geophysics Research Directorate, Air Force Cambridge Research Center, Air Research and Development Command, Cambridge, Massachusetts

(Received March 2, 1954)

The photolysis of nitrous oxide at 1849 A has been studied and the quantum yield ratios $\phi N_2O/\phi N_2$, $\phi N_2O/\phi O_2$, and $\phi N_2O/\phi NO$ measured. The former two ratios compare well with the same ratios at 1470 A and the latter ratio is pressure dependent. It appears that the photolysis mechanism at 1849 A is similar to that at 1470 A. The absorption coefficient of N_2O is calculated from the photolysis data and found to compare well with previous work.

I. INTRODUCTION

PREVIOUS work[1] on the photolysis of nitrous oxide has raised a question regarding the similarity of the decomposition mechanisms using 1470 A light and light of longer wavelength. In attempting to reconcile the data at 1470 A with the work of Noyes[2] at λλ1850–1950 A, it became necessary to discuss the nature of the absorption in these wavelength regions. Reference to the absorption spectrum[3] shows that we need consider two continua, one extending from 1380 A to 1600 A, and the other from 1600 A to 2100 A. It was suggested on spectroscopic grounds that the initial dissociation of N_2O induced by absorption of light in both these wavelength regions leads to nitrogen molecules and oxygen atoms. The data on photolysis at 1470 A was shown to be explainable on the basis of a four-step mechanism, but the results of Noyes[2] could be explained by (1) to (4)[1] and by the addition of three more steps.[1] In order to show that the different conclusions cannot be accounted for on the basis of wavelength differences, the present work describes some experiments on N_2O photolysis using a low-pressure quartz mercury arc. From this lamp the strongest mercury line absorbed by N_2O is that at 1849 A. Since the continuum in this region is quite flat and extends from 1600 A to 2100 A, it appears safe to conclude that absorption of 1849 A produces the same effect on N_2O as does absorption of the Al spark lines between 1850 A–1950 A.

II. EXPERIMENTAL

The lamp used for these measurements is shown in Fig. 1. The quartz section was sealed into the reaction vessel through graded seals. Since both 1849 A and 2537 A are produced, a Vycor tube which transmits only above 2100 A was fitted around the quartz as a filter. This filter was provided with sealed-in iron rods so that it could be moved over the quartz section by using a magnet on the outside of the reaction vessel. When this filter was in place over the quartz section of the lamp, the amount of N_2O decomposition was reduced to less than two percent of that produced by the unfiltered light. Even this small amount of decomposition was probably produced by unfiltered light emanating from the ends of the filter tube and also by the action of unfiltered light on the small amount of gas between the filter and the quartz section. Furthermore, examination of the work of Sponer and Bonner[4] on N_2O absorption as well as of that by Zelikoff, Watanabe, and Inn[3] shows that the absorption of 2537 A by N_2O is only about 10^{-4} times that at 1849 A, the absorption coefficient[3] at 1849 A being about 3.7 cm^{-1}. It may be concluded that in these experiments the "active" radiation lies below 2100 A and consists chiefly of 1849 A.

The electrodes used were heated filaments of thoriated tungsten similar to those used in previous work.[1] Stable operating conditions were obtained at 260 volts and 100 milliamperes dc using a voltage regulated power supply. Electric air blowers were used to cool the reaction vessel and electrodes, maintaining the temperature at about 50°C. The lamp filling consisted of a small drop of mercury and about 8 mm argon. The nitrous oxide pressures ranged from 1.2 mm to 34.4 mm and were read on an Alphatron pressure gauge previously calibrated for N_2O. This gauge was used in order to avoid using a mercury manometer which might have introduced mercury vapor into the reaction vessel. To insure that the N_2O decomposition would not be mercury photosensitized the reaction vessel was always pumped out to less than 10^{-5} mm before adding N_2O. Furthermore, at no time during the construction and use of the apparatus was mercury vapor allowed in contact with the reaction vessel. The N_2O used in this work was prepared and tested in the same manner as that previously described.[1]

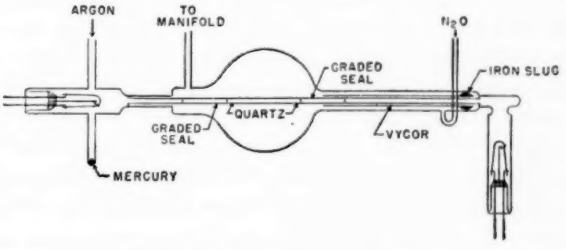

FIG. 1. Mercury resonance lamp.

[1] M. Zelikoff and L. M. Aschenbrand, J. Chem. Phys. (same issue as part I).
[2] W. A. Noyes, Jr., J. Chem. Phys. **5**, 807 (1937).
[3] Zelikoff, Watanabe, and Inn, J. Chem. Phys. **21**, 1643 (1953).
[4] H. Sponer and L. G. Bonner, J. Chem. Phys. **8**, 33 (1940).

TABLE I. Results of N_2O photolysis at 1849 A.

Run No.	mm N_2O pressure	Exposure time in sec	% N_2O decomposed	Products % N_2	% NO	% O_2	Ratios $\phi N_2O/\phi N_2$	$\phi N_2O/\phi NO$	$\phi N_2O/\phi O_2$
1	1.22	300	12.1	11.1	4.9	4.1	1.0_9	2.4_8	2.9_5
2	2.19	300	11.2	9.4	5.2	3.5	1.1_9	2.1_5	3.2_0
3	2.81	900	25.9	19.4	11.5	7.2	1.3_3	2.2_5	3.5_9
4	2.84	300	11.7	8.5	4.8	3.1	1.3_7	2.4_3	3.7_7
5	2.96	300	11.0	7.9	5.6	3.0	1.3_9	1.9_7	3.6_7
6	3.00	300	10.1	7.4	4.8	2.9	1.3_7	2.1_0	3.4_8
7	3.27	300	11.5	8.8	5.0	3.2	1.3_0	2.3_0	3.5_9
8	5.28	300	9.1	7.9	5.3	2.9	1.1_5	1.7_1	3.1_3
9	5.57	300	8.3	7.0	5.4	2.5	1.1_9	1.5_4	3.3_2
10	5.66	300	9.1	6.8	4.7	2.6	1.3_4	1.9_4	3.5_0
11	5.71	900	23.7	17.7	11.4	6.5	1.3_3	2.0_7	3.6_4
12	6.03	300	10.7	8.5	5.7	3.3	1.2_5	1.8_7	3.2_4
13	11.2	300	9.4	8.2	5.1	2.9	1.1_5	1.8_4	3.2_4
14	11.4	300	8.7	6.8	5.3	2.4	1.2_8	1.6_4	3.6_2
15	11.6	900	21.8	16.3	10.9	6.1	1.3_3	2.0_0	3.5_7
16	12.4	300	8.0	6.3	4.6	2.3	1.2_7	1.7_4	3.4_8
17	16.0	300	7.7	6.3	4.5	2.3	1.2_2	1.7_1	3.3_4
18	16.8	300	7.8	6.4	4.6	2.3	1.2_1	1.6_9	3.3_9
19	17.2	300	7.9	6.3	5.2	2.0	1.2_5	1.5_1	3.9_5
20	17.3	300	6.7	5.4	3.9	2.0	1.2_4	1.7_2	3.3_5
21	22.6	300	7.0	5.9	4.8	2.0	1.1_8	1.4_5	3.5_0
22	23.2	300	6.8	5.6	4.6	1.8	1.2_1	1.4_7	3.7_7
23	23.4	300	6.1	5.0	3.7	1.8	1.2_2	1.6_4	3.3_9
24	34.4	300	4.8	4.4	3.1	1.5	1.0_9	1.5_4	3.2_0
Averages							$1.2_4 \pm .07$		$3.4_7 \pm 0.20$

Since the quantum yield of N_2O decomposition in this wavelength region can be calculated from the data of Noyes[2] it was possible to measure the output of the lamp using N_2O as an actinometer. This turned out to be about 2×10^{17} quanta/sec of light below 2100 A absorbed by N_2O. This light, as pointed out before, was predominantly 1849 A. This measurement involves the assumption that all energy absorbed by N_2O in this region produces dissociation, and the validity of this assumption can be seen from the nature of the absorption spectrum.[3] Most of the runs made were of five minutes duration. At the end of each run the gas was sampled and analyzed on a Consolidated Engineering Corporation Analytical Mass Spectrometer.

III. RESULTS AND DISCUSSION

Since Noyes[2] has already made an energy measurement to determine the quantum yield of nitrous oxide disappearance, this was not repeated in the present work. The value of Noyes for ϕN_2O is 1.45. In the previous work at 1470 A,[1] ϕN_2O was measured as 1.7. To show the similarity in mechanism of N_2O photolysis at 1470 A and 1849 A, it is sufficient to compare the ratios $\phi N_2O/\phi N_2$, $\phi N_2O/\phi NO$, and $\phi N_2O/\phi O_2$ at the two wavelengths. For these experiments, Table I lists the initial N_2O pressure, exposure time, the percentage of N_2O decomposed, the percentage of products formed and the above-mentioned ratios. Table II shows a comparison of the average value of these ratios for the present work, for N_2O at 1470 A[1] and for Noyes' results.[2] These figures suggest rather strongly that the photolysis at 1849 A leads to the same reaction mechanism as does that at 1470 A. This similarity has already been suggested[1] and can be considered as evidence supporting the potential energy diagram of N_2O worked out previously.[3]

The effect of added oxygen on the quantum yield of N_2O should be negligible since O_2 dissociation is slight at 1849 A.[5] The absence of an O_2 effect was confirmed experimentally in this work. The effect of added N_2 was also negligible, since N_2 does not absorb 1849 A light. The amount of NO produced in these reaction mixtures was low, since the extent of decomposition of N_2O was usually kept <10 percent. Also NO was found experimentally to decompose very much more slowly than does N_2O for these wavelengths. It is not surprising therefore that added NO was found to be without effect on the rate of N_2O decomposition, provided the added NO did not exceed a few percent of the total gases present.

It has been pointed out that the N_2O photolysis data at 1470 A can be accounted for on the basis of steps (1) to (4) and that the mechanism at 1849 A is similar. It is, therefore, interesting to examine the data of Noyes[2] considering that $\phi N_2=1.4$, the value given by the present work rather than $\phi N_2=1$, the value assumed by Noyes. According to the latter,

$$\phi N_2+\phi NO=1.9. \quad \text{(a)}$$

Inserting our value for ϕN_2, we find $\phi NO=0.5$. Also according to Noyes,

$$\phi N_2O=\phi N_2+\tfrac{1}{2}\phi NO. \quad \text{(b)}$$

Therefore, we arrive at $\phi N_2O=1.65$. Finally, ϕO_2 can be calculated as $\simeq 0.58$.

Thus, by inserting $\phi N_2=1.4$ into Noyes' data, ϕN_2O and ϕO_2 are found to be practically identical with the values of this work. The value $\phi NO=0.5$ agrees fairly well with the average value of this work. Good agreement should not be expected here since we found ϕNO to be pressure dependent, whereas Noyes did not.

Further examination of the data in this paper suggests that it is possible to estimate from it the approximate value of the absorption coefficient (α) of N_2O, where α is defined by $I/I_0=\exp(-\alpha x)$. x is the layer thickness of N_2O reduced to NTP. Since the absorbing path length varies in the lamp and since some indeterminate errors may exist in the absolute value of the pressure measurement, one cannot expect very much accuracy. Probably the largest error is that occasioned by the measurement of I_0, the intensity of light entering the gas. The number of N_2O molecules decomposed per second was used as a measure of the number of quanta absorbed per second, and this was plotted against N_2O pressure. The resulting exponential curve was extrapolated approximately to "infinite" pressure

TABLE II. Comparison of quantum yield ratios.

	$\phi N_2O/\phi N_2$	$\phi N_2O/\phi O_2$	$\phi N_2O/\phi NO$
This work	1.24 ± 0.07	3.47 ± 0.2	pressure dependent
N_2O at 1470 A	1.2	3.4	pressure dependent
Noyes	1.45	5.3	no pressure dependence

[5] Watanabe, Inn, and Zelikoff, J. Chem. Phys. **21**, 1026 (1953).

at which the light should be completely absorbed and the value for I_0 determined as the number of quanta absorbed per second when absorption is complete. The intensity of light transmitted by the gas I can be measured by subtracting from I_0 the number of quanta absorbed per second (ΔI). ΔI can be easily calculated at each pressure from the product of the pressure and percent decomposition. Thus, taking the average absorbing path length as 5 cm, it is possible to calculate the absorption coefficient. It must be noted here that all runs used for these calculations are of 300 seconds duration. The average of 21 values of α (in cm^{-1}) is 5.1 ± 0.5. This value can be compared to the value 3.7 cm^{-1} at 1849 A measured previously.[3] Considering the nature of the calculation, particularly the I_0 extrapolation, the agreement is surprising. Moreover, the value 5.1 is the integrated value of several lines. The agreement must be considered as evidence supporting the contention that the "active" light in these experiments consists primarily of 1849 A and that the amount of 2537 A absorbed is negligible.

IV. CONCLUSIONS

Comparison of the data on N_2O photolysis at 1849 A with that at 1470 A shows that a strong similarity exists between the decomposition mechanisms at the two wavelengths. Thus the evidence suggests that the initial act of absorption leads to N_2+O and that the NO produced arises from the action of oxygen atoms on N_2O. Insertion of the value $\phi N_2=1.4$ into the data of Noyes results in values of ϕN_2O, ϕO_2, and ϕNO in good agreement with those of the present work.

THE JOURNAL OF CHEMICAL PHYSICS VOLUME 22, NUMBER 10 OCTOBER, 1954

Application of the Hertz Theory of Impact to Explosion Phenomena

M. P. MURGAI
Defence Science Laboratory, N.P.L. Buildings, Pusa, New Delhi-12, India
(Received March 8, 1954)

Pressure and time of impact have been calculated by Hertz theory of impact, taking data from some experiments on explosion. The calculated temperature rise, by adiabatic compression of an entrapped gas bubble, is within a reasonable range of that obtained experimentally. The calculated times have been compared with experimental observations on impact explosion delays. The adiabatic compression of solids has been referred to.

1. INTRODUCTION

FROM their well-controlled experiments on the mechanism of the initiation of explosion Bowden *et al.*[1] have concluded that the explosion always starts from a local hot spot formed inside the body of the explosive. The hot spot may result from, among other causes such as viscous heating, rubbing against a grit particle, etc., the adiabatic compression of an entrapped gas bubble. Very often in these experiments a thin layer of the explosive is placed between two steel blocks, and a striker is thrown from different heights until the explosion occurs. When the explosive is disposed on the anvil in such a manner as to enclose an air bubble (e.g., in a ring or a parallel layered formation), or when no special precautions are taken to make it free from one (in which case some air is always likely to be present), the impact energies required for explosion are small as compared to those in observations on samples "absolutely" free from air. In the latter case the mechanism of hot spot formation supposed to be operative is that of viscous heating, while in the former the temperature rise is presumably due to the passage of a pressure pulse through the explosive, which causes adiabatic compression. Though there have been some general attempts to estimate the pressures obtained under these conditions, there seems to be no straightforward calculation. For example, Gray[2] made measurements of pressures resulting from cavity strikers with a piezoelectric gauge, etc. Eirich and Tabor[3] calculated the value of the pressure obtained in a liquid film enclosed between flat surfaces. An assessment of the upper limit of the pressures, reached on impact, has been made from considerations of flow strength of metals.[4] Simple observations on colliding surfaces reveal that plastic deformation occurs at the point of impact, from which it would appear that very high pressures—amounting to yield pressure of metals—are produced there. The pressures reached at the region of impact are very high, but those acting on the explosive under the upper steel block are obviously different. We report here some calculations on the estimates of these pressures. Strictly speaking, they would entail the knowledge of the nature of the plastic deformation of the impacting surfaces in these experiments on explosion. In the

[1] F. P. Bowden and A. D. Yoffe, *The Initiation and Growth of Explosion in Liquids and Solids* (Cambridge University Press, New York, 1952).

[2] P. Gray, Research (London) **2**, 392 (1949).

[3] F. R. Eirich and D. Tabor, Proc. Cambridge Phil. Soc. **44**, 566 (1948).

[4] F. P. Bowden and D. Tabor, *The Friction and Lubrication of Solids* (Oxford University Press, New York, 1950).

absence of any such detailed information, this has been investigated on the basis of the Hertz theory of impact, which essentially applies to elastic collisions.

2. HERTZ THEORY OF IMPACT*

The time of impact τ between a sphere and a plane is given by

$$\tau = 2.9432\alpha_1/v, \tag{1}$$

where v is the velocity of approach of the ball, $\omega r!$ the plane, and

$$\alpha_1 = \left[\frac{15\pi v^2(\phi_1+\phi_2)m_1m_2}{16(m_1+m_2)}\right]^{2/5}\left(\frac{1}{r_1}\right)^{1/5}.$$

r_1 is the radius of the spherical ball, m_1 its weight, m_2 the weight of the anvil, and

$$\phi_1+\phi_2 = \frac{2(1-\sigma)^2}{\pi V_c^2\rho(1-2\sigma)}.$$

σ is the Poissons ratio of the material of which the ball and the anvil are made (assumed to be the same in this case, namely steel) ρ the density, and V_c the velocity of the compression waves, given by

$$V_c = \left(\frac{k+(4/3)\mu}{\rho}\right)^{\frac{1}{2}}.$$

Here k is the volume elasticity and μ the shear modulus. If F is the force of impact and A is the area of the anvil, the pressure acting on the explosive p_a is given by

$$p_a = \frac{4a^3}{3\pi r_1 A(\phi_1+\phi_2)}, \tag{2}$$

where a is the radius of the circle of contact and is equal to $(\alpha_1 r_1)^{\frac{1}{2}}$. The pressure p_i acting at the point of impact is very large indeed, and becomes known from considerations relating to F and a. If the upper anvil is not there and the striker falls on the explosive directly, p_i gives the order of pressure acting on the explosive. The exact determination will entail the knowledge of the elastic as well as the plastic properties of the explosive. The results reported here relate to the calculation of p_a.

TABLE I.

Explosive	Weight of ball in gm	Height of fall in cm	Time of impact, calc μsec	Impact explosion time, obs μsec	Pressure of impact, calc atmos	Rise in temperature °C Calc	Obs
	1860	18.0	167	···	27.0 (Spread as a ring)	497	460–500
		40	157	···	43.6 (Spread as a continuous layer)	610	
PETN (5,6)	1860	60	148	131	···	···	
	530	155	145	65	···	···	
	250	180	150	103	···	···	
Nitroglycerine[a]	112	[b]	···	···	15.0	348	450–480
Mercury fulminate[c]	225	100	160	100	64.3 Efficiency >50%	714	630–690

[a] A. Yoffe, Proc. Roy. Soc. (London) **A198**, 373 (1949).
[b] This result has been calculated from a graph between efficiency and temperature.
[c] F. P. Bowden and O. A. Gurton, Proc. Roy. Soc. (London) **A198**, 350 (1949).

* For details see Love, *The Mathematical Theory of Elasticity* (Dover Publications, New York), p. 198.

TABLE II.

Substance	$\Delta T \times 10^4$ °C
Copper	4
Sodium	58
Glycerine	53
Toluene	223

3. RESULTS AND DISCUSSION

Having calculated the pressure p_a by Eq. (2) the temperature rise by adiabatic compression of an entrapped gas bubble can be calculated by the relation

$$T = T_0\left(\frac{p_a}{p_0}\right)^{(\gamma-1)/\gamma}, \tag{3}$$

where p_0, T_0 are the original pressure and temperature, and γ is the ratio of the specific heats of the gas concerned. The results of calculation are shown in Table I. The source of data in each case is mentioned underneath the explosive.

The results for PETN and nitroglycerine refer to 50 percent efficiency, while those for mercury fulminate are presumably for greater explosion efficiency. The data available on other explosives are not suited to this treatment. These calculations give, therefore, for cases where efficiency of explosion is 50 percent, a value for the pressure which will result (by the adiabatic compression of a gas bubble) in a temperature rise that is within reasonable range of the minimum temperature (given in the last column) required for explosion as found out experimentally by volume compression.[5] In the present attempt no account of the effect of squeezing out of the explosive layer between the two anvils has been taken, as was done by Eirich and Tabor.[3] During this process some greater pressures will be developed (the upper anvil here corresponds to the hammer in reference 3). As this effect is more marked in the case of liquids than solids, this would explain the low value of the pressure obtained in the case of nitroglycerine.

Comparison of the calculated time of impact with the impact explosion delay measured experimentally, as given above, incidentally confirms the experimental observation made by Rideal and Robertson[6] regarding the fact that the explosion always precedes rebound in these experiments.

[5] F. P. Bowden and O. A. Gurton, Proc. Roy. Soc. (London) **A198**, 337 (1949).
[6] E. K. Rideal and A. J. B. Robertson, Proc. Roy. Soc. (London) **A195**, 135 (1948).

4. ADIABATIC COMPRESSION OF SOLIDS

Having calculated the temperature rise by adiabatic compression of an entrapped gas bubble by pressures obtained in these impact experiments, it is of interest to estimate the increase in the temperature of the explosive itself, under similar conditions. We give in Table II the temperature rise per atmosphere caused by adiabatic compression of some of the liquids and solids. If S be the entropy, and pressure and temperature be regarded as independent variables, we have

$$dS=\left(\frac{\partial s}{\partial p}\right)_T dp+\left(\frac{\partial s}{\partial T}\right)_p dT. \tag{4}$$

For an adiabatic process, by virtue of the following thermodynamic relations

$$\left(\frac{\partial s}{\partial \mathrm{T}}\right)_p=\frac{C_p}{T},$$

$$\left(\frac{\partial s}{\partial p}\right)_T=-\left(\frac{\partial V}{\partial T}\right)_p,$$

we have the rise in temperature ΔT per atmosphere given by

$$\Delta T=\frac{7.262\alpha}{\rho C_p},$$

where α is the coefficient of cubical expansion, ρ the density, and C_p the specific heat in Cal/gm/deg. The value of ΔT given in Table II, is quite small, a fact perhaps also obvious intuitively. But it makes the problem theoretically complete, as it were, in the sense that it shows that the temperature rise of the solid or the liquid explosive alone, by pressures obtained in these experiments, is never more than a few degrees, thus supporting the hypothesis that the presence of an entrapped gas bubble gives rise to the optimum temperature required for explosion. The value of α for explosives is not available, but this value of ΔT would give the correct order of the rise in temperature even in explosives.

The author is grateful to Professor D. S. Kothari, Scientific Adviser to the Ministry of Defence, Government of India, for his suggestions, interest, and permission to publish this work.

THE JOURNAL OF CHEMICAL PHYSICS VOLUME 22, NUMBER 10 OCTOBER, 1954

Electron Trap Distributions in Phosphors

J. M. HONIG
Department of Chemistry, Purdue University, Lafayette, Indiana
(Received April 8, 1954)

The possible interpretation of long lifetime phosphorescence decay in terms of the electron trap mechanism is briefly reviewed. It is then shown how the distribution of activation energies among filled traps may be computed from the experimentally observed decay curves. The decay curves can be expressed as a Laplace transform of the distribution density function for activation energies, and the latter can then be calculated by inversion of the transform. Several examples are given in illustration of the procedure. The limitations inherent in the procedure are briefly discussed, and it is pointed out how the method might be used to test the applicability of the simple electron-trap model to experimental data.

1. INTRODUCTION

LONG lifetime phosphorescence in ionic crystals can be interpreted by several alternative mechanisms.[1] One of these postulates the existence of "electron traps" in the solid. It is supposed that upon (optical) excitation of the crystal these traps are filled by electrons originally associated with luminescence centers. If the excitation source is removed, the electrons remain localized about the trap until they acquire sufficient thermal energy to effect a transfer into the conduction band. From there they undergo (possibly via intermediate stages) a radiative transition into the ground state of an empty luminescence center.

Usually it is assumed that the rate of radiative transition into the ground state is much faster than the rate of occurrence of the activation step which raises the electron from the trap into the conduction band. Also it is assumed that retrapping effects may be neglected.[1,2] Under these conditions the intensity of phosphorescence is governed by the rate of activation.

Using this very simple model it may be shown[2] that the intensity of the afterglow radiation decreases with time according to the relation

$$I_\epsilon=Cn_0b_0e^{-\epsilon/kT}\exp(-b_0te^{-\epsilon/kT}) \tag{1}$$

where C is a constant, n_0 is the number of filled electron traps at time $t=0$, b_0 is the attempt frequency for escape of a trapped electron, ϵ the activation energy (i.e., the distance on the energy scale between the electron trap level and the bottom level of the conduction

[1] See, for example, H. W. Leverenz, *Introduction to Solid Luminescence* (John Wiley and Sons, Inc., New York, 1950).

[2] J. T. Randall and M. H. F. Wilkins, Proc. Roy. Soc. (London) **A184**, 390 (1945).

band), and T is the absolute temperature. The attempt frequency b_0 is a function of temperature but is assumed independent of t or ϵ.[3,4]

The foregoing theory predicts an exponential decrease of I with time. Deviations of experimental data from the exponential decay law can be attributed to two causes. Either the mechanism just outlined is not applicable[5–7] or else the deviation arises from the fact that different traps are associated with different energy levels. Under the latter alternative Eq. (1) represents the contribution to the total intensity due to electrons localized at traps of energy ϵ. The over-all contribution is obtained by summing terms of this type; in the limit of a continuous distribution of activation energies among traps one finds

$$I(t,T)=\int_0^\infty Cb_0e^{-\epsilon/kT}\exp(-b_0te^{-\epsilon/kT})N(\epsilon)d\epsilon, \quad (2)$$

where $N(\epsilon)d\epsilon$ is the number of filled traps associated with an activation energy in the range ϵ to $\epsilon+d\epsilon$. $N(\epsilon)d\epsilon$ is not necessarily the number of available traps in that energy range since not all traps may have been filled in the excitation process.

We must further take account of the restriction

$$N_0=\int_0^\infty N(\epsilon)d\epsilon, \quad (3)$$

where N_0 is the total number of filled traps upon cessation of the excitation process.

The purpose of this paper is to show how the unknown distribution density function $N(\epsilon)$ can be calculated by inversion of the integral (2), once the function $I(t,T)$ is specified from the experimental data. It is hoped that these calculations will aid in deciding whether deviations of experimental data from exponential decay laws are compatible with a distribution of ϵ values among traps or whether a different model must be chosen to explain the data.

The customary procedure in the past has been to use trial functions for $N(\epsilon)$ on the right-hand side of Eq. (2), to carry out the indicated integrations, and to compare the calculated functions I with that observed experimentally.[2,8] The method discussed below eliminates the trial and error procedure, indicates conditions of uniqueness and applicability of the method, and provides for an interpretation of empirical constants in the analytic representation of the experimental data.

[3] N. F. Mott and C. W. Gurney, *Electronic Processes in Ionic Crystals* (Oxford University Press, New York, 1948), second edition.
[4] F. E. Williams and H. Eyring, J. Chem. Phys. **15**, 229 (1947).
[5] V. V. Antonov-Romanovskii, Doklady Akad. Nauk. SSSR **85**, 517 (1952).
[6] V. V. Antonov-Romanovskii, Bull. acad. sci. USSR Sér. phys. **10**, 554 (1946).
[7] For review of other models, see also references 1, 3, 4.
[8] D. Curie, Compt. rend. **229**, 193, 1321 (1949).

2. FORMALISTIC INVERSION

We suppose that the experimentally observed phosphorescence decay curve has been fitted by some empirical function $I(t,T)$. To invert the integral (2) introduce the change in variable

$$Z=e^{-\epsilon/kT} \quad (4)$$

into (2) and write

$$J(t,T)=\frac{I}{Cb_0kT}=\int_0^1 e^{-b_0tZ}F(Z)dZ, \quad (5)$$

where

$$F(Z)=N(-kT\ \ln Z). \quad (6)$$

Now let

$$s=b_0t; \quad (7)$$

then

$$K(s)=\int_0^1 e^{-sZ}F(Z)dZ=J(s/b_0,T). \quad (8)$$

It becomes convenient at this point to introduce a function $F_1(Z)$ defined by

$$K(s)=\int_0^\infty e^{-sZ}F_1(Z)dZ=\mathfrak{L}\{F_1(Z)\}. \quad (9)$$

In Eq. (9), $K(s)$ is known as the Laplace transform of $F_1(Z)$, as indicated by the symbolic relation on the right-hand side. The motivation for the introduction of Eq. (9) is that standard mathematical procedures are available for the determination of $F_1(Z)$ once the function $K(s)$ is specified.[9–11] In such operations s is regarded as a complex variable; the inversion of Eq. (9) can be shown to lead to the relation

$$F_1(Z)=\frac{1}{2\pi i}\lim_{\beta\to\infty}\int_{\gamma-i\beta}^{\gamma+i\beta}e^{Zs}K(s)ds=\mathfrak{L}^{-1}\{K(s)\}, \quad (10)$$

where $F_1(Z)=\mathfrak{L}^{-1}\{K(s)\}$ is known as the inverse Laplace transform of $K(s)$. Under suitable conditions, $F_1(Z)$ can alternatively be specified as a sum of the residues of the function $e^{Zs}K(s)$. For a thorough discussion of these matters the reader is referred to the standard treatises.[9–11] Fortunately, it is seldom necessary to carry out actual computations, since tables are available in the literature[9,10] which correlate the functions $K(s)$ and $F_1(Z)$.

Use will be made of the tabulated results in the examples to be given below.

Since $F_1(Z)$ is presumed to be available from tables after specification of the function $K(s)$, there remains only the task of finding the desired distribution function $F(Z)$. Comparison indicates that Eq. (9)

[9] R. V. Churchill, *Modern Operational Mathematics in Engineering* (McGraw-Hill Book Company, Inc., New York, 1944).
[10] G. Doetsch, *Theorie und Anwendung der Laplace-Transformation* (Verlag Julius Springer, Berlin, 1937).
[11] D. V. Widder, *The Laplace Transform* (Princeton University Press, Princeton, 1941).

reduces to Eq. (8) upon setting

$$F_1(Z)=F(Z) \text{ for } 0\leqslant Z\leqslant 1, \quad (11a)$$
$$=0 \quad \text{for } Z>1. \quad (11b)$$

Concerning uniqueness, there exists a theorem to the effect that any two functions with the same Laplace transform differ by at most a null function $F_0(Z)$ such that $\int_0^Z F_0(t)dt=0$. For most applications this represents a very mild restriction. Thus, if a $K(s)$ is specified for which $F_1(Z)$ is of the form (11), such a solution is essentially unique; hence $F(z)$ is determined except for the possible presence of null functions.

Before discussing the implications of the above method, a few examples are cited in illustration of the inversion procedure.

3. EXAMPLES

Suppose the experimental decay curve is found to be of the form

$$I=(ACkT/t)[\exp(-b_0te^{-\epsilon_m/kT})-e^{-b_0t}]; \quad (12)$$

then

$$K(s)=Ae^{-Z_ms}/s-Ae^{-s}/s, \quad (13)$$

where

$$Z_m=e^{-\epsilon_m/kT}. \quad (14)$$

Use is now made of the theorem that if $F_1(Z)=\mathfrak{L}^{-1}\{f(s)\}$ is the inverse Laplace transform of $f(s)$ then the function

$$\begin{cases} F_1(Z-b) & (Z\geqslant b) \\ 0 & (0\leqslant Z<b) \end{cases} \quad (15)$$

is the inverse Laplace transform of $e^{-bs}f(s)$. Since $\mathfrak{L}^{-1}\{A/s\}=A$ for $Z\geqslant 0$, it follows that inversion of Eq. (13) yields

$$F_1(Z)=\begin{cases} A & \text{for } Z\geqslant Z_m \\ 0 & \text{for } 0\leqslant Z<Z_m \end{cases}-\begin{cases} A & \text{for } Z\geqslant 1 \\ 0 & \text{for } 0\leqslant Z<1; \end{cases} \quad (16)$$

i.e., one obtains the step function

$$F_1(Z)=\begin{cases} A & \text{for } Z_m\leqslant Z\leqslant 1 \\ 0 & \text{otherwise} \end{cases}. \quad (17)$$

Equation (17) identically fulfills requirement (11b) and thus represents an acceptable distribution function. Use of relations (11a), (4), (6), and (14) leads to the desired distribution function in terms of ϵ.

$$N(\epsilon)=\begin{cases} A & \text{for } 0\leqslant\epsilon\leqslant\epsilon_m \\ 0 & \text{otherwise.} \end{cases} \quad (18)$$

The constant A can be determined by use of the normalization condition (3). In the limit as $\epsilon_m\to\infty$, relations (12) and (18) reduce to those derived by Randall and Wilkins.[2] It is impossible, however, to maintain a uniform trap distribution over an infinite energy range without having an infinite number of traps available; use of the limit $\epsilon_m=\infty$ in these relations is therefore unrealistic. The example also illustrates that the upper and lower limits on ϵ are determined by the parameters appearing in the representation of $I(t,T)$; in this instance the parameter ϵ_m of Eq. (12) is the upper limit of the energy ϵ.

As a second example, one might examine the relation

$$I(t,T)=(ACkT/b_0t^2)[\exp(-b_0te^{-\epsilon_m/kT}) \times(1+b_0te^{-\epsilon_m/kT})-e^{-b_0t}(1+b_0t)] \quad (19)$$

which reduces to

$$K(s)=(AZ_m/s)e^{-sZ_m}-(A/s^2)e^{-sZ_m} -(A/s)e^{-s}-(A/s^2)e^{-s}. \quad (20)$$

According to the tabulated results, $F_1(Z)=\mathfrak{L}^{-1}\{A/s^2\}=AZ$. Use of the theorem cited in conjunction with Eq. (15) then leads to the function

$$\begin{aligned} F_1(Z)=&\begin{cases} AZ_m & Z\geqslant Z_m \\ 0 & \text{for } 0\leqslant Z<Z_m \end{cases} \\ &+\begin{cases} A(Z-Z_m) & Z\geqslant Z_m \\ 0 & \text{for } 0\leqslant Z<Z_m \end{cases} \\ &-\begin{cases} A & Z\geqslant 1 \\ 0 & \text{for } 0\leqslant Z<1 \end{cases} \\ &-\begin{cases} A(Z-1) & Z\geqslant 1 \\ 0 & \text{for } 0\leqslant Z<Z_m \end{cases} \\ =&\begin{cases} AZ & \text{for } Z_m\leqslant Z\leqslant 1 \\ 0 & \text{otherwise.} \end{cases} \end{aligned} \quad (21)$$

Here, the requirement (11b) is again identically fulfilled and thus $F(Z)=AZ$ in the range $Z_m\leqslant Z\leqslant 1$. Converting to $N(\epsilon)$ one obtains the exponentially decreasing distribution

$$N(\epsilon)=Ae^{-\epsilon/kT} \quad (0\leqslant\epsilon\leqslant\epsilon_m). \quad (22)$$

Again, A can be determined by use of Eq. (3). It is to be noted also that the parameters of Eq. (19) determine the range of ϵ values.

4. DISCUSSION

The application of the mathematical techniques described above is subject to several restrictions. (a) To insure that the inversion integral (10) converges to $F_1(Z)$ irrespective of the choice of γ, it is sufficient to impose the requirement that $K(s)$ be analytic and of order s^{-k} in some half-plane $R(s)\geqslant\gamma_0$ where $\gamma_0\leqslant\gamma$ and $k>1$ are real constants. (b) Equation (11) or comparison of Eqs. (8) and (9) shows that if a function $K(s)$ is to be correlated with the distribution of traps $F(Z)$ then the condition $F_1(Z)=0$ for $Z>1$ must hold. Requirement (11b) imposes a very severe restriction on

the class of functions capable of inversion to $F(Z)$. This class is limited to those functions $K(s)$ whose inverse Laplace transform automatically vanishes in the range $Z>1$. Clearly, if the experimental data lead to functions $K(s)$ which do not satisfy conditions (a) and (b) then such data cannot be interpreted in terms of the electron trap mechanism described in the introduction. In some cases it may thus be possible to rule out the applicability of this mechanism on a purely mathematical basis. The physical interpretation of condition (11b) is that any decay curve leading to an electron trap distribution which involves negative values of ϵ must be ruled out.

By way of illustration it might be noted that the hyperbolic decay law $I=ACkT/t$ is not compatible with the mechanism of Sec. 1. For, while the corresponding inverse Laplace transform is easily shown to be $F_1(Z)=A$, the inversion procedure imposes no restriction on Z other than $Z\geqslant 0$. Condition (11b) is therefore violated, and it is incorrect to set $F(Z)=A$. This fact may be verified by substituting A for $F(Z)$ in Eq. (5); it is found that the integral does not converge to the hyperbolic decay law.[12] Similar remarks apply to the attempted use of the "ideal bimolecular decay law" $I=ACkT/b_0t^2$.

If the empirical decay curve obeys conditions (a) and (b) it may be possible to pass judgment on the applicability of the mechanism by examining the parameters involved in the calculations. For example, if the phosphorescence decay data follow Eq. (12) and if the electron trap mechanism is to apply then the "decay constant" $b_0e^{-\epsilon_m/kT}$ for the first exponential term in the bracket can be determined from the decay curve. A check on the calculations is provided by ascertaining whether or not this constant obeys the predicted temperature dependence. Assuming this is the case, ϵ_m can now be evaluated by curve fitting. Should this lead to unreasonable results, the applicability of the mechanism is clearly in doubt. A second check is provided by computing N_0 according to Eq. (3) using the values A and ϵ_m obtained from Eq. (12). This calculated quantity N_0 may be compared to the number of impurity centers deliberately introduced into the phosphors. Any large discrepancies occurring here would clearly constitute an internal inconsistency in the mechanism.

It should be pointed out that the mathematical procedure must be applied with caution, the reason being that $F(Z)$ and $K(s)$ are related by an integral equation. Integration always represents a "smoothing out" process. Thus the distribution function $F(Z)$ may assume a variety of different functional forms without appreciably affecting the function $K(s)$. Conversely, $K(s)$ must be known with great precision in order that the computations will yield the correct distribution function $F(Z)$. This means that the experimental data must show a minimal amount of scatter, and also that the empirical decay curve $I(t,T)$ must fit the experimental data very closely over a wide range of experimental conditions. Undoubtedly, one of the chief obstacles in the application of the theory is the difficulty of deciding which of a variety of possible interpolation equations $I(t,T)$ best represent a set of data. It may likewise be extremely difficult to ascertain whether the experimental points can or cannot be represented by an acceptable $K(s)$ function which satisfies conditions (a) and (b).

[12] The expression $I=ACkT/t$ is regained only by using ∞ as the upper limit in Eq. (5): this choice involves the physically unacceptable region $\epsilon<0$.

5. ACKNOWLEDGMENT

It is a pleasure to acknowledge the helpful criticism of the manuscript by Mrs. Henry Feuer.

Fluorescence of Nitrogen Dioxide*

DAN NEUBERGER† AND A. B. F. DUNCAN
Department of Chemistry, University of Rochester, Rochester, New York

(Received January 22, 1954)

The mean lifetime of fluorescence of NO_2 vapor was measured at pressures in the range 12 to 0.6 microns by a direct electronic method. A linear dependence of lifetime on pressure was found, and extrapolation to zero pressure gave 44 microseconds for the lifetime in absence of collisions. The fluorescence spectrum in the region 4600–8000 A was photographed with 4358 and 5461 A excitation, with somewhat different results. Interpretation of the results appears to require two excited electronic levels, one of which is not connected optically with the normal state and which is responsible for the long-lived fluorescence.

THE fluorescence of NO_2 has been studied previously by Norrish[1] and by Baxter,[2] and their principal results may be summarized briefly as a background for the present work. Norrish found that the fluorescence spectrum excited either by 4358 A or 4070 A consisted mainly of two broad bands, with approximate wavelengths 5600–6050 A and 6250–6550 A, and a few less intense, narrow bands in the blue region. He observed also that the second fluorescence band was excited preferentially by 4358 A while the first band was excited preferentially by 4070 A. These observations will be discussed in a later section, since they are not supported by results of the present work. The quantum yield of photochemical decomposition is negligible above 4000 A. Baxter measured the fluorescence yield with 4070 and 4358 A excitation, and studied the quenching of fluorescence by NO_2 itself, and by other gases. The former process was shown to be more effective, and quenching was shown to follow a Stern-Volmer mechanism. Baxter obtained a value for the product $\sigma^2\tau$, where σ is the cross section for quenching, and τ is the mean lifetime of the state from which fluorescence occurred. He assumed that $\tau=10^{-7}$ sec, corresponding to an allowed transition, and obtained a cross section about ten times the kinetic theory value. However Heil[3] showed subsequently that $\tau=10^{-5}$ sec by a diffusion method.

The purpose of the present work was to obtain direct measurements of τ for NO_2, excited to fluorescence under various conditions, and to obtain photographs of the fluorescence spectrum under comparable conditions. It was hoped that such measurements would lead to a better understanding of the nature of the electronic state, or states concerned with the fluorescence. Photographs showing details of the absorption spectrum in the region 4300–9000 A were not available, and the spectrum was rephotographed at various pressures, but it was not possible to make any additional contribution toward the interpretation of this spectrum.

EXPERIMENTAL DETAILS

The equipment for the most part was conventional, and it will be described only briefly. The NO_2[4] was claimed to have a minimum purity of 99 percent, with 0.01 percent H_2O and lower nitrogen oxides as the only impurities. These impurities were removed by drying with P_2O_5, and vacuum pumping and distillation at -80°C. The purified solid was completely white, and it was kept at all times at -80°C, covered with black felt to avoid possible photodecomposition. NO_2 vapor from this solid was handled in a mercury-free vacuum system. Apiezon-N grease was satisfactory for the lubrication of stopcocks at the low pressures of NO_2 used here. Low pressures were measured directly with a calibrated quartz gauge;[5] higher pressures were obtained by immersion of the solid in constant low temperature baths, and the NO_2 pressure was estimated from the total vapor curve[6] of $NO_2-N_2O_4$, and the equilibrium data[7] for this system. There was no interference of N_2O_4 in any of these experiments, either because of the low total pressure, or because of low absorption coefficients of N_2O_4 at the wavelengths used.

LIFETIME MEASUREMENTS

The method of Kaskan and Duncan[8] was used to obtain single flashes of about 5 μsec duration. A 1 μf capacitor was fully charged to 10 000 v and discharged between tungsten electrodes 7.5 cm apart through a 3 mm i.d. quartz tube filled with argon at 4 cm pressure. Light from the flash was filtered by the combinations shown in Table I, and entered a glass cell containing freshly purified NO_2. The fluorescence emerged through a plane end window at 90° to the incident light, and was received by a 931 A photomultiplier tube, selected for high sensitivity. A Corning 3484 filter was placed

* This work was supported in part under Contract N6onr-241, Task Order X, with the U. S. Office of Naval Research, and under Contract DA-30-115-ORD-295 with the Office of Ordnance Research.

† Part of a dissertation presented to the Faculty of the Graduate School of the University of Rochester in partial fulfillment of the requirements for the degree of Doctor of Philosophy.

[1] R. G. W. Norrish, J. Chem. Soc. 1611 (1929).
[2] W. P. Baxter, J. Am. Chem. Soc. **52**, 3920 (1930).
[3] O. Heil, Z. Physik **77**, 563 (1932).
[4] Obtained from the Matheson Company.
[5] A. S. Coolidge, J. Am. Chem. Soc. **45**, 1637 (1923).
[6] W. F. Giauque and J. D. Kemp, J. Chem. Phys. **6**, 40 (1938).
[7] F. H. Verhoek and F. Daniels, J. Am. Chem. Soc. **53**, 1250 (1931).
[8] W. E. Kaskan and A. B. F. Duncan, J. Chem. Phys. **16**, 223 (1948).

TABLE I. Filters for lifetime studies.

Spectral region transmitted	Filter combination	Percent transmitted at maximum
3300–3900 A	Corning No. 5860	30% at 3600 A
3750–4150	Corning Nos. 3060, 4308, 5970	10% at 3950
4050–4700	Corning Nos. 3389, 5113	18% at 4300
4400–5000	Corning Nos. 3387, 5113 (1/2 standard thickness)	12% at 4650
5200–5700	B. and L. interference filter for 5461 A and Wratten No. 55	18% at 5461

between the photomultiplier and end window in most experiments, to absorb all radiation below 5200 A. The output of the photomultiplier was fed to the vertical deflection plates of a DuMont 303 oscillograph, and timing marks were supplied to the horizontal plates. The tracings of decay of fluorescence were photographed on plates, and the coordinates of points on the curves were measured with a precision comparator. The precision was limited by the finite width of the tracings, and duplicate measurements from a trace usually agreed within 0.5 percent.

The mean lifetime τ was obtained as the slope of $\log I - t$ curves, drawn from five to eight points of the decay curves. The $\log I - t$ curves were always straight lines, showing that the decay was exponential, and the precision in τ obtained in this way varied from 0.6 to 4.4 percent.

SPECTROGRAPHIC MEASUREMENTS

Fluorescence spectra were excited in a Raman excitation unit.[9] For 4358 A excitation, the sample tube was surrounded by a double thickness of Wratten 2A gelatin filter, 1 cm of saturated $NaNO_2$ in H_2O, and 2 cm of a solution containing 88 g $CuSO_4$, 200 ml conc. NH_4OH to 750 ml H_2O. This filter combination eliminated effectively all other Hg lines. For 5461 A excitation, 1 cm of 1.5 M $Nd(NO_3)_3$ and 2.5 cm of 1.25 M $CuSO_4$ were used in conjunction with a Wratten No. 55 filter around the sample tube. A Wratten No. 22 filter was placed before the spectrograph slit to remove all radiation below 5500 A. A three-prism spectrograph with glass elements (f 2.8 camera lens) was used to record the spectra; the reciprocal dispersion was 37 A/mm at 4358 A and 300 A/mm at 7200 A. Eastman 103a-F and I-N plates were used.

Pressures of NO_2 varied from 1 to 40 mm, and exposure times were from 10 minutes to 4 hours. To show that the spectra observed were all actually due to NO_2, blank experiments were made in which the NO_2 was frozen out in a side trap attached to the fluorescence tube, and exposures were made for comparable times.

For measurement of absorption spectra, the NO_2 was contained in a cylindrical quartz cell, one meter long, with plane windows sealed on, and provided with a side tube for adjustment of pressure. The sides were painted flat black to avoid photodecomposition by extraneous light. A tungsten strip filament lamp was the source, and spectra were recorded with a Bausch and Lomb No. 3027 spectrograph.

[9] Harrison, Lord, and Loofbourow, *Practical Spectroscopy* (Prentice-Hall, New York, 1948), p. 513.

RESULTS

The results on mean lifetime of fluorescence are based on a large number of observations at thirteen different pressures in the range 12 to 0.6 microns. Values of $1/\tau$ were plotted against pressure and a straight line was obtained, which indicates that a Stern-Volmer mechanism is obeyed in this pressure range. The principal results are shown in Fig. 1. Since τ could be measured at pressures as low as 6×10^{-4} mm, an extrapolation to zero pressure probably is justified. The extrapolated value τ_0 represents the mean lifetime in the absence of collisions, and is related theoretically to the transition probability from the fluorescing state to the normal state. τ_0 was found to be 44.5 microseconds, accurate to ±4 percent. The principal error arises from ambiguity in the slope of the plot. Approximately the same lifetime was found with 3950, 4300 and 4650 A exciting radiation. No fluorescence, and hence no lifetime, could be measured with 3600 A excitation. No lifetime trace could be seen with 5461 A excitation, which may be because of insufficient intensity or too short lifetime. It is believed that the latter cause is the true one; it appears that the intensity of fluorescence should have been sufficient.

Excitation of NO_2 at low pressures (about one mm) with 4358 A produces an emission which is apparently continuous at the low resolution used. Emission extends from near the exciting line to about 8000 A, the long

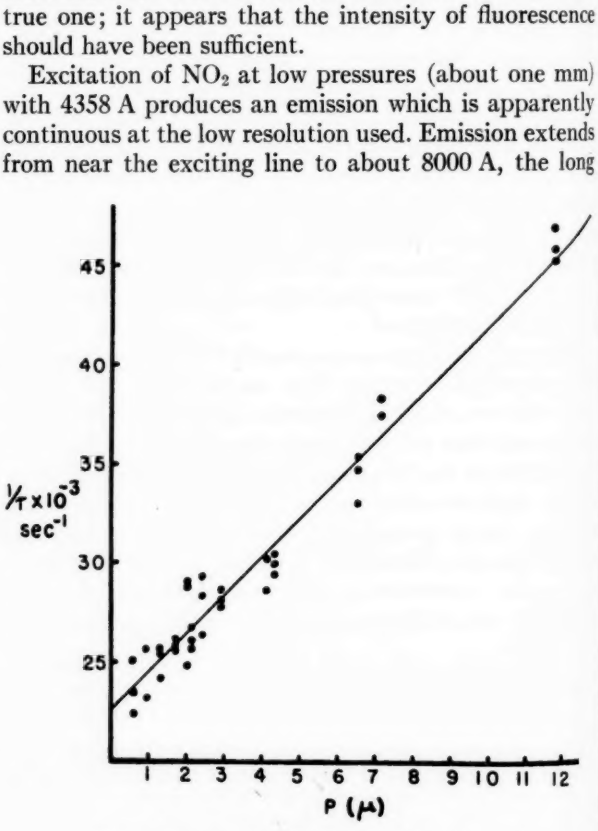

FIG. 1. Reciprocal of lifetime as a function of pressure (in microns).

wave limit of observation. At higher pressures, some of the fluorescence is reabsorbed leading to observation of the usual absorption spectrum against the background of continuous emission. It is interesting to note that the fluorescence spectrum at higher pressures contained the two bands observed by Norrish,[1] but investigation over a wide pressure range showed that the minimum between the two bands corresponded exactly to a maximum in the absorption spectrum. This fact is clear also from an examination of the spectrophotometric data of Dixon.[10] No support could be obtained here for the observation of Norrish that the intensity distribution between the two "bands" (or regions) which he observed in fluorescence was dependent on the wavelength of excitation. Direct measurement by photoelectric methods in the regions of the two "bands" showed that their relative intensities were independent of the wavelength of excitation. It appears that the intensity of emission increases continuously toward longer wavelengths, but this may not be real, because of the difficulties introduced by self-absorption.

Since a continuous fluorescence spectrum is somewhat unusual for such a simple molecule at low pressures, the question of spurious origin was investigated carefully by blank experiments. Blanks with NO_2 completely frozen out, and blanks taken with no NO_2, but air at one atmosphere in the cell, showed that the continuous emission could not be caused by molecular light scattering, or by scattering of filter solutions or other equipment. The emission must be attributed, therefore, to NO_2 or to a possible decomposition product. The possibility that emission originated from recombination of decomposition products was explored. Ultraviolet excitation, which is photochemically active, does not produce any emission, while pure 4358 A, which appears to be completely inactive, produces the emission in question. This is in complete agreement with the work of other investigators. Emission by excited species, either directly or after reabsorption of radiation, appears unlikely for the same reasons. All these observations lead to the conclusion that the fluorescent emission must be attributed to NO_2.

With 5461 A excitation, the over-all intensity is weaker than with 4358 A excitation. An apparently continuous emission, increasing in intensity with wavelength, has superimposed on it six narrow and relatively more intense bands, and two broad indistinct bands whose wavelengths could not be measured. The narrow bands can be interpreted in terms of normal state frequencies,[11] $\nu_1=1322.5$, $\nu_2=750.9$, and $\nu_3=1616.0$. An interpretation is suggested in Table II. The possibility that these narrow bands are not caused by NO_2 fluorescence was investigated. Blank experiments with air in the cell, and with NO_2 frozen out eliminated the possibility of spurious origin or Rayleigh scattering. It is not expected that a Raman spectrum could result from exciting light within the absorption band. The vibrational frequencies do not agree with those reported for N_2O_4. Furthermore, the pressures are too low, and exposures too short, for production of a Raman spectrum of this molecule.

TABLE II. Fluorescence bands excited by 5461 A.

Observed $\Delta\nu$ (cm^{-1}) from 18 313 cm^{-1}	Assignment	Calculated frequencies from preceding column
1343	ν_1	1323
2094	$\nu_1+\nu_2$	2073
2653	$2\nu_1$	2645
2835	$\nu_1+2\nu_2$	2824
3028	$(\nu_1+\nu_3)$?	2938
3393	$2\nu_1+\nu_2$	3396

The absorption spectra obtained here were not suitable for intensity measurements needed for calculation of the transition probability to the electronic state reached by absorption. The data of Hall and Blacet[12] for the region 2600 to 5000 A, and the data of Dixon[10] for the region 5000 to 7000 A were used to obtain the integrated absorption coefficient. The former data give NO_2 absorption separated from N_2O_4 absorption. The absorption coefficients are very small at the extreme wavelengths, and the absorption curve shows a broad maximum near 4000 A. It was assumed that the entire absorption belonged to one electronic transition. The estimated f number is about 0.01, which represents a minimum value, and the corresponding mean lifetime would be 2.6×10^{-7} sec for a purely radiative transition back to the normal state.

DISCUSSION AND CONCLUSIONS

The principal results of the present work may be summarized as follows:

(1) A fluorescence spectrum, apparently continuous at low dispersion, is excited by 4358 A. It begins near the exciting line and extends to the long wave limit of observation at about 8000 A.

(2) The mean lifetime of fluorescence excited by 4358 A is relatively long; the value extrapolated to zero pressure is about 4.4×10^{-5} sec.

(3) The integrated absorption coefficient to the state reached by absorption corresponds to a mean lifetime of about 2.6×10^{-7} sec for a purely radiative transition back to the normal state.

(4) The fluorescence excited by 5461 A is weaker, for equivalent quanta absorbed, and no lifetime could be measured, probably because it was too short.

(5) The fluorescence spectrum excited by 5461 A shows relatively sharp emission bands superimposed on apparently continuous emission.

This discussion proposes to give some explanation of these observations, some of which are apparently conflicting.

[10] J. K. Dixon, J. Chem. Phys. **8**, 157 (1940).
[11] G. E. Moore, J. Opt. Soc. Am. **43**, 1045 (1953).
[12] T. C. Hall, Jr., and F. E. Blacet, J. Chem. Phys. **20**, 1745 (1952).

Little is known definitely about the electronic levels of NO_2 from a theoretical standpoint. The most recent discussion of this subject has been given by Walsh,[13] based on correlation diagrams of molecular orbitals of AB_2 molecules, in which the binding energies of the orbitals are plotted schematically against the angle BAB. The NO_2 molecule is bent to an angle of 134°,[11] and is thus almost exactly midway between a linear and a right-angled form. From Walsh's diagram, the most easily excited electron probably comes from an orbital of symmetry type A_1. Since the ground state has electronic symmetry A_1, the excited states reached by absorption are $^2A_1$, $^2B_1$, and $^2B_2$, but without quantitative calculations no definite predictions can be made about the symmetry type of the lowest excited level. However, it appears from the diagram that a number of states of all symmetries, including $^2A_2$, may lie not far above the ground state. A careful examination of the absorption spectrum and absorption coefficients provides no evidence (abrupt changes in intensity or in spacing) that more than one excited state is below 22 946 cm^{-1} (4358 A). Examination of the partially resolved structure of the absorption shows that there are no strong central maxima in the vibrational transitions, which suggests that the electric moment lies in the direction of the twofold axis. If this is correct, the upper electronic state probably is $^2A_1$.

The fluorescence spectrum and lifetime measurements were obtained at such low pressures that the time between collisions is of the same order of magnitude as the average lifetime of an allowed transition. This means that a large fraction of molecules will fluoresce from the higher vibrational levels reached by absorption before deactivation by collision, and that the fluorescence spectrum will begin near the exciting line. This is observed with both exciting lines. The apparently continuous nature of the fluorescence is ascribed to lack of resolution of emission which comes from a series of closely spaced and partly overlapping upper levels to a similar series of lower levels. This argument is supported by the fact that the absorption spectrum near 4358 A is almost continuous. The appearance of relatively sharp emission bands from 5461 A excitation is ascribed to a more simple absorption spectrum in this region.

No simple explanation can be offered for the fact that the fluorescence is weaker with 5461 than with 4358 A excitation. It is possible that fluorescence is quenched more efficiently at the longer wavelength because of the smaller energy difference between normal and excited molecules. A somewhat artificial argument, which appears necessary, however, to account for the long lifetime of fluorescence with 4358 A excitation, may explain partly the weaker fluorescence with 5461 A. This argument assumes the existence of an additional electronic state with symmetry $^2A_2$ between 18 312 cm^{-1} (5461 A) and 22 946 cm^{-1} (4358 A) above the ground state, probably slightly below 22 946 cm^{-1}. The over-all symmetries of electronic-vibrational levels of this state will be A_2 and B_2, while in the excited state reached by absorption the levels will be A_1 and B_1. It is expected that resonance transfer can occur readily between levels of the A_1 and A_2 excited electronic states, but the optical transition probability back to the ground state will be small, since it is allowed only by the perturbation of a vibration with symmetry B_2 in the upper state. The lifetime of 4.4×10^{-5} sec is a reasonable value for a transition of this nature. Furthermore, molecules in an A_2 state are expected to be fairly resistant to quenching by collision with normal A_1 molecules, which may account partly for the apparently higher efficiency of fluorescence at 4358 A as compared with 5461 A, if it is assumed that molecules excited by the latter wavelength have no opportunity to reach the A_2 level.

But it appears probable that not all of the fluorescence spectrum comes from the A_2 state, and perhaps emission occurs from both A_1 and A_2 states. Emission with two lifetimes, one 2.6×10^{-7} sec and the other 4.4×10^{-5} sec, estimated from the integrated absorption coefficient to the A_1 state, could not have been detected in these experiments. Even when the initial intensity of fluorescence from the A_1 state is many times the intensity from the A_2 state, a decay constant $k(A_1)=1/(2.6\times10^{-7})$ will give only negligible contribution compared with $k(A_2)=1/(4.4\times10^{-5})$ to the measured intensity after a few microseconds, and the decay tracings would appear to be exponential over most of their length.

[13] A. D. Walsh, J. Chem. Soc. 2266 (1953).

THE JOURNAL OF CHEMICAL PHYSICS VOLUME 22, NUMBER 10 OCTOBER, 1954

Thermodynamics of Alcohol-Hydrocarbon Mixtures

CARL B. KRETSCHMER AND RICHARD WIEBE
Motor Fuels Evaluation Section, Northern Utilization Research Branch, Agricultural Research Service, U. S. Department of Agriculture, Peoria, Illinois

(Received April 27, 1954)

The thermodynamic properties of alcohol-hydrocarbon mixtures are explained on the basis of association of the alcohol to form polymers of all orders from two to infinity. Our treatment differs from that of Redlich and Kister in using the Flory-Huggins expression for free energy, and an equilibrium constant in terms of concentrations rather than mole fractions. The equations derived are in satisfactory agreement with vapor-pressure data for several systems. They also agree with the experimental energy of mixing and excess entropy for ethanol-methylcyclohexane solutions. For mixtures of alcohols with aromatic hydrocarbons, it is necessary to assume that each alcohol monomer or polymer can combine with one molecule of hydrocarbon.

I. INTRODUCTION

It is now well-known that the properties of hydrogen-bonding substances such as alcohols may be explained by the concept of "continued association." This means that the substance consists of an equilibrium mixture of single molecules with linear polymers of all orders from two to infinity. The concept of continued association was introduced by Lassettre.[1] Tobolsky and Blatz,[2] Flory,[3] Redlich and Kister,[4] and Scatchard[5] have derived equations for the free energy of mixing with a nonassociating solvent, based on this model. The treatment of Redlich and Kister is the only one which has been compared with experiment. It is quite successful in representing the behavior of methanol in mixtures with various hydrocarbons.

Tompa[6] and Barker[7,8] have initiated a more fundamental attack on the problem by constructing the partition function for the arrangement of molecules on a lattice, when the energy of nearest neighbor interaction depends on the relative orientations of the molecules concerned. Their treatments predict the correct shapes of curves for the excess entropy and heat of mixing of alcohol-hydrocarbon solutions, and Barker[8] has obtained good agreement with the experimental data for methanol-carbon tetrachloride and methanol-benzene solutions. However, the mathematical complexity of these theories is considerable.

It is the purpose of the present paper to investigate whether a simpler treatment based on continued association can predict the free energy, entropy, and heat of mixing of solutions of alcohols in nonassociating solvents. Of course, the concept of association can be regarded merely as a mathematical device for taking into account some of the departures from random spatial and orientational distribution, caused by the intermolecular forces.

[1] E. N. Lassettre, J. Am. Chem. Soc. **59**, 1383 (1937).
[2] A. V. Tobolsky and P. J. Blatz, J. Chem. Phys. **13**, 379 (1945).
[3] P. J. Flory, J. Chem. Phys. **14**, 49 (1946).
[4] O. Redlich and A. T. Kister, J. Chem. Phys. **15**, 849 (1947).
[5] G. Scatchard, Chem. Revs. **44**, 7 (1949).
[6] H. Tompa, J. Chem. Phys. **21**, 250 (1953).
[7] J. A. Barker, J. Chem. Phys. **20**, 794 (1952).
[8] J. A. Barker, J. Chem. Phys. **20**, 1526 (1952).

II. LIST OF SYMBOLS

A	Helmholtz free energy
b	constant in Flory-Huggins equation
c	concentration, moles/ml
E	energy
F	Gibbs free energy
H	enthalpy
K, K', k	equilibrium constants
n	number of moles
R	gas constant
S	entropy
T	absolute temperature
V	volume of one *true* mole of solution
V_x	volume of one stoichiometric mole of solution
v	molal volume
x	mole fraction
α	coefficient of thermal expansion
β	coefficient of compressibility
γ	activity coefficient
ϕ	volume fraction

Subscripts

a	alcohol, stoichiometric
h	hydrocarbon, stoichiometric
0	hydrocarbon, free
1, 2, $\cdots i \cdots$	species consisting of 1, 2, $\cdots i$, $\cdots$ alcohol molecules
$i0$	species consisting of i alcohol molecules and one hydrocarbon molecule
V	constant volume

Superscripts

M	change on mixing
E	excess of property over that of ideal solution
0	property of pure component.

III. DERIVATION OF EQUATIONS

One stoichiometric mole of an alcohol-hydrocarbon solution contains x_a moles of alcohol and x_h moles of hydrocarbon, the alcohol being present as n_1 moles of monomer, n_2 moles of dimer, $\cdots n_i$ moles of i-mer, $\cdots$.

The quantities n_i satisfy the relationship

$$\sum_{i=1}^{\infty} in_i = x_a. \tag{1}$$

The Flory-Huggins equation for the Helmholtz free energy of the solution per stoichiometric mole at constant volume may be written[9]

$$A_V = x_h A_h^0 + RT \ln\phi_h + \sum_{i=1}^{\infty} n_i (A_i^0 + RT \ln\phi_i) + bV_x \phi_h \phi_a. \tag{2}$$

The term $bV_x\phi_h\phi_a$ includes both an energy of mixing and an entropy component. The partial molal free energies obtained by differentiating Eq. (2) are

$$\bar{A}_h = A_h^0 + RT\left(\ln\phi_h + 1 - \frac{v_h}{V}\right) + bv_h\phi_a^2, \tag{3}$$

and

$$\bar{A}_i = A_i^0 + RT\left(\ln\phi_i + 1 - \frac{v_i}{V}\right) + bv_i\phi_h^2. \tag{4}$$

V is the volume of one true mole of solution:

$$\frac{1}{V} = \frac{\phi_h}{v_h} + \sum_{i=1}^{\infty} \frac{\phi_i}{v_i}.$$

For equilibrium in the reaction

$$(\text{alcohol})_{i-1} + \text{alcohol} \rightleftarrows (\text{alcohol})_i, \tag{5}$$

we must have

$$\bar{A}_i - \bar{A}_{i-1} - \bar{A}_1 = 0, \tag{6a}$$

$$RT\left(\ln\frac{\phi_i}{\phi_{i-1}\phi_1} - 1\right) + A_i^0 - A_{i-1}^0 - A_1^0 = 0. \tag{6b}$$

We have assumed that there is no volume change accompanying reaction (5), so that $v_i = iv_1$. Reaction (5), occurring between isolated molecules, is accompanied by a free energy change

$$\Delta A = \Delta E - T\Delta S, \tag{7}$$

which is assumed to be independent of i. For the reaction between the pure polymeric species, there is an additional entropy change of $R\ln(v_i/v_{i-1}v_1)$ which comes from the differences in molal volumes of the polymers. Then

$$RT[\ln(\phi_i/\phi_{i-1}\phi_1) - 1] = -\Delta A + RT\ln(v_i/v_{i-1}v_1),$$
$$RT\ln(c_i/c_{i-1}c_1) = -\Delta A + RT = RT\ln K'. \tag{8}$$

Thus the equilibrium constant for the polymerization reactions is independent of i only if it is written as a ratio of concentrations rather than mole fractions or volume fractions, as was pointed out by Flory.[10] Redlich and Kister's theory[4] differs from ours in using the ideal solution entropy of mixing, and an equilibrium constant expressed in terms of mole fractions.

We can now write

$$c_i = K'c_1c_{i-1} = c_1(K'c_1)^{i-1}, \tag{9}$$

and

$$\phi_a = \phi_1/(1-K\phi_1)^2, \tag{10}$$

where

$$K = K'/v_1. \tag{11}$$
$$1/V = \phi_h/v_h + \phi_a(1-K\phi_1)/v_1.$$

The addition of dn_a moles of alcohol to a solution changes its free energy by the amount $dA = \bar{A}_a dn_a$ and changes the number of moles of each polymeric species present by amounts dn_i such that

$$dn_a = \sum_{i=1}^{\infty} i dn_i.$$

The free energy change can also be written in the form

$$dA = \sum_{i=1}^{\infty} \bar{A}_i dn_i.$$

From Eq. (6a),

$$\bar{A}_i = i\bar{A}_1.$$

Then

$$dA = \sum_{i=1}^{\infty} i\bar{A}_1 dn_i = \bar{A}_1 dn_a,$$

and

$$\bar{A}_a = \bar{A}_1. \tag{12}$$

Thus we have for the partial molal free energies of the alcohol and hydrocarbon

$$\bar{A}_a = A_a^0 + RT\left(\ln\frac{\phi_1}{\phi_1^0} - \frac{v_1}{V} + \frac{v_1}{V^0}\right) + bv_1\phi_h^2, \tag{13}$$

$$\bar{A}_h = A_h^0 + RT\left(\ln\phi_h + 1 - \frac{v_h}{V}\right) + bv_h\phi_a^2. \tag{3}$$

Since the difference between the Helmholtz free energy of mixing at constant volume and the Gibbs free energy

TABLE I. Experimental data and parameters of Eq. (14).

System	Temp., °C	v_1, ml	v_h, ml	K	$\frac{10^3 b}{2.3RT}$
Ethanol-isooctane[a]	50	60.37	171.28	112	1.62
Ethanol-methylcyclohexane[b]	35	59.33	129.83	170	2.12
Ethanol-methylcyclohexane[b]	55	60.73	132.92	100	2.10
Ethanol-toluene[c]	55	60.73	110.48	25	1.70
Methanol-*n*-heptane[d]	59	42.50	154.27	150	3.15

[a] Kretschmer, Nowakowska, and Wiebe, J. Am. Chem. Soc. **70**, 1785 (1948).
[b] C. B. Kretschmer and R. Wiebe, J. Am. Chem. Soc. **71**, 3176 (1949).
[c] C. B. Kretschmer and R. Wiebe, J. Am. Chem. Soc. **71**, 1793 (1949).
[d] Benedict, Johnson, Solomon, and Rubin, Trans. Am. Inst. Chem. Engrs. **41**, 371 (1945).

[9] J. H. Hildebrand and R. L. Scott, *The Solubility of Nonelectrolytes* (Reinhold Publishing Company, New York, 1950), third edition, p. 349.

[10] P. J. Flory, J. Chem. Phys. **12**, 425 (1944).

of mixing at constant pressure is negligible,[11] Eqs. (3) and (13) may be taken as giving the partial molal Gibbs free energies at constant pressure, which are the quantities ordinarily measured. These equations are identical with the equations on p. 31 of Scatchard's paper,[5] with f taken equal to 2, but no application to experimental data was made in that paper.

Equations (3), (11), and (13) give

$$\log\frac{\gamma_a\phi_a}{\gamma_h\phi_1}-\frac{v_h-v_1}{2.3}\left\{\frac{\phi_h}{v_h}+\frac{\phi_a(1-K\phi_1)}{v_1}\right\}-\log\frac{v_1}{\phi_1^0 v_h}+\frac{K\phi_1^0}{2.3}=\frac{b}{2.3RT}(v_1\phi_h^2-v_h\phi_a^2), \quad (14)$$

which can be compared with experimental data. The volume fraction of monomeric alcohol, ϕ_1, is obtained by solving Eq. (10).

$$\phi_1=[2K\phi_a+1-(4K\phi_a+1)^{\frac{1}{2}}]/2K^2\phi_a. \quad (15)$$

The correct value of K is obtained by plotting the left-hand side of Eq. (14), calculated for various values of K, against $v_1\phi_h^2-v_h\phi_a^2$, and choosing the value that gives the best straight line passing through the origin.

IV. COMPARISON WITH EXPERIMENTAL DATA

The experimental data listed in Table I were used to test Eq. (14). Molal volumes of the liquids, used in calculating volume fractions, were either taken from the references cited in Table I or selected from the literature. For ethanol-isooctane solutions, gas-imperfection corrections were calculated by the method of Scatchard and Ticknor,[12] using recently published values[13] of the second virial coefficient of ethanol. The effect on the activity coefficients of the higher virial coefficients of ethanol was shown by calculation to be negligible. For the other systems, the gas-imperfection corrections, given in the references cited, were used.

The values of K and b obtained by fitting Eq. (14) to these data are also listed in Table I. The nature of the agreement is shown in Fig. 1. The maximum deviation in the value of γ_a/γ_h is less than 8 percent, corresponding to an error of less than 0.02 in the mole fraction of alcohol in the vapor. In general, the agreement is considerably better than this, and we consider the fit to be fairly satisfactory for an equation with only two adjustable parameters. For the data on ethanol in methylcyclohexane, not shown in Fig. 1, the maximum deviation in γ_a/γ_h is 2 percent. The individual activity coefficients, γ_a and γ_h, for ethanol-methylcyclohexane solutions at 55° were also found to be represented by Eqs. (3) and (13) with the values of K and b given in Table I, with a maximum deviation of 2 percent. This is a necessary result, since Eqs. (3) and (13) satisfy the Gibbs-Duhem relation, and the data were known to satisfy this relation reasonably closely.

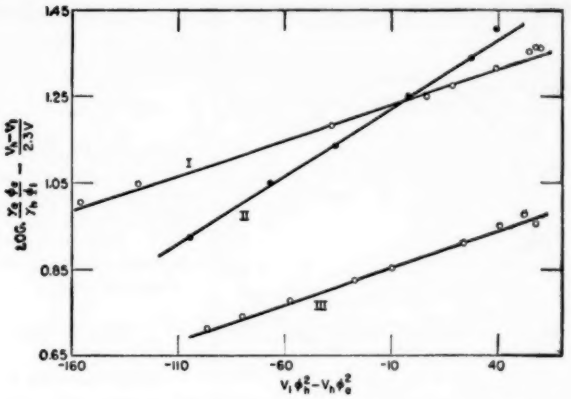

FIG. 1. Application of Eq. (14) to data on (I) ethanol in isooctane, 50°, (II) methanol in n-heptane, 59°, and (III) ethanol in toluene, 55°.

The values of K found for ethanol-methylcyclohexane solutions at 35° and 55° yield a value of -5375 cal/mole for ΔE in Eq. (7). This has an uncertainty of possibly 1000 cal/mole, because the fit of Eq. (14) to the data is not very sensitive to the value of K. It is a reasonable figure for the energy of formation of a hydrogen bond. The value of K for ethanol-isooctane solutions at 50° is consistent with the values for ethanol-methylcyclohexane solutions. The reason for the low value of K for ethanol-toluene solutions will be discussed later.

V. ENERGY AND ENTROPY OF MIXING

Our theory gives for the energy of mixing at constant volume

$$E_V{}^M=bV_x\phi_a\phi_h+K\Delta E x_a(\phi_1-\phi_1{}^0), \quad (16)$$

and for the excess entropy,

$$S_V{}^E=-R[x_h\ln(\phi_h/x_h)+x_a\ln(\phi_1/\phi_1{}^0x_a)]+K(\Delta E/T-R)x_a(\phi_1-\phi_1{}^0). \quad (17)$$

We have neglected for the moment the entropy component of b. Reference (b) of Table I gives heats of mixing and excess entropies for the system ethanol-methylcyclohexane at 35°. These were calculated from the observed temperature variation of $F_p{}^E$, with the assumption that $H_p{}^M$ does not vary with temperature. From Eq. (16), we can obtain a better estimate of the temperature variation of $H_p{}^M$. Using this estimate, we have recalculated $S_p{}^E$ and $H_p{}^M$ from the experimental data on this system, and have converted these functions to those for the mixing process at constant volume by use of the relations

$$E_V{}^M\cong H_p{}^M-TV_x{}^M\alpha/\beta \quad (18)$$

and

$$S_V{}^E\cong S_p{}^E-V_x{}^M\alpha/\beta \quad (19)$$

[11] Reference 9, p. 139.

[12] G. Scatchard and L. B. Ticknor, J. Am. Chem. Soc. **74**, 3724 (1952).

[13] C. B. Kretschmer and R. Wiebe, J. Am. Chem. Soc. **76**, 2579 (1954).

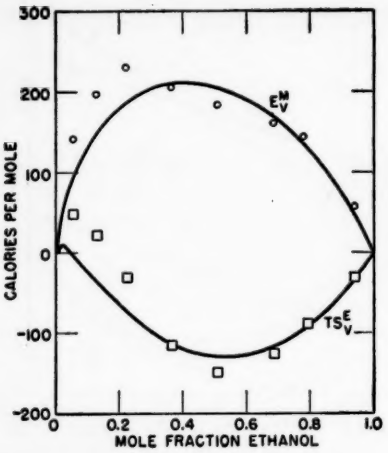

FIG. 2. Thermodynamic functions of ethanol-methylcyclohexane solutions at 35°. Curves: theoretical values. Points: observed values.

given by Scatchard.[5] Since the maximum value of $H_p^M - E_V^M$ is only about 30 cal, no great accuracy is required in the conversion. We used the measured values of V_x^M at 25° given in the reference cited, and estimated α as 1.2×10^{-3} deg^{-1} and β as 1.2×10^{-4} atmos^{-1}.

Figure 2 shows values of E_V^M and S_V^E, calculated from the experimental vapor pressures as just described, and values calculated from Eqs. (16) and (17). It might be argued that, since Eq. (14) reproduces the data satisfactorily at both temperatures, Eqs. (16) and (17) would necessarily give the same result as the direct calculation of E_V^M and S_V^E from the data. However, the latter calculation involves small differences between the free energies at 35° and 55°, and Eq. (14) does not fit the data so exactly that we can be sure it will reproduce the experimental energy and entropy. Therefore it is gratifying to find that Eqs. (16) and (17) agree with the experimental points within the uncertainty of the latter, which is about 50 cal/mole for E_V^M and TS_V^E calculated from the difference between free energies at 35° and 55°. Our equations correctly predict the unsymmetrical shapes of the energy and entropy curves, including the small region of positive excess entropy at low mole fractions of alcohol. This particular feature is also predicted by the treatments of Tompa[6] and Barker,[7,8] and it is reasonable to assume that it would appear in the continued-association theory of Redlich and Kister[4] as well.

VI. ALCOHOL-SOLVENT INTERACTIONS

The volume fraction of monomer in pure alcohol is given by Eq. (15) with $\phi_a=1$. Therefore K should be the same for solutions of a given alcohol in all nonpolar solvents at a given temperature, and it is necessary to modify the theory to account for the low value of K found for ethanol-toluene solutions at 55°. It is assumed that each alcohol polymer or monomer can combine with one molecule of aromatic hydrocarbon, the aromatic nucleus acting as an electron donor in hydrogen bond formation. The equilibrium constant for this process is

$$k=c_{i0}/c_i c_0, \tag{20}$$

and k is assumed to be independent of the degree of polymerization i. When the mathematical steps outlined above are carried out for this model, it develops that the behavior of the system can still be represented by Eqs. (14) and (15), to a good approximation, but with K replaced by $Kv_1/(v_1+k)$. Thus, for the ethanol-toluene system at 55°, $k=183$. This means that, at low alcohol concentrations, somewhat more than one-half of the alcohol polymers are associated with toluene molecules.

VII. RELATION TO OTHER WORK

Scatchard, Kavanagh, and Ticknor[14] have discussed the behavior of mixtures of water and hydrogen peroxide on the basis of the Flory-Huggins free-energy equation and the concept of continued association. They obtained good agreement with their measured values of the thermodynamic functions of the mixtures. Their treatment differs in detail from that of the present paper, since water and hydrogen peroxide have more than two bonding sites per molecule and can form three-dimensional polymeric networks.

Prigogine and Desmyter[15] have proposed an equation for solutions of alcohols in nonpolar solvents, which may be expressed as

$$\gamma_a/\gamma_h=(\phi_1 v_1)/(\phi_a \phi_1^0 v_h). \tag{21}$$

Equation (21) may be obtained by neglecting the nonlogarithmic terms in our Eq. (14). These authors avoided reference to the state of the pure alcohol by using activity coefficients based on an infinitely dilute solution of alcohol in nonpolar solvent as the reference state for both components. They showed that the major portion of the nonideal behavior of such solutions could be accounted for by Eq. (21), using values of ϕ_1/ϕ_a derived from infrared light-absorption measurements.

Coggeshall and Saier[16] have studied the association of alcohols and phenols in carbon tetrachloride by means of infrared light-absorption measurements, and have concluded that the equilibrium constant for dimer formation must be only $\frac{1}{3}$ to $\frac{2}{3}$ as large as that for the higher polymers, to explain their measurements satisfactorily.

A smaller equilibrium constant for dimer formation would improve the agreement of our treatment with the experimental data at low alcohol concentrations, but at the cost of introducing an additional adjustable

[14] Scatchard, Kavanagh, and Ticknor, J. Am. Chem. Soc. 74, 3715 (1952).
[15] I. Prigogine and A. Desmyter, Trans. Faraday Soc. 47, 1137 (1951).
[16] N. D. Coggeshall and E. L. Saier, J. Am. Chem. Soc. 73, 5414 (1951).

parameter, and a considerable increase in the difficulty of the calculations. A simple way to achieve approximately the same result would be to make $\phi_i/(\phi_{i-1}\phi_1)$ a constant, rather than $c_i/(c_{i-1}c_1)$. This would make the concentration equilibrium constant for dimer formation half as large as that for a very long polymer or, in general,

$$K_i=c_i/(c_{i-1}c_1)=K_\infty(i-1)/i, \tag{22}$$

and would give a very simple relation between ϕ_1 and ϕ_a.

THE JOURNAL OF CHEMICAL PHYSICS VOLUME 22, NUMBER 10 OCTOBER, 1954

Deviations from Additivity of the Intermolecular Field at High Densities*

LAURENS JANSEN AND ZAKA I. SLAWSKY
Department of Chemistry, University of Maryland, College Park, Maryland
(Received February 22, 1954)

The intermolecular field of an assembly of neutral atoms or molecules is usually assumed to be additive with respect to isolated pairs. Nonadditive effects have been calculated in the first-order forces by Rosen and in the second-order forces by Axilrod and Teller. For the evaluation of second-order forces between two molecules at high densities the zero-order wave function must be made antisymmetric with respect to nearest neighbors. It is shown that this correction results in a decrease of the second-order forces compared to an isolated pair of molecules, and may be interpreted as a screening effect. The method is based on the model of the caged atom or molecule.

A. INTRODUCTION

FOR the statistical evaluation of physical properties of compressed gases, of liquids and solids the intermolecular field is usually assumed to be additive, i.e., the potential field at all densities may be written as a sum of terms referring to isolated pairs of molecules. This statement is known as the "additivity of intermolecular forces." The assumption of additivity is obviously not valid for molecules which tend to associate or for molecules which form hydrogen bonds. We restrict ourselves to forces between spherically symmetric atoms, especially argon, and we exclude from consideration the types of forces mentioned above.

Consider a group of three identical spherically symmetric atoms, a, b, and c, with closed shells of electrons. The intermolecular field between these atoms (molecules) will be evaluated by applying perturbation theory, on the basis of the valence bond method which is useful for simple systems. The total zero-order wave function is written as

$$\Psi_0=\sum_\lambda(-1)^\lambda P_\lambda\Psi_a\Psi_b\Psi_c, \tag{1}$$

where P_λ is any permutation operator of the symmetric group on $3n$ particles; n is the number of electrons per molecule. The group consists of $(3n)!$ elements and λ is even or odd for even or odd permutations, respectively. The Hamiltonian for the system of three molecules is

$$\mathrm{H}=\mathrm{H}_0+\mathrm{H}_{abc}', \tag{2}$$

where H_0 is the Hamiltonian for three unperturbed atoms (molecules) and H_{abc}' is the interaction operator. First-order perturbation theory gives the repulsive interaction between the atoms. From the calculations by Rosen[1] it appears that the first-order forces between three helium atoms are not equal to the sum of interactions between isolated pairs; this means that first-order forces do not have the property of additivity. Since the overlap of wave functions is greatest in the equilateral triangular configuration, the contribution of nonadditivity is larger in this case than for other configurations having the same triangular perimeter. Rosen obtained the result

$$\frac{E_{abc}}{E_{ab}+E_{ac}+E_{bc}}=-1.15e^{-0.33(3R)}$$

for the equilateral configuration; R is the distance between pairs, in units of Bohr radii, E_{abc} is the nonadditive contribution, E_{ab} is the first-order interaction between pair ab, etc. For the linear symmetric case the result is

$$\frac{E_{abc}}{E_{ab}+E_{ac}+E_{bc}}=+9.8e^{-0.66(4R)},$$

with R, $2R$ the distance between pairs. For the equilateral triangle the error involved in neglecting nonadditivity is one percent or less for $R\geqslant 4.8$ units of Bohr radii. The error involved for the linear symmetric case has the opposite sign and is always smaller than for the equilateral triangle in the region considered ($R\geqslant 1.8$ Bohr radii). For large distances $E_{abc}/3E_{ab}=I$ is a good approximation in the equilateral case; I is the overlap integral. Therefore the effect of nonadditivity is

* Supported by the U. S. Office of Naval Research under Contract Nonr-595(02).

[1] P. Rosen, J. Chem. Phys. **21**, 1007 (1953).

negligible if the overlap integral is small compared with unity. On increasing the distances between the three atoms, the first-order forces decrease rapidly. The second-order forces (dispersion forces) become predominant and the evaluation of this term may at large distances be based on a zero-order wave function which is a simple product of atomic wave functions

$$\Psi_0=\Psi_a\cdot\Psi_b\cdot\Psi_c \tag{1'}$$

and the Hamiltonian

$$\mathrm{H}=\mathrm{H}_0+\mathrm{H}_{abc}'. \tag{2}$$

London[2] and Margenau[3] have shown that the dispersion forces are additive in this second-order approximation. Axilrod and Teller[4,5] applied third-order perturbation theory to the dispersion forces between neutral atoms. It was observed that this order reflects the interaction between triplets of atoms, giving rise to a nonadditive term in the dipole dispersion field. The magnitude of the triple dipole interaction can be illustrated by comparing it with the dipole-dipole interaction for three rare gas atoms, as calculated for three isolated pairs. For convenience we consider again two configurations of the triplet of atoms, an equilateral triangle and a collinear array. The results are $E_{abc}/(E_{ab}+E_{ac}+E_{bc})=-(11/32)\alpha/R^3$ for the equilateral triangle, and $+(4/43)\alpha/R^3$ for the collinear array. E_{ab}, etc. are the second-order forces between the different pairs, counted negative. The polarizability of an atom is α and R, $2R$ is the distance between pairs. The results show that the attractive field is decreased in the equilateral triangle and increased in the case of the collinear array as compared to the additive sum of pairs. For the crystals of neon, argon, krypton, and xenon $(11/32)\alpha/R^3$ is 0.0041, 0.0099, 0.0139, and 0.0166, respectively. Axilrod[6] summed the third-order interaction energy for crystals of the heavy rare gases. The third-order energy is positive, thus decreasing the attractive field between the particles, and amounts to two to nine percent of the cohesive energy. It is not possible on this basis to explain why the heavy rare gases crystallize in the face-centered cubic lattice instead of in the somewhat more closely packed structure of hexagonal symmetry. Axilrod evaluated the difference in third-order interaction energy between the f.c.c. and h.c.p. lattices and found that, although this nonadditive effect favors the cubic structure, the difference between the two structures is less than 0.01 percent of the cohesive energy.

The nonadditivity calculations of Rosen and Axilrod are straightforward extensions of the evaluation of first- and second-order forces between two atoms or molecules. It may be expected that for the calculation of second-order forces the simple-product wave function is a poor approximation at the densities of the crystals and that exchange terms should be taken into account. For instance, if of the three atoms a, b, c two are close together (a,b) and one is far apart (c), then the total wave function can be written as

$$\Psi_0=[\textstyle\sum_\lambda(-1)^\lambda P_\lambda\Psi_a\cdot\Psi_b]\cdot\Psi_c; \tag{1''}$$

i.e., the dispersion forces between (ab) and (c), as calculated on the basis of isolated pairs, may be affected by the exchange terms between a and b. The purpose of the following calculation is to indicate a method by which the effect of exchange terms on the dispersion forces can be estimated based on the model of the "caged" atom or molecule.

B. FORMALISM

Consider a system of N identical spherically symmetric atoms $a, b, \ldots N$ with closed shells of electrons. The model of the caged atom is based on the assumption that the exchange interaction between the atoms may be replaced by an ordinary potential term. For the evaluation of second-order forces this means that we may start with a zero-order wave function which is a simple product of atomic wave functions

$$\Psi_d=\Psi_{d_a}\cdot\Psi_{d_b}\cdot\Psi_{d_c}\cdots \tag{3}$$

and the Hamiltonian

$$\mathfrak{H}=\mathfrak{H}_0+\mathrm{H}', \tag{4}$$

where H′ is the usual interaction operator. The operator $\mathfrak{H}_0$ includes the potential term for the exchange interaction between the atoms

$$\mathfrak{H}_0=\textstyle\sum_a\mathfrak{H}_{0a}, \tag{5}$$

where

$$\mathfrak{H}_{0a}=\mathrm{H}_{0a}+V_a(r). \tag{6}$$

H_{0a} is the Hamiltonian for a free atom a, and $V_a(r)$ is the potential term replacing the effect of exchange; r is the distance from the center of atom a. The wave functions Ψ_{d_a}, Ψ_{d_b} . . . are solutions of the equations

$$\mathfrak{H}_{0a}\Psi_{d_a}=(E_{0a}+E_a')\Psi_{d_a}. \tag{7}$$

E_{0a} is the energy of the ground state of a free atom and E_a' is the first-order interaction of atom a with the surrounding atoms; E_a' is a function of the density of the system. Solutions of the wave Eq. (7) are possible if, e.g., $V_a(r)$ has the form of a boundary condition

$$\begin{aligned} V_a(r)&=0 \qquad \text{for } r<R \\ &=\infty \qquad \text{for } r\geqslant R. \end{aligned} \tag{8}$$

R is called the radius of the "cage" of atom a. In principle, the value of R can be determined if E_{0a} and E_a' are known (from solutions for the free atom and of the determinantal wave equation for the first-order interaction). In practice, one solves the wave equation (7)

[2] F. London, Z. Physik. Chem. **B11**, 222 (1930).
[3] H. Margenau, Revs. Modern Phys. **11**, 1 (1939).
[4] B. M. Axilrod and E. Teller, J. Chem. Phys. **11**, 299 (1943).
[5] B. M. Axilrod, J. Chem. Phys. **17**, 1349 (1949); **19**, 719 (1951).
[6] B. M. Axilrod, J. Chem. Phys. **19**, 724 (1951).

with the condition (8) for different values of R. Then it is assumed that the pressure

$$P=-(1/4\pi R^2)\cdot\partial E_a'/\partial R,$$

which the electron "gas" of atom a exerts on the wall of the cage, balances the external pressure of the whole gas.[7] In doing so, a rough model of the effect of exchange terms is used. The wave equation (7) has been solved for hydrogen atoms,[8–10] helium atoms,[11] the hydrogen molecule ion,[12] and argon atoms.[7,13]

Second-Order Forces

With the new zero-order wave functions (3), (4), (5), (7) perturbation theory is applied up to the second order. The first-order change in energy is identically zero, and in second order the dispersion forces are again additive, but now with respect to the new unperturbed state of caged atoms. If we write for the attractive field between a pair of caged atoms $\varphi_{ij}^{(d)}$, then we have for the total second-order forces

$$\varphi^{(d)}=\tfrac{1}{2}\sum_{i,j}{}'\varphi_{ij}^{(d)}. \tag{9}$$

On the other hand the dispersion forces in a system consisting of isolated pairs of atoms are

$$\varphi^{(0)}=\tfrac{1}{2}\sum_{i,j}{}'\varphi_{ij}^{(0)}. \tag{9'}$$

If $\varphi^{(d)}\neq\varphi^{(0)}$, then the dispersion forces are nonadditive with respect to isolated pairs. London's expression for the dipole dispersion field between two atoms is

$$\varphi_{ij}^{(0)}=-3V_0\alpha_0^2/4r_{ij}^6, \tag{10}$$

where V_0 is the first ionization potential of a free atom and α is its polarizability; r is the distance between the centers of the two atoms. In the same approximation we obtain for the dipole dispersion forces between a pair of "caged" atoms

$$\varphi_{ij}^{(d)}=-3V_d\alpha_d^2/4r_{ij}^6. \tag{10'}$$

Here V_d is the first ionization potential of a caged atom in its unperturbed state (7); α_d is the polarizability of a caged atom. As follows from the calculations on the caged atom or molecule, both V_d and α_d are smaller than their values for the free atom. Physically speaking the exchange terms compress the electron clouds of the caged atom and this results in a decrease of the intrinsic dipole moment and an increase of the fundamental frequencies of the electrons. Consequently, the second-order forces are weaker than calculated for isolated pairs. If we take a pair of atoms ij, then a measure of the nonadditive effect will be given by

$$(\varphi_{ij}^{(d)}-\varphi_{ij}^{(0)})/\varphi_{ij}^{(0)}=2\Delta\alpha/\alpha_0+\Delta V/V_0, \tag{11}$$

where we have substituted $\alpha_d=\alpha_0+\Delta\alpha$, $V_d=V_0+\Delta V$, and only linear terms have been taken into account. The values of $\Delta\alpha/\alpha_0$ and $\Delta V/V_0$ must be taken from the theoretical calculations on the caged atom; for argon from references 7 and 13. At a temperature of 25°C and a density of 600 Amagat we find for argon $\Delta\alpha/\alpha_0=-3.2\times10^{-2}$. However, it is difficult to give an accurate estimate of $\Delta V/V_0$. For the ground state of helium we replace $\Delta V/V_0$ by approximately $\Delta E/E_0$, where E_0 is the energy of the ground state of a free helium atom. From reference 11 we have at a pressure of 5×10^4 atmos $\Delta E/E_0=-0.014$ and $\Delta\alpha/\alpha_0=-0.168$. For argon we take as a lower theoretical limit of $2\Delta\alpha/\alpha_0+\Delta V/V_0$ a value of -6×10^{-2}. Equation (11) may be rewritten in terms of any set of intermolecular parameters; for instance we have for a Lennard-Jones potential field: $\varphi_{ij}^{(0)}=-4\epsilon(\sigma/r_{ij})^6$ and a corresponding expression for $\varphi_{ij}^{(d)}$. Then we have for the change in the quantity $\epsilon\sigma^6$

$$\Delta(\epsilon\sigma^6)=(2\Delta\alpha/\alpha_0+\Delta V/V_0)(\epsilon\sigma^6)^{(0)}, \tag{12}$$

where the superscript (0) refers to the values of the intermolecular parameters as determined from low density measurements of the second virial coefficient, etc.

C. THERMODYNAMIC FUNCTIONS

For the calculation of thermodynamic functions, including this nonadditive part of the dipole dispersion field, we write for the second-order forces between two molecules

$$\varphi_{ij}^{(d)}=\varphi_{ij}^{(0)}+(2\Delta\alpha/\alpha_0+\Delta V/V_0)(-4\epsilon\sigma^6/r_{ij}^6) \tag{13}$$

with values of ϵ and σ as determined from low density data. Next it is assumed that the atoms may be considered fixed at the centers of their cells as far as the nonadditive part of (13) is concerned; i.e., the distance r_{ij} may be replaced by the distance between the centers of cells i and j, R_{ij}. With this approximation the partition function is a product of two parts and the thermodynamic functions are additive in the two parts of the field. It should be noted that the contribution of the nonadditive effect in (13) is independent of temperature in this approximation. For the internal energy $U=U_0+\Delta U$ we obtain

$$\Delta U=-2N(2\Delta\alpha/\alpha_0+\Delta V/V_0)\times(\epsilon\sigma^6/R_0^6)\cdot\sum_{j=2}^{N}(R_0/R_{1j})^6, \tag{14}$$

where R_0 is the distance between nearest neighbors in

[7] C. A. ten Seldam, thesis, Utrecht (1953).
[8] Michels, de Boer, and Bijl, Physica **4**, 981 (1937).
[9] A. Michels and S. R. de Groot, Physica **16**, 183 (1950).
[10] A. Sommerfeld and H. Welker, Ann. Physik **32**, 56 (1938).
[11] C. A. ten Seldam and S. R. de Groot, Physica **18**, 891, 905 (1952).
[12] T. L. Cottrell, Trans. Faraday Soc. **47**, 337 (1951).
[13] C. A. ten Seldam and S. R. de Groot, Physica **18**, 910 (1952).

the lattice.

$$\sum_{j=2}^{N}(R_0/R_{1j})^6=14.4;$$

for a face-centered cubic array[14] at a density of 600 Amagat we have $R_0=4.3$A. The values of ϵ and σ as determined from low density pvT data, are 165×10^{-16} *ergs* and 3.405A, respectively.[15] When these values are inserted into (14) we obtain for ΔU a value of about $+100$ cal per mole. On account of the model used for the evaluation of this nonadditive effect, this value is probably too high. The result indicates, however, that the use of a simple-product type of wave function for the calculation of second-order forces at high densities overestimates the magnitude of the dipole dispersion field.

D. RELATIVE MAGNITUDE EFFECTS

In terms of perturbation theory the nonadditivity calculated by Rosen is a first-order effect, the influence of exchange terms on the dispersion forces between two atoms is of the second order, whereas Axilrod's nonadditive effect is of third order. Evidently this does not imply that the relative magnitude of these effects has always this same order. The nonadditivity in the first-order forces will predominate at the highest densities. In the crystals of the heavy rare gases the first-order forces are only about half as large as the second-order forces and the three nonadditive effects might be of comparable magnitude. Quantitative comparison between these calculations and experimental values of the sublimation energies of crystals at absolute zero is possible only if the intermolecular field between two molecules is accurately known. It will not be attempted to give such a comparison on the basis of the Lennard-Jones potential field, because there are numerous indications that this potential field does not accurately represent the interaction field at small distances between the molecules.

Kihara[16] has shown that the Lennard-Jones $(6, n)$ potential field fails to explain the absolute stability of the f.c.c. crystal structure as compared to the hexagonal one for any acceptable value of n, if additivity of intermolecular forces is assumed.† For an additive "exp-six" potential of the form

$$\varphi(r)=\frac{\epsilon}{1-6/\alpha}\left[\frac{6}{\alpha}e^{\alpha(1-r/r_m)}-\left(\frac{r_m}{r}\right)^6\right], \qquad (15)$$

the cubic structure can become more stable than the hexagonal one for $\alpha<8.675$ (Kihara[16]). The separation distance between two molecules is r; ϵ is the depth of the potential energy minimum, r_m is the position of the minimum, and α is a parameter which is a measure of the steepness of the repulsion energy. To avoid effects due to nonadditivity at high densities the accurate determination of the parameters ϵ, α, and r_m in (12) must be based on experimental second virial coefficients and measurements of transport properties at moderate densities and at high temperatures. This has been done recently by Mason and W. E. Rice[17] for helium and hydrogen. They showed that a potential of the form (12) is definitely superior to the Lennard-Jones (6,12) potential. A combination of high temperature measurements at moderate densities with accurate data on the sublimation energies of the crystals at 0°K and on zero-point energies will give information on the importance of nonadditive effects at high densities.

[14] J. E. Lennard-Jones and A. E. Ingham, Proc. Roy. Soc. (London) **A107**, 636 (1925).
[15] A. Michels and H. Wijker, Physica **15**, 627 (1949).
[16] T. Kihara, Revs. Modern Phys. **25**, 831 (1953).
† Kihara assumes that the zero-point energy does not play any essential role regarding the stability of the cubic closest packed structure, since helium, in spite of its large zero-point energy, seems to crystallize in the hexagonal closest packing.
[17] E. A. Mason and W. E. Rice, J. Chem. Phys. **22**, 522 (1954).

Oxidation Ions in Hydrocarbons on Ultraviolet Irradiation

ANDREW GEMANT
Engineering Laboratory and Research Department, The Detroit Edison Company, Detroit, Michigan
(Received March 24, 1954)

Ultraviolet irradiation, mostly in the presence of a peroxide, increases the electrical conductivity, thus produces oxidation ions in solutions of aromatic diols, to a lesser extent in those of monohydroxyl compounds, and to a still lesser, but measurable, extent in a hydrocarbon itself, namely *o*-xylene. Ultraviolet spectroscopy permits identification of the chief oxidation products: *o*-phthalic aldehyde in the case of *o*-xylene. The ions are probably oxidation intermediates of relative stability. Whereas the anion can be derived from the acids, the cations are probably oxonium-type ions, derivable from the *o*-aldehydes formed.

SCOPE OF STUDY

PREVIOUS studies[1] have established the existence of organic ions in hydrocarbon solvents: negative ions of the type of anions of aliphatic acids, and positive ions of the type of ammonium cations. Whereas the former results easily on oxidation of hydrocarbons, the latter is usually not present at marked concentrations. Ions that occur in a hydrocarbon as a result of oxidation will be called oxidation ions. In a further search for oxidation ions in hydrocarbons,[2] the existence of ions of the nature of semiquinones was indicated. As a source of such oxidation-ions ortho-dihydroxyl aromatic compounds were found to be effective, yielding both anions and cations on oxidation.

Since increased electrical conductivity is a generally observed effect on hydrocarbon oxidation, it is likely that oxidation ions are formed not only from ortho-dihydroxyl compounds, but from a larger variety of sources, including hydrocarbons themselves. The purpose of this study was, first, to ascertain what types of compounds, besides the aromatic diols, lead to ion formation; second, to draw conclusions from these findings concerning the possible structure of the ions.

In the present study a method of oxidation was used, considered to resemble natural conditions under which hydrocarbons often oxidize. One of these conditions is excitation of electronic states, which is often, though not always, of importance. In the presence of a high electric field and subsequent discharges excitation of molecules certainly occurs. Ultraviolet irradiation was, therefore, chosen as a means for initiating oxidation processes. A second condition is the frequent presence of organic peroxides, formed by a foregoing primary oxidation process. In many of the following experiments an organic peroxide was, therefore, added to the system.

The action of the ultraviolet light is twofold. First, as mentioned, excited electronic states result, favoring chemical reactions. In the presence of a peroxide, the excitation can lead to dissociation into radicals of the peroxide,[3] promoting oxidation of the hydrocarbon. Second, ozone is produced from the oxygen of the air, also contributing to the oxidation process.

The ultraviolet source consisted of four G.E. germicidal lamps, 90 percent of their output being at 2537 A. The samples in open Pyrex containers were at about 15 cm from the source; the intensity at that spot was about 2500 μwatts/cm^2. Evaporated solvent was replaced before each conductivity measurement; the latter was carried out in Balsbaugh cells, using a variable-frequency power-factor bridge.

The peroxide used was benzoyl peroxide, recrystallized from the Eastman product. Its good solubility in hydrocarbons, its relative stability, and its ability to oxidize organic solvents[4] are of advantage in such a study; it was employed at the low concentration of 20 millimole/liter.

EXPERIMENTAL RESULTS ON ELECTRICAL CONDUCTIVITY

Figure 1 presents the electrical conductivity of solutions of *p*-butylcatechol, which was shown[2] to produce ions on oxidation by inorganic solid oxidants. Curve 1 shows the large effect obtainable on ultraviolet irradiation in the presence of peroxide. The effect can be, partially at least, reversed by reduction in a hydrogen stream on platinum black catalyst, as shown in the curve H_2, indicating that the ions formed are capable of

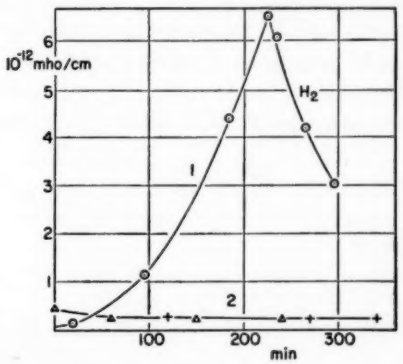

FIG. 1. Electrical conductivity of benzenediol solutions *vs* time of ultraviolet irradiation in the presence of 20 mM/l benzoyl peroxide. Curve 1: 10 mM/l butylcatechol in benzene; oxidation followed by reduction (H_2); 2 (Δ): 6 mM/l butylhydroquinone in benzene; 2 (+): benzene.

[1] Andrew Germant, J. Chem. Phys. **14**, 424 (1946).
[2] Andrew Gemant, J. Electrochem. Soc. **100**, 320 (1953).
[3] Milas, Kurz, and Anslow, J. Am. Chem. Soc. **59**, 543 (1937).
[4] Henry Gilman, *Organic Chemistry* (John Wiley and Sons, Inc., New York, 1953), Vol. IV, p. 1132.

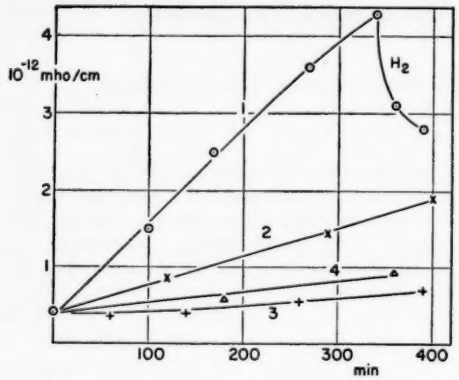

FIG. 2. Conductivity of methyl benzenes *vs* time of ultraviolet irradiation (20 mM/l benzoyl peroxide). Curve 1: *o*-xylene (with reduction curve H_2); 2: *o*- and *p*-xylene 1:1; 3: *p*-xylene; 4: toluene.

reduction. In Curve 2, the triangles refer to a solution of butylhydroquinone, indicating that only the ortho-, but not the para-, diol produces the effect. The crosses in Curve 2 refer to a control test for the solvent alone, which was also negative.

Whereas in acid-amine-phenol systems the conductivity data should be corrected for changes in dielectric constant, such corrections are not necessary in the case of oxidation-ions, since the effect of the dielectric constant on conductivity was shown[2] to be small. It is also worth mentioning that the conductivity effects observed are not caused by a possible production of water.[2]

Having thus established the usefulness of the method, the main results are presented in Fig. 2, proving the formation of ions directly from a hydrocarbon. Curve 1 gives the effect obtainable with *o*-xylene, in contrast to the very small effect with *p*-xylene (3), as well as toluene (4). A mixture of equal parts of *o*- and *p*-xylene (2) gives an effect smaller than *o*-xylene. The effect is partially reversed on reduction in a hydrogen stream (H_2). Thus, ion formation is found not only with a diol, but with an aromatic hydrocarbon, provided the latter possesses side groups, easily attacked by oxidants, in the ortho position.

Figure 3 provides further information, showing the

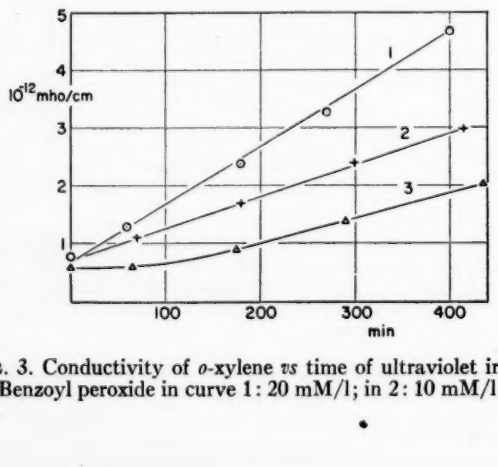

FIG. 3. Conductivity of *o*-xylene *vs* time of ultraviolet irradiation. Benzoyl peroxide in curve 1: 20 mM/l; in 2: 10 mM/l; in 3: none.

effect of the peroxide concentration. In Curve 1 it is 20 millimole/liter, in 2, 10 millimole/liter, giving a smaller conductivity than in 1. The peroxide is not absolutely necessary: Curve 3 shows the result of irradiation of the pure solvent, giving a measurable effect. This is in keeping with the statements above on the photochemical action of the irradiation.

Figure 4 presents the increases in conductivity on irradiating solutions of phenols: *o*-cresol (1), phenol and 3–4 dimethylphenol (2) in the presence of peroxide, 3–4 dimethylphenol (3) in the absence of peroxide. Since the CH group adjoining the COH group oxidizes preferentially,[5] phenols exhibit ion production similar to diols and *o*-xylene.

In Figs. 1 to 4 the conductivity increment on irradiation for 300–400 minutes is throughout about 5×10^{-12} mho/cm. However, the specific effectiveness of the three groups of compounds is quite different, as may be seen from the difference in concentration. The diols are active at 3 to 6 millimole/liter, the phenols at 50 to 200 millimole/liter, whereas 1 liter of *o*-xylene contains

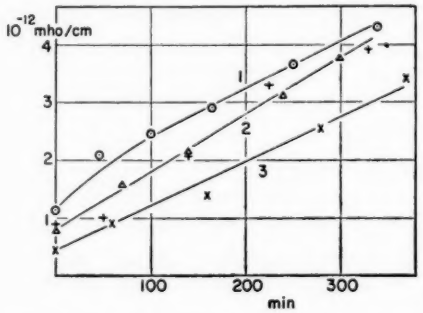

FIG. 4. Conductivity of phenol solutions *vs* time of ultraviolet irradiation. Solvent: benzene. Benzoyl peroxide in curve 1 and 2: 20 mM/l; in 3: none. 1: *o*-cresol, 200 mM/l; 2 (+): phenol, 200 mM/l; 2 (Δ) and 3: 3–4 dimethylphenol, 100 mM/l.

about 8 moles. Hence, the specific effectiveness decreases in the approximate ratios: 2000:25:1.

The effect of the concentrations of both substrate and peroxide is shown for 3–4 dimethylphenol in Table I.

Table II shows that the peroxide does not produce ions in the solutions studied, if ultraviolet irradiation is absent; the latter is essential in this arrangement.

Table III gives results on simultaneous measurements of electrical conductivity and acidity by titration upon irradiation. In agreement with the data presented above, a marked increase in conductivity is observed only with phenol solutions and *o*-xylene. In contrast to this, there is in every case an increase of acidity, although varying in magnitude. A comparison of the data between *o*- and *p*-xylene in presence of peroxide is particularly striking. The increase in acidity is a measure of the extent of oxidation, and the data show that absence of the conductivity effect is not caused by an absence of oxidation. The latter is evidently not a sufficient

[5] Cross, Bevan, and Heiberg, Ber. deut. chem. Ges. **33**, 2015 (1910).

criterion for ion formation. Ions are produced only if the conditions mentioned above concerning the structure of the substrate are fulfilled. This conclusion is important in attempting to ascribe certain structures to the ionic species formed.

EXPERIMENTAL RESULTS ON ABSORPTION SPECTROSCOPY

For this purpose it is useful to know the composition of the compounds formed on oxidation. In most cases this aim can be achieved only approximately, since with progressing oxidation a variety of compounds is produced; besides monomers, dimers and finally polymers are often formed. For this reason it is often advantageous to oxidize only for a short time, permitting only the primary products to form.

TABLE I. Increase in conductivity (10^{-12} mho/cm), on irradiating for 300-min solutions of various concentrations, (mM/l), of dimethylphenol and benzoyl peroxide in benzene.

Phenol \ Peroxide	10	20	40
25	...	1.7	...
50	...	2.3	...
100	2.4	3.0	4.1

From the chemical nature of the substrate one may see what types of compounds result from oxidation. A possible way of gaining more information on this point is by absorption spectroscopy. By comparing the spectra of oxidized samples with spectra of known compounds that might be among the products, an identification of at least part of the latter may be made.

Figure 5 presents such an analysis on *p*-butylcatechol,

TABLE II. Effect of benzoyl peroxide, 20 mM/l, in the absence of ultraviolet irradiation (380 minutes).

Hydrocarbon	Solute	Concentration mM/liter	Increase of conductivity 10^{-12} mho/cm
Benzene	Butylcatechol	10	0.15
Benzene	3–4 dimethyl-phenol	100	−0.15
o-Xylene	...	...	−0.06

by plotting the logarithm of the absorption coefficient as a function of wavelength in the ultraviolet. Curve 1 is the spectrum of butylcatechol, obtained with a Beckman spectrophotometer, the absorption coefficients for wavelengths larger than 330 mμ dropping to very small values, and curve 3, after Goldschmidt and Graef,[6] is that of *o*-quinone, a substance similar to the probable oxidation product. Curve 2 is the spectrum of a butylcatechol solution, oxidized by $KMnO_4$ for 1 minute. Since the solution contains a mixture in this case, the total concentration c_0 of which is known, only

[6] Landolt-Börnstein, *Zahlenwerte und Funktionen* (Springer, Berlin, 1951), Vol. I, Part 3/II, p. 307.

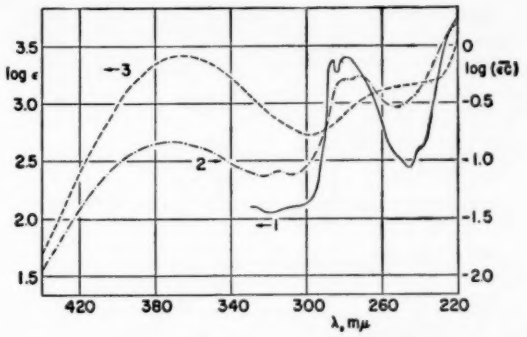

FIG. 5. Extinction coefficient *vs* wavelength. Curve 1: *p*-butylcatechol in isooctane; 2: same, oxidized by $KMnO_4$ for 1 min; 3: *o*-quinone in ether (Goldschmidt and Graef). Arrows on numbers point toward ordinates.

the average product $\bar{\epsilon}c$ of the mixture can be calculated from the absorption measured. The right-hand ordinate is thus valid for curve 2. The total concentration was 3×10^{-4} mole/l, and the two ordinates are aligned in a manner that permits a direct comparison of the three curves. The peak of 280 mμ of the diol is clearly present in the oxidation product, indicating a concentration about 30 percent smaller than before oxidation. The characteristic broad peak of the quinone at 370 mμ is also clearly present in curve 2, indicating quinone as an oxidation product at a concentration about 20 percent of the total.

A similar analysis on 1–2 naphthodiol is presented in Fig. 6. Curve 1 is the spectrum of the diol, curve 3 of 1–2 naphthoquinone, and curve 2 of the diol oxidized for 2 minutes. The latter shows the peak of the diol at around 290 mμ, indicating a concentration drop of about 30 percent. It also shows the broad peak of the quinone at 400 mμ at a concentration of about 30 percent of the total.

Figure 7 presents the spectra of *o*-xylene oxidation products. In this case the irradiated xylene samples (no peroxide was used) were extracted with water, the oxidation products having a finite solubility in water. Since *o*-xylene itself is soluble in water (0.013 g in 100 g), a saturated solution was used for comparison in the

TABLE III. Increase of conductivity and acidity during 300 minutes of irradiation.

Hydrocarbon	Solute	Concentration mM/l	Benzoyl peroxide 20 mM/l	Increase of Conductivity 10^{-12} mho/cm	Acidity, 10^{-3} N
Benzene	...	...	+	−0.07	2.5
Benzene	Heptaldehyde	42	+	0.20	11.1
o-Xylene	...	...	+	2.8	12.2
o-Xylene	...	...	−	1.1	5.1
p-Xylene	...	...	+	−0.08	10.5
p-Xylene	...	...	−	0.03	1.8
Benzene	3–4 Dimethyl-phenol	100	+	3.0	9.3
Benzene	3–4 Dimethyl-phenol	100	−	1.8	0.5

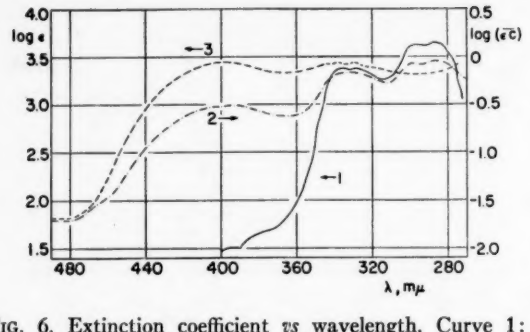

FIG. 6. Extinction coefficient *vs* wavelength. Curve 1: 1–2 naphthodiol; 2: same, oxidized by $KMnO_4$ for 2 min; 3: 1–2 naphthoquinone. Solvent: benzene. Arrows point toward ordinates.

Beckman. With progressing oxidation (8, 15, and 60 minutes) the absorption increases, as may be expected. Whereas curves 1 and 2, particularly the latter, show good details, the last is not any longer useful, probably because of the multiplicity of products formed.

The oxidation products of *o*-xylene are varied, such as *o*-toluic aldehyde, *o*-toluic acid, *o*-phthalic acid, and others.[7] In order to see which was prevalent in the present case, the spectra of three compounds are shown in Fig. 8, in which curves 2 and 3 refer to *o*-phthalic anhydride and *o*-phthalic acid, and curve 1, after Carmack, Moore, and Balis,[8] to *o*-phthalic aldehyde. There is a noticeable similarity between the latter curve and curve 2 of Fig. 7: a peak at 260 (270), a shoulder at 220 (230), and a second peak at 210 (220) mμ. Hence, compounds obtainable from the side-chain oxidation of *o*-xylene, particularly the aldehyde, appear to be formed as a result of ultraviolet irradiation.

DISCUSSION OF IONIC STRUCTURES

Assignment of structures to the oxidation ions formed directly from a hydrocarbon on the basis of this study can be done only in a tentative manner. Considering, however, that basic information on the chemical nature of ions in hydrocarbons has been lacking up to now, such

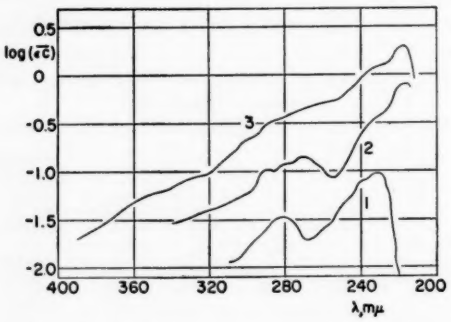

FIG. 7. Extinction coefficient *vs* wavelength for *o*-xylene products on irradiation. Solvent: water. Time of irradiation: Curve 1: 8 min; 2: 15 min; 3: 60 min.

[7] Beilstein, *Handbuch der Organischen Chemie* (Springer, Berlin, 1922), Vol. 5, p. 362.
[8] Carmack, Moore, and Balis, J. Am. Chem. Soc. **72**, 844 (1950).

an answer based on experimental data is nevertheless of some value.

It is found that dissolving in a hydrocarbon initial and final oxidation products, like a diol and dione, or an aldehyde and acid, does not produce increased electrical conductivity. One may conclude that the ions are not formed by an equilibrium process from the initial and final compounds. It is likely, then, that the ions are found among the intermediate oxidation products, and, although perhaps not stable in a thermodynamic sense, they may be relatively stable. This conclusion is in keeping with observations indicating gradual decrease with time of conductivities obtained from oxidation.

There are two possible ways for ions to exist in such solutions: either as ion radicals, having an odd electron, or as ions with completed shells. A definitive decision is not possible on the basis of the present data; perhaps measurements of the magnetic permeability might help. It appears, however, that an explanation by the second mechanism is more plausible. The following evidences may be cited.

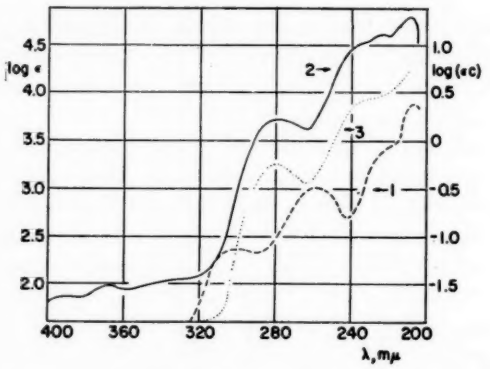

FIG. 8. Extinction coefficient *vs* wavelength. Curve 1: *o*-phthalic aldehyde (Carmack, Moore, and Balis); 2: *o*-phthalic anhydride; 3: *o*-phthalic acid. Solvent: water. Arrows point toward ordinates.

(1) Negative ions originating from acids are compounds with completed electronic shells, having lost a proton.

(2) The previously studied amine solutions[1] revealed the existence of cations of the ammonium type in which a nitrogen atom has a completed octet to which a proton is attached. By analogy it appears likely that oxidation cations contain an oxygen atom with an added proton, i.e., the ions are oxonium type ions. The existence of ions of this nature is known.[9]

(3) Results of the present paper show ortho compounds as ion parents, and ortho side-chain oxidation as leading to ion formation. This preference is explainable on the basis of the added proton being located between the two ortho side groups, closing a ring, as in chelate-type structures.

(4) The ions, as mentioned, are not formed by an equilibrium. If oxonium-type cations are assumed, then

[9] W. Hückel, *Theoretische Grundlagen der Organischen Chemie* (Akademische Verlagsgesellschaft, Leipzig, 1952), Vol. I, p. 127.

the kinetics of ion formation can be explained via radicals, the occurrence of which among oxidation intermediates is generally accepted.[4] The chemical equations, showing only the pertinent part of the molecules, indicate a possible and admittedly hypothetical kinetics of ion formation from *o*-xylene (I). An intermediate oxidation product II has one alcohol and one aldehyde group. On further oxidation this forms the free radical III. Another free radical, IV, forms from further oxidation of phthalic acid. There are probably also other radicals present. Free radicals have a tendency to dimerize or combine, and of the various

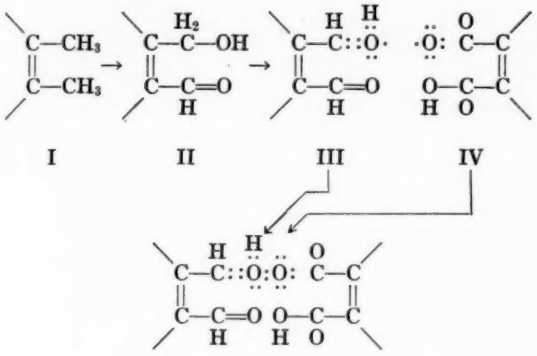

I II III IV

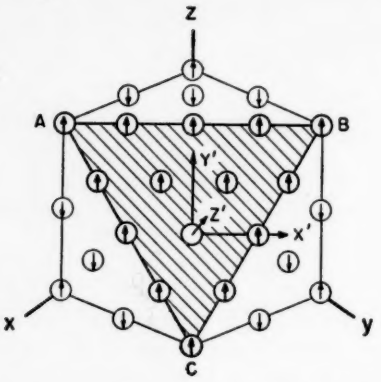

FIG. 1. A spin plane of MnO with axes x', y', z' which label the directions of zero torque for the magnetic dipole energy. The (x,y,z) crystal axes are the directions of spin alignment found experimentally; the (x',y',z') axes are the directions of spin alignment as calculated from just the magnetic dipole interactions. In terms of the direction cosines with reference to the $(x,y,z$ axes) the (x',y',z') axes are given as

$$x'=\left(-\frac{1}{\sqrt{2}},\frac{1}{\sqrt{2}},0\right),$$
$$y'=\left(-\frac{1}{\sqrt{6}},\frac{1}{\sqrt{6}},\frac{2}{\sqrt{6}}\right),$$
$$z'=\left(\frac{1}{\sqrt{3}},\frac{1}{\sqrt{3}},\frac{1}{\sqrt{3}}\right).$$

A. MnO

The classical dipole energy of MnO can be written as

$$E=-\tfrac{1}{2}\mathbf{M}_A\cdot\mathbf{H}^{AA}-\mathbf{M}_A\cdot\mathbf{H}^{BA}-\tfrac{1}{2}\mathbf{M}_B\cdot H^{BB}, \quad (2)$$

where M_A is the magnetization of sublattice A, and H^{BA} is the field at a lattice point A arising from the spins on lattice B; the other terms are defined in a similar way. Defining the magnetization direction of spin systems A and B relative to the crystal axes (as shown in Fig. 1) by $[\alpha\beta\gamma]$ and $[\alpha'\beta'\gamma']$, respectively, we may write

$$\mathbf{H}^{BA}=\alpha'(\mathbf{i}H_{xx}{}^{BA}+\mathbf{j}H_{xy}{}^{BA}+\mathbf{k}H_{xz}{}^{BA})+\beta'(\mathbf{i}H_{yx}{}^{BA}+\mathbf{j}H_{yy}{}^{BA}+\mathbf{k}H_{yz}{}^{BA})+\gamma'(\mathbf{i}H_{zx}{}^{BA}+\mathbf{j}H_{zy}{}^{BA}+\mathbf{k}H_{zz}{}^{BA}); \quad (3)$$

$$M_A=|M_A|(\mathbf{i}\alpha+\mathbf{j}\beta+\mathbf{k}\gamma). \quad (4)$$

Here $H_{ji}{}^{BA}$ is the ith component of the field at an A lattice point arising from spins on the B lattice aligned in the j direction, and $|M_A|$ is the magnitude of the magnetization.

Each sublattice contains 16 atoms per unit cell. As an aid in computing the magnetic fields, each sublattice, A and B, is itself further subdivided into four f.c.c. lattices, each containing four atoms per unit cell. The fields of an f.c.c. lattice at certain selected high symmetry points have been computed by McKeehan.[4] It was found that by using the symmetry properties of an f.c.c. lattice the points at which we needed the fields could all be transformed into McKeehan's points. As an example of the method the fields for MnO are computed in the Appendix. In all cases the fields were computed for a spherical specimen. The results are as follows:

$$H_{ij}{}^{BA}=57.41\frac{(2S)\mu_B}{a_0{}^3}, \quad i\neq j$$
$$=0, \quad i=j \quad (5)$$

and

$$H_{ij}{}^{AA}=H_{ij}{}^{BB}=-57.41\frac{(2S)\mu^B}{a_0{}^3} \quad i\neq j$$
$$=0 \quad i=j, \quad (6)$$

where μ_B = Bohr magnetron, S = electron spin, a_0 = lattice constant.

Substitution of these values in Eqs. (3) and (4) gives for the energy, Eq. (2),

$$E=\underbrace{\frac{(16)(57.41)(2S)^2\mu_B{}^2}{a_0{}^6}}_{K}[\alpha\beta+\beta\gamma+\alpha\gamma+\alpha'\beta'+\beta'\gamma'+\alpha'\gamma'-\alpha'\beta-\alpha\beta'-\beta'\gamma-\beta\gamma'-\alpha'\gamma-\alpha\gamma'], \quad (7)$$

where $a_0=8.86$ A, and S for Mn^{++} is taken to be 5/2. The value of K is then found to be 4.09×10^6 ergs/cm^3, which is unusually high.

We see by inspection that the energy will be zero when the spins are aligned along any one of the [001] axes. It turns out further that the [001] directions are not preferred directions for the dipolar interaction alone. This is seen by calculating the torque on one of the sublattices:

$$\begin{aligned}\mathbf{T}_A=\mathbf{M}_A\times[\mathbf{H}^{AA}+\mathbf{H}^{BA}]=&-K\{\mathbf{i}[\alpha(\beta-\gamma)+\beta^2-\gamma^2]\\&+\mathbf{j}[\beta(\gamma-\alpha)+\gamma^2-\alpha^2]+\mathbf{k}[\gamma(\alpha-\beta)+\alpha^2-\beta^2]\}\\&+K\{\mathbf{i}[\beta(\alpha'+\beta')-\gamma(\alpha'+\gamma')]\\&+\mathbf{j}[\gamma(\beta'+\gamma')-\alpha(\alpha'+\beta')]\\&+\mathbf{k}[\alpha(\alpha'+\gamma')-\beta(\beta'+\gamma')]\}. \quad (8)\end{aligned}$$

The torque for the spins of the two sublattices aligned antiparallel along the z axis will then be

$$\mathbf{T}_A\left\{\begin{matrix}\gamma=1 & \alpha=\beta=0\\ \gamma'=1 & \alpha'=\beta'=0\end{matrix}\right\}=2K[\mathbf{i}-\mathbf{j}]. \quad (9)$$

A nonzero torque implies that the direction chosen is not an extremum of the energy. Shull[3] finds, however, that the spins are aligned along the [001] axes. We must therefore conclude that there must be another important source of anisotropy energy. An interaction of quadrupole form is an obvious possibility. Before considering the form of the quadrupole interaction it is of interest to choose a set of axes along which the dipolar torque will be zero. These new axes, x', y', z', are also

[4] L. W. McKeehan, Phys. Rev. **43**, 913 (1933).

shown in Fig. 1. The energy and torque in the new set of axes are

$$E=K[-\tfrac{1}{2}(\alpha^2+\beta^2)+\gamma^2-\tfrac{1}{2}(\alpha'^2+\beta'^2)+\gamma'^2] \\ -K[-(\alpha'\alpha+\beta'\beta)+2\gamma'\gamma], \quad (10)$$

and

$$\mathbf{T}_A=K[\mathbf{i}'3\beta\gamma+\mathbf{j}'3\alpha\gamma]-K[\mathbf{i}'(2\beta\gamma'+\gamma\beta') \\ +\mathbf{j}'(2\alpha\gamma'+\gamma\alpha')+\mathbf{k}'(\alpha\beta'-\beta\alpha')]. \quad (11)$$

For the spins antiparallel the energy surface will be an ellipsoid of revolution with the minor axes in the $x'y'$ plane and the major axis in the z' direction. The dipole energy in the plane is ($E=-2K$), perpendicular to the plane ($E=4K$) and in the direction of the crystal axes ($E=0$).

The general form of the quadrupole energy[5] is

$$H_{qp}=\sum_{k>j} K_{jk}r_{jk}^{-4}(\mathbf{S}_{Aj}\cdot\mathbf{r}_{jk})^2(\mathbf{S}_{Ak}\cdot\mathbf{r}_{jk})^2 \\ +\sum_{k>j} K_{jk}'r_{jk}^{-4}(\mathbf{S}_{Bj}\cdot\mathbf{r}_{jk})^2(\mathbf{S}_{Bk}\cdot\mathbf{r}_{jk})^2 \\ +\sum_{k,j} K_{jk}''r_{jk}^{-4}(\mathbf{S}_{Bj}\cdot\mathbf{r}_{jk})^2(\mathbf{S}_{Ak}\cdot\mathbf{r}_{jk})^2. \quad (12)$$

Summing over only nearest neighbors and treating the spins classically, the quadrupole energy simplifies in the crystal axes coordinates to

$$E_{qp}=2K_1[(\alpha-\beta)^4+(\alpha-\gamma)^4+(\beta-\gamma)^4] \\ +2K_1[(\alpha'-\beta')^4+(\alpha'-\gamma')^4+(\beta'-\alpha')^4] \\ +2K_2[(\alpha+\beta)^2(\alpha'+\beta')^2+(\alpha+\gamma)^2(\alpha'+\gamma')^2 \\ +(\beta+\gamma)^2(\beta'+\gamma')^2]. \quad (13)$$

The total spin anisotropy energy is then the sum of the magnetic dipole and quadrupole energies. The exchange energy does not enter as it depends on the mutual spin directions which we take to be antiparallel. We find the energies in the three directions to be

		Dipole	Quadrupole	
E_{001}	=	0	$8K_1+4K_2$	
$E_{x'y'\text{ plane}}$	=	$-2K$	$18K_1+K_2$	(14)
E_{111}	=	$4K$	$(32/3)K_2$.	

Since the [001] axes are known to be the easy direction of spin alignment, we must have

$$K>2K_1-\frac{5}{3}K_2, \\ K<5K_1-\tfrac{3}{2}K_2. \quad (15)$$

These are conditions easily satisfied. A more stringent condition would be that the energy be an extremum along a [001] axis, but this would require that the spin axes be exactly in the [001] direction and not just in that direction plus or minus a few degrees. A deviation would not be observed from the neutron diffraction results. Without further restrictions on the quadrupole constants one can only conclude that the [001] axes are energetically possible; the restrictions on K_1 and K_2 are too broad to give a range for the value of the anisotropy field H_A, but it would be quite fortuitous for H_A to be particularly low.

[5] F. Keffer and C. Kittel, Phys. Rev. **85**, 329 (1952); J. H. Van Vleck, Phys. Rev. **52**, 1178 (1937).

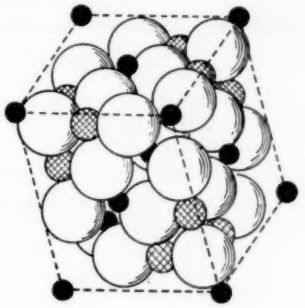

FIG. 2. The spinel unit cell containing $8[\alpha^{++}\beta_2^{+++}O_4]$. The large spheres are oxygen, the black spheres tetrahedral sites, and the cross-hatched spheres octehedral sites.

B. SPINEL STRUCTURE

There are two limits of the spinel structure $[\alpha^{++}\beta_2^{+++}O_4]$, the normal and the inverse spinel. In a unit cell, Fig. 2, for both types, there are 16 octahedral and 8 tetrahedral sites occupied. The normal spinel has the tetrahedral sites occupied by the α^{++} ions, and the octahedral sites occupied by the β^{+++} ions; the inverse spinel has the tetrahedral sites occupied by half the β^{+++} ions and the octahedral sites occupied at random by the α^{++} ions and the other half of the β^{+++} ions. It is found that the octahedral-tetrahedral exchange coupling is such as to produce an antiparallel alignment of the spins on the two types of sites.[6-8] Based on this model the calculation of the magnetic energy for the normal and inverse structure is the same except that for the inverse structure we take one-half the sum of the spins of the α^{++} and β^{+++} ions as the spin value for the octahedral sites. The result of such a calculation, using the same methods as in Section A, is that both spinel structure dipolar energies are zero, independent of direction. This of course satisfies the requirement of cubic symmetry.

I wish to thank Professor Kittel for suggesting this problem and for his helpful suggestions.

This research has been supported in part by the U. S. Office of Naval Research and the U. S. Signal Corps.

APPENDIX

There were four symmetry operations used to help find the necessary field components.

1. Given a point in an f.c.c. lattice (a,b,c) the field will be the same for any point obtained by adding one-half a lattice spacing to any two of the three coordinates.

[6] L. Neel, Ann. phys. **3**, 139 (1948).
[7] Shull, Wollan, and Koehler, Phys. Rev. **84**, 912 (1951).
[8] J. M. Hastings and L. M. Corliss, Revs. Modern Phys. **25**, 114 (1953).

TABLE I.

Field point	Field components
Spins in x direction	
(1/2,0,0)	(0,0,0)
(1/4,1/4,0)	(17.57,57.41,0)
(0,1/4,1/4)	(−35.14,0,0)
(0,0,0)	(0,0,0)
Spins in y direction	
(0,1/2,0)	(0,0,0)
(0,1/4,1/4)	(0,17.47,57.41)
(1/4,0,1/4)	(0,−35.14,0)
(0,0,0)	(0,0,0)
Spins in z direction	
(0,0,1/2)	(0,0,0)
(1/4,0,1/4)	(57.41,0,17.57)
(1/4,1/4,0)	(0,0,−35.14)
(0,0,0)	(0,0,0)

The notation

$$(a,b,c)\overset{1}{\equiv}(a,\ b+\tfrac{1}{2},\ c+\tfrac{1}{2})$$

will be used to indicate an example of operation (1).

2. If the spins on an f.c.c. lattice are pointed in the z direction, a point with coordinates (a,b,c) has the same field as a point with coordinates $(1-a,\ b,\ c)$ except for a sign difference in the x components of the field. The notation

$$(a,b,c)\overset{2}{\equiv}(\bar{1}-a,\ b,\ c),$$

will be used to indicate an example of operation (2).

3. If the spins are pointed in the z direction a point with its x and y coordinates interchanged will have its x and y field components interchanged. The notation for operation (3) will be

$$(a,b,c)\overset{3}{\equiv}P(x,y)(b,a,c),$$

where $P(x,y)$ means that the x and y field components for the point (b,a,c) are to be interchanged so as to equal the field at the point (a,b,c).

4. If the spins are pointed in the z direction a point with its z component "c" replaced by $1-c$ will have its z field component unchanged, but will have a change of sign in the x and y field components. The notation

$$(a,b,c)\overset{4}{\equiv}(\bar{a},\ \bar{b},\ 1-c),$$

will indicate operation (4).

As an example of the use of these operations, the field components for MnO will be computed. McKeehan[4] gives a table of field components for spins on an f.c.c. lattice aligned in the x direction; in Table I the values are also given for the spins aligned in the y and z directions.

The coordinates of a lattice point B with respect to each of the four f.c.c. lattices of A are

(0,0,1/2), (3/4,1/2,1/4), (3/4,1/4,1/2), (1/2,3/4,1/4).

The term $H_{iz}^{AB}/(2S\mu_B/a_0^3)$ will then be equal to the sum of the x field components at point B arising from the spins on the four f.c.c. lattices aligned in the i direction.

For the spins on the A lattice aligned in the x direction:

Field point		Field component
(0,0,1/2)	$\overset{1}{\equiv}$(1/2,1/2,1/2) $\overset{1}{\equiv}$(1/2,0,0)	(0,0,0)
(3/4,1/2,1/4)	$\overset{3}{\equiv}P(yz)$(3/4,1/4,1/2) $\overset{2}{\equiv}$(1/4,1/4,0)	(17.57,0,57.41)
(3/4,1/4,1/2)	$\overset{2}{\equiv}$(1/4,1/4,0)	(17.57,57.41,0)
(1/2,3/4,1/4)	$\overset{1}{\equiv}$(0,1/4,1/4)	(−35.14,0,0)
	Total	(0,57.41,57.41)

Thus

$$H_{xx}^{AB}=0,\quad H_{xy}^{AB}=(57.41)\frac{2S\mu_B}{a_0^3},\quad H_{xz}^{AB}=57.41\frac{2S\mu_B}{a_0^3}.$$

In the same way one can show that

$$H_{yx}^{AB}=57.41\frac{2S\mu_B}{a_0^3},\quad H_{yy}^{AB}=0,\quad H_{yz}^{AB}=57.41\frac{2S\mu_B}{a_0^3},$$

$$H_{zx}^{AB}=57.41\frac{2S\mu_B}{a_0^3},\quad H_{zy}^{AB}=57.41\frac{2S\mu_B}{a_0^3},\quad H_{zz}^{AB}=0.$$

We also must calculate the field components at a B lattice arising from the spins on the B lattice. The coordinates of a lattice point B with respect to each of the four f.c.c. lattices of B are

(3/4,3/4,1/2), (3/4,0,1/4), (0,1/2,1/2), (0,3/4,3/4).

For the spins on the B lattice aligned in the x direction:

Field point		Field component
(3/4,3/4,1/2)	$\overset{1}{\equiv}$(1/4,3/4,0) $\overset{2}{\equiv}$(1/4,$\bar{1}$/4,0)	(17.57,−57.41,0)
(3/4,0,1/4)	$\overset{3}{\equiv}P(y,z)$(3/4,1/4,1/4,0)	(17.57,0,−57.41)
	$\overset{4}{\equiv}P(y,z)$(1/4,$\bar{1}$/4,0)	
(0,1/2,1/2)	$\overset{1}{\equiv}$(0,0,0)	(0,0,0)
(0,3/4,1/4)	$\overset{2}{\equiv}$(0,$\bar{1}$/4,1/4)	(−35.14,0,0)
	Total	(0,−57.41,−57.41)

Thus

$$H_{xx}^{BB}=0,\quad H_{xy}^{BB}=-57.41\frac{2S\mu_B}{a_0^3},$$

$$H_{xz}^{BB}=-57.41\frac{2S\mu_B}{a_0^3},$$

or in general

$$H_{ij}^{BB}=-57.41\frac{2S\mu_B}{a_0^3}\quad i\neq j$$

$$H_{ii}^{BB}=0.$$

THE JOURNAL OF CHEMICAL PHYSICS VOLUME 22, NUMBER 10 OCTOBER, 1954

N-Particle Distribution Functions*

H. L. FRISCH†
Physics Department, Syracuse University, Syracuse, New York
(Received April 2, 1954)

An investigation of a certain class of approximate solutions of the Yvon-Born-Green recurrence relations for the lower-dimensional molecular distribution functions has been presented, based on a particular mechanism of exclusion of interactions among "clusters" composed of successively larger number of molecules. This mechanism leads to a chain of equations for the approximate distribution functions which (a) converge to the exact molecular distribution function after a finite number of approximations, (b) are linear in the dependent variable just like the Yvon-Born-Green recurrence relations, and (c) are time reversible. The connection between these equations and certain natural generalizations of Boltzmann's equation to other than binary collisions is obtained. Finally the application of this hierarchy to certain problems of fluids at equilibrium has been indicated.

I. INTRODUCTION

A SYSTEM consisting of a large number of similar components (molecules) may be treated with the help of the methods of statistical mechanics, which amount essentially to constructing the Liouville equation of the Gibbs ensemble and then attempting to obtain rigorous solutions. The unknown in this case is the distribution function in the phase space of the system whose dimensionality is the product of the number of dimensions of the phase space of a single molecule and the number of molecules. The rigorous treatment of this Liouville equation is, however, prohibitive. In many problems interest centers only on the lowest-dimensional distribution functions, i.e., the one-, two-, and three-particle distribution functions in terms of which most physically interesting macroscopic parameters of these systems can be expressed. Given the Liouville equation in the phase space of N isolated molecules, a number of workers, among them Yvon,[1] Born and Green,[2] and Kirkwood,[3] have obtained the distribution functions of q molecules f_q, $q=1,2,3,\cdots$, by integrating the Liouville equation over the coordinates of $(N-q)$ molecules. This procedure yields a hierarchy of differential equations determining the successive distribution functions. The differential equation for f_q contains in one (differentiated) term the distribution function of $q+1$ molecules. Hence, this procedure fails to give a self-contained mathematical problem in a lower-dimensional space unless the next-higher-dimensional distribution function is assumed to be determined by the lower ones. Such assumptions have been made by various authors, leaving, however, always the question of validity of these *ad hoc* assumptions. The plan of the present paper is to replace these assumptions by a (convergent) approximation method for finding the lower-dimensional distribution functions. Successive approximations to these distribution functions will reflect the assumptions of neglect of all but binary interactions ("collisions"), all but binary and ternary interactions between molecules, etc. The differential equations satisfied by these successive approximations to f_q are linear, first-order differential equations, the $N-q+1$th approximation satisfying the same differential equation and boundary conditions satisfied by f_q.

Alternatively to these methods based on Liouville's equation, Boltzmann treated systems consisting of a large number of similar components in the phase space of an individual molecule, by assuming that the motion of each molecule in its phase space was determined by the internal dynamics of the molecule itself as well as the averaged action of all the other molecules in its vicinity. The resulting equation, which deals with the distribution function of a single molecule, takes into account only binary interactions and has the form of an integro-differential equation. This equation is more nearly manageable than the Liouville equation in gamma space. There has, however, always been a question as to the validity of the Boltzmann equation and its relationship to the Liouville equation. The present paper will in part devote itself to elucidating certain aspects of this problem.

The Hamiltonian H_N of an isolated system consisting of N "indistinguishable" particles (molecules) will be defined as

$$H_N=\sum_{j=1}^{N}\left\{\frac{1}{2m}(\mathbf{p}_j)^2+\Phi_j+\sum_{i\neq j=1}^{N-1}\phi^{(i;j)}\right\}$$
$$=H_{N-1}+\frac{1}{2m}(\mathbf{p}_N)^2+\Phi_N+\sum_{i=1}^{N-1}\phi^{(i;N)},$$

where m and $\mathbf{p}_N$ is the mass and momentum of the Nth particle, Φ_j the external potential acting on the jth particle, $\phi^{(i;j)}$ the interparticle potential between the ith and jth particle, and H_{N-1} is the Hamiltonian of

* This research was supported by the United States Air Force, through the Office of Scientific Research of the Air Research and Development Command.
† Present address: Department of Chemistry, University of Southern California, Los Angeles 7, California.
[1] J. Yvon, *La theorie statistique des fluides* (Hermann and Cie, Paris, 1935).
[2] M. Born and H. S. Green, Proc. Roy. Soc. (London) **A188**, 10 (1947).
[3] J. G. Kirkwood, J. Chem. Phys. **14**, 180 (1946).

the remaining $N-1$ particles. The position and velocity of the ith particle are given by the vectors $\mathbf{x}_i$ and $\xi_i=\mathbf{p}_i/m$, respectively. In the case of simple fluids, $\phi^{(i;j)}$ is assumed to depend only on the distance between the ith and jth particle. To facilitate the construction of ensembles of such systems, Born and Green[2] have defined the probability distribution $f_q(\mathbf{x}_1,\cdots,\xi_q;t)$, $q=0,1,\cdots,N$, of selecting any q particles from the totality of N of them with positions and velocities in the range $\mathbf{x}_1$ and $\mathbf{x}_1+d\mathbf{x}_1,\cdots,\xi_q$ and $\xi_q+d\xi_q$, to be a symmetric function in the coordinates of the q particles. The quantity f_N satisfies Liouville's equation

$$\frac{\partial f_N}{\partial t}+[f_N, H_N]=0. \tag{1}$$

Introducing for convenience the Born integral operator,

$$\chi_q\cdots=\int\int\cdots d\mathbf{x}_q d\xi_q,$$

then the f_q are so normalized as to satisfy

$$\chi_{q+1}f_{q+1}=(N-q)f_q \tag{2}$$

with $f_0=1$.

The successive application of the integral operator χ_q $(q=N, N-1,\cdots, N-q-1)$ on Eq. (1) leads to the Born-Green hierarchy[2]

$$\frac{\partial f_q}{\partial t}+[f_q,H_q]=\frac{df_q}{dt}=S_{q+1}, \tag{3a}$$

where the "statistical term" S_{q+1} is given by

$$S_{q+1}=\sum_{i=1}^{q}\chi_{q+1}[\phi^{(i;q+1)},f_{q+1}]=\mathcal{S}_{q+1}f_{q+1}. \tag{3b}$$

Since f_{q+1} has to be known in order that f_q may be found, Eq. (3) as it stands cannot be used for the direct computation of the f_q. These equations are merely suggestive in that they show that the influence on any of the q particles exerted by the remaining $(N-q)$ is exhibited in the single "statistical term" S_{q+1} and depends on only the next higher distribution function.

II. THE APPROXIMATION PROCEDURE

In order to simplify the discussion of the approximation method, we formally introduce the generating functions $f_q(\mathbf{x}_1,\cdots,\xi_q;t;\lambda)=f_q(\lambda)$, $q=1,2,\cdots,N$; which are to possess the following properties:

(a) $f_q(\lambda)$ is a symmetric function of its arguments $(\mathbf{x}_i,\xi_i)$; $i=1,\cdots,q$, and a single "dimensionless" parameter λ, where $0\leqslant\lambda\leqslant 1$.

(b) $f_N(\lambda)$ satisfies Liouville's equation

$$\frac{df_N(\lambda)}{dt}=\frac{\partial f_N(\lambda)}{\partial t}+[f_N(\lambda),H_N]=0.$$

(c) As λ approaches zero, $f_q(\lambda)$ is to approach the probability distribution in the phase space of q isolated particles $f_q^{(0)}$, which satisfies $df_q^{(0)}/dt=0$. As λ approaches one, $f_q(\lambda)$ is to approach the f_q of the Born-Green hierarchy.

These conditions can be satisfied if $f_q(\lambda)$ is taken to be a solution of the equation

$$\frac{df_q(\lambda)}{dt}=\frac{\partial f_q(\lambda)}{\partial t}+[f_q(\lambda),H_q]=\lambda\mathcal{S}_{q+1}f_{q+1}(\lambda), \tag{4}$$

$q=1,2,\cdots,N$. The definition of $f_q(\lambda)$ is completed by requiring that the initial value of $f_q(\lambda)$ be independent of λ and identical with the initial value of the corresponding distribution function f_q of the Born-Green hierarchy.

The introduction of the parameter λ corresponds physically to surrounding any group of q particles by a membrane separating them from the remaining $(N-q)$ particles. The membrane transmits but imperfectly the interparticle interactions between any one of the q particles and any one of the $(N-q)$ particles; the parameter λ representing the "translucence" of the membrane; i.e., as $\lambda\to 1$ the membrane becomes a perfect conductor and as $\lambda\to 0$ the membrane becomes a perfect insulator.

The basic idea of our approximation method may now be stated. We assume that $f_q(\lambda)$ can be expanded in a polynomial in λ,

$$f_q(\lambda)=f_q^{(0)}+\sum_{j=1}^{N-q}\lambda^j\{f_q^{(j)}-f_q^{(j-1)}\}, \tag{5a}$$

where the successive approximations to f_q, $f_q^{(j)}$ satisfy the linear, first-order partial differential equations

$$\begin{aligned} &df_q^{(0)}/dt=0,\\ &df_q^{(j)}/dt=\mathcal{S}_{q+1}f_{q+1}^{(j-1)}, \quad j=1,2,\cdots. \end{aligned} \tag{5b}$$

On substituting Eqs. (5) in Eqs. (4) and collecting coefficients of equal powers of λ, we verify the convergence of $f_q^{(j)}$ to f_q, i.e.,

$$\lim_{j\to N-q} f_q^{(j)}=f_q=\lim_{\lambda\to 1} f_q(\lambda).$$

The quantity $f_q^{(j)}$ corresponds to that approximation to f_q which results if we neglect all interactions involving more than $q+j$ particles.‡ If f_q is known at any time t_0, $f_q(\mathbf{x}_1^0,\cdots,\xi_q^0;t_0)$, (Cauchy data), then by virtue of the definition of the generating function

‡ This method of approximating the molecular distribution functions does not lead to power series in any quantity, not in the density, activity, or even λ, i.e., the $f_q^{(j)}$ are not functions of λ. The generating function of the $f_q^{(j)}$, $f_q(\lambda)$, is not itself a molecular distribution function; it is not an infinite power series in λ but a polynomial (of degree $N-q$) in λ. The λ itself never appears in the end results. The method does not lead to a generalized virial development of the molecular distribution functions in powers of a chosen physical parameter.

$f_q(\lambda)$, Eqs. (5b) must possess unique solutions under the initial conditions

$$f_q^{(j)} \to f_q^{(j-1)} \to \cdots \to f_q^{(0)} \to f_q(\mathbf{x}_1^0, \cdots, \xi_q^0; t_0) \quad (5c)$$

as $t \to t_0$.

To summarize we have found a convergent hierarchy of approximations to the lower-dimensional distribution functions satisfying the Yvon-Born-Green recurrence relations. The solutions of Eqs. (5b) are reversible in the sense that for every solution of these equations another is obtained by reversing the signs of t and the velocities ξ_i. For $j=1$ this assertion holds since $f_q^{(0)}$ is a solution of Liouville's equation and for $j=2,3,\cdots,(N-q)$ it follows by induction. This statement, in turn, implies that these equations cannot be used as a basis for a theory of irreversible processes without adjoining to them some mechanism by which irreversibility can be introduced. In the next section we will show this can be done by assuming an analog of Boltzmann's "Stosszahlansatz."

For attenuated systems, such as dilute gases, the one-particle distribution function f_1, which is the physically most interesting one, is very well approximated by $f_1^{(1)}$, obtained by neglecting all but binary interactions. By a well-known mean-free-path argument one can show that a necessary condition for the validity of this assumption is that $n\sigma^3 \ll 1$, where n is the number density of molecules and σ the "effective molecular diameter." For central interparticle forces, $f_1^{(1)}$ may be explicitly obtained as a solution of

$$\begin{aligned} &df_2^{(0)}/dt = 0, \qquad && f_2^{(0)}(t_0) = f_2(t_0); \\ &df_1^{(1)}/dt = S_2 f_2^{(0)}, && f_1^{(1)}(t_0) = f_1(t_0). \end{aligned} \quad (6)$$

Since general methods of finding explicit solutions of Eq. (6) under these conditions are well known,[4] they need not be discussed here. In principle, at least the higher approximations to f_1 can be found from Eqs. (5). We should recognize though that in common with other approximation schemes, e.g., the Yvon-Born-Green recurrence relations in conjunction with Kirkwood's superposition principle, the procedure outlined in this section is limited in that explicit solutions of Eqs. (5) for large values of j, i.e., for higher approximations to the molecular distribution functions, are hard to find at least for nonstationary systems. In particular, explicit solutions of $df_q^{(0)}/dt = 0$ for $q \geq 3$ are not generally known. The scheme of approximations can still be usefully employed if we restrict ourselves to consideration of systems not far from equilibrium in which the higher-dimensional distribution functions vary very slowly with time. In this case approximate f_q's can be obtained by setting $f_{q+k}^{(0)}$, $k=1,2,\cdots$, in Eqs. (5) equal to the corresponding equilibrium probability densities. The validity of this procedure must then be verified anew for every system considered.

III. RELATION TO BOLTZMANN'S EQUATION

Recently[4–7] a number of authors have discussed the relationship between Boltzmann's equation and Liouville's equation. For a derivation of Boltzmann's equation from Liouville's equation certain additional assumptions ("molecular chaos," etc.) have to be made, whose consistency with Liouville's equation requires a separate investigation. Grad[8] has discussed some of these assumptions in detail, the chief being (1) point molecules, (2) complete collisions, (3) slowly varying one-molecule distribution function, and (4) molecular chaos. The relation of these derivations and the approximation procedure of the preceding section arises from the second assumption, which is merely a stronger statement of the neglect of all but binary collisions; we may start therefore from Eq. (6) expressing $f_1^{(1)}$ in terms of $f_2^{(0)}$. The various derivations differ in at least two important respects, first the interpretation of the molecular chaos assumption and second in the introduction of a mechanism for the irreversibility of the Boltzmann equation. The approaches of both Kirkwood[5] and Schönberg[6] involve the introduction of special time averages, so that the Boltzmann equation is satisfied by a "time-coarse-grained" distribution function. Irreversibility is introduced in the course of this averaging. Kirkwood[5] averages the distribution function over a time interval along the real motion, while Schönberg[6] averages instead the effect of the interaction along a virtual motion of a two-particle system. We shall follow the presentation of Schönberg. Denote by $\theta(\tau_1(t), \tau_2(t))$ the time of collision corresponding to a collision finishing when the two particles are at the points $\tau_1(t)$ and $\tau_2(t)$ of phase space; it will be treated as a first-order infinitesimal quantity in connection with the space variation of the distribution functions.[6] The time average is now defined by

$$\frac{1}{\theta}\int_{t-\theta}^{t} f_1^{(1)}(\tau_1, t)dt' = \bar{f}_1^{(1)}.$$

Applying this method of time averaging to both sides of Eq. (6), one obtains[6]

$$\frac{d}{dt}\bar{f}_1^{(1)} = \frac{1}{m}\int_{-\infty}^{\infty} d\xi_2 \int_V \{\bar{f}_2^{(0)}(\mathbf{x}_1, \xi_1^+, \mathbf{x}_2, \xi_2^+; t) - \bar{f}_2^{(0)}(\tau_1, \tau_2; t)\} |\xi_1 - \xi_2| d\mathbf{q}_2 \quad (7)$$

with

$$\xi_i^+ = \xi_i(t-\theta), \quad i=1,2; \quad d\mathbf{q}_2 = d\mathbf{x}_2^{(1)} d\mathbf{x}_2^{(1)}.$$

The right-hand side of Eq. (7) can now be identified with the collision integral of Boltzmann by introducing

[4] R. Courant and D. Hilbert, *Methoden der Mathematischer Physik* (J. Springer, Berlin, 1937), Vol. II, Chap. 2.
[5] J. G. Kirkwood, J. Chem. Phys. **15**, 72 (1947); Kirkwood, Buff, and Green, J. Chem. Phys. **17**, 988 (1949).
[6] M. Schönberg, Nuovo cimento **10**, 419 (1953).
[7] M. S. Green, Phys. Rev. **94**, 792 (1954).
[8] H. Grad, Comm. Pure Appl. Math. **2**, 331 (1949).

the molecular chaos hypothesis in terms of the modified distribution functions. This hypothesis must allow us to express $\bar{f}_2^{(0)}$ as the product

$$\left(\frac{N-1}{N}\right)\bar{f}_1^{(1)}(\tau_1,t)\bar{f}_1^{(1)}(\tau_2,t). \tag{8}$$

Except in equilibrium this hypothesis has never been rigorously justified. Since a correlation between the velocities of two molecules not in collision can arise only from a past collision or a previous collision of the two molecules with a same third molecule, it is clear that the error inherent in this assumption is greatly reduced in the limit as N, and the total volume in which the molecules are contained is allowed to approach infinity. Thus Eq. (7) becomes

$$\frac{d}{dt}\bar{f}_1^{(1)}=\frac{1}{m}\int_{-\infty}^{\infty}d\xi_2\int_V\{\bar{f}_1^{(1)}(\mathbf{x}_1,\xi_1^+;t)\bar{f}_1^{(1)}(\mathbf{x}_2,\xi_2^+;t) - \bar{f}_1^{(1)}(\tau_1;t)\bar{f}_1^{(1)}(\tau_2;t)\}|\xi_1-\xi_2|\,d\mathbf{q}_2. \tag{9}$$

Applying this procedure to the next higher approximation in Eqs. (5) yields a generalization of Boltzmann's equation to ternary collisions. Schönberg has shown that the form of that equation is given by

$$\frac{d}{dt}\bar{f}_2^{(2)}=\frac{1}{m}\int_{-\infty}^{\infty}d\xi_3\int_V\{\bar{f}_3^{(1)}(\mathbf{x}_1,\xi_1^+,\mathbf{x}_2,\xi_2^+,\mathbf{x}_3,\xi_3;t) - \bar{f}_3^{(1)}(\tau_1,\tau_2,\tau_3;t)\}|\xi_3-\xi_1-\xi_2|\,d\mathbf{q}_3$$

where

$$\xi_1^+=\tfrac{1}{2}\{\xi_b(t-\theta')+\xi_r(t)\},\quad \xi_2^+=\tfrac{1}{2}\{\xi_b(t-\theta')-\xi_r(t)\},$$

$$\xi_3^+=\xi_3(t-\theta'),\quad \theta'=\theta(\tau_1,\tau_2,\tau_3),\quad \xi_r=\xi_1-\xi_2,$$

and

$$\xi_b=\xi_1+\xi_2.$$

Using a three-particle analog of the molecular chaos assumption suggested by the superposition principle of Kirkwood and Boggs[9] completes the analogy to the ordinary Boltzmann equation. This process can be continued. While these equations can presumably be applied to less dilute gases than Eq. (8), the increase in mathematical complexity resulting therefrom seriously curtails their practical applicability.

IV. SYSTEMS IN EQUILIBRIUM

One of the principal problems of the theory of fluids at rest is concerned with the finding of suitable approximations to the radial distribution function $n_2(\mathbf{r})$ and its higher analogs defined by

$$n_q(\mathbf{x}_1,\cdots,\mathbf{x}_q)=\int^{(q)}\cdots\int f_q(\mathbf{x}_1,\cdots,\xi_q)d\xi_1^{(q)}\cdots d\xi_q$$

with

$$\partial f_q/\partial t=0.$$

For sufficiently large values of N, f_N will be given by Boltzmann's distribution

$$f_N=\exp\beta(F_N-H_N),$$

where $\beta=1/kT$, k is Boltzmann's constant, T the absolute temperature, and F_N the free energy of the N-particle system. As N increases the labor entailed in the calculation of the n_q as well as F_N directly from this relation soon becomes prohibitive. We will show that the approximation scheme previously outlined can be used to obtain simple approximations for at least the lower n_q's. As for nonstationary systems, we can define the $f_q(\lambda)$ and $f_q^{(j)}$, the latter satisfying the (equilibrium) recurrence relations:

$$[f_q^{(j)},H_q]=\mathcal{S}_{q+1}f_{q+1}^{(j-1)},\quad j=1,2,\cdots,$$

i.e.,

$$\sum_{i'=1}^{q}\left\{\xi_{i'}\cdot\frac{\partial f_q^{(j)}}{\partial\mathbf{x}_{i'}}+\frac{1}{m}\left(\mathbf{F}_{i'}-\sum_{k\neq i}\frac{\partial\phi^{(i';k)}}{\partial\mathbf{x}_i}\right)\cdot\frac{\partial f_q^{(j)}}{\partial\xi_{i'}}\right\} =\sum_{i'=1}^{q}\frac{1}{m}\int\int\frac{\partial f_{q+1}^{(j-1)}}{\partial\xi_{i'}}\cdot\frac{\partial\phi^{(i';q+1)}}{\partial\mathbf{x}_{i'}}d\mathbf{x}_{q+1}d\xi_{q+1}; \tag{11a}$$

and

$$[f_q^{(0)},H_q]=0,$$

i.e., we choose§

$$f_q^{(0)}=\exp\beta(F_q-H_q),$$

where $\mathbf{F}_{i'}$ is the force on the i'th particle due to an external potential. The jth approximation to n_q, $n_q^{(j)}$ is obtained by integrating $f_q^{(j)}$ over the velocities $\xi_1,\cdots,\xi_q$. Equations (11a) can be transformed into linear recurrence relations for the $n_q^{(j)}$ by multiplying Eq. (11a) by ξ_i, $1\leqslant i\leqslant q$, and integrating over the velocities $\xi_1,\cdots,\xi_q$, taking for convenience $\mathbf{F}_i\equiv 0$,

$$\frac{1}{(-\beta)}\frac{\partial n_q^{(j)}}{\partial\mathbf{x}_i}=n_q^{(j)}\sum_{k=1}^{q}\frac{\partial\phi^{(i;k)}}{\partial\mathbf{x}_i} +\int n_{q+1}^{(j-1)}\frac{\partial\phi^{(i;q+1)}}{\partial\mathbf{x}_i}d\mathbf{x}_{q+1} \tag{11b}$$

with

$$n_q^{(0)}=\gamma^q\exp\beta\{F_q-\sum_{i\neq j=1}^{q}\phi^{(i;j)}\},\quad \gamma=(2\pi/\beta m)^{\frac{1}{2}}.$$

A first approximation to the radial distribution function $n_2(\mathbf{r})$ in a liquid can be immediately obtained from Eq. (11b) by taking $q=2$, $j=1$, $\mathbf{r}=\mathbf{x}_2-\mathbf{x}_1$, $\mathbf{s}=\mathbf{x}_3-\mathbf{x}_1$,

[9] J. G. Kirkwood and E. M. Boggs, J. Chem. Phys. **10**, 394 (1942).

§ By choosing this solution for $f_q^{(0)}$ we insure convergence of the successive approximations.

$t=\mathbf{x}_2-\mathbf{x}_3$, and $l^2=r^2+s^2-2rs\cos\theta$,

$$\frac{1}{(-\beta)}\frac{\partial n_2^{(1)}}{\partial \mathbf{x}_1}=n_2^{(1)}\frac{\partial \phi^{(1;2)}}{\partial \mathbf{x}_1}+\int n_3^{(0)}(r,s,l)\frac{\partial \phi^{(1;3)}}{\partial \mathbf{x}_1}d\mathbf{x}_3$$

with

$$n_3^{(0)}(r,s,l)=\gamma^3\exp\{\beta[F_3-\phi(r)-\phi(s)-\phi(l)]\}$$

$$=a_3\exp\{-\beta[\phi(r)+\phi(s)+\phi(l)]\},$$

$$a_3=\gamma^3\exp(+\beta F_3)$$

$$=\left[\int\int\int\exp\{-\beta[\phi(r)+\phi(s)+\phi(l)]\}drdsdt/6\right]^{-1}.\|$$

This in turn can be written as

$$\exp[-\beta\phi(r)]\frac{d}{dr}\{n_2^{(1)}\exp[\beta\phi(r)]\}$$

$$=-2\pi\beta\int_0^\infty\int_0^\pi n_3^{(0)}(r,s,l)\phi'(s)\cos\theta\sin\theta d\theta s^2ds$$

$$=\pi\beta\int_0^\infty\int_{|r-s|}^{|r+s|}n_3^{(0)}(r,s,l)t\left(\frac{l^2-s^2}{r^2}-1\right)dl\phi'(s)ds$$

$$=-I(r)$$

which on integration over r gives

$$\frac{n_2^{(1)}}{n^2}=\exp[-\beta\phi(r)]\left\{1+\int_r^\infty\frac{I(r')}{n^2}\times\exp[\beta\phi(r')]dr'\right\},\quad(12a)$$

n being the number density. The critical values of r are then solutions of the transcendental equation

$$n^2\beta\phi'(r)\exp[-\beta\phi(r)]\times\left\{1+\int_r^\infty\frac{I(r')}{n^2}\exp[\beta\phi(r')]dr'\right\}+I(r)=0.\quad(12b)$$

A better estimate of the radial distribution function would be given by $n_2^{(2)}(r)$ whose calculation presents no extreme expenditure of labor. Equations (11) and their generating functions may help to elucidate certain aspects of condensation in fluids. Whether these relations can be used for a theory of condensation is strongly dependent on the sensitivity of the partition function of the N molecules to being approximated by a chain of products of partition functions of various molecular clusters in the way obtainable from Eqs. (11).

The author wishes to acknowledge helpful discussions in connection with this problem with P. G. Bergmann and E. P. Gross of Syracuse University as well as M. S. Green of the University of Maryland.

Note added in proof.—After this paper had been accepted for publication the author came across a paper by N. Bogolubov [J. Phys. (U.S.S.R.) **10**, 265 (1946)] whose approach in some respects is related to that of the author.

‖ That is, $6/a_3$ is the configurational partition function for three particles.

Millimeter Wave Spectra and Centrifugal Stretching Constants of the Methyl Halides*

W. J. ORVILLE THOMAS,† J. T. COX, AND WALTER GORDY
Department of Physics, Duke University, Durham, North Carolina

(Received May 7, 1954)

High J transitions of the methyl halides have been measured and have been used to calculate accurate values for the centrifugal distortion constants.

The values obtained for B_O, D_{JJ}, and D_{JK} are (in Mc/sec and kc/sec, respectively); $CH_3 \cdot F^{19}$, 25 536.11, 59.3, 445; $CH_3 \cdot Cl^{35}$, 13 292.86, 18.1, 198; $CH_3 \cdot Br^{79}$, 9568.20, 9.9, 128.3; $CH_3 \cdot Br^{81}$, 9531.82, 9.7, 127.4; $CH_3 \cdot I^{127}$, 7501.30, 6.28, 98.5.

The new D_{JJ} value for $CH_3 \cdot Cl^{35}$ is in good agreement with the value of 18.4 kc/sec theoretically predicted by Chang and Dennison.

For all four molecules the D_{JJ} constants were found to be in good agreement with those predicted from Kratzer's formula

$$D_{JJ}=4B_O^3/\omega^2,$$

where ω is the vibrational frequency corresponding to the stretching of the carbon halogen bond.

I. INTRODUCTION

THIS paper represents part of a program of accurate measurement of microwave absorptions in the spectral region of one to three millimeter wavelength where more accurate values may be obtained for the centrifugal distortion constants of molecules through study of higher J transitions. Already these constants have been evaluated approximately for the methyl halides from measurements below 100 kMc. In this frequency range, the centrifugal stretching terms, particularly those in D_{JJ}, are too small to be measured with high accuracy. Recently methods have been developed in this laboratory[1a] which allow precision measurements by microwave electronic methods down to one millimeter wavelength and even into the submillimeter wave region.[1b] Because of these developments, and because of the new theoretical predictions of the stretching constants of methyl chloride by Chang and Dennison,[2] we have considered it worth while to measure rotational transitions of the methyl halides in the one-to-three millimeter range in order to obtain more accurate values of the centrifugal distortion constants.

The centrifugal distortion constants can be obtained in a theoretical manner by use of the values of the force constants occurring in the potential function governing the vibrations of the molecule. Using accurate values for the force constants, Chang and Dennison[2] have obtained the values $D_{JJ}=18.4$ kc/sec, $D_{JK}=189$ kc/sec for $CH_3 \cdot Cl^{35}$. The theoretical value for D_{JJ} differs by some 40 percent from the experimental values of Simmons and Anderson,[3] and that obtained from infrared data by Pickworth and Thompson.[4]

TABLE I. The hyperfine structure of the $J=2\rightarrow3$ rotational transition for $CH_3 \cdot Cl^{35}$.

K Transition	F Transition	ν (observed) Mc/sec	ν (calculated)[a] Mc/sec
0	7/2→9/2 5/2→7/2	79 756.00	79 756.10
	3/2→5/2 1/2→3/2	79 751.44	79 751.46
1	7/2→9/2	79 756.00	79 756.03
	5/2→7/2	79 751.44	79.751.34
	1/2→3/2	79 756.00	79 755.89
2	7/2→9/2 7/2→7/2 7/2→5/2	79 756.00	79 755.86

[a] Calculated using the data given in Table VIII.

II. EXPERIMENTAL

The spectrometer used was of the simple video type with absorption cells of coin silver G-, H-, and K-band wave guide. Crystal harmonic generators driven by reflex klystron tubes were used as energy sources, and the single crystal system was employed for detection. The harmonic generator and detector employed are those described by King and Gordy.[1a] Fourth, sixth, seventh, and eighth harmonics of the fundamental of the klystron power were used in the different measurements.

Frequency measurements were made at the klystron fundamental by use of a secondary frequency standard which was monitored by comparison of the lowest frequency in the multiplier chain, 5 Mc/sec, with the standard 5-Mc/sec signal broadcast by station WWV.

The absorption cell was immersed in dry ice. Gas pressures of about 10^{-2} mm Hg were used.

* This research was supported by the U. S. Air Force through the Office of Scientific Research of the Air Research and Development Command.

† Visiting Fulbright Scholar, 1953–1954. On sabbatical leave from The Edward Davies Chemical Laboratories, University College of Wales, Aberystwyth, Wales.

[1] (a) W. C. King and Walter Gordy, Phys. Rev. **90**, 319 (1953); **93**, 407 (1954). (b) Charles A. Burrus and Walter Gordy, Phys. Rev. **93**, 897 (1954).

[2] Tsu-Shen Chang and D. M. Dennison, J. Chem. Phys. **21**, 1293 (1953).

[3] J. W. Simmons and W. E. Anderson, Phys. Rev. **80**, 338 (1950).

[4] J. Pickworth and H. W. Thompson, Trans. Faraday Soc. **50**, 218 (1954).

III. RESULTS

The observed frequencies for the different transitions which were measured in the present work are given in Tables I to VI. The $J=0\rightarrow1$ transition of methyl fluoride, which has been already measured in the 1 to 3 millimeter range, was remeasured leading to a value of $\nu=51\,071.98$ Mc/sec. The rotational spectra of methyl chloride, bromide, and iodide each have hyperfine structure arising from the nuclear quadrupole interaction of the halogen nuclei. These hyperfine structures are analyzed with the help of the numerical tables given in the book by Gordy, Smith, and Trambarulo.[5] The calculated hyperfine frequencies are given in the tables for comparison with the observed values. Relative intensity measurements of the different hyperfine components were made with accuracy sufficient only for identification of the patterns and are not given in the tables.

TABLE II. The hyperfine structure of the $J=3\rightarrow4$ rotational transition for $CH_3\cdot Cl^{35}$.

K Transition	F Transition	ν (observed) Mc/sec	ν (calculated) Mc/sec
0	9/2→11/2 7/2→9/2	106 338.75	106 338.81
	9/2→9/2	106 320.08	106 320.08
	7/2→7/2	106 345.33	106 345.37
	5/2→7/2 3/2→5/2	106 336.59	106 336.63
	5/2→5/2	106 355.35	106 355.36
1	9/2→11/2	106 337.70	106 337.77
	7/2→9/2	106 335.79	106 335.89
	7/2→7/2	106 341.52	106 341.48
	5/2→5/2	106 350.77	106 350.84
	3/2→5/2	106 336.59	106 336.79
2	9/2→11/2	106 334.53	106 334.62
	9/2→9/2 7/2→9/2	106 327.02	106 327.13
3	9/2→11/2	106 392.24	106 329.40
	9/2→9/2	106 335.79	106 335.95
	7/2→9/2	106 312.37	106 312.55
	7/1→7/2	106 310.31	106 310.25
	5/2→7/2	106 321.24	106 321.17
	5/2→5/2	106 314.52	106 314.62

Second-order quadrupole coupling effects which in methyl bromide and methyl iodide can be easily detected in low J transitions are entirely negligible for the high J transitions measured here.

From an analysis of the hyperfine multiplets the hypothetical ν_0's given in Table VII are obtained. They represent the frequencies at which the unsplit rotational lines would occur if there were no nuclear quadrupole interaction. These ν_0's are then employed with the usual formula for the symmetric rotor,

$$\nu_0=2B_O(J+1)-2D_{JK}(J+1)K^2-4D_{JJ}(J+1)^3$$

[5] Gordy, Smith, and Trambarulo, *Microwave Spectroscopy* (John Wiley and Sons, Inc., New York, 1953).

TABLE III. The hyperfine structure of the $J=5\rightarrow6$ rotational transition for $CH_3\cdot Cl^{35}$.

K Transition	F Transition	ν (observed) Mc/sec	ν (calculated) Mc/sec
0	13/2→15/2 11/2→13/2	159 499.02	159 498.97
	13/2→13/2	159 480.29	159 480.24
	9/2→11/2 7/2→9/2	159 498.25	159 498.11
1	13/2→15/2		159 496.77
	11/2→13/2	159 495.99[a]	159 496.24
	9/2→11/2		159 495.59
	7/2→9/2		159 496.11
	13/2→13/2	159 479.25	159 479.39
2	13/2→15/2	159 490.27	159 490.21
	11/2→13/2	159 488.13	159 488.07
	9/2→11/2	159 488.13	159 488.06
	7/2→9/2	159 490.27	159 490.20
3	13/2→15/2	159 479.25	159 479.26
	11/2→13/2	159 474.48	159 474.44
	9/2→11/2	159 475.47	159 475.49
	7/2→9/2	159 480.29	159 480.31
4	13/2→15/2	159 463.92	159 463.89
	11/2→13/2	159 455.37	159 455.33
	7/2→9/2	159 466.53	159 466.43

[a] Center of broad unresolved band.

to give the distortion constants D_{JK} and D_{JJ}, as well as B_O (Table VIII). It is obvious that D_{JJ} must be evaluated before an exact measurement of B_O can be made since for even the lowest $J=0\rightarrow1$ transition the last centrifugal stretching term does not vanish entirely.

The values derived for ν_0 and B_O, the nuclear quadrupole coupling eQq, and the distortion constants,

TABLE IV. The hyperfine structure of the $J=7\rightarrow8$ rotational transition for $CH_3\cdot Br^{79}$.

K Transition	F Transition	ν (observed) Mc/sec	ν (calculated) Mc/sec
0	17/2→19/2 15/2→17/2	153 069.61	153 069.58
	13/2→15/2 11/2→13/2	153 073.09	153 073.14
1	17/2→19/2	153 066.92	153 066.88
	15/2→17/2	153 068.60	153 068.59
	13/2→15/2	153 071.60	153 071.66
2	17/2→19/2	153 058.75	153 058.76
	15/2→17/2	153 065.61	153 065.64
3	17/2→19/2	153 045.22	153 045.24
	15/2→17/2	153 060.67	153 060.70
	13/2→15/2	153 059.73	153 059.78
	11/2→13/2	153 044.21	153 044.31
4	17/2→19/2	153 026.32	153 026.30
	15/2→17/2	153 053.70	153 053.79
	13/2→15/2	153 049.30	153 049.38
	11/2→13/2	153 021.82	153 021.89
5	17/2→19/2	153 001.93	153 001.96
	13/2→15/2	153 035.98	153 036.02
	11/2→13/2	152 992.98	152 993.12
6	15/2→17/2	153 034.03	153 034.07
	13/2→15/2	153 019.63	153 019.63

TABLE V. The hyperfine structure of the $J=7\rightarrow8$ rotational transition for $CH_3\cdot Br^{81}$.

K Transition	F Transition	ν (observed) Mc/sec	ν (calculated) Mc/sec
0	17/2→19/2 15/2→17/2	152 488.14	152 488.13
	13/2→15/2 11/2→13/2	152 491.10	152 491.11
1	17/2→19/2	152 485.61	152 485.55
	15/2→17/2	152 487.03	152 486.98
	15/2→15/2	152 466.19	152 466.30
	13/2→15/2	152 489.56	152 489.54
	11/2→13/2	152 488.14	152 488.11
2	17/2→19/2	152 477.87	152 477.80
	15/2→17/2	152 483.60	152 483.55
	13/2→15/2	152 484.89	152 484.86
	11/2→13/2	152 479.20	152 479.11
3	17/2→19/2	152 464.97	152 464.89
	15/2→17/2	152 477.87	152 477.81
	13/2→15/2	152 477.06	152 477.04
4	17/2→19/2	152 446.88	152 446.81
	17/2→17/2	152 487.03	152 487.01
	15/2→17/2	152 469.84	152 469.78
	13/2→15/2	152 466.19	152 466.09
	11/2→13/2	152 443.13	152 443.12
5	15/2→17/2	152 459.44	152 459.46
	13/2→15/2	152 452.02	152 452.03
6	15/2→17/2	152 446.88	152 446.84

D_{JJ} and D_{JK}, are given in Table VIII. Because of the selection rules which allow no change in K, the constant D_{KK} cannot be evaluated from measurements of this type; it should be positive in sign.

IV. DISCUSSION

The energy term containing D_{JK} arises from the interaction of the rotations of the molecule about the A and B axes. Examination of Table VII shows that as K increases the rotational frequencies ν_0 decrease since $D_{JK}>0$. This indicates that the effective moment of inertia I_b of the molecule about the B axis increases with K. This seems surprising when it is remembered that an increase in K, which increases the rotational frequency of the molecule about the CX bond, will be expected to decrease α (Fig. 1) which in turn should decrease I_b.

Simmons and Anderson[3] have suggested that the positive sign for D_{JK} indicates a considerable lengthening of the CH bonds. However, a significant lengthening of the CH bond would not be expected because of the relatively large stretching force constant of this bond compared with the bond bending constant and the C—Hal stretching constant. A simple calculation for methyl chloride shows that if α and d_{C-Hal} were to remain unchanged, an increase of 0.005A in d_{CH} would be required to account for the displacement of the rotational line in the $J=5\rightarrow6$ transition from the value found for $K=0$ to that found for $K=5$. Actually there is a reduction in the centrifugal force tending to stretch the C—Hal bond because an increase in K must be accompanied by a decrease in the end over end rotational momentum, so that the total angular momentum will remain the same. This effect, as well as the expected decrease in angle α in Fig. 1 already mentioned, will tend to decrease I_b. Thus the increase in d_{CH}, if it is to account for the observed increase in I_b, must be actually greater than 0.005A. From the known force constant $k_{CH}=5\times10^5$ dyne/cm, it is easy to estimate the energy required to stretch the three CH bonds by 0.005A. It is $\Delta E=(\frac{3}{2}k_{CH})(\Delta d_{CH})^2=7.5\times10^{-5}$ erg per molecule, an amount which is orders of magnitude

TABLE VI. The hyperfine structure of the J=7→8 rotational transition for $CH_3\cdot I^{127}$.

K Transition	F Transition	ν (observed) Mc/sec	ν (calculated) Mc/sec
0	19/2→21/2	120 012.42	120 012.35
	17/2→19/2	120 015.95	120 015.94
	17/2→17/2	119 919.48	119 919.24
	15/2→17/2	120 008.43	120 008.50
	13/2→15/2	119 998.90	119 998.96
	11/2→13/2	119 994.36	119 994.47
	9/2→11/2	120 000.34	120 000.42
1	19/2→21/2	120 012.99	120 012.95
	17/2→19/2	120 012.42	120 012.54
	17/2→17/2	119 920.02	119 919.87
	15/2→17/2	120 004.25	120 004.35
	15/2→15/2	120 070.89	120 070.68
	13/2→15/2	119 996.05	119 996.14
	11/2→13/2	119 993.97	119 994.07
	9/2→11/2	120 002.44[a]	120 002.69
2	19/2→21/2	120 014.89	120 014.78
	17/2→19/2	120 002.44[a]	120 002.34
	17/2→17/2	119 921.72	119 921.75
	15/2→17/2	119 991.88	119 991.89
	13/2→15/2	119 987.78[a]	119 987.68
	11/2→13/2	119 992.78	119 992.88
	9/2→11/2	120 009.33	120 009.53
3	19/2→21/2	120 017.88	120 017.82
	17/2→19/2	119 985.10	119 985.32
	15/2→17/2	119 971.10	119 971.11
	13/2→15/2	119 973.48	119 973.59
	11/2→13/2	119 990.79	119 990.89
	9/2→11/2	120 020.67	120 020.91
4	19/2→21/2	120 022.18	120 022.06
	17/2→19/2	119 961.23	119 961.50
	15/2→17/2	119 941.94	119 942.02
	13/2→15/2	119 953.94	119 953.84
	13/2→13/2	120 014.89	120 014.91
	11/2→13/2	119 987.78[a]	119 988.10
	9/2→11/2	120 036.54	120 036.84
5	19/2→21/2	120 027.60	120 027.53
	17/2→19/2	119 930.63	119 930.88
	15/2→17/2	119.904.58	119 904.62
	13/2→15/2	119 928.43	119 928.46
	11/2→13/2	119 984.47	119 984.52
	9/2→11/2	120 057.13	120 057.32
6	19/2→21/2	120 034.26	120 034.20
	17/2→19/2	119 893.31	119 893.45
	17/2→17/2	119 941.94	119 941.80
	15/2→17/2	119 858.79	119 858.91
	13/2→15/2	119 897.38	119 897.44
	11/2→13/2	119 980.18	119 980.13
	9/2→11/2	120 082.48	120 082.36

[a] Broad unresolved band.

TABLE VII. Frequencies of the hypothetical unsplit rotational lines ν_0 in the methyl halides.

J Transition	K Transition	Mc/sec
	$CH_3 \cdot Cl^{35}$	
	0	79 755.11
2→3	1	79 754.12
	2	79 750.65
	0	106 338.20
	1	106 336.58
3→4	2	106 331.80
	3	106 323.92
	0	159 498.77
	1	159 496.12
5→6	2	159 489.25
	3	159 477.30
	4	159 460.70
	$CH_3 \cdot I^{127}$	
	0	120 007.86
	1	120 006.28
	2	120 001.51
7→8	3	119 993.58
	4	119 982.57
	5	119 968.38
	6	119 951.13
	$CH_3 \cdot Br^{79}$	
	0	153 070.91
	1	153 068.87
	2	153 062.69
7→8	3	153 052.40
	4	153 038.02
	5	153 019.52
	6	152 996.96
	$CH_3 \cdot Br^{81}$	
	0	152 489.25
	1	152 487.24
	2	152 481.15
7→8	3	152 470.96
	4	152 456.69
	5	152 438.29
	6	152 415.92

larger than the total rotational energy of the states involved. Clearly the molecular distortion must come about primarily through a shifting of the internal energy of the molecule from one bond to another rather than through a total decrease in molecular rotational energy. This energy shift, we believe, takes place through changes in the C orbital hybridization which would be expected to accompany the decrease in angle α. The mechanism of distortion is then as follows: the increase of angular momentum about the symmetry axis tends through the increased centrifugal force to make the CH_3 group more nearly planar and hence to increase the s character in the three C orbitals which bond to hydrogens. (For a completely planar structure each of these orbitals would have 33 percent s character as contrasted with 25 percent s character for the usual tetrahedral carbon bonding.) As a consequence, the s character of the C orbital bonding to the Hal must be reduced for proper normalization. The combined effect is to make the CH bonds stronger and the C-Hal bond weaker. Both because of the small mass of H and the strong force constant of the CH bond, we can neglect the small direct effects of changes in size and shape of the CH_3 group upon the moment of inertia I_b in comparison to the indirect effects which decrease the s character and hence cause a lengthening of the C−Hal bond. An increase of only 0.0004A in the C−Cl bond length would account for the 60-Mc separation of the $K=0$ and $K=5$ lines in the $J=5\rightarrow6$ transition. Assuming that this increase is caused by a change in the

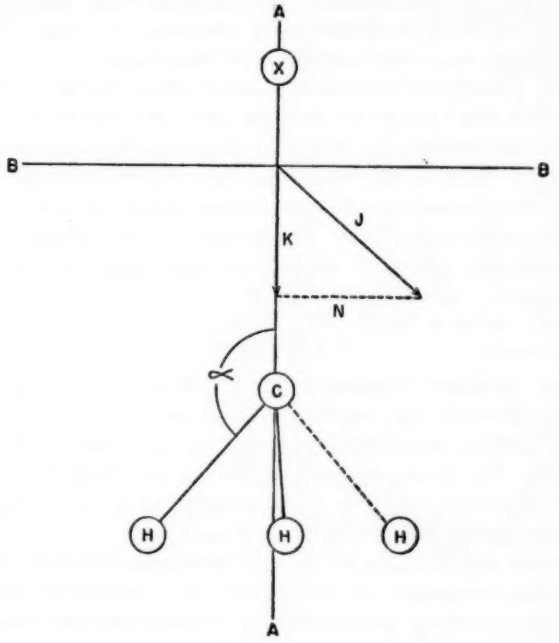

FIG. 1. Structural figure for the methyl halides.

TABLE VIII. Observed spectral constants in the methyl halides.

Molecule		Previous values	New values
$CH_3 \cdot F^{19}$	B_0	25 536.12 Mc	25 536.11±0.01 Mc
	D_{JJ}	57.8 kc	59.3 ±0.20 kc
	D_{JK}	445.0 kc	445.0 ±5.00 kc
$CH_3 \cdot Cl^{35}$	B_0	13 292.95 Mc	13 292.86±0.03 Mc
	D_{JJ}	26.4 kc	18.1 ±0.50 kc
	D_{JK}	189.0 kc	198.0 ±5.00 kc
	eQq	−75.33 Mc	−74.9 ±0.10 Mc
$CH_3 \cdot Br^{79}$	B_0	9568.19 Mc	9568.20±0.01 Mc
	D_{JJ}	11.1 kc	9.9 ±0.20 kc
	D_{JK}	129.4 kc	128.3 ±0.50 kc
	eQq	577.3 Mc	577.3 Mc
$CH_3 \cdot Br^{81}$	B_0	9531.85 Mc	9531.82±0.01 Mc
	D_{JJ}	10.7 kc	9.7 ±0.20 kc
	D_{JK}	129.0 kc	127.4 ±0.50 kc
	eQq	482.4 kc	482.4 Mc
$CH_3 \cdot I^{127}$	B_0	7501.31 Mc	7501.30±0.01 Mc
	D_{JJ}	7.95 kc	6.28±0.10 kc
	D_{JK}	99.4 kc	98.5 ±0.50 kc
	eQq	−1934.0 Mc	−1934.0 Mc

covalent radius of the carbon atom an estimate of the resulting change in hybridization can be obtained from the fact that as the effective covalent radius of C in a CH bond increases by 0.04A the hybridization changes from sp to sp_3 type. A proportional change here would require only 0.25 percent decrease in s character or increase in p character of the C orbital to account for the needed C−Cl bond lengthening. From this change in hybridization an increase in ∠HCH of only 5.0′ is expected with a shortening of 0.00018A in the CH bond. The latter, however, would be partly compensated by the centrifugal force tending to lengthen the CH bond.

By arguments similar to those given above, one might conclude that because end over end rotation alone would tend to make ∠HCH smaller, it might increase the s character of the C orbital bonding to the

TABLE IX. Observed and calculated values of D_{JJ}(kc/sec).

Molecule	Observed	Calculated Kratzer's approx
$CH_3 \cdot F$	59.3[a]	67.5
$CH_3 \cdot Cl$	18.1	19.5
$CH_3 \cdot Br$	9.9	10.4
$CH_3 \cdot I$	6.28	6.62

[a] Calculated with the remeasured 0→1 frequency (ν=51 071.98 Mc) and the frequencies of the higher transition given in reference 1.

halogen sufficiently to make the C—Hal bond shorter and D_{JJ} negative. Actually D_{JJ} is positive, and we must conclude that the end over end rotation is less effective in distorting the bond angle and thus varying the hybridization than is the much more rapid rotation about the symmetry axis when $K \neq 0$. The expected change in hybridization for end over end rotation, while although evidently not sufficient to make D_{JJ} negative, may tend to reduce its magnitude.

If we neglect entirely the small effects of distortion of the CH_3 group by the end over end rotation and assume that the D_{JJ} term arises mainly from a stretching of the C—Hal bond, we can regard the methyl halide molecules as simple diatomic molecules with the CH_3 group replaced by a composite "atom" of mass 15. With this simplified model we can apply Kratzer's formula[6]

$$D_{JJ}=4B_0^3/\omega^2$$

for diatomic molecules. The stretching constants calculated in this way agree with the observed values remarkably well, as may be seen by an examination of Table IX. From this agreement we conclude that the principal distortion by the end over end rotation alone is the stretching of the C—Hal bond.

The values obtained for the distortion constants for methyl chloride are in satisfactory agreement with those predicted theoretically by Chang and Dennison.[2] This measure of agreement between the microwave parameters and those obtained theoretically from infrared data may be taken as an indirect confirmation of the satisfactory nature of the valence force potential function proposed for the methyl chloride molecule by Chang and Dennison.

[6] A. Kratzer, Z. Physik **3**, 289 (1920).

A number of reliable values for D_{JJ} and D_{JK} in the methyl halides are now known. In Fig. 2 the values of log D_{JJ} are plotted against $\log B_0^3/\omega^2$, where ω is the frequency [$\nu_3(a_1)$ in Herzberg's notation] of the C—X bond stretching vibration. The C—X stretching frequency, $\nu_3(a_1)$, goes over into the deformation frequency $\nu_4(f_2)$ of methane when the mass of X is decreased continuously.[7] With this frequency value it is found that the points corresponding to methane and the methyl halides lie on a straight line. The frequency $\nu_6(e)$ in the $CH_3 \cdot X$ molecules also goes over into $\nu_4(f_2)$ in methane. In Fig. 2 the values of log D_{JK} are plotted against $\log B_0^3/\nu_6^2$. A linear relationship is found which intersects the D_{JJ} plot at the point corresponding to methane. This is essentially a plot of

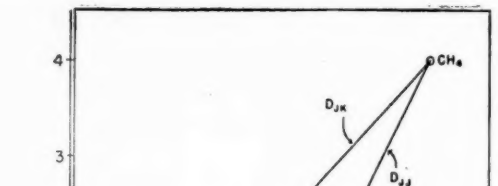

FIG. 2. Relation of D_{JJ} and D_{JK} to B and ω for methane and methyl halides.

Kratzer's relation which strictly applies only to diatomic molecules. Hence it appears purely fortuitous that the point for methane falls on this curve. Boyd and Thompson[8] plotted $\log B_0$ against log D_{JJ} and D_{JK} and obtained linear relationship for the methyl halides. With the more precise values for the stretching constants obtained here this relationship is found to be nonlinear.

[7] J. Wagner, Z. physik Chem. **B40**, 36 (1938).
[8] D. R. J. Boyd and H. W. Thompson, Trans. Faraday Soc. **49**, 1281 (1953).

Rotational Constants of GeH_3D and $GeHD_3$†

LOUIS P. LINDEMAN AND M. KENT WILSON
Mallinckrodt Chemical Laboratory, Harvard University, Cambridge, Massachusetts
(Received March 29, 1954)

The analysis of the rotational structure of the Ge−D stretching fundamental of GeH_3D yields the following values:

$$B''=1.95_7, \quad B''-B'=0.014_2\pm0.0017, \quad \nu_0=1520.4\pm0.2\ \text{cm}^{-1}.$$

A similar analysis of the Ge−H stretching mode in GeD_3H yields for this molecule:

$$B''=1.66_5, \quad B''-B'=0.012_8, \quad \nu_0=2112.4\pm0.2\ \text{cm}^{-1}.$$

The germanium-hydrogen distance obtained under the assumption that it is unchanged by isotopic substitution is $1.52_9\pm0.003$ and $1.52_5\pm0.005$ in GeH_3D and $GeHD_3$, respectively.

INTRODUCTION

RECENT microwave determinations of the Ge−H distance in substituted germanes[1,2] have indicated that the Ge-H distance in these compounds is considerably larger than the value 1.48A reported by Straley, Tindal, and Nielsen[3] for GeH_4. Their analysis of the GeH_4 spectrum is complicated by the presence of strong perturbations in $\nu_4(f_2)$ caused by Coriolis coupling to the infrared inactive band, $\nu_2(e)$. A similar situation exists in SiH_4,[4] and recently[5] it was shown by an investigation of the Si−D stretching fundamental in SiH_3D that the Si−H distance was longer than that reported in SiH_4 and, indeed, was more in agreement with the bond distances obtained from microwave data on halosilanes. The determination of the Si−H distance in SiH_3D is considerably easier than in SiH_4 since only one band need be analyzed and no perturbations occur with the Si−D stretching mode. Analogous arguments apply to GeH_3D and $GeHD_3$ concerning their superiority over GeH_4 in the determination of the Ge−H distance. Accordingly, the present paper reports the analysis of the Ge−H stretching mode in $GeHD_3$ and the Ge−D stretching vibration in GeH_3D.

EXPERIMENTAL

The GeH_3D used in this investigation was prepared by the following sequence of reactions:

$$GeCl_4+Ge \xrightarrow{350^\circ} GeCl_2$$

$$GeCl_2+DCl \longrightarrow GeDCl_3$$

$$GeDCl_3+LiAlH_4 \longrightarrow GeDH_3.$$

Because of contamination of the DCl with HCl the intermediate product, $GeDCl_3$ contained about five percent $GeHCl_3$. The reaction with $LiAlH_4$ was carried out by condensing the $GeDCl_3$ and anhydrous ether into a trap containing the $LiAlH_4$ cooled to liquid nitrogen temperature. As the mixture was allowed to warm up to room temperature a vigorous reaction took place with the evolution of considerable noncondensable gas. The product was freed of noncondensables by slowly passing the evolved gas through a U-trap cooled in liquid nitrogen. The ether was then removed by several bulb-to-bulb distillations at low temperature. The yield was poor and the final product contained a large proportion of GeH_4. However, this impurity caused no interference in the spectral region of interest.

The GeD_3H was obtained as a minor product from the reaction of $GeCl_4$ with $LiAlD_4$ using tetrahydrofuran as a solvent. The final product purified as above contained about 20 percent GeD_3H and the rest the expected GeD_4. There was no interference by the GeD_4 on the ν_1 band of GeD_3H.

The spectra were obtained with a Perkin-Elmer Model 12-C spectrograph modified for double-pass operation and equipped with a CaF_2 prism. The instrument was calibrated in the 1600-cm^{-1} region by water vapor lines whose frequencies were taken from the work of Nielsen[6] and Benedict, Claassen, and Shaw[7] and in the 2100-cm^{-1} region by the CO frequencies reported by Lagemann, Nielsen, and Dickey.[8] In order to reduce the water vapor absorption to a tolerable value in the 1600-cm^{-1} region the instrument was continuously flushed with dry nitrogen.

In Figs. 1 and 2 are reproduced the tracings of ν_2 in GeH_3D and ν_1 in $GeHD_3$, respectively. In both figures the dotted curve is the spectrum of the empty cell. The frequencies of the rotational lines and their assignments are listed in Tables I and II.

DISCUSSION

The frequencies of the rotational lines in a parallel band of a symmetric top molecule when the effect of

† This work was supported in whole or in part by the United States Air Force under Contract AF 18(600)-590 monitored by the U. S. Office of Scientific Research.

[1] Dailey, Mays, and Townes, Phys. Rev. **76**, 136 (1949).
[2] Venkateswarlu, Mockler, and Gordy, J. Chem. Phys. **21**, 1713 (1953).
[3] Straley, Tindal, and Nielsen, Phys. Rev. **62**, 161 (1942).
[4] Tindal, Straley, and Nielsen, Phys. Rev. **62**, 151 (1952).
[5] S. R. Polo and M. K. Wilson, J. Chem. Phys. (to be published): the rotational constants of SiHD.
[6] H. H. Nielsen, Phys. Rev. **59**, 565 (1941).
[7] Benedict, Claassen, and Shaw, J. Research Natl. Bur. Standards **49**, 91 (1952).
[8] Lagemann, Nielsen, and Dickey, Phys. Rev. **72**, 284 (1947).

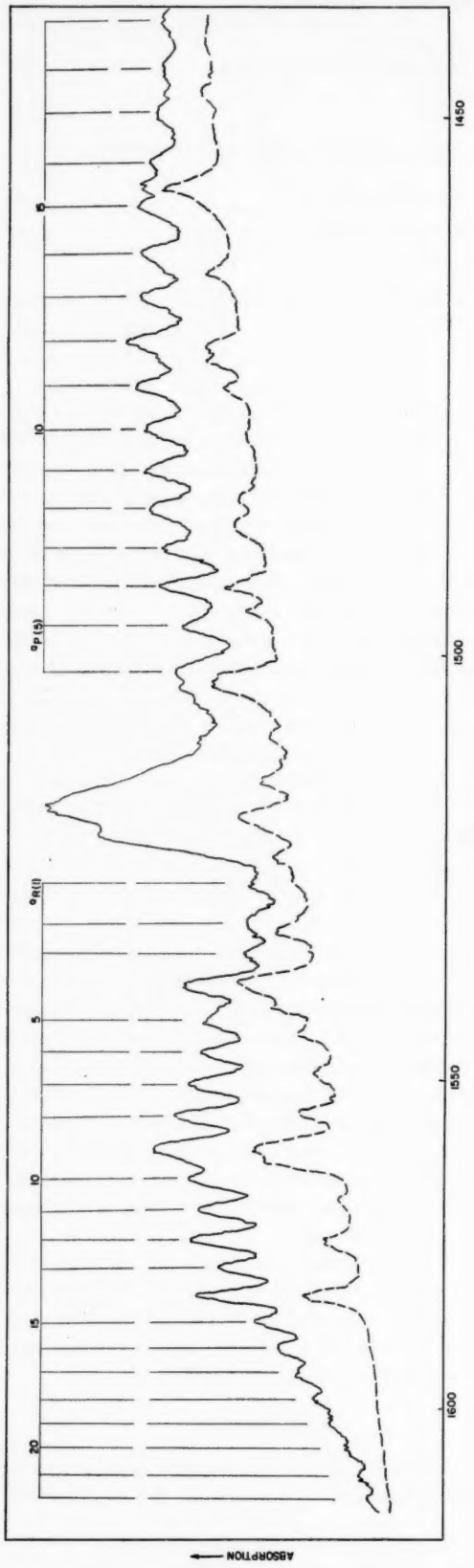

FIG. 1. The Ge-D stretching fundamental, ν_2 of GeH_3D. The dotted curve indicates the absorption due to water vapor.

TABLE I. Observed frequencies of the rotational lines of the ν_1 fundamental of $GeHD_3$.

J	$R(J)$ (cm^{-1})	$P(J)$ (cm^{-1})
6	2135.4	...
7	38.4	2088.6
8	41.5	85.0
9	44.4	81.4
10	47.4	77.6
11	50.3	74.5
12	53.3	70.6
13	56.2	66.9
14	59.3	63.5
15	62.2	59.8
16	65.2	56.4
17	68.2	52.5
18	71.2	49.9
19	74.2	46.0
20	78.5	42.3
21	80.1	38.9
22	...	34.9

centrifugal distortion is neglected are given by

$$P(J)=\nu_0+(B'+B'')J+(B'-B'')J^2$$

and

$$R(J)=\nu_0+(B'+B'')(J+1)+(B'-B'')(J+1)^2$$

where B' and B'' are the rotational constants in the upper and lower vibrational states, respectively, and J is the rotational quantum number of the lower state. The values of the rotational constants can be obtained from the combination differences

$$\Delta_2F''(J)=R(J-1)-P(J+1)$$
$$=4B''(J+\tfrac{1}{2})$$

and

$$\Delta_2F'(J)=R(J)-P(J)$$
$$=4B'(J+\tfrac{1}{2}).$$

TABLE II. Observed frequencies of the rotational lines of the ν_2 fundamental of GeH_3D.

J	$R(J)$ (cm^{-1})	$P(J)$ (cm^{-1})
1	1527.9	...
2	31.9	1512.4
3	35.9	08.5
4	...	05.2
5	43.3	00.5
6	47.3	1496.3
7	50.7	92.5
8	54.2	88.4
9	58.1	84.4
10	61.7	80.3
11	65.3	75.4
12	68.9	71.8
13	72.3	67.2
14	...	63.2
15	78.9	58.4
16	82.3	54.5
17	85.5	49.1
18	88.8	45.4
19	92.0	41.1
20	94.6	...
21	98.9	...
22	1601.9	...

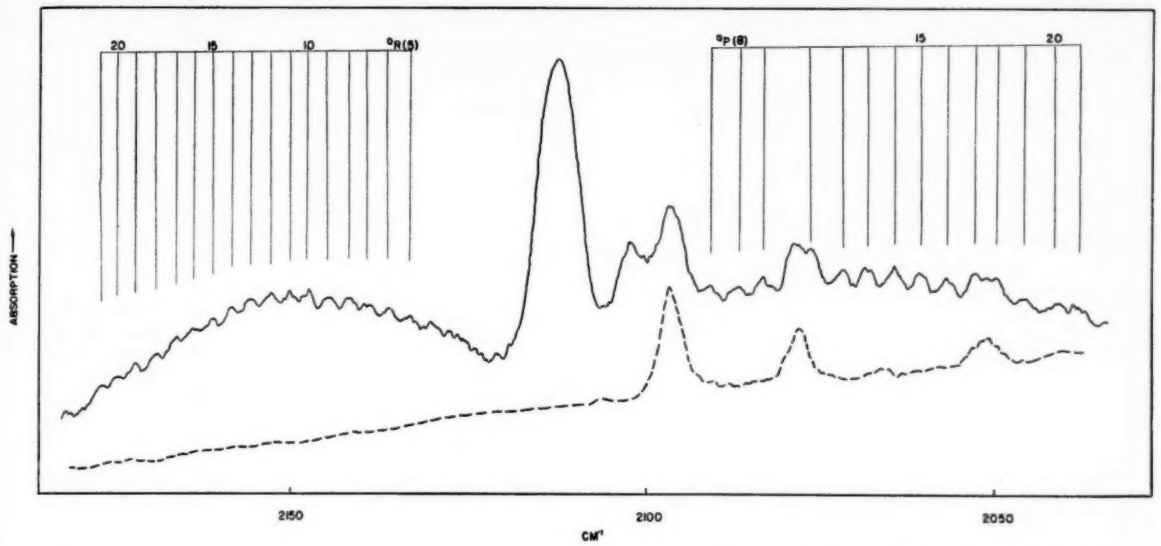

FIG. 2. The Ge—H stretching fundamental, ν_1, of $GeHD_3$. The dotted curve indicates the blank in this region.

In Figs. 3 and 4, $\Delta_2F''-4B''(J+\frac{1}{2})$ is plotted *versus* $J+\frac{1}{2}$ for GeH_3D and $GeHD_3$ with some indication of the limits of error.

The moment of inertia one obtains from an analysis of a parallel band of a symmetric top molecule is that about an axis perpendicular to the symmetry axis. If tetrahedral angles are assumed for both GeD_3H and $GeDH_3$ and the further reasonable assumption is made that the Ge—D and Ge—H bond distances are equal, this moment of inertia for GeX_3Y is given by

$$I=\frac{4m_X(3m_X+5m_Y)+m_{Ge}(5m_X+3m_Y)}{m_{Ge}+3m_X+m_Y}r^2$$

where r is the bond distance. The bond distances obtained in this manner from the observed rotational constants are given in Table III.

The value of the band center and the difference in the rotational constants in the upper and lower states may be obtained from the sum

$$R(J-1)+P(J)=2\nu_0+2(B'-B'')J^2.$$

In Figs. 5 and 6 $R(J-1)+P(J)$ is plotted as a function of J^2 and the values of and $B'-B''$ for both bands are included in Table III.

The average germanium-hydrogen distance of 1.52_7 ± 0.005A obtained in this investigation is in excellent agreement with the value of 1.52A found in GeH_3Cl by Dailey, Mays, and Townes.[1] Venkateswarlu, Mockler, and Gordy[2] from a microwave investigation of $GeHCl_3$

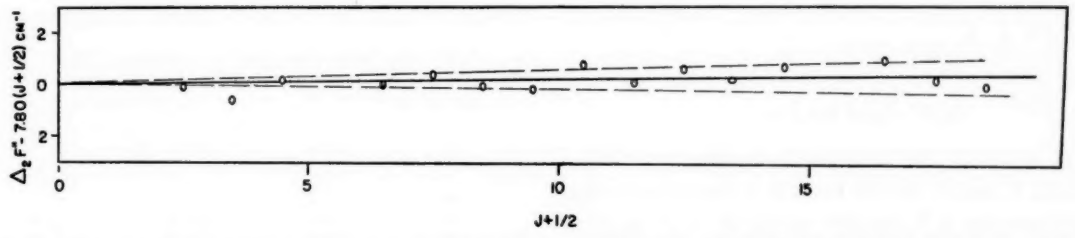

FIG. 3. Plot of $\Delta F_2''-7.80(J+1/2)$ cm^{-1} *vs* $J+1/2$ for the determination of B'' for GeH_3D. The dotted lines indicate the limits of error assigned in determining the slope.

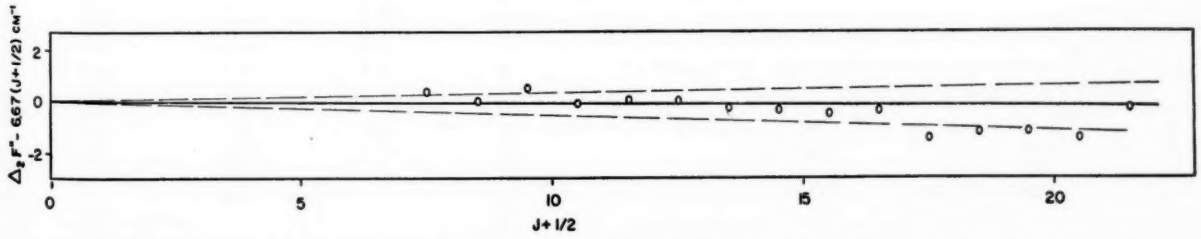

FIG. 4. Plot of $\Delta F_2''-6.67(J+1/2)$ cm^{-1} *vs* $J+1/2$ for the determination of B'' for $GeHD_3$. The dotted lines indicate the limits of error assigned in determining the slope.

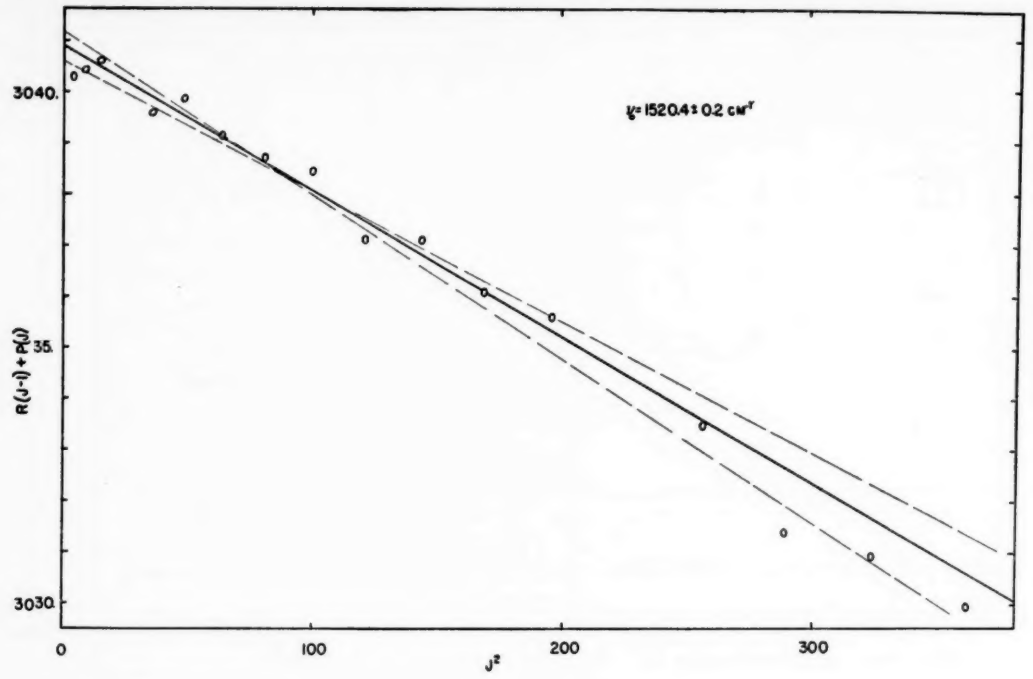

FIG. 5. Determination of the band origin for ν_2 of GeH_3D.

report a Ge—H distance of 1.55±0.04 A. The larger limits of error in these compounds stem from the fact that the moments of inertia are relatively insensitive to the Ge—H distance. Thus, although very accurate values of the I_B moment of inertia are obtainable by investigation of the microwave spectrum, the bond distances are not necessarily determined with the same accuracy.

A possible explanation can be advanced for the low value of the Ge—H distance reported in GeH_4.[3] The rotational constants for a molecule possessing tetrahedral symmetry can be determined if the rotational spacing of both infrared active fundamentals is known. Thus,

$$2(B''-\zeta_3 B')=\Delta\nu_3$$

and

$$2(B''-\zeta_4 B')=\Delta\nu_4$$

where $\Delta\nu_3$ and $\Delta\nu_4$ are the corresponding rotational spacings and ζ_3 and ζ_4 are the Coriolis interaction terms. For this discussion it is possible to set $B''=B'$ without introducing appreciable error. Since $\zeta_3+\zeta_4=\frac{1}{2}$,[9] there is obtained by adding the foregoing two equations the result

$$3B''=\Delta\nu_3+\Delta\nu_4.$$

There seems to be little doubt about the correct value for $\Delta\nu_3$ for GeH_4 as this band is well behaved. A tracing of this band taken with the Perkin-Elmer 12-C spectrograph yields a spacing of 5.62 cm^{-1} which is in excellent agreement with the value of 5.60 reported by Straley, Tindal, and Nielsen.[3] Therefore, the difficulty appears to be in the spacing of the relatively complicated ν_4 band. The outstanding feature of STN's assignments in this band is the discrepancy between the spacings of the P and R branches. In the R branch the spacing was reasonably uniform with an average value of about 2.3 cm^{-1}; however, in the P branch the spacing jumped

TABLE III. Molecular constants of GeH_3D and $GeHD_3$.

	GeH_3D	$GeHD_3$
B''	1.95_7 ±0.005 cm^{-1}	1.66_5 ±0.012 cm^{-1}
$B''-B'$	0.014 cm^{-1}	0.013 cm^{-1}
γ_{Ge-H}	1.52_9 ±0.003A	1.52_5 ±0.005A
ν_0	1520.4±0.2 cm^{-1}	2112.4±0.2 cm^{-1}

[9] Herzberg, *Infrared and Raman Spectra* (D. Van Nostrand Company, Inc., New York, 1951), p. 448.

TABLE IV. New assignment of rotational lines of the ν_4 fundamental of GeH_4.

J	$R(J)$	$P(J)$	$\frac{1}{2}\left(\frac{R(J-1)-P(J+1)}{J+\frac{1}{2}}\right)=\Delta\nu$
0	819.7	...	
1	22.0	814.1[a]	2.46
2	24.3	12.2[a]	2.63
3	26.4	08.8	2.63
4	28.9	05.5	2.51
5	31.2	03.3	2.50
6	33.0	01.4[a]	2.45
7	35.5	799.4	2.51
8	37.9	95.4	2.48
9	39.0	93.1	2.47
10		91.6[a]	2.38
11	45.0	88.2	2.42
12	47.3	85.2	2.48
13		82.9[a]	2.45
14		81.1	
			average 2.50

[a] Measured in this investigation. All other values taken from Table II of reference 3.

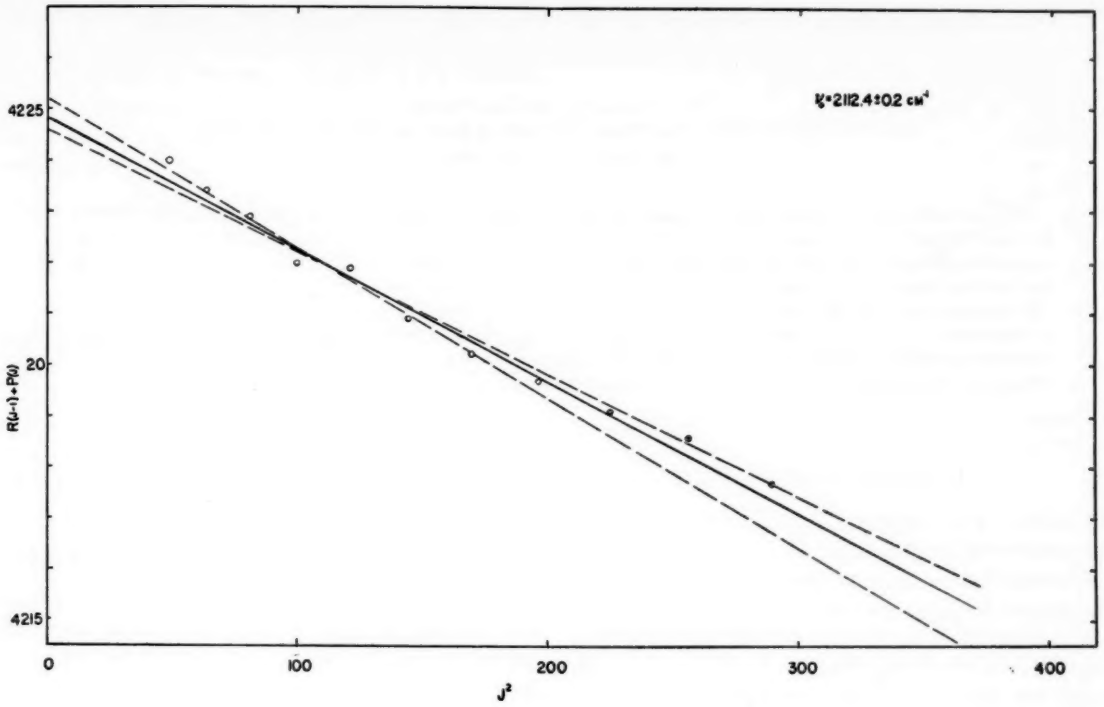

FIG. 6. Determination of the band origin for ν_1 of $GeHD_3$.

to 3.7 cm^{-1}. A mean value of 3.0 cm^{-1} for the entire band was used by STN. We felt that a new assignment possibly could be made for the rotational levels in the P branch and such a reassignment is contained in Table IV. The frequencies for the most part are taken directly from Table II of reference 3. For lines that were not listed in reference 3 we have taken values obtained with a Perkin-Elmer Model 21 spectrophotometer using a NaCl prism. Using these data a spacing of 2.50 cm^{-1} is found for ν_4 and the Ge—H distance in GeH_4 is calculated to be 1.52_4 which is in excellent agreement with the results on GeH_3D, $GeHD_3$, and GeH_3Cl.

Approximate Treatment of the Viscosity of Idealized Liquids. I. The Collisional Contribution

F. C. COLLINS AND H. RAFFEL
Department of Chemistry, Polytechnic Institute of Brooklyn, Brooklyn, New York
(Received March 23, 1954)

The instantaneous transport of momentum across the bodies of molecules occurs upon molecular collision in a rigid sphere liquid undergoing viscous flow. The contribution of this effect to the viscosity is calculated on a quasi-equilibrium basis for a liquid consisting of hard spherical molecules. The calculation makes use of the free volume theory, a correction being introduced to take account of the blocking effect of third neighbors. The equation so obtained may be expressed in terms of the adiabatic compressibility of the liquid and its heat of vaporization. The calculated viscosity contributions are of the order of a quarter to a half of the experimental viscosities for various low molecular weight liquids investigated. The temperature coefficients of the viscosity contributions are also lower than those of the experimental viscosities.

INTRODUCTION

THE viscosity of idealized hard sphere liquids can be considered as the sum of two contributions: (1) that caused by the instantaneous transport of momentum normal to the plane of viscous flow across the bodies of molecules upon collision, and (2) that resulting from the unbalanced attractive force field exerted upon the molecules because of the perturbation of the Maxwell-Boltzmann distribution of their neighbors in space by the viscous flow. This paper concerns itself with the collisional transport of momentum.

This contribution to the viscosity of dense gases has been dealt with by Enskog[1] and by Chapman and Cowling.[2] The present treatment is patterned after their methods of calculation. The theory is quasi-equilibrium as it assumes a Maxwell-Boltzmann distribution of peculiar molecular velocities about the mean mass motion at each point in the medium. The treatment departs from the Chapman-Enskog theory, however, in assuming that the concentration of the centers of the nearest neighbors around a given collision sphere is given by the reciprocal of the molecular free volume[3,4] instead of the reciprocal of the molecular volume. Account must be taken of the fact that only a small fraction of the surface of the collision sphere is accessible for collision by any given neighbor, the remaining area being blocked by third neighbors. In these calculations, it is assumed that the accessible area is that contiguous to the free space in which the given molecular center is confined. Calculation of the exact magnitude of this accessible area turns out to be unnecessary as it cancels in the calculation. The free volume likewise does not appear explicitly in the final equation for the viscosity coefficient. The related ratio of the incompressible and molecular volumes which does appear may be obtained from the velocity of sound in the given liquid.[5]

THE PHENOMENOLOGICAL PRESSURE TENSOR

The general method of the calculation is to calculate the momentum flux, arising from molecular collisions, across an arbitrary element of surface δS and to compare the resulting equation with the momentum flux expressed in terms of the phenomenological pressure tensor $\mathbf{P}$. It is to be noted at the outset that the probability that the surface element δS cuts through a molecular body is very high compared to the probability that it lies in a free space which may be traversed by a molecular center. Accordingly, the transport of momentum by the motion of molecular centers across the reference surface element is negligible compared to its transport by collision. The momentum flux $\mathbf{Q}$ in terms of the pressure tensor is

$$\mathbf{Q}=\mathbf{P}(\mathbf{r})\cdot\mathbf{n}\delta S, \tag{1}$$

where $\mathbf{n}$ is the unit normal to the surface element δS and $\mathbf{r}$ denotes the position of the volume element in which the surface δS is located relative to an arbitrary origin. The present treatment will be confined to Newtonian liquids for which the pressure tensor has the form[6]

$$\mathbf{P}=\left[p+\left(\frac{2\eta}{3}-\phi\right)\frac{\partial}{\partial\mathbf{r}}\cdot\mathbf{c}_0\right]\mathbf{U}-2\eta\left(\frac{\partial\mathbf{c}_0}{\partial\mathbf{r}}\right)^{\ddagger} \tag{2}$$

where p is the hydrostatic pressure, η the shear viscosity, and ϕ the bulk, or dilatation, viscosity. The symbol $\mathbf{U}$ stands for the unit tensor, $(\partial/\partial\mathbf{r})\cdot\mathbf{c}_0$ is the divergence of the mass, or mean molecular, velocity at $\mathbf{r}$, and $(\partial\mathbf{c}_0/\partial\mathbf{r})^{\ddagger}$ is the symmetrical rate of strain tensor.

DYNAMICS AND FREQUENCY OF COLLISIONS IN A RIGID SPHERE LIQUID

As a preliminary to the calculation of the momentum flux, it is necessary to obtain the probability that any given molecule suffers a collision which is characterized

[1] D. Enskog, Kgl. Svenska Vetenskapsakad. Handl. **63**, No. 4, 1 (1921).
[2] S. Chapman and T. G. Cowling, *Mathematical Theory of Non-Uniform Gases* (Cambridge University Press, Cambridge, 1939).
[3] H. Eyring and J. O. Hirschfelder, J. Phys. Chem. **41**, 249 (1937).
[4] J. E. Lennard-Jones and A. F. Devonshire, Proc. Roy. Soc. (London) **A163**, 61 (1937).
[5] F. C. Collins and M. H. Navidi, J. Chem. Phys. **22**, 1254 (1954).
[6] See Kirkwood, Buff, and Green, J. Chem. Phys. **17**, 988 (1949).

by collision parameters within a specified range of values. In making this calculation it will be assumed that the distribution of peculiar velocities of the nearest neighbors is independent of the velocity of the given molecule and that the distribution obeys the Maxwell-Boltzmann relation:

$$f(\mathbf{C}(\mathbf{r}))=(m/2\pi kT)^{\frac{3}{2}}\exp[-mC^2(\mathbf{r})/2kT]$$
$$=(m/2\pi kT)^{\frac{3}{2}}\exp\{-m[\mathbf{c}-\mathbf{c}_0(\mathbf{r})]^2/2kT\}$$
$$=f(\mathbf{r}), \tag{3}$$

where $\mathbf{c}_0(\mathbf{r})$ is the local average velocity of molecules in the volume element $(\mathbf{r}, \mathbf{r}+d\mathbf{r})$, $\mathbf{c}$ is the velocity of a molecule at $\mathbf{r}$, and $\mathbf{C}$ is the peculiar velocity, $\mathbf{C}(\mathbf{r})=\mathbf{c}-\mathbf{c}_0(\mathbf{r})$. To facilitate the calculations we will assume that the liquid is in a steady state with respect to shear and that its density and temperature are uniform throughout.

The molecule 1 under consideration will be represented by a "collision sphere" of radius σ equal to the diameter of the molecule. The center of the representative nearest neighbor 2 will then be confined to a free volume cavity formed by the collision spheres of its neighbors, see Fig. 1. The calculation of the magnitude v_f of the free volume will be discussed in a later section of this paper. In order for a collision within the time dt to occur with the relative velocity, $\mathbf{g}=\mathbf{c}_2-\mathbf{c}_1$, and orientation $\mathbf{k}$ of the line of centers at collision, it is necessary that the center of molecule 2 lie within slant cylinder of volume $\sigma^2\mathbf{g}\cdot\mathbf{k}d\mathbf{k}dt$ with its base on the collision sphere of molecule 1. It is further required that the direction of g be such that the product $\mathbf{g}\cdot\mathbf{k}$ be positive in order for collision to ensue.

The probability that the center of the second molecule lies within the above element of volume and that the respective molecules have the velocities $\mathbf{c}_1$ and $\mathbf{c}_2$ before collision is then from Eq. (3):

$$\frac{\sigma^2\mathbf{g}\cdot\mathbf{k}d\mathbf{k}dt}{v_f}f(\mathbf{r}_1)f(\mathbf{r}_2)d\mathbf{c}_1d\mathbf{c}_2, \tag{4}$$

where v_f is again the molecular free volume. The orientations which may be assumed by the unit vector $\mathbf{k}$ are limited by the presence of the third neighbors whose collision spheres overlap the collision sphere of molecule 1. If $\mathbf{k}_0$ is a unit vector directed from the center of the free volume cavity toward the center of molecule 1, and Ω is the angle between the vectors $\mathbf{k}$ and $\mathbf{k}_0$, then

$$d\mathbf{k}_0=2\pi\sin\Omega d\Omega/4\pi \quad 0\leqslant\Omega\leqslant\Omega^*, \tag{5}$$

where Ω^* is the average maximum value of Ω. The fraction of the area of the collision sphere of the reference molecule 1 accessible for collision by the particular neighbor 2 is obtained by integrating Eq. (5) between the specified limits. The area of the collision sphere with which collisions can occur involving any of the ν nearest neighbors is then

$$\nu\sigma^2\tfrac{1}{2}(1-\cos\Omega^*).$$

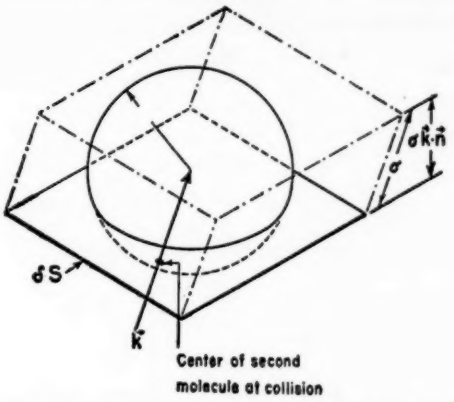

FIG. 1. Requirements for the mechanics of a collision in order that momentum transport take place across the surface δS upon collision.

The foregoing device of using the unit vector $\mathbf{k}$ as z axis as reference for the orientation of the vector $\mathbf{k}_0$ now leaves $\mathbf{k}$ free to assume any orientation. The differential frequency of collisions of a molecule having velocity $\mathbf{c}_1$ with neighbors having the velocity $\mathbf{c}_2$ is then

$$dZ=\nu\sigma^2(1-\cos\Omega^*)\frac{\mathbf{g}\cdot\mathbf{k}}{2v_f}f(\mathbf{r}_1)f(\mathbf{r}_2)d\mathbf{c}_1d\mathbf{c}_2d\mathbf{k}. \tag{6}$$

TRANSPORT OF MOMENTUM BY MOLECULAR COLLISION

For the transport of momentum across an arbitrary surface element δS by a molecular collision, it is required that the centers of the colliding molecules lie on opposite sides of the surface element and that the line joining their centers cut it. This requires that the center of molecule 1 lie within the volume $\sigma\mathbf{k}\cdot\mathbf{n}\delta S$, where $\mathbf{n}$ is the unit normal to the surface δS. The *a priori* probability of this occurrence is $\sigma\mathbf{k}\cdot\mathbf{n}\delta S/v$, where v is the molecular volume. Combining this probability with Eq. (6), we obtain for the differential frequency of those collisions with momentum transport across δS:

$$dW=\frac{\sigma\mathbf{k}\cdot\mathbf{n}\delta S}{v}\frac{\nu\sigma^2(1-\cos\Omega^*)}{2v_f}\mathbf{g}\cdot\mathbf{k}f(\mathbf{r}_1)f(\mathbf{r}_2)d\mathbf{c}_1d\mathbf{c}_2d\mathbf{k}. \tag{7}$$

The velocity distribution functions $f(\mathbf{r}_1)$ and $f(\mathbf{r}_2)$ must be evaluated at the points at which the given molecules are located at collision. This raises a difficulty because the positions of the centers of the molecules at collision relative to the surface element δS are not uniquely defined. We will here make use of a device discussed by Chapman and Cowling in their treatment of the Enskog theory of dense gases. The centers of the two molecules will be assumed to be exactly at their mean positions, $\mathbf{r}+\frac{1}{2}\sigma\mathbf{k}$ and $\mathbf{r}-\frac{1}{2}\sigma\mathbf{k}$, respectively, where $\mathbf{r}$ is the location of the surface element δS. The velocity distributions then become $f(\mathbf{r}+\frac{1}{2}\sigma\mathbf{k})$ and $f(\mathbf{r}-\frac{1}{2}\sigma\mathbf{k})$. This approximation may be expected to contribute a negligible error except at very high rates of shear. These velocity distributions may be expanded around the

point $\mathbf{r}$ as follows:

$$f(\mathbf{r}+\tfrac{1}{2}\sigma\mathbf{k})$$
$$=f(\mathbf{r})+\tfrac{1}{2}\sigma\mathbf{k}\cdot\frac{\partial}{\partial\mathbf{r}}f(\mathbf{r})$$
$$=f(\mathbf{r})+\tfrac{1}{2}\sigma\mathbf{k}\cdot\frac{\partial}{\partial\mathbf{r}}\left\{\left(\frac{m}{2\pi kT}\right)^{\frac{3}{2}}\exp\left[-\frac{m(\mathbf{c}-\mathbf{c}_0(\mathbf{r}))^2}{2kT}\right]\right\}$$
$$=f(\mathbf{r})\left\{1+\frac{\sigma m}{2kT}\mathbf{k}\cdot\left[\mathbf{C}(\mathbf{r})\cdot\frac{\partial}{\partial\mathbf{r}}\mathbf{c}_0(\mathbf{r})\right]\right\}, \tag{8}$$

with a corresponding expression for $f(\mathbf{r}-\frac{1}{2}\sigma\mathbf{k})$.

Each collision transports an amount of momentum $m(\mathbf{c}_1'-\mathbf{c}_1)$ from molecule 2 to molecule 1, $\mathbf{c}_1'$ being the velocity of the first molecule after collision. From the principles of conservation of energy and momentum in the collision of rigid spheres, we have

$$m(\mathbf{c}_1'-\mathbf{c}_1)=m\mathbf{g}\cdot\mathbf{kk}. \tag{9}$$

Then the total transport of momentum per unit area is

$$\mathbf{Q}=\frac{\nu\sigma^3(1-\cos\Omega^*)}{2vv_f}\int m\mathbf{g}\cdot\mathbf{kkk}\cdot\mathbf{n}\cdot\mathbf{g}\cdot\mathbf{k}f(\mathbf{r}+\tfrac{1}{2}\sigma\mathbf{k})f(\mathbf{r}-\tfrac{1}{2}\sigma\mathbf{k})d\mathbf{c}_1d\mathbf{c}_2d\mathbf{k}, \tag{10}$$

where the integration is over all allowed values of the collision parameters. The product $\mathbf{g}\cdot\mathbf{k}$ must be positive for the collision to take place, and the product $\mathbf{k}\cdot\mathbf{n}$ must be positive for the momentum flux to have the correct sign. Because of the symmetry of collisions, it is possible to allow the integration to extend over all values of $\mathbf{k}\cdot\mathbf{n}$ and then to divide the result by two.

The analysis involved in the integration of Eq. (10) will be facilitated if we make the following substitutions:

$$f_1(\mathbf{r})f_2(\mathbf{r})=\left(\frac{m}{2\pi kT}\right)^3\exp[-m(C_1^2+C_2^2)/2kT]$$
$$=\left(\frac{m}{2\pi kT}\right)^3\exp\left[-m\left(\frac{g^2}{4}+G^2\right)\Big/2kT\right], \tag{11}$$

where $\mathbf{G}=(\mathbf{c}_1+\mathbf{c}_2)/2$,

$$\frac{\partial}{\partial\mathbf{r}}\ln[f_1(\mathbf{r})/f_2(\mathbf{r})]=\frac{\partial}{\partial\mathbf{r}}[-m(C_1^2-C_2^2)/2kT]$$
$$=\frac{\partial}{\partial\mathbf{r}}\{-m[(c_1^2-c_2^2)-\mathbf{c}_0\cdot(2\mathbf{c}_1-\mathbf{c}_0-2\mathbf{c}_2+\mathbf{c}_0)]/2kT\}$$
$$=\left(\frac{m}{kT}\right)\left(\frac{\partial}{\partial\mathbf{r}}\mathbf{c}_0\right)\cdot(\mathbf{C}_1-\mathbf{C}_2)$$
$$=-\left(\frac{m}{kT}\right)\left(\frac{\partial}{\partial\mathbf{r}}\mathbf{c}_0\right)\cdot\mathbf{g}. \tag{12}$$

In the convenient notation of Chapman and Cowling[7]

$$(\mathbf{a}\cdot\mathbf{d})(\mathbf{b}\cdot\mathbf{c})=\mathbf{ab}:\mathbf{cd},$$

whence

$$(\mathbf{g}\cdot\mathbf{k})^2=\mathbf{gg}:\mathbf{kk} \tag{13}$$

and

$$\mathbf{k}\cdot\frac{\partial\mathbf{c}_0}{\partial\mathbf{r}}\cdot\mathbf{g}=\frac{\partial\mathbf{c}_0}{\partial\mathbf{r}}:\mathbf{gk}=\frac{(\partial\mathbf{c}_0)^*}{\partial\mathbf{r}}:\mathbf{kg}, \tag{14}$$

where $(\partial\mathbf{c}_0/\partial\mathbf{r})^*$ and $\mathbf{kg}$ are the conjugate tensors of $\partial\mathbf{c}_0/\partial\mathbf{r}$ and $\mathbf{gk}$. Upon introducing the substitutions (11) to (14), Eq. (10) becomes

$$\mathbf{Q}=\left(\frac{m}{2\pi\mathbf{kT}}\right)^3\frac{\rho\nu\sigma^3(1-\cos\Omega^*)}{4v_f}\times\int\exp\left[-m\left(\frac{g^2}{4}+G^2\right)\Big/2kT\right]\mathbf{kkkk}:\mathbf{gg}dgd\mathbf{G}d\mathbf{k}$$
$$-\left(\frac{m}{2\pi kT}\right)^4\frac{\rho\nu\sigma^4(1-\cos\Omega^*)}{8v_f}\times\int\exp\left[-m\left(\frac{g^2}{4}+G^2\right)\Big/2kT\right]\times\frac{\partial\mathbf{c}_0}{\partial\mathbf{r}}:\mathbf{kkkkk}:\mathbf{ggg}dgd\mathbf{G}d\mathbf{k}. \tag{15}$$

The limits of the indicated integrations are as follows: (a) All orientations of the vector $\mathbf{G}$ and the unit vector $\mathbf{k}$ are allowed, and the magnitude of $\mathbf{G}$ may assume any value. (b) The vector $\mathbf{g}$ is limited by the condition $\mathbf{g}\cdot\mathbf{k}\geqslant 0$ for any given orientation of $\mathbf{k}$. If $\mathbf{g}$ is measured with $\mathbf{k}$ as the z axis, so that

$$\mathbf{g}=g\sin\xi\cos\epsilon\mathbf{i}+g\sin\xi\sin\epsilon\mathbf{j}+g\cos\xi\mathbf{k},$$

then the integration limits for $\mathbf{g}$ are $0\leqslant\xi\leqslant\pi/2$, $0\leqslant\epsilon\leqslant 2\pi$, and $0\leqslant g<\infty$.

The first integral of Eq. (15) is then integrated as follows:

$$\int f_1(\mathbf{r})f_2(\mathbf{r})\mathbf{gg}dgd\mathbf{G}$$
$$=\left(\frac{m}{2\pi kT}\right)^3\int\exp\left(-\frac{mg^2}{4kT}\right)\mathbf{gg}dg\times\int_0^\infty\exp\left(-\frac{mG^2}{kT}\right)4\pi G^2dG$$
$$=\left(\frac{m}{2\pi kT}\right)^3\left(\frac{\pi kT}{m}\right)^{\frac{1}{2}}\int_0^\infty\exp\left(-\frac{mg^2}{4kT}\right)g^4dg\times\int_0^{\pi/2}[2\pi\cos^2\xi\mathbf{kk}+\pi\sin^2\xi(\mathbf{ii}+\mathbf{jj})]\sin\xi d\xi$$

[7] Reference 2, p. 18.

$$=\left(\frac{m}{2\pi kT}\right)^{3}\left(\frac{\pi kT}{m}\right)^{\frac{3}{2}}\frac{3\pi^{\frac{1}{2}}}{8}\left(\frac{4kT}{m}\right)^{5/2}\times\frac{2\pi}{3}(\mathbf{ii}+\mathbf{jj}+\mathbf{kk}). \quad (16)$$

The first integral of Eq. (15) is then

$$I_1=\frac{kT\nu\sigma^3(1-\cos\Omega^*)}{4vv_f}\int(\mathbf{ii}+\mathbf{jj}+\mathbf{kk}):\mathbf{kkkk}d\mathbf{k}, \quad (17)$$

where the indicated integration is now over all orientations of the vector $\mathbf{k}$ with respect to the axes $\mathbf{x}, \mathbf{y}, \mathbf{z}$, fixed in space. The double dot product is simply scalar unity because of orthogonality and Eq. (17) reduces simply to

$$I_1=\frac{\pi kT\nu\sigma^3(1-\cos\Omega^*)}{3vv_f}\mathbf{U}, \quad (18)$$

where $\mathbf{U}$ is the second-order unit tensor.

The nonzero term of the second integral of Eq. (14) contains the factor

$$\int\exp\left(-\frac{mG^2}{kT}\right)d\mathbf{G}=(\pi kT/m)^{\frac{3}{2}},$$

while the integration over g is

$$\int\mathbf{ggg}\exp(-mg^2/4kT)d\mathbf{g}.$$

Upon integrating the terms of the third-order tensor $\mathbf{ggg}$ with respect to ϵ $(0\leqslant\epsilon\leqslant 2\pi)$, the only remaining nonzero terms are

$$g^3[2\pi\cos^3\xi\mathbf{kkk}+\pi\sin^2\xi\cos\xi(\mathbf{kii}+\mathbf{iki}+\mathbf{iik}+\mathbf{kjj}+\mathbf{jkj}+\mathbf{jjk})]\exp[-mg^2/4kT]g^2dg.$$

In the double dot product of this result with $\mathbf{kk}$, all terms vanish because of orthogonality except the first. The contribution of the second integral of Eq. (15) is then

$$I_2=-\left(\frac{m}{2\pi kT}\right)^{3}\frac{\rho\nu\sigma^4(1-\cos\Omega^*)}{8v_f}\times\left(\frac{\pi kT}{m}\right)^{\frac{1}{2}}\int\int_0^\infty\left(\frac{m}{kT}\right)\frac{\partial\mathbf{c}_0}{\partial\mathbf{r}}:\mathbf{kkk}\times\mathbf{kk}:(g^3 2\pi\cos^3\xi)\mathbf{kkk}\exp\left(-\frac{mg^2}{4kT}\right)g^2dgd\mathbf{k}. \quad (19)$$

Noting that $\mathbf{kk}:\mathbf{kk}=1$ and carrying out the integration with respect to g, we obtain

$$I_2=-\left(\frac{m}{2\pi kT}\right)^{3}\frac{\rho\nu\sigma^4(1-\cos\Omega^*)}{8v_f}\times\left(\frac{\pi kT}{m}\right)^{\frac{1}{2}}\left(\frac{m}{kT}\right)\frac{\partial\mathbf{c}_0}{\partial\mathbf{r}}:\int\mathbf{kkkk}d\mathbf{k}, \quad (20)$$

where the indicated integration is over all orientations of the unit vector $\mathbf{k}$. The integral in Eq. (20) may be symbolized by

$$\mathbf{T}:\int\mathbf{kkkk}d\mathbf{k}, \quad (21)$$

where $\mathbf{T}$ is a second-order tensor and

$$\mathbf{k}=\mathbf{z}\cos\theta+\mathbf{x}\sin\theta\cos\varphi+\mathbf{y}\sin\theta\sin\varphi.$$

Then

$$\mathbf{kk}=\begin{pmatrix}\cos^2\theta & \cos\theta\sin\theta\cos\varphi & \cos\theta\sin\theta\sin\varphi\\ \cos\theta\sin\theta\cos\varphi & \sin^2\theta\cos^2\varphi & \sin^2\theta\cos\varphi\sin\varphi\\ \cos\theta\sin\theta\sin\varphi & \sin^2\theta\cos\varphi\sin\varphi & \sin^2\theta\sin^2\varphi\end{pmatrix} \quad (22)$$

and upon carrying out the integration of Eq. (20) over all products of the components of Eq. (22), the only nonzero terms are the following:

$$\mathbf{zzzz}\int_0^{2\pi}\int_0^{\pi}\cos^4\theta\sin\theta d\theta d\varphi=\tfrac{4}{5}\pi\mathbf{zzzz}$$

$$\mathbf{xxxx}\int_0^{2\pi}\int_0^{\pi}\sin^5\theta\cos^4\varphi d\theta d\varphi=\tfrac{4}{5}\pi\mathbf{xxxx}$$

$$\mathbf{yyyy}\int_0^{2\pi}\int_0^{\pi}\sin^5\theta\sin^4\varphi d\theta d\varphi=\tfrac{4}{5}\pi\mathbf{yyyy}$$

$$[P(\mathbf{zzxx})+P(\mathbf{zzyy})]\times\int_0^{\pi}\pi\cos^2\theta\sin^3\theta d\theta=\frac{4}{15}\pi[P(\mathbf{zzxx})+P(\mathbf{zzyy})] \quad (23)$$

$$P(\mathbf{xxyy})\int_0^{2\pi}\int_0^{\pi}\sin^5\theta\sin^2\varphi d\theta d\varphi=\frac{4}{15}\pi P(\mathbf{xxyy}).$$

Here $P(\mathbf{aabb})$ denotes the sum over all nonduplicate permutations of the vectors:

$$P(\mathbf{aabb})=\mathbf{aabb}+\mathbf{abab}+\mathbf{abba}+\mathbf{baab}+\mathbf{bbaa}.$$

It is convenient at this point to separate the components of Eq. (23) into diagonal and nondiagonal terms as follows:

$$\mathbf{T}:\int\mathbf{kkkk}=\frac{4\pi}{15}\mathbf{U}(\mathbf{T}:\mathbf{U})+\frac{8\pi}{15}\times\begin{pmatrix}T_{zz} & \frac{1}{2}(T_{zx}+T_{xz}) & \frac{1}{2}(T_{zy}+T_{yz})\\ \frac{1}{2}(T_{zx}+T_{xz}) & T_{xx} & \frac{1}{2}(T_{xy}+T_{yx})\\ \frac{1}{2}(T_{zy}+T_{yz}) & \frac{1}{2}(T_{xy}+T_{yx}) & T_{yy}\end{pmatrix}=\frac{4\pi}{15}\mathbf{U}(\mathbf{T}:\mathbf{U})+\frac{8\pi}{15}\mathbf{T}^{\ddagger}, \quad (24)$$

where $(\mathbf{T})^{\ddagger}=\frac{1}{2}[\mathbf{T}+\mathbf{T}^*]$, $\mathbf{T}^*$ being the tensor conjugate to $\mathbf{T}$.

Upon combining Eqs. (18), (20), and (24) we have for the total transport of momentum by collision across the volume element, δS:

$$\mathbf{Q}=\left[\frac{\pi kT\nu\sigma^3(1-\cos\Omega^*)}{3vv_f}-\frac{2}{15}\times\frac{\nu\sigma^4(\pi mkT)^{\frac{1}{2}}(1-\cos\Omega^*)}{vv_f}\left(\frac{\partial}{\partial\mathbf{r}}\cdot\mathbf{c}_0\right)\right]\mathbf{U}-\frac{4}{15}\frac{\nu\sigma^4(\pi mkT)^{\frac{1}{2}}(1-\cos\Omega^*)}{vv_f}\left(\frac{\partial\mathbf{c}_0}{\partial\mathbf{r}}\right)^{\ddagger}. \quad (25)$$

Equation (22) may now be compared term by term with the phenomenological Eq. (2). This leads to

$$p_c=\frac{\pi kT\nu\sigma^3(1-\cos\Omega^*)}{3vv_f}, \quad (26)$$

$$\phi_s=0, \quad (27)$$

$$\eta_c=\frac{2\nu\sigma^4(\pi mkT)^{\frac{1}{2}}(1-\cos\Omega^*)}{15vv_f}. \quad (28)$$

The bulk or dilatational viscosity contribution ϕ_s is zero as required by our initial assumption that the liquid is in a steady state of viscous shear. The calculated collisional contribution η_c to the shear viscosity coefficient may be greatly simplified by making use of Eq. (26) and the free volume equation of state.[5] According to the free volume theory, the translational part of the molecular partition function is

$$Q=\frac{(2\pi mkT)^{\frac{3}{2}}}{h^3}v_f\exp[-U(v)/kT], \quad (29)$$

where $U(v)$ is the mean or smoothed potential within the free volume and the other symbols have their usual significance. The free volume is related to the molecular and incompressible volumes as follows:

$$v_f=\alpha(v^{\frac{1}{3}}-v_0^{\frac{1}{3}})^3, \quad (30)$$

where α is a constant of the order of 4. The external pressure is then

$$p=\left[\frac{\partial}{\partial v}(kT\ln Q)\right]_T=\frac{kT}{v[1-(v_0/v)^{\frac{1}{3}}]}-\left(\frac{\partial U}{\partial v}\right)_T\simeq 0. \quad (31)$$

The internal kinetic pressure is nearly equal to the cohesive pressure $(\partial U/\partial v)_T$ and may be set equal to the collisional hydrostatic pressure, Eq. (26).

By combining Eqs. (26), (28), (30), and (31), the following simple expression results for the shear viscosity

$$\eta_c=\frac{2}{5}\frac{\sigma(mkT)^{\frac{1}{2}}}{\pi^{\frac{1}{2}}v[1-(v_0/v)^{\frac{1}{3}}]}. \quad (32)$$

COMPARISON OF THE CALCULATED COLLISIONAL VISCOSITY CONTRIBUTION WITH EXPERIMENT

The various quantities appearing in Eq. (32) can be approximately evaluated from various experimental measurements. The ratio v_0/v of the "incompressible" volume to the molecular volume can be obtained readily from the velocity of sound in the liquid by use of the following equation:[5]

$$u_s=\frac{1-\frac{2}{3}(v_0/v)^{\frac{1}{3}}}{1-(v_0/v)^{\frac{1}{3}}}\left\{\frac{C_pRT/M}{C_p[1-\frac{2}{3}(v_0/v)^{\frac{1}{3}}]-R}\right\}^{\frac{1}{2}}, \quad (33)$$

where C_p is the molar specific heat and M is the molecular weight. The collision radius σ may be assumed to be related to the incompressible volume in the same way that the mean distance a between nearest neighbors is related to the molecular volume v, *viz.*:

$$\sigma=\beta v_0^{\frac{1}{3}},\qquad a=\beta v^{\frac{1}{3}}. \quad (34)$$

The constant β depends on the type of liquid quasi-lattice assumed. It is $2^{1/6}$ for a close-packed cubic lattice and does not change significantly when the number of nearest neighbors varies somewhat.[5]

TABLE I. Comparison of calculated values of the collisional contribution to the viscosity coefficients with experimental viscosity coefficients for various liquids at several temperatures.

Compound	t °C	u_s M/sec	$(v_0/v)^{\frac{1}{3}}$	v $(\text{A}^\circ)^3$	σ A°	η_c C_p	η_{exp} C_p	η_c/η_{exp}
Benzene	10	1374	0.9138	145.81	5.344	0.216	0.758	0.285
	20	1327	0.9091	147.42	5.336	0.206	0.652	0.316
	30	1280	0.9039	149.39	5.329	0.195	0.564	0.346
	40	1234	0.8985	151.23	5.319	0.185	0.503	0.368
	50	1184	0.8923	153.20	5.305	0.175	0.442	0.395
Chlorobenzene	10	1326	0.9271	167.65	5.680	0.283	0.912	0.311
	20	1289	0.9235	169.20	5.676	0.272	0.799	0.341
	30	1249	0.9195	170.77	5.668	0.260	0.715	0.364
Bromobenzene	30	1139	0.9259	175.90	5.764	0.330	0.985	0.335
Iodobenzene	30	1087	0.9323	186.86	5.922	0.398	1.417	0.281
Chloroform	20	1001	0.9004	133.28	5.111	0.246	0.58	0.424
	30	967.7	0.8952	135.08	5.103	0.234	0.514	0.456
	40	933.4	0.8893	136.83	5.092	0.222	0.461	0.482
	50	899.9	0.8831	138.75	5.080	0.210	0.424	0.496
Bromoform	20	931	0.9287	145.20	5.424	0.487	2.02	0.241
	30	910	0.9257	146.53	5.423	0.471	1.741	0.270
Carbon tetrachloride	20	937.8	0.9078	160.18	5.478	0.269	0.969	0.278
	30	907.0	0.9028	162.16	5.470	0.256	0.843	0.304
	40	876.0	0.8975	164.32	5.462	0.244	0.739	0.330
	50	845.3	0.8918	166.38	5.450	0.231	0.651	0.354
Ethyl bromide	10	935	0.8871	122.24	4.892	0.213	0.441	0.482
	20	900	0.8806	123.88	4.877	0.201	0.402	0.501
	30	866	0.8736	125.67	4.862	0.190	0.348	0.546
Ethyl iodide	20	876	0.9003	133.83	5.116	0.280	0.592	0.473
	30	848	0.8951	135.40	5.108	0.267	0.540	0.495
	40	820	0.8896	137.07	5.096	0.254	0.495	0.514

Calculated values of the collisional viscosity coefficient contribution for a number of simple organic liquids at various temperatures, using data for velocity of sound from Lagemann, McMillan, and Woolf[8] are presented in Table I. The ratio of the collisional contribution to the experimental viscosity coefficient is of the order of about a quarter to a half for the several liquids investigated. The temperature coefficient of the collisional contribution is about one-third of the experimental coefficient indicating that the collisional contribution becomes more significant at higher temperatures.

[8] Lagemann, McMillan, and Woolf, J. Chem. Phys. **17**, 369 (1949).

The numerical comparison indicates that the molecular collision process makes a significant contribution to the viscosity coefficient of idealized liquids. The ratio of the collisional viscosity contribution to the experimental viscosity shows relatively large variation among the various liquids investigated. In order to give a qualitative interpretation of this variation, it will be necessary to know the order of magnitude of the viscosity contribution due to unbalanced intermolecular force field arising from the perturbation of the distribution of nearest neighbors due to viscous flow. The calculation of this contribution is in progress and will be presented later.

THE JOURNAL OF CHEMICAL PHYSICS VOLUME 22, NUMBER 10 OCTOBER, 1954

Theory of the Interaction of Hindered Internal Rotation with Over-All Rotations. I. Symmetric Rotors: Methyl Silane*

DANIEL KIVELSON
Research Laboratory of Electronics and Department of Physics, Massachusetts Institute of Technology, Cambridge, Massachusetts

(Received May 6, 1954)

An approximate theory of the interactions of hindered internal rotation with over-all rotations of symmetric rotors is given. This treatment considers the interdependence of hindered internal rotation and vibrations and their effect upon the rotational energy levels. The resulting expression for the frequencies of $\Delta K=0$, $\Delta J=1$ transitions is

$$\nu=2J[B_v+F_v(m|1-\cos 3\theta|m)+G_v(m|\Pi_z^2|m)+L_vK(m|\Pi_z|m)],$$

where B_v, F_v, G_v, and L_v are constants independent of the rotational quantum numbers, m represents the basis that diagonalizes the Hamiltonian corresponding to pure internal rotation, Π_z is the internal angular momentum operator, and θ is the angle of internal rotation. Procedures for evaluating $(m|1-\cos 3\theta|m)$ and $(m|\Pi_z^n|m)$ in terms of a parameter α are given.

This theory has been applied to the $J=0\rightarrow 1$ transitions of methyl silane. The parameters B_v, F_v, G_v, and α were obtained empirically and were then used to calculate frequencies. The agreement between observed and calculated values was quite good. Furthermore, the anomalous ordering of the lines observed by Lide and Coles[1] is explained by these calculations. Assuming a cosine potential, the barrier height V_0 is proportional to the parameter α. The value of V_0 was set at 558 cm$^{-1}\pm$17 cm^{-1}. The constant B_v, which is the rotational constant in the ground torsional state for the limiting case of $V_0=0$, is 10985.79 Mc/sec and 9636.50 Mc/sec for CH_3SiH_3 and CH_3SiD_3, respectively.

I. INTRODUCTION

THE microwave spectra of methyl silane[1] and other symmetric rotor molecules[2] in which internal rotation can take place have been investigated by several workers. Each over-all rotational line has several fairly intense satellite lines. These satellite lines have been explained qualitatively by the fact that an appreciable fraction of the total number of molecules is found in low-lying torsional states and that the rotational constants are different in each torsional state. Furthermore, each line corresponding to a different torsional state is split into a multiplet. This multiplet structure arises from centrifugal distortion effects and from the so-called tunneling phenomenon.

In this paper an approximate theory of the interaction of hindered internal rotation (torsion) with over-all rotations is considered. The theory is then used to explain in detail the structure of the $J=0\rightarrow 1$ transition lines in methyl silane and to determine the height of the hindering "barrier."

II. THEORY

The moments of inertia of a symmetric rotor are not directly dependent upon the torsional normal coordi-

* This work was supported in part by the Signal Corps, the Air Materiel Command, and the U. S. Office of Naval Research.

[1] David R. Lide and Donald K. Coles, Phys. Rev. **80**, 911 (1950).

[2] J. Sheridan and W. Gordy, (CH_3SiF_3), J. Chem. Phys. **19**, 965 (1951); Minden, Mays, and Dailey, (CH_3SiF_3), Phys. Rev. **78**, 347A (1950); Dailey, Shulman, and Minden, (CH_3CF_3), Phys. Rev. **75**, 1319 (1949); H. Minden and B. Dailey, (CH_3CF_3) and (CH_3SiF_3), Phys. Rev. **82**, 338A (1951); Bak, Hansen, and Rastrup-Andersen, ($CH_3-C\equiv C-CF_3$), J. Chem. Phys. **21**, 1612*L* (1953).

nate, that is, upon the angle of internal rotation.[3] Thus, if the molecule could be kept rigid except for the torsional motion, the rotational constants would be independent of the torsional frequency or of the speed of internal rotation. This implies that the internal rotation affects the rotational constants only in a higher order through the interactions between the internal rotation and the other vibrational modes.

As a first approximation to the solution of the problem, the torsional mode can be separated from the other vibrational modes.[4] To a higher order, however, the interactions between the torsional and the vibrational modes must be considered. The Hamiltonian can be written in the form

$$\mathbf{H}=\tfrac{1}{2}\sum\mu_{\alpha\beta}\mathbf{P}_\alpha\mathbf{P}_\beta+\mathbf{H}_I+\mathbf{H}_v, \tag{1}$$

where $\mathbf{H}_I$ is essentially the part of the Hamiltonian that is connected with internal rotation; $\mathbf{H}_v$ is the part that is concerned with the other vibrational modes; $\mathbf{P}_\alpha$ is the component of total angular momentum along the α-principal axis; and $\mu_{\alpha\beta}$ is the $\alpha\beta$ component of the instantaneous inertia tensor. The term $\mathbf{H}_I$ depends upon the vibrational modes but represents pure internal rotation if the vibrational modes are damped out [see Eqs. (28) and (11)]; $\mathbf{H}_v$, in turn, depends upon the torsional motion, while $\mu_{\alpha\beta}$ is a function of the vibrational coordinates and hence, indirectly, a function of the angle of internal rotation.

This Hamiltonian can be treated in a manner similar to that proposed by Wilson and Howard.[5] $\mathbf{H}_v$ can be diagonalized although it remains a function of θ, the torsional angle. Let $v(\theta)$ be the set of quantum numbers indicating the basis in which $\mathbf{H}_v$ is diagonal, and let $W_v(\theta)$ be the corresponding set of eigenvalues. Then if a Van Vleck transformation[6] is applied, in order to diagonalize $\mathbf{H}_v$, the Hamiltonian takes on the form

$$\begin{aligned}\mathbf{H}=&\mathbf{W}_v(\theta)\\&+\tfrac{1}{2}\sum_{\alpha,\beta}(v(\theta)|\mu_{\alpha\beta}|v(\theta))\mathbf{P}_\alpha\mathbf{P}_\beta+(v(\theta)|\mathbf{H}_I|v(\theta))\\&+\sum_{v'}{}'(v(\theta)|\tfrac{1}{2}\sum_{\alpha,\beta}\mu_{\alpha\beta}\mathbf{P}_\alpha\mathbf{P}_\beta+\mathbf{H}_I|v'(\theta))\\&\times(v'(\theta)|\tfrac{1}{2}\sum_{\alpha,\beta}\mu_{\alpha\beta}\mathbf{P}_\alpha\mathbf{P}_\beta+\mathbf{H}_I|v(\theta))\\&\times[h\nu_{vv'}(\theta)]^{-1}+\cdots,\end{aligned} \tag{2}$$

where $\sum_{v'}{}'$ means the sum over all v' except $v'=v$, and

$$h\nu_{vv'}(\theta)=W_{v'}(\theta)-W_v(\theta). \tag{3}$$

This approximation is valid only if the terms containing $\mathbf{P}_\alpha\mathbf{P}_\beta\mathbf{P}_\gamma\mathbf{P}_\delta$ or $\mathbf{P}_\alpha\mathbf{P}_\beta\mathbf{H}_I$ are small with respect to terms characterized by $\mathbf{P}_\alpha\mathbf{P}_\beta$, and if the terms containing $(v|\mathbf{H}_I|v')(v'|\mathbf{H}_I|v)$ are small compared to the $(v|\mathbf{H}_I|v)$ term. These conditions hold quite well wherever the vibrational frequencies are considerably larger than those of over-all and internal rotation.

The expressions $(v(\theta)|\mu_{\alpha\beta}|v(\theta))$ and $W_v(\theta)$ are symmetric functions of θ, the angle of internal rotation, and for the molecules under consideration they have a period of $2\pi/3$. Thus these functions can be expanded in terms of a Fourier series of cosines. In particular, the expansion can be carried out so that the series is of the form

$$f(\theta)=f(0)+\sum_{\tau=1}a_\tau(1-\cos3\tau\theta). \tag{4}$$

If rapid convergence is assumed only the first two terms need be retained.

The Hamiltonian can now be written in the approximate form

$$\begin{aligned}\mathbf{H}=&\mathbf{W}_v(0)+\omega_v(1-\cos3\theta)\\&+(v(\theta)|\mathbf{H}_I|v(\theta))+\tfrac{1}{2}\sum_{\alpha,\beta}[\bar{\mu}_v]_{\alpha\beta}\mathbf{P}_\alpha\mathbf{P}_\beta\\&+\sum_{\alpha,\beta}(f_v)_{\alpha\beta}(1-\cos3\theta)\mathbf{P}_\alpha\mathbf{P}_\beta+\tfrac{1}{2}\sum_{v'}{}'\sum_{\alpha,\beta}(v|\mu_{\alpha\beta}|v')\\&\times[\mathbf{P}_\alpha\mathbf{P}_\beta(v'|\mathbf{H}_I|v)+(v'|\mathbf{H}_I|v)\mathbf{P}_\alpha\mathbf{P}_\beta](h\nu_{vv'})^{-1}\\&+\tfrac{1}{4}\sum_{v'}{}'\sum_{\alpha\beta\gamma\delta}(v|\mu_{\alpha\beta}|v')(v'|\mu_{\gamma\delta}|v)(h\nu_{vv'})^{-1}\\&\times\mathbf{P}_\alpha\mathbf{P}_\beta\mathbf{P}_\gamma\mathbf{P}_\delta+\sum_{v'}{}'(v|\mathbf{H}_I|v')(v'|\mathbf{H}_I|v)\\&\times(h\nu_{vv'})^{-1}+\cdots,\end{aligned} \tag{5}$$

where v represents the basis that diagonalizes $\mathbf{W}_v(0)$, the vibrational energy when $\theta=0$; $[\bar{\mu}_v]_{\alpha\beta}$ is the average value of $\mu_{\alpha\beta}$ in the vibrational state given by v; $(f_v)_{\alpha\beta}$ and ω_v are Fourier coefficients and are constant for a given vibrational state, that is, they are independent of internal and over-all rotations. The last four sums in Eq. (5) are correction terms and are generally quite small. Since these correction terms will be considered only to first order their dependence on θ through $v(\theta)$ may be neglected, for this dependence affects the results in a higher order.

If r represents the basis that diagonalizes the "effective" rigid rotor Hamiltonian given by

$$\tfrac{1}{2}\sum_{\alpha,\beta}[\bar{\mu}_v]_{\alpha\beta}\mathbf{P}_\alpha\mathbf{P}_\beta, \tag{6}$$

and rM represents the basis that diagonalizes the internal rotational Hamiltonian

$$(v(\theta)|\mathbf{H}_I|v(\theta)), \tag{7}$$

one can obtain a first-order energy expression by taking the diagonal element of the Hamiltonian of Eq. (5) in the rM basis. However, since the last four sums in Eq. (5) are merely correction terms, they may be evaluated to a suitable degree of accuracy by taking the

[3] This is also true of the CH_3NO_2, CH_3OH, CH_3NH_2 types of molecule but is not true if neither group is a symmetric rotor. See footnote 19.

[4] In this article vibrational modes mean all internal modes of motion other than torsion (hindered internal rotation).

[5] E. B. Wilson, Jr., and J. B. Howard, J. Chem. Phys. **4**, 260 (1936).

[6] E. C. Kemble, *The Fundamental Principles of Quantum Mechanics* (McGraw-Hill Book Company, Inc., New York, 1937), p. 394.

diagonal element in the rm basis, the basis that diagonalizes

$$(v(0)|\mathbf{H}_I|v(0)). \tag{7a}$$

Since the first two terms in Eq. (5) are vibrational terms they may be neglected in the present problem. The third and the last term do not involve over-all rotation either and need not be considered here. Neglecting the next to last sum in Eq. (5), the ordinary centrifugal distortion term, the over-all rotational energy may be written as

$$\begin{aligned} W_r=&\tfrac{1}{2}\sum_{\alpha,\beta}[\bar{\mu}_v]_{\alpha\beta}(r|\mathbf{P}_\alpha\mathbf{P}_\beta|r)\\ &+\sum_{\alpha,\beta}(f_v)_{\alpha\beta}(m|1-\cos 3\theta|m)(r|\mathbf{P}_\alpha\mathbf{P}_\beta|r)\\ &+\tfrac{1}{2}\sum_{v'}{}'\sum_{\alpha,\beta}(v|\mu_{\alpha\beta}/h\nu_{vv'}|v')\\ &\times(rm|\{(v'|\mathbf{H}_I|v)\mathbf{P}_\alpha\mathbf{P}_\beta+\mathbf{P}_\alpha\mathbf{P}_\beta(v'|\mathbf{H}_I|v)\}|rm). \end{aligned} \tag{8}$$

In writing this expression the fact that m and r are separable is used.[7] The first sum, the energy of an "effective" rigid rotor, can be treated by standard methods.[8] The last two sums require more discussion.

III. EVALUATION OF TERMS WITH H_I

Consider the Hamiltonian for over-all rotational motion and internal rotational motion

$$\mathbf{H}'=\tfrac{1}{2}\sum\eta_{\alpha\beta}\mathbf{p}_\alpha\mathbf{p}_\beta+\tfrac{1}{2}\sum\rho_{\alpha\beta}\mathbf{p}_\alpha\mathbf{p}_\beta+V_I. \tag{9}$$

V_I is the torsional potential energy, $\boldsymbol{\eta}$ and $\boldsymbol{\rho}$ are the inverse instantaneous inertia tensors of the two parts of the molecule that can rotate with respect to each other, and $\mathbf{p}_\alpha$ and $\mathbf{p}_\alpha$ are the corresponding components of angular momentum along the α-principal axis of the entire molecule.[9]

The total angular momentum $\mathbf{P}$ is equal to $\mathbf{p}+\mathbf{p}$. Equation (9) can be rewritten as

$$\begin{aligned} \mathbf{H}'=&\tfrac{1}{2}\sum\mu_{\alpha\beta}\mathbf{P}_\alpha\mathbf{P}_\beta\\ &+\tfrac{1}{2}\sum[(\rho_{\alpha\beta}-\mu_{\alpha\beta})\mathbf{P}_\alpha\mathbf{P}_\beta-\rho_{\alpha\beta}(\mathbf{P}_\alpha\mathbf{p}_\beta+\mathbf{p}_\alpha\mathbf{P}_\beta)\\ &+(\eta_{\alpha\beta}+\rho_{\alpha\beta})\mathbf{p}_\alpha\mathbf{p}_\beta]+V_I, \end{aligned} \tag{10}$$

where $\mu_{\alpha\beta}$ is the inverse instantaneous inertia tensor of the entire molecule. The first term represents over-all rotation; the remainder represents internal rotation, i.e., $\mathbf{H}_I$.

In the special case of a symmetric rotor with no vibrations other than hindered internal rotation governed by a cosine potential, Eq. (9) takes on the form

$$\begin{aligned} \mathbf{H}'=&\tfrac{1}{2}\sum\mu_{\alpha\alpha}{}^{(0)}\mathbf{P}_\alpha{}^2+\tfrac{1}{2}(\rho_{zz}{}^{(0)}\eta_{zz}{}^{(0)}/\mu_{zz}{}^{(0)})\mathbf{\Pi}_z{}^2\\ &+\tfrac{1}{2}V_0(1-\cos 3\theta); \end{aligned} \tag{11}$$

where the superscript (0) indicates equilibrium values, and

$$\mathbf{\Pi}_z=\mathbf{p}_z-(\mu_{zz}{}^{(0)}/\eta_{zz}{}^{(0)})\mathbf{P}_z \tag{12}$$

$$(\mu_{\alpha\alpha}{}^{(0)})^{-1}=(\eta_{\alpha\alpha}{}^{(0)})^{-1}+(\rho_{\alpha\alpha}{}^{(0)})^{-1}. \tag{13}$$

The Hamiltonian of Eq. (11) is diagonal in the quantum numbers m and r already defined.

The third sum in Eq. (8), S_3, can be evaluated by means of Eqs. (10)–(13). The resulting expression for a symmetric rotor is

$$\begin{aligned} S_3=&b_1(m|\mathbf{\Pi}z^2|m)J(J+1)+b_2(m|\mathbf{\Pi}z^2|m)K^2\\ &+b_3(m|\mathbf{\Pi}_z|m)KJ(J+1)+b_4(m|\mathbf{\Pi}_z|m)K^3\\ &+b_5(m|\mathbf{\Pi}_z|m)K+b_6K^2(m|1-\cos 3\theta|m)\\ &+b_7J(J+1)(m|1-\cos 3\theta|m), \end{aligned} \tag{14}$$

where J is the quantum number of over-all rotation and K is the component of angular momentum along the figure axis. The b_i's depend upon the vibrational quantum numbers, v, evaluated at $\theta=0$, but they are independent of the rotational quantum numbers.[3] Terms of the order $\mathbf{P}^4$ have been neglected[10] [see Appendix I for a derivation of Eq. (14)].

The transition frequencies for over-all rotations of a symmetric rotor of the type discussed here may be obtained by combining Eqs. (8) and (14) together with the selection rules $\Delta J=1$, $\Delta K=0$. The rotational frequencies are given by the relation

$$\nu=2\mathfrak{B}_{vm}J, \tag{15}$$

where J is the rotal angular momentum quantum number of the higher state and

$$\begin{aligned} \mathfrak{B}_{vm}=&B_v+F_v(m|1-\cos 3\theta|m)+G_v(m|\mathbf{\Pi}_z{}^2|m)\\ &+L_vK(m|\mathbf{\Pi}_z|m). \end{aligned} \tag{16}$$

In Eq. (16)

$$B_v=\tfrac{1}{2}(\bar{\mu}_v)_{xx}. \tag{17}$$

The other terms are discussed below.

IV. EVALUATION OF TERMS INVOLVING θ

The energy of hindered internal rotation, W_m, may be expressed in terms of a reduced energy R_m.[11]

$$W_m=(V_0/4\alpha)R_m+\tfrac{1}{2}V_0, \tag{18}$$

where V_0 is the barrier height of a cosine potential as seen in Eq. (13) and

$$\alpha=(C/C_1C_2)^{\frac{1}{4}}V_0. \tag{19}$$

C, C_1, and C_2 are the rotational constants[12] about the

[7] H. H. Nielsen, Phys. Rev. **40**, 445 (1932).
[8] King, Hainder, and Cross, J. Chem. Phys. **11**, 27 (1943).
[9] If the molecule vibrates, the α axis is given by the Eckart conditions; C. Eckart, Phys. Rev. **47**, 552 (1935).
[10] Terms of order $\mathbf{P}^4$ can be lumped together with the usual centrifugal distortion terms. See D. Kivelson and E. B. Wilson, Jr., J. Chem. Phys. **20**, 1575 (1952).
[11] J. S. Koehler and D. M. Dennison, Phys. Rev. **57**, 1006 (1940).
[12] $C=h/8\pi^2cI_c$, where I_c is the moment of inertia about the figure axis. C_1 and C_2 are defined in a similar way. C, C_1, and C_2 are proportional to $\mu_{zz}{}^{(0)}$, $\rho_{zz}{}^{(0)}$, $\eta_{zz}{}^{(0)}$, respectively.

figure axis of the entire molecule, the first, and the second part of the molecule, respectively. Dennison and Koehler[11] have obtained the relation

$$R_m=(\tau+\sigma)^2+\alpha^2/T_{\tau+3}+\alpha^2/T_{\tau-3}, \tag{20}$$

where τ is an integer, $\sigma=-KC/C_1$,[13] and T is given by the recurrence relation

$$T_{\tau\pm3}=R_m-(\sigma+\tau\pm3)^2-\alpha^2/T_{\tau\pm6}. \tag{21}$$

From Eqs. (11) and (18) one can obtain[14] the relations

$$(m|\mathbf{\Pi}_z^2|m)=R_m-\alpha(\partial R_m/\partial\alpha)_\sigma \tag{22}$$

and

$$(\partial R_m/\partial\alpha)_\sigma=A_m^{-1}B_m, \tag{23}$$

where

$$A_m=[1+(\alpha/T_{\tau+3})^2+(\alpha/T_{\tau+3})^2(\alpha/T_{\tau+6})^2+\cdots +(\alpha/T_{\tau-3})^2+(\alpha/T_{\tau-3})^2(\alpha/T_{\tau-6})^2+\cdots] \tag{24}$$

$$\alpha B_m=2[\alpha^2/T_{\tau+3}+(\alpha/T_{\tau+3})^2\alpha^2/T_{\tau+6} +(\alpha/T_{\tau+3})^2(\alpha/T_{\tau+6})^2\alpha^2/T_{\tau+9}+\cdots +\alpha^2/T_{\tau-3}+(\alpha/T_{\tau-3})^2\alpha^2/T_{\tau-6} +(\alpha/T_{\tau-3})^2(\alpha/T_{\tau-6})^2\alpha^2/T_{\tau-9}+\cdots]. \tag{25}$$

By the use of standard techniques,[14] $(m|1-\cos3\theta|m)$ may be expressed in terms of R_m and $(m|\mathbf{\Pi}_z^2|m)$. The resulting relation is

$$(m|1-\cos3\theta|m)=(1/2\alpha)[R_m+2\alpha-(m|\mathbf{\Pi}_z^2|m)]. \tag{26}$$

The expression $(m|\mathbf{\Pi}_z|m)$ appearing in Eq. (16) is evaluated in Appendix II. Since only $J=0\rightarrow1$ transitions will be considered here, $K=0$, and the coefficient of $(m|\mathbf{\Pi}_z|m)$ vanishes. It should be mentioned that if higher J transitions are treated this term, as well as the terms in $\mathbf{P}^4$, the ordinary centrifugal distortion terms, should be included.

V. METHYL SILANE

Methyl silane is a good molecule to consider in the present study for it is about the lightest symmetric rotor, capable of internal rotation, that absorbs in the microwave region. The $J=0\rightarrow1$ transition has been observed and measured by Lide and Coles,[1] and their data is given in Table I.[15] It is seen that this over-all rotational transition has a complicated fine structure. Lide and Coles were able to assign these satellite lines by means of intensity measurements. The frequency decreases with increasing quantum number n, the torsional quantum number corresponding to the limiting case of a high barrier. The lines corresponding to each n are split further into two components labeled by k, the quantum number corresponding to the limiting case of free internal rotation. This subsplitting is in accordance with the theory of hindered internal rotation developed by Koehler and Dennison.[11] For higher J transitions, the rotational quantum number K need not be zero and, according to the theory, each n line would be split into three components in addition to the splitting that might arise from ordinary centrifugal distortion effects.

The data on methyl silane exhibits an anomalous ordering of the satellite lines. The internal rotational energy levels as given by the Koehler and Dennison theory increase with increasing n and with increasing k. However, the measurements of Lide and Coles show that the satellite lines are not ordered in this manner with respect to k, although they are ordered properly with respect to n (see Fig. 1). This inversion in the ordering means that the origin of the fine structure must be caused by effects other than centrifugal distortion. It should be noted that there are two $k=3$ and two $k=6$ lines as predicted by the Koehler and Dennison theory.

For the $J=0\rightarrow1$ transition, $K=0$ and Eqs. (15) and (16) reduce to

$$\nu/2=B_v+F_v(m|1-\cos3\theta|m)+G_v(m|\mathbf{\Pi}_z^2|m). \tag{27}$$

The problem is to fit the constants in this equation to the data given in Table I. There are four constants to be determined, B_v, F_v, G_v, and α. Alpha is proportional to the barrier height assuming a cosine potential, and enters into the expressions $(m|1-\cos3\theta|m)$ and $(m|\mathbf{\Pi}_z^2|m)$ as demonstrated above. (It should be noted that m stands for the two pseudo-quantum numbers n, k.) Here $(m|1-\cos3\theta|m)$ and $(m|\mathbf{\Pi}_z^2|m)$ were calculated for α equal to 12 and 13.5, and for each of these values the parameters B_v, F_v, and G_v were taken in order to give the exact frequencies for the $(n=0)$, $(n=1,\ k=2)$, and $(n=3,\ k=5)$ lines. The other fre-

TABLE I. Frequencies of $J=0\rightarrow1$ transitions for methyl silane.

n	k	Frequencies observed by Lide and Coles[a] (Mc/sec)	Calculated frequencies[c] (Mc/sec)
0	0,1[b]	21937.92	(21937.92)
1	3	21873.08	21873.00
1	2	21872.38	(21872.38)
2	4	21814.20	21812.48
2	3	21808.71	21808.05
3	6	21768.83	21767.51
3	5	21758.78	(21758.78)
4	6[d]?	21737.77	21736.25
4	7[d]?	21706.87	21734.10

[a] See reference 15.
[b] These two lines could not be resolved. The calculated value is the average of the two. The calculated frequency difference between these two lines is less than 0.05 Mc/sec.
[c] Values in parentheses agree exactly with the observed frequencies since they were used to determine the constants.
[d] The questioned assignments could not be made unambiguously (see references 1 and 15).

[13] K is the quantum number of the z component of total angular momentum.
[14] The technique for obtaining these terms involves holding σ constant, differentiating the Hamiltonian of Eq. (11) with respect to α, and combining the result with Eq. (18). See reference 10. $\mathbf{\Pi}_z$ is given in units of $\hbar$.
[15] The values of the frequencies were given to the author by Dr. David R. Lide.

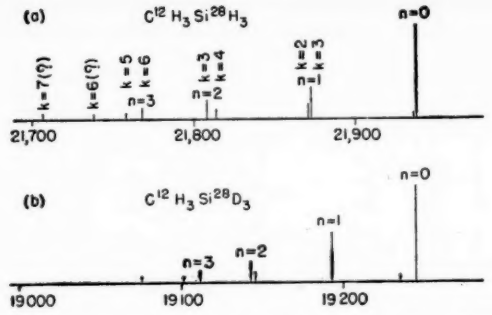

FIG. 1. The $J=0\rightarrow1$ transitions in methyl silane (see reference 1).

quencies were then calculated and compared with the experimental results. These calculated frequencies were all found to lie above the experimental ones, but those calculated on the basis of α equal to 13.5 agreed more closely with the observed values. Values of $(m|1-\cos3\theta|m)$ and $(m|\mathbf{\Pi}_z^2|m)$ were then obtained for larger values of α by extrapolation. Since the actual calculations for these two quantities are lengthy, it is well to try and approximate the best value of α as closely as possible by extrapolation or by interpolation. It was seen that the calculated frequencies decreased with increasing α and that they agreed quite closely with the experimental values for α equal to 17. The calculations were carried out in full for this value of α, and these detailed calculations agreed quite well with the results obtained by extrapolation. The final values of the constants are

$$\alpha=17.0\pm0.5,$$
$$B_v=10985.79 \text{ Mc/sec}\pm0.05 \text{ Mc/sec},$$
$$F_v=-65.322 \text{ Mc/sec}\pm0.8 \text{ Mc/sec},$$
$$G_v=-0.8824 \text{ Mc/sec}\pm0.04 \text{ Mc/sec}.$$

The calculated frequencies are given in Table I.

The estimated errors given above are based solely on the uncertainty in the determination of the best value of α according to the procedure outlined. The agreement between the experimental and the calculated frequencies does not fall within experimental error for all the lines, which means that the theory is not exact and that the parameters determined above have a limited significance. The corrections to the theory are probably to be found in some of the terms discarded in the approximations made in section II. As a possible indication of the importance of these neglected terms, the term $N_v(m|\mathbf{\Pi}_z^2|m)(m|1-\cos3\theta|m)$ was added to Eq. (27) and the problem reinvestigated. It was found that this term contributed very little and that the other four parameters were only slightly affected by it. However, the change is great enough to indicate that the agreement between calculated and observed frequencies might well fall within experimental error if all terms of this order were kept. It was not felt, however, that the data justified the determination of so many parameters.

If instead of a good fit for all of the lines an exact fit is obtained for four low-lying torsional states, i.e., the first four lines in Table I, the value of α is considerably smaller (approximately 13), and the agreement with experiment for the lines in the higher torsional states is poor. The discarded terms discussed in the preceding paragraph are less important for the low-lying torsional levels, which is an argument in favor of this method of determination. However, these four levels do not involve relations that are sufficiently independent to yield good values for the constants. Furthermore, the rather close agreement, except for the $k=7$ line, between the values calculated on the basis of $\alpha=17$ and the frequencies obtained by Lide and Coles appears to justify the original procedure. These calculations also properly predict the anomalous ordering of the levels. This anomalous ordering arises in the evaluation of $(m|1-\cos3\theta|m)$, see Table II, and is explained by the fact that the probability of finding an atom under the barrier is not solely dependent upon the height of the given energy level; it is also dependent upon the symmetry of the wave function.

Lide and Coles were unable to assign the $k=7$ line with any degree of certainty. Thus it is very likely that the discrepancy between the measured and the calculated frequency for this line is the result of an improper assignment. Of course it is possible that the assignment is correct and that the calculations are not valid for the higher torsional states. However, the close fit for the next highest torsional state seems to justify the former explanation. Further experimental work on the subject is contemplated.

It should be mentioned that calculations were also carried out for $\alpha=10.5$, and rough calculations were made for surrounding values. It was seen that Eq. (27) had a hyperbolic type of singularity for some value of α between 10.5 and 12. The calculated frequencies fell below the observed frequencies on the lower "branch." The calculated frequencies increased with decreasing α, but appeared to approach asymptotically to values of the frequencies below the observed values. One must be careful of this singularity or else it may be difficult to approach the solution by extrapolation.

TABLE II. Calculations related to the torsional energy levels of methyl silane.

n	k	R	$(m\|\mathbf{\Pi}_z^2\|m)$	$(m\|1-\cos3\theta\|m)$	W_m-W_0 (cm^{-1})[a]
0	1	−22.2222	5.5799	0.182291	0.0262
0	0	−22.2252	5.5627	0.182709	0.0000
1	3	0.0495	15.5377	0.544465	183
1	2	−0.0502	15.0366	0.556270	182
2	4	19.4083	22.1968	0.917985	342
2	3	18.2792	17.9776	1.008870	332
3	6	38.5136	35.8872	1.077247	498
3	5	32.3815	20.3406	1.354144	448
4	6	42.4574	28.1325	1.421320	531
4	7	52.2939	45.2915	1.205953	611

[a] W_m and W_0 are the torsional energy levels corresponding to the $m=(n,R)$ and $(n=0, k=0)$ levels, respectively. $W_0=96.6$ cm^{-1}.

B_v can be interpreted as the ordinary rotational constant, that is, the rotational constant averaged over a vibrational state v. B_v is evaluated at $\theta=0°$. $G_v(m|\Pi_z^2|m)$ is a centrifugal distortion term that includes part of the effects of the speed of internal rotation upon the vibrations and, hence, upon the rotational constant. G_v can, in principle, be evaluated by combining the results given above with techniques used in calculating constants of centrifugal distortion.[16] In practice, however, this is a formidable task that involves the knowledge of all of the force constants.

The term $F_v(m|1-\cos 3\theta|m)$ includes part of the centrifugal distortion effect discussed above and also accounts for the dependence of the vibrational modes upon the angle θ. One might picture the two functional groups pushed apart as the angle θ moves from 0 to $\pi/3$, that is, from equilibrium to the point of maximum barrier. Also, as the groups are pushed apart, the vibrational characteristics of the molecule might be changed. In order to calculate F_v, one would have to make assumptions concerning the changes in interatomic distances and in the vibrational frequencies with changes in the angle of internal rotation. This problem might be worth a more thorough study.

The parameter α is proportional to the barrier height, V_0, of a cosine potential. See Eq. (19). Assuming that the value of the rotational constants C_1 and C_2 are those of CH_4 and SiH_4, respectively, and that C is the corresponding rotational constant about the figure axis of SiH_3CH_3, one has

$$C_1=5.252\ \text{cm}^{-1},\ \text{(see reference 17)}$$
$$C_2=2.965\ \text{cm}^{-1},\ \text{(see reference 17)}$$
$$C=1.895\ \text{cm}^{-1}.$$

Then

$$V_0=558\ \text{cm}^{-1}\pm 17\ \text{cm}^{-1},$$

which is just above the upper limit set on V_0 by means of intensity measurements made by Lide and Coles. From this the energy level spacings of the torsional states can be computed. See Table II. It is seen that the $n=1$ torsional level is 183 cm^{-1} above the ground state. This is in exact agreement with the results obtained by Lide and Coles.

The barrier height should be almost the same in CH_3SiD_3 as it is in CH_3SiH_3. However, the value of α for the deuterated species is increased to 20.74, provided that C_2 is taken as 1.482 cm^{-1} and C is changed accordingly. With this value of α, the constants B_v, G_v, and F_v were determined by means of the $(k=0)$, $(n=1,\ k=3)$, $(n=3,\ k=5)$ lines, and the frequencies of the remaining lines were calculated. The comparison between the theoretical frequencies and those measured by Lide and Coles are given in Table III. The agreement between the calculated and the experimental frequencies could probably be improved by altering α slightly, but the data did not warrant the extra work.

TABLE III. Frequencies for $J=0\rightarrow 1$ transitions for CH_3SiD_3.

n	k	Frequencies observed by Lide and Coles[a] (Mc/sec)	Calculated frequencies (Mc/sec)[c]
0	0,1[b]	19245.56	(19245.56)
1	2,3[b]	19192.76	(19192.76)
2	4?[d]	19144.38	19144.28
2	3?[d]	19142.69	19143.19
3	6	19110.41	19103.00
3	5	19100.57	(19100.57)

[a] See reference 15.
[b] These two lines could not be resolved.
[c] Values in parentheses were used to determine the constants $B_v=9636.50$ Mc/sec, $F_v=-52.868$ Mc/sec, $G_v=-0.8012$ Mc/sec.
[d] The questioned assignments could not be made unambiguously because of the presence of another line at 19145.39 Mc/sec.

The theory stated above gives a satisfactory explanation of the satellite lines in the $J=0\rightarrow 1$ transition of a symmetric rotor with internal rotation. It explains the anomalous ordering and gives a quantitative fit. Furthermore, a reasonably precise value of the potential barrier has been obtained. The dependence of the splitting upon barrier shape has not been investigated here although the assumption of a cosine potential seems justified in view of the recent work of Pitzer and Hollenberg.[18]

A small-oscillations treatment of the torsional mode of vibration of a symmetric rotor indicates that this mode should not be infrared active. However, if the "wobbling" motion, already discussed in connection with the F_v term, is superposed upon the hindered internal rotation, transitions between torsional states should be active, though weak, in the infrared. This phenomenon is being investigated, and it is hoped that it will yield more information concerning the potential barrier.

In a forthcoming paper the interactions between internal and over-all rotations will be treated for the case of asymmetric rotors.

ACKNOWLEDGMENT

The author is indebted to Dr. David R. Lide for supplying unpublished data and for helpful discussions on the subject of internal rotation. He would like to thank Professor M. W. P. Strandberg and Professor E. Bright Wilson, Jr., for their interest in the work and for their suggestions. He is grateful to Miss Ethel Ginsburgh for her assistance in carrying out the numerical work.

APPENDIX I

To evaluate the third sum in Eq. (8) one must divide the Hamiltonian of Eq. (10) into two parts, the over-all rotational part, consisting of the first sum, and the

[16] D. Kivelson and E. B. Wilson, Jr., J. Chem. Phys. **21**, 1229 (1953).
[17] G. Herzberg, *Molecular Spectra and Molecular Structure: II. Infrared and Raman Spectra of Polyatomic Molecules* (D. Van Nostrand Company, Inc., New York, 1949), p. 456.
[18] K. B. Pitzer and J. L. Hollenberg, J. Am. Chem. Soc. **75**, 2123 (1953).

internal rotational part, $\mathbf{H}_I$, consisting of the remaining terms. Thus

$$(v|\mathbf{H}_I|v')=\sum_{\alpha,\beta}[(v|\tfrac{1}{2}\{\rho_{\alpha\beta}-\mu_{\alpha\beta}\}|v')\mathbf{P}_\alpha\mathbf{P}_\beta - (v|\rho_{\alpha\beta}\{\mathbf{P}_\alpha\mathbf{p}_\beta+\mathbf{p}_\beta\mathbf{P}_\alpha\}|v') +(v|\{\rho_{\alpha\beta}+\eta_{\alpha\beta}\}\mathbf{p}_\alpha\mathbf{p}_\beta|v')+(v|V_I|v')]. \quad (28)$$

This element must then be multiplied by

$$(v'|\sum_{\gamma\delta}\mu_{\gamma\delta}/h\nu_{vv'}|v)\mathbf{P}_\gamma\mathbf{P}_\delta. \quad (29)$$

Next the substitution

$$\mathbf{p}_\alpha=\mathbf{\Pi}_\alpha+(\mu_{\alpha\alpha}/\eta_{\alpha\alpha})\mathbf{P}_\alpha \quad (30)$$

must be made. The terms of order $\mathbf{P}^4$ are neglected. Even in the vibrating molecule there is only one degree of freedom allowed to the internal rotation although it may no longer be along the z axis. Thus the component of the internal angular momentum operator in the vibrating molecule may be written as

$$\mathbf{\Pi}_\alpha=a_{\alpha z}\mathbf{\Pi}_z \quad (31)$$

and the potential as

$$V_I=a_I(1-\cos 3\theta), \quad (32)$$

where $a_{\alpha z}$ and a_I are functions of v but are independent of J, K, m.[19] After making all of these substitutions one then sums the product described above over v', excluding $v'=v$. The result is of the form

$$S_3'=\sum_{\alpha,\beta,\gamma}[A_{\alpha\beta}{}^{(1)}\mathbf{P}_\alpha\mathbf{P}_\beta\mathbf{\Pi}_z{}^2+A_{\alpha\beta\gamma}{}^{(2)}\mathbf{P}_\alpha\mathbf{P}_\beta\mathbf{P}_\gamma\mathbf{\Pi}_z +A_{\alpha\beta}{}^{(3)}(1-\cos 3\theta)\mathbf{P}_\alpha\mathbf{P}_\beta] \quad (33)$$

where the $A^{(i)}$'s are functions of v but are independent of the rotational quantum numbers.[19] The $(rm|mr)$ element must now be taken where r represents the two symmetric rotor quantum numbers K and J. It is readily seen that Eq. (14) is the resulting expression for S_3.[8,11]

A more detailed derivation will be given in an ensuing paper.

[19] Actually these constants may depend upon θ and, hence, upon m. If the vibrations distort the molecule so that neither functional group remains a symmetric rotor, the moments of inertia and, hence, the rotational constants depend directly upon θ.

APPENDIX II

The expression $(m|\mathbf{\Pi}_z|m)$ appearing in Eq. (16) may be evaluated in units of $\hbar$ by the following procedure. Consider the Hamiltonian

$$\mathfrak{H}=\mathbf{H}_I+Q(C_1C_2/C)\mathbf{\Pi}_z=(C_1C_2/C)\mathbf{\Pi}_z{}^2 +\tfrac{1}{2}V_0(1-\cos 3\theta)+Q(C_1C_2/C)\mathbf{\Pi}_z. \quad (34)$$

If $\mathcal{E}$ is an eigenvalue of this Hamiltonian, then one has[20]

$$(C/C_1C_2)(\partial\mathcal{E}/\partial Q)_{Q=0}=(m|\mathbf{\Pi}_z|m). \quad (35)$$

Equation (18) still holds, provided that ϵ is substituted for W and that R is now a function of Q. $R(Q)$ is given by Eqs. (20)–(21) in which $(\sigma+\tau\pm 3n)^2$ is replaced by $(\sigma+\tau\pm 3n)^2+Q(\sigma+\tau\pm 3n)$. One can now obtain the expression

$$(\partial\mathcal{E}/\partial Q)_{Q=0}=(\partial R/\partial Q)_{Q=0}=A_m{}^{-1}D_m, \quad (36)$$

where

$$D_m=(\tau+\sigma)+(\alpha/T_{\tau+3})^2(\tau+\sigma+3) +(\alpha^2/T_{\tau+3}T_{\tau+6})^2(\tau+\sigma+6)+\cdots +(\alpha/T_{\tau-3})^2(\tau+\sigma-3) +(\alpha^2/T_{\tau-3}T_{\tau-6})^2(\tau+\sigma-6)+\cdots \quad (37)$$

and A_m is given by Eq. (24). This technique could be used to evaluate $(m|\mathbf{\Pi}_z{}^t|m)$ where t is any positive integer.

By squaring $\mathbf{H}_I$ and following a procedure similar to that described here and in reference (10), terms of the form $(m|\cos^2 3\theta|m)$ and $(m|\mathbf{\Pi}_z{}^2\cdot\cos 3\theta+(\cos 3\theta)\cdot\mathbf{\Pi}_z{}^2|m)$ can be evaluated. These expressions would be of interest if higher-order terms were kept in the expansions of Eqs. (2) and (4).

[20] See section IV of reference 10.

Elementary Processes in the Radiation Chemistry of Water

KEITH J. LAIDLER
Department of Chemistry, The Catholic University of America, Washington, D. C.
(Received December 11, 1953)

Schematic potential-energy diagrams are constructed for ground and excited states of H_2O, H_2O^+ and H_2O^-, making use of thermochemical, spectroscopic, and electron-impact data. On electron impact a gaseous water molecule is raised to various states of H_2O, H_2O^+ and H_2O^-, which may subsequently decompose to give H, O, H_2, and OH and the ions H^+, H^-, O^+, O^-, OH^+, and H_2^+. The exact mechanisms by which these atoms, radicals, and ions are produced are discussed in detail with reference to the potential-energy curves, due attention being paid to the appropriate correlation and selection rules. It is concluded that the production of O^- at 173 kcal electron energy probably proceeds via a $^2A_1$, $^2B_1$, $^2A_2$, or $^2B_2$ state of H_2O^- which decomposes into $2H+O^-$ without the prior formation of OH^-. The production of O^+ at 437 kcal must necessarily proceed via a $^4A_2$ or $^4B_2$ state of H_2O^+, while H_2^+ at 530 kcal must involve the formation of a $^2A_2$ or $^2B_2$ state; both these latter states are stable with respect to the simple breaking of an O—H bond. The nonappearance of OH^- in electron-impact experiments is shown to be related to the high stability of OH^-, states of H_2O^- which correlate with $H+OH^-$ being of very high energy. The bearing of the treatment on the radiation chemistry of liquid water is briefly considered.

WHEN water is subjected to the action of ionizing radiation there are produced atoms, radicals, and ions in their ground states and in various states of excitation. Of the atoms and radicals, some are produced directly, others indirectly from ions by secondary reactions. A theoretical discussion of the direct formation of the hydrogen atom and the hydroxyl radical has recently been given by Niira,[1,2] who has been particularly concerned with the question of the abnormal rotation of the hydroxyl radical produced in electrical discharges through water vapor. The present paper is devoted to a discussion of the detailed mechanisms involved in the formation of ions when water vapor is subjected to the action of high-energy electrons.

The procedure adopted in the present paper consists of combining conclusions from purely theoretical considerations with the results of thermochemical, radiochemical and spectroscopic investigations. In view of the uncertainties attached to quantum-mechanical calculations, particularly for excited states, it has not been thought that a completely theoretical discussion of this complex problem would be useful at the present time. Semiquantitative theoretical conclusions have therefore been combined with experimental data, and a self-consistent scheme has been worked out. The methods employed in the construction of the potential-energy surfaces are equivalent to those used in previous publications,[3–6] and discussed in a recent review.[7] Previous theoretical treatments of the elementary processes in radiochemical reactions have been presented by Eyring, Hirschfelder, and Taylor[8,9] and by Magee and Burton.[10,11] The experimental data employed in the present treatment are the spectroscopic data[12] for the OH radical and the OH^+ ion, the electron-impact data of Mann, Hustrulid, and Tate[13] and various thermochemical data. The thermochemical values that have been used, together with their source, are listed in Table I.

In Table II are listed the ions that are detected in the electron-impact experiments,[13] in order of increasing appearance potential. In the fifth column are given the over-all reactions which are believed, on the basis of the following theoretical treatment, to account for the various ions. It will be seen from the last column that the minimum energy required to produce the ion by the process indicated is always less than the appearance potential. The over-all processes given are not always the ones by which the particular ions are produced with the minimum expenditure of energy; other reactions producing the ions with less energy can sometimes be written down, but there may be no mechanism by which they can occur.

THE POTENTIAL-ENERGY SURFACES

In Fig. 1 are given the potential-energy curves for the various states of OH, OH^+, and OH^-. In the case of OH^- the only experimental values available are the electron affinities of O and of OH; the values used are 51 and 48 kcal, respectively (see Table I).

The following considerations are relevant to the

[1] K. Niira, J. Phys. Soc., Japan **4**, 230 (1949).
[2] K. Niira, J. Phys. Soc., Japan **7**, 193 (1952).
[3] K. J. Laidler, J. Chem. Phys. **10**, 34 (1942).
[4] K. J. Laidler, J. Chem. Phys. **10**, 43 (1942).
[5] K. J. Laidler, J. Chem. Phys. **15**, 712 (1947).
[6] V. F. Griffing and K. J. Laidler, *Third Symposium on Combustion, Flame and Explosion Phenomena* (Williams and Wilkins Company, Baltimore, 1949), p. 432.
[7] K. J. Laidler and K. E. Shuler, Chem. Revs. **48**, 153 (1951).
[8] Eyring, Hirschfelder, and Taylor, J. Chem. Phys. **4**, 479 (1936).
[9] Eyring, Hirschfelder, and Taylor, J. Chem. Phys., **4**, 570 (1936).
[10] J. L. Magee and M. Burton, J. Am. Chem. Soc. **72**, 1965 (1950).
[11] J. L. Magee and M. Burton, J. Am. Chem. Soc. **73**, 523 (1951).
[12] G. Herzberg, *Spectra of Diatomic Molecules* (D. Van Nostrand Company, Inc., New York, 1950), pp. 560–1.
[13] Mann, Hustrulid, and Tate, Phys. Rev. **58**, 340 (1940).

states of OH^-. The O^- ion is isoelectronic with the fluorine atom, and therefore probably has a ^2P_u ground state and a ^4P_g first excited state. The combination $H(^2S_g)+O^-(^2P_u)$ gives the following states of OH^-: $^1\Sigma^+$, $^3\Sigma^+$, $^1\Pi$, $^3\Pi$. The electronic structure of the OH radical is $K(2s\sigma)^2(2p\sigma)^2(2p\pi)^3$, and the OH^- ion in the ground state is presumably made by filling the $(2p\pi)$ orbital; this gives rise to $K(2s\sigma)^2(2p\sigma)^2(2p\pi)^4$, which corresponds to the $^1\Sigma^+$ state. Excited states can correspond to $K(2s\sigma)^2(2p\sigma)^2(2p\pi)^3(3s\sigma)$, which give rise to $^1\Pi$ and $^3\Pi$ states, or to $K(2s\sigma)^2(2p\sigma)^2(2p\pi)^3(3p\pi)$, which can give the states $^1\Sigma^+$, $^1\Sigma^-$, $^1\Delta$, $^3\Sigma^+$, $^3\Sigma^-$, and $^3\Delta$.

The correlations relevant to the various states of H_2O, H_2O^+ and H_2O^- were worked out using the method of Shuler.[14] The symmetry of these triatomic species is C_{2v}, and when they are dissociated by the continuous increase of one O—H distance, with the other kept fixed, they pass through a series of intermediate configurations of symmetry C_s (one plane of symmetry). The system under consideration therefore consists of a triatomic configuration of symmetry C_{2v} (isosceles triangle), an intermediate configuration of symmetry C_s, and a configuration consisting of a diatomic molecule of symmetry $C_{\infty v}$ together with an atom. In order to establish the over-all correlations it is therefore necessary to correlate C_{2v} with C_s, and then C_s with $C_{\infty v}$ and the atom. The former correlations are shown in Table III, and the latter in Table IV, which is taken from Shuler's paper. It is clear from these tables that the A and B states may occur interchangeably; in the following discussion and figures A and B states have been employed arbitrarily and may in all cases be exchanged for one another.

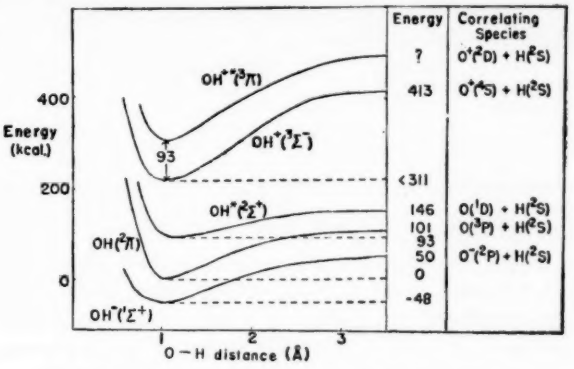

FIG. 1. Potential-energy curves for the O—H system.

The correlations obtained in this way are given in Tables V and VI. Figure 2 shows schematic potential-energy curves for various states of H_2O, H_2O^+, and H_2O^-, energy being represented as a function of H—OH distance. This figure is to be regarded as a section through the potential energy surface (see Fig. 3) corresponding to a fixed H—O distance in the OH radical or ion. The exact form of the curves shown in Fig. 2 is not known, but in constructing these the available electron-impact data and the correlation rules have

TABLE 1. Thermochemical data.

Substance	State	Standard ΔH of formation at 25°C (kcal)	Energy with respect to gaseous atom or atoms (kcal)	Source
H	^2S_g	52.1	0	a
H*	^2S_g	287.2	235.1	b
H**	^2S_g	330.7	278.6	b
H^+	^1S_g	363.8	311.7	b
H^-	^1S_g	34.9	−17.2	c
O	^3P_g	59.2	0	a
O^+	^4S_u	371.4	312.2	b
O^-	^2P_u	8.5	−50.7	b, c
H_2	$^1\Sigma_g^+$	0	−104.2	a
H_2^+	$^2\Sigma_g^+$	355.7	251.5	d
OH	$^2\Pi$	10.1	−101.2	a
OH*	$^2\Sigma^+$	103.5	−7.8	d
OH^+	$^3\Sigma^-$	321	210	e
OH^{+*}	$^3\Pi$	406	295	d, e
OH^-	$^1\Sigma^+$	−38.3	−149.6	c
H_2O	$^1B_1$ or $^1B_2$	−57.8	−221.2	a

[a] F. D. Rossini *et al.*, *Selected Values of Chemical Thermodynamic Properties* (U. S. National Bureau of Standards, 1949).
[b] G. Herzberg, *Atomic Spectra and Atomic Structure* (Prentice-Hall, Inc., New York, 1937).
[c] H. S. W. Massey, *Negative Ions* (Cambridge University Press, Cambridge, 1950).
[d] G. Herzberg, *Spectra of Diatomic Molecules* (D. Van Nostrand Company, Inc., New York, 1950).
[e] Present work.

TABLE II. Data for the appearance of various ions on electron impact.

Ion	Appearance potential ev	Appearance potential kcal	Intensity at 100 volts	Probable over-all process	Theoretical minimum energy kcal
H^-	5.6	129	0.6	$H_2O+e\rightarrow OH+H^-$	103
O^-	7.5	173	1.5	$H_2O+e\rightarrow 2H+O^-$	171
H_2O^+	13.0	300	100	$H_2O+e\rightarrow H_2O^++2e$	(300)
H_3O^+	13.8	318	...	$\left.\begin{matrix}H_2O+e\rightarrow H_2O^++2e\\ H_2O^++H_2O\rightarrow H_3O^++OH\end{matrix}\right\}$	~250
OH^+	18.7	431	23.2	$H_2O+e\rightarrow H+OH^++2e$	<431
O^+	18.8	433	2.0	$H_2O+e\rightarrow H_2+O^++2e$	429
H^+	19.5	450	5.0	$H_2O+e\rightarrow OH+H^++2e$	432
H_2^+	23.0	530	0.07	$H_2O+e\rightarrow H_2^++O+2e$	473
O^-	23.7	546	...	$H_2O+e\rightarrow H^*+H+O^-$	406
O^+	26.0	599	1.7	$H_2O+e\rightarrow H_2+O^++2e$	429
O^+	28.1	648	...	...	...
O^-	36.0	830	...	...	...

[14] K. E. Shuler, J. Chem. Phys. **21**, 624 (1953).

TABLE III. Correlation table for groups C_{2v} and C_s.

Representations of C_{2v}	Corresponding representations of C_s
A_1, B_1	A'
A_2, B_2	A''

been taken into consideration. Unfortunately there is not enough information to enable a unique diagram to be constructed, and Fig. 2 must be regarded as one of many possibilities. A study of such a diagram is, however, instructive from the standpoint of the interpretation of electron-impact experiments.

One point needs special discussion in connection with the states of H_2O^-. Since the lowest state ($^1\Sigma^+$) of OH^- has a completed valence shell the approach of an $H(^2S_g)$ atom will be associated with strong repulsion; the state of H_2O^- produced is a $^2A_1$ (or $^2B_2$) state, and it is shown as a highly repulsive state in Fig. 2. This state probably does not contribute to the production of ions in electron-impact experiments, at any rate at low energies. The formation of O^- at 173 kcal does, however, require that there is a state of H_2O^- at this level, and in accordance with a suggestion of Dr. C. A. McDowell it is supposed that this is a $^2A_1$, $^2B_1$, $^2A_2$, or $^2B_2$ state arising from the $^2\Pi$ state of OH^- rather than the lowest state. This state of OH^- is probably unstable with respect to dissociation into $H(^2S_g)+O^-(^2P_u)$.

MECHANISMS OF ION FORMATION

In the light of the preceding discussion the following detailed mechanisms, consistent with the Franck-Condon principle and obeying the correlation and selection rules, are suggested for the formation of the various ions in the electron-impact experiments.

H^- (129 kcal)

At an electron energy of 129 kcal the water molecule is raised to a repulsive $^2A_1$ or $^2A_2$ state of H_2O^-, which at once dissociates into $H^-(^1S)+OH(^2\Pi)$.

O^- (173 kcal)

There are two possibilities for the formation of this ion. In the first place, the water molecules might be excited to a state of H_2O^- which is unstable with respect to the dissociation

$$H_2O^- \rightarrow 2H+O^-. \quad (1)$$

The reaction $e+H_2O^- \rightarrow 2H+O^-$ is actually endothermic by 171 kcal, so that the electrons provide just enough energy for this to occur. If this is the situation the H_2O^- state produced cannot be the $^2A_1$ state which correlates with $H(^2S)+OH^-(^1\Sigma^-)$, since in that case OH^- ions would be obtained, and these have not been observed. The state may, however, be a $^2A_1$ or $^2A_2$ state which correlates with $H(^2S)+OH^{-*}(^2\Pi)$, the latter being a repulsive state of OH^-. There is not, however, enough excess energy to allow this repulsive state of OH^- to be formed, so that it must be supposed that the H_2O^- decomposes directly into $2H+O^-$. The way in which this can occur is shown in Fig. 3, in which the relevant potential-energy surfaces are drawn schematically. It is seen that the surface of the H_2O^- ($^2A_1$ or $^2A_2$) state has something of the shape of a pointed spade; after electronic excitation the system moves directly along a horizontal path towards the outer edge of the cube, which corresponds to $2H+O^-$.

The second possibility is that the interaction between an electron and a water molecule gives rise to a state of H_2O^- which undergoes rearrangement into $H_2(^1\Sigma_g^+)+O^-(^2P_u)$; this could be an $^2A_1$, $^2A_2$, $^2B_1$ or $^2B_2$ state.

TABLE IV. Correlation table for groups C_s and $C_{\infty v}$+atom.

	S_g	S_u	P_g	P_u	D_g	D_u
Σ^+	A'	A''	$A'+2A''$	$2A'+A''$	$3A'+2A''$	$2A'+3A''$
Σ^-	A''	A'	$2A'+A''$	$A'+2A''$	$2A'+3A''$	$3A'+2A''$
Π, Δ, etc.	$A'+A''$	$A'+A''$	$3A'+3A''$	$3A'+3A''$	$5A'+5A''$	$5A'+5A''$

TABLE V. Correlations for the various states of H_2O and H_2O^+.

Reactants	Energy level of reactants with respect to H_2O (kcal)	Product	Intermediate states (C_s)	States of product (C_{2v})
$H(^2S_g)+OH(^2\Pi)$	120.0	H_2O	$^1A', ^3A', ^1A'', ^3A''$	$^1A_1, ^3A_1, ^1A_2, ^3A_2$
$H(^2S_g)+OH^*(^2\Sigma^-)$	213.0	H_2O	$^1A'', ^3A''$	$^1A_2(2), ^3A_2(2)$
$H^*(^2S_g)+OH(^2\Pi)$	355.1	H_2O	$^1A', ^3A', ^1A'', ^3A''$	$^1A_1, ^3A_1, ^1A_2, ^3A_2$
$H^+(^1S_g)+OH^-(^1\Sigma^-)$	383.3	H_2O	$^1A''$	$^1A_2(2)$
$H(^2S_g)+OH^+(^3\Sigma^-)$	431	H_2O^+	$^2A'', ^4A''$	$^2A_2(2), ^4A_2(2)$
$H^+(^1S_g)+OH(^2\Pi)$	432	H_2O^+	$^2A', ^2A''$	$^2A_1, ^2A_2$
$H(^2S_g)+OH^{+*}(^3\Pi)$	516	H_2O^+	$^2A', ^4A', ^2A'', ^4A''$	$^2A_1, ^4A_1, ^2A_2, ^4A_2$
$H^+(^1S_g)+OH^*(^2\Sigma^-)$	525	H_2O^+	$^2A''$	$^2A_2$
$H^+(^2S_g)+OH^+(^3\Sigma^-)$	668	H_2O^+	$^2A'', ^4A''$	$^2A_2(2), ^4A_2(2)$

This possibility cannot be excluded, but the correspondence between the appearance potential (173 kcal) and the endothermicity of the reaction producing 2H+O⁻ (171 kcal) makes us favor the first possibility, and this is the one shown in the figures.

H_2O^+ (300 kcal)

This is attributed to excitation of the H_2O to a $^2A_2$ state of H_2O^+, which correlates with $H(^2S)+OH^+(^2\Sigma)$, the exact level of which is not known. The H_2O^+ in this $^2A_2$ state is stable with respect to any kind of dissociation, the levels of $H+OH^+$, H^++OH, H_2+O^+, and H_2^++O all being considerably higher than 300 kcal.

H_3O^+ (318 kcal)

This ion must inevitably be produced by a bimolecular process, and Mann, Hustrulid, and Tate[13] in fact find that its intensity is proportional to the square of the pressure. Possible reactions are

$$H_2O^+ + H_2O \rightarrow H_3O^+ + OH + \sim 50 \text{ kcal} \quad (2)$$

$$H_2O^+ + H \rightarrow H_3O^+ + \sim 170 \text{ kcal}. \quad (3)$$

Of these the latter is more likely on purely energetic grounds, but the hydrogen atom concentration may be too low for it to be significant. In any case the reaction forming H_3O^+ apparently has an activation energy of 18 kcal, so that the H_2O^+ reacting must have this amount of excess energy in its vibrational modes.

TABLE VI. Correlations for the various states of H_2O^-.

Reactants	Energy level of reactants with respect to H_2O (kcal)	Intermediate states (C_{2v})	States of products (C_{2v})
$H(^2S_g)+OH^-(^1\Sigma^+)$	72[a]	$^2A'(2)$	$^2A_1(2)$
$H^-(^1S_g)+OH(^2\Pi)$	101.9	$^2A', {}^2A''$	$^2A_1, {}^2A_2$
$H^*(^2S_g)+OH^-(^1\Sigma^-)$	267.5[a]	$^2A'(2)$	$^2A_1(2)$
$H(^2S_g)+OH^{-*}(^3\Sigma^+)$	···	$^2A'(2), {}^4A'(2)$	$^2A_1(2), {}^4A_1(2)$
$H(^2S_g)+OH^{-*}(^1\Pi)$	···	$^2A', {}^2A''$	$^2A_1, {}^2A_2$
$H(^2S_g)+OH^{-*}(^3\Pi)$	···	$^2A', {}^4A', {}^2A'', {}^4A''$	$^2A_1, {}^4A_1, {}^2A_2, {}^4A_2$
$H(^2S_g)+OH^{-*}(^1\Delta)$	···	$^2A', {}^2A''$	$^2A_1, {}^2A_2$
$H(^2S_g)+OH^{-*}(^3\Delta)$	···	$^2A', {}^4A', {}^2A'', {}^4A''$	$^2A_1, {}^4A_1, {}^2A_2, {}^4A_2$
$H(^2S_g)+OH^{-*}(^1\Sigma^-)$	···	$^2A''(2)$	$^2A_2(2)$
$H(^2S_g)+OH^{-*}(^3\Sigma^-)$	···	$^2A''(2), {}^4A''(2)$	$^2A_2(2), {}^4A_2(2)$
$H^-(^1S_g)+OH^*(^3\Sigma^+)$	···	$^2A'(2)$	$^2A_1(2)$

[a] These values are consistent with a value of 48 kcal for the electron affinity of $OH(^2\Pi)$.

OH^+ (431 kcal)

The appearance of this ion must be due to the initial formation of an H_2O^+ state which is unstable with respect to $H+OH^+$; this means that the level of $H+OH^+$ with respect to H_2O must be not greater than 431 kcal, a conclusion that leads to a lower limit of 321 kcal for the standard ΔH of formation of the OH^+ ion (see Table I).

The species produced at 431 kcal could be a $^2A_2$ which correlates with $H(^2S)+OH^+(^3\Sigma^-)$, or it could be any other state of the same multiplicity which "crosses" this $^2A_2$ state. In Fig. 2 it is shown as a $^2B_1$ or $^2B_2$, and reaction will involve a transition (at point *a*) from this state to the $^2A_2$ state followed by dissociation into $H(^2S)+OH^+(^3\Sigma^-)$. The over-all process may therefore

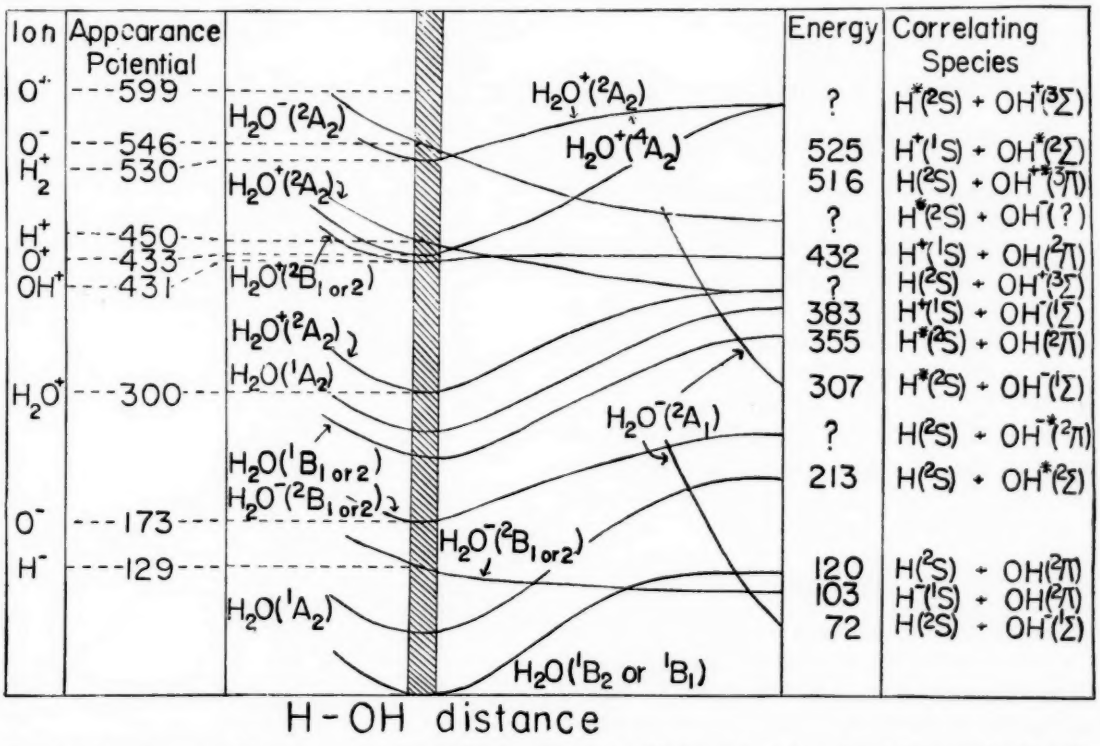

FIG. 2. Schematic potential-energy curves for the H−OH system; in this figure the letters *A* and *B* are used arbitrarily and may be interchanged.

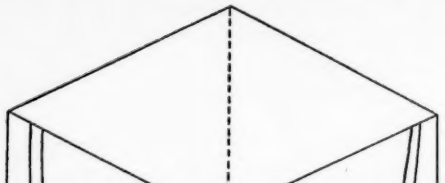

FIG. 3. Potential-energy surfaces relevant to the formation of O^- at 173 kcal.

be represented as

$$e(431\text{ kcal})+H_2O\rightarrow H_2O^+(^2B_1 \text{ or } ^2B_2)\rightarrow H_2O^+(^2A_2)\rightarrow H(^2S_g)+OH^+(^3\Sigma^-). \quad (4)$$

The path of the reaction is shown in Fig. 4 which shows the relevant part of Fig. 2 on a larger scale and shows the resonance splitting.

O^+ (437 kcal)

The formation of O^+ at 437 must be due to the process

$$e+H_2O\rightarrow H_2O^+\rightarrow H_2+O^+, \quad (5)$$

since there is insufficient energy for the production of $2H+O^+$. Since H_2 is $^1\Sigma_g^+$ and the lowest state of O^+ is ^4S_u, it follows from Tables III and IV that the H_2O^+ state must be a $^4A_2$ (or $^4B_2$) state. Since this species dissociates into H_2+O^+ rather than to H^++OH or $H+OH^+$ it is necessary that it correlate with H^++OH or $H+OH^+$ at a higher level than 437 kcal; a correlation with $H^*(^2S_g)+OH^+(^3\Sigma^-)$ is shown in Fig. 2. The nonappearance of H_2O^+ at this level implies that decomposition of the molecule to H_2+O^+ is a rapid one. Transitions to repulsive state such as $^2A_2$ are of course forbidden by the spin conservation rule.

H^+ (450 kcal)

The production of this ion must be due to the formation of a state of H_2O^+ which either correlates with H^++OH or "crosses" a state that does so. In Figs. 2 and 4 excitation is shown as giving rise to initially a $^2A_2$ state; the system then undergoes a radiationless transition to the $^2B_1$ or $^2B_2$ state which is unstable with respect to H^++OH; the over-all reaction is therefore

$$e(450\text{ kcal})+H_2O\rightarrow H_2O^+(^2A_2)\rightarrow H_2O^+(^2B_1 \text{ or } ^2B_2)\rightarrow H^+(^1S_g)+OH(^2\Pi). \quad (6)$$

The course of the reaction is represented by the dotted line in Fig. 4.

H_2^+ (530 kcal)

The production of H_2^+ must be due to a process of the type $H_2O^+\rightarrow H_2^++O$, and since H_2^+ is $^2\Sigma_g^+$ and O is ^3P_g, the possible states for the H_2O^+ are $^2A_1$, $^2A_2$, $^2B_1$, $^2B_2$, $^4A_1$, $^4A_2$, $^4B_1$, and $^4B_2$. The lowest species above 530 kcal that will give any of these states is $H^*(^2S)+OH(^3\Sigma^-)$, which will give rise to $^2A_2$ and $^4A_2$, the latter being concerned in the production of O^+ at 433 kcal. We therefore conclude tentatively that the process is

$$e+H_2O\rightarrow H_2O^+(^2A_2)\rightarrow H_2^+(^2\Sigma_g^+)+O(^3P_g). \quad (7)$$

O^- (546 kcal)

Various possibilities exist for the formation of O^- at 546 kcal. There is ample energy for the products to be $2H+O^-$, so that a state of H_2O^- may be produced which is unstable with respect to $2H+O^-$. One possibility for this is shown in Fig. 2; electron capture produces H_2O^- in a $^2A_2$ state which correlates with $H^*(^2S_g)+OH^{-*}$, the latter being some repulsive state of OH^-. The process need not, however, involve the intermediate formation of OH^{-*}; the system may pass directly from H_2O^- to $2H+O^-$, as was the case in the production of O^- at 173 kcal.

Alternatively the H_2O^- ion produced may be stable with respect to the simple rupture of an O—H bond, but may undergo an intramolecular rearrangement to H_2+O^-; in this case the H_2O^- would have to be in a $^2A_1$, $^2B_1$, $^2A_2$, or $^2B_2$ state.

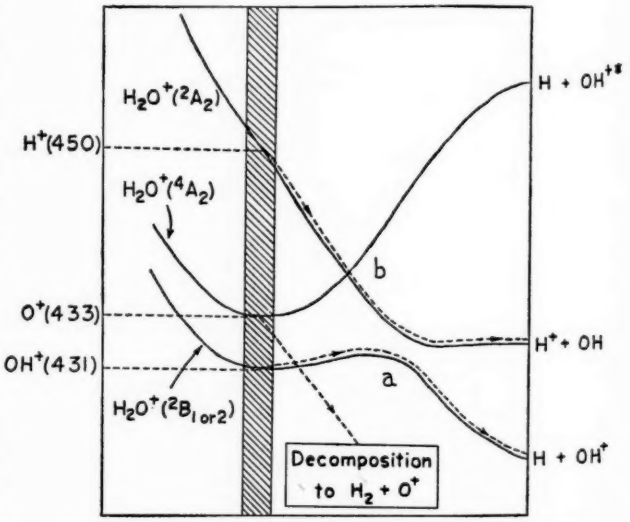

FIG. 4. Enlarged (and distorted) version of part of Fig. 2.

DISCUSSION

One point of special interest that arises relates to the nonappearance of the stable ion OH^-; this ion is conspicuous by its absence in radiation experiments with water, and also with other substances such as methyl alcohol. At first sight OH^- might be expected to arise from the dissociation of H_2O^- (either in its ground or an excited state), but more detailed consideration reveals why this does not take place. The stable states of OH^- (e.g., the $^1\Sigma^+$ ground state) have such stable electronic configurations that the approach to them of a hydrogen atom (or some radical such as CH_3) gives rise to very strong repulsion; the resulting negative ion therefore plays no role in connection with electronic excitation. The states of H_2O^- (or CH_3OH^-, etc.) which are produced by electron attachment must therefore correlate with less stable and probably repulsive states of the OH^- ion. They therefore decompose into O^- rather than into OH^-.

This conclusion as to the nonappearance of OH^- is of interest in view of the fact that primary reactions involving the formation of this ion are generally postulated in discussions of the radiation chemistry of liquid water and of aqueous solutions. In view of the above considerations we prefer to regard OH^- as produced in liquid water by secondary reactions as

$$H^-+H_2O\rightarrow H_2+OH^- \tag{8}$$

and

$$O^-+H_2O\rightarrow OH+OH^- \tag{9}$$

which can probably occur very readily. Other secondary processes which may take place in the liquid state are

$$H^++H_2O\rightarrow H_3O^+ \tag{10}$$

$$OH^++H_2O\rightarrow H^++H_2O_2 \quad \text{or} \quad 2OH \tag{11}$$

$$O^++H_2O\rightarrow H^++HO_2. \tag{12}$$

Haissinsky and Magat[15,16] have pointed out that when aqueous solutions are irradiated OH radicals play a much more important role than H atoms. The scheme formulated in the present paper is consistent with this. Hydroxyl radicals are produced in the primary processes

$$H_2O+e\rightarrow OH+H^- \text{ (at 129 kcal)}, \tag{13}$$

$$H_2O+e\rightarrow OH+H^++2e \text{ (at 450 kcal)}, \tag{14}$$

and in the secondary processes

$$H_2O^++H_2O\rightarrow H_3O^++OH, \tag{15}$$

$$O^-+H_2O\rightarrow OH+OH^-, \tag{16}$$

$$OH^++H_2O\rightarrow H^++2OH. \tag{17}$$

Hydrogen atoms are only produced in the primary processes

$$H_2O+e\rightarrow 2H+O^- \text{ (at 173 kcal)}, \tag{18}$$

$$H_2O+e\rightarrow H+OH^++2e \text{ (at 431 kcal)}, \tag{19}$$

in the first of which there will be considerable primary recombination.

This explanation differs slightly from that of Haissinsky and Magat who postulate the reaction

$$H_2O+e\rightarrow H_2+O^-. \tag{20}$$

However, we consider this to be unlikely in view of the very short life of $H_2O^-(^2A_2)$; we prefer reaction (18) followed by primary recombination.

In conclusion it must be emphasized that it is not valid to make predictions as to the relative probabilities of reactions on the basis of purely energetic considerations; owing to the crossing of potential-energy surfaces (Fig. 2) the products obtained are frequently not the ones of lowest energy.

The author is grateful to Dr. K. E. Shuler and Dr. G. Herzberg for valuable suggestions. He has also derived much help from detailed comments made by Dr. C. A. McDowell on the basis of a preliminary draft of the paper.

[15] M. Haissinsky and M. Magat, Compt. rend. **233**, 954 (1951).
[16] M. Haissinsky, Discussions Faraday Soc. **12**, 133 (1952).

The Relative Abundance of HT and HTO in the Atmosphere

P. HARTECK
Contribution from the Walker Chemical Laboratory of Rensselaer Polytechnic Institute, Troy, New York
(Received March 2, 1954)

A kinetic discussion of the HT and HTO formation in the atmosphere indicates that the ratio of about 1 HT to 1000 HTO in nature and the very high T concentration of 4.10^{-15} in atmospheric hydrogen compared with about 3.10^{-18} in normal rain water can only be understood by means of a photochemical reaction. Since the tritium atoms are quickly removed by oxygen molecules in three-body collisions and form the TO_2 radical which in turn forms HTO, the TO_2 must be photochemically dissociated. The T atoms thus set free collide repeatedly with hydrogen atoms and undergo to a certain extent the exchange reaction $H_2+T=HT+H$. On the other hand, the T atoms or TO_2 radicals may react with ozone to form a OT radical which combines with the hydrogen of the atmosphere into HTO. In low altitudes the reaction of TO_2 with air polluting bodies form HTO predominately. The ratio of these reactions is responsible for the ratio of HT and HTO in nature with the HTO brought down into the surface waters by rainfall.

INTRODUCTION

TRITIUM is observed in the hydrogen[1] of the atmosphere as well as in all bodies of water covering the earth.[2] A number of tritium concentrations calculated and observed, are tabulated in the appendix. Note that the largest concentration of tritium observed in the atmosphere is in atmospheric hydrogen. With the relative concentration of hydrogen in the atmosphere as 5×10^{-7}, and the relative concentration of HT in hydrogen as $7.6\pm1.1\times10^{-15}$, the relative concentration of HT in the atmosphere is therefore 3.8×10^{-21}. Thus, the total amount of T on the earth is 0.7 mole as HT and about one thousand moles as HTO.

Under certain conditions, tritium concentrations are found to be relatively high in rain water and much higher than in sea water or in water which has had no contact with rain water in tens of years.[3] This difference may be readily understood if we consider the exchange rate of "old" water with fresh rain water, the formation of HTO in the atmosphere, and the radioactive decay rate (half-life) of tritium ($12\frac{1}{2}$ years).

Faltings and Harteck[1] assumed the concentration of tritium to be greater in atmospheric hydrogen than in rainwater. Their first attempt at the detection of tritium was therefore made with atmospheric hydrogen. It should be noted that initially no investigation of tritium in heavy water was made since nuclear physicists did not report the presence of radioactivity even after handling tons of heavy water. The assumption of a greater concentration of tritium in atmospheric hydrogen than in rain water has now been verified, being larger by several orders of magnitude. However, the total amount of tritium present in the bodies of water on the surface of the earth is about 1000 times that in the hydrogen of the atmosphere. An explanation of this phenomenon is the principal purpose of this paper. The problems connected with the formation and the escape of He_3 from the earth's atmosphere are not discussed in this paper (see reference 1a).

DISCUSSION

The tritium found in nature is formed by cosmic radiation, partly by direct disintegration of the atoms of air and partly by the reaction of fast neutrons with nitrogen as indicated by Fireman.[4] The tritium atoms or tritium ions, initially formed, have a high kinetic energy, and by collision with air molecules become thermal tritium atoms. These tritium atoms will undergo a chemical reaction and form HT and HTO.

The two reactions of primary importance to be considered initially are: First, the most probable reaction for a H or T atom in air at pressures ranging from atmospheric to very low pressures is the formation of HO_2 or TO_2 in a three-body collision with oxygen.

$$T+O_2+M=TO_2+M. \qquad (1)$$

Thus HO_2 and therefore TO_2 are rather stable radicals which would, normally, undergo other reactions and finally form H_2O and HTO but not H_2 or HT (in the atmosphere).

The second possibility is an exchange reaction which occurs when a T atom collides with a H_2 molecule. In the atmosphere, the relative H_2 concentration is 5×10^{-7}. This reaction was carefully studied with parahydrogen.[5]

$$H_{2(para)}+H=H+H_{2(normal)}$$

and correspondingly,

$$T+H_2=HT=H. \qquad (II)$$

Next consider a hypothetical case of the absence of a photochemical reaction in the atmosphere, with no

[1] V. Faltings and P. Harteck, Z. Naturforsch. **5a**, 439 (1950); (a) Nature **166**, 1109 (1950).
[2] Grosse, Johnston, Wolfgang, and Libby, Science **113**, 1 (1951); H. Suess, Trans. Geophysical Union **34**, 343 (1953); and latest measurements by Grosse, Kirschenbaum, Kulp, and Broecker, Phys. Rev. **93**, 250 (1954).
[3] W. F. Libby, Phys. Rev. **91**, 442 (1953).
[4] E. L. Fireman, Phys. Rev. **91**, 922 (1953).
[5] K. H. Geib and P. Harteck, Z. physik. Chem., Bodenstein-Festband 849 (1931); A. Farkas, Z. physik Chem. **B**, **1a**, 419 (1930); A. Farkas, *Orthohydrogen, Parahydrogen and Heavy Hydrogen* (Cambridge University Press, Cambridge, 1935).

ozone, radicals or atoms, present. Therefore the tritium atoms formed by cosmic radiation have only two possibilities to react, (a) to form the radical TO_2 in a 3-body collision with oxygen according to reaction (I) or (b), to form an exchange reaction with H_2 according to reaction (II).

Since the TO_2 radical is not dissociated thermally, it finally forms HTO. Reaction (1) and (2) results in the equation for the ratio of HT to HTO as

$$\frac{d[\mathrm{HT}]}{d[\mathrm{HTO}]}=\frac{k_{\mathrm{II}}[\mathrm{H_2}]}{k_{\mathrm{I}}[\mathrm{O_2}][\mathrm{M}]}. \qquad \text{(III)}$$

If we introduce particle concentrations per cubic centimeter and the values of the reaction coefficients:[6]

$$k_{\mathrm{I}}=3.0\times10^{-33}\left(\frac{T}{273}\right)^{\frac{1}{2}} \quad \text{and} \quad 3.0\times10^{-35}\left(\frac{T}{273}\right)^{\frac{1}{2}}$$

$$k_{\mathrm{II}}=5\times10^{-11}\times e^{-7000/1.98T}.$$

We obtain the relationship

$$\frac{d[\mathrm{HT}]}{d[\mathrm{HTO}]}=\frac{5\times10^{-11}\times e^{-7000/1.98\times T}\times[\mathrm{H_2}]}{3.0\times10^{-33}\left(\frac{T}{273}\right)^{\frac{1}{2}}[\mathrm{O_2}][\mathrm{M}]}$$

and

$$\frac{5\times10^{-11}\times e^{-7000/1.98T}[\mathrm{H_2}]}{3.0\times10^{-35}\left(\frac{T}{273}\right)^{\frac{1}{2}}\times[\mathrm{O_2}][\mathrm{M}]}. \qquad \text{(IV)}$$

In Table I the data for calculating the ratio of HT to HTO are presented. T_1 is the temperature obtained from NACA data, and T_2 the temperature measured directly by rocket ascension. Columns 4 through 7 list the particle concentration (i.e., number of particles in one cubic centimeter); n_{M} (for all particles); $n_{\mathrm{H_2}}$ (for the H_2 molecules); n_{O} (for the O atoms); and $n_{\mathrm{O_3}}$ (for the ozone molecule), each varying with altitude.

To calculate k_2 (column 15), NACA temperatures were adopted. Rocket temperatures would give much smaller values for k_2 in regions above 40 kilometers. In column 9 and 13 the life times (duration of existence) of T atoms are listed corresponding to reaction (I). According to the results of F. Paneth[7] the gases of the atmosphere mix rather quickly up to altitudes of 60 km. Thus it is possible to calculate from column 10 an average ratio from HT to HTO which has a value of about 10^{-7} for $k_1=3.0\times10^{-33}$ and 10^{-5} for $k_1=3.0\times10^{-35}$. Therefore the former value is about 4 decades and the

TABLE I.

1	2	3	4	5	6	7	8	9	10	11	12	13	14	15	16	17	18	19
Altitude km	T_1 NACA	T_2 Rocket	n_{M}	$n_{\mathrm{H_2}}$	n_{O}	$n_{\mathrm{O_3}}$	$\frac{C}{C_0}$	L_T in sec $k_1=3.10^{-33}$	$\frac{\mathrm{HT}}{\mathrm{HTO}}$ $k_1=3.10^{-33}$	$\frac{L_T}{k_1}+\frac{L_{TO_2}}{k_1=3.10^{-33}}$	Time till T had reacted in sec $k_1=3.10^{-33}$	L_T in sec $k_1=3.10^{-35}$	Time till T had reacted in sec $k_1=3.10^{-35}$	k_{II} for NACAT	$\frac{k_{\mathrm{II}}}{k_{\mathrm{III}}}$ Temp $=T_1$	$\frac{k_{\mathrm{II}}}{k_{\mathrm{III}}}$ Temp $=T_2$	$\frac{\mathrm{H_2}}{\mathrm{O_3}}$	$\frac{\mathrm{HT}}{\mathrm{HTO}}$ Temp $=T_1$
0	280		$2.6\cdot10^{19}$	$1.3\cdot10^{23}$	$\sim10^{4}$	$\sim4\cdot10^{11}$	1	$2.5\cdot10^{-6}$	$7.5\cdot10^{-9}$	$2.5\cdot10^{-7}$	10^{0}	$2.5\cdot10^{-4}$	10^{4}	$2.3\cdot10^{-16}$	0.027		32	(0.86)
10	230		$8\cdot10^{18}$	$4\cdot10^{22}$	$\sim10^{5}$	$1.5\cdot10^{12}$	$3.1\cdot10^{-1}$	$2.5\cdot10^{-5}$	$1.6\cdot10^{-9}$	$2.5\cdot10^{-6}$	$2\cdot10^{0}$	$2.5\cdot10^{-3}$	$2\cdot10^{2}$	$1.6\cdot10^{-17}$	0.012		2.7	$3.2\cdot10^{-2}$
20	220		$1.7\cdot10^{18}$	$8.5\cdot10^{21}$	$\sim10^{8}$	$2\cdot10^{12}$	$6.5\cdot10^{-2}$	$6\cdot10^{-4}$	$4.3\cdot10^{-9}$	$6\cdot10^{-5}$	10^{7}	$6\cdot10^{-2}$	10^{5}	$8.5\cdot10^{-18}$	0.010		$4.2\cdot10^{-1}$	$4.2\cdot10^{-3}$
30	220	225	$4.2\cdot10^{17}$	$2.1\cdot10^{21}$	$1.7\cdot10^{9}$	$2.5\cdot10^{13}$	$1.6\cdot10^{-2}$	$9.5\cdot10^{-3}$	$1.7\cdot10^{-8}$	$9.5\cdot10^{-4}$	$6.5\cdot10^{5}$	$9.5\cdot10^{-1}$	$6.5\cdot10^{3}$	$8.5\cdot10^{-18}$	0.010	0.011	$8\cdot10^{-2}$	$8\cdot10^{-4}$
40	270	265	$8.5\cdot10^{16}$	$4.3\cdot10^{20}$	$2\cdot10^{10}$	$4.6\cdot10^{11}$	$3.3\cdot10^{-3}$	$2.3\cdot10^{-1}$	$1.5\cdot10^{-6}$	$2.3\cdot10^{-2}$	$1.2\cdot10^{4}$	23	$1.2\cdot10^{2}$	$1.5\cdot10^{-16}$	0.024	0.022	$9\cdot10^{-2}$	$2.0\cdot10^{-3}$
50	350	280	$2.3\cdot10^{16}$	$1.2\cdot10^{19}$	$4.4\cdot10^{10}$	$5.5\cdot10^{10}$	$8.9\cdot10^{-4}$	3.1	$1.1\cdot10^{-4}$	$2,4\cdot10^{-1}$	$7\cdot10^{2}$	$3.1\cdot10^{2}$	7	$2.8\cdot10^{-15}$	0.056	0.027	$2\cdot10^{-1}$	$5.4\cdot10^{-3}$
60	350	260	$7.5\cdot10^{15}$	$3.7\cdot10^{18}$	$1.0\cdot10^{11}$	$7.3\cdot10^{9}$	$2.9\cdot10^{-4}$	$3\cdot10^{+1}$	$7.3\cdot10^{-4}$	0.88	10^{3}	$7\cdot10^{3}$	10	$2.8\cdot10^{-15}$	0.056	0.021	$5\cdot10^{-1}$	$1\cdot10^{-2}$
70	290	215	$2.0\cdot10^{15}$	$1\cdot10^{18}$	$1.9\cdot10^{11}$	$6\cdot10^{8}$	$7.7\cdot10^{-5}$	$4.3\cdot10^{+2}$	$1.5\cdot10^{-4}$	0.98	$2\cdot10^{4}$	$4\cdot10^{4}$	$2\cdot10^{2}$	$3.6\cdot10^{-16}$	0.031	0.009	1.7	$1.5\cdot10^{-2}$

[6] The values for $k_1=3.0\times10^{-33}$ and 3.0×10^{-35} are the most probable value and lower limit which is feasible according to similar reactions indicated in the literature of M. Bodenstein and Schenk, Z. physik Chem. **B, 20**, 420 (1933); L. Farkas and H. Sachsse, Z. physik Chem. **B, 27**, 111 (1934); Bates and Cook, J. Am. Chem. Soc. **57**, 1775 (1935).

[7] F. Paneth, Phys. Rev. **84**, 846 (1951).

latter about 2 decades, less than had been found in nature experimentally.

Had rocket temperatures been utilized, the results corresponding to reaction (IV) would indicate less HT in the altitudes concerned, and the difference, with the amount of HT actually found in nature, would increase. The result shows that the kinetics of the HT formation cannot be determined by the reaction mechanism indicated in the foregoing. Thus photochemical reactions may be responsible for the behavior of the tritium in the atmosphere.

The following facts indicate that only *one* photochemical reaction, namely, the photochemical decomposition of TO_2, is possible which could produce a measurable amount of HT (0.1 percent).

(A) The atmosphere contains 5×10^{-7} elementary hydrogen and detectable amounts of methane. Hydrogen is formed at altitudes above 60 kilometers by means of the photochemical decomposition of water vapor, which arrives at these altitudes by its transport velocity, owing to diffusion and convection in the upper layers of the atmosphere.[8] Since this process produces only relatively small amounts of hydrogen, the average life time of the hydrogen molecules (and therefore also of the methane) in the atmosphere must cover a period of years. Therefore all photochemical reactions and mechanism which indicate a rapid attack on molecular hydrogen for example by O atoms to form H_2O cannot be considered.

(B) The thermal equilibria

$$H_2+HDO\rightleftarrows HD+H_2O \qquad (V)$$

$$H_2+HTO\rightleftarrows HT+H_2O \qquad (VI)$$

indicate that the concentration of D in HDO should be 3.5 to 6 times larger than in HD, and by analogy the *T* concentration should be 4.5 to 8 times larger in the HTO than in HT.[8a] Experimentally it has been shown that in the atmosphere the D concentration in HD is slightly larger than in HDO[8b] and the T concentration about 10^3 times larger in HT than in HTO.[1] In higher altitudes where the HTO formed is not readily diluted by the normal H_2O, the difference in the tritium concentration may not be as large. But all this indicates that the thermal equilibrium according to Eqs. (V) and (VI) is not at all established in the atmosphere. These two facts show that all mechanisms which involve reasonable atom or radical concentrations cannot be considered, since H atoms or OH radicals would catalyze reactions (V) and (VI), and therefore the only feasible explanation for the HT formation is as will be shown the photodecomposition of TO_2.

Since the HO_2 and TO_2 radicals have not been spectroscopically identified, the absorption spectrum is not known. However, from reaction kinetics the binding energy of the T atom in the TO_2 is not more than 40 kilocalories (most probable value may lie between 30 and 40 kilocalories); thus light of wavelengths shorter than 6500A has sufficient energy to dissociate TO_2 photochemically. With the absorption spectrum of TO_2 not known, there is a high probability that in the region between 3000A and 6500A (the sun emits radiation with high intensity in this region), there is at least one wavelength interval in which TO_2 radicals may absorb sunlight very strongly.

Since an absorption coefficient α of 1 means that a single molecule will absorb a light quanta passing through 1 square centimeter with a probability of 0.85×10^{-19}, and since the number of light quanta which are emitted by the sun and pass through 1 square centimeter at wavelengths between 3000 and 6000A is about 2.4×10^{17}, an estimated average absorption coefficient of 5 means that TO_2 may have a lifetime of about 10 seconds in the incident sun light. It should be emphasized that this is only an estimate with a probable error of a factor of 3. In comparison, the lifetime of ozone in altitudes above 50 km, where the strong photodissociation occurs, is about two minutes. But ozone has only a small absorption coefficient in the visible spectrum ($\alpha=0.06$ at 6000A) and has a high absorption coefficient at wavelengths shorter than 2800A, ($\alpha=140$ at 2600A), where the number of light quanta emitted by the sun decrease rapidly. Thus ozone has a longer lifetime in the sunlight than should be expected for TO_2. Fortunately, the lifetime of TO_2 in sunlight is not too important, since it does not enter directly in the equation for the formation of HT. Column (11) lists the ratio of the lifetimes of T atoms to the sum of the lifetimes T and TO_2, provided that one TO_2 is dissociated every 10 seconds by sunlight.

At this point, a discussion of the effect of ozone, and the oxygen-atoms formed photochemically from ozone, on the HT formation is necessary. Fortunately, ozone concentration has recently been measured at altitudes up to 70 kilometers and the oxygen-atom concentration calculated for this range of altitudes.[9] A discussion of this problem is possible since the kinetic analysis of the reaction between hydrogen and oxygen[10,11] is well known, and the limits of error for the reaction coefficients involved in this problem are reasonable.

A discussion of the kinetics of ozone formation in the upper atmosphere is included in the fine work of Johnson, Purcell, Tousey, and Watanabe,[9] and will be omitted here. This paper also lists the O atom concentrations. The reaction coefficient used for

[8] P. Harteck and J. H. D. Jensen, Z. Naturforsch. **3a**, 591 (1948).

[8a] H. Urey, J. Chem. Soc. **1947**, 562.

[8b] P. Harteck and H. Suess, Naturwiss. **36**, 218 (1949).

[9] Johnson, Purcell, Tousey, and Watanabe, J. Geophys. Research **57**, 157 (1952).

[10] B. Lewis and G. Von Elbe, *Combustion, Flames and Explosions of Gases* (Academic Press, Inc., New York, 1951), and the literature from this book.

[11] D. A. Bates M. C. Nicolet, J. Geophys. Research **55**, 1950.

reaction

$$O_2+O+M=O_3+M \qquad \text{(VII)}$$

is given as 7×10^{-35}.[12]

To explain the ratio of the HT−HTO formation, the TO_2 must be repeatedly dissociated photochemically into T and O_2. If the atmosphere is free from dust and gaseous pollutions, the T atoms, formed photochemically have a probability to react according to reaction (II) or with ozone which is in fact the largest "impurity" or chemical reactive substance in the atmosphere in the altitudes concerned. The reactions to be considered are:

$$T+O_3=TO+O_2+77 \text{ kcal};\quad 5 \text{ kcal heat of act.} \qquad \text{(VIII)}$$

$$TO_2+O_3=TO+2O_2+37 \text{ kcal};\quad 10 \text{ kcal heat of act.} \qquad \text{(IX)}$$

$$TO_2+O=TO+O_2+61 \text{ kcal};\quad 2 \text{ kcal heat of act.} \qquad \text{(X)}$$

$$TO+H_2=HTO+H\ 17 \text{ kcal};\quad 6 \text{ kcal heat of act.} \qquad \text{(XI)}$$

$$TO+H_2=H_2O+T+16 \text{ kcal};\quad 6 \text{ kcal heat of act.} \qquad \text{(XII)}$$

All these reaction are exothermic and have a relatively small heat of activation. The values of this heat of activation have either been taken from the compilation of K. H. Geib[13] or estimated by the author.

In reactions (VIII), (IX), and (X), tritium is undergoing an irreversible reaction if followed by reaction (XI).[14] Which of the reactions becomes predominant depends upon the heat of activation and the relative concentration of ozone and oxygen atoms. In the vicinity of the earth's surface where the lifetime of T atoms is only 2.5×10^{-6} second, reaction (IX) may be larger than reaction (VIII). But in the vicinity of the earth's surface where the air is polluted, the TO_2 radical will react faster with these pollutions than the ozone. Thus, in layers of the air in which the amount of ozone is markedly reduced by air pollution, the TO_2 will be consumed and form HTO or it will be dissolved in the clouds, and with rain, will wash out of the atmosphere. But where the altitude is more than 20 kilometers above the earth's surface, the air may be reasonably pure. Since the H_2 concentrations in these altitudes are still of the same order of magnitude or larger than the O_3 concentrations, the largest amount of HT may be formed there. Above 20-kilometers altitudes, the ozone, and above 40 kilometers the O atom concentration, becomes larger than the amount of H_2. Therefore OT will be formed by reaction (VIII) to (X) and less HT according to reaction (II)[14,14a] will be formed. However, since the total amount of the atmosphere above 40 kilometers is only a fraction of a percent, the reactions which occur above this altitude are only of minor importance. In addition to the above examples, there is another way in which HT may be formed. It is known that the hydrogen of the atmosphere has a photochemical origin by photodecomposition of water vapor. At very high altitudes (80 km) where the atmosphere has a pressure of less than 10^{-5} atmos and where the radical concentrations become high, HT and HTO will indeed be formed by the reactions:

$$T+H+M=HT+M \qquad \text{(XIII)}$$

$$OH+T+M=HTO+M \qquad \text{(XIV)}$$

where M is a third particle in the three-body collision. However, the amount which forms in this altitude is very small compared with the amount of HT and HTO formed in the lower levels of the atmosphere. For completeness, the exchange reactions of H and T atom with H_2O by K. H. Geib and E. W. R. Steacie[16] should be included. These are

$$H_2O+D=HDO+H \qquad \text{(XV)}$$

$$D_2O+H=HDO+D. \qquad \text{(XVI)}$$

The heats of activation are 12 ± 1 and 11 ± 1 kcal, respectively. Thus, the exchange reaction with T atoms has about the same heat of activation, i.e.,

$$H_2O+T=HTO+H \qquad \text{(XVII)}$$

$$HTO+H=H_2O+T. \qquad \text{(XVIII)}$$

Equation (XVII) may have a reaction coefficient $k_{XVII}=5\times10^{-11}\times e^{-12\,000/RT}$.

Since the H_2 concentration in the atmosphere is 5×10^{-7}, and the humidity on the surface of the earth seldom reaches a value of 4×10^{-2}, and above the cold trap at 10-km altitude, it is only about 5×10^{-5}, the HTO formation by Eq. (XVII) in altitudes above 10 km can be neglected in comparison with the other reactions. In the area surrounding the surface of the earth, especially in a tropical climate, a T atom would react faster by reaction (XVII) than by reaction (II). However, under these conditions the T atom and TO_2 radical would normally form HTO by reacting with air polluting bodies, and condensed water vapor.[17]

[12] It seems to this author that the reaction coefficient of 7×10^{-35} lies on the lower limit of feasibility.

[13] K. H. Geib, *Ergebnisse der exacten Naturwissenschaften* (Verlag Julius Springer, Berlin, 1938, 1936), p. 44 to 105.

[14] In Table I column (19) the effect of the O atoms is not considered because we do not know enough of this reaction and it never becomes dominant for our problem.

[14a] A reaction corresponding to (XII) has the effect of favoring the formation of HT since a T atom is set free once again.

[16] K. H. Geib and E. W. R. Steacie, Z. physik. Chem. **B, 29**, 215 (1935).

[17] For completeness, a discussion of two possible reactions of the TO_2 radicals with atmospheric hydrogen is required. These reactions are:

(1) $TO_2+H_2=HTO_2+H+$about 0 to 10 kcal
(2) $TO_2+H_2=HO_2+HT+1$ kcal.

In possibility (1), B. Lewis and G. von Elbe (see reference 10) indicate a reaction coefficient, K_1 of $10^{-11.7}\times e^{-24\,000/RT}$. Because of

To obtain a simple formula for the ratio of HT to HTO formation in the atmosphere we consider reactions (I), (II), and (VIII) only, and the sun's irradiation which dissociates the TO_2. Thus we obtain the simple relation:

$$\frac{k_{II}}{k_{VIII}}=\frac{5\times10^{-11}\times e^{-7000/RT}}{5\times10^{-11}\times e^{-5000/RT}}=e^{-2000/RT}$$

and

$$\frac{d[HT]}{d[HTO]}=\frac{k_{II}[H_2]}{k_{VIII}[O_3]}=\frac{[H_2]\times e^{-2000/RT}}{[O_3]} \quad \text{(XIX)}$$

where R is the gas constant equivalent to 1.985 cal. From column 19, Table I, it can be seen that in the vicinity of the earth's surface, a large amount of the T should become HT. However, since the time in which reaction (XIX) could occur is long (see columns 12 and 14), before reaction II can occur, almost all the TO_2 radicals will be consumed by air impurities and condensed water. In an altitude of about 10 kilometers, 3.2 percent of the T atoms should enter HT. However, in this region, a reasonable amount of TO_2 may still be consumed by air impurities and by water condensate since the lifetime of TO_2 is still relatively high so that it may reach, by convection, the lower levels of the atmosphere where water condenses out. In altitudes above 20 kilometers, the HT formation may reach the values, according to the formula (XIX), listed in column 19, Table I. A summation of the HT formation over all levels give an amount of about 0.1 percent of HT.

A better knowledge of all kinetic parameters involved would make it necessary to take into consideration also effects, as the dependence of the cosmic radiation with altitude, and the fact that overnight the photochemical reactions are stopped.

It should be emphasized that photochemical reactions occurring in the atmosphere often need very large time intervals. For example, it takes a few weeks for the photochemical ozone cycle to be completed; i.e., it takes some weeks for the O atoms which are formed at 30-kilometers altitude by photochemical dissociation of oxygen to reform oxygen molecules, during which time the immediately formed ozone has been dissociated photochemically thousands of times, with the reformation of ozone, until finally one oxygen atom with ozone forms two oxygen molecules ($O_3+O=2O_2$).

And it takes about a week for a tritium atom formed at 30-kilometers altitude to end its reaction by undergoing an exchange reaction with H_2 according to reaction (II) or with ozone according to reaction (VIII), during which time the rapidly formed TO_2 has been repeatedly photochemically dissociated.

It has been shown from previous data that about 1 per mil of tritium should go into atmospheric hydrogen and 99.9 percent into rain water. The following is a method to determine the absolute amounts of tritium in atmospheric hydrogen and rain water. Assuming that the average rain fall is about 5 moles per square centimeter, which is equivalent to 36 inches per year measured with a rain gauge, and the tritium content is 3×10^{-15}, then the total rain fall on the earth per year will contain $5.1\times10^{+18}\times3\times10^{-18}\times5\times2=153$ moles of T. With an average lifetime of 18 years for tritium, this results in a stationary tritium balance of 2750 g atoms. In the atmosphere there is an equivalent of a 0.4 cm^3 or 1.8×10^{-5} moles of hydrogen per square centimeter over the total altitude. This evaluates for the total atmosphere, with a ratio of T to H of 3.8×10^{-15} in the atmosphere, to

$$1.8\times10^{-5}\times7.6\times10^{-15}\times5.1\times10^{18}=0.70$$

g atoms tritium.

This means that in the stationary state 0.025 percent tritium is in atmospheric hydrogen. This number can be better evaluated in the future when the total balance of tritium in the world has been more accurately measured.[3] But if the HT in the atmosphere becomes oxidized with a reasonable velocity by oxygen atoms and excited ozone molecules as compared with the decay constant of tritium, the mean lifetime of the tritium in atmospheric hydrogen may be reduced by a few years. Therefore, primarily about 1 per mil of the tritium must go into atmospheric hydrogen. The measurement of the exact balance of tritium in atmosphere is an extremely difficult undertaking. Knowledge of the amount of rain fall per year, the tritium content and additional meteriological data (i.e., the re-evaporation of the rain fall on the earth's surface and the exchange of the moisture content of the atmosphere with this large body of water covering the earth's surface) is necessary. Since the tritium concentration in atmosperic hydrogen is 3.8×10^{-15} and that of tritium in rain water is 3×10^{-18}, a ratio of 1 to 1000 results (see appendix). With much less HTO in the water of the seas, the ratio of the T concentration in atmospheric hydrogen and sea water may be of the order of 10^{+5}. The tritium concentration in atmospheric hydrogen should remain fairly stable, whereas tritium concentration in rain water may vary with locality as shown by Libby.[3]

CONCLUSION

An explanation has been given to show why there is about 1000 times more T present in the bodies of water on the surface of the earth than in the hydrogen of the atmosphere and why the T concentration in HT is about 1000 times larger than in the rain water.

(A) Tritium is formed through cosmic radiation and is proportional to the concentration of the air and the intensity of the radiation.

its high heat of activation (24 kcal), this reaction can be neglected. In case (2), a large impairment of the chemical bonding of the H_2 molecule is involved (during the formation of HT), which should be associated with a high heat of activation. Thus, reaction (2) may also be disregarded.

TABLE II.

Samples[a]	HT conc.	Ratio T/H	Remarks
1. Atmospheric hydrogen	$7.6\times10^{-15}\pm2.5\times10^{-15}$	$3.8\times10^{-15}\pm1.25\times10^{-15}$	Total amount of HT in the earth atmosphere 0.7 ± 0.2 gram atoms
2. Atmospheric hydrogen[b] enriched by electrolysis by 26 ± 2 times	$1.9\times10^{-13}\pm0.2\times10^{-13}$	$0.95\times10^{-13}\pm0.1\times10^{-13}$	Total amount of HT on the earth atmosphere 0.6 ± 0.06 moles (calculated value)
	Ratio T/H	Ratio T/H Calculated for natural abundance	
3. Heavy water from Norway 99.5 percent D: year 1943	$7.5\times10^{-14}\pm10$ percent	$3.5\times10^{-18}\pm0.7\times10^{-18}$	Yields to a total amount of about 2000 moles HTO on the earth
	Ratio T/H		
4. Heavy water from Norway 99.95 percent D: year 1937	$4.5\times10^{-13}\pm10$ percent	...	For samples with a D content over 99.9 percent the natural abundance T/H could be calculated only with a much larger limit of error

[a] The age of all samples was considered and the tritium concentrations are corrected for the time when the samples had been collected.
[b] Atmospheric hydrogen was prepared in the year 1948/1949 through the generosity of Linde A. G. München in the Plant of Hamburg.

(B) Tritium atoms will react with oxygen to form TO_2 or undergo an exchange reaction with H_2 to form HT. This alone does not determine the reaction mechanism for the observed ratio of HT and HTO.

(C) The reactions that must be considered are: the photochemical dissociation of TO_2 and the reactions with ozone according to (VIII) to (XII).

(D) Altitude affects the reaction. Below 5 km, air pollutions, clouds and rain will tend to consume the TO_2 and form HTO. In regions from 10 to 40 km mostly HT will be formed. In regions above 40 km, the concentrations are so small that they do not contribute readily to the total HT.

APPENDIX

In our first paper, we estimated that atmospheric hydrogen contained about one mole of tritium atoms. Later, V. Faltings made more exact measurements for the tritium content in atmospheric hydrogen and heavy water. The measurements were made with the same counting system, but the filling technique had been improved.[18] In the earlier experiments, acetylene was hydrogenated with atmospheric hydrogen to atmospheric ethane, with a resultant pressure in the counter of 40 mm as ethane. In the improved system, Faltings counted with a filling pressure of 295- to 350-mm atmospheric hydrogen or deuterium, to which about 10 mm of toluene had been added. This method was simpler and direct, with a greater amount of atmospheric hydrogen introduced into the counter. In Table II, the tritium concentration of atmospheric hydrogen is listed. In addition, some tritium determinations of heavy water are tabulated. This heavy water was made in Norway by Norsk Hydro, which also provided Libby with his first samples. The tritium concentrations in heavy water found by Libby and ourselves were almost identical, but in the paper by A. Grosse and Libby, the tritium concentrations which were calculated for rain water from the tritium concentration in the heavy water samples were listed with about 10^{-18}, with a large limit of error. Since I had the opportunity to study the process of deuterium production very carefully at Norsk Hydro, I was able to report the tritium concentrations with smaller limits of error. These correlate readily with the data given by Libby[3] for tritium concentrations in rain samples of other origins.

[18] V. Faltings, Naturwiss. **40**, 409 (1953).

Dielectric Properties of Wool-Water Systems at 3000 and 9300 Megacycles

J. J. WINDLE AND T. M. SHAW
Western Utilization Research Branch, Agricultural Research Service, United States Department of Agriculture, Albany 6, California

(Received August 17, 1953)

The dielectric constant ϵ' and dielectric loss ϵ'' for wool-water systems have been determined at frequencies of 3000 and 9300 Mc by a cavity resonator method. The water content of the wool fibers was varied between 0 and 14 percent of the weight of the dry wool. The upper limit of 14 percent is approximately one-half the amount of water wool will absorb in a saturated atmosphere at 25°C. The increased dielectric loss in the systems studied and the resultant attenuation of microwave power prevented measurements from being made at water contents in excess of approximately 14 percent.

The results of the measurements show that both ϵ' and ϵ'' increase with increasing water content. The results have been analyzed in terms of a sorption theory proposed by Cassie which shows that the water sorbed by wool consists of localized water which is intimately bound to polar sites in the wool and mobile water which constitutes the remainder sorbed. The dielectric constant of the localized water is found to be 5.8 at both frequencies. This result compares favorably with the microwave dielectric constant of irrotationally bound water obtained by Buchanan *et al.* from studies of protein hydration. It has been found that ϵ' and ϵ'' of the mobile water are less than for liquid water if the dielectric properties of the wool are assumed to be unaffected by water sorption. The alternate assumption (in which ϵ' and ϵ'' for the mobile water are set equal to those of liquid water) is discussed.

INTRODUCTION

THE interpretation of the dielectric properties of proteins containing various amounts of sorbed water requires a knowledge of the interactions between the protein and the sorbed water and the influence of the sorbed water on the protein-protein interactions. Information concerning the protein-water interactions has been derived, on the whole, from sorption studies. Although these studies do not give information about the detailed microscopic interactions involved, they are in general agreement that in the initial stages of sorption the water is intimately bound or localized[1] on polar sites in the protein[2] and that in subsequent stages of sorption the water is mobile or free and possesses many of the properties of liquid water. At this time, the present state of knowledge concerning the structure of proteins does not permit a more detailed analysis of the sorption process to be made. The successful interpretation of the dielectric data in terms of a sorption theory is not in itself sufficient proof of the theory. Nevertheless, such information should lead to a better understanding of the molecular structure of proteins, the mechanism of their water sorption and the properties of the sorbed water.

An analysis of the sorption isotherm for wool has been made by Cassie[3] in terms of his theory of multimolecular absorption.[4] In this theory a certain fraction of the sorbed water is localized at polar sites in the fiber and the remainder is sorbed without the evolution of heat under attractive forces like those in liquid water. Cassie has determined the number of moles of localized and mobile water sorbed at any vapor pressure between 0–100 percent relative humidity.

The dielectric properties of a material can be specified completely by the complex dielectric constant $\epsilon=\epsilon'-j\epsilon''$. The real part ϵ' is called the dielectric constant and the imaginary part ϵ'' is called the dielectric loss factor. For polar materials the dielectric constant may be expressed by the Kirkwood[5] formula

$$\frac{(\epsilon'-1)(2\epsilon'+1)}{9\epsilon'}\frac{M}{\rho}=P, \tag{1}$$

where M is the molecular weight, ρ is the density, and P is the molecular polarization of the material.

In the present work the variation with water content of ϵ' and ϵ'' for wool-water systems has been determined at frequencies of 3×10^9 ($\lambda=10$ cm) and 9.3×10^9 cps ($\lambda=3.2$ cm). The results have been analyzed in terms of Cassie's theory of localized and mobile water by extending the Kirkwood relation (1) to include a mixture of polar materials.[6]

EXPERIMENTAL

The experimental techniques employed for the determination of ϵ' and the theory of the method have

[1] In this paper the term "localized" will be used and refers to that water which is believed to be attached directly to polar groups in the protein. The term mobile will refer to all other sorbed water which is probably only indirectly attached through other water molecules.

[2] A. D. McLaren and J. W. Rowen, J. Polymer Sci. **7**, 311 (1951).

[3] A. B. D. Cassie, Trans. Faraday Soc. **41**, 458 (1945).

[4] A. B. D. Cassie, Trans. Faraday Soc. **41**, 450 (1945). This theory has been criticized and corrected by T. L. Hill, J. Chem. Phys. **14**, 263 (1946) but Cassie's results are unaffected.

[5] J. G. Kirkwood, J. Chem. Phys. **7**, 911 (1939).

[6] G. King [Trans. Faraday Soc. **43**, 601 (1947)], has made a similar study for horn keratin at lower frequencies and has applied Cassie's analysis and the Debye equation to his data. We have found that Table II in King's paper is in error (confirmed by a private communication with King). We have been unable to rectify the errors and therefore cannot utilize the results of his analysis.

been discussed in an earlier publication.[7] Briefly, ϵ' is calculated from the change in resonant frequency (f_0-f) of a cylindrical cavity resonator which occurs when a thin cylindrical bundle of fibers is placed coaxially in the resonator. The change in resonant frequency is given by equation (1a) from reference 7.

$$(f_0-f)=\frac{f_0}{0.539}\frac{V_s}{V_c}(\epsilon'-1),$$

where f is the frequency of the cavity resonator containing the dielectric specimen, f_0 is the frequency of the empty resonator, ϵ' is the dielectric constant of the specimen, V_c is the volume of the resonator, and V_s is the volume of the specimen.

The microwave technique discussed for fibers, in reference 7 has been improved by a modification of the resonant cavity.[8] A slot has been cut parallel to the direction of current flow in the walls of the resonator. Fiber holders, in which a parallel bundle of fibers can be tautly mounted, have been fitted to the slot so that the fiber bundle will be precisely positioned coaxially within the resonator. This modification has greatly reduced the time required to place a conditioned fiber specimen in the resonator and insures that the dimensions of the parallel bundle of fibers will remain fixed throughout the course of the measurement. While mounted in the holders, the fibers can be conditioned by humidification at 25°C in evacuated desiccators containing an appropriate concentration of sulfuric acid. It was determined experimentally that 24 hours was ample to establish moisture equilibrium for a typical fiber bundle weighing of the order of 0.015 g. The fibers were dried in evacuated desiccators over magnesium perchlorate at 25°C. The fibers were considered to be dry when (f_0-f) for the specimens remained constant with further desiccation. The water content of the fibers was determined from the sorption isotherm for wool.[9]

In general, the room humidity will not be the same as that for the conditioned fibers; thus when removed from the desiccators and placed in the cavity for measurement, the fiber bundle will lose or gain water. These changes in water content were minimized by making the electrical measurements immediately after the fibers were removed from the constant humidity chamber. A small correction was made for the moisture change which occurred during the time required (about 20 seconds) to make the measurement. This was done by making three successive determinations of (f_0-f) in a total elapsed time of about 100 seconds.[10] The variation of (f_0-f) with time was found to be linear in every case. The value of (f_0-f) at zero time was obtained by extrapolation and was assumed to be the value appropriate to the fiber when in equilibrium with the atmosphere of the evacuated desiccator. It is estimated that the values of ϵ' obtained in this way are accurate to within ± 2 percent.

The dielectric loss is given by the equation[11]

$$\epsilon''=0.269\frac{a^2}{c^2}\left(\frac{1}{Q_1}-\frac{1}{Q_2}\right) \qquad (2)$$

where a is the radius of the resonator and c is the radius of the specimen. Q_1 is the Q of the resonator containing the test specimen and Q_2 is the Q when the test specimen is replaced by a loss-free dielectric of the same permittivity and dimensions so that the resonant frequency is unchanged. Equation (2) is an approximate formula which is valid when thin specimens are used. A complete discussion of the limitations of Eq. (2) and the derivation of the exact formula are given in reference 11.

Q_1 can be determined experimentally, but Q_2 cannot since, in general, a loss-free dielectric of the same permittivity as the test specimen will not be available. When thin specimens of relatively high loss, such as wool, are used, however, Q_2 can be approximated by the Q of the air-filled resonator because the resonant frequency is changed only slightly due to the test specimen. For the specimens studied here the maximum change in frequency is less than 0.5 percent of the resonant frequency.

In the present work, the cavity resonance curve is presented on a cathode ray oscilloscope.[7] The oscilloscope presentation permits a measurement of Q by means of the relation $Q=f/\delta f$ where f is the resonant frequency and δf is the difference in frequency at the two half-power points of the cavity resonance curve. Substituting for Q_1 and Q_2 in Eq. (2) gives

$$\epsilon''=0.269\frac{a^2}{c^2}\frac{1}{f}(\delta f_1-\delta f_2). \qquad (3)$$

Equation (3) has been checked and found to be valid for materials of known loss and dimensions comparable to the specimens studied. In testing Eq. (3) the method of Sproull and Linder[12] was used to determine δf. For hygroscopic materials such as wool, a more rapid method for the determination of δf was found to be necessary. In the present work, δf was measured from a photograph of an oscilloscope presentation of the cavity resonance curve taken immediately after the fiber specimen was placed in the cavity. For this purpose,

[7] T. M. Shaw and J. J. Windle, J. Appl. Phys. **21**, 956 (1950).
[8] T. M. Shaw and J. J. Windle, Phys. Rev. **91**, 218 (1953).
[9] J. B. Speakman and C. A. Cooper, J. Text. Inst. **27**, T183 (1936).
[10] In 100 seconds dry wool will pick up about 3 percent water from an atmosphere of approximately 40 percent R.H. For the moist fiber, the loss or gain of water will be less the closer the relative humidity of the constant humidity chamber is to the R.H. of the room.
[11] Horner, Taylor, Dunsmuir, Lamb, and Jackson, J. Inst. Elec. Engrs. London **93**, 53 (1946).
[12] R. L. Sproull and E. G. Linder, Proc. Inst. Radio Engrs. **34**, 305 (1946).

Eq. (3) can be written

$$\epsilon''=0.269\frac{a^2\alpha}{c^2 f}(\delta l_1-\delta l_2), \quad (4)$$

where δl_1 and δl_2 are the widths at half-height as measured from the photographs. The factor α is a constant to convert the width to megacycles and was determined experimentally by measuring the dielectric loss of materials for which the values of ϵ' and ϵ'' lay in the range of those for the wool-water systems studied. It is estimated that the values of ϵ'' obtained in this way are accurate to within ± 10 percent.

In the calculation of the values of ϵ' and ϵ'' from the experimental data, account has been taken of the transverse swelling of the wool fibers.[13] All the measurements to be discussed have been made with the electric field parallel to the fiber axis. Measurements were made at 25°C in a constant temperature room.

RESULTS AND DISCUSSION

Dielectric Constant

A direct extension of the Kirkwood formula (1) to a mixture of polar materials gives the relation

$$\frac{(\epsilon'-1)(2\epsilon'+1)}{9\epsilon'}\frac{\Sigma M_i X_i}{\rho}=\Sigma P_i X_i, \quad (5)$$

where M_i, X_i, P_i are the molecular weight, mole fraction, and molecular polarization, respectively, of the ith component; ϵ' and ρ are the dielectric constant and density of the mixture. In terms of Cassie's analysis, the wool-water system is a mixture composed of three components: wool, localized water, and mobile water. For the wool-water system Eq. (5) becomes

$$\frac{(\epsilon'-1)(2\epsilon'+1)}{9\epsilon'}\frac{M_k X_k+M_w X_w}{\rho}=P_k X_k+P_l X_l+P_m X_m, \quad (6)$$

where M_k is the average molecular weight of amino acid residues in wool, M_w is the molecular weight of water, X_k, X_w are the mole fractions of the wool and sorbed water, respectively, X_l, X_m are the mole fractions of the localized and mobile water, respectively, $(X_w=X_l+X_m)$, and P_k, P_l, P_m are the molar polarizations of the dry wool, localized water, and mobile water, respectively. The values of X_k, X_w, X_l, X_m are obtained from Cassie's analysis of the absorption isotherm for wool.[3]

Figure 1 shows the variation of ϵ' for wool fibers (New Zealand, medium)[14] for water contents between zero and 14 percent at 3×10^9 and 9.3×10^9 cps. The circles represent the experimental points. Their radius indicates the estimated uncertainty in the water content. The vertical line indicates the estimated experimental error in the dielectric constant.

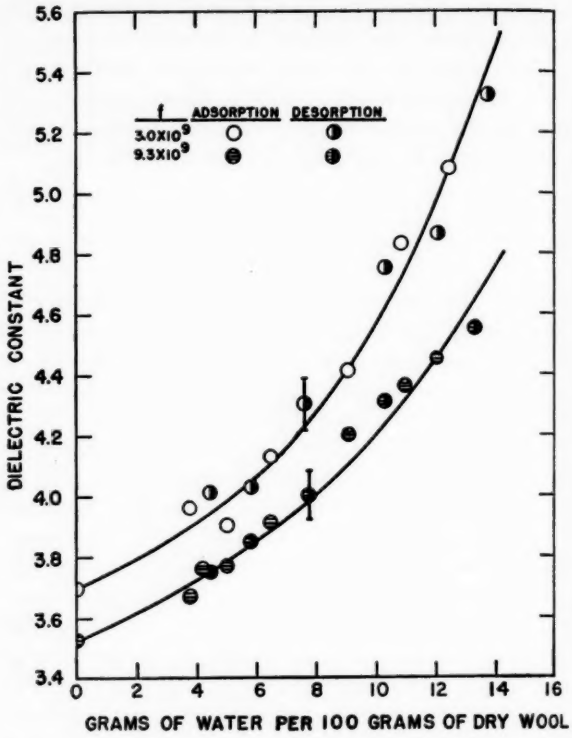

FIG. 1. A comparison of the experimental values of the dielectric constant of wool-water systems with the theoretical relationship (solid curves) calculated from Eq. (6). The radius of the circles indicates the estimated experimental error in the water content. The estimated experimental error in the dielectric constant, as indicated by the vertical line, is ± 2 percent. The points at zero water content represent both absorption and desorption dry values.

In each case the solid curve has been calculated using Eq. (6) and the values of the polarizations of the components given in Table I.

The values of the polarization of the wool P_k were obtained directly from Eq. (1) using the value of ϵ' measured for the dry fibers and Astbury's value of 118 for the average value of the molecular weight of the amino acid residues in wool. The polarizations of the localized and mobile water, in each case, were obtained from the best smooth curve passed through the experimental points by applying Legendre's method of least squares to the solution of Eq. (6) for P_l and P_m. The agreement between the calculated curve and the experimental points is well within the limits of the estimated experimental error and indicates that the observed variation of the microwave dielectric constant of the wool-water system with water content can be interpreted satisfactorily in terms of a simple three component mixture. Moreover, the values found for the polarizations of the localized and mobile water are plausible and are consistent with the picture of water sorption employed.

[13] F. L. Warburton, J. Text. Inst. **38**, T64 (1947).
[14] W. von Bergen and J. H. Wakelin, Text. Res. J. **22**, 123 (1952).

Localized Water

According to the theory, the molecules of localized water are intimately bound to sites throughout the wool molecule. In this view, the localized water is not required to form a continuum or layer possessing a structure of its own. It can be considered as a random distribution of individual water molecules more or less rigidly attached to isolated polar groups in the wool. (Since wool is better than 80 percent amorphous a random distribution of sites seems likely.) If these localized water molecules are sufficiently restricted at microwave frequencies so that they are unable to rotate in the field, then they can contribute to the dielectric constant only through their electronic and atomic polarizations. The dielectric constant of the localized water therefore should be essentially constant at microwave frequencies, and the molar polarization of such an arrangement of water molecules should be about the same as that of liquid water determined at frequencies so high that only electronic and atomic polarizations can contribute to the dielectric constant. The high frequency dielectric constant of water has been found to be 5.5 ± 1,[15,16] which corresponds to a molar polarization calculated by Eq. (1) of 19.6 ± 4.0 cc. From Table I, the average molar polarization of the localized water is 20.8 cc and the values of P_l are essentially the same at both microwave frequencies. The close agreement between these two polarizations tend to confirm the properties suggested for the localized water.

In an entirely different type of investigation of protein hydration Buchanan *et al.*[17] have analyzed microwave dielectric measurements on six aqueous protein solutions in terms of water "irrotationally bound" to the proteins, i.e., unable to rotate in the high frequency field. They found that a value "slightly higher than 5.5" for the dielectric constant of the irrotationally bound water was required to give the best agreement with their experimental results. This value compares favorably with the dielectric constant of 5.8 for localized water calculated from its molar polarization. They also give estimates of the amount of water irrotationally bound to the proteins and although their study did not include wool, a comparison shows that the amount of localized water sorbed by wool at saturation is of the same order of magnitude as the amount of water irrotationally bound to the proteins. These facts suggest that irrotational water and localized water are synonymous, and are taken as further confirmation of the interpretation of the dielectric behavior of the wool-water system presented here.

TABLE I. Polarization of dry wool, localized water, and mobile water at 3×10^9 and 9.3×10^9 cps.[a]

f(cps)	P_k(cc)	P_l(cc)	P_m(cc)
3×10^9	61.6	20.9	242
9.3×10^9	58.0	20.7	150

[a] The polarizations of liquid water calculated from Saxton's values of ϵ' by the use of Eq. (1) are 302 and 238 at 3×10^9 and 9.3×10^9 cps, respectively.

Mobile Water

According to Cassie's theory, the mobile water is viewed as being sorbed with no evolution of heat and under attractive forces like those in liquid water. The dielectric properties of the mobile water therefore should be identical with the dielectric properties of liquid water. A comparison of the values of P_m from Table I with the polarizations of liquid water (see footnote to Table I) shows that this is not the case. At both frequencies the value of P_m is less than the corresponding polarization for liquid water. This difference is too large to be attributed to experimental errors alone. Without seriously altering the theory or encumbering it with additional terms, two possible explanations for this discrepancy are suggested.

In the first of the two ways to be discussed for resolving the above discrepancy concerning the polarization of the mobile water, the assumption is made that P_k is not constant as was assumed originally but must decrease with increasing water content. A change in the polarization of the wool is to be expected as a result of the interaction of the sorbed water with the wool, the change in the polarization of the sorbed water upon localization already having been taken into account. A calculation shows that this decrease amounts to about 20 percent of P_k at 14 percent water content and it is of interest to speculate on a possible mechanism for it.

Thus far, it has been assumed that the polarization of the wool is a function of frequency only and is independent of water content. The usual arguments given for this assumption are that at microwave frequencies the only contributions to the dielectric constant arise from electronic and atomic polarizations which are assumed to be independent of water content and that dipole rotation, whether or not it may be facilitated by any plasticizing action of the sorbed water, is not active because of the high frequencies involved. This latter assumption is supported by some unpublished data on the variation of the dielectric constant of dry horn keratin with temperature at 3×10^9 cps which shows a temperature dependence opposite to that observed when dipoles are active. It seems as if there is much less basis for assuming that the atomic polarization is independent of water content in a molecule as complex as is wool. For wool at microwave frequencies, the magnitude of the atomic polarization is a large fraction ($\sim$45 percent) of P_k. Now it is observed that in infrared spectroscopy of proteins the absorption bands are affected by molecular association resulting, for example, from hydrogen bond formation with water

[15] Collie, Hasted, and Ritson, Proc. Phys. Soc. (London) **60**, 145 (1948).
[16] J. A. Saxton, Proc. Roy. Soc. (London) **A213**, 473 (1952).
[17] Buchanan, Haggis, Hasted, and Robinson, Proc. Roy. Soc. (London) **A213**, 379 (1952).

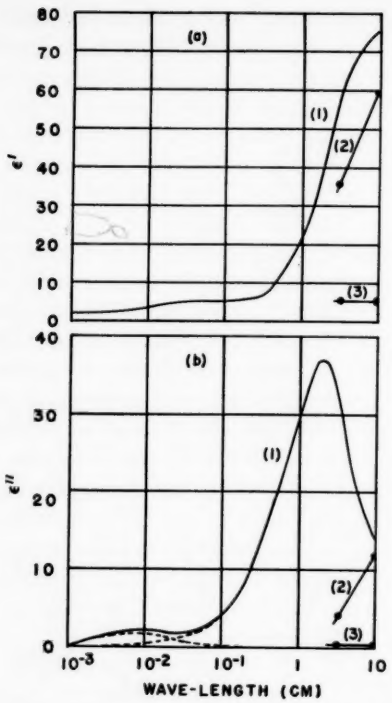

FIG. 2. The variation of $\epsilon'(a)$ and $\epsilon''(b)$ with wavelength. (1) Liquid water (see reference 16); (2) mobile water; (3) localized water. The dashed curves of part (b) show the components of ϵ'' due to Debye dispersion and resonance absorption.

sorption. The effects of such association must also be reflected in the microwave atomic polarization. Although it is not yet possible to calculate the magnitude of such effects for wool, it would seem, in view of its very large atomic polarization, that a change in P_k of the order of 20 percent is not unreasonable. In assuming that the properties of the mobile water are unaffected by absorption, only the interaction between the localized water and wool can be responsible for the decrease in P_k. There is some evidence that the localized sites in the wool are associated with the carbonyl group in the peptide linkage.[3] Work is in progress on the possible effects of this linkage and its associated hydrogen bond on the dielectric constant.

In the second possibility to be considered concerning the polarization of the mobile water the original assumption is retained, that the polarization of the mobile water is unaffected by water sorption. It is found that the complex dielectric constant of the mobile water is not the same as that of liquid water. A comparison between the dielectric constants and dielectric loss factors for liquid water, mobile water, and localized water is given in Fig. 2(a),(b), where the variation of ϵ' and ϵ'' with wavelength is shown. The data for liquid water were taken from reference 16. The solid curves for the mobile and localized water represent our experimental results. The dipole dispersion which occurs for liquid water in the microwave region ($\lambda = 1$–10 cm) appears to be shifted to longer wavelengths for mobile water and presumably to much longer wavelengths for the localized water. This result indicates that the mobile water may suffer some restriction to rotation greater than that found in liquid water and therefore may be influenced by the localized water or indirectly by the wool.

There is one piece of evidence to suggest that this may be the case. Buchanan *et al.*[17] have estimated the maximum hydration of what they call bound water, i.e., water carried through the solution by the protein (included in this estimate is the amount of water irrotationally bound). Bound water differs from nonhydrated water in that it is attached to its binding molecules by bonds broken less often than water-water bonds. A comparison between the amounts of water sorbed at saturation vapor pressure for four of the proteins for which these data are available[18] out of the six studied by Buchanan *et al.* shows that the maximum amount of bound water ranges from about one-half to three-fourths of the maximum amount of water the proteins can sorb. This would indicate then that at least part of the water sorbed in addition to the localized water is not identical to liquid water. It is not possible to make an estimate of the microwave dielectric properties of the bound water from the data of Buchanan, but the complex dielectric constant should be intermediate to that of the localized and liquid water as indeed it has been found to be for the mobile water.

The suggestion that the water sorbed in addition to the localized water is not like liquid water but may have properties varying continuously between localized and liquid water has been proposed by others.[2] We have not attempted to apply these theories, however, because they lack the simplicity of Cassie's theory, which we have shown is sufficient to interpret our results.

Dielectric Loss Factor

The dielectric loss factor of a mixture of dielectrics, each with a dielectric loss factor ϵ_i'' and mole fraction X_i can be expressed by the relation,

$$\epsilon'' = \sum \epsilon_i'' X_i. \tag{7}$$

For the three-component system, wool, localized water, and mobile water, Eq. (7) becomes

$$\epsilon'' = \epsilon_k'' X_k + \epsilon_l'' X_l + \epsilon_m'' X_m. \tag{8}$$

The value of ϵ'' for the system and ϵ_k'' for the dry wool are measured directly as explained in the experimental section. As was the case for the polarization of the wool,

TABLE II. Dielectric loss factor for dry wool, localized water, and mobile water at 3×10^9 and 9.3×10^9 cps.

f(cps)	ϵ_k''	ϵ_l''	ϵ_m''
3×10^9	0.106 ± 0.01	0.226 ± 0.023	11.8 ± 1.2
9.3×10^9	0.070 ± 0.007	0.276 ± 0.028	3.8 ± 0.4

[18] H. B. Bull, J. Am. Chem. Soc. **66**, 1499 (1944).

ϵ_k'' also initially is assumed to be independent of the water content. Figure 3 shows the experimentally determined variation of ϵ'' with water content for 3×10^9 and 9.3×10^9 cps. The method of least squares has been applied to curves of Fig. 3, and ϵ_l'' and ϵ_m'' have been calculated from Eq. (8). In Table II the values of ϵ_k'', ϵ_l'' and ϵ_m'' have been summarized for each frequency.

Localized Water

The dielectric constant of the localized water has been found to be the same as the high frequency dielectric constant of liquid water, and it might be expected therefore that its dielectric loss factor would be the same as the high frequency dielectric loss factor of liquid water. From Fig. 2(b), the dielectric loss factor corresponding to the high frequency ($\lambda=10^{-1}-10^{-2}$ cm) dielectric constant of 5.5 for liquid water is of the order of 3. A comparison of this value with the values of $\epsilon_l''\sim0.25$ given in Table II shows that ϵ_l'' is only about one-tenth that of water.

This difference can be explained as follows: According to Fig. 2b, the dielectric loss factor for liquid water in the region $\lambda=10^{-2}-10^{-1}$ cm is the sum of the high frequency wing of the Debye type loss, the maximum of which occurs in the microwave region for liquid water, and the low frequency wing of a resonance absorption[16] (both shown as dashed curves between $\lambda=10^{-3}-10^{-1}$ cm). For the localized water, however, there is no evidence for any Debye type rotation in the microwave region and the dielectric loss factor should result from the resonance absorption only. For liquid water, the dielectric loss factor for the resonance absorption ranges from about 0.1 to 10^{-1} cm to about 1.6 at 10^{-2} cm. The fact that the values of ϵ_l'' are found to be intermediate to these suggests that the dielectric loss factor for localized water is very much like that for liquid water at high frequencies in the absence of any Debye absorption.

Mobile Water

The dielectric loss factors for the mobile water shown in Table II and Fig. 2b were determined with the assumption that the dielectric loss of the wool was independent of water content and equal to that found for dry wool. Most of the discussion on the dielectric constant of the mobile water can be applied to its dielectric loss factor. If the loss factor for the wool is independent of water content then the values of ϵ_m'' also indicate that the dispersion of the mobile water is shifted to lower frequencies. On the other hand, if the assumption is made that the dielectric loss factor of the mobile water is the same as that of liquid water, it is found that the dielectric loss of the system, calculated from Eq. (8), is much greater than the experimental value and no reasonable assumptions concerning the dielectric loss of the wool will serve to bring the values into agreement. This result indicates that the dielectric properties of the mobile water are probably not greatly different from the values shown in Tables I and II.

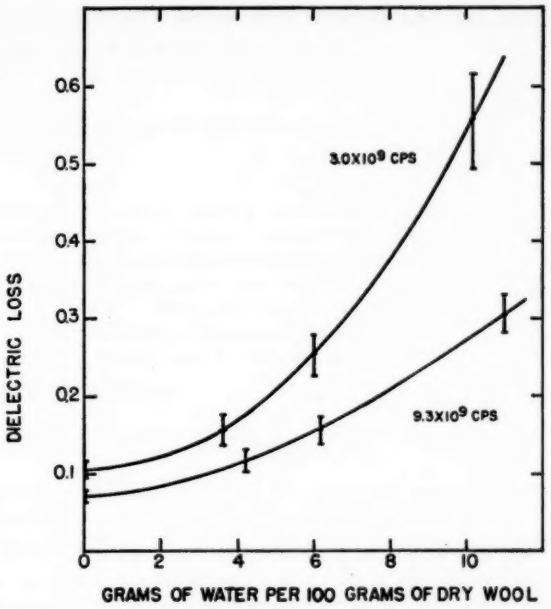

FIG. 3. Experimental value of the dielectric loss *vs* water content.

ACKNOWLEDGMENT

The authors would like to thank Dr. K. J. Palmer for his interest and suggestions during the course of this work.

Tables of Statistical Electron Distributions for Atoms with Degree of Ionization Zero to Four and of the Corresponding Electrostatic Potentials

L. H. THOMAS
Watson Scientific Computing Laboratory, Columbia University, New York, New York
(Received January 14, 1954)

The potential and electron density in statistical distributions for atoms according to Dirac's equation and Jensen's boundary conditions are given as functions of radial distance on a logarithmic scale for neutral atoms and for singly charged positive ions, at uniform interval of a parameter γ. A simple interpolation only is required to obtain them for any particular atomic number. The values of the separate terms in the energy of the distribution are also given.

Tables at a closer interval in radial distance and for positive ions up to charge four can be obtained from the Watson Laboratory, free of charge. They are also available on punched cards.

INTRODUCTION

THE largest advances in the theory of the approximate statistical electron distributions for atoms in their normal states were the demonstration by Dirac[1] that a statistical distribution could be regarded as an approximation to the density matrix which is equivalent to a Hartree-Fock approximation, and that a term representing exchange interaction could be included in the differential equation satisfied by the distribution, and the recognition by Jensen[2] that boundary conditions should be obtained from the same minimum problem as the differential equation. It then became possible to find distributions for neutral atoms and for positive ions with boundary conditions based on a theory rather than on intuition or on attempts to fit empirical data. Reference will not be made here to the large literature but only to the books of Brillouin[3] and Gombas[4] for the theory and many applications.

The most extensive tabulations hitherto published are those of Kwai Umeda[5] with Brillouin's boundary conditions for a neutral atom giving the potential and its derivative as functions of radial distance and that of Metropolis and Reitz[6] giving functions for various boundary conditions which cover positive ions, neutral atoms, and infinite distributions. The following tables give the potential and the electron density as functions of radial distance on a logarithmic scale for neutral atoms and for positive ions of charge one to four units, for uniformly increasing values of a parameter γ. The functions can be interpolated directly for any atomic number. In addition values of the separate terms in the energy of the distribution are given for each degree of ionization and for each atomic number.

[1] P. A. M. Dirac, Proc. Cambridge Phil. Soc. **26**, 376 (1930).
[2] H. Jensen, Z. Physik **93**, 232 (1935).
[3] L. Brillouin, *L'atom de Thomas-Fermi et la méthode de champ "self-consistent"* (Herman & Cie., Paris, 1934).
[4] P. Gombas, *Die Statistische Theorie des Atoms und ihre Anwendungen* (Springer-Verlag, Wien, 1949).
[5] Kwai Umeda, J. Fac. Sci., Hokkaido Univ. Ser. II, Vol. III, 171 (1942).
[6] N. Metropolis and J. R. Reitz, J. Chem. Phys. **19**, 555 (1951).

OUTLINE OF THE THEORETICAL BACKGROUND

The Schrödinger equation for a many electron problem has the form

$$\{H_1+H_2+\cdots+V_{12}+\cdots\}\psi=W\psi,$$

where ψ, a function of all the coordinates of all the electrons, must satisfy the Pauli condition that it should change sign when all the coordinates of any pair of particles are interchanged. This is the same as saying that the energy

$$W=\int\bar{\psi}\{H_1+H_2+\cdots+V_{12}+\cdots\}\psi d\mathrm{r}\Big/\int\bar{\psi}\psi d\mathrm{r}$$

is stationary, or for the ground state, a minimum, subject to the Pauli condition, and where the integration is over all the coordinates of all the electrons.

If we neglect V_{rs} in zero approximation, the solutions are antisymmetrical linear combinations of wave functions that, to satisfy the Pauli condition, are products of functions of the coordinates of the separate electrons, of the form, for n electrons,

$$\begin{vmatrix}\psi_1(1), & \psi_1(2), & \cdots, & \psi_1(n)\\ \psi_2(1), & \psi_2(2), & \cdots, & \psi_2(n)\\ \cdots, & \cdots, & \cdots, & \cdots\\ \psi_n(1), & \psi_2(2), & \cdots, & \psi_n(n)\end{vmatrix}$$

suitably normalized. The Hartree-Fock approximation is to take functions that make the energy a minimum when required to be of this form, and leads to equations for separate wave functions in the fields due to the remainder with extra terms for exchange energy.

For a function of the foregoing form we can construct a "Dirac density matrix"

$$\rho(\mathrm{r},\mathrm{r}')=\psi_1(\mathrm{r})\bar{\psi}_1(\mathrm{r}')+\psi_2(\mathrm{r})\bar{\psi}_2(\mathrm{r}')+\cdots$$

where r stands for all the coordinates of a single electron, including spin, r′ for another set of coordinates. This matrix will satisfy the conditions

$$\int\rho(\mathrm{r},\mathrm{r}')\rho(\mathrm{r}',\mathrm{r}'')d\mathrm{r}'=\rho(\mathrm{r},\mathrm{r}''),$$

$$\int\rho(\mathrm{r},\mathrm{r})d\mathrm{r}=n$$

provided that $\psi_1(\mathrm{r})$, $\psi_2(\mathrm{r})$, $\cdots$ are normalized in the ordinary way, and the integration includes summation over spin. Conversely, a function of r and r′ satisfying these conditions specifies the functions $\psi_1(\mathrm{r})$, $\psi_2(\mathrm{r})$, $\cdots\psi_n(\mathrm{r})$.

This function in quantum mechanics is a special case of a density matrix corresponding to the particle distribution function of a gas in the phase space of a single particle.

Dirac showed that the Hartree-Fock equations could be expressed simply in terms of the density matrix by the condition that

$$W=\int\{H(\mathrm{r})\rho(\mathrm{r},\mathrm{r}')\}_{\mathrm{r}'=\mathrm{r}}d\mathrm{r}+\tfrac{1}{2}\int\int\{\rho(\mathrm{r}_1,\mathrm{r}_1)\rho(\mathrm{r}_2,\mathrm{r}_2)-\rho(\mathrm{r}_1,\mathrm{r}_2)\rho(\mathrm{r}_2,\mathrm{r}_1)\}V(\mathrm{r}_1,\mathrm{r}_2)d\mathrm{r}_1d\mathrm{r}_2$$

should be stationary subject to the foregoing conditions.

If each "self-consistent" equation is like a wave equation with a kinetic energy and an effective potential field, we may expect to be able to approximate near any position r by a set of plane waves $\exp(2\pi i/h)(\mathrm{p}\cdot\mathrm{r})$ with values of p distributed uniformly within a sphere of radius, say P, at a rate 2, for the two directions of spin, for each h^3 of phase space, and, approximately replacing the sum by an integral, we have

$$\rho(\mathrm{r},\mathrm{r}')=\int_{|\mathrm{P}|<P}\frac{1}{h^3}\mathrm{e}^{(2\pi i/h)(\mathrm{p}\cdot\mathrm{r}-\mathrm{r}')}d\mathrm{p}\delta(s_1,s_2),$$

where for definiteness we take $P=P(\frac{1}{2}|\mathrm{r}+\mathrm{r}'|)$, so that $\rho(\mathrm{r},\mathrm{r}')$ depends on a function of a single set of space variables, $\frac{1}{2}(\mathrm{r}+\mathrm{r}')$, and we have separated off the spin factor, $\delta(s_1,s_2)$. Thus

$$\rho(\mathrm{r},\mathrm{r}')=\frac{1}{2\pi^2|\mathrm{r}-\mathrm{r}'|}\left(\sin\frac{2\pi P|\mathrm{r}-\mathrm{r}'|}{h}-\frac{2\pi P|\mathrm{r}-\mathrm{r}'|}{h}\times\cos\frac{2\pi P|\mathrm{r}-\mathrm{r}'|}{h}\right)\delta(s_1,s_2).$$

This expression, though Hermitian so that it can be substituted in W, does not satisfy

$$\int\rho(\mathrm{r},\mathrm{r}')\rho(\mathrm{r}',\mathrm{r}'')d\mathrm{r}'=\rho(\mathrm{r},\mathrm{r}'')$$

exactly; integration still includes summation over spin.

We obtain the statistical field satisfying Dirac's differential equation and Jensen's boundary conditions by choosing the function P to make W a minimum subject to

$$\int\rho(\mathrm{r},\mathrm{r})d\mathrm{r}=n.$$

THE DIRAC-JENSEN EQUATIONS

Using atomic units, with Planck's constant $h=2\pi$, electronic mass $m=1$, and charge $e=1$, we may take for an atom of atomic number Z

$$H=\tfrac{1}{2}p^2-\frac{Z}{r},$$

while

$$V_{12}=\frac{1}{r_{12}}.$$

We have then for the charge density, putting $\mathrm{r}'=\mathrm{r}$ and summing over spin,

$$\rho=\frac{1}{3\pi^2}P^3$$

giving total charge

$$E=\frac{4}{3\pi}\int P^3r^2dr.$$

Substituting in the integral, the energy W is the sum of four terms:

the kinetic energy $\quad K=\dfrac{2}{5\pi}\displaystyle\int P^5r^2dr,$

the exchange energy $\quad U=-\dfrac{1}{\pi^2}\displaystyle\int P^4r^2dr,$

the potential energy $\quad V=-Z\dfrac{4}{3\pi}\displaystyle\int P^3rdr,$

and the potential interaction

$$I=\frac{1}{2}\int\int\frac{P_1^3}{3\pi^2}\frac{P_2^3}{3\pi^2}\frac{1}{r_{12}}dr_1dr_2.$$

The problem of choosing a function P to make W a minimum subject to $E=n$ leads directly to either $P>5/4\pi$ or $P=0$, so that there is a finite boundary at which $P=5/4\pi$; and within this P must satisfy the equation

$$\tfrac{1}{2}P_1^2-\frac{1}{\pi}P_1-\lambda=\frac{Z}{r_1}-\int\frac{\rho_2}{r_{12}}dr_2=\phi_1 \text{ say},$$

the potential λ being a multiplier corresponding to the condition $E=n$.

Hence the potential ϕ satisfies the differential equation

$$\nabla^2\phi=4\pi\rho,$$

where ρ is given in terms of P and so of ϕ, and at the boundary

$$\phi=\frac{Z-E}{r}=-\frac{15}{32\pi^2}-\lambda,\quad\frac{d\phi}{dr}=-\frac{Z-E}{r^2}.$$

The terms of W satisfy the two integral relations, which include the virial equation,

$$5K+4U+3V+6I=\lambda 3E$$
$$-I=V+2K+U.$$

TABLE I. Radius and energy against atomic number.

Z	γ	r_0	K	−V	−U	Z	γ	r_0	K	−V	−U
						54	3.4785	3.5881	8645.4	20038.5	174.6
						55	3.4935	3.5958	9021.3	20911.9	179.9
						56	3.5082	3.6034	9406.5	21806.6	185.4
5	1.3329	2.2211	36.1	79.8	3.5	57	3.5226	3.6108	9800.8	22722.8	190.9
6	1.5034	2.3588	54.7	122.1	4.7	58	3.5367	3.6180	10204.5	23660.6	196.4
7	1.6480	2.4697	77.8	174.7	6.1	59	3.5506	3.6251	10617.4	24620.1	202.1
8	1.7734	2.5620	105.6	238.2	7.6	60	3.5642	3.6320	11039.7	25601.4	207.8
9	1.8840	2.6406	138.3	313.1	9.2	61	3.5775	3.6388	11471.5	26604.7	213.5
10	1.9826	2.7089	176.1	399.8	10.9	62	3.5906	3.6454	11912.7	27630.0	219.3
11	2.0716	2.7690	219.1	498.7	12.8	63	3.6034	3.6519	12363.5	28677.5	225.2
12	2.1525	2.8225	267.6	610.2	14.7	64	3.6161	3.6583	12823.8	29747.3	231.1
13	2.2268	2.8708	321.7	734.6	16.8	65	3.6285	3.6646	13293.7	30839.4	237.1
14	2.2953	2.9146	381.5	872.4	18.9	66	3.6406	3.6708	13773.3	31954.2	243.2
15	2.3588	2.9547	447.1	1023.8	21.2	67	3.6526	3.6768	14262.6	33091.6	249.3
16	2.4181	2.9916	518.8	1189.0	23.6	68	3.6644	3.6827	14761.7	34251.7	255.5
17	2.4736	3.0257	596.6	1368.6	26.0	69	3.6760	3.6885	15270.7	35434.8	261.7
18	2.5257	3.0574	680.6	1562.6	28.6	70	3.6874	3.6942	15789.5	36640.8	268.0
19	2.5747	3.0870	771.0	1771.4	31.3	71	3.6986	3.6998	16318.2	37870.0	274.4
20	2.6211	3.1147	867.8	1995.3	34.0	72	3.7096	3.7053	16856.9	39122.4	280.8
21	2.6651	3.1406	971.3	2234.4	36.8	73	3.7205	3.7108	17405.6	40398.1	287.3
22	2.7068	3.1652	1081.4	2489.1	39.8	74	3.7311	3.7161	17964.4	41697.2	293.8
23	2.7466	3.1883	1198.3	2759.6	42.8	75	3.7417	3.7213	18533.3	43019.9	300.4
24	2.7845	3.2103	1322.1	3046.1	45.9	76	3.7520	3.7265	19112.3	44366.2	307.1
25	2.8208	3.2311	1452.9	3348.8	49.1	77	3.7623	3.7315	19701.5	45736.3	313.8
26	2.8556	3.2510	1590.8	3668.0	52.3	78	3.7723	3.7365	20301.0	47130.2	320.6
27	2.8889	3.2699	1735.8	4003.9	55.7	79	3.7822	3.7415	20910.7	48548.1	327.4
28	2.9209	3.2879	1888.1	4356.6	59.1	80	3.7920	3.7463	21530.8	49990.0	334.3
29	2.9517	3.3052	2047.7	4726.4	62.6	81	3.8017	3.7511	22161.2	51456.1	341.2
30	2.9813	3.3218	2214.8	5113.5	66.2	82	3.8112	3.7557	22802.0	52946.3	348.2
31	3.0099	3.3376	2389.4	5518.1	69.9	83	3.8206	3.7603	23453.3	54461.0	355.3
32	3.0374	3.3529	2571.5	5940.3	73.7	84	3.8298	3.7649	24115.1	56000.2	362.4
33	3.0641	3.3675	2761.4	6380.4	77.5	85	3.8389	3.7694	24787.4	57563.7	369.6
34	3.0898	3.3817	2958.9	6838.5	81.4	86	3.8479	3.7738	25470.3	59151.9	376.8
35	3.1147	3.3953	3164.3	7314.8	85.4	87	3.8568	3.7782	26163.8	60765.0	384.1
36	3.1389	3.4084	3377.6	7809.5	89.4	88	3.8656	3.7825	26867.9	62402.7	391.4
37	3.1623	3.4211	3598.9	8322.8	93.6	89	3.8742	3.7867	27582.7	64065.3	398.8
38	3.1850	3.4334	3828.3	8854.7	97.8	90	3.8828	3.7909	28308.3	65753.1	406.2
39	3.2071	3.4453	4065.7	9405.6	102.0	91	3.8912	3.7950	29044.6	67465.8	413.7
40	3.2286	3.4568	4311.3	9975.5	106.4	92	3.8996	3.7990	29791.7	69203.6	421.3
41	3.2495	3.4679	4565.2	10564.6	110.8	93	3.9078	3.8030	30549.7	70967.0	428.9
42	3.2698	3.4788	4827.3	11173.0	115.3	94	3.9159	3.8070	31318.6	72755.7	436.6
43	3.2896	3.4893	5097.9	11800.9	119.9	95	3.9239	3.8109	32098.4	74569.7	444.3
44	3.3089	3.4995	5376.9	12448.6	124.5	96	3.9319	3.8148	32889.1	76409.2	452.0
45	3.3277	3.5094	5664.4	13116.0	129.2	97	3.9397	3.8185	33690.9	78274.6	459.9
46	3.3460	3.5191	5960.5	13803.5	134.0	98	3.9475	3.8223	34503.7	80165.5	467.7
47	3.3639	3.5285	6265.3	14511.0	138.8	99	3.9551	3.8260	35327.5	82082.1	475.7
48	3.3814	3.5377	6578.7	15238.8	143.7	100	3.9627	3.8297	36162.4	84024.6	483.7
49	3.3985	3.5466	6900.9	15987.0	148.7	101	3.9702	3.8333	37008.5	85993.2	491.7
50	3.4152	3.5553	7232.0	16755.7	153.7	102	3.9776	3.8369	37865.8	87987.9	499.8
51	3.4316	3.5638	7571.8	17545.0	158.8	103	3.9849	3.8404	38734.3	90008.6	507.9
52	3.4476	3.5721	7920.7	18355.2	164.0	104	3.9921	3.8439	39614.0	92055.4	516.1
53	3.4632	3.5802	8278.5	19186.4	169.3	105	3.9993	3.8473	40504.8	94128.2	524.4

N = 1

TABLE I.—*Continued.*

Z	γ	r_0	K	−V	−U	Z	γ	r_0	K	−V	−U
2	2.9800	3.3210	4.7	10.2	.9	54	5.8615	4.6577	8646.1	20053.4	174.7
3	3.3407	3.5163	11.5	25.6	1.6	55	5.8757	4.6633	9022.0	20927.0	180.1
4	3.6009	3.6507	21.9	49.2	2.6	56	5.8897	4.6689	9407.1	21821.9	185.5
5	3.8040	3.7522	36.3	82.0	3.6	57	5.9034	4.6743	9801.3	22738.3	191.0
6	3.9702	3.8333	54.9	124.6	4.9	58	5.9168	4.6796	10204.9	23676.2	196.6
7	4.1105	3.9004	78.0	177.5	6.2	59	5.9300	4.6848	10617.8	24635.9	202.2
8	4.2317	3.9575	105.8	241.3	7.7	60	5.9429	4.6899	11040.0	25617.5	207.9
9	4.3382	4.0070	138.5	316.5	9.3	61	5.9555	4.6949	11471.7	26621.0	213.6
10	4.4332	4.0507	176.3	403.5	11.1	62	5.9680	4.6998	11912.9	27646.6	219.5
11	4.5187	4.0895	219.3	502.6	12.9	63	5.9802	4.7046	12363.6	28694.4	225.3
12	4.5965	4.1246	267.8	614.4	14.9	64	5.9922	4.7093	12823.9	29764.5	231.3
13	4.6677	4.1564	321.9	739.1	16.9	65	6.0040	4.7140	13293.8	30857.1	237.3
14	4.7334	4.1855	381.6	877.1	19.1	66	6.0156	4.7185	13773.4	31972.1	243.3
15	4.7942	4.2123	447.3	1028.8	21.4	67	6.0270	4.7230	14262.7	33109.9	249.5
16	4.8509	4.2372	518.9	1194.3	23.7	68	6.0382	4.7274	14761.9	34270.5	255.7
17	4.9038	4.2602	596.7	1374.1	26.2	69	6.0492	4.7317	15270.8	35453.9	261.9
18	4.9536	4.2818	680.7	1568.3	28.8	70	6.0601	4.7359	15789.6	36660.3	268.2
19	5.0005	4.3020	771.0	1777.4	31.4	71	6.0707	4.7401	16318.4	37889.8	274.6
20	5.0448	4.3210	867.9	2001.5	34.2	72	6.0812	4.7442	16857.1	39142.5	281.0
21	5.0868	4.3390	971.3	2241.0	37.0	73	6.0915	4.7482	17405.8	40418.5	287.5
22	5.1267	4.3559	1081.4	2495.9	39.9	74	6.1017	4.7522	17964.6	41717.9	294.0
23	5.1646	4.3720	1198.3	2766.6	42.9	75	6.1117	4.7561	18533.5	43040.9	300.6
24	5.2008	4.3873	1322.1	3053.4	46.0	76	6.1216	4.7599	19112.5	44387.4	307.2
25	5.2353	4.4019	1452.9	3356.4	49.2	77	6.1313	4.7637	19701.8	45757.8	314.0
26	5.2684	4.4158	1590.7	3675.8	52.5	78	6.1409	4.7674	20301.2	47151.9	320.7
27	5.3001	4.4290	1735.8	4011.9	55.8	79	6.1503	4.7710	20910.9	48569.9	327.6
28	5.3306	4.4417	1888.1	4364.9	59.3	80	6.1596	4.7746	21531.0	50011.9	334.4
29	5.3598	4.4539	2047.8	4735.1	62.8	81	6.1688	4.7782	22161.4	51478.0	341.4
30	5.3881	4.4656	2214.8	5122.4	66.4	82	6.1778	4.7817	22802.2	52968.5	348.4
31	5.4153	4.4769	2389.5	5527.3	70.1	83	6.1867	4.7851	23453.4	54483.2	355.4
32	5.4415	4.4877	2571.6	5949.8	73.8	84	6.1955	4.7885	24115.2	56022.3	362.5
33	5.4669	4.4982	2761.5	6390.1	77.6	85	6.2041	4.7919	24787.4	57585.9	369.7
34	5.4915	4.5083	2959.1	6848.5	81.5	86	6.2127	4.7952	25470.3	59174.2	376.9
35	5.5153	4.5180	3164.6	7325.0	85.5	87	6.2211	4.7984	26163.8	60787.1	384.2
36	5.5383	4.5275	3377.9	7820.0	89.6	88	6.2294	4.8016	26867.9	62424.9	391.5
37	5.5606	4.5366	3599.2	8333.5	93.7	89	6.2376	4.8048	27582.7	64087.4	398.9
38	5.5823	4.5454	3828.6	8865.7	97.9	90	6.2458	4.8079	28308.3	65775.3	406.4
39	5.6033	4.5540	4066.1	9416.8	102.2	91	6.2538	4.8110	29044.6	67487.9	413.9
40	5.6238	4.5623	4311.7	9987.0	106.5	92	6.2616	4.8140	29791.8	69225.8	421.4
41	5.6437	4.5703	4565.7	10576.3	111.0	93	6.2694	4.8170	30549.7	70989.0	429.0
42	5.6630	4.5781	4827.9	11185.0	115.4	94	6.2771	4.8200	31318.6	72777.5	436.7
43	5.6818	4.5857	5098.5	11813.3	120.0	95	6.2848	4.8229	32098.5	74591.6	444.4
44	5.7002	4.5932	5377.6	12461.2	124.6	96	6.2923	4.8258	32889.3	76431.1	452.2
45	5.7181	4.6003	5665.2	13128.9	129.3	97	6.2997	4.8286	33691.1	78296.5	460.0
46	5.7355	4.6074	5961.3	13816.6	134.1	98	6.3070	4.8315	34504.0	80187.4	467.9
47	5.7526	4.6142	6266.1	14524.4	138.9	99	6.3143	4.8342	35327.9	82104.2	475.8
48	5.7692	4.6209	6579.6	15252.5	143.8	100	6.3214	4.8370	36163.0	84046.9	483.8
49	5.7855	4.6274	6901.9	16001.0	148.8	101	6.3285	4.8397	37009.3	86015.8	491.8
50	5.8013	4.6337	7232.9	16770.0	153.9	102	6.3355	4.8423	37866.8	88010.6	499.9
51	5.8169	4.6399	7572.8	17559.5	159.0	103	6.3424	4.8450	38735.5	90031.7	508.0
52	5.8320	4.6460	7921.5	18369.8	164.1	104	6.3493	4.8476	39615.5	92079.1	516.2
53	5.8469	4.6519	8279.3	19201.1	169.4	105	6.3560	4.8502	40506.9	94153.0	524.5

N = 0

TABLE II. Values of $r\varphi$.

	r/r_0	.00316228	.00398107	.00501187	.00630957	.00794328	.01000000	.01258926	.01584893	.01995262	.02511887	.03162278	.03981072	.05011872
γ	Z													
2.0	.6056	.5961	.5938	.5908	.5872	.5827	.5771	.5703	.5620	.5518	.5394	.5244	.5065	.4852
2.2	.7865	.7730	.7696	.7655	.7603	.7540	.7461	.7365	.7248	.7106	.6934	.6726	.6479	.6187
2.4	1.0098	.9908	.9861	.9803	.9731	.9643	.9534	.9401	.9239	.9043	.8807	.8524	.8188	.7793
2.6	1.2857	1.2592	1.2527	1.2446	1.2347	1.2225	1.2076	1.1894	1.1672	1.1405	1.1084	1.0702	1.0250	.9723
2.8	1.6266	1.5900	1.5811	1.5701	1.5565	1.5398	1.5195	1.4946	1.4646	1.4285	1.3853	1.3341	1.2739	1.2040
3.0	2.0460	1.9958	1.9836	1.9686	1.9501	1.9275	1.8999	1.8665	1.8261	1.7776	1.7200	1.6519	1.5723	1.4804
3.2	2.5640	2.4956	2.4791	2.4587	2.4337	2.4032	2.3660	2.3211	2.2670	2.2024	2.1258	2.0357	1.9311	1.8110
3.4	3.2042	3.1112	3.0888	3.0613	3.0276	2.9866	2.9368	2.8766	2.8046	2.7187	2.6174	2.4990	2.3621	2.2060
3.6	3.9959	3.8699	3.8397	3.8026	3.7574	3.7024	3.6358	3.5557	3.4599	3.3463	3.2128	3.0576	2.8793	2.6772
3.8	4.9781	4.8077	4.7670	4.7173	4.6566	4.5830	4.4942	4.3876	4.2606	4.1107	3.9354	3.7325	3.5008	3.2401
4.0	6.1997	5.9692	5.9145	5.8478	5.7665	5.6682	5.5498	5.4082	5.2402	5.0427	4.8127	4.5481	4.2478	3.9124
4.2	7.7255	7.4138	7.3403	7.2507	7.1418	7.0105	6.8527	6.6648	6.4426	6.1825	5.8811	5.5365	5.1479	4.7170
4.4	9.6377	9.2157	9.1168	8.9964	8.8506	8.6750	8.4648	8.2152	7.9214	7.5789	7.1843	6.7356	6.2332	5.6804
4.6	12.0472	11.4747	11.3414	11.1794	10.9837	10.7485	10.4682	10.1364	9.7473	9.2962	8.7791	8.1950	7.5456	6.8367
4.8	15.0988	14.3199	14.1397	13.9211	13.6578	13.3424	12.9675	12.5256	12.0099	11.4147	10.7366	9.9756	9.1359	8.2270
5.0	18.9896	17.9256	17.6810	17.3853	17.0298	16.6054	16.1027	15.5126	14.8272	14.0403	13.1495	12.1565	11.0696	9.9037
5.2	23.9775	22.5175	22.1843	21.7824	21.3008	20.7277	20.0514	19.2610	18.3473	17.3045	16.1315	14.8339	13.4251	11.9281
5.4	30.4348	28.4191	27.9626	27.4135	26.7575	25.9796	25.0654	24.0018	22.7790	21.3918	19.8421	18.1412	16.3110	14.3853
5.6	38.8396	36.0392	35.4103	34.6560	33.7577	32.6964	31.4546	30.0172	28.3738	26.5217	24.4680	22.2324	19.8494	17.3683
5.8	49.9151	45.9919	45.1187	44.0747	42.8356	41.3780	39.6802	37.7255	35.5044	33.0184	30.2836	27.3331	24.2195	21.0137
6.0	64.6578	59.1100	57.8873	56.4301	54.7075	52.6898	50.3515	47.6748	44.6533	41.2970	37.6359	33.7240	29.6397	25.4839
6.2	84.5200	76.5893	74.8602	72.8068	70.3894	67.5714	64.3236	60.6290	56.4883	51.9261	46.9951	41.7804	36.3979	30.9905
6.4	111.7860	100.2887	97.8111	94.8809	91.4469	87.4648	82.9029	77.7491	72.0181	65.7595	59.0624	52.0587	44.9190	37.8436
.8	2.7941	2.7578	2.7488	2.7377	2.7240	2.7072	2.6866	2.6614	2.6306	2.5933	2.5485	2.4948	2.4312	2.3564
1.0	3.4872	3.4324	3.4190	3.4024	3.3819	3.3568	3.3261	3.2885	3.2430	3.1882	3.1222	3.0438	2.9512	2.8431
1.2	4.3337	4.2537	4.2341	4.2101	4.1805	4.1443	4.1000	4.0461	3.9810	3.9026	3.8090	3.6982	3.5680	3.4171
1.4	5.3729	5.2586	5.2308	5.1968	5.1548	5.1035	5.0410	4.9654	4.8740	4.7647	4.6347	4.4814	4.3025	4.0964
1.6	6.6507	6.4898	6.4510	6.4032	6.3447	6.2733	6.1865	6.0817	5.9557	5.8054	5.6276	5.4190	5.1771	4.9002
1.8	8.2298	8.0053	7.9514	7.8853	7.8045	7.7060	7.5868	7.4431	7.2710	7.0666	6.8259	6.5453	6.2219	5.8542
2.0	10.1874	9.8764	9.8021	9.7112	9.6002	9.4654	9.3026	9.1071	8.8740	8.5982	8.2750	7.9002	7.4712	6.9872
2.2	12.6299	12.2004	12.0984	11.9738	11.8222	11.6383	11.4170	11.1522	10.8376	10.4671	10.0353	9.5377	8.9719	8.3384
2.4	15.6872	15.0952	14.9556	14.7852	14.5785	14.3285	14.0285	13.6708	13.2477	12.7517	12.1769	11.5187	10.7755	9.9502
2.6	19.5377	18.7222	18.5310	18.2982	18.0164	17.6768	17.2706	16.7880	16.2196	15.5569	14.7931	13.9243	12.9507	11.8788
2.8	24.4214	23.2959	23.0338	22.7156	22.3311	21.8693	21.3188	20.6675	19.9041	19.0186	18.0043	16.8584	15.5848	14.1946
3.0	30.6500	29.0928	28.7326	28.2965	27.7711	27.1423	26.3952	25.5151	24.4886	23.3048	21.9573	20.4463	18.7806	16.9798
3.2	38.6743	36.5098	36.0133	35.4131	34.6925	33.8329	32.8157	31.6230	30.2391	28.6526	26.8591	24.8636	22.6833	20.3492
3.4	49.0869	46.0620	45.3736	44.5441	43.5512	42.3712	40.9807	39.3581	37.4861	35.3538	32.9608	30.3202	27.4619	24.4343
3.6	62.7300	58.4735	57.5132	56.3599	54.9839	53.3550	51.4442	49.2264	46.6828	43.8054	40.6015	37.0972	33.3415	29.4073
3.8	80.8257	74.7837	73.4338	71.8173	69.8959	67.6312	64.9880	61.9370	58.4605	54.5568	50.2462	45.5761	40.6241	35.4980
4.0	105.0980	96.4358	94.5204	92.2347	89.5288	86.3546	82.6691	78.4415	73.6574	68.3285	62.4972	56.2436	49.6876	42.9868
4.2	138.1140	125.5465	122.7986	119.5325	115.6832	111.1899	106.0038	100.0940	93.4578	86.1291	78.1879	69.7650	61.0425	52.2477

O = N

I = N

TABLE II.—*Continued.*

	r/r_0	.06309574	.07943282	.10000000	.12589254	.15848932	.19952623	.25118866	.31622777	.39810717	.50118724	.63095735	.79432824	1.00000000
γ	Z													
2.0	.6056	.4606	.4327	.4010	.3654	.3260	.2830	.2369	.1884	.1383	.0878	.0382	−.0090	−.0542
2.2	.7865	.5841	.5450	.5010	.4520	.3983	.3403	.2787	.2144	.1484	.0820	.0167	−.0464	−.1078
2.4	1.0098	.7344	.6837	.6270	.5646	.4971	.4251	.3495	.2713	.1917	.1120	.0338	−.0417	−.1154
2.6	1.2857	.9222	.8579	.7858	.7066	.6213	.5308	.4362	.3386	.2391	.1396	.0412	−.0564	−.1504
2.8	1.6266	1.1523	1.0715	.9815	.8827	.7763	.6632	.5449	.4229	.2985	.1741	.0511	−.0703	−.1875
3.0	2.0460	1.4307	1.3299	1.2181	1.0951	.9628	.8226	.6757	.5243	.3699	.2156	.0631	−.0866	−.2305
3.2	2.5640	1.7650	1.6398	1.5017	1.3498	1.1867	1.0136	.8324	.6457	.4552	.2649	.0772	−.1057	−.2809
3.4	3.2042	2.1648	2.0101	1.8398	1.6529	1.4527	1.2398	1.0178	.7892	.5559	.3233	.0938	−.1283	−.3407
3.6	3.9959	2.6417	2.4519	2.2439	2.0150	1.7705	1.5107	1.2398	.9606	.6762	.3929	.1138	−.1552	−.4119
3.8	4.9781	3.2090	2.9776	2.7248	2.4459	2.1486	1.8331	1.5044	1.1653	.8199	.4759	.1376	−.1873	−.4967
4.0	6.1997	3.8824	3.6010	3.2948	2.9570	2.5971	2.2154	1.8178	1.4076	.9899	.5741	.1658	−.2253	−.5971
4.2	7.7255	4.6801	4.3408	3.9707	3.5636	3.1297	2.6691	2.1899	1.6953	1.1919	.6906	.1992	−.2701	−.7154
4.4	9.6377	5.6234	5.2145	4.7701	4.2801	3.7589	3.2049	2.6292	2.0347	1.4299	.8276	.2383	−.3227	−.8541
4.6	12.0472	6.7370	6.2469	5.7133	5.1259	4.5016	3.8378	3.1475	2.4355	1.7110	.9895	.2845	−.3847	−1.0170
4.8	15.0988	8.0503	7.4623	6.8251	6.1229	5.3764	4.5829	3.7589	2.9081	2.0429	1.1809	.3392	−.4581	−1.2099
5.0	18.9896	9.5977	8.8944	8.1327	7.2938	6.4037	5.4581	4.4757	3.4617	2.4307	1.4046	.4031	−.5443	−1.4370
5.2	23.9775	11.4191	10.5777	9.6665	8.6665	7.6088	6.4821	5.3133	4.1079	2.8837	1.6656	.4776	−.6447	−1.7000
5.4	30.4348	13.5610	12.5553	11.4737	10.2833	9.0251	7.6867	6.2990	4.8661	3.4139	1.9705	.5646	−.7615	−2.0066
5.6	38.8396	16.0772	14.8756	13.5900	12.1756	10.6837	9.0944	7.4519	5.7519	4.0329	2.3256	.6661	−.8972	−2.3615
5.8	49.9151	19.0313	17.6005	16.0696	14.3889	12.6259	10.7466	8.8042	6.7923	4.7586	2.7419	.7846	−1.0545	−2.7737
6.0	64.6578	22.4990	20.7973	18.9837	16.9933	14.9107	12.6867	10.3900	8.0123	5.6109	3.2307	.9232	−1.2369	−3.2505
6.2	84.5200	26.5702	24.5515	22.4000	20.0435	17.5837	14.9594	12.2469	9.4419	6.6077	3.8031	1.0851	−1.4484	−3.8037
6.4	111.7860	31.3520	28.9553	26.4080	23.6299	20.7199	17.6228	14.4253	11.1179	7.7777	4.4756	1.2755	−1.6935	−4.4469
.8	2.7941	2.2693	2.1703	2.0581	1.9317	1.7904	1.6339	1.4624	1.2763	1.0760	.8622	.6358	.3980	.1500
1.0	3.4872	2.7344	2.6116	2.4756	2.3254	2.1606	1.9811	1.7870	1.5787	1.3568	1.1221	.8757	.6188	.3525
1.2	4.3337	3.3139	3.1625	2.9955	2.8120	2.6118	2.3951	2.1624	1.9145	1.6538	1.3814	1.0982	.8054	.5040
1.4	5.3729	4.0284	3.8417	3.6369	3.4134	3.1708	2.9096	2.6305	2.3344	2.0221	1.6955	1.3597	1.0161	.6660
1.6	6.6507	4.8900	4.6597	4.4098	4.1394	3.8481	3.5365	3.2057	2.8572	2.4929	2.1150	1.7260	1.3264	.8760
1.8	8.2298	5.9124	5.6299	5.3260	4.9995	4.6499	4.2781	3.8857	3.4748	3.0477	2.6071	2.1560	1.6977	1.1888
2.0	10.1874	7.1109	6.7702	6.4035	6.0102	5.5894	5.1423	4.6710	4.1781	3.6665	3.1393	2.5997	2.0500	1.4939
2.2	12.6299	8.5030	8.0941	7.6562	7.1882	6.6892	6.1607	5.5955	5.0062	4.3940	3.7624	3.1165	2.4594	1.8000
2.4	15.6872	10.1080	9.6224	9.1008	8.5432	7.9484	7.3184	6.6475	5.9477	5.2221	4.4723	3.7054	2.9256	2.1444
2.6	19.5377	11.9477	11.3744	10.7561	10.0977	9.3944	8.6485	7.8577	7.0307	6.1732	5.2874	4.3827	3.4624	2.5408
2.8	24.4214	14.0464	13.3703	12.6446	11.8691	11.0438	10.1688	9.2442	8.2702	7.2618	6.2196	5.1557	4.0748	2.9931
3.0	30.6500	16.4312	15.6373	14.7877	13.8824	12.9214	11.9048	10.8328	9.7055	8.5229	7.3004	6.0525	4.7855	3.5195
3.2	38.6743	19.1319	18.2048	17.2196	16.1763	15.0749	13.9154	12.6980	11.4228	10.0898	8.6992	7.2511	5.7455	4.2327
3.4	49.0869	22.1814	21.1109	19.9722	18.7654	17.4904	16.1473	14.7362	13.2572	11.7304	10.1459	8.5040	6.8048	5.0484
3.6	62.7300	25.6154	24.3917	23.0948	21.7247	20.2815	18.7652	17.1760	15.5140	13.7793	11.9720	10.0973	8.1654	6.1763
3.8	80.8257	29.4729	28.0866	26.6277	25.0962	23.4922	21.8158	20.0671	18.2462	16.3532	14.3882	12.3513	10.2426	8.0622
4.0	105.0980	33.7961	32.2381	30.6084	28.9071	27.1343	25.2901	23.3746	21.3879	19.3301	17.2014	15.0020	12.7321	10.3919
4.2	138.1140	38.6312	36.8930	35.0844	33.2055	31.2564	29.2372	27.1480	24.9889	22.7601	20.4617	18.0939	15.6569	13.1508

TABLE II.—*Continued.*

		r/r_0	.06309574	.07943282	.10000000	.12589254	.15848932	.19952623	.25118865	.31622777	.39810717	.50118724	.63095735	.79432824	1.00000000
	γ	Z													
O=N	2.0	.6056	.4600	.4307	.3970	.3588	.3163	.2701	.2213	.1713	.1223	.0770	.0388	.0113	.0000
	2.2	.7865	.5845	.5449	.4997	.4490	.3932	.3332	.2706	.2075	.1467	.0914	.0455	.0131	.0000
	2.4	1.0098	.7333	.6806	.6209	.5545	.4823	.4056	.3266	.2481	.1736	.1070	.0527	.0150	.0000
	2.6	1.2857	.9113	.8417	.7637	.6779	.5855	.4885	.3900	.2934	.2032	.1240	.0603	.0170	.0000
	2.8	1.6266	1.1237	1.0329	.9319	.8219	.7047	.5833	.4616	.3440	.2358	.1423	.0686	.0192	.0000
	3.0	2.0460	1.3756	1.2580	1.1285	.9887	.8415	.6908	.5417	.3998	.2713	.1620	.0772	.0214	.0000
	3.2	2.5640	1.6751	1.5238	1.3586	1.1822	.9986	.8129	.6316	.4617	.3101	.1832	.0864	.0237	.0000
	3.4	3.2042	2.0306	1.8370	1.6276	1.4062	1.1784	.9511	.7321	.5299	.3522	.2059	.0961	.0261	.0000
	3.6	3.9959	2.4519	2.2053	1.9411	1.6649	1.3839	1.1071	.8441	.6048	.3978	.2301	.1063	.0286	.0000
	3.8	4.9781	2.9517	2.6388	2.3069	1.9635	1.6185	1.2830	.9688	.6871	.4473	.2560	.1170	.0312	.0000
	4.0	6.1997	3.5443	3.1485	2.7329	2.3078	1.8860	1.4811	1.1074	.7773	.5006	.2835	.1282	.0338	.0000
	4.2	7.7255	4.2481	3.7487	3.2297	2.7050	2.1908	1.7041	1.2612	.8760	.5582	.3128	.1400	.0366	.0000
	4.4	9.6377	5.0841	4.4552	3.8086	3.1627	2.5379	1.9546	1.4317	.9838	.6202	.3439	.1524	.0394	.0000
	4.6	12.0472	6.0791	5.2881	4.4840	3.6905	2.9332	2.2362	1.6206	1.1016	.6869	.3768	.1653	.0424	.0000
	4.8	15.0988	7.2648	6.2709	5.2721	4.2990	3.3830	2.5522	1.8296	1.2300	.7586	.4117	.1788	.0454	.0000
	5.0	18.9896	8.6815	7.4328	6.1933	5.0015	3.8954	2.9071	2.0609	1.3700	.8355	.4486	.1928	.0486	.0000
	5.2	23.9775	10.3751	8.8068	7.2696	5.8116	4.4781	3.3048	2.3163	1.5221	.9179	.4875	.2074	.0518	.0000
	5.4	30.4348	12.4096	10.4384	8.5317	6.7487	5.1426	3.7517	2.5988	1.6879	1.0064	.5287	.2227	.0551	.0000
	5.6	38.8396	14.8521	12.3734	10.0086	7.8307	5.8978	4.2516	2.9099	1.8676	1.1007	.5720	.2385	.0585	.0000
	5.8	49.9151	17.8021	14.6807	11.7456	9.0838	6.7597	4.8132	3.2537	2.0630	1.2018	.6176	.2549	.0620	.0000
	6.0	64.6578	21.3748	17.4373	13.7906	10.5367	7.7428	5.4433	3.6332	2.2753	1.3097	.6657	.2720	.0655	.0000
	6.2	84.5200	25.7174	20.7397	16.2048	12.2230	8.8650	6.1504	4.0519	2.5055	1.4250	.7162	.2897	.0692	.0000
	6.4	111.7860	31.0457	24.7304	19.0739	14.1946	10.1546	6.9489	4.5166	2.7568	1.5489	.7698	.3082	.0730	.0000
I=N	.8	2.7941	2.2694	2.1697	2.0570	1.9321	1.7968	1.6543	1.5093	1.3683	1.2394	1.1314	1.0531	1.0103	1.0000
	1.0	3.4872	2.7183	2.5762	2.4173	2.2428	2.0559	1.8614	1.6659	1.4784	1.3091	1.1689	1.0683	1.0134	1.0000
	1.2	4.3337	3.2440	3.0487	2.8322	2.5970	2.3478	2.0918	1.8379	1.5976	1.3835	1.2086	1.0841	1.0166	1.0000
	1.4	5.3729	3.8620	3.5996	3.3115	3.0019	2.6778	2.3488	2.0271	1.7269	1.4632	1.2505	1.1008	1.0200	1.0000
	1.6	6.6507	4.5878	4.2412	3.8643	3.4639	3.0497	2.6348	2.2347	1.8667	1.5480	1.2945	1.1181	1.0235	1.0000
	1.8	8.2298	5.4427	4.9903	4.5036	3.9921	3.4698	2.9536	2.4628	2.0180	1.6386	1.3409	1.1362	1.0271	1.0000
	2.0	10.1874	6.4501	5.8653	5.2425	4.5958	3.9439	3.3084	2.7130	2.1816	1.7349	1.3895	1.1549	1.0309	1.0000
	2.2	12.6299	7.6416	6.8905	6.0992	5.2877	4.4803	3.7042	2.9882	2.3586	1.8378	1.4407	1.1743	1.0348	1.0000
	2.4	15.6872	9.0506	8.0909	7.0915	6.0793	5.0858	4.1448	3.2898	2.5498	1.9470	1.4943	1.1945	1.0388	1.0000
	2.6	19.5377	10.7215	9.5000	8.2430	6.9862	5.7702	4.6355	3.6205	2.7561	2.0631	1.5505	1.2153	1.0429	1.0000
	2.8	24.4214	12.7089	11.1582	9.5821	8.0274	6.5448	5.1826	3.9836	2.9791	2.1867	1.6093	1.2369	1.0471	1.0000
	3.0	30.6500	15.0753	13.1105	11.1392	9.2217	7.4206	5.7916	4.3812	3.2193	2.3176	1.6708	1.2591	1.0514	1.0000
	3.2	38.6743	17.9082	15.4205	12.9579	10.5972	8.4141	6.4718	4.8183	3.4790	2.4571	1.7353	1.2822	1.0558	1.0000
	3.4	49.0869	21.3044	18.1557	15.0824	12.1806	9.5402	7.2302	5.2974	3.7590	2.6049	1.8027	1.3060	1.0604	1.0000
	3.6	62.7300	25.3903	21.4038	17.5695	14.0062	10.8177	8.0763	5.8229	4.0609	2.7617	1.8730	1.3305	1.0650	1.0000
	3.8	80.8257	30.3321	25.2784	20.4924	16.1192	12.2706	9.0221	6.4002	4.3870	2.9282	1.9466	1.3558	1.0698	1.0000
	4.0	105.0980	36.3275	29.9108	23.9325	18.5639	13.9237	10.0791	7.0339	4.7386	3.1048	2.0234	1.3819	1.0746	1.0000
	4.2	138.1140	43.6363	35.4711	27.9962	21.3997	15.8068	11.2612	7.7298	5.1178	3.2921	2.1036	1.4087	1.0796	1.0000

TABLE III. Values of $r^{\frac{1}{2}}\rho$.

	r/r_0	.00316228	.00398107	.00501187	.00630957	.00794328	.01000000	.01258926	.01584893	.01995262	.02511887	.03162278	.03981072	.05011872
γ	Z													
2.0	.6056	.0476	.0478	.0480	.0481	.0483	.0483	.0483	.0483	.0481	.0477	.0472	.0464	.0453
2.2	.7865	.0698	.0699	.0701	.0702	.0702	.0701	.0699	.0695	.0689	.0680	.0669	.0653	.0633
2.4	1.0098	.1006	.1006	.1007	.1006	.1004	.1000	.0994	.0985	.0972	.0956	.0934	.0906	.0872
2.6	1.2857	.1432	.1431	.1429	.1425	.1419	.1410	.1397	.1380	.1357	.1327	.1289	.1243	.1187
2.8	1.6266	.2021	.2017	.2011	.2002	.1989	.1971	.1947	.1916	.1876	.1826	.1765	.1690	.1601
3.0	2.0460	.2828	.2819	.2806	.2788	.2764	.2732	.2691	.2639	.2573	.2493	.2395	.2278	.2142
3.2	2.5640	.3937	.3919	.3895	.3863	.3821	.3768	.3699	.3615	.3510	.3383	.3232	.3054	.2849
3.4	3.2042	.5458	.5426	.5385	.5331	.5261	.5174	.5064	.4930	.4766	.4571	.4341	.4074	.3770
3.6	3.9959	.7544	.7490	.7421	.7332	.7220	.7081	.6909	.6701	.6450	.6154	.5808	.5413	.4969
3.8	4.9781	1.0412	1.0323	1.0210	1.0069	.9892	.9675	.9409	.9090	.8710	.8265	.7752	.7172	.6529
4.0	6.1997	1.4361	1.4218	1.4039	1.3816	1.3541	1.3205	1.2799	1.2315	1.1745	1.1083	1.0328	.9484	.8559
4.2	7.7255	1.9822	1.9597	1.9316	1.8969	1.8544	1.8030	1.7413	1.6684	1.5833	1.4855	1.3750	1.2527	1.1204
4.4	9.6377	2.7402	2.7049	2.6611	2.6075	2.5424	2.4641	2.3710	2.2617	2.1352	1.9912	1.8301	1.6538	1.4654
4.6	12.0472	3.7983	3.7431	3.6754	3.5929	3.4934	3.3746	3.2343	3.0709	2.8834	2.6718	2.4376	2.1841	1.9164
4.8	15.0988	5.2839	5.1982	5.0934	4.9668	4.8149	4.6348	4.4237	4.1796	3.9018	3.5912	3.2511	2.8869	2.5073
5.0	18.9896	7.3857	7.2524	7.0906	6.8960	6.6640	6.3907	6.0726	5.7076	5.2958	4.8397	4.3453	3.8223	3.2842
5.2	23.9775	10.3792	10.1718	9.9213	9.6217	9.2667	8.8510	8.3706	7.8238	7.2121	6.5413	5.8221	5.0705	4.3076
5.4	30.4348	14.6915	14.3671	13.9775	13.5139	12.9680	12.3329	11.6043	10.7816	9.8697	8.8796	7.8302	6.7475	5.6641
5.6	38.8396	20.9477	20.4379	19.8287	19.1078	18.2639	17.2887	16.1784	14.9352	13.5701	12.1039	10.5682	9.0051	7.4640
5.8	49.9151	30.1558	29.3478	28.3872	27.2566	25.9416	24.4326	22.7280	20.8363	18.7797	16.5957	14.3372	12.0707	9.8712
6.0	64.6578	43.8797	42.5861	41.0561	39.2657	37.1971	34.8406	32.2006	29.2986	26.1772	22.9022	19.5610	16.2582	13.1060
6.2	84.5200	64.6390	62.5422	60.0754	57.2069	53.9151	50.1949	46.0642	41.5692	36.7898	31.8393	26.8614	22.0194	17.4800
6.4	111.7860	96.7453	93.2884	89.2455	84.5748	79.2548	73.2935	66.7383	59.6830	52.2739	44.7063	37.2150	30.0537	23.4671
.8	2.7941	.4500	.4492	.4481	.4465	.4443	.4414	.4375	.4324	.4259	.4178	.4077	.3952	.3803
1.0	3.4872	.6240	.6223	.6200	.6168	.6125	.6070	.6000	.5910	.5798	.5659	.5489	.5285	.5043
1.2	4.3337	.8597	.8564	.8520	.8461	.8387	.8291	.8170	.8020	.7834	.7608	.7337	.7014	.6637
1.4	5.3729	1.1799	1.1739	1.1662	1.1562	1.1436	1.1277	1.1080	1.0836	1.0540	1.0184	.9760	.9263	.8692
1.6	6.6507	1.6152	1.6050	1.5920	1.5756	1.5550	1.5294	1.4979	1.4595	1.4133	1.3583	1.2936	1.2188	1.1337
1.8	8.2298	2.2093	2.1927	2.1715	2.1451	2.1122	2.0719	2.0226	1.9631	1.8921	1.8084	1.7112	1.6000	1.4751
2.0	10.1874	3.0231	2.9961	2.9624	2.9206	2.8691	2.8061	2.7301	2.6390	2.5314	2.4056	2.2610	2.0975	1.9161
2.2	12.6299	4.1444	4.1017	4.0485	3.9831	3.9030	3.8060	3.6896	3.5514	3.3893	3.2017	2.9882	2.7494	2.4878
2.4	15.6872	5.6958	5.6285	5.5454	5.4438	5.3203	5.1717	4.9946	4.7859	4.5431	4.2649	3.9514	3.6047	3.2296
2.6	19.5377	7.8568	7.7514	7.6223	7.4650	7.2752	7.0483	6.7797	6.4656	6.1032	5.6918	5.2328	4.7310	4.1952
2.8	24.4214	10.8911	10.7266	10.5259	10.2831	9.9916	9.6453	9.2382	8.7658	8.2254	7.6174	6.9462	6.2213	5.4573
3.0	30.6500	15.1810	14.9240	14.6122	14.2368	13.7890	13.2601	12.6427	11.9318	11.1255	10.2270	9.2459	8.1990	7.1109
3.2	38.6743	21.3174	20.9148	20.4284	19.8462	19.1555	18.3448	17.4053	16.3320	15.1253	13.7943	12.3571	10.8434	9.2921
3.4	49.0869	30.1761	29.5416	28.7795	27.8716	26.8009	25.5527	24.1164	22.4888	20.6764	18.6980	16.5873	14.3934	12.1788
3.6	62.7300	43.1163	42.1098	40.9068	39.4814	37.8103	35.8751	33.6656	31.1835	28.4464	25.4921	22.3795	19.1894	16.0196
3.8	80.8257	62.3011	60.6888	58.7703	56.5103	53.8778	50.8511	47.4233	43.6076	39.4439	35.0023	30.3851	25.7237	21.1690
4.0	105.0980	91.1485	88.5346	85.4406	81.8168	77.6245	72.8404	67.4694	61.5492	55.1610	48.4329	41.5379	34.6871	28.1114
4.2	138.1140	135.2802	130.9798	125.9188	120.0293	113.2630	105.6061	97.0888	87.8009	77.8994	67.6121	57.2309	47.0916	37.5428

O = N

I = N

TABLE III.—*Continued.*

	r/r_0	.06309574	.07943282	.10000000	.12589254	.15848932	.19952623	.25118865	.31622777	.39810717	.50118723	.63095734	.79432823	1.0000000
γ	Z													
2.0	.6056	.0440	.0424	.0405	.0384	.0361	.0337	.0312	.0287	.0262	.0237	.0213	.0190	.0169
2.2	.7865	.0610	.0585	.0557	.0527	.0495	.0461	.0427	.0392	.0358	.0324	.0291	.0260	.0231
2.4	1.0098	.0833	.0791	.0746	.0699	.0650	.0600	.0550	.0501	.0453	.0407	.0364	.0324	.0287
2.6	1.2857	.1120	.1060	.0995	.0927	.0857	.0786	.0716	.0647	.0580	.0517	.0458	.0403	.0353
2.8	1.6266	.1498	.1414	.1324	.1230	.1132	.1033	.0933	.0835	.0741	.0652	.0569	.0494	.0425
3.0	2.0460	.1992	.1879	.1757	.1629	.1496	.1360	.1224	.1089	.0958	.0834	.0719	.0614	.0520
3.2	2.5640	.2631	.2482	.2321	.2150	.1973	.1793	.1613	.1435	.1262	.1098	.0945	.0806	.0681
3.4	3.2042	.3449	.3254	.3042	.2817	.2584	.2348	.2111	.1877	.1650	.1434	.1233	.1050	.0885
3.6	3.9959	.4484	.4230	.3953	.3659	.3355	.3047	.2738	.2432	.2136	.1855	.1594	.1356	.1142
3.8	4.9781	.5780	.5451	.5092	.4711	.4318	.3920	.3521	.3126	.2744	.2381	.2045	.1738	.1462
4.0	6.1997	.7387	.6963	.6502	.6012	.5508	.4998	.4488	.3982	.3493	.3029	.2598	.2206	.1854
4.2	7.7255	.9362	.8822	.8232	.7609	.6967	.6321	.5674	.5033	.4412	.3823	.3276	.2778	.2332
4.4	9.6377	1.1766	1.1085	1.0341	.9553	.8748	.7932	.7117	.6312	.5531	.4791	.4103	.3476	.2915
4.6	12.0472	1.4677	1.3817	1.2877	1.1894	1.0887	.9869	.8853	.7849	.6876	.5954	.5097	.4317	.3618
4.8	15.0988	1.8230	1.7145	1.5972	1.4744	1.3487	1.2220	.9961	.8708	.7627	.6602	.5648	.4780	.4004
5.0	18.9896	2.2577	2.1211	1.9741	1.8209	1.6650	1.5083	1.3523	1.1980	1.0490	.9076	.7762	.6567	.5498
5.2	23.9775	2.7900	2.6179	2.4340	2.2434	2.0509	1.8567	1.6648	1.4748	1.2910	1.1170	.9549	.8076	.6759
5.4	30.4348	3.4417	3.2261	2.9973	2.7604	2.5220	2.2827	2.0463	1.8123	1.5862	1.3721	1.1727	.9918	.8297
5.6	38.8396	4.2387	3.9705	3.6862	3.3923	3.0979	2.8033	2.5134	2.2258	1.9480	1.6848	1.4398	1.2174	1.0183
5.8	49.9151	5.2111	4.8777	4.5259	4.1636	3.8015	3.4400	3.0837	2.7312	2.3900	2.0671	1.7665	1.4935	1.2490
6.0	64.6578	6.4028	5.9906	5.5553	5.1103	4.6657	4.2217	3.7837	3.3509	2.9327	2.5364	2.1677	1.8324	1.5327
6.2	84.5200	7.8662	7.3566	6.8216	6.2741	5.7282	5.1837	4.6457	4.1145	3.6010	3.1142	2.6617	2.2496	1.8815
6.4	111.7860	9.6618	9.0346	8.3777	7.7048	7.0335	6.3660	5.7054	5.0527	4.4218	3.8246	3.2685	2.7628	2.3104
.8	2.7941	.3630	.3432	.3211	.2971	.2719	.2460	.2200	.1943	.1693	.1455	.1232	.1033	.0858
1.0	3.4872	.4756	.4497	.4207	.3892	.3562	.3223	.2883	.2545	.2218	.1906	.1614	.1353	.1124
1.2	4.3337	.6060	.5730	.5360	.4958	.4537	.4105	.3671	.3241	.2824	.2427	.2056	.1723	.1431
1.4	5.3729	.7625	.7209	.6744	.6238	.5708	.5164	.4620	.4078	.3553	.3054	.2587	.2168	.1800
1.6	6.6507	.9477	.8960	.8382	.7754	.7094	.6417	.5741	.5069	.4416	.3795	.3215	.2694	.2237
1.8	8.2298	1.1647	1.1012	1.0300	.9528	.8717	.7886	.7055	.6229	.5426	.4663	.3951	.3310	.2749
2.0	10.1874	1.4172	1.3398	1.2533	1.1593	1.0607	.9596	.8585	.7579	.6601	.5673	.4806	.4027	.3344
2.2	12.6299	1.7095	1.6164	1.5119	1.3987	1.2797	1.1579	1.0360	.9145	.7966	.6846	.5799	.4859	.4035
2.4	15.6872	2.0463	1.9352	1.8104	1.6748	1.5323	1.3864	1.2404	1.0950	.9537	.8196	.6943	.5817	.4831
2.6	19.5377	2.4331	2.3010	2.1527	1.9916	1.8225	1.6488	1.4751	1.3020	1.1339	.9744	.8254	.6916	.5743
2.8	24.4214	2.8756	2.7195	2.5441	2.3541	2.1539	1.9486	1.7433	1.5388	1.3402	1.1516	.9756	.8174	.6788
3.0	30.6500	3.3799	3.1969	2.9911	2.7673	2.5324	2.2910	2.0496	1.8089	1.5753	1.3535	1.1465	.9606	.7977
3.2	38.6743	3.9525	3.7385	3.4973	3.2362	2.9614	2.6788	2.3969	2.1156	1.8422	1.5829	1.3406	1.1232	.9328
3.4	49.0869	4.6000	4.3510	4.0697	3.7655	3.4457	3.1170	2.7886	2.4614	2.1434	1.8413	1.5594	1.3067	1.0850
3.6	62.7300	5.3291	5.0410	4.7151	4.3631	3.9929	3.6120	3.2315	2.8523	2.4839	2.1341	1.8069	1.5141	1.2571
3.8	80.8257	6.1466	5.8141	5.4387	5.0325	4.6061	4.1670	3.7280	3.2901	2.8651	2.4614	2.0841	1.7461	1.4496
4.0	105.0980	7.0595	6.6771	6.2466	5.7797	5.2896	4.7851	4.2810	3.7784	3.2901	2.8264	2.3931	2.0048	1.6643
4.2	138.1140	8.0747	7.6387	7.1459	6.6124	6.0514	5.4732	4.8962	4.3220	3.7633	3.2324	2.7367	2.2926	1.9031

		4.0	105.0980	91.1485	88.5346	85.4406	81.8168	77.6245	72.8404	67.4694	61.5492	55.1610	48.4329	41.5379	34.6871	28.1114
		4.2	138.1140	135.2802	130.9798	125.9188	120.0293	113.2630	105.6061	97.0888	87.8009	77.8994	67.6121	57.2309	47.0916	37.5428

TABLE III.—*Continued.*

		r/r_0	.06309574	.07943282	.10000000	.12589254	.15848932	.19952623	.25118865	.31622777	.39810717	.50118724	.63095735	.79432824	1.00000000
	γ	Z													
N = 0	2.0	.6056	.0439	.0422	.0400	.0374	.0344	.0310	.0273	.0234	.0195	.0157	.0123	.0096	.0095
	2.2	.7865	.0608	.0578	.0542	.0500	.0453	.0401	.0346	.0291	.0236	.0185	.0141	.0107	.0103
	2.4	1.0098	.0830	.0781	.0723	.0658	.0587	.0511	.0433	.0356	.0283	.0216	.0160	.0117	.0109
	2.6	1.2857	.1120	.1043	.0955	.0858	.0754	.0645	.0537	.0432	.0335	.0250	.0180	.0127	.0116
	2.8	1.6266	.1498	.1380	.1249	.1108	.0959	.0807	.0659	.0520	.0394	.0287	.0201	.0138	.0121
	3.0	2.0460	.1986	.1812	.1621	.1418	.1209	.1002	.0803	.0620	.0460	.0328	.0223	.0149	.0129
	3.2	2.5640	.2618	.2363	.2090	.1804	.1516	.1235	.0972	.0736	.0535	.0372	.0247	.0160	.0136
	3.4	3.2042	.3433	.3066	.2679	.2282	.1889	.1513	.1169	.0868	.0618	.0419	.0272	.0172	.0142
	3.6	3.9959	.4482	.3961	.3419	.2873	.2342	.1845	.1400	.1019	.0710	.0471	.0298	.0184	.0148
	3.8	4.9781	.5833	.5098	.4347	.3602	.2891	.2240	.1668	.1191	.0812	.0527	.0326	.0196	.0155
	4.0	6.1997	.7571	.6543	.5508	.4500	.3556	.2708	.1980	.1386	.0926	.0588	.0356	.0208	.0161
	4.2	7.7255	.9809	.8380	.6962	.5606	.4360	.3263	.2342	.1607	.1051	.0654	.0386	.0221	.0167
	4.4	9.6377	1.2693	1.0714	.8782	.6967	.5331	.3920	.2761	.1858	.1190	.0725	.0419	.0234	.0172
	4.6	12.0472	1.6417	1.3685	1.1062	.8642	.6503	.4697	.3246	.2141	.1344	.0801	.0453	.0247	.0178
	4.8	15.0988	2.1231	1.7469	1.3920	1.0705	.7919	.5616	.3807	.2461	.1513	.0883	.0488	.0261	.0184
	5.0	18.9896	2.7474	2.2302	1.7508	1.3246	.9628	.6702	.4455	.2822	.1699	.0971	.0526	.0274	.0190
	5.2	23.9775	3.5580	2.8477	2.2010	1.6374	1.1689	.7982	.5202	.3228	.1904	.1065	.0565	.0288	.0195
	5.4	30.4348	4.6162	3.6403	2.7684	2.0238	1.4181	.9497	.6065	.3686	.2129	.1167	.0606	.0303	.0201
	5.6	38.8396	5.9979	4.6570	3.4823	2.5002	1.7184	1.1280	.7057	.4201	.2376	.1275	.0649	.0317	.0207
	5.8	49.9151	7.8147	5.9692	4.3852	3.0897	2.0819	1.3388	.8201	.4780	.2647	.1391	.0694	.0332	.0212
	6.0	64.6578	10.2127	7.6676	5.5294	3.8202	2.5217	1.5877	.9520	.5430	.2944	.1516	.0740	.0347	.0218
	6.2	84.5200	13.3936	9.8740	6.9842	4.7266	3.0544	1.8816	1.1038	.6161	.3270	.1649	.0789	.0363	.0223
	6.4	111.7860	17.6600	12.7691	8.8482	5.8606	3.7041	2.2311	1.2797	.6986	.3629	.1792	.0841	.0378	.0228
N = 1	.8	2.7941	.3624	.3416	.3176	.2906	.2609	.2290	.1958	.1620	.1288	.0968	.0666	.0375	.0048
	1.0	3.4872	.4760	.4435	.4070	.3669	.3238	.2788	.2332	.1886	.1463	.1075	.0725	.0405	.0057
	1.2	4.3337	.6204	.5715	.5177	.4596	.3987	.3368	.2759	.2180	.1651	.1185	.0783	.0433	.0065
	1.4	5.3729	.8045	.7326	.6548	.5727	.4885	.4048	.3247	.2509	.1855	.1300	.0841	.0460	.0073
	1.6	6.6507	1.0387	.9351	.8247	.7103	.5956	.4843	.3804	.2874	.2076	.1421	.0900	.0485	.0081
	1.8	8.2298	1.3377	1.1900	1.0353	.8782	.7237	.5774	.4442	.3282	.2316	.1548	.0960	.0510	.0088
	2.0	10.1874	1.7192	1.5109	1.2965	1.0826	.8768	.6862	.5171	.3736	.2576	.1682	.1021	.0535	.0095
	2.2	12.6299	2.2079	1.9162	1.6211	1.3323	1.0602	.8139	.6006	.4244	.2860	.1825	.1084	.0559	.0103
	2.4	15.6872	2.8338	2.4278	2.0242	1.6369	1.2794	.9631	.6959	.4810	.3168	.1975	.1148	.0583	.0109
	2.6	19.5377	3.6379	3.0752	2.5257	2.0086	1.5416	1.1378	.8050	.5442	.3503	.2135	.1215	.0607	.0116
	2.8	24.4214	4.6743	3.8968	3.1513	2.4636	1.8557	1.3423	.9296	.6146	.3867	.2304	.1283	.0630	.0123
	3.0	30.6500	6.0127	4.9405	3.9316	3.0198	2.2317	1.5816	1.0720	.6930	.4262	.2482	.1353	.0654	.0129
	3.2	38.6743	7.7514	6.2735	4.9096	3.7028	2.6832	1.8623	1.2350	.7806	.4692	.2672	.1426	.0678	.0136
	3.4	49.0869	10.0156	7.9787	6.1363	4.5414	3.2251	2.1912	1.4212	.8782	.5159	.2873	.1501	.0702	.0142
	3.6	62.7300	12.9776	10.1676	7.6789	5.5729	3.8762	2.5768	1.6340	.9868	.5666	.3085	.1579	.0725	.0148
	3.8	80.8257	16.8776	12.9934	9.6280	6.8474	4.6606	3.0297	1.8777	1.1080	.6218	.3311	.1659	.0749	.0155
	4.0	105.0980	22.0361	16.6535	12.0962	8.4224	5.6065	3.5618	2.1565	1.2431	.6817	.3549	.1742	.0773	.0161
	4.2	138.1140	28.9025	21.4186	15.2361	10.3748	6.7488	4.1874	2.4756	1.3936	.7467	.3802	.1827	.0798	.0167

For any particular degree of ionization $Z-E=N$, say, $r\phi$ and $r^2d\phi/dr$ are given at the boundary, and we can find solutions of the differential equation by integrating inwards for various values of the radius, r_0 of the outer boundary, leading to solutions for various values of Z.

THE NUMERICAL INTEGRATIONS

For the numerical integration a transformation was made to a logarithmic scale for the ratio of radial distance to that of the outer boundary so that

$$r=r_0e^{-v}$$

and a new dependent variable w was taken such that

$$\frac{1}{2}\left(P-\frac{1}{\pi}\right)^2=\phi+\lambda+\frac{1}{2\pi^2}=\frac{9\pi^2}{128}\frac{w}{r^{1/2}r_0^{7/2}}.$$

If we put $\gamma=(8/3\pi^2)r_0^2$, the equation for w becomes

$$\frac{d^2w}{dy^2}=\tfrac{1}{4}w+e^{-(5/2)v}\{e^{\frac{1}{2}v}w^{\frac{1}{2}}+\gamma\}^3$$

with the conditions at the outer boundary, $y=0$,

$$w^{\frac{1}{2}}=\frac{2}{3\pi^2}r_0^2=\tfrac{1}{4}\gamma,$$

$$\frac{dw}{dy}+\tfrac{1}{2}w=\frac{128}{9\pi^2}r_0^3(Z-E)=\frac{128}{9\pi^2}\left(\frac{3\pi^2}{8}\right)^{\frac{1}{3}}\gamma^{\frac{1}{3}}(Z-E).$$

while as $y\to\infty$, towards the nucleus,

$$e^{-\frac{1}{2}v}w\to\frac{128}{9\pi^2}r_0^3Z=\left(\frac{32\pi^2}{3}\right)^{\frac{1}{3}}\gamma^{\frac{1}{3}}Z.$$

This differential equation was integrated by the Gauss-Jackson-Numerov[7] method for which with little extra trouble the truncation error is proportional to the sixth derivative. Over most of the range of r an interval of y was used such as to give ten steps for a tenfold decrease in r. Near the outer boundary a finer interval was used, increased from time to time by doubling, till the regular interval was reached. When a radius of $10^{-6}r_0$ was reached, the final values were extrapolated to find Z.

This was done for $Z-E$, $=N$, $=0$, 1, 2, 3, and 4, at interval 0.2 in γ so as to cover values of Z up to 105. The resulting functions were differenced with γ to remove gross errors, and they vary sufficiently smoothly with γ for each value of r/r_0 so that they can be interpolated to integral values of Z with the accuracy to which they were computed.

At the same time integrals of the solution were computed, namely,

$$\int e^{-\frac{1}{2}v}(e^{-\frac{1}{2}v}w^{\frac{1}{2}}+\gamma e^{-\frac{1}{2}v})^3dy=-2\pi^2\gamma^2\frac{V}{Z},$$

$$\int e^{-\frac{1}{2}v}(e^{-\frac{1}{2}v}w^{\frac{1}{2}}+\gamma e^{-\frac{1}{2}v})^3dy=\frac{4\sqrt{2}\pi}{\sqrt{3}}\gamma^{\frac{1}{2}}E,$$

$$\int e^{-(5/4)v}w^{\frac{1}{2}}(e^{-\frac{1}{2}v}w^{\frac{1}{2}}+\gamma e^{-\frac{1}{2}v})^3dy=\frac{16\sqrt{2}\pi}{3\sqrt{3}}\gamma^{5/2}(-\pi^2U-\tfrac{3}{4}E),$$

$$\int e^{-v}w(e^{-\frac{1}{2}v}w^{\frac{1}{2}}+\gamma e^{-\frac{1}{2}v})^3dy$$

$$=\frac{16\sqrt{2}\pi^2}{3\sqrt{3}}\gamma^{7/2}\left(\frac{5\pi}{2}K+2\pi U+\frac{3}{4\pi}E\right),$$

and from these values of E, K, U, and V were obtained. That E should have the correct value, and that the equation obtained by eliminating I from the integral relations should be satisfied, served as over-all checks on the computing of each solution.

Values of γ for integral Z were found by inverse interpolation, and these and the corresponding values of r_0 and interpolated values of K, U, and V are given for integral values of Z and for $N=0$, 1, 2, 3, and 4, in Table I.

Table II contains the value of $r\phi$ for the values of N, γ, and r/r_0, used in the integrations, and Table III the corresponding values of $r^{\frac{1}{2}}\rho$.

The tables have been reproduced photographically from sheets typed by an I.B.M. card operated typewriter from the checked cards.

The integrations were done on the International Business Machines Corporation's Selective Sequence Electronic Calculator by Mr. William McClellan, Miss P. K. Brown, and Mr. Sherwood Skillman at various times from 1948 to 1950.

The checking, interpolation, and preparation of copy was carried out at the Watson Scientific Computing Laboratory by Bernd Zondek.

These tables may be obtained free of charge from the Watson Scientific Computing Laboratory, 612 West 116th Street, New York 27, New York, and the values are also available on punched cards.

Abbreviated tables, for $N=0$ and 1 only, follow.

ARRANGEMENT AND USE OF THE TABLES

In Table I there will be found for each atomic number Z and for each degree of ionization $N=0$ and 1, values of the radius r_0 and of the terms K, the kinetic energy V, the potential energy of the electrons in the nuclear field, and U, the exchange energy, for a statistical electron distribution according to Dirac's equation and Jensen's boundary condition. In addition, there are values of γ for interpolating in Tables II and III. The units are atomic units, for radius that of the first

[7] B. V. Numerov, Monthly Notices Roy. Astron. Soc. **84**, 592 (1924); J. Jackson, Monthly Notices Roy. Astron. Soc. **84**, 602 (1924).

Bohr orbit of hydrogen, 0.53×10^{-8} cm, for energy twice the ionization energy of hydrogen, 4.30×10^{-11} erg. Note that the total energy is equal to $-K$.

In Table II there will be found for uniform interval 0.2 in γ and for degrees of ionization $N=0$ and 1, in columns headed by the values of r/r_0, values of the product of the radial distance and the potential, $r\phi$ at radius r in the distribution. The values of r/r_0 start at $10^{-2.5}$ and proceed at a constant ratio of increase, ten values per decade (the full tables start at 10^{-6} and have a finer interval near $r=r_0$). To find the values of $r\phi$ for integral values of Z, direct interpolation is required between values in the same vertical column, with the value of γ found in Table I for the relevant values of Z and N. Four or five point Lagrangian interpolation is as accurate as the tables, but for most purposes linear interpolation will be sufficient.

In Table III for the charge density ρ, values of $r^4\rho$ are given in the same way as the values of $r\phi$ in Table II.

The units of potential and charge density are again atomic units, 9×10^{-2} esu/cm for potential, 3.2×10^{15} esu/cm^3 for charge density.

THE JOURNAL OF CHEMICAL PHYSICS VOLUME 22, NUMBER 10 OCTOBER, 1954

Investigation of Rotational Isomers with Ultrasound

JOHN KARPOVICH*
Imperial College of Science and Technology, London, England
(Received April 14, 1954)

Sound absorption measurements in organic liquids have revealed relaxation processes in some cyclohexane derivatives, cyclohexene, methyl formate, ethyl acetoacetate, acetic anhydride, and methyl benzoate. Additional absorption measurements have been made in the relaxation regions of formic acid, ethyl formate, methyl acetate, and ethyl acetate.

A study of cyclohexane derivatives and other similar ring molecules has led to the identification of the mechanism responsible for the relaxations in these liquids. The relaxation phenomena are attributed to the disturbance by the sound wave of equilibria between rotational isomers. The restricted rotation occurs about the single bonds in the ring during the conversion from one chair configuration to another.

The relaxation in cyclohexene is caused by the disturbance of the equilibrium between pseudochair and boat configurations, again involving rotation about single C−C bonds.

The relaxations in esters of the carboxylic acids are attributed to rotational isomers which arise from rotation about C−O bonds.

Infrared absorption bands at about 1160 and 1185 cm^{-1} in the formates and acetates are identified with rotational isomers of the type postulated for the relaxations in these liquids.

1. INTRODUCTION

THE sound absorption in most organic liquids is proportional to the square of the frequency, as predicted by the classical formulas for shear viscosity[1] and heat conduction[2] losses, but is usually of greater magnitude than the sum of these two losses.[3] In a few organic liquids the absorption has been found to obey the laws of a relaxation process[4–6] rather than be proportional to the square of the frequency. The organic liquids in which relaxations have been observed previous to this investigation are shown in Table I.

It is generally understood that an acoustic relaxation process is the result of a perturbation by the sound wave of a chemical equilibrium in the liquid. Spakowski[7] suggested that the relaxation in acetic acid was due to

TABLE I. Organic liquids with relaxations reported previous to this investigation.

No.	Liquid	Relaxation frequency at 20°C Mc	Observers
1	Formic acid	Unknown	Bazulin[a]
2	Ethyl formate	Unknown	Liebermann[b]
3	Acetic acid	0.556	Lamb and Pinkerton[c]
4	Methyl acetate	Unknown	Biquard[d]
5	Ethyl acetate	11.4	Pinkerton[e]
6	Propionic acid	2.02	Lamb and Huddart[f]
7	Toluene	0.1	Moen[g]
8	Carbon disulfide	72.1	Lamb and Andreae[h]

[a] P. Bazulin, J. Exptl. Theoret. Phys. (U.S.S.R.) **8**, 457 (1938).
[b] L. N. Liebermann, Phys. Rev. **75**, 1415 (1949).
[c] See reference 4.
[d] P. Biquard, Ann. phys. **6**, 195 (1936).
[e] J. M. M. Pinkerton, Colloquium over Ultrasonore Trillingen, 117 (1951).
[f] See reference 5.
[g] C. J. Moen, J. Acoust. Soc. Am. **23**, 62 (1951).
[h] See reference 6.

* This paper is extracted from a thesis submitted as partial fulfillment for the requirements for the degree of Doctor of Philosophy at the University of London. The author is now with the Physical Research Laboratory of the Dow Chemical Company, Midland, Michigan.

[1] G. G. Stokes, Proc. Cambridge Phil. Soc. **8**, 287 (1845).
[2] G. Kirchhoff, Pogg. Ann. Phys. **134**, 177 (1868).
[3] J. M. M. Pinkerton, Proc. Phys. Soc. (London) **B62**, 129 (1949).
[4] J. Lamb and J. M. M. Pinkerton, Proc. Roy. Soc. (London) **199A**, 114 (1949).
[5] J. Lamb and D. H. A. Huddart, Trans. Faraday Soc. **46**, 540 (1950).
[6] J. Lamb and J. H. Andreae, Nature **167**, 898 (1951).
[7] B. Spakowski, Acad. Sci. (U.S.S.R.) **18**, 169 (1938).

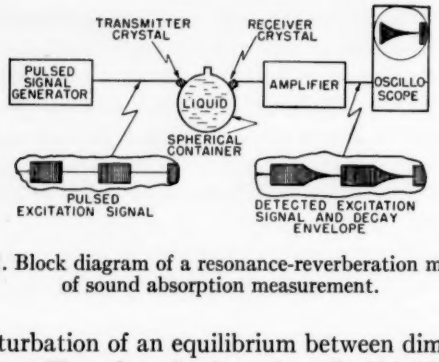

FIG. 1. Block diagram of a resonance-reverberation method of sound absorption measurement.

the perturbation of an equilibrium between dimers and monomers. The relaxation in carbon disulfide[6] has been attributed to the excitation of different vibrational states of the molecule, similar to the interpretations given for the relaxations observed in a number of triatomic gas molecules.[8]

The development of a resonance-reverberation method for sound absorption measurements† has made it possible to study liquids in the frequency range of 20 to 600 kc. A block diagram of the experimental arrangement is shown in Fig. 1. The spherical glass container is filled with the liquid to be studied, and is excited with an intermittent train of continuous sound waves generated by a piezoelectric element. A second piezoelectric element detects the manner in which the sound energy dies away after the excitation stops. The decay pattern, which has a time constant inversely proportional to the sound absorption of the system, is displayed on an oscilloscope. The wall loss must be separated from the total absorption of the system to obtain the absorption due to the liquid alone. This was accomplished by calibrating the liquid container with a number of carefully chosen liquids of known absorption. The absorption values of the calibration liquids were obtained by extrapolation from higher frequency measurements, assuming that no relaxation occurred in the region of the extrapolation. The liquids were chosen so that calibration curves could be prepared over a wide range of absorption. The absorption coefficient of a liquid of unknown absorption is obtained by reference to the calibration curves. Liquid containers as small as 5 ml can be used with this method. Relaxations were observed in the frequency range of this technique.[9] These relaxations have been attributed to the perturbation of the equilibria between rotational isomers.

2. RELATION BETWEEN SOUND ABSORPTION AND MOLECULAR REACTION RATE CONSTANTS

The sound absorption in liquids which exhibit relaxation phenomena characterized by one relaxation time will obey the following expression:

$$\alpha/f^2=B+\frac{A}{1+(f/f_c)^2}, \tag{1}$$

where α is the absorption coefficient; f is the frequency of the sound wave; f_c is the relaxation frequency; B is the value of α/f^2 where $f\gg f_c$; and A is the increase of α/f^2 due to the relaxation process.

The terms in Eq. (1) are illustrated in Fig. 2. It is usually considered that the observed values of α/f^2, which are higher than the "classical" value, correspond to $A+B$ in Fig. 2, and that at higher frequencies the absorption will "relax" to the classical value.[10]

Equation (1) may be written as the absorption per wavelength μ caused by the relaxation process (see Fig. 2).

$$\mu=\alpha'\lambda=\frac{Acf}{1+(f/f_c)^2}, \tag{2}$$

where α' represents the absorption due to the relaxation process only, λ is the wavelength, and c is the phase velocity of the sound wave.

The relaxation parameters which are significant for molecular reaction studies are μ_{max} and f_c. These parameters are determined by measuring α, f, and c experimentally.

A two state reaction of the type necessary for an acoustic relaxation may be described by the following relation:

$$dn_2/dt=k_{12}n_1-k_{21}n_2, \tag{3}$$

where n_1 is the fraction of gram molecular weight in state 1; n_2 is the fraction of gram molecular weight in state 2; k_{12} is the rate constant for the transition 1→2; k_{21} is the rate constant for the transition 2→1; and t is time.

At equilibrium the relative populations in the two states are given by

$$n_2/n_1=k_{12}/k_{21}=\frac{\exp(-\Delta E_1/RT)}{\exp(-\Delta E_2/RT)}=\exp(-\Delta E/RT), \tag{4}$$

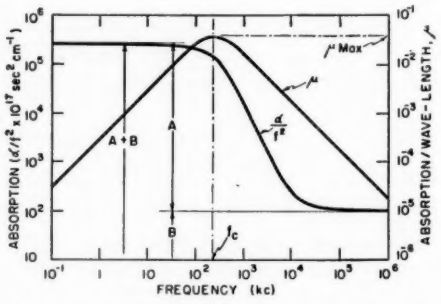

FIG. 2. Curves associated with an acoustic relaxation which illustrate the terms appearing in the expression for an acoustic relaxation.

[8] E. F. Fricke, J. Acoust. Soc. Am. **12**, 245 (1940).

† The paper describing the resonance-reverberation method has been submitted to *The Journal of the Acoustical Society of America* for publication.

[9] J. Karpovich, J. Chem. Phys. **21**, 1120 (1953).

[10] C. Kittel, Repts. Phys. Soc. Progr. Phys. **11**, 205 (1946–47).

where ΔE_1 is the activation energy in the direction 1→2; ΔE_2 is the activation energy in the direction 2→1; ΔE is the energy difference between the two states; R is the gas constant; and T is the absolute temperature.

Figure 3 is the potential energy diagram of the two-state condition represented by Eq. (3). The relaxation frequency may be expressed in terms of reaction rate and energy parameters as follows:[11,4]

$$f_c=\frac{(k_{12}+k_{21})}{2\pi}. \tag{5}$$

For most practical cases, $k_{21}\gg k_{12}$, so expression (5) becomes

$$f_c\approx\frac{k_{21}}{2\pi}$$

$$\approx M\exp(-\Delta E_2/RT), \tag{6}$$

where the factor M has the dimensions of time^{-1}.

It can be shown that ΔE is a complicated function of μ_{max}. Herzfeld[12] has made such a theoretical development assuming that the sound wave is a thermal mechanism of perturbation, and Hall[13] has made a parallel development assuming that the sound wave is a pressure mechanism.

Two conditions must be satisfied to observe a relaxation in a liquid when using longitudinal sound waves as the means of perturbation. First, it is necessary that the molecules of the liquid are capable of existing in more than one state with *different* energies. Secondly, the relaxation frequency must be within the frequency range of experimental methods of measuring sound absorption.

3. CYCLOHEXANE DERIVATIVES

A low-frequency relaxation process was observed in methylcyclohexane, whereas no similar anomalous absorption was found in cyclohexane. These sound absorption results may be explained by the peculiar

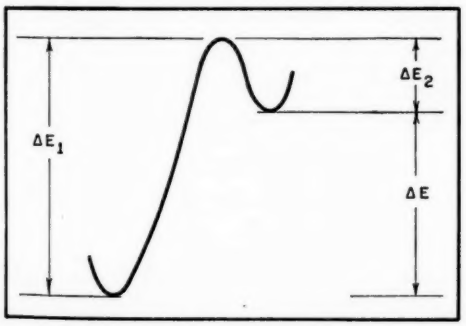

FIG. 3. A two-state potential energy diagram of the type necessary for the occurrence of an acoustic relaxation.

[11] W. T. Richards, Revs. Modern Phys. **11**, 36 (1939).
[12] K. F. Herzfeld, J. Acoust. Soc. Am. **13**, 33 (1941).
[13] L. Hall, Phys. Rev. **73**, 775 (1948).

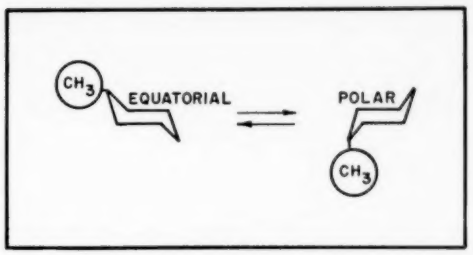

FIG. 4. The polar-equatorial type of rotational isomers of methyl cyclohexane.

steric properties of the hydrogen atoms of the cyclohexane molecule. The hydrogen atoms in the chair configuration can be divided into two types called *polar* and *equatorial*.[14] If the carbon ring in the chair configuration is imagined to be horizontal, there are three polar hydrogens above and three below the ring, while the other six hydrogen atoms lie in the *equatorial* belt around the carbon ring. Each carbon has one polar and one equatorial hydrogen. If the cyclohexane ring passes into the opposite chair configuration by rotation about the C−C bonds, all hydrogens originally equatorial become polar, and vice versa. As long as all substituent groups are hydrogen atoms, both chair configurations have the same potential energy, but when one of the hydrogens is replaced with another group, rotational isomers with different energies become possible. Figure 4 illustrates the polar-equatorial type of rotational isomers in methylcyclohexane. The relaxation process may well be due to the perturbation of the equilibrium between these readily interconvertible configurations. A number of cyclohexane derivatives and related ring molecules were studied in order to find additional evidence for this postulate. Figure 5 shows the frequency dependence of the absorption of some of these molecules. Table II is a list of the cyclohexane derivatives and related ring molecules which have been studied, and their sound absorption parameters.

Other monosubstituted cyclohexane derivatives which were studied included cyclohexanol, cyclohexylamine, and dicyclohexylamine. All of these molecules exhibit the same type of polar-equatorial isomerisms as methylcyclohexane, and all of them exhibit relaxations.

From a study of a model of cyclohexanone, one can see that this molecule does not exhibit the polar-equatorial properties of monosubstituted cyclohexane derivatives. No relaxation was observed.

o-Methyl cyclohexanone has a methyl group which can exhibit polar-equatorial isomers. A relaxation was observed in this liquid.

Several di-substituted cyclohexane derivatives were studied. The isomers of *trans*-4-methylcyclohexanol are shown in Fig. 6. Beckett, Pitzer, and Spitzer[14] estimate that the energy difference between the isomers in *trans*-1-4-dimethylcyclohexane will be twice that in methyl

[14] Beckett, Pitzer, and Spitzer, J. Am. Chem. Soc. **69**, 2488 (1947).

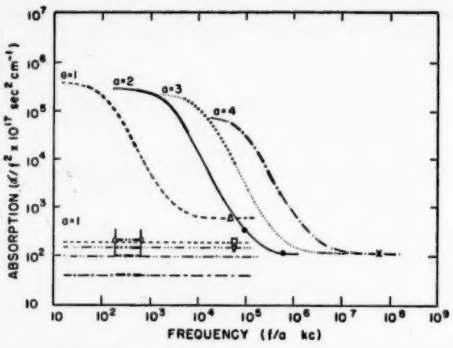

FIG. 5. The frequency dependence of the sound absorption of some cyclohexane derivatives and related ring molecules. The curves have been shifted along the frequency axis by multiples of a log cycle as indicated in the figure. The heavy line portion of the curves represents the region of the resonance-reverberation data. The data at 52 Mc were supplied by Andreae [J. H. Andreae (unpublished). Absorption and sound velocity measurements obtained with a pulse technique were used with the kind permission of J. H. Andreae], and the point at 8.5 Mc for methyl cyclohexane was obtained from Hazzard [G. W. Hazzard, J. Acoust. Soc. Am. **22**, 29 (1950)]. The curves have been extended beyond the limits of the experimental data as predicted by the appropriate theoretical relationship. The temperatures at which the data were taken are shown in Table II.

△ — — — — — cyclohexanol
● ——————— methylcyclohexane
····· cyclohexylamine
× —·—·—·— cyclohexene
□ — — — — — cyclohexane
▽ —··—··— 1,4-dioxan
| | {*cis*-1,3-dimethylcyclohexane
○ ——··—— ○ {*trans*-1,3-dimethylcyclohexane
| | {1,1-dimethylcyclohexane
—·—·—·— cyclohexanone
— — — — — — — methylcyclopentane

cyclohexane. It is not likely that a replacement of one of the methyl groups by a hydroxyl group will greatly alter the expected energy difference between the isomers. The relaxation observed in *trans*-4-methylcyclohexanol indicates that the energy difference between the isomers is greater than in methylcyclohexane.

In 1,1-dimethylcyclohexane and in *trans*-1,3-dimethylcyclohexane, the chair configurations will both have one polar and one equatorial methyl group; hence there will be no energy difference between the isomers. No relaxations were observed.

Cis-1,3-dimethylcyclohexane will exhibit polar-equatorial isomers with different potential energies. Figure 7 shows the configurations of the rotational isomers. It is clear from Fig. 7 that the methyl groups in the polar position will encounter considerable steric interaction since both are on the same side of the plane. Beckett, Pitzer, and Spitzer[14] have assigned an energy

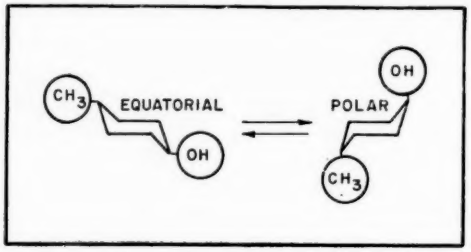

FIG. 6. The polar-equatorial type of rotational isomers of *trans*-4-methylcyclohexanol.

difference of 5.4 kcal/mole to the isomers of *cis*-1,3 dimethylcyclohexane as compared to 1.6 kcal/mole for methylcyclohexane. It is not likely that the activation energy for the equatorial to polar transition in these two molecules will differ greatly since the same number of bonds are involved in the rotation. The activation energy for the reverse process will therefore be smaller in *cis*-1,3-dimethylcyclohexane than in methyl cyclohexane, and the relaxation frequency will be higher

TABLE II. Cyclohexane derivatives and related ring molecules and their sound absorption parameters. The values of α/f^2 only are tabulated for liquids which exhibit no relaxation in the frequency range studied. The measurements on liquids number 5, 7, and 9 were qualitative, and are compared to methylcyclohexane. Measurements on liquids number 10, 11, and 12 were made in 5-cc spherical vessels which were not calibrated to obtain greater accuracy. See Eq. (1) and Fig. 2 for the significance of A and B.

No.	Liquid	Temp. °C	Relaxation frequency Mc	$A \times 10^{-17}$ sec² cm⁻¹	$B \times 10^{-17}$ sec² cm⁻¹	$\alpha/f^2 \times 10^{-17}$ sec² cm⁻¹
1	Cyclohexane	22	None observed			197
2	Methylcyclohexane	25	0.22	260 000	100	
3	Cyclohexanol	32	0.12	351 000	540	
4	Cyclohexylamine	19	0.11	210 000	100	
5	Dicyclohexylamine	19	~0.22	~260 000	···	
6	Cyclohexanone	24	None observed			98
7	*o*-Methylcyclohexanone	18	~0.22	~260 000	···	
8	1-4-Dioxan	25	None observed			136
9	*Trans*-4-methylcyclohexanol	18	~0.22	~260 000	···	
10	1-1-dimethylcyclohexane	19	None observed			200±150
11	*Trans*-1-3 dimethylcyclohexane	18	None observed			200±150
12	*Cis*-1-3 dimethylcyclohexane	19	None observed			200±150
13	Methylcyclopentane	15	None observed			38
14	Cyclohexene	36	0.08	74 000	127	

(see Eq. 6). The experimental results support this analysis since the absorption between 0.5 and 0.6 Mc is very low, and there is no indication of a relaxation similar to the one observed in methylcyclohexane.

Methylcyclopentane is a five-membered ring with a methyl group, similar in this respect to methylcyclohexane. Kilpatrick, Pitzer, and Spitzer[15] have studied the structure of this molecule, and state that the torsional forces about the single bonds are in opposition to the forces tending to maintain tetrahedral bond angles. Thus the latter forces tend to keep all five carbon atoms coplanar while the torsional forces tend to "pucker" the ring. A study of the model of methylcyclopentane indicates that it does not exhibit the polar-equatorial atomic configurations common to the cyclohexane ring. No relaxation was observed.

The study of cyclohexane derivatives and similar ring molecules is presented as the basis for the postulate that the relaxations observed in these liquids are caused by the disturbance by the sound wave of an equilibrium between rotational isomers of the polar-equatorial type.

4. CYCLOHEXENE

A relaxation was observed in cyclohexene (Fig. 5 and Table II) which is attributed to a disturbed equilibrium between pseudochair and boat configurations. The pseudochair form corresponds to the model suggested by Lister[16] which he states is the most stable

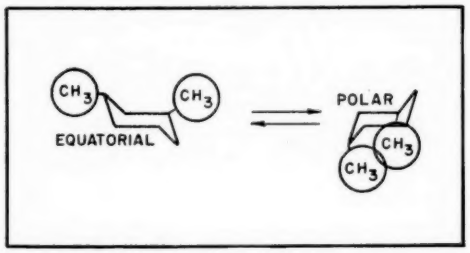

FIG. 7. The polar-equatorial type of rotational isomers of *cis*-1,3-dimethylcyclohexane.

configuration. The two configurations are shown in Fig. 8. These two configurations correspond to the chair and boat in cyclohexane, yet no anomaly was observed in cyclohexane. A study of the models of the two molecules in the boat forms reveals a distinct difference in the spacial configuration which may account for this apparent inconsistency. The double C—C bond in cyclohexene causes the two hydrogen atoms pointing together from the "fore" and "aft" of the boat configurations to be further apart in cyclohexene than in cyclohexane as shown in Fig. 9. In addition, the four hydrogen atoms below the "boat" in cyclohexane inter-

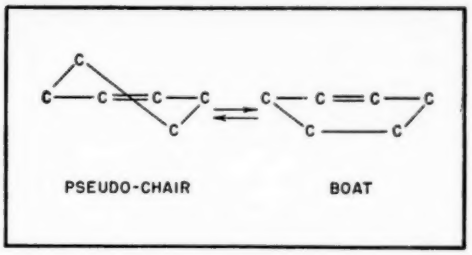

FIG. 8. The pseudochair and boat rotational isomer configurations of cyclohexene.

act to make this form less stable. The energy difference between the isomers in cyclohexene should therefore be less than between the isomers in cyclohexane. If the forward activation energies for the isomeric conversion in both molecules is of the same order of magnitude, then the reverse activation energy in cyclohexene will be greater, and the relaxation frequency will be lower (see Eq. 6).

5. SUBSTANCES CONTAINING THE CARBOXYL GROUP

The sound absorption coefficients of several liquids containing the carboxyl group have been measured as a function of frequency, and relaxations have been observed in all of them. Figure 10 shows the frequency dependency of the absorption, and Table III lists the sound absorption parameters.

Before discussing the sound absorption results further, it is necessary to know something about molecular association in these liquids. Fenton and Garner[17] have shown that acetic acid is almost completely associated into double molecules even at the boiling point. Formic and propionic acids are also considered to be associated into double molecules in the liquid phase. Pauling and Brockway[18] determined the configuration of the double molecule of formic acid by electron diffraction measurements. It was found to be a planar ring, the two molecules being joined by two hydrogen bonds.

The chemical equilibrium which is disturbed by the sound wave in the carboxylic acids is probably that between dimers and monomers.[7]

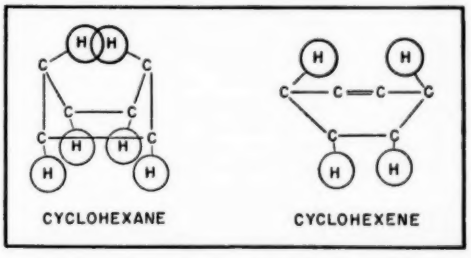

FIG. 9. A comparison of the "boat" configurations of cyclohexane with cyclohexene, illustrating the difference in steric properties.

[15] Kilpatrick, Pitzer, and Spitzer, J. Am. Chem. Soc. **69**, 2483 (1947).
[16] M. W. Lister, J. Am. Chem. Soc. **63**, 143 (1941).
[17] T. M. Fenton and W. E. Garner, J. Chem. Soc. **1930**, 694.
[18] L. Pauling and L. O. Brockway, Proc. Natl. Acad. Sci. U. S. **20**, 336 (1934).

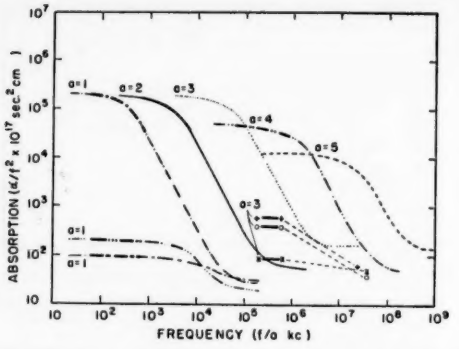

FIG. 10. The frequency dependence of the sound absorption of liquids with the carboxyl group. The curves have been shifted along the frequency axis by multiples of a log cycle as indicated in the figure. The heavy line portion of the curves represents the region of the resonance-reverberation data. The data of other contributors has not been plotted with the exception of three high frequency points for acetic anhydride, ethyl acetoacetate and methyl benzoate obtained from Andreae [J. H. Andreae (unpublished). Absorption and sound velocity measurements obtained with a pulse technique were used with the kind permission of J. H. Andreae]. The origin of other contributing data can be found in the "observers" column in Table III. The curves have been extended beyond the limits of the experimental data as predicted by the appropriate theoretical relationship. The temperatures at which the data were taken are shown in Table III.

—·—·—·— ethyl formate
————————methyl formate
·····acetic acid
—·—·—·—·formic acid
— — — — —propionic acid
+————+acetic anhydride
O————Oethyl acetoacetate
—···—···—methyl acetate
—·—·—·— ethyl acetate
×————×methyl benzoate

It is quite likely that a form of weaker internal hydrogen bonding exists in the esters, as in *o*-chlorophenol and catechol,[19,20] with one of the hydrogens of the alkyl group being joined to the carbonyl group. Spectroscopic studies of *o*-chlorophenol and catechol give evidence of restricted rotation about the C—O bond.[19,20] The lower energy configuration of the esters is that in which there is an internal hydrogen bond. This configuration will further be stabilized by the planarity of the

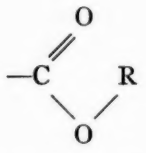

group in view of the possibility of resonance involving a structure of the type

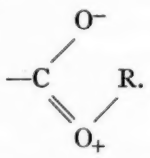

The higher energy configuration may well be the other planar form, namely

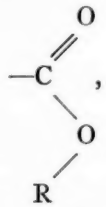

since in this form also there is probably an appreciable resonance energy.

The suggested configurations for the esters may be used to account for the difference in the relaxation frequencies between the liquids studied. The acetates have larger alkyl groups which will encounter steric interaction in the higher energy configurations, increasing the energy level of those configurations. This condition results in a high reverse rate constant, or a short

TABLE III. Liquids with the carboxyl group, and their sound absorption parameters. Most of the sound absorption parameters have been determined with the results of the resonance-reverberation measurements in conjunction with results of other investigators. The symbol # appears in the "observers" column when resonance-reverberation measurements have contributed to the determination of the sound absorption parameters. See Eq. (1) and Fig. 2 for the significance of A and B.

No.	Liquid	Temp. °C	Relaxation frequency Mc	$A \times 10^{-17}$ sec² cm⁻¹	$B \times 10^{-17}$ sec² cm⁻¹	Observers
1	Formic acid	21	1.33	46 000	50	# (a)
2	Methyl formate	25	0.35	160 000	50	# (b)
3	Ethyl formate	25	0.4	192 000	26	# (c)
4	Acetic acid	20	0.556	160 000	151	(d)
5	Methyl acetate	20	6.8	196	22	# (e)
6	Ethyl acetate	20	11.8	63	35	# (f)
7	Propionic acid	21	2.02	11 470	130	(g)
8	Ethyl acetoacetate	16	···	~340	···	# (b)
9	Methyl benzoate	26	···	~33	···	# (b)
10	Acetic anhydride	20	···	~550	···	# (b)

a—See a in Table I.
b—See J. H. Andreae in Fig. 5 (or Fig. 10) caption.
c—See b in Table I.
d—See reference 4.
e—See d in Table I.
f—See e in Table I.
g—See reference 5.

[19] O. R. Wulf and V. Liddell, J. Am. Chem. Soc. **57**, 1464 (1935).
[20] L. Pauling, J. Am. Chem. Soc. **58**, 94 (1936).

"lifetime" in the higher energy configuration. This is consistent with a higher relaxation frequency.

The infrared spectra of some of these liquids has been examined in an attempt to make a correlation of the sound absorption results with spectroscopic data. Thompson and Torkington[21] (see Fig. 11) have studied the vibrational spectra of the esters of carboxylic acids, and have observed what they describe as "interesting bands" at about 1160 cm^{-1} and 1185 cm^{-1} in the formates. They also identify a strong band in the acetates at 1245 cm^{-1} as analogous to those at 1160 cm^{-1} and 1185 cm^{-1} in the formates. They suggest that these bands are connected with the C—O bond in the

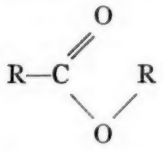

group but do not define them any further. A qualitative correlation of the vibrational bands mentioned above can be made with the sound absorption results. It is suggested that the two bands in the formates and the single band in the acetates are due to the presence of the postulated rotational isomers.

The band at 1160 cm^{-1} in the formates decreases in intensity as the alkyl group increases in size, while the frequency remains almost constant throughout the series. This band is assigned to the higher energy isomer. The decrease in intensity as the alkyl group increases is due to increase in steric interaction. As the steric interaction increases, the energy difference increases; consequently, the populations of the higher energy configuration decreases. The band 1185 cm^{-1} falls from about 1214 cm^{-1} in methyl formate and 1195 cm^{-1} in ethyl formate to a steady value of about 1185 cm^{-1} in the higher homologs. This band corresponds to the lower energy isomer.

In the acetates only *one band* was observed at 1245 cm^{-1}. The absence of the second band is not clarified by Thompson and Torkington. The energy difference between the two postulated states in the acetates is probably greater than that between the two postulated states in the formates owing to the greater steric interaction in the higher energy forms of the acetates. This larger energy difference in the acetates means a more

[21] H. W. Thompson and P. Torkington, J. Chem. Soc. **1945**, 640.

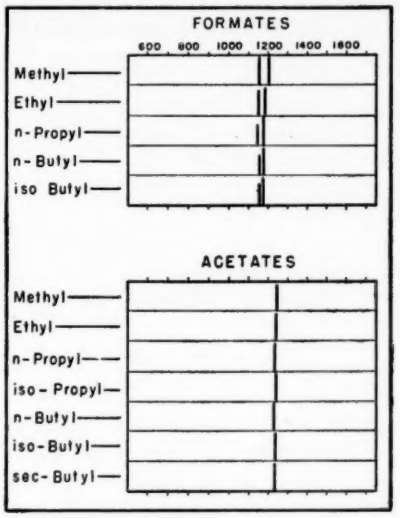

FIG. 11. Some infrared absorption bands in formates and acetates. This figure was extracted from Thompson and Torkington (see reference 21) with the kind permission of the authors and the Journal of Chemical Society (London). The absorption bands shown are identified with the C—O bond, and the double bands in the formates are attributed to rotational isomers of the type involving rotation about the C—O bond.

sparsely populated higher energy state [Eq. (4)]. This could account for the absence of the second band in the acetates. The band at 1245 cm^{-1} is attributed to the lower energy isomer. It may be possible to observe the higher energy isomer band for the C—O bond vibration by heating the liquid and using a high resolution spectroscope.

A complete study of the sound absorption parameters as a function of temperature would enable the determination of both the energy difference between the rotational isomers and the associated barrier energies.

The application of sound absorption measurements to liquids illustrates the usefulness of this method for the study of chemical processes with rapid reversible reactions. This method may find further application in the study of excitation, dissociation and other rapid reversible chemical processes.

The author wishes to express his gratitude to Professor Willis Jackson for offering facilities for carrying out this program of research. The author is also grateful to Mr. J. H. Andreae, Mr. J. E. Piercy, Dr. N. Sheppard, Dr. A. E. Braude, Dr. G. J. Szasz, Dr. W. C. Price, and Professor H. C. Longuet-Higgins for interesting discussions.

Letters to the Editor

THIS section will accept reports of new work, provided these are terse and contain few figures, and especially few half-tone cuts. The Editorial Board will not hold itself responsible for opinions expressed by the correspondents. Contributions to this section should not exceed 600 words in length and must reach the office of the Editor not later than the 15th of the second month preceding that of the issue in which the Letter is to appear. No proof will be sent to the authors. A publication charge of $15.00 per Letter is made which, when honored, will entitle the Institution to 100 free reprints.

Calculation of the Concentration of Atomic Hydrogen at a Cathode. II.

HUGH W. SALZBERG AND SIGMUND SCHULDINER
Columbia University, New York City, and Naval Research Laboratory, Washington, D. C.
(Received January 26, 1953)

IN a letter published by Bockris and Parsons[1] they contest our calculation of the concentration of atomic hydrogen at a cathode.[2] We believe, however, that the results stated in our letter are correct and that the equation of Bockris and co-workers is still incorrect in magnitude by a factor of 10^9 in terms of the rate of reaction. This is because their choice of standard states is incompatible with their choice of a minimum free energy of activation and also because they have omitted a probability factor from their equation.

The absolute rate theory of Glasstone, Laidler, and Eyring,[3] on which these calculations are based, requires the standard state to be in terms of molecules per unit volume, or area, and the minimum free energy of activation for a reaction to be zero. A standard state which is defined in terms of moles per unit area would require a minimum free energy of activation which is a negative quantity, namely, $-RT\ln N$, where N is Avogadro's number. Bockris and co-workers have used a standard state in terms of moles per cm² with, however, a minimum free energy of zero, thus arbitrarily increasing their activation energy by $RT\ln N$ and thus decreasing the maximum rate by a factor of N. The arbitrary and unreal nature of their standard state is indicated both by the negative value of the minimum free energy of activation and by the fact that a mole per cm² is a concentration of about 6×10^7 molecules per square angstrom unit.

The insertion of the probability factor $s/2L$ is necessary since two atoms will combine only when they are in adjacent positions on the surface. This treatment has been worked out in detail in standard textbooks on kinetics.[4,5] The suggestion of Bockris and Parsons that the entropy of activation accounts for the probability factor is not correct since entropy of activation has nothing to do with two particles not being close enough to each other to react. Any implication that the activated complex is mobile is also incorrect, since the activated complex must be adsorbed on a site for the heat of reaction to be dissipated to the third body (the surface). Even if the hydrogen atoms on the surface were mobile, a probability factor would be necessary since the calculation is concerned with the number of atomic pairs on the surface at any instant.

Bockris and co-workers have in essence calculated a maximum rate for combination of any two atoms on a surface, since the specific nature of the gas is removed from the calculation by assuming a zero activation energy. The experimental work of Goodeve and Jack[6] however shows combination rates 10^5 times greater than the maximum found by Bockris *et al.* This is clear experimental evidence that the calculation of Bockris and co-workers is incorrect. The rates of reaction found by Goodeve and Jack do however agree with our calculation.

The experimental evidence quoted by Bockris and Parsons in justification of their calculation is certainly not conclusive. It has been shown[7] that the limiting current density they found for a platinum cathode in acid solution could very well be due to trace impurities in the solution, rather than a saturation of the surface with adsorbed hydrogen.

As Bockris and Parsons have pointed out in their letter,[1] our criticism of the dimensions of their equation is incorrect. Their choice of standard state automatically fixes the units of their results. Also, we were in error in our equation when we used standard free energies of activation in the same equation with partition functions. However, since we assigned the value of unity to the ratio of partition functions, this did not affect the value of our calculation. Our Eq. (4)[2] should read

$$r=(kT/h)H^2(2/L)\exp(-\Delta G^*/RT)$$

where: r is the rate of a molecular combination; (kT/h) is the frequency factor; H is the number of hydrogen atoms per cm² of cathode surface; L is the number of active sites per cm² of cathode surface; ΔG^* is the standard free energy of activation. This is the free energy difference between the reactants (hydrogen atoms on the surface) and the activated complex adsorbed on the surface, each in its standard state of one molecule per cm²; R and T are the gas constant and the absolute temperature, respectively.

We wish to thank Professor K. J. Laidler of the Catholic University of America for his explanation of the minimum free energy of activation required by each choice of standard state in the absolute rate theory.

[1] J. O'M. Bockris and R. Parsons, J. Chem. Phys. **21**, 569 (1953).
[2] H. W. Salzberg and S. Schuldiner, J. Chem. Phys. **20**, 1495 (1952).
[3] Glasstone, Laidler, and Eyring, *Theory of Rate Processes* (McGraw-Hill Book Company, Inc., New York, 1941), pp. 160–191.
[4] K. J. Laidler, *Chemical Kinetics* (McGraw-Hill Book Company, Inc., New York, 1950), p. 157, Eq. (32).
[5] E. S. Amis, *Kinetics of Chemical Change in Solutions* (Macmillan Company, New York, 1949), pp. 277–278.
[6] Goodeve and Jack, Discussions Faraday Soc. **4**, 89 (1948).
[7] S. Schuldiner, J. Electrochem. Soc. **99**, 493 (1952).

Calculation of the Concentration of Atomic Hydrogen at a Cathode. II

J. O'M. BOCKRIS AND ROGER PARSONS
University of Pennsylvania, Philadelphia, Pennsylvania and University College, Dundee, Scotland
(Received May 26, 1954)

SALZBURG and Schuldiner[1] have withdrawn their contention[2] that the dimensions of an equation used by us[3] are incorrect and have conceded the error in their own equation.[4] They now differ from us in respect to (i) a probability term; (ii) an alleged limitation on the choice of standard states; (iii) the mechanism of hydrogen evolution on Pt at high current densities.

(i) The probability factor proposed[1,2] is required only when the adsorbed atoms are immobile. We assumed them to be mobile[5] and to behave as a two-dimensional gas in contact with a third body. Thus, by analogy to a three-dimensional gas, no probability factor exists. Support for mobility is by analogy with Ni and Fe systems (dependence of heat of adsorption on coverage).[6] Entropy of adsorption measurements for H on Hg[7] give the same conclusion.

(ii) Any standard states may be used in the reaction rate theory and their correspondence to physical reality is not of moment.* It appears that both the present authors and Salzburg and Schuldiner are incorrect in suggesting that there is a minimum *free energy* of activation of zero for a maximum rate of combination.† But it is reasonable to set the *energy* of activation as zero in considering the maximum rate of a reaction: the entropy of activation will then be fixed by the model assumed and the standard state employed. Consider,

$$2H\rightarrow HH^x\rightarrow H_2 \qquad (1)$$

occurring on a metal surface. Then,

$$v=\frac{kT}{h}c_H{}^2\frac{F^x}{F_H{}^2}\exp\left[-\frac{\Delta E_0}{kT}\right] \quad (2)$$

where these terms have the significance usual in rate theory. F_H corresponds to two degrees of translational motion and one degree of vibrational (perpendicular to the surface); F^x to two degrees of translational motion, one of rotation, two of vibration (perpendicular to the surface and assumed to be the same in the initial and activated state). One obtains with (2)

$$v=4\left(\frac{kT}{\pi m}\right)^{\frac{1}{2}}c_H{}^2\frac{r}{\sigma}\exp\left[-\frac{\Delta E_0}{kT}\right] \quad (3)$$

where σ is a symmetry factor, here 2, and r is the distance between the centers of the activated complex. The result is essentially the same as the corresponding kinetic expression:[2]

$$v=\left(\frac{8kT}{\pi m}\right)^{\frac{1}{2}}c_H{}^2\frac{r}{2}\exp\left[-\frac{E}{kT}\right] \quad (4)$$

if E is identified with ΔE_0.

The entropy term for the model mobile atom and mobile activated complex is,

$$\exp\left[\frac{\Delta S^{0\ddagger}}{k}\right]=\frac{2r}{\sigma}\left[\frac{\pi h^2}{2mkT}\right]. \quad (5)$$

which ($T=300°$, $r=10^{-8}$, $m_H=1.67\ 10^{-24}=1.43\ 10^{-16}$). The standard states are *molecules cm*$^{-2}$ for both states. If we change to moles cm^{-2}, i.e., the standard states used in our paper,[3] the entropy factor becomes $1.43\ 10^{-16}N_0=8.6\ 10^7$, and utilizing this in the original equation we obtain results in agreement with (4).

Hence, the model used by us, treated by rate theory, is in accord with kinetic theory and gives similar results to the latter on the assumption that, for maximum rate, $\Delta H^{0\ddagger}=0$, whatever the standard states. Conversely, the comparison made by Salzburg and Schuldiner with (4) is invalid because their deduction involves a different model from that of (4).

(iii) The electrochemical mechanism for desorption of H when $b\simeq 0.1$ remains the most probable one. $\Delta H^{0\ddagger}$ for the combination[9] is not necessarily zero and hence the surface may approach saturation at the current densities at which the break occurs. Alternative theories (e.g., H_2O discharge) involve energetic difficulties.[10]

We wish to thank Professor H. Eyring, of the University of Utah, for helpful discussions regarding standard states used in the absolute reaction rate theory.

* See e.g., the use of the "unreal" standard state of 1 mole cm^{-2} by Glasstone, Laidler, and Eyring (reference 8).

† Although, with standard states of moles cm^{-2}, this accords with the simplest interpretation of the observed change of Tafel slope in the H evolution reaction on Pt[3].

[1] H. W. Salzburg and S. Schuldiner, J. Chem. Phys. **22**, 1774 (1954), preceding letter.
[2] H. W. Salzburg and S. Schuldinger, J. Chem. Phys. **20**, 1495 (1952).
[3] Parsons and Bockris, Trans. Faraday Soc. **47**, 914 (1951); Bockris and Potter, J. Electrochem. Soc., **99**, 169 (1952).
[4] Bockris and Parsons, J. Chem. Phys. **21**, 569 (1953).
[5] Goodeve and Jack, Discussions Faraday Soc. **1952**, 493.
[6] Beeck, *Advances in Catalysis* **II**, 194 (1949).
[7] Law, thesis (London, 1951), p. 170.
[8] Glasstone, Laidler, and Eyring, *Theory of Rate Processes* (McGraw-Hill Book Company, Inc., New York, 1941), p. 397.
[9] See Schechter, Acta Physicochim. **10**, 379 (1939).
[10] See Bockris, *Modern Aspects of Electrochemistry* (London, 1954), Chapter IV.

On a Supposed Raman Spectrum of Gaseous Bromine

R. F. Barrow
Physical Chemistry Laboratory, Oxford University, Oxford, England
(Received August 10, 1954)

ONLY one report of a Raman spectrum of bromine appears so far to have been recorded. This was given by Stammreich[1] who illuminated the vapor at 900 mm pressure with He 5875.6. He observed shifts at 316.8, 631.3, and 944.5 cm^{-1}. Now although it is possible indeed that the Raman fundamental might be photographed under the experimental conditions employed, the intensities of the overtones are, as Stammreich noted, likely to be several orders of magnitude smaller. Moreover, the observed shifts fit poorly with those calculated from the known values of the vibrational constants (see Table I) on the assumption that the shifts are $G''(1)-G''(0)$, $G''(2)-G''(0)$, and $G''(3)-G''(0)$, respectively.

A more plausible interpretation of these observations is that the lines are really lines of a resonance fluorescence series. The wave number of the exciting line is 17014.8 cm^{-1}. There is only one strong absorption band in this region, the 13.2 band of the system $B^3\pi o_u{}^+-X'\Sigma_g{}^+$, with head at 17033.7 cm^{-1} (Brown[2]). The "Raman spectrum" may then be interpreted as the series dropping from $v'=13$ to $v''=2$, 3, 4, and 5. Re-absorption probably prevented observation of the anti-Stokes lines with $v''=0,1$. The numerical evidence in support of this interpretation is shown in

Table I.

Observed shift	Calculated Raman shift	Calculated resonance shift
316.8 cm^{-1}	$G''(1)-G''(0)=321.5$ cm^{-1}	$G''(3)-G''(2)=316.9$ cm^{-1}
631.3	$G''(2)-G''(0)=640.7$	$G''(4)-G''(2)=631.5$
944.5	$G''(3)-G''(0)=957.6$	$G''(5)-G''(2)=943.8$

Table I. The calculated values are with

$$G_v''=323.81(v''+\tfrac{1}{2})-1.15(v''+\tfrac{1}{2})^2:$$

these values of the vibrational constants (which refer to $Br^{79}Br^{81}$) are taken from Plumley.[3] It may be objected that the pressure (900 mm) is high for the observation of a resonance spectrum. However, Plumley[3] found that the self-quenching in bromine is much weaker than in iodine, and observed appreciable intensity of resonance series at pressures as high as 100 mm. There is little doubt that the decay with increasing pressure is sufficiently slow for observation of a series at 900 mm pressure under conditions such as are used for the study of the feeble Raman spectra of gases.

[1] H. Stammreich, Phys. Rev. **78**, 79 (1950).
[2] W. G. Brown, Phys. Rev. **38**, 1179 (1931).
[3] H. J. Plumley, Phys. Rev. **45**, 678 (1934).

Vapor Pressure and Viscosity of Liquids

Shashanka Shekhar Mitra, *Department of Physics*
and
Dhirendra Nath Chakravarty, *Department of Chemistry, Allahabad University, Allahabad 2, India*
(Received August 9, 1954)

THE temperature dependence of vapor pressure and viscosity of liquids being similar (one increasing and the other decreasing) it seems that they are governed by parallel mechanisms. By eliminating temperature between Wrede's[1] vapor pressure formula and Andrade[2]-Reynolds[3] viscosity formula one arrives at a simple relationship connecting these two fundamental properties of a liquid. The relation is

$$\log p+n\log\eta=C \quad (1)$$

where p represents vapor pressure, η viscosity and n and C being constants. This equation has been given and tested by many authors.[4–11] In fact for certain simple liquids the plot of $\log p$ against $\log\eta$ yields a straight line, but for many of them, especially, the associated ones the deviations from the straight line are frequent. The inadequacy of Eq. (1) has been discussed by one of us[12] in a previous note and has been attributed to the approximate nature of Wrede-Andrade type of function. It was shown that for these liquids Eq. (1) should be modified to

$$\log p+n\log\eta+n'(\log\eta)^2=C. \quad (2)$$

In the present communication the deviation will be discussed in further detail. If at any temperature T_0 the vapor pressure and

viscosity are represented, respectively, by p_0 and η_0 then (1) can be rewritten in the form

$$\log p - \log p_0 - n(\log \eta_0 - \log \eta) = 0$$

or,

$$n = \frac{\log p - \log p_0}{\log \eta_0 - \log \eta}. \tag{3}$$

If a liquid follows (1) then n must be independent of temperature. But that is not the case with many of the liquids particularly the associated ones, as is evidenced from the column IV of Tables I and II, which show the case for water and ethyl alcohol. Hence n

TABLE I. Water.

T°K	p mm	$\eta \times 10^3$ (cgs)	n	$K \times 10^2$
273	4.579	17.93	...	...
283	9.209	13.11	2.2314	158.6
293	17.54	10.06	2.3232	157.9
303	31.82	8.00	2.4021	157.6
313	55.32	6.57	2.4818	157.4
323	92.51	5.50	2.5422	157.3
333	149.38	4.69	2.5983	157.5
343	233.7	4.06	2.6476	157.6
353	355.1	3.56	2.6897	157.9
363	525.8	3.16	2.7325	158.2
373	760.0	2.84	2.7741	158.6

TABLE II. Ethyl alcohol.

T°K	p mm	$\eta \times 10^3$ (cgs)	n	$K \times 10^2$
273	12.2	17.90	...	...
283	23.6	17.52	30.803	353.1
293	43.9	17.16	30.214	353.6
303	78.8	16.81	29.676	354.0
313	135.3	16.47	28.920	354.1
323	222.2	16.13	27.880	353.6
333	352.7	15.81	27.090	353.4
343	542.5	15.49	26.242	353.1

may be represented by some function of temperature:

$$n = f(T). \tag{4}$$

When n and T are plotted on a logarithmic graph, a straight line is obtained showing the function of the type

$$n = \frac{T^a}{b} \tag{4a}$$

or

$$a \log T - \log n = K, \tag{5}$$

where a, b, and K are constants. The constancy of K is shown in the column V of the tables. The value of a is 0.7889 and 1.1995 for water and ethyl alcohol, respectively, and T_0 has been taken to be 273°K. It has been found that n may also be represented as

$$n = \frac{(\log T)^c}{d} \tag{4b}$$

where c and d are two other constants.

Equations (4a) and (4b) connect vapor pressure and viscosity of liquids involving temperature too, whereas Eq. (2) may be regarded as a temperature-independent relation begween them.

The authors are grateful to Professor S. Ghosh and Dr. K. Majumdar for their interest in the investigation. They also thank Dr. A. K. Dey and Mr. Y. P. Varshni for helpful discussions.

[1] Wrede, Ann. Physik **104**, 612 (1858).
[2] Andrade, Phil Mag. **17**, 497, 698 (1934).
[3] Reynolds, Trans. Roy. Soc. (London) **177**, 157 (1886).
[4] Stoel, Z. physik. Chem. **11**, 126 (1893).
[5] Stoel. J. Phys. Chem. **1**, 700 (1897).
[6] Porter, Phil. Mag. **23**, 458 (1912).
[7] Prasad, Current Sci. **1**, 237 (1933).
[8] Rente and Senggert, Ind. Eng. Chem. **26**, 550 (1934).
[9] Lucatu, Compt. rend. **207**, 1403 (1938).
[10] Cheu and Hu, J. Chinese Chem. Soc. **12**, 29 (1945).
[11] Cheu and Yi, J. Chinese Chem. Soc. **12**, 44 (1945).
[12] S. S. Mitra, J. Chem. Phys. **22**, 250 (1954); Erratum, **22**, 1471 (1954)

Free Electron Model for Tropolone

SADHAN BASU
Indian Association for the Cultivation of Science, Calcutta 32, India
(Received July 27, 1954)

IT has been shown by Dewar[1] that the absorption spectra and the orientation effect in electrophilic substitution of tropolone can be predicted fairly accurately by molecular orbital calculation. The purpose of the present note is to show that exactly the same result is obtained by "free electron approximation" treatment.[2] The cyanine-like character of tropolone anion (I), makes it well suited for the purpose.

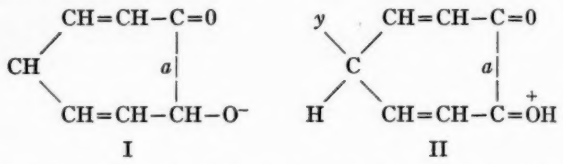

I II

The box dimension for the π electrons in the anion is 8 l, where l is the C−C bond length in benzene (=1.41 A) and there are in all 10 electrons, one for each carbon atom and 3 for two terminal oxygen atoms, which will occupy 5 lowest levels. The energy levels are given by

$$E = \left(\frac{h^2}{8m}\right)\frac{n^2}{L^2} \tag{1}$$

(where L is the total length of the box) and the wavelength for the first transition by

$$\lambda = 329.7\frac{L^2}{(2n+1)}. \tag{2}$$

From this equation the calculated value for the first absorption maximum for tropolone anion comes out to be equal to 382.4 mμ as compared to 396 mμ given by Doering and Knox,[3] and attributed to the ion by Dewar. In the un-ionized form the application of free electron theory is not justified; still we may use it as a first approximation. In this case the box dimension is 7 l with 8 π electrons, which will fill up 4 lowest energy levels. The calculated wavelength for first transition comes out to be 356 mμ. Cook *et al.*[4] have reported an absorption at 352 mμ for tropolone in alcohol, while Doering and Knox reported an absorption at 368 mμ. In both case agreement appears to be as good as MO calculation. Difference from MO calculation is that only principal absorption maximum can be predicted accurately by free electron treatment.

Relative ease of electrophilic substitution at ortho, meta, and para positions can be predicted from the difference in π-electron energies of tropolone and the quinonoid transition states, like II. Total π-electron energy of each structure was calculated using Eq. (1) and their difference from parent tropolone (non-ionic) are listed in Table I. It is evident that the difference is minimum

TABLE I.

Substitution	ΔE_π
ortho	$1.90K$[a]
meta	2.52
para	1.00

[a] K stands for $h^2/8ml^2$.

for para substitution, hence this reaction will be most favored. The same conclusion has also been arrived at by MO calculation. (In all these deductions bond "a" in I and II has been taken to be predominantly single in character).

[1] Dewar, Nature **166**, 790 (1950).
[2] Bayliss, J. Chem. Phys. **16**, 287 (1948); Kuhn, Helv. Chem. Acta **31**, 1441 (1948).
[3] Doering and Knox, J. Am. Chem. Soc. **72**, 2305 (1950).
[4] Cook *et al.*, Chem & Indust. 426 (1950).

Backscattering from Targets of Low Atomic Number Bombarded with 1–2 Mev Electrons*

JEROME SALDICK AND AUGUSTINE O. ALLEN
Brookhaven National Laboratory, Upton, Long Island, New York
(Received July 26, 1954)

IN a recent article[1] we estimated the fraction of "high-energy secondaries" ("HES"),[2] including deflected primaries together with true high-energy secondaries,[3] which would be scattered back from an aqueous solution bombarded with perpendicularly incident 1- and 2-Mev electrons. This fraction was measured for thick targets of Al, Fe, W, Pt, and Pb. Interpolation between $Z=0$ and $Z=13$ was made on the assumption that the fraction varied linearly with Z. Subsequently, we have obtained data for Mg, C, Be, and (at 1 Mev only) Li. The results, given in Fig. 1,

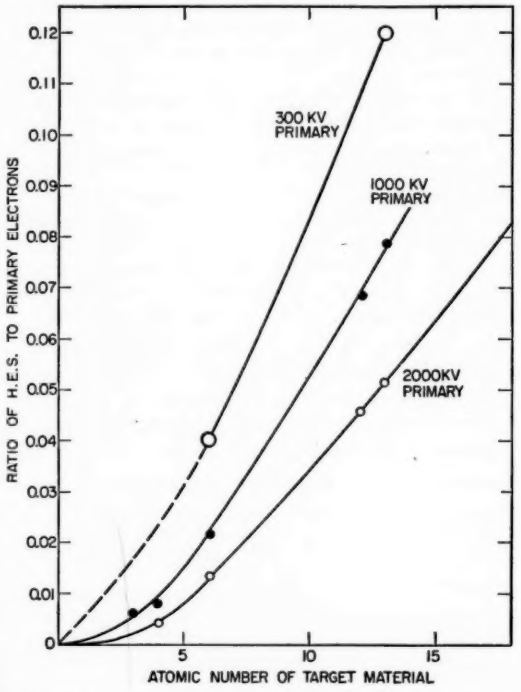

FIG. 1. Ratio of high-energy secondary to primary electrons as a function of atomic number of target material. Data for 300 kv taken from reference 2.

show definitely that the fraction increases nonlinearly with Z in the range of low Z.

According to the new data, "HES," as fraction of total primary beam, for our $0.8N$ H_2SO_4 solutions ($Z_{eff}=6.74$), should be 0.0168 at 2 Mev and 0.0278 at 1 Mev, as compared to the formerly assumed values of 0.0371 and 0.0404. Since we assume the "HES" have on the average 15 percent of the energy of the primary electrons, the previously reported values of G for $FeSO_4$ solutions should be increased by 85 percent of the difference between the old and new HES values, or 1.73 percent at 2 Mev and 1.07 percent at 1 Mev. The reported value of G, however, was assigned a probable error of ± 3 percent. This revision of the backscattering correction, and any small additional correction required by consideration of true high-energy secondaries from the aluminum window on the Van de Graaff machine do not, therefore, affect our conclusions, and are important to dose measurement only when greater accuracy is sought.

* Research performed under the auspices of the U. S. Atomic Energy Commission.
[1] J. Saldick and A. O. Allen, J. Chem. Phys. **22**, 438 (1954).
[2] J. G. Trump and R. J. Van de Graaff, Phys. Rev. **75**, 44 (1949).
[3] Marshall, Shatas, and Pomerantz, Bull. Am. Phys. Soc. **29**, 46(A) (1954).

I. Experimental Verification of the Mie Theory of Light Scattering*†

WILFRIED HELLER, JOSEPH N. EPEL, AND RICHARD M. TABIBIAN
Chemistry Department, Wayne University, Detroit, Michigan
(Received July 27, 1954)

SEVERAL thorough investigations published during the past 45 years[1] left little doubt that the Mie theory of light scattering[2] is in essential agreement with the facts. There has, however, been no rigorous quantitative proof which presupposes (a) the use of a system with spherical particles as uniform in size as possible, (b) an exact knowledge of their density and refractive index, (c) an optical precision instrument, and (d) a fairly reliable independent method of comparative size determinations. While one or two of these requirements could be met, not all could be complied with satisfactorily in the past. Polystyrene and polyvinyl toluene lattices of remarkably small degree of heterodispersion[3] were used in the present investigation. A separate study by Thomas L. Pugh in this laboratory showed that the colloidal spheres had a density of 1.057 and 1.026 and a refractive index of 1.625 and 1.595, respectively (25°C).[4] This note is concerned with particle size determinations from the specific turbidity obtained by transmission measurements using a precision apparatus constructed in this laboratory in conjunction with K. Herrington.[5] Its characteristics pertinent to the data given here are (a) a solid angle of the primary and secondary beam of 0.7° and 0.8°, respectively, and (b) a quantitative exclusion of primary and secondary parasite light. Since shadow casting showed no perceptible flattening out of the apparently rigid polymer spheres, electron microscopy was used as the independent comparative second method. In view of the well-known systematic variation of electron-optical diameters with the instrument used,[6] an additional set of electron-optical diameters, obtained by Dr. E. B. Bradford of the Dow Chemical Company, was also considered.

The first column in Table I gives the experimental specific turbidities observed at 5461 a.u. and extrapolated to zero concentration (c in g 100 g^{-1}). The second column contains the optical particle diameter D_0 calculated by interpolation from the theoretical specific turbidities given in a preceding preliminary note.[7] Columns 3 and 4 show the electron microscopic diameters, D_E and column 5 defines, by the standard deviation σ, the spread of the size distribution curve in the lattices used. Most of the latter data were compiled in this laboratory.

Excluding from a comparison the unsatisfactory sample with the smallest particle diameter, the average percent deviation of the electron optical diameters from the optical ones is +14.5 (Watson) and +6.8 (Bradford) for polystyrene, and +5.2 for

TABLE I.

$(\tau/c)_0$ cm^{-1}	D_0 mμ	D_E in Bradford	mμ Watson	σ
5.1*	58	45	65	8
22.9	109	119	···	4
37.0	132	132	···	2
49.4*	132	135	155	16
42.7	141	144	···	4
59.0*	152	150	180	20
62.7	171	177	···	4
104.2*	206	219	258	10
110.9*	215	223	260	17
109.4*	212	230	218	9
113.0*	217	254	258	10
126.0*	232	252	263	35
126.0*	232	259	289	7
158.4*	262	275	299	47
204	350	···	373	11
246	410	439	···	6
269	446	470	···	5
310	511	535	···	9
331	548	595	···	7
397	705	770	···	11

* Starred data refer to polystyrene, others pertain to polyvinyl toluene.

polyvinyl toluene. The maximum deviation in the latter systems —which in every respect were more satisfactory than polystyrene —amounts to +8.4 percent. It is noteworthy that all deviations, except one, are positive, which is possibly accounted for by minute flattening out of the spheres in electron microscopy.[4] The systematic error in electron microscopy should not exceed, but may be as large as, ±5 percent and the nonsystematic error is assumed to be about ±1 percent. The combined error in measurements of τ and c approximates ±3 percent for particles whose diameters are less than 200 mμ and ±2 percent for larger particles. Taking all this into account, the agreement between optical and electron optical diameters must be considered as excellent. Consequently, it can be stated, without reservations, that the Mie theory is in quantitative agreement with the facts.

* The exploratory first part of this work (J. N. Epel) was supported by a grant from the Research Corporation, the later large scale investigations (Richard M. Tabibian) were supported by the U. S. Office of Naval Research.

† Electron microscopy by John H. L. Watson, Edsel B. Ford Institute for Medical Research, Detroit, Michigan.

[1] Beginning with W. Steubing, Ann. Physik **26**, 329 (1908).

[2] G. Mie, Ann. Physik **25**, 377 (1908).

[3] These lattices were prepared by the Dow Research Laboratories, Midland, Michigan and kindly given to us by Dr. R. S. Spencer and Dr. F. Towsley and, more recently, by Dr. J. W. Vanderhoff.

[4] The refractive index decreased with increasing particle size, possibly due to a decrease in the contribution of the highly refractive stabilizing agent adsorbed at the surface of the particles. The values given are extrapolations to zero diameter. Use of the present mean values of a continuing investigation on diameters between 0 and 400 mμ, 1.607 and 1.588, respectively, would reduce the average percent deviation between optical and electron-optical diameters to less than 5 percent for both systems.

[5] Unpublished work presented at 116th Meeting of the American Chemical Society, September, 1949, Atlantic City, New Jersey.

[6] See, e.g., Ch. H. Gerould, J. Appl. Phys. **21**, 183 (1950).

[7] W. Heller and W. J. Pangonis, J. Chem. Phys. **22**, 948 (1954).

"Steric Protection" of Hydrophobic Colloidal Particles by Adsorption of Flexible Macromolecules*

WILFRIED HELLER AND THOMAS L. PUGH
Chemistry Department, Wayne University, Detroit, Michigan
(Received July 30, 1954)

THE two classical principles for protecting non-ionogenic hydrophobic particles in an aqueous medium are (a) adsorption of capillary active, preferably amphipathic, long chain ions which may provide a sufficiently high surface potential and charge density (e.g. soaps); (b) adsorption of rigid non-ionizing strongly hydrophilic macromolecules[1] which—after monolayer formation—impart upon the particles the typical stability of a hydrophilic colloid (e.g. natural or synthetic polysaccharides and derivatives). The responsible factor may be a critical reduction in the difference of cohesive energy densities of colloid and medium due to indirect hydration. Both principles may apply to a single protective agent (e.g. proteins). A third possibility arose as a consequence of work done by W. Tanaka on the adsorption isotherms of flexible macromolecules.[2] It leads to the following picture of the mechanism of adsorption: (a) flexible molecules of the moderately high weight used (up to $M=6000$) neither "stand up" (like soaps) nor lie flat (like proteins) but most likely assume a configuration roughly described by a V or W,[3] i.e., they are anchored into the surface with only a few segments; (b) with increasing surface coverage, and with increasing molecular weight, at equal surface coverage, additional molecules require more and more time to reach physical contact with the surface (and also to diffuse away from it). Assuming a V configuration, the most probable distance of a terminal segment from the surface proper would be of the order of magnitude of 10′ a.u. Assuming negligible interpenetration of the polymeric peripheries of two colliding colloidal particles—which appears justified in the light of related results by Flory[4]—their nearest possible approach would be characterized by a distance of the same order of magnitude. Distances of this order are large enough to make the negative interaction energy of two colloidal particles as small or smaller than their thermal energy. An inability to effectively aggregate, i.e., a stabilization which may be called "steric protection" should therefore be expected in such cases.[5]

TABLE I.

M polymer:	600	4000	6000	9000
γ^a:	18.0±2.5	22±5	47±5	480±30

[a] γ in absence of polymer: 12.5±2.5.

Tests were carried out by studying the effect of polyethylene glycols[6] upon the stability of gold sols using a modification of Zsigmondy's gold number. (The same materials had been used for the adsorption experiments.) Protection, towards coagulation by KCl, increased with increasing polymer concentration—without intermediate sensitization—until an approximately constant optimum was reached at about 1.50 g of polymer per liter mixture. Table I gives the protective action near this optimum (1.00 g per liter mixture) as a function of M at 21°–24°C. γ represents the concentration of KCl, in millimoles per liter mixture, which leads, after exactly 24 hours, to a red→blue shift in color (transmission) for a Au concentration of 89.0 mg per liter mixture.

The protective action increases throughout with M, but an enormous increase begins in the neighborhood of $M=6000$. The amount of polymer adsorbed is, according to Tanaka, practically independent of M at $M=6000$. Only one plausible explanation of the sudden rise in protective efficiency appears therefore possible, i.e., the attainment at or near this M, of the critical minimum distance between colloidal particles above which "steric protection" becomes fully effective. Since it is very difficult to desorb such high molecular weight material completely, the significance of this type of protection for permanent stabilization of hydrophobic colloids is apparent.

* This work was carried out with the support of the U. S. Office of Naval Research.

[1] Their hydrophilic monomers are also effective, although considerably less, as the retardation of thixotropic sol-gel transformation by sucrose and amino acids indicates [W. Heller, Compt. rend. **203**, 1507 (1936)].

[2] For a preliminary publication of some of these results, see W. Heller and W. Tanaka, Phys. Rev. **82**, 301 (1951).

[3] Recent theoretical work [Simha, Frisch, and Eirich, J. Phys. Chem. **57**, 584 (1953)] seems to support this picture and seems to indicate that the V configuration is more probable in our case.

[4] P. J. Flory, J. Chem. Phys. **13**, 453 (1945).

[5] M. van der Waarden offered previously essentially the same explanation for the stabilization of charcoal suspensions in organic liquids by means of low molecular weight (up to C_{16}) hydrocarbon derivatives. [J. Colloid Sci. **5**, 317 (1950)]. See also E. L. Mackor and J. H. van der Waals, J. Colloid Sci. **7**, 535 (1952).

[6] Samples, which we purified by reprecipitation, were kindly provided by the Carbide and Carbon Chemical Company and also by the Texas Division of the Dow Chemical Company.

On the Absolute Turbidity of Water*

RICHARD W. FESSENDEN AND RICHARD S. STEIN
Department of Chemistry, University of Massachusetts, Amherst, Massachusetts
(Received July 26, 1954)

GORING and Napier have recently reported a value of 1.76×10^{-5} cm^{-1} for the turbidity of water at a wavelength of 5461 angstrom units.[1] We wish to report some measurements of this quantity.

Scattering measurements were made at 5461 A at $\theta=90°$ using a modified Zimm type apparatus.[2,3] Solutions were filtered by suction directly into the scattering cell using a "Millipore" type filter† with Type HA 0.5 micron pore size membrane type filter disks. The scattering was measured relative to that of carefully purified benzene. The intensities were corrected using refraction correction factors.[3]

Aqueous solutions of a number of salts were studied. It was found that a lower turbidity was obtained for very dilute salt

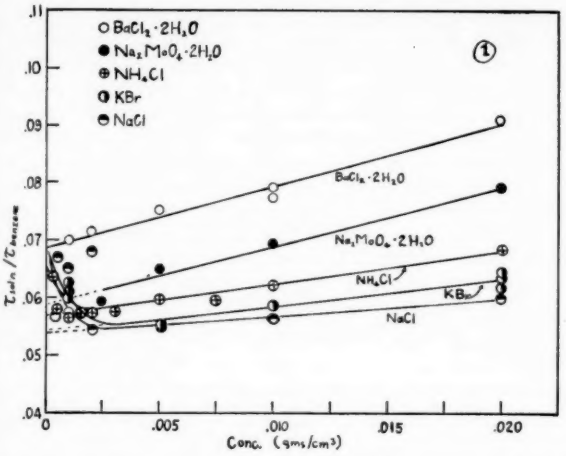

FIG. 1. The relative turbidites at $\theta = 90$, $\lambda = 5461$ A for aqueous solutions of a number of salts.

solutions than for pure water. This presumably occurred because of the electrolyte aiding in the precipitation and removal of colloidal impurities from the water. It was therefore concluded that the best value for the turbidity of water could be obtained by extrapolating that of a dilute salt solution to infinite dilution.

The relative turbidites obtained by doing this for NaCl, $BaCl_2 \cdot 2H_2O$, $Na_2MoO_4 \cdot 2H_2O$, NH_4Cl, and KBr are plotted in Fig. 1. The average intercept is 0.0577 ± 9 percent. It is noted that the higher-valent salts give higher intercepts. This may result from curvature of the plots at low concentrations arising from the lower activity coefficients for these salts. The average turbidity calculated using Zimm and Carr's value for the turbidity of benzene of 2.83×10^{-4} cm^{-1} is $1.63 \times 10^{-5} \pm 10$ percent. This agrees, within the limits of experimental error, with Goring and Napier's value. The average molecular weights for the salts calculated from the slopes of Fig. 1 and the refractive index increments are of the correct order of magnitude.

* This work constitutes part of a Senior Honors Research Problem by Mr. Fessenden at the University of Massachusetts.
† Lovell Chemical Company, Watertown, Massachusetts.
[1] D. A. I. Goring and P. G. Napier, J. Chem. Phys. **22**, 147 (1954).
[2] B. H. Zimm, J. Chem. Phys. **16**, 1099 (1948).
[3] C. I. Carr, Jr., and B. H. Zimm, J. Chem. Phys. **18**, 1616 (1950).

The Liquid System Ozone-Oxygen*

A. C. JENKINS AND C. M. BIRDSALL
Laboratory of the Linde Air Products Company, A Division of Union Carbide and Carbon Corporation, Tonawanda, New York
(Received June 25, 1954)

IN a Letter to the Editor of this Journal, H. J. Schumacher[1] presented a temperature-composition diagram of the system ozone-oxygen at atmospheric pressure. When this diagram was published we had just completed work on a similar diagram, which gave no indication of any azeotropic maximum; Schumacher's diagram shows a maximum at -105.3°C.

Furthermore, we found that at one atmosphere pressure there is a region in which two liquid phases co-exist at constant temperature over the liquid composition range of about 21 to 65 mole-percent ozone. Schumacher's data show no two liquid phase region at one atmosphere, but indicate that the liquid curve is just above the consolute temperature.

In order to confirm our data we determined the time-temperature curve shown in Fig. 1. Ano zone-oxygen mixture with an initial composition of 3.5 mole-percent ozone was allowed to boil off at approximately one atmosphere pressure (757 mm) and the temperature of the liquid observed continuously. This curve indicates that a two-liquid phase region, not shown in Schumacher's diagram, exists at the pressure of the experiment.

The time-temperature curve also shows that there is no maximum at -105.3°C. At the end of the two-liquid phase region the temperature rises rapidly until it reaches the boiling point of pure ozone. (Our normal boiling point for pure ozone[2] was -111.9°C ± 0.3°C which is in agreement with the boiling point reported by Riesenfeld and Beja.[3]) The temperature remains at -111.9°C until the volume of liquid is too small for further temperature measurements. If Schumacher's diagram were correct the temperature would reach a maximum of -105.3°C and stay constant, since the liquid and vapor would have the same composition at this point and no further change in composition or temperature would occur.

We have carefully examined the published reports of Schumacher's complete work[4] in an effort to explain his results. His liquid compositions in the ozone-rich region, in both his solubility diagram and in his temperature-composition diagram, are lower in ozone than ours by as much as 20 mole-percent. This suggests that Schumacher's method of vaporizing the entire ozone-rich liquid sample before analysis may have resulted in partial decomposition of the ozone, a procedure which would lead to low results. It will be noted that no measurements were made, or at least

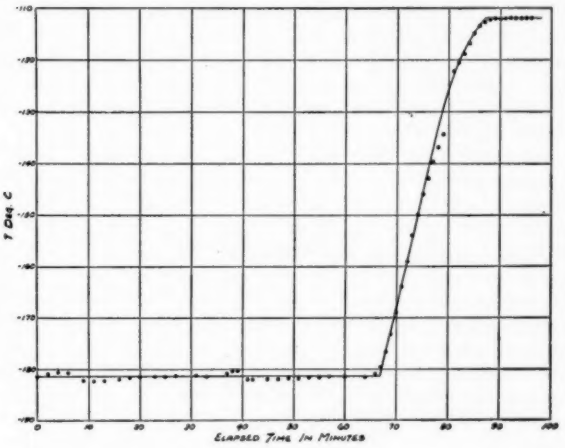

FIG. 1.

none was reported, at one atmosphere pressure in that part of the temperature-composition diagram which would include the two-liquid phase region; apparently it was *assumed* in drawing the curve that this region was above the consolute temperature.

Schumacher states that in his thermostat, the resistance thermometer was located between the vessel containing the sample and the heating coil. No mention is made of any precautions to assure temperature equilibrium between the thermometer and sample bulb. It appears possible that the thermometer recorded a temperature between that of the heating coil and sample vessel, rather than the true temperature of the sample. Since it would be necessary to supply heat continuously to overcome the cooling effect of the outer liquid-nitrogen bath, this would result in the maximum temperature's being too high.

From our extensive work on liquid and vapor compositions and vapor pressures of ozone-oxygen mixtures and on the properties of pure liquid ozone, we must conclude that (1) there is no azeotropic maximum in the temperature-composition diagram, and (2) a two liquid phase region exists at atmospheric pressure for ozone-oxygen mixtures.

We would like to acknowledge the help of Mr. F. S. DiPaolo in carrying out the experiments described in this letter.

* This work was performed under Contract NOa(s)10945 for the Bureau of Aeronautics, United States Navy.
[1] H. J. Schumacher, J. Chem. Phys. **21**, 1610–1611 (1953).
[2] A. C. Jenkins and C. M. Birdsall, J. Chem. Phys. **20**, 1158–1161 (1952).
[3] E. H. Riesenfeld and M. Beja, Medd. Netenskapsakad. Nobelinst. **6**, No. 7, 1 (1923).
[4] H. J. Schumacher, Anales asoc. quím. argentina **41**, 208–229 (1953).

Distribution of Kinetic and Potential Energy in Vibrating Molecules

WILLIAM J. TAYLOR
McPherson Chemical Laboratory, The Ohio State University, Columbus, Ohio
(Received July 16, 1954)

IN carrying out a normal coordinate calculation for a molecule, it is desirable to obtain some indication of the form of the normal modes, Q_α, Q_β, $\cdots$, in addition to their (squared) frequencies, λ_α, λ_β, $\cdots$. The latter are obtained, in Wilson's **G**-matrix method[1] by solving the secular equation $|\mathbf{GF}-\lambda\mathbf{I}|=0$. **G** is the reciprocal of the kinetic energy matrix, and **F** the potential energy matrix, both expressed in terms of a set of internal coordinates, R_i, R_j, $\cdots$; **I** is the unit matrix. For a symmetric molecule, each symmetry type may be dealt with separately, and the R_i's will be assumed to represent symmetry coordinates.

The form of the normal modes may be determined by finding the transformation **L** connecting the R_i's and Q_α's, $\mathbf{R}=\mathbf{LQ}$. Here **L** is a square matrix $[L_{i\alpha}]$, and $\mathbf{R}=\{R_i, \cdots\}$, $\mathbf{Q}=\{Q_\alpha, \cdots\}$, are column vectors. If a single normal mode, Q_α, is excited with unit amplitude, the amplitudes of the R_i's are given by the αth column of **L**, or $R_i=L_{i\alpha}$. The transformation **L** may be determined by solving the eigenvector equation $\mathbf{GFL}=\mathbf{L\Lambda}$, where $\mathbf{\Lambda}$ is the diagonal matrix of the λ_α's. This matrix equation is equivalent for each α, to a set of simultaneous homogeneous linear equations,[1] $(\mathbf{GF}-\lambda_\alpha\mathbf{I})\mathbf{L}_\alpha=0$, for the elements of $\mathbf{L}_\alpha$, the αth column of **L** (αth eigenvector). The $\mathbf{L}_\alpha$ may be "normalized" by means of the relation $\mathbf{L}_\alpha'\mathbf{FL}_\alpha=\lambda_\alpha$.

The solution for the quantities $L_{i\alpha}$ would seem to provide a complete answer to the question of the form of the normal modes. However, the $L_{i\alpha}$'s suffer from the disadvantage that they are not invariant to the unit used in defining the internal coordinates, R_i. This is particularly troublesome if some of the R_i's represent stretching coordinates (linear units), and others represent bending coordinates (angular units). One method of handling this situation is the multiplication of each bending coordinate by a length, for example, a bond length, but the arbitrary nature of this device makes it rather unsatisfying. For this, and other reasons, several workers[2] have suggested that the distribution of potential energy among the R_i's be used as a criterion of the form of the normal modes. The potential energy matrix for the Q_α's is $\mathbf{L'FL}=\mathbf{\Lambda}$ (diagonal matrix), so that the force constant for Q_α is $\lambda_\alpha=\sum_{ij}L_{i\alpha}L_{j\alpha}F_{ij}=\sum_{ij}\lambda_{ij}{}^\alpha$, say. The quantities $\lambda_{ij}{}^\alpha=L_{i\alpha}L_{j\alpha}F_{ij}$ are invariant to the choice of units for R_i and R_j. From this viewpoint, Q_α is regarded as being predominantly the motion R_i, and λ_α the characteristic frequency of R_i, if $\lambda_{ii}{}^\alpha$ is the dominant term in the preceding sum (the diagonal terms $\lambda_{ii}{}^\alpha$, as well as λ_α, are non-negative).

The purpose of the present note is to point out that a criterion for the form of the normal modes based on the distribution of potential energy alone is incomplete, and may be misleading, in spite of its undoubted usefulness in many cases. To obtain a complete picture, the distribution of kinetic energy must also be considered. The kinetic energy matrix for the Q_α's is $\mathbf{L'G^{-1}L}=\mathbf{I}$ (unit matrix), so that the mass for Q_α is $1=\sum_{ij}L_{i\alpha}L_{j\alpha}(\mathbf{G}^{-1})_{ij}=\sum_{ij}\eta_{ij}{}^\alpha$, say. The quantities $\eta_{ij}{}^\alpha=L_{i\alpha}L_{j\alpha}(\mathbf{G}^{-1})_{ij}$ are also invariant, and indicate the distribution of kinetic energy when Q_α is excited, just as the $\lambda_{ij}{}^\alpha$'s indicate the distribution of potential energy ($\eta_{ii}{}^\alpha$ is non-negative). They are generalizations of the quantities introduced for Cartesian coordinates by E. Teller.[3] The $\eta_{ij}{}^\alpha$'s satisfy a sum rule:

$$\sum_\alpha \eta_{ij}{}^\alpha=(\mathbf{G}^{-1})_{ij}\sum_\alpha L_{i\alpha}L_{j\alpha}=(\mathbf{G}^{-1})_{ij}(\mathbf{LL}')_{ij}=(\mathbf{G}^{-1})_{ij}G_{ij}.$$

Here we have used the relation $\mathbf{LL}'=\mathbf{G}$, which follows from the fundamental relation, $\mathbf{L'G^{-1}L}=\mathbf{I}$. If **G** is diagonal, as for Cartesian coordinates, one obtains Teller's result, $\sum_\alpha \eta_{ij}{}^\alpha=\delta_{ij}$. A similar sum rule may be obtained for the $\lambda_{ij}{}^\alpha$'s: $\sum_\alpha \lambda_{ij}{}^\alpha=F_{ij}G_{ij}$.

If the potential energy of the normal coordinate Q_α or $\lambda_\alpha=\sum_{ij}\lambda_{ij}{}^\alpha$ is predominantly contributed by R_i, then $\lambda_\alpha\sim\lambda_{ii}{}^\alpha$, or $\lambda_\alpha\sim L_{i\alpha}{}^2F_{ii}$: Similarly, if the kinetic energy of Q_α, or $\sum_{ij}\eta_{ij}{}^\alpha(=1)$, is contributed predominantly by R_i, then $L_{i\alpha}{}^2(\mathbf{G}^{-1})_{ii}\sim 1$. Therefore, when *both* these conditions are satisfied, $\lambda_\alpha\sim F_{ii}/(\mathbf{G}^{-1})_{ii}$, or $\lambda_\alpha\sim\lambda_i{}^0$, where $\lambda_i{}^0=F_{ii}/(\mathbf{G}^{-1})_{ii}$ is the frequency the coordinate R_i would have if it were not coupled to the other coordinates. The frequency λ_α may then be said to be a characteristic frequency of the coordinate R_i (for example, a bond stretching or bending).[4]

The distribution of kinetic energy depends on the elements of $\mathbf{G}^{-1}$, whereas it is **G** that is most readily computed (using Wilson's method[1]). However $\mathbf{G}^{-1}$ may be obtained without direct reciprocation of **G** as follows:[5] from $\mathbf{L'FL}=\mathbf{\Lambda}$, one obtains $\mathbf{L}^{-1}=\mathbf{\Lambda}^{-1}\mathbf{L'F}$, and using the relation $\mathbf{L'G^{-1}L}=\mathbf{I}$, one then has $\mathbf{G}^{-1}=(\mathbf{L}^{-1})'\mathbf{L}^{-1}$. An alternative procedure[1] is to solve the equations $\mathbf{FG}(\mathbf{L}^{-1})'=(\mathbf{L}^{-1})'\mathbf{\Lambda}$, instead of $\mathbf{GFL}=\mathbf{L\Lambda}$, thus obtaining $\mathbf{L}^{-1}$ directly (normalize by $\mathbf{L}^{-1}\mathbf{G}(\mathbf{L}^{-1})'=\mathbf{I}$). Then $\mathbf{G}^{-1}=(\mathbf{L}^{-1})'\mathbf{L}^{-1}$, and $\mathbf{L}=\mathbf{G}(\mathbf{L}^{-1})'$.

[1] E. B. Wilson, Jr., J. Chem. Phys. **7**, 1047 (1939); **9**, 76 (1941). The section on page 82 of Wilson's second paper is of particular interest in the present connection, and the notation of this section will be followed closely.
[2] O. Burkard, Proc. Indian Acad. Sci. **8**, 365 (1938); J. Wagner, Z. physik. Chem. **B45**, 69 (1939); P. Torkington, J. Chem. Phys. **17**, 357 (1949); Y. Morino and K. Kuchitsu, J. Chem. Phys. **20**, 1809 (1952).
[3] E. Teller, *Hand- und Jahrbuch der Chemischen Physik* (Akademische Verlagsgesellschaft, Leipzig, 1934), volume 9, section 2.
[4] The present analysis is oversimplified for modes and frequencies characteristic of structural groups containing several internal coordinates, R_i, R_j, $\cdots$ The characteristic frequencies are then roots of the corresponding submatrices of **F** and $\mathbf{G}^{-1}$, and are affected by coupling between coordinates within the group. The obvious generalization of the preceding result is as follows: the potential *and* kinetic energies of a normal mode must be contributed predominantly by the internal coordinates within a structural group, if the mode and its frequency are to be regarded as characteristic of the group.
[5] B. L. Crawford, Jr., and W. L. Fletcher, J. Chem. Phys. **19**, 141 (1951).

Photochemical Reactions of Cyclo-Octatetraene

IKUZO TANAKA AND MICHIO OKUDA
Laboratory of Physical Chemistry, Tokyo Institute of Technology Ookayama, Neguro-ku, Tokyo, Japan
(Received August 12, 1954)

CYCLO-OCTATETRAENE (C.O.T.) has the absorption of light at 2750 A and near 1950 A.[1] They both show continuous spectra at room temperature. The strong band below 2000 A may be due to the $^1A_1-{}^1E$ transition and the 2800 A weak band to the $^1A_1-{}^1A_1$ or the $^1A_1-{}^1A_2$ transition.[2] It has been shown, by means of absorption spectra, that when irradiated with a mercury vapor lamp C.O.T. undergoes photochemical reactions according to the following processes:

(1) Photolysis[3]: C.O.T.→benzene+acetylene
(2) Photoisomerization[4]: C.O.T.→styrene
(3) Formation of unknown substances:
Unknown gaseous substances are detected by absorption spectra at 2913 A, 2913–2895 A(d), 2847–2820 A(d), 2810–2785 A(d), 2670–2720 A(d).

The benzene obtained by photolysis was quantitatively determined by means of a spectrometer, and the quantum yield for benzene was about 0.1.[3] After irradiation, the gaseous products being not condensed by dry ice were analyzed by a mass spectrometer.

The mass spectra were measured with a Hitachi R-M type mass spectrometer, which arranged a sector-type magnet with a 90 deflection. The instrumental conditions were as follows: the

TABLE I.

	Relative intensity	
m/e	Product	Acetylene
12	1.4	2.3
13	4.7	6.4
24	6.0	8.3
25	23	23
26	100	100
27	4.5	4.1
28	3.0	2.8

TABLE II.[a]

Irradiated time	C.O.T. Pressure	Acetylene (mole)	Photon (mole)	Quantum yield
(a) 30 min	7.0 mm Hg	$2.70 \cdot 10^{-6}$	$2.62 \cdot 10^{-5}$	0.103
(a) 30 min	6.2	3.00	2.80	0.107
(a) 30 min	6.7	3.00	2.97	0.101
(b) 60	7.0	3.28	5.46	0.060
(c) 120	4.2	3.40	7.40	0.046

[a] Reaction temperature is (a) 27.5°C, (b) 30.7°C, (c) 19.4°C.

electron energy is 100 ev; ion accelerating potential is 890 v. The mass spectra of pure acetylene and that gaseous product were compared in Table I. Thus, the gaseous product may be taken to consist of acetylene only. The acetylene was quantitatively determined by pressure change. The quantum yield for acetylene was shown in Table II. The quantum yields for both benzene and acetylene which were separately determined coincide with each other.

Therefore, from this fact it is shown that benzene and acetylene are not produced by the different processes, but by the identical process, that is

$$C_8H_8 \rightarrow C_6H_6 + C_2H_2.$$

The incident surface of the reaction vessel was covered by the membrane of the yellow substance which might be regarded as the polymer of acetylene like cuprene, so the quantum yield for acetylene was slightly influenced by reaction time.

The styrene obtained by photoisomerization was quantitatively determined by means of a spectrometer as in the case of benzene. One of the observed values was as follows.

The quanta of photons absorbed $\cdots 4.2 \times 10^{18}$
The quantity of produced styrene $\cdots 1.7 \times 10^{16}$.

From these values, the quantum yield for styrene is about 0.004, which is about 1/25 to that for benzene.

[1] Miyakawa, Tanaka, and Uemura, Bull. Chem. Soc. Japan **24**, 136 (1951).
[2] I. Tanaka, and S. Shida, Bull. Chem. Soc. Japan, **23**, 54 (1950), Mori, Tanaka, and Shida, *ibid.* **23**, 168 (1950). We have calculated the energy levels of C.O.T. as the symmetry of D_{2d}.
[3] Tanaka, Miyakawa, and Shida, Bull. Chem. Soc. Japan **24**, 119 (1951).
[4] I. Tanaka, J. Chem. Soc. Japan, Pure. Chem. Sect. **75**, 100 (1954).

Cell for Measurements of Polarization Voltages in Melted Electrolytes

R. PIONTELLI AND G. MONTANELLI
Laboratory of Electrochemistry, Chemical Physics and Metallurgy, Politecnico of Milan, Milan, Italy
(Received July 26, 1954)

THE polarization phenomena at electrodes are perhaps the most important aspects of studies on electrode processes. The overvoltages are studied by measuring the voltage between terminals of a tensiometric cell formed by coupling the electrode under study through a suitable "junction" with a reference electrode.

As the main sources of systematic error one must consider:

1. Disturbance of the current distribution on the electrode surface caused by the use of "capillary" (for instance of the classic Luggin-Haber type) realizing the "junction."

2. Spurious contribution included in the measured voltages, when the solution interposed between electrode surface and reference electrode is transversed by the current or it has non-uniform and variable composition.

One of us has developed the theory of these errors.[1] The results of this, backed by systematic experimentation on "model cells"[2] have led to the realization of two entirely new arrangements, which eliminate the errors involved in the Luggin-Haber capillary method. Some cells for the polarization measurements in aqueous and nonaqueous electrolytes have been realized on this basis and they have given very good results.[3]

The problem of studying polarization in melted electrolytes, although strictly similar in principle, involves in practice many additional difficulties. On the application of the above principles we have now realized for this purpose a cell of which Fig. 1 gives the main details. *E* is a graphite body, placed in an insulating

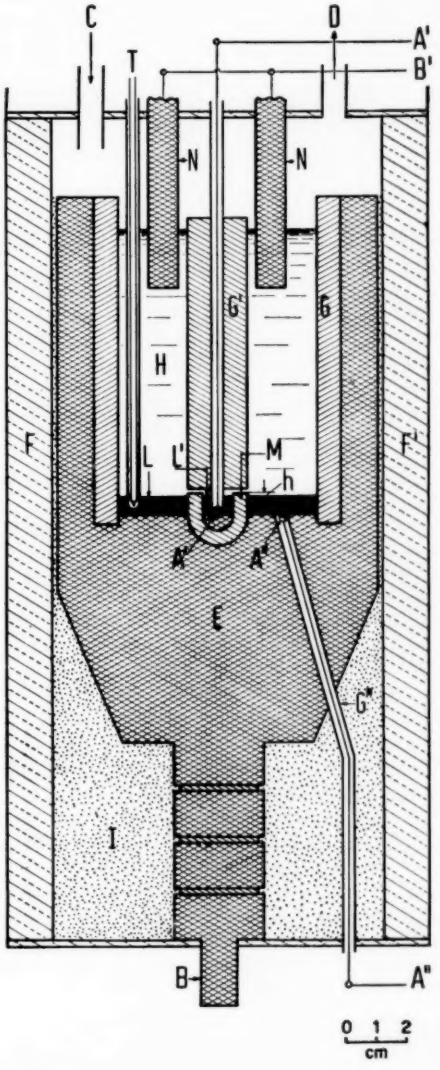

FIG. 1. Cell (sectional view).

support *I*, and lined internally by an insulating wall *G*. The assembly is placed in an electric furnace *FF'*.

For working the cell at constant temperature and under controlled atmosphere (N_2,*A*), are provided the thermocouple *T* and gas inlet and outlet tubes *C* and *D*. *L* is the metal of the electrode under study, *N* the electrodes of opposite polarity, *H* the bath. The current supply is connected to *B* and *B'*.

The metallic part *L'*[4] of the reference electrode supported on graphite is contained in a cup *M* of insulating material (sintered corundum) and is connected by means of a special lead *A'A'* (graphite and platinum) to the voltage measuring apparatus

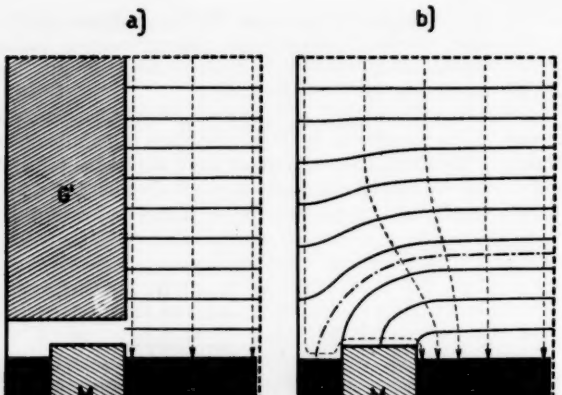

FIG. 2. Current distribution near reference electrode. (a) with insulating sheath G'. (b) without G'.

(oscillograph, potentiometer), to which is also connected the polarized electrode through a similar lead $A''A''$. The symmetrical arrangement avoids thermoelectric and other sources of trouble. For studying overvoltages, in the case of aluminum electrolysis, we have recently utilized quite a similar arrangement,[5] in which the lead $A'A'$ was, however, covered only by a thin insulating wall. This caused some residual perturbation in the current distribution and the correction of this error has required experiments on models.

The lead $A'A'$ in the present cell is on the contrary contained in a thick insulating sheath $G'G'$ leaving only a cylindrical slit to provide the junction between reference and polarized electrode. The current distribution is thus uniform while the main part of the junction electrolyte does not carry any current. The improvement thus realized is explained in principle by the results given in Fig. 2 of experiments conducted on model cells [lead anodes in aqueous solution: 0.5 M $Pb(NH_2SO_3)_2$].

The systematic error involved by the new cell corresponds in practice only to the ohmic voltage in a thin layer of electrolyte (whose thickness, h in Fig. 1, may be in practice of the order of 1 mm) and its magnitude can be evaluated by the knowledge of h, electrolytic conductivity, and current density.

The new cell has been utilized with excellent results for measurements of overvoltages on lead electrodes in melted lead chloride.

The matter is given in detail in a paper in preparation. Dr. B. Rivolta has given very valuable help in the experiments on models and Mr. R. Manocha in those on overvoltages at the $Pb/PbCl_2$ electrode.

[1] R. Piontelli, Gazz. Chim. Ital. **83**, 357, 370 (1953).
[2] Piontelli, Bianchi, and Aletti, Z. Elektrochem. **56**, 86 (1952).
[3] Piontelli, Bianchi, Bertocci, Guerci, and Rivolta, Z. Electrochem. **58**, 54 (1954); Piontelli, Bertocci, Bianchi, Guerci, and Poli, *ibid.* **58**, 86 (1954).
[4] As the reference electrode, in the cases in which in the absence of current an equilibrium voltage is reached, one may adopt for L' the same metal as that of the polarized electrode.
[5] R. Piontelli and G. Montanelli, Alluminio **22**, 672 (1953).

Microwave Absorption by the Nonpolar Gas CO_2

G. BIRNBAUM, A. A. MARYOTT, AND P. F. WACKER
National Bureau of Standards, Washington, D. C.
(Received August 12, 1954)

ABSORPTION of microwave radiation has been detected in the nonpolar gas CO_2.[1] Using tunable cavity resonators designed to operate well above atmospheric pressure, measurements were made up to 60 atmospheres and at wavelengths of 1.29 and 3.30 cm. At 45 atmos and 25°C, the absorption was 1.4×10^{-4} cm^{-1} at 1.29 cm, and 2.3×10^{-5} at 3.30 cm. The absorption was found to increase roughly as the square of the gas density.

Tests with He did not reveal any effects attributable to distortion of the cavity. A number of gases, such as A, Ch_4, and SF_6, having a wide range of dielectric constants and a loss which was shown to be negligible, were used to determine the changes in cavity characteristics (transmission and Q) accompanying tuning.

As identical results were obtained with CO_2 generated from dry ice and with CO_2 of different degrees of purity from a variety of commercial sources, the absorption is undoubtedly not due to impurities. Errors due to the gas being adsorbed upon or absorbed in the walls of the cavity were ruled out by (1) the use of cavities operating in $TE_{0,1,n}$ and $TE_{1,1,n}$ modes, (2) the use of both copper- and silver-lined cavities, and (3) studies of the variation of Q with time after the admission or withdrawal of gas.

It is suggested that the observed absorption is due to dipoles induced by the quadrupoles of the nearby molecules. The selection rules for such a process are the same as those for the rotational Raman effect,[2] namely, $\Delta J=0, \pm2$. To determine the absorption due to this mechanism, Mizushima's[3] analysis of pressure-induced infrared absorption was adapted to the present case, the Van Vleck-Weiskopf line shape and Smith and Howard's value for the quadrupole moment[4] were assumed, and a rough estimate made for $\Delta\nu$. The absorption so computed is of the same order of magnitude as that observed and is primarily due to nonresonant transitions ($\Delta J=0$). Further work on this problem is in progress.

[1] G. Birnbaum and A. A. Maryott, Phys. Rev. **95**, 622A (1954).
[2] C. M. Lewis and W. V. Houston, Phys. Rev. **44**, 905 (1933).
[3] M. Mizushima, Phys. Rev. **76**, 1268L (1949).
[4] W. V. Smith and R. Howard, Phys. Rev. **79**, 132 (1950).

Proton Magnetic Resonance and Structure of Ammonium Hydroxide*

H. S. GUTOWSKY AND S. FUJIWARA †
Noyes Chemical Laboratory, University of Illinois, Urbana, Illinois
(Received July 28, 1954)

IT is conventional to use the formula NH_4OH to represent the molecular state of NH_3 in aqueous solution. This formula is most likely an oversimplification. In fact there is considerable argument against the existence of discrete NH_4OH molecules. Davis[1] has commented on the problem recently, emphasizing the weak noncovalent character of the NH_3-H_2O interaction, and concluding that the system is better described by the equation

$$NH_3+H_2O\leftrightarrows NH_4^++OH^-. \quad (1)$$

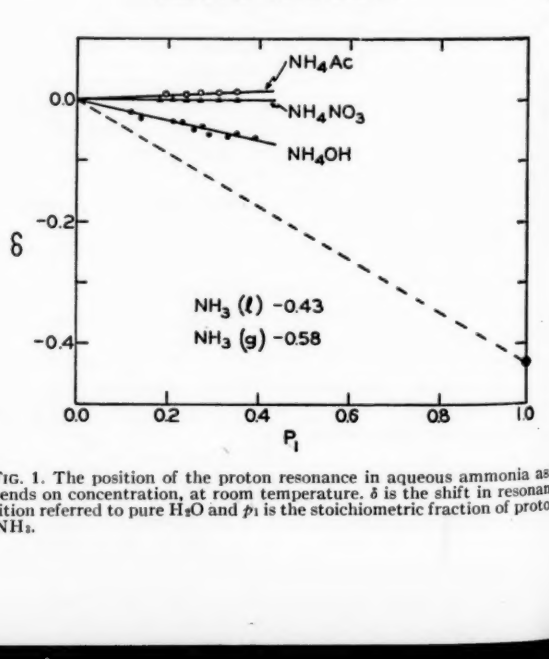

FIG. 1. The position of the proton resonance in aqueous ammonia as it depends on concentration, at room temperature. δ is the shift in resonance position referred to pure H_2O and p_1 is the stoichiometric fraction of protons as NH_3.

Van Velden and Ketalaar[2] arrived earlier at much the same conclusions.

The experimental evidence is conflicting. Rao[3] found that aqueous ammonia exhibited the same Raman spectrum as liquid NH_3, suggesting no new important molecular species are present in solution. But the infrared spectra of the solid ammonia hydrates show[4] absorption bands found neither in ice nor in solid NH_3. Early thermodynamic arguments[5] were based on the partition of NH_3 between H_2O and immiscible organic liquids and indicated that half or more of the NH_3 remained free in the aqueous solutions. However, Khakham[6] reinvestigated the problem by this method and found only 5 to 10 percent free NH_3.

An independent method is offered by nuclear magnetic resonance. Chemical shifts in the resonance position are a sensitive indication of differences in the electronic environment of nuclei and have proven useful in studying the structure of other solutions.[7] Figure 1 gives the proton resonance position observed[7] in aqueous NH_3 as a function of concentration, at room temperature and a field of 4200 oersteds.

The resonance at all concentrations was a single narrow line (<1 millioersted). If discrete molecular species existed with lifetimes longer than about[7] 10^{-3} sec, separate resonance lines would have been found for each species. The conclusion that there is fast proton exchange agrees with the inferences of Eigen[8] and with the unsuccessful attempts[9] to observe directly the exchange rate between D_2O and NH_3.

When chemical exchange produces a single resonance line, its position is a number average of the resonance positions for the nuclei in the absence of that exchange. If Eq. (1) represented the true molecular state of the solutions, the resonance position in the solutions δ_s should be given as[7]

$$\delta_s = p_1\delta_{NH_3} + p_2\delta_{H_2O}, \tag{2}$$

and defining $\delta_{H_2O} \equiv 0$ as was done experimentally,

$$\delta_s = p_1\delta_{NH_3}. \tag{3}$$

p_1 is the fraction of the protons in NH_3, and δ_{NH_3} and δ_{H_2O} represent the proton resonance positions of pure NH_3 and H_2O. The small concentrations of NH_4^+ and OH^- are completely negligible in writing Eq. (2).

The observed δ_s values in Fig. 1 are plotted against the stoichiometric p_1. The dotted line represents Eq. (3) using the δ_{NH_3} value from the liquid. The large deviation of this line from the observed data is strong evidence that the structural model of free NH_3 and H_2O is inadequate. Our data show there are significant interactions between NH_3 and H_2O, but the state is a very dynamic one. Eigen[8] has arrived at a similar model from supersonic absorption measurements.

The importance of hydrogen bonding in the solutions is shown by the systematic increase in the δ values of NH_3 (g),[10] NH_3 (l) and the aqueous solutions. However, whether one wishes to describe the state of association as NH_4OH molecules or $NH_3 \cdot H_2O$ complexes seems at this point a matter primarily of personal preference or convention. We are attempting to learn more about the different molecular species actually present, by cooling the solutions to decrease the exchange rate so separate resonance lines can be resolved.

* Supported by the U. S. Office of Naval Research and by a Grant-in-Aid from E. I. duPont de Nemours and Company.
† University of Illinois Post-doctoral Fellow.
[1] J. B. Davis, J. Chem. Ed. **30**, 511 (1953).
[2] P. F. van Velden and J. A. A. Ketelaar, Chem. Weekblad **43**, 401 (1947).
[3] B. P. Rao, Proc. Indian Acad. Sci. **20A**, 292 (1944).
[4] R. D. Waldron and D. F. Hornig, J. Am. Chem. Soc. **75**, 6079 (1953).
[5] These results are reviewed by N. V. Sidgwick, *The Chemical Elements and Their Compounds* (The Clarendon Press, Oxford, 1950) Vol. 1, p. 658.
[6] I. B. Khakham, Zhur. Obschchei Khim. **18**, 1215 (1948); Chem. Abstracts **43**, 6891[h] (1949).
[7] H. S. Gutowsky and A. Saika, J. Chem. Phys. **21**, 1688 (1953).
[8] M. Eigen, Z. Physik. Chem., Neue Folge **1**, 176 (1954).
[9] A. I. Brodskii and L. V. Sulima, Doklady Akad. Nauk S. S. S. R. **74**, 513 (1950); Chem. Abstracts **45**, 424[b] (1951).
[10] R. A. Ogg, Jr., J. Chem. Phys. **22**, 560 (1954).

Paramagnetic Resonance Absorption in Triphenylmethyl and Dimesitylmethyl

H. S. JARRETT AND G. J. SLOAN *
Chemical Department, Experimental Station, E. I. du Pont de Nemours and Company, Wilmington 98, Delaware
(Received August 9, 1954)

PARAMAGNETIC resonance absorption spectra of solutions of triphenylmethyl and of dimesitylmethyl in benzene have been observed in this laboratory. The structure in these spectra is presumed to be hyperfine, being caused by dipole-dipole interaction between the magnetic moments of the hydrogen nuclei and the unpaired electron. Since an unpaired electron density would not be expected on the hydrogen atoms, the magnetic moments probably couple through the chemical bond in a manner similar to the hyperfine interactions observed in nuclear magnetic resonance. The rapid tumbling of the free-radical molecule averages out spatial and anisotropic dipole-dipole coupling.

The equipment used in obtaining these spectra has been described previously.[1] The measurements were made at approximately 24 kmc/sec at room temperature. The homogeneity of the static magnetic field as determined by nuclear resonance was approximately 0.05 oersted. Complete dissociation of the dimers, hexaphenylethane or tetramesitylethane, into free radicals is assumed when concentrations of the radicals in benzene solution are given.

The derivative of the resonance absorption spectrum (Fig. 1)

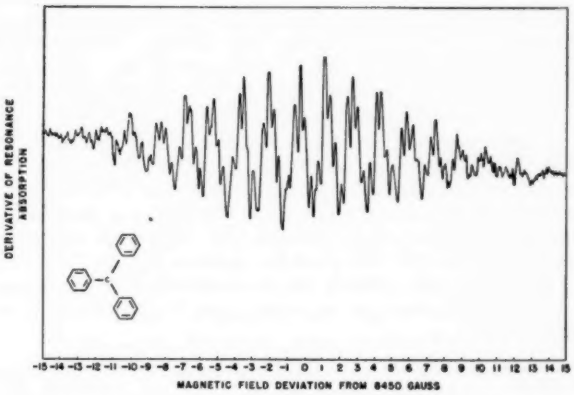
DERIVATIVE OF RESONANCE ABSORPTION
-15 -14 -13 -12 -11 -10 -9 -8 -7 -6 -5 -4 -3 -2 -1 0 1 2 3 4 5 6 7 8 9 10 11 12 13 14 15
MAGNETIC FIELD DEVIATION FROM 8450 GAUSS

FIG. 1. Derivative of the paramegnatic resonance absorption spectrum of triphenylmethyl

of a 0.001 molar solution of triphenylmethyl consists, approximately, of groups of four closely spaced hyperfine structure lines. Eighteen such groups of lines are observed above the noise background if the modulating field amplitude is less than 0.1 oersted. However, if the amplitude is greater than 0.1 oersted, the sensitivity is increased and 21 instead of 18 groups of lines are observed in the resonance spectrum, but the individual hyperfine structure lines of which these major groups are composed become unresolved. At 0.1 molar concentration in benzene, only the 21 major peaks can be resolved and at 1.0 molar no fine structure can be observed. Exchange narrowing was not detected at the higher concentrations. A total of 196 hyperfine structure lines is theoretically possible if it is assumed (1) that hyperfine coupling from a particular hydrogen exists when there is an unpaired electron density on the adjacent carbon atom, (2) that all the ortho-, para-, and meta-positions, respectively, of the three phenyl rings are equivalent, and (3) an unpaired electron density exists at each carbon position. Complete interpretation of this complex spectrum based on the unpaired electron density at the various carbon positions would be extremely difficult.

Dimesitylmethyl was examined to determine if there is a large hyperfine structure splitting by the methyl hydrogen consistent with a large unpaired electron density on the methyl carbon and

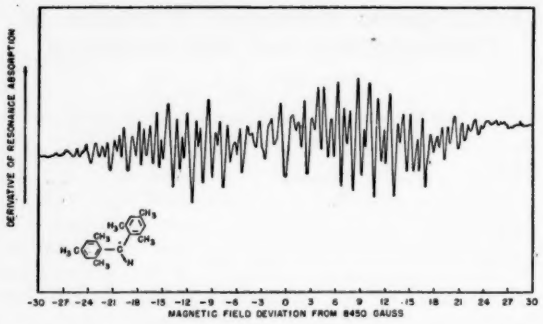
DERIVATIVE OF RESONANCE ABSORPTION
-30 -27 -24 -21 -18 -15 -12 -9 -6 -3 0 3 6 9 12 15 18 21 24 27 30
MAGNETIC FIELD DEVIATION FROM 8450 GAUSS

FIG. 2. Derivative of the paramagnetic resonance absorption spectrum of dimesitylmethyl.

if the reduction of the number of hydrogen atoms attached to the phenyl rings gives a simpler resonance spectrum. Since the ortho- and para-positions on the phenyl rings contain methyl groups, the hyperfine structure would be expected to arise entirely from the four meta-hydrogens. There would then be five hyperfine structure lines with a Gaussian intensity distribution. If there is in addition a large methyl hydrogen splitting, a spectrum of two sets of five lines each should be observed. The measured spectrum (Fig. 2) does not conform with this simple expectation. It is apparent that although there are indeed two sets of peaks separated by 24 oersteds, each set contains many more than five lines. Molecular orbital calculations assuming a planar molecule indicate that because of hyperconjugation the electron density on the para-methyl group is greater by a factor of 400 than the density on the ortho-methyl groups. If this is true, the hydrogen nuclei of the para-methyl groups would exist in the π-electron system and a large hyperfine coupling with the unpaired electron would result. If the hydrogen atoms of the para-methyl groups are assumed to be equivalent, each of the hyperfine structure peaks discussed above would be split into seven peaks to give for the whole spectrum two sets of 35 peaks each. This result is in qualitative agreement with the spectrum shown in Fig. 2.

The authors wish to thank Dr. R. E. Merrifield of this laboratory for carrying out the molecular orbital calculations on dimesitylmethyl.

* Present address: 2nd Army Area Med. Lab., Ft. Geo. G. Meade, Maryland.

Stability and Structure of Bunsen Flame*

MAHINDER S. UBEROI
Department of Aeronautical Engineering, University of Michigan, Ann Arbor, Michigan
(Received August 6, 1954)

A LEAN propane-air flame was established on $\frac{3}{4}$-in. diameter tube and the flow upstream of the flame was made uniform by using a number of very fine screens. As the volume flow was decreased at constant mixture ratio the tip of the flame changed from concave to convex (see Fig. 1). The following is offered as a tentative explanation of the phenomenon.

FIG. 1. Change of flame shape with decreasing volume flow (from left to right).

Far upstream of the flame the unburned gas flow is parallel and the flow bends away from the burner axis before reaching the flame. Since the velocity component normal to the flame is increased considerably after combustion and the flame is concave towards the unburned gas, the burned gases are further bent away from the burner axis. Assuming constant flame speed the pressure drop across the flame is the same for every streamline and there is no pressure drop towards the burner axis to make the diverging flow parallel. For a flame convex towards the unburned gas, the flow also bends away from the burner axis before reaching the flame but after going through the flame the burned gases are bent towards the burner axis. The pressure is higher in the central than in the outer streamlines and this bends the streamlines away from the center. An equilibrium is reached further downstream where the flow becomes parallel and pressure becomes uniform.

In practice the concave Bunsen burner flame is realized because the flame speed increases as we go from the base to the tip of the flame; i.e., going through the flame the central streamlines experience more pressure drop than the outer streamlines. This pressure drop toward the center makes the diverging burned gases parallel. As the height of the flame decreases the curvature decreases and change in flame speed at the tip is not big enough to support a concave flame. These considerations apply quite generally but it is not possible to demonstrate this for the usual Bunsen burner. The usual burner has a boundary layer at the wall (in the above experiment we decreased this considerably by using very fine screens) and the flame flashes back at the rim before the volume flow is low enough for the flame curvature to change at the tip.

In view of the above considerations, the usual assumption that the shape of the Bunsen burner flame and the flow field can be determined by assuming constant flame speed is untenable. Other theoretical considerations and detail flow field measurements supporting these views will be reported elsewhere.

* This work is a part of the research program supported by the U. S. Office of Naval Research under Contract NONR 1224-02.

Mass Spectrometric Detection of Free OH Radical in the Thermal Decomposition Products of H_2O Vapor

T. TSUCHIYA
Tokyo Chemical Industrial Research Institute, 58, 1, Nakameguro, Tokyo, Japan
(Received July 14, 1954)

SEVERAL methods have been reported in the past for the detection of the free hydroxyl radical OH: and these were recently re-examined by the microwave spectral method.[1] Consequently, it has become apparent that of these methods only the one in which the intensity of the OH absorption spectrum is measured in the ultraviolet region can give satisfactory results.

In an experiment preliminary to the series in our research on the mechanism of thermal decomposition of gas molecules, free OH radicals were detected with the mass spectrometer by subjecting H_2O vapor to pyrolysis on a platinum filament.

The work was carried out with a 60° or Nier type mass spectrometer made by the Scientific Research Institute.[2] A small auxiliary platinum filament similar to that described by Robertson[3] was installed in the ionization chamber for the pyrolysis of gas molecules. The temperature of this filament was measured with an optical pyrometer. Throughout the experiment the heating temperature was 1200°C. Electron energies were measured with a calibrated dc meter capable of being read to an accuracy of 0.1 percent of full scale reading. The H_2O was an ordinary distilled

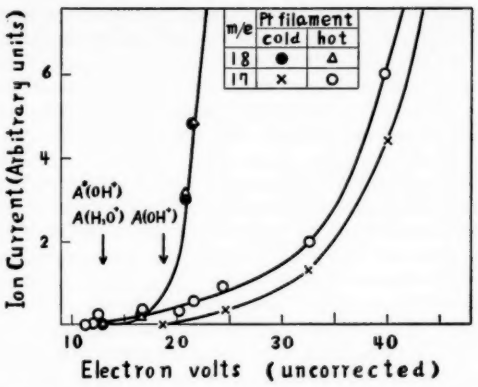

FIG. 1. Ionization efficiency curves for $m/e=17$ and 18, with hot and cold Pt filaments, small background spectra included.

sample, and was introduced into the ionization chamber as a molecular beam.

Heating of the Pt filament produces the following effects on the mass spectra of H_2O.

1. The appearance potential of OH^+ ions decreases from its normal value of $A(OH^+)=18.7$ ev[4] to a new value $A^*(OH^+)$ which is nearly equal to the appearance potential of the parent ion, $A(H_2O^+)=13.0$ ev[4] (Fig. 1).

2. The appearance potential of H^+ also decreases by roughly about 2 ev.

3. As seen in Fig. 1, practically no change at all occurs in the H_2O^+ ionization efficiency curve.

4. Under ordinary operating conditions, electron energy at 70 ev, the ratio of intensities N, of $m/e=17$ ions to $m/e=18$ ions, is always larger than when measured with an unheated Pt filament. In one example cold filament value of $N=0.35$ increased to 0.63 after heating the Pt filament for one minute.

5. At $m/e=16$, a spectrum appears: the ratio of its intensity to that of H_2O^+ is about 1/10.

6. Turning off the electron current and using just the heated Pt filament alone produces no H_2O spectra at all

Effect 3 gives no indication of the presence of excited H_2O molecules.

From the hot Pt filament curve I in Fig. 2, it is seen that near $A(OH^+)$, where the cold filament curve II becomes zero, the amount of OH^+ shows a markedly uniform and continuous increase relative to that of H_2O^+, as the electron energy is lowered.

In accordance with these facts and effects 4, 5 and 6, we can reasonably expect that new particles such as free OH radicals are being formed thermally.[5] Taking into account effects 2 and 6, the main decomposition mechanism would be $H_2O \rightarrow OH+H$.

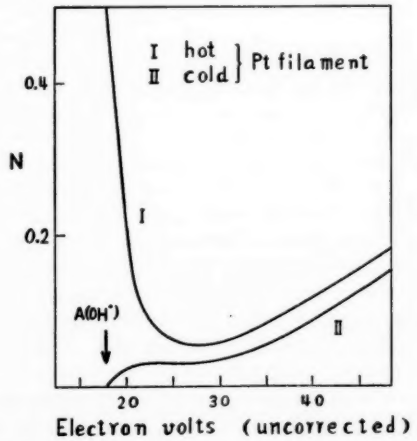

FIG. 2. Intensity ratio N between the $m/e=17$ spectrum and the $m/e=18$ spectrum, *vs* electron energy.

The ionization potential $I(OH)$ of the OH radical is reported to be ≤ 13.6 ev.[4] Neglecting the small effects due to vertical transition favored by the Franck-Condon principle[6] and the possibility of thermally produced OH radicals being in excited states, $A^*(OH)$ equals $I(OH)$. Again from consideration of this appearance potential, effect 1, namely that $A^*(OH^+)$ nearly equals $A(H_2O^+)=13.0$ ev, can also be explained beautifully by assuming free OH radicals to be present.

Precise measurement of the appearance potential of the OH radical is now in progress.

[1] Sanders, Schawlow, Dousmanis, and Townes, J. Chem. Phys. **22**, 245 (1954).
[2] Nishina Research Laboratory, Kagaku Kenkyujo Hokoku, **27**, 435 (1951). In Japanese.
[3] A. J. B. Robertson, Proc. Roy. Soc. (London) **A199**, 394 (1949).
[4] Mann, Hustrulid, and Tate, Phys. Rev. **58**, 340 (1940).
[5] G. C. Eltenton, J. Chem. Phys. **15**, 455 (1947).
[6] R. E. Honig, J. Chem. Phys. **16**, 105 (1948).

Note on the Hybrids in the Nontetrahedral Carbon Atom

M. MASHIMA
Faculty of Liberal Arts, Saga University, Saga, Japan
(Received July 28, 1954)

THE hybrid orbitals in the nontetrahedral carbon atom have been investigated by a number of authors.[1-5] Coulson and Moffitt[3] especially have given an exact treatment of the bent bonds in some strained hydrocarbons. However, Kilpatrick and Spitzer's[2] criterion for the bent bonds was improved here.

With no loss in generality, bonding orbitals in a quadrivalent carbon atom are formed as follows:[2]

$$f_1=as+bp_z+(1/2)^{\frac{1}{2}}p_x,$$
$$f_2=as+bp_z-(1/2)^{\frac{1}{2}}p_x,$$
$$f_3=bs-ap_z+(1/2)^{\frac{1}{2}}p_y,$$
$$f_4=bs-ap_z-(1/2)^{\frac{1}{2}}p_y,$$
$$b=+(1/2-a^2)^{\frac{1}{2}}.$$

The equivalent orbitals f_1 and f_2 are used to form the two C−C bonds, and have their maximum values in the XZ plane. f_3 and f_4 (taken in the YZ plane) are equivalent. The bond strength of f_1 is given by the expression:

$$S=a+(1/2-a^2)^{\frac{1}{2}}3^{\frac{1}{2}}\cos\theta+(3/2)^{\frac{1}{2}}\sin\theta. \quad (1)$$

The condition $dS/da=0$ now being used, the following relations are obtained:[2]

$$a=(1/2+6\cos^2\theta_0)^{\frac{1}{2}}, \quad b=(3\cos^2\theta_0/2+6\cos^2\theta_0)^{\frac{1}{2}},$$

where θ_0 is not an angle at which S has the maximum value, but equated to θ which is contained in the equation obtained by $dS/da=0$. Thus Eq. (1) becomes as follows:

$$S=(1/2+6\cos^2\theta_0)^{\frac{1}{2}}+(3\cos^2\theta_0/2+6\cos^2\theta_0)^{\frac{1}{2}}3^{\frac{1}{2}}\cos\theta + (3/2)^{\frac{1}{2}}\sin\theta. \quad (2)$$

By setting $\theta=\theta_0$ in Eq. (2), f_1 has a value a particular direction θ_0. But it has the maximum value in a direction θ differing from θ_0. The angular dependence of the bond strength of f_1 at $\theta_0=30°$ is shown in Fig. 1.

As the measure of binding power, Kilpatrick and Spitzer[2] have used S_{θ_0} which is the numerical value of S in the bond direction. However, it is evident from Fig. 1 that the cosine of S in the bond direction has the greatest value at any angle $\theta_0+\beta$. (β is an angle between new direction and bond direction.) The numerical value of $S\cdot\cos\beta(=S_\beta)$ is given by the expression:

$$S_\beta=\cos\beta\{a+(1/2-a^2)^{\frac{1}{2}}3^{\frac{1}{2}}\cos(\beta+\alpha/2)+(3/2)^{\frac{1}{2}}\sin(\beta+\alpha/2), \quad (3)$$

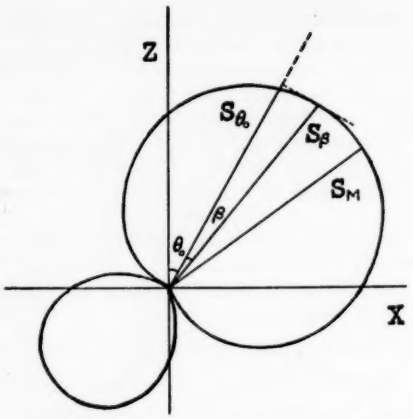

FIG. 1. The angular dependence of S at $\theta_0=30°$. S_{θ_0} is the value 1.887 (see reference 6) at $\theta=\theta_0$. S_M is the maximum value 1.985 at $\theta=50°\ 14'$. See the text for S_β.

where $\alpha/2=\theta_0$, α is the angle between two C−C bonds in lower cycloparaffins. The maximum value of S_β is obtained by setting simultaneously $dS_\beta/d\beta=0$ and $dS_\beta/da=0$. Thus the following equations are obtained:

$$a\cdot\sin\beta=(3/2)^{\frac{1}{2}}\cos(2\beta+\alpha/2)-3^{\frac{1}{2}}(1/2-a^2)^{\frac{1}{2}}\sin(2\beta+\alpha/2), \quad (4)$$

$$a=\{1/2+6\cos^2(\beta+\alpha/2)\}^{\frac{1}{2}}. \quad (5)$$

By solving Eqs. (4) and (5) we can obtain $S_\beta=1.932$, $\beta=9°\ 23'$ for $\alpha=60°$ (cyclopropane); $S_\beta=1.989$, $\beta=3°\ 3'$ for $\alpha=90°$ (cyclobutane). S_β being used as the bond strength, the bond is considerably stronger than the bond formed with S_{θ_0}. Then S has the maximum value in a direction θ_M, that is, the bond is bent. From Eqs. (1) and (5), and the condition $dS/d\theta=0$, θ_M is easily obtained. Thus a strained angle is calculated by $\theta_M-\alpha/2$.

The HCH angle θ_{34} (between the bonds formed with f_3 and f_4) is given by $\tan\theta_{34}=-2\{1+3\cos^2(\beta+\alpha/2)\}^{\frac{1}{2}}/3\cos^2(\beta+\alpha/2)$. Then it is assumed that the hybrid orbitals have their maxima in the directions of the C−H bonds.

For cyclopropane the calculated values of the strained angle $\theta_M-\alpha/2$, the greatest value S_β of $S\cdot\cos\beta$, the HCH angle θ_{34}, and the maximum value S_{f3} (used to form the C−H bond) are given in Table I with the experimental value[7] and Coulson and Moffitt's calculations.[3] The agreement of the calculated value with experiment may be to a great extent fortuitous.

TABLE I.

	$\theta_M-\alpha/2$	S_β	<HCH	S_{f3}
Calculated	21° 18′	1.932	118° 12′	1.994
Coulson and Moffitt	22°	···	116°	···
Experimental	···	···	118.2°±2°	···

[1] G. H. Duffey, J. Chem. Phys. **14**, 342 (1946).
[2] J. E. Kilpatrick and R. Spitzer, J. Chem. Phys. **14**, 463 (1946).
[3] C. A. Coulson and W. E. Moffitt, J. Chem. Phys. **15**, 151 (1947); Phil. Mag. **40**, 1 (1949).
[4] P. Torkington, J. Chem. Phys. **19**, 528 (1951).
[5] M. Mashima, J. Chem. Soc. Japan, Pure Chem. Sect. **73**, 531 (1952).
[6] See reference 2, Table I.
[7] O. Bastiansen and O. Hassel, Tids. Kjemi Bergvesev Met. **6**, 71 (1946).

Infrared Spectra of Chemisorbed Carbon Monoxide

R. P. EISCHENS, W. A. PLISKIN, AND S. A. FRANCIS
Beacon Laboratories, The Texas Company, Beacon, New York
(Received June 21, 1954)

SPECTRA attributed to CO chemisorbed on Cu, Pt, Pd, and Ni have been obtained. The metals were dispersed by making slurries with Cab-o-sil[1] and solutions of metal salts. Samples were deposited on CaF_2 plates by evaporation of the slurry. The sample thickness was about 0.012 g/cm² and the metal content, after reduction in H_2 at 200–350°C, was 7–10 percent. The sample cell was a Pyrex cylinder fitted with two side tubes. The CaF_2 plates were sealed to the ends of the cylinder with silicone putty. A Perkin-Elmer spectrometer equivalent to Model 12C with a CaF_2 prism was used.

After reduction the samples were cooled to room temperature in H_2, the H_2 purged with nitrogen and CO passed through the cell for 10 minutes. The sample was then transferred to the spectrometer and the gaseous CO removed by purging with N_2 or H_2. The spectra, corrected for background, obtained after removal of the gaseous CO are shown in Fig. 1.

Rotation of the molecule causes the fundamental vibration of gaseous CO to appear as a doublet with transmission minima at 4.60 microns and 4.72 microns. The wavelength corresponding to the pure vibrational transition would be at 4.67 microns. Bands, attributed to CO bonded to a single metal atom, are found at 4.70 microns for Cu, 4.83 microns for Pt, 4.92 and 5.24 microns for Ni, and 4.87 and 5.22 microns for Pd. The spectrum of CO chemisorbed on Cu includes some gaseous CO at a pressure of 10 cm, indicated by the dotted line. In the spectra shown a N_2 purge was used with the Cu and Pt samples and a H_2 purge with the Ni and Pd. The admission of H_2 to a sample with chemisorbed CO shifts the major bands toward longer wavelengths by about 0.05 micron and broadens the bands. The bands of the Ni and Pd samples were broader than those of the Pt sample even before admission of H_2. The H_2 treatment also appears to increase the intensity of the 5.5 micron bands for the Pt and Pd spectra.

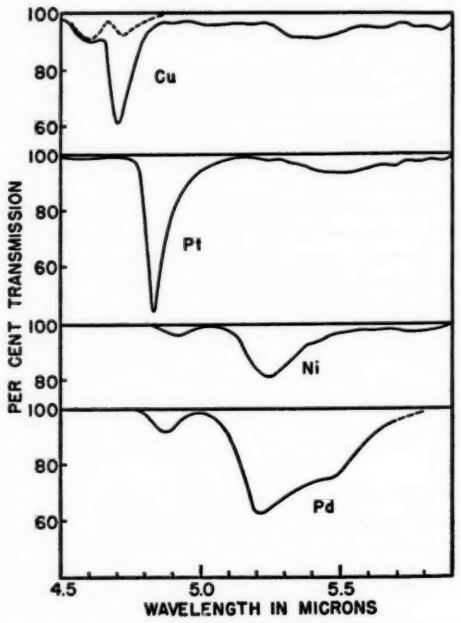

FIG. 1. Infrared spectra of chemisorbed CO on various metals.

The weak bands found in the 5.5 micron region for Cu, Pt, and Pd systems are attributed to CO molecules bridged between two metal atoms as in iron nonacarbonyl. In the spectrum of iron nonacarbonyl the stretching of the carbon-oxygen double bond in the bridged molecules produces a band at 5.5 microns instead of the 5.8 microns usually found for the carbonyl group. This difference has been attributed to the strain imposed by distortion of the angle between the two metal-carbon bonds.[2] A reproducible technique for obtaining the spectrum of CO chemisorbed on Fe has not yet been developed. Partially successful experiments

indicate that this system has a transmission minimum at 5.77 microns with a weaker band at 5.35 microns.[3]

It is likely that the magnitude of the displacement of the positions of the major bands from the wavelength corresponding to the pure vibrational transition of gaseous CO is a measure of the strength of the metal-carbon bond. The spectra show that there are two types of bonds to single metal atoms when CO is chemisorbed on Ni or Pd. Moreover, the broadness of these bands is evidence that there are greater differences among the bonds contributing to each band than there are in the case of CO on Pt. The theory that carbon monoxide is chemisorbed as a molecule and bonded to the metal through the carbon appears to be confirmed by the infrared spectra.

We are grateful to Dr. L. C. Roess for his interest and encouragement and to E. J. Bane for his help with the experimental work.

[1] Nonporous spheres of silica 0.015–0.02 micron in diameter, obtained from Godfrey L. Cabot, Inc., Boston, Massachusetts.
[2] R. K. Sheline, J. Am. Chem. Soc. **73**, 1615 (1951).
[3] R. P. Eischens and J. E. Mapes, unpublished results.

Bromine Quadrupole Spectra and Hammett's Sigma Values*

P. J. Bray
Department of Physics, Rensselaer Polytechnic Institute, Troy, New York
(Received August 6, 1954)

SOME additional bromine pure quadrupole resonances in organic compounds have been detected with a self-quenching superregenerative oscillator in the 150 to 300 Mcps region. Table I lists the frequencies measured at liquid nitrogen termperature.

The Br^{81} values listed in column 4 of Table I should be compared with the values in column 5. These latter values are predicted from the graph of Bray and Barnes[1] of Br^{81} resonance frequencies *versus* sigma values for the substituents on bromobenzene. In such comparisons, agreement must be considered satisfactory if the values are within several megayccles per second of each other since crystal structure effects often displace resonances by 1 or 2 megacycles per second and sigma values are neither exactly known nor constant for the same substituent from compound to compound. For those bromobenzene substituents in Table I for which sigma values of the substituents are not known, the listed Br^{81} frequency is used with the frequency *versus* sigma value plot of reference 1 to secure an estimate of the sigma values. Most such compounds in Table I contain a substitutent in the ortho position with respect to the bromine and the predicted sigma value must be considered only a crude measure of the type of effects produced by meta and para substitution.

From 2,4-dimethylbenzene and the known[2] sigma value for m-CH_3 substitution a sigma value of -0.75 is predicted for o-CH_3 substitution. Similarly, from 2-bromo-4-methylaniline a sigma value between -0.47 and -0.77 is predicted for o-NH_2 substitition. This latter range of values should be compared with the value predicted in the same manner for o-NH_2 substitution from the o-bromoaniline Br^{81} resonance frequency in reference 1.

The p-bromophenol Br^{79} resonance frequencies[1] 274.795 and 271.500 or 269.283 and 268.222 Mcps (two crystalline phases with two resonances in each phase) complete the bromophenol set of resonances. Comparision of the p-bromo-n,n-diethylaniline resonances with the 265.57 Mcps[3,4] value for p-bromoaniline shows the minor effect of substituting diethylaniline for aniline on the benzene ring as far as the electron distribution in the para position on the ring is concerned.

The Cl^{35} resonance in benzoyl chloride has been reported[5] at 29.93 Mcps at liquid nitrogen temperature. The usual multiplication factor of 6.5 between Cl^{35} and Br^{81} resonances would predict a value of about 194 Mcps for benzoyl bromide. It took very little searching to find the 192 Mcps resonance reported. The Cl^{35} resonance in acetyl chloride would be predicted at about 27.7 Mcps on the basis of the acetyl bromide value of Table I. The resonance has not been found, though the Cl in COCl resonances in dichloro-and trichloro-acetyl chloride have been found.[6,7]

Room temperature measurements on bromoacetic acid have been reported by three laboratories.[3,4,8] Shimomura and coworkers[8] reported a doublet at room temperature which could not be resolved by the other investigators.[3,4] The existence of a doublet is quite clear at liquid nitrogen temperature even though the lines

TABLE I.

Compound	S/N[a]	Br^{79} frequency (megacycles per second)	Br^{18} frequency (megacycles per second)	Br^{81} predicted frequency[b]	Substitutent	Sigma value
o-bromophenol BrC_6H_4OH	15	275.884 ±0.020	230.48[c]		o −OH	0.50[d]
m-bromophenol BrC_6H_4OH	<2	272.745 ±0.080	227.86[c]	226.6	m −OH	−0.002[e]
p-bromophenetole $BrC_6H_4OC_2H_5$	5 to 7	266.818 ±0.020	222.91[c]	224.5	p −OC_2H_5	−0.25[f]
p-bromophenyl phenyl ether $BrC_6H_4OC_6H_5$	20	272.500 ±0.020	227.65[c]	226.4	p −OC_6H_5	−0.028[e]
p-bromo-n,n-diethylaniline $BrC_6H_4N(C_2H_5)_2$	8 to 10	263.444 ±0.020	220.09[c]		p −$N(C_2H_5)_2$	−0.82[d]
	8 to 10	262.906 ±0.020	219.64[c]			−0.87[d]
2-bromo-1,4-dimethylbenzene $BrC_6H_3(CH_3)_2$	15	263.332 ±0.020	219.99[c]		o −CH_3 + m −CH_3	−0.82[d]
2-bromo-4-methylaniline 2-Br-4-CH_3-$C_6H_3NH_2$	5	265.974 ±0.065	222.20[c]		o −NH_2 + m −CH_3	−0.54[d]
	5	263.222 ±0.065	219.90[c]			−0.84[d]
1-bromonaphthalene $C_{10}H_7Br$	6	267.895 ±0.075	223.81[c]			
benzoyl bromide C_6H_5COBr	3 to 4		191.868 ±0.070			
acetyl bromide CH_3COBr	7		181.350 ±0.070			
	7		180.140 ±0.070			
	7		179.536 ±0.070			
	7		178.082 ±0.070			
bromoacetic acid $CH_2BrCOOH$	2 to 2½	286.74 ±0.08				
	2 to 2½	284.55 ±0.08				

[a] Signal-to-noise ratio as observed on oscilloscope.
[b] Predicted from the frequency *versus* sigma value plot of reference 1 on basis of known sigma value for the substituent.
[c] Not measured accurately but calculated from $f_{Br^{79}} = 1.1970 f_{Br^{81}}$.
[d] Predicted from the listed Br^{81} frequency and the frequency *versus* sigma value plot of reference 1.
[e] H. H. Jaffe, Chem. Revs. **53**, 191 (1953).
[f] See reference 2.

are weak. Integration of the signal out of the noise for these weak resonances was greatly aided by the use of a Polaroid Land camera for securing time exposures of the pattern on the oscilloscope screen.

* Research supported by grants from the National Science Foundation and the Rensselaer Polytechnic Institute Research Grants Committee.

[1] P. J. Bray and R. G. Barnes, J. Chem. Phys. (to be published).
[2] L. P. Hammett, *Physical Organic Chemistry* (McGraw-Hill Book Company, Inc., New York, 1940).
[3] P. J. Bray, J. Chem. Phys. **22**, 950 (1954).
[4] Barnes, Miller, and Wooten, J. Chem. Phys. **22**, 946 (1954).
[5] D. W. McCall and H. S. Gutowsky, J. Chem. Phys. **21**, 1300 (1953).
[6] P. J. Bray, J. Chem. Phys. (to be published).
[7] H. C. Allen, J. Am. Chem. Soc. **74**, 6074 (1952).
[8] Shimomura, Kushida, Inoue, and Imaeda, J. Chem. Phys. **22**, 350 (1954).

Improved Approximate Solutions of Flame Equations for Flames Governed by Simple Chemical Reactions

KENNETH A. WILDE
Rohm and Hass Company, Redstone Research Division, Huntsville, Alabama
(Received July 26, 1954)

THERE has been considerable recent interest in obtaining numerical[1] and approximate analytical[2-5] solutions of the flame equations for simple cases, e.g., one-dimensional, laminar, premixed flames governed by a first-order reaction, $A \rightarrow B$. We present here a method of obtaining an approximate analytical solution which is within the accuracy of the numerical integration for a wide range of parameters. The equation to be solved to give an eigenvalue, the flame velocity, is, for the above case,

$$\frac{dG}{d\theta}\ \frac{1}{\mu^2}\frac{(1-\epsilon)}{(\theta-G)}e^{-E/RT}, \tag{1}$$

where G=fraction of mass flow of B; ϵ=mole fraction of B; $\theta=T-T_0/T_f-T_0$; T_0=initial temperature; T_f=adiabatic flame temperature; E/RT=conventional Arrhenius exponent; $\mu=M(c_p/B\rho\lambda)^{\frac{1}{2}}$, where μ=dimensionless mass flame velocity; M=mass flow rate; c_p=heat capacity; B=kinetic frequency factor; λ=thermal conductivity.

With the condition that $\delta\equiv D\rho c_p/\lambda=1$ we have $\epsilon\equiv\theta^1$, where D is the usual Fick's law constant. The boundary conditions are

$$G=0 \quad \text{when} \quad \theta=0, \quad G=1 \quad \text{when} \quad \theta=1.$$

Following Adams[3] we partially integrate (1) to obtain

$$\mu^2=\frac{\int_0^1 f(\theta)d\theta}{\frac{1}{2}-\int_0^1 Gd\theta}. \tag{2}$$

Adams evaluates both integrals by approximating both G and the Arrhenius term by θ^n, where n is found by matching derivatives at T_f. Actually, this only need be done for the integral in the denominator, since the other can be evaluated exactly. Employing $G=\theta^{n+1}$ suggested, from an examination of numerical composition-temperature profiles, by Hirschfelder, Curtiss, and Campbell,[6] we obtain from (2):

$$\mu^2=\frac{2\eta(\eta\varphi+2)}{\varphi^3}\left[Ei(-\eta)\left(\frac{1}{\eta}+\frac{1}{2}\right)+\left(\frac{1}{2\eta^2}+\frac{1}{2\eta}\right)e^{-\eta}\right] \tag{3}$$

where

$$\eta=\frac{E}{RT_f}=\text{dimensionless activation energy}$$

$$\varphi=1-\frac{T_0}{T_f}, \quad Ei(-\eta)=\int_\infty^\eta \frac{e^{-x}}{x}dx.$$

Another approximate solution for the same case can be devised using the ignition temperature concept as applied by Hirschfelder and Kihara.[7] An analytical solution of the equations which they integrated numerically can be obtained as follows:

Replace G and $\exp\left(+\frac{E}{RT_f}-\frac{E}{RT}\right)$ in (1) by

$$\begin{cases}\left(\frac{\theta-\theta_i}{1-\theta_i}\right)^2 & 1>\theta>\theta_i \\ \text{zero} & \theta_i>\theta>0\end{cases} \tag{4}$$

where θ_i is a dimensionless "ignition temperature," $(T_i-T_0)/(T_f-T_0)$.

$$\mu^2=\frac{(1-\theta_i)^2e^{-\eta}}{2(1+2\theta_i)}. \tag{5}$$

We have not yet specified a means of relating θ_i to the other parameters of the system. A way which is immediately suggested is to match the derivatives of the exact and approximate reaction rate expressions, as with the Adams method. The result is

$$\theta_i=1-\frac{2}{\eta\varphi}. \tag{6}$$

It is undoubtedly an overextension of the model to associate θ_i with any experimental ignition temperature or lean-limit temperature, but such a semiempirical approach may prove useful in certain situations.

The results of Eqs. (3) and (5) are compared with the numerical results of Friedman and Burke in Table I, setting $\varphi=1$,[8] and $\delta=D\rho c_p/\lambda=1$.[9] The results of several other approximate methods are given for comparison.

TABLE I. Comparison of dimensionless burning velocities.

			Adams		Corner[b]	
η	Numerical integration[a]	Eq. (3) μ	μ	% error	μ	% error
2	0.167	0.172	0.260	+55	...	...
4	0.0365	0.0368	0.0460	+31	0.552	+51
7	0.00507	0.00503	0.00572	+13	0.00551	+8.7
10	$8.33(10^{-4})$	$8.33(10^{-4})$	$9.11(10^{-4})$	+9.4	$7.94(10^{-4})$	−4.7
15	$4.74(10^{-5})$	$4.77(10^{-5})$	$5.07(10^{-5})$	+6.5	$4.10(10^{-5})$	−13.5
22	$1.00(10^{-6})$	...	$1.05(10^{-6})$	+5.0	$0.790(10^{-6})$	−21

	Zeldovitch and Frank-Kamenetsky[c]		Eq. (5)	
η	μ	% error	μ	% error
2	0.260	+55	0.260	+55
4	0.0478	+31	0.0338	−7.4
7	0.00610	+17	0.00392	+23
10	$9.53(10^{-4})$	+14.4	$5.91(10^{-4})$	+29
15	$5.24(10^{-5})$	+10.5	$3.17(10^{-5})$	+33
22	$1.07(10^{-6})$	+7.0	$0.64(10^{-6})$	+36

[a] See reference 1. [b] See reference 4. [c] See reference 5.

Von Karman and Penner[2] employ a procedure similar to that used here and obtain a good analytical solution for $\eta\sim10$. The agreement of Eq. (3) with the numerical integration seems to be within the precision of the numerical integrations, ±2 percent. The other solutions, considering their approximations, are reasonably satisfactory. In fact, the solution of a single-reaction model apparently can be made much more reliable than the model itself. The question still remains as to how reliable and useful a description of a complex reaction in terms of "one-dimensional" kinetics can be.

[1] R. Friedman and E. Burke, J. Chem. Phys. **21**, 710 (1953).
[2] T. von Karman and S. S. Penner, *Selected Combustion Problems, Combustion Colloquium, Cambridge, December, 1953.* (Butterworth's Publications, Ltd., London, 1952), p. 5.
[3] E. N. Adams, U. Wisconsin Report CF-957, Part V (1949). See also J. O. Hirschfelder, *et al.*, *Third Symposium on Combustion, Flames and Detonations* (Williams and Wilkins, Baltimore, 1949), p. 128.
[4] J. Corner, Proc. Roy. Soc. (London) **A198**, 388 (1949).
[5] Y. B. Zeldovitch and D. A. Frank-Kamenetsky, N.A.C.A. Tech. Memos 1026 and 1084.
[6] Hirschfelder, Curtiss, and Campbell, *Fourth Symposium on Combustion* (Williams and Wilkins, Baltimore, 1952), p. 204.
[7] J. O. Hirschfelder and T. Kihara, U. Wisconsin Report CM-766, February, 1953.
[8] They use a slightly different form of the Arrhenius exponential: $\exp[-E/RT_f(T_f-T_0/T-T_0)]$. It has the advantage that no cold boundary flame holder is needed, but for comparison purposes its effect is to neglect T_0 in comparison with T_f. That is, their work sets $\varphi=1$.
[9] Zero energy flux is thus assumed. Most of the approximate methods can (formally) consider the case $\delta\neq1$.

Substituted Methanes. XXIV. Potential Constants for CCl_2F_2

JEROME M. DOWLING
Spectroscopy Laboratory, Department of Physics, Illinois Institute of Technology, Chicago 16, Illinois*
(Received July 30, 1954)

RECENTLY Claassen[1] has obtained the Raman spectra of some chlorofluormethanes in the gaseous state. For CCl_2F_2 eight of the nine fundamentals were observed and assigned. Comparison with previous Raman and infrared spectral data led to a choice between 446 K and 473 K for the missing b_2 fundamental. On the basis of a sum rule and thermodynamic arguments, Claassen assigned the 446 K band as this fundamental.

To help ascertain a value for this fundamental, the writer has carried out a normal coordinate treatment (Wilson FG Matrix method[2]) for this molecule with a potential energy function

TABLE I. Observed and calculated wave numbers for CCl_2F_2.

Fundamental	Type	Wave numbers in kaysers Observed	Calculated
ν_1	a_1	1099	1098
ν_2	a_1	667.2	671
ν_3	a_1	457.5	455
ν_4	a_1	261.5	263
ν_5	a_2	322	322
ν_6	b_1	922	922
ν_7	b_1	435	433
ν_8	b_2	1162	1162
ν_9	b_2	446	446

containing all possible second-degree terms. The F and G matrix elements are formally the same as those of Decker *et al.*[3] and will therefore not be listed here. Potential constants were transferred from CF_3Cl,[4] CCl_3F,[5] CF_2Br_2,[3] and CCl_2Br_2.[6]

The calculations favored the 446 K band as the b_2 fundamental. Unfortunately, they do not completely rule out the other possibility since it was possible to modify the potential constants sufficiently to reproduce the 473 K band as the b_2 frequency.

TABLE II. Potential constants for CCl_2F_2.[a]

Constant	Value	Constant	Value
f_r	5.8468[b]	$f_{cc'l}$	−0.23360
f_{rl}	1.0048	f_{cc}	−0.10860
f_α	3.4017	f_{ll}	2.0480
$f_{\alpha l}$	0.80800	f_{cl}	1.3994
$f_{c\alpha}$	0.31458	f_{cc}	1.0700
f_{rll}	0.29270	$f_{cc'l}$	0.06730
$f_{r\alpha l}$	0.30557	$f_{cc'l'}$	0.11043
$f_{c'l}$	0.31729	f_{cll}	0.06083
$f_{c\alpha}$	0.36040	$f_{cc'l}$	0.06236
$f_{r\alpha l'}$	−0.15278	$f_{cc'l'}$	−0.15550
$f_{\alpha ll}$	−0.20895	$f_{cc'll}$	0.10211

[a] Bond constants and bond-bond interaction constants are in md/A; bond angle interaction constants are in md/rad; and angle, and angle interaction constants, are in md A/rad².
[b] This number of significant figures is not justified but is necessary to give best reproduction of the observed wave numbers and to secure internal consistency in the calculations.

The calculated values of the wave numbers corresponding to the fundamental frequencies are compared with the probable values determined by Claassen in Table I. The potential constants used to calculate the F matrix elements are given in Table II. To calculate the G matrix elements the C−F and C−Cl bond distances[7] were taken as 1.35 and 1.74 A, respectively, and the masses of the C, F, and Cl atoms were taken as 12.010, 19.000, and 35.457 awu, respectively.

Thermodynamic properties also were calculated assuming a rigid rotor, harmonic oscillator approximation. The values so obtained agree with the calculated values of Pitzer and Gelles[8] to within 0.04 cal deg^{-1} mole^{-1} and therefore will not be given here.

Acknowledgments.—This investigation was part of a research program which has been aided during the present year by a contract with the Office of Ordnance Research, U. S. Army; and by grants from the Research Corporation, the Socony-Vacuum Laboratories, and the American Academy of Arts and Sciences. The author and his associates are thankful for this assistance.

* Publication No. 107.
[1] H. H. Claassen, J. Chem. Phys. **22**, 50 (1954).
[2] E. B. Wilson, Jr., J. Chem. Phys. **7**, 1047 (1939); **9**, 76 (1941).
[3] Decker, Meister, Cleveland, and Bernstein, J. Chem. Phys. **21**, 1781 (1953).
[4] Decker, Meister, and Cleveland, J. Chem. Phys. **19**, 784 (1951).
[5] Zietlow, Cleveland, and Meister, J. Chem. Phys. **18**, 1076 (1950).
[6] Davis, Cleveland, and Meister, J. Chem. Phys. **20**, 454 (1952).
[7] L. O. Brockway, J. Chem. Phys. **41**, 747 (1937).
[8] E. Gelles and K. Pitzer, J. Am. Chem. Soc. **75**, 5259 (1953).

Electron-Induced Water Decomposition and Its Relation to Mass Spectrometric C_3^+ Measurements in Graphite Vapor

DWIGHT A. HUTCHISON
Chemistry Division, Argonne National Laboratory, Lemont, Illinois
(Received July 21, 1954)

RECENTLY, mass spectrometric measurements of variations in background peaks have been made as a function of hydrogen pressure in the ion source of a 60° direction-focusing instrument.[1] The results have been interpreted as follows: The electron beam which ionizes molecules in the mass spectrometer ion source induces a chemical reaction in the residual H_2O, O_2, and H_2 to form the dimer, $(H_2O)_2^+$.

The purposes of this note are to present preliminary results on this reaction and to discuss briefly the relation of these data to those of Honig[2] and Chupka and Inghram,[3] who made measurements on graphite vapor and ascribed their mass 36 ion peak to C_3^+.

In the present work normal isotopic H_2 was employed, and the larger positive ion background peaks in the mass range 1–50 were studied. Currents were recorded with a vibrating reed electrometer, and magnetic scanning was employed.

The experimental data are presented in Table I and Figs. 1 and 2. These data were taken with an electron beam energy of 50.0 volts. For comparison with the graphite measurements,[2,3] data were taken at 20.0 volts, and the linear increase of mass 36 with mass 18 was observed.

If the usual stoichiometry for decomposition of H_2O to form H_2 and O_2 applies, then under steady-state conditions one should expect a linear plot of the square root of the oxygen concentration *vs* the water concentration as shown in Fig. 1.

Since in Table I the mass 36 increases linearly with mass 18, the assignment of the major part of the mass 36 to the dimer $(H_2O)_2^+$ seems quite probable. For further evidence D_2 was employed, and the linear increase of mass 40 with mass 20 was observed as shown in Fig. 2. From these data it is believed that the formation of $(H_2O)_2^+$ and $(D_2O)_2^+$ has been observed. In a similar manner evidence has been obtained for OH^+, H_3O^+, H_4O^+,

TABLE I. Observed peak heights[a] when H_2 was introduced into the ion source.

Mass 2 ±2	Mass 18 ±0.1	Mass 32 ±0.04	Mass 36 ±0.04
136	7.3	0.90	0.12
280	14.0	0.70	0.17
414	19.6	0.58	0.20
514	23.1	0.49	0.21
654	27.9	0.42	0.22
741	30.7	0.37	0.23

[a] Peak heights have been corrected for background except for mass 32 since residual oxygen is consumed in the reaction.

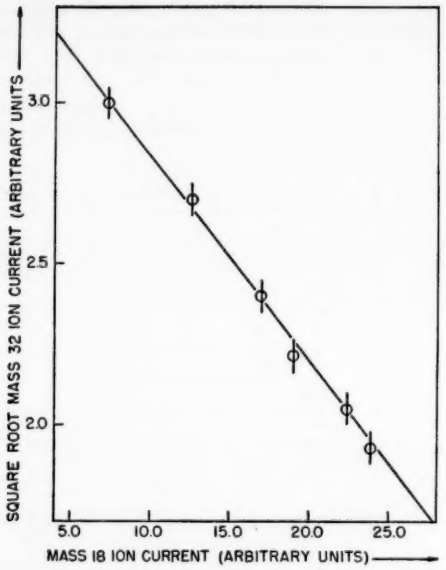

FIG. 1. Plot of the square root of the mass 32 ion current *vs* the mass 18 ion current. Circle diameters indicate the estimated errors in the mass 18 ion current and the vertical lines represent estimated errors in the square root of the mass 32 ion currents. The negative slope is due to the fact that oxygen is depleted to form water and its dimer ions.

and their dimer ions. These data and the kinetics and mechanisms of the various ion formations will be the subject of a paper in the near future.

In recent measurements on graphite vapor the conditions[4] were such that the formation of water dimer ions was highly probable. Even under the best of vacuum conditions, 10^{-7} to 10^{-9} mm Hg, obtained through bakeout and prolonged pumping, it has been

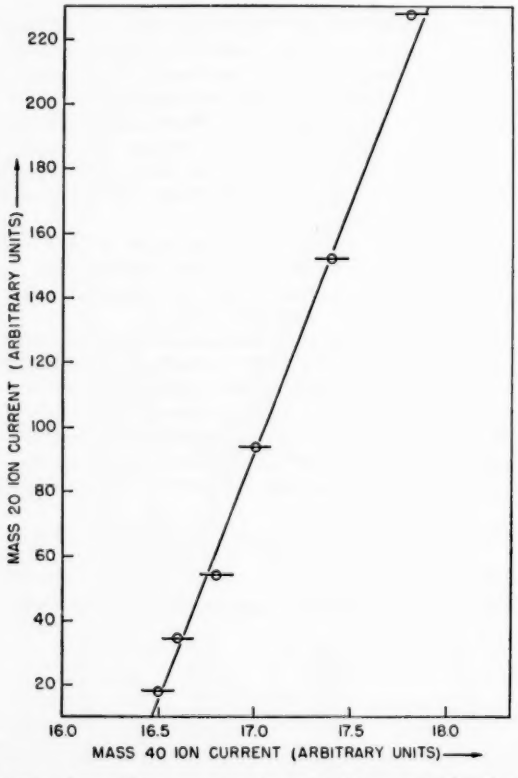

FIG. 2. Plot of mass 20 ion current *vs* the mass 40 ion current when deuterium was introduced into the mass spectrometer.

observed by the writer that small changes in ion-source temperature cause quite large changes in the mass 18 peak due to liberation of adsorbed water from metal and glass surfaces of the ion source and the surrounding tube envelope. It is interesting to compare Honig's[2] values, $C_1^+:C_3^+=1.0:6.7$, with Chupka and Inghram's[3] values, 1.0:1.6, which were obtained under approximately similar conditions except that no bakeout was employed by Honig.[4] It is felt that variations in these results can be attributed to $(H_2O)_2^+$.

These workers[2-4] have ascribed their residual mass 36 peak to HCl^+ on the basis of an approximate ratio of mass 36 to mass 38 being near the natural abundance of the chlorine isotopes. From the present work a ratio of 3.7 ± 0.1 has been obtained, which exceeds the accepted value[5] by 21 percent. Since the writer's work showed the mass 38 peak to increase with the mass 18 peak, it would seem that $(H_3O)_2^+$ rather than HCl^{37+} would be an experimentally more justified assignment for the mass 38 peak.

It would appear that an investigation of possible secondary reactions induced by the electron beam should be made before assignment of a given mass ion to a certain molecular ion structure. As stated previously,[2,3] there must be determined the ionization cross sections of proposed molecular species, their precise appearance potentials, their excess kinetic energy, etc. before reasonable conclusions can be made. Ion structure assignments to observed masses in graphite vapor must be considered only as preliminary until the potentialities of the mass spectrometric art are more fully realized. In light of the present work one can state that some fraction, or possibly all, of the measured C_3^+ can be interpreted as $(H_2O)_2^+$.

Acknowledgment is due Mr. L. G. Pobo for his assistance in the collection of these data.

[1] Designed by and constructed under the writer's direction. To be described later.
[2] R. E. Honig, J. Chem. Phys. **22**, 126 (1954).
[3] W. A. Chupka and M. G. Inghram, J. Chem. Phys. **21**, 1313 (1953).
[4] From conversation with R. E. Honig and with M. G. Inghram at the Second Annual Meeting of the ASTM E-14 Committee on Mass Spectrometry, May 23–28, 1954, New Orleans.
[5] K. T. Bainbridge and A. O. Nier, Preliminary Report No. 9, Nuclear Science Series, Division of Mathematics and Physical Sciences, National Research Council.

A Quantum-Mechanical Equation of Reaction Rates

IWAO YASUMORI AND KENJI FUEKI
Laboratory of Physical Chemistry, Tokyo Institute of Technology, Ookayama, Meguro-ku, Tokyo, Japan
(Received July 8, 1954)

ATTEMPTS have been made by several investigators to calculate the transmission through a potential barrier of a mass point representing the reacting system so that, on the basis of these results, the rate equation might be formulated.[1]

Following such a principle and using a potential barrier of more natural form for chemical problems, we have obtained a quantum-mechanical rate equation which gives some theoretical basis for the approximations used in the absolute reaction rate (ARR) theory.

The wave equation which expresses a displacement reaction $A+BC\rightarrow AB+C$ of linear configuration, is

$$\left[-\frac{\hbar^2}{2\mu}\frac{\partial^2}{\partial\rho^2}-\frac{\hbar^2}{2m}\frac{\partial^2}{\partial\rho^2}+V(r,\rho)\right]\Psi(r,\rho)=E_t\Psi(r,\rho), \quad (1)$$

where $\mu=m_A(m_B+m_C)/(m_A+m_B+m_C)$, $m=m_Bm_C/(m_B+m_C)$, ρ is the displacement of the $B-C$ distance from its equilibrium value and r is the displacement of the distance between A and the center of mass of the molecule BC from its value at the top of the barrier.

Confining the problem to the case where the reaction path lies parallel to the r axis, one may take the potential barrier function $V(r,\rho)$ as follows: (Fig. 1)

$$V(r,\rho)=V_r(r)+[a_0-aV_r(r)]\rho^2. \quad (2)$$

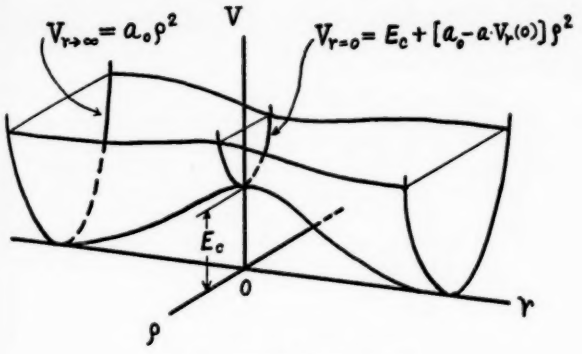

FIG. 1. Potential energy barrier.

Then, by the use of $\Psi(r,\rho)$ in the expanded form

$$\Psi(r,\rho)=\Sigma_n \psi_n(\rho)\cdot F_n(r), \tag{3}$$

where $\psi_n(\rho)$ is the normalized eigenfunction for the equation

$$\left[-\frac{\hbar^2}{2m}\frac{d^2}{d\rho^2}+a_0\rho^2\right]\psi_n(\rho)=E_n\psi_n(\rho), \tag{4}$$

one obtains

$$\left[\frac{\hbar^2}{2\mu}\frac{d^2}{dr^2}+E_l-V_r(r)\,(1-a\rho^2{}_{n,n})\right]F_n(r)$$
$$=-aV_r(r)[\rho^2{}_{n,n-2}\cdot F_{n-2}(r)+\rho^2{}_{n,n+2}\cdot F_{n+2}(r)],$$
$$n=0,\ 1,\ 2,\ \cdots, \tag{5}$$

where $E_l=E_i-E_n$ and $\rho_{kl}{}^2=\int_{-\infty}^{+\infty}\psi_k{}^*(\rho)\rho^2\psi_l(\rho)d\rho$.

This set of simultaneous differential equations can not be solved rigorously. But, when $a\rho_{kl}{}^2$ ($k=n,\ l=n,\ n\pm2$) is sufficiently small in comparison with unity, the right-hand side of Eq. (5) may approximately be taken equal to zero.[2]

Moreover, if one takes the Eckart potential[3] $V_r(r)=E_c/\cosh^2(\pi r/l)$ as the actual one, Eq. (5) can be solved and then the transmission coefficient κ_n is obtained as follows:

$$\kappa_n=\frac{\cosh(4\pi\alpha)-1}{\cosh(4\pi\alpha)+\cosh(2\pi\delta)}\simeq\frac{e^{4\pi\alpha}}{e^{4\pi\alpha}+e^{2\pi\delta}}, \tag{6}$$

where $\alpha=\frac{1}{2}[E_l/C]^{\frac{1}{2}}$, $\delta=[E_c(1-a\rho^2{}_{n,n})/C-\frac{1}{4}]^{\frac{1}{2}}$, $C=\hbar^2/8\mu l^2$.

From Eq. (6), one can easily find $\partial\kappa_n/\partial a>0$. This means that κ_n may increase or decrease according as the curvature of vibrational potential at the barrier becomes smaller or larger. Assuming the initial states in thermal equilibrium, one can obtain, by the help of the approximate form of κ_n, the rate equation[4,5]

$$k=\frac{kT}{h}\frac{f^{\ddagger}_{tr}}{F_A\cdot F_{BC}}\exp\left(\frac{h\nu_0}{2kT}\right)\sum_n\left[1+2\sum_{m=1}^{\infty}\left\{(C/4\pi^2kT)^m\right.\right.$$
$$\left.\left.\cdot L_{2m}(x_n)\cdot\sum_{p=1}^{\infty}\frac{(-1)^p}{p^{2m}}\right\}\right]\exp(-y_n{}^2), \tag{7}$$

where

$$L_{2m}(x_n)=-\left[\exp(x^2)\frac{d^{(2m)}}{dx^{(2m)}}\exp(-x^2)\right]_{x=x_n},$$
$$x_n{}^2=\frac{1}{kT}\left[E_c-h\left(\frac{\nu_0{}^2-\nu^{\ddagger 2}}{2\nu_0}\right)(n+\tfrac{1}{2})-C/4\right],$$
$$y_n{}^2=x_n{}^2+\frac{h\nu_0}{kT}(n+\tfrac{1}{2}),$$

ν_0 and $\nu^{\ddagger}$ are the vibrational frequencies deduced from the relations $a_0=2\pi^2m\nu_0{}^2$ and $a_0-aV_r(0)=2\pi^2m\nu^{\ddagger 2}$, respectively.

As $(C/4\pi^2kT)$ approaches to zero, the above equation turns formally to that of the ARR theory, i.e.,

$$k=\frac{kT}{h}\frac{f^{\ddagger}_{tr}}{F_A\cdot F_{BC}}\left[1-\exp\left(-\frac{h\nu_a}{kT}\right)\right]^{-1}$$
$$\times\exp\left[-\frac{1}{kT}(E_c+\tfrac{1}{2}h\nu_a-\tfrac{1}{2}h\nu_0)\right]. \tag{8}$$

But it is to be noted that the term corresponding to the vibrational partition function of the "activated complex" includes $\nu_a=(\nu_0{}^2+\nu^{\ddagger 2})/2\nu_0$, instead of $\nu^{\ddagger}$, as the frequency.

As an example, the deviation of the ARR equation (k_A), from Eq. (7) is estimated for the hydrogen atom-molecule reaction which seems to show the largest quantum effect (Table I). When

TABLE I. Ratio of calculated rates for the reaction $H+H_2\to H_2+H$.[a]

Temp. °K	300	500	1000	2000
$(k_A/k)_1$[b]	0.974	1.029	1.030	1.022
$(k_A/k)_2$[c]	0.193	0.574	0.873	0.971

[a] $h\nu_0=12.56$, $h\nu^{\ddagger}=10.36$ and $E_c=7.63$ kcal/mole are used (see reference 6).
[b] Values for $l=3.65$ A. In this case the curvature of reaction path at the top of the barrier is equal to that obtained by the semiempirical method.
[c] Values for $l=1.15$ A.

$a\rho_{kl}{}^2$ is not so small, the problem must be treated by the more elaborate method. Detailed discussion will be published elsewhere.

We are much indebted to Dr. S. Shida for his kind guidance.

[1] J. O. Hirschfelder and E. Wigner, J. Chem. Phys. **7**, 616 (1939); E. Bauer and Ta-You Wu, J. Chem. Phys. **21**, 726 (1953); F. A. Matsen, J. Chem. Phys. **22**, 165 (1954). Also see Eyring, Walter, and Kimball, *Quantum Chemistry* (John Wiley & Sons, Inc., New York, 1949), Chap. XVI, p. 299.
[2] This condition also means that $aV_r(r)$ is much smaller than a_0.
[3] C. Eckart, Phys. Rev. **35**, 1303 (1930).
[4] Excluding the rotational term only, $f^{\ddagger}_{tr}$, F_A, and F_{BC} are defined by the usual manner in the rate theory.
[5] If the restrictions for energies, $E_i<E_{n-2}$ and $E_c<2h\rho_0$, are assumed, $\psi_0(\rho)F_0(r)$ and $\psi_1(\rho)F_1(r)$ would be good approximations for $\Psi(r,\rho)$, independent of $a\rho_{kl}{}^2$. In this case the summation is taken for $n=0$, 1 and a correction term, $-\exp(-E_{n-2}/kT)$, is added inside the summation.
[6] Hirschfelder, Eyring, and Topley, J. Chem. Phys. **4**, 170 (1936).

Erratum: Rotational Energy Transfer in Diatomic Molecules

[J. Chem. Phys. **22**, 1189 (1954)]

ROBERT BROUT
Department of Chemistry, University of Rochester, Rochester 3, New York

THE following corrections should be made: In connection with formula (2)

$k_J=(2\mu(kT+\Delta\epsilon)/\hbar^2)^{\frac{1}{2}}$

$\Delta\epsilon$ = energy difference between rotational levels j and $j-2$.

In connection with formula (5)

$$k_{\rm rot}{}^2=2\mu kT_{\rm rot}/\hbar^2 \quad \text{where} \quad kT_{\rm rot}=\hbar^2/2I.$$

Formula (8) should have the factor $(c\lambda^2/16)$ rather than $(c\lambda^2/10)$

Erratum: The Infrared Spectrum and Molecular Constants of Sulfur Dioxide

R. D. SHELTON, A. H. NIELSEN, AND W. H. FLETCHER
Department of Physics, University of Tennessee, Knoxville, Tennessee

[J. Chem. Phys. **21**, 2178 (1953)]

THROUGH an oversight in proofreading, X_{23} found in line 7 of the second column of the text on page 2182 reads 0.390 cm^{-1}. It should read -3.90 cm^{-1}.

Errata: Symmetry and Stability in Diborane and in Borine

[J. Chem. Phys. **22**, 536 (1954)]

G. W. CASTELLAN
The Department of Chemistry, The Catholic University of America, Washington, D. C.

IN the above-named article the statement that the outermost pair of electrons in diborane are in an orbitally degenerate state led to a misinterpretation in the application of the Jahn-

Teller theorem to the case of diborane. It is true that the π_g molecular orbitals (MO's) are orbitally degenerate, but the antisymmetrized product (AP) of lowest energy built from them is not. In order to use the Jahn-Teller theorem, one must consider the total electronic wave function, that is, the AP rather than the MO's. The argument as presented therefore is not correct.

It is still possible, although unlikely, that the ethane structure for diborane is unacceptable because of symmetry. Mulliken[1] lists three electronic configurations which are close to one another in energy. The ground-state configuration yields states having symmetries $^3A_{2g}$, ^1E_g, and $^1A_{1g}$. Of these, $^3A_{2g}$ seems likely to have the lowest energy. If this is really the ground state, then symmetry does not rule out the ethane-like structure. The two other configurations yield states of symmetry ^3E_u, ^1E_u, ^1E_g in addition to a number of nondegenerate states. One of these states of symmetry E might conceivably lie so low as to actually be the ground state. In this case, symmetry would not admit the ethane structure for diborane.

With regard to the magnitude of the effect produced by the Jahn-Teller theorem, in the footnote on p. 537 of *Symmetry and Stability in Diborane and in Borine*, a reference is made to the work of Griffing and Macek. This work should not have been quoted in this connection; the reference to it was occasioned by the above-mentioned confusion over MO and AP symmetry. However, the reference to the work of Hirschfelder is valid.

The application of the Jahn-Teller theorem to borine is being re-examined.

The author wishes to express his thanks to Dr. Joseph T. Vanderslice for helpful discussions.

[1] R. S. Mulliken, Chem. Revs. **41**, 207 (1947).